Blind and semi-blind signal processing for telecommunications and biomedical engineering

Vicente Zarzoso

Mémoire en vue de l'obtention de

l'HABILITATION À DIRIGER DES RECHERCHES

Université de Nice - Sophia Antipolis

U.F.R. Sciences

TRAITEMENT AVEUGLE ET SEMI-AVEUGLE DU SIGNAL POUR LES TÉLÉCOMMUNICATIONS ET LE GÉNIE BIOMÉDICAL

Vicente ZARZOSO

Présenté le

9 novembre 2009

devant le jury :

M. Pierre Comon	Président
M. Sergio Cerutti	Rapporteur
M. Christian Jutten	Rapporteur
M. John McWhirter	Rapporteur
M. Éric Moreau	Examinateur
M. Jean-Marc Vesin	Examinateur

Résumé

Ce rapport résume mes activités de recherche depuis l'obtention de mon doctorat. Je me suis penché sur le problème fondamental de l'estimation de signaux sources à partir de l'observation de mesures corrompues de ces signaux, dans des scénarios où les données mesurées peuvent être considérées comme une transformation linéaire inconnue des sources. Deux problèmes classiques de ce type sont la déconvolution ou égalisation de canaux introduisant des distortions linéaires, et la séparation de sources dans des mélanges linéaires. L'approche dite *aveugle* essaie d'exploiter un moindre nombre d'hypothèses sur le problème à résoudre : celles-ci se réduisent typiquement à l'indépendance statistique des sources et l'inversibilité du canal ou de la matrice de mélange caractérisant le milieu de propagation. Malgré les avantages qui ont suscité l'intérêt pour ces techniques depuis les années soixante-dix, les critères aveugles présentent aussi quelques inconvénients importants, tels que l'existence d'ambiguïtés dans l'estimation, la présence d'extrema locaux associés à des solutions parasites, et un coût de calcul élevé souvent lié à une convergence lente.

Ma recherche s'est consacrée à la conception de nouvelles techniques d'estimation de signal visant à pallier aux inconvénients de l'approche aveugle et donc à améliorer ses performances. Une attention particulière a été portée sur deux applications dans les télécommunications et le génie biomédical : l'égalisation et la séparation de sources dans des canaux de communications numériques, et l'extraction de l'activité auriculaire à partir des enregistrements de surface chez les patients souffrant de fibrillation auriculaire. La plupart des techniques proposées peuvent être considérées comme étant *semi-aveugles*, dans le sens où elles visent à exploiter des informations a priori sur le problème étudié autres que l'indépendance des sources ; par exemple, l'existence de symboles pilotes dans les systèmes de communications ou des propriétés spécifiques de la source atriale dans la fibrillation auriculaire. Dans les télécommunications, les approches que j'ai explorées incluent des solutions algébriques aux fonctions de contraste basées sur la modulation numérique, la combinaison de contrastes aveugles et supervisés dans des critères semi-aveugles, et une technique d'optimisation itérative basée sur un pas d'adaptation calculé algébriquement. Nos efforts visant à extraire le signal atrial dans des enregistrements de fibrillation auriculaire nous ont permis non seulement de dégager de nouvelles fonctions de contraste basées sur les statistiques de second ordre et d'ordre élevé incorporant l'information a priori sur les statistiques des sources, mais aussi d'aboutir à de nouveaux résultats d'impact clinique et physiologique sur ce trouble cardiaque encore mal compris. Ce rapport se conclut en proposant quelques perspectives pour la continuation de ces travaux.

Ces recherches ont été menées en collaboration avec un nombre de collègues en France et à l'étranger, et ont également compris le co-encadrement de plusieurs doctorants. Les contributions qui en ont découlé ont donné lieu à plus de soixante publications dans des journaux, des conférences et des ouvrages collectifs à caractère international. Quelques-unes de ces publications sont jointes à ce document.

Mots-clés : algèbre tensorielle, analyse en composantes indépendantes, analyse en composantes principales, critères basés sur l'alphabet fini, critère à module constant, déconvolution, égalisation du canal, électrocardiogramme, fibrillation auriculaire, filtrage spatio-temporel, fonctions de contraste, information a priori, kurtosis, modulations numériques, optimisation itérative, optimisation du pas d'adaptation, problèmes inverses, séparation de sources, statistiques de second ordre, statistiques d'ordre élevé, techniques aveugles, techniques semi-aveugles, traitement d'antenne, traitement statistique du signal.

BLIND AND SEMI-BLIND SIGNAL PROCESSING FOR TELECOMMUNICATIONS AND BIOMEDICAL ENGINEERING

Report submitted in accordance with the requirements of the

University of Nice - Sophia Antipolis
Faculty of Science

to obtain the

AUTHORIZATION TO SUPERVISE RESEARCH

Vicente Zarzoso

Defended on

November 9, 2009

in front of the jury:

Pierre Comon	Chairman
Sergio Cerutti	Reviewer
Christian Jutten	Reviewer
John McWhirter	Reviewer
Éric Moreau	Examiner
Jean-Marc Vesin	Examiner

Abstract

The present report summarizes the research activities that I have carried out since completion of my PhD. My attention has focused on the fundamental signal processing problem of source signal estimation from the observation of corrupted measurements, in scenarios where the measured data can be considered as unknown linear transformations of the sources. Two typical problems of this kind are the deconvolution or equalization of channels introducing linear distortions and source separation in linear mixtures. The *blind* approach makes as few assumptions as possible about the problem in hand: these typically reduce to the statistical independence of the sources and the invertibility of the channel or mixing matrix characterizing the propagation medium. Despite the advantages that have driven the interest in these techniques since the 70's, blind criteria also present some important drawbacks such as the existence of estimation ambiguities, the presence of local extrema leading to spurious solutions, and a high computational complexity often linked to slow convergence.

My research has been devoted to the design of novel signal estimation techniques alleviating the drawbacks and thus improving the performance of the blind approach. Special emphasis has been laid on two specific applications in telecommunications and biomedical engineering: equalization and source separation in digital communication channels and atrial activity extraction in surface electrocardiogram recordings of atrial fibrillation patients. Most of the proposed techniques can be considered as *semi-blind* in that they aim at exploiting available prior information about the problems under study other than source independence; e.g., the existence of training data in communication systems or specific properties about the atrial source in atrial fibrillation. In communications, the approaches that I have explored include algebraic solutions to contrast functions based on digital modulations, the combination of blind and training-based contrasts into semi-blind criteria, and an iterative optimization technique with an optimal step-size coefficient computed algebraically. Our efforts to extract the atrial signal in multi-lead atrial fibrillation recordings has led not only to new contrast functions based on second- and higher-order statistics incorporating priors about the source statistics, but also to novel results of clinical and physiological significance about this challenging cardiac condition. The report concludes by proposing some possible avenues for the continuation of this work.

This investigation has been carried out in collaboration with a number of colleagues in France and abroad, and has also comprised the joint supervision of several PhD students. The resulting contributions have given rise to over sixty publications in international journals, conferences and book chapters. A compilation of selected

publications is attached to this document.

Keywords: alphabet-based criteria, array signal processing, atrial fibrillation, blind techniques, channel equalization, constant modulus, contrast functions, deconvolution, digital modulations, electrocardiogram, higher-order statistics, independent component analysis, inverse problems, iterative optimization, kurtosis, principal component analysis, prior information, second-order statistics, semi-blind techniques, source separation, space-time filtering, statistical signal processing, step-size optimization, tensor algebra.

Acknowledgments

A large part of the work summarized in this report has been made possible by the participation of many individuals, and citing them all would probably fill many pages.

First of all, I feel indebted to Pierre Comon, Olivier Meste and Tarek Hamel, for their constant support and encouragement, for believing in me, since I arrived at the I3S Laboratory. Many other people have greatly contributed to making my work at I3S very pleasant. I will just mention here Viviane Rosello, Micheline Hagnère and Sabine Barrère. I am also very grateful to my teaching colleagues at the GEII Department, IUT Nice - Côte d'Azur, for the friendly work atmosphere.

Doing research is all about learning and discovering new things, and I have learnt so many from all the collaborators I have worked with over the years, including the students I have helped supervise. Their knowledge, skills and enthusiasm have been a continuous source of stimulation. My collaborations with Pietro Bonizzi, Narcís Cardona, Francisco Castells, Pierre Comon, Adriana Dapena, Yumang Feng, Jorge Igual, Kostas Kokkinakis, Olivier Meste, José Millet, Juan José Murillo, Asoke K. Nandi, Héctor J. Pérez-Iglesias, Ronald Phlypo, José J. Rieta, Ludwig Rota, Addisson Salazar, Luis Vergara and Wenhuan Xu have been as enjoyable as rewarding, and often excitingly challenging.

I would like to express my most sincere gratitude to Sergio Cerutti, Pierre Comon, Christian Jutten, John McWhirter, Éric Moreau and Jean-Marc Vesin for willingly accepting to be part of the jury. I feel honored that such renowned researchers have spent some of their precious time and energy to evaluate my work.

Olivier Meste, Hervé Rix and Gérard Favier, colleagues at I3S, sacrificed valuable time from their busy timetables to carefully read a preliminary version of this report and give me some interesting suggestions. Together with Luc Deneire, they also offered me useful advice for my defense preparation. I thank them for their feedback.

Last but not least, I am infinitely grateful to my family. Without their love, everything else would have been impossible, if not just meaningless. My wife, Caroline, has been particularly loving, patient and supportive over the preparation of my HDR.

Contents

Acronyms

AA	atrial activity
ABS	average beat subtraction
ACMA	analytic constant modulus algorithm
ACPA	analytic constant power algorithm
AEML	alternative extended maximum likelihood
AF	atrial fibrillation
AFL	atrial flutter
AML	approximate maximum likelihood
ANC	adaptive noise cancellation
APF	alphabet polynomial fitting
ASTRE	former Signal Processing for Communications Research Group, now part of the SIGNAL team at the I3S Lab
AV	atrio-ventricular
BIOMED	former Biomedical Signal Processing Research Group, now part of the SIGNAL team at the I3S Lab
BPSK	binary phase shift keying
BSPM	body surface potential mapping
BSS	blind source separation
CCI	co-channel interference
CF	Comon's formula
CFAE	complex fractionated atrial electrogram
CHU	university hospital
CM	constant modulus
CMA	constant modulus algorithm
CoM	contrast maximization
CP	constant power
CPA	constant power algorithm
DERA	Defence Evaluation and Research Agency, UK
DFT	discrete Fourier transform
ECG	electrocardiogram
EML	extended maximum likelihood
ETSIT	Higher Telecommunications Engineering School at UPV
EVD	eigenvalue decomposition
FIR	finite impulse response
GEII	Electrical Engineering and Industrial Data Processing Department
HOS	higher-order statistics
I3S	Computer Science, Signals and Systems Laboratory of Sophia Antipolis, France
ICA	independent component analysis

i.i.d.	independent and identically distributed
ISI	intersymbol interference
ISM	industrial, scientific and medical frequency band
IUT	University Institute of Technology
JADE	joint approximate diagonalization of eigenmatrices
KM	kurtosis maximization
KSP	kurtosis sign priors
KVP	kurtosis value priors
LMS	least mean squares
LS	least squares
MAP	maximum a posteriori
MaxViT	maximum variance in tails
MIMO	multiple input multiple output
MISO	multiple input single output
ML	maximum likelihood
MMSE	minimum mean square error
MSK	minimum shift keying
NSR	normal sinus rhythm
OS-CMA	optimal step-size constant modulus algorithm
OS-CPA	optimal step-size constant power algorithm
OSTBC	orthogonal space-time block coding
PCA	principal component analysis
pdf	probability density function
PEDR	bonus for research and doctoral supervision
PSK	phase shift keying
QPSK	quadrature phase shift keying
RACMA	real analytic constant modulus algorithm
RF	radiofrequency
SC	spectral concentration
SIMO	single input multiple output
SISO	single input single output
SNR	signal-to-noise ratio
SOBI	second-order blind identification
SOS	second-order statistics
SPC	Signal Processing for Communications Research Group at the University of Liverpool, UK
STC	spatiotemporal QRST cancellation
SVD	singular value decomposition
UPV	Polytechnic University of Valencia, Spain
VA	ventricular activity
V-BLAST	vertical Bell Labs layered space-time architecture
WDA	wavelength dependent attenuator
WDM	wavelength division multiplexing
ZF	zero forcing

Chapter 1

Extended CV

1.1 Personal Details

Name:	Vicente ZARZOSO
Birth date and place:	Sep. 12, 1973, Valencia (Spain)
Nationality:	Spanish
Family status:	married since July 15, 2005 one child since Sep. 28, 2007
Personal address:	96 Corniche Fleurie, Sirius-B, 06200 Nice, France

Professional address:	Laboratoire I3S, Les Algorithmes - Euclide-B
	2000 route des Lucioles, BP 121
	06903 Sophia Antipolis Cedex, France
	Tel: +33 (0)4 92 94 27 95
	Fax: +33 (0)4 92 94 28 96
	`zarzoso@i3s.unice.fr`
	`http://www.i3s.unice.fr/~zarzoso`

1.2 Career Evolution

Since 2005 **Lecturer/researcher (maître de conférences)**
Teaching: Département de Génie Électrique et Informatique Industrielle (GEII), IUT Nice - Côte d'Azur, Univ. Nice - Sophia Antipolis.
Research: Laboratoire d'Informatique, Signaux et Systèmes de Sophia Antipolis (I3S).

In Jan. 2007, I was promoted to grade 3 (*3ème échelon*) of the *maîtres de conférences* salary scale.

Since Sep. 2007, I have been in receipt of a Bonus for Research and Doctoral Supervision (*Prime d'encadrement doctoral et de recherche, PEDR*) from the French Ministry of Education.

2000–2005 **Research Fellow, Royal Academy of Engineering, UK**
Department of Electrical Engineering & Electronics, University of Liverpool, UK.
Topic: blind signal separation for communications and biomedical engineering.

1999 **PhD, University of Liverpool, UK**
Thesis: "Closed-Form Higher-Order Estimators for Blind Separation of Independent Source Signals in Instantaneous Linear Mixtures" (PhD viva: Oct. 14, 1999).
Supervisor: Prof. Asoke K. Nandi.
Funding: University Scholarships; my first year was also partially funded by the Defence Evaluation and Research Agency (DERA) of the UK.
I was awarded the *Robert Legget Prize* (2000) for an especially distinguished thesis submitted to the Faculty of Engineering.

1996 **MEng Telecommunications, Universidad Politécnica de Valencia (UPV), Spain**
I graduated with the *highest distinction (rank: 1st)* at the Escuela Técnica Superior de Ingenieros de Telecomunicación (ETSIT).

1.3 Research Activities

1.3.1 Research Areas

My research has focused on the fundamental signal processing problem of signal estimation in linear mixtures, including blind channel equalization, blind source separation (BSS) and independent component analysis (ICA). I am interested in the theoretical aspects at the heart of these techniques as well as their practical application to telecommunications and biomedical engineering. Details about these activities can be found in Chapters 3 and 4.

Since 2005: my activities have lain at the interface between two groups of the I3S Lab: the Signal Processing for Communications (ASTRE) group, leaded by Pierre Comon, and the Biomedical Signal Processing (BIOMED) group, leaded by Hervé Rix.[1]

- In the area of signal processing for communications, I have worked on the following topics:
  - blind and semi-blind channel equalization based on the finite alphabet property of digital communication signals;
  - efficient iterative optimization with optimal step-size selection for channel equalization and source separation;
  - contrasts for BSS/ICA incorporating prior information about the signals of interest.

[1] In 2008, both groups merged into the SIGNAL research team.

Publications: [P4, P5, P8, P9, P14, P15, P37, P40, P41].[2]

- In biomedical signal processing, I have contributed to the topic of:
  - atrial activity analysis in atrial fibrillation episodes using BSS/ICA-based techniques exploiting prior information.

    Publications: [P1, P2, P3, P6, P10, P11, P13, P25, P26, P28, P29, P30, P31, P32, P33, P34, P35, P36, P38].

  Publications involving a close collaboration between the ASTRE and BIOMED groups: [P5, P11, P14, P26, P30, P32, P38],

  Publications issued from students' supervision: [P1, P2, P3, P5, P6, P13, P14, P25, P28, P29, P31, P32, P33, P34, P35, P36, P38].

2000–2005: my postdoctoral research was carried out at the Signal Processing and Communications (SPC) research group, leaded by Asoke K. Nandi, University of Liverpool, UK. The final two years comprised a stay at the I3S Lab (Sec. 1.3.4).

- The topics covered during this period include the application of BSS/ICA techniques to:
  - space-time equalization in wireless digital communication systems;
  - optical transmission monitoring;
  - atrial activity extraction in atrial fibrillation episodes.

  Publications: [P12, P17, P18, P19, P20, P21, P22, P23, P24, P42, P43, P44, P45, P46, P47, P48, P49, P50, P51, P52, P53, P54, P55, P56, P57, P58, P59, P60, P61, P62, P63, P64, P65, P66, P67]

  Publications issued from students' supervision: [P22, P42, P45, P51, P52, P58, P59, P61].

1995–1999: my MEng final year project and the first two years of my PhD studies took place at the Department of Electrical & Electronic Eng., University of Strathclyde, Glasgow, UK, under the supervision of Asoke K. Nandi. My PhD then concluded at the University of Liverpool.

- Topics:
  - closed-form estimators for BSS/ICA in the two-signal case;
  - application to non-invasive fetal activity extraction from maternal skin electrode recordings.

  Publications: [P69]– [P90].

[2] Underlined publications are attached to this report.

1.3.2 Thematic Mobility

Before 2003 My research focused on generic theoretical aspects of *blind signal processing* and, in particular, the problems of *BSS/ICA*. The performance of the BSS/ICA techniques that I developed were illustrated on signals issued from biomedical applications such as non-invasive *fetal electrocardiogram extraction* during pregnancy and, since 2000, non-invasive *atrial activity extraction in atrial fibrillation* episodes.

2003–2005 My postdoctoral stay at the I3S Lab (ASTRE group) allowed me to deepen my understanding of the theoretical aspects of blind and *semi-blind signal processing*, with particular emphasis on applications related to *telecommunications* and *biomedical engineering*. Semi-blind techniques incorporate prior information into purely blind techniques, generating algorithms more adapted to the particular problem under study and thus yielding improved performance.

Since 2005 My research has been shared between the ASTRE and BIOMED groups (now SIGNAL team) of the I3S Lab, where

- I have been gaining further understanding of theoretical aspects of blind and semi-blind signal processing;
- I have been searching for more specific semi-blind techniques for *atrial fibrillation analysis*.

1.3.3 Geographic Mobility

My studies and professional activities have taken place in four universities of three different countries:

1991–1995 **Universidad Politécnica de Valencia, Spain**
First four years of MEng in Telecommunications.

1995–1999 **University of Strathclyde, Glasgow, UK**
Erasmus year followed by my first two years of PhD studies.

1999–2003 **University of Liverpool, UK**
End of my PhD studies and first three years of my postdoctoral research, funded by the Royal Academy of Engineering.

2003– **Université de Nice - Sophia Antipolis, France**
Two-year postdoctoral stay at I3S Lab.
Permanent lecturer/researcher position since Sep. 2005.

1.3.4 International Collaborations and Invitations by Foreign Universities

2006– **Institute Biomedical Technology (IbiTech), Universiteit Gent, Belgium**
Collaborators: Ronald Phlypo (PhD student) and Ignace Lemahieu.
Topic: atrial activity extraction from surface recordings of atrial fibrillation by exploiting prior information about the signal of interest (Secs. 4.6–4.7, pp. 60–68.)
Publications: [P1, P3, P5, P6, P11, P13, P14, P32, P33, P34, P36, P38].

2006– **Departamento de Electrónica y Sistemas, Universidad de la Coruña, Spain**
Collaborators: Héctor J. Pérez-Iglesias and Adriana Dapena.
Topic: application of BSS/ICA techniques based on the eigenvalue decomposition of second- and fourth-order cumulant matrices to blind channel estimation in space-time coded communications systems (Sec. 3.6.2, pp. 48–49).
Publications: [P7, P16, P27, P39].

2004– **Departamento de Señal y Comunicaciones, Universidad de Sevilla, Spain**
Collaborator: Juan J. Murillo-Fuentes.
Topic: algebraic solutions to ICA based on fourth-order statistics (Sec. 2.4.1, p. 24).
Publications: [P18, P44, P49].

2003– **Groupe ASTRE, Laboratoire I3S**
2005 *Collaborator:* Pierre Comon.
Topic: during my postdoctoral stay, we worked on algebraic and iterative solutions for blind and semi-blind channel equalization based on digital signal alphabets (Secs. 3.3–3.5, pp. 30–46, and Sec. 3.6.1, pp. 46–48).
Stay funded by a "Research Fellowship" awarded by the Royal Academy of Engineering, UK.
Publications: [P12, P17, P19, P42, P43, P45, P46].

12/03– **Departamento de Comunicaciones, UPV**
01/04 *Collaborators:* Óscar Lázaro, Gema Piñero and Narcís Cardona.
Topic: blind channel estimation in 3rd-generation (UMTS) mobile telephony systems with distributed antennas.
Stay funded by "Programa de Incentivo a la Investigación de la UPV 2003 — Estancias en la UPV de Investigadores de Prestigio."
The stay included a talk to the members of the department on the fundamentals of blind channel identification (Sec. 1.3.7).

12/01– **Departamento de Comunicaciones, UPV**
01/02 *Collaborators:* Jorge Igual and Luis Vergara.
Topic: space-time MIMO channel equalization using BSS/ICA techniques (Sec. 3.2, pp. 28–30).
Stay funded by "Programa de Incentivo a la Investigación de la UPV 2001 — Estancias en la UPV de Investigadores de Prestigio."
Publications: [P53, P60].

2000– **Grupo de Bioingeniería, UPV**
Collaborators: José J. Rieta, Francisco Castells and José Millet.
Topic: biomedical signal processing applications, with focus on atrial fibrillation analysis (Secs. 4.4–4.5, pp. 58–60, and Sec. 4.9.2, pp. 70–71).
Stay partly funded by the Consejo Superior de Investigaciones Científicas (CSIC) [Spanish National Research Council].
Publications: [P2, P20, P21, P25, P48, P56, P57, P63, P67, P73, P79].

1.3.5 Students' Supervision

My implication in the supervision of *PhD students* is summarized in Table 1.1. I have helped supervise six students of five different nationalities from three different universities. Four of these students have successfully completed their PhD, whereas the two others are still pursuing their degree. This supervisory work has resulted in the publication of a book chapter [P11], three journal articles [P13, P14, P22] and sixteen conference papers [P25, P28, P29, P31, P32, P33, P34, P35, P36, P38, P42, P45, P51, P58, P59, P61] (Sec. 1.3.6). In addition, another book chapter [P1] is being prepared, while four journal articles [P2, P3, P5, P6] have been submitted for publication.

I have also contributed to the supervision of several *MSc students*' projects in the UK:

Student	Topic	Year	Publications
K. Kokkinakis	Blind audio source separation	2001	—
S. Punnoose	Blind multicarrier equalization	2002	—
L. Sarperi	Blind deconvolution of digital communication channels	2002	[P52]

In addition, I have supervised the following *final year project students*:

Students	School	Topic	Year
J. Thaon C. Beaussieux	IUT GEII	Digital filtering of biomedical signals: a Java demonstrator	2007
J. Neveux J. Aumard	IUT GEII	Digital filtering of biomedical signals: a Java demonstrator	2008
M. Zahri S. Canavese	IUT GEII	Atrial fibrillation signal database	2009
J. Neveux N. Bessou	ENSEA Cergy-Pontoise	Atrial fibrillation signal database	2009

University	Student	Country of origin	Topic	Period	super-vision	Other co-supervisors	Publications
Nice Sophia Antipolis (France)	P. Bonizzi	Italy	Atrial activity analysis in atrial fibrillation episodes (Secs. 4.8–4.9, pp. 69–71.) Expected completion: June 2010	2006–	50%	O. Meste	[P1, P2, P25, P28, P29, P31, P35]
	L. Rota	France	Blind multi-user channel equalization (Sec. 3.6.1, pp. 46–48)	2001–2004	15%	P. Comon S. Icart	[P42, P45]
Gent (Belgium)	R. Phlypo	Belgium	Biomedical signal extraction based on ICA with prior information (Secs. 4.6–4.7, pp. 60–68.) Supervision started on Oct. 1, 2006; expected completion: Dec. 2009	2004–	50%	I. Lemahieu	[P1, P3, P5, P6, P11, P13, P14, P32, P33, P34, P36, P38]
Liverpool (UK)	Y. Feng	China	Optical transmission monitoring (Sec. 3.6.3, p. 49)	2000–2004	25%	A. K. Nandi	[P22, P58, P59, P61]
	K. Kokkinakis	Greece	Blind separation of convolutive mixtures of speech	2001–2005	25%	A. K. Nandi	[P51]
	W. Xu	China	Blind multi-user detection	2000–2004	10%	A. K. Nandi	—

Table 1.1: Summary of PhD students' supervision.

1.3.6 Publications

My list of publications appears at the end of the present document (pp. 93–102). The number of articles *published or in press* can be summarized as follows:

	Chapters	Journals	Conferences
Total	6	21	54
First author	6	16	26
Supervision	1	3	16
Collaborations	—	5	17

Implication in article composition, including works under review and in preparation:

- Main author of research work and paper writing (56):
  [P4, P5, P8, P9, P10, P11, P12, P14, P15, P17, P18, P19, P23, P24, P26, P30, P37, P40, P41, P42, P43, P44, P45, P46, P47, P50, P53, P54, P55, P60, P62, P64, P65, P66, P69, P70, P71, P72, P73, P74, P75, P76, P77, P78, P79, P80, P81, P82, P83, P84, P85, P86, P87, P88, P89, P90].
- Collaborator in research work and paper writing (30):
  [P1, P2, P3, P6, P7, P13, P16, P20, P21, P22, P25, P27, P28, P29, P31, P32, P33, P34, P35, P36, P38, P39, P48, P49, P51, P52, P58, P59, P61, P67].
- Collaborator in research work, without direct implication in paper writing (3):
  [P56, P57, P63].

Invited conference contributions (3): [P26, P30, P39].

1.3.7 Presentations and Seminars

I was an *invited lecturer* at the 6th International Summer School on Biomedical Signal Processing, Siena, Italy, July 10–17, 2007, organized by the IEEE Engineering in Medicine and Biology Society (EMBS). I delivered two lectures on "Blind source separation: theory and methods" (1.5h) and "Application of BSS to cardiac signal extraction" (1.5h). The content of these lectures was later expanded into book chapter [P10].

Talks at international conferences (16): [P26, P30, P37, P40, P41, P47, P53, P59, P60, P64, P82, P83, P85, P86, P87, P88]; invited: [P26, P30].

Poster presentations at international conferences (11): [P43, P44, P46, P50, P52, P61, P62, P65, P66, P84, P89].

I obtained an *Award for meritorious final-year project poster presentation* at the Department of Electrical & Electronic Engineering, University of Strathclyde, Glasgow (1996).

Seminars:

July 7 2009 "Quelques résultats et perspectives sur l'analyse de la fibrillation auriculaire"
Dépt. Cardiologie, Centre Hospitalier Princesse Grace, Monaco.

May 22 2008 "Égalisation robuste du canal de communication numérique"
Laboratoire I3S, Signals, Images and Systems Research Pole seminar.

Sep. 4 2007 "Égalisation robuste du canal de communication numérique"
École Nationale d'Ingénieurs de Monastir, Tunisia, Département de Génie Électrique, visiting researcher seminar invited by Hassani Messaoud.

Mar. 15 2006 "Extraction de l'activité auriculaire par des techniques de séparation aveugle de sources"
Laboratoire I3S, Doctoral Student Association (ADSTIC) seminar.

Mar. 31 2005 "Analyse de la fibrillation auriculaire par des techniques de séparation aveugle de sources"
Laboratoire des Images et des Signaux (LIS, now GIPSA-Lab), Grenoble.

Dec. 7 2004 "Cardiac signal extraction by blind source separation techniques"
Laboratoire I3S, seminar invited by Luc Pronzato (then SIROCCO project leader, now I3S Lab Director).

Nov. 3 2004 "Optimal step-size constant modulus algorithm for blind equalization"
University of Liverpool, Dept. Electrical Eng. & Electronics, SPC Group seminar.

Jan. 19 2004 "Blind processing of digital communication signals"
UPV, Departamento de Comunicaciones, visiting researcher's seminar invited by Narcís Cardona.

Nov. 18 2003 "Application of independent component analysis to blind MIMO equalization"
Laboratoire I3S, ASTRE team seminar.

Nov. 28 2002 "Blind space-time equalization for future wireless digital communication systems"
University of Liverpool, Dept. Electrical Eng. & Electronics, departmental seminar.

1.3.8 Reviewing and Chairing

Area Chair of the "Signal Processing Theory, Detection and Estimation" Track at EUSIPCO-2009, 17th European Signal Processing Conference, Glasgow, UK, Aug. 24-28, 2009. I managed the review of 15 submissions on this area.

Technical program committee member of the International Conference on Independent Component Analysis and Signal Separation 2004 (I reviewed 5 papers), 2006 (6 papers), 2007 (5 papers) and 2009 (4 papers).

Reviewer of international conferences: IEEE International Conference on Acoustics, Speech and Signal Processing 2008 (2) and 2009 (2), IEEE Engineering in Medicine and Biology Conference 2007 (2) and 2008 (5), IEEE Workshop on Statistical Signal Processing 2009 (1), IEEE International Symposium on Information Theory 2007 (1), IEEE International Conference on Communications 2006 (1), IEEE International Symposium on Circuits and Systems 2005 (4), European Signal Processing Conference 2006 (1).

Reviewer of international journals: IEEE Transactions on Signal Processing (11), IEEE Transactions on Biomedical Engineering (11), IEEE Signal Processing Letters (8), IEEE Transactions on Neural Networks (2), IEEE Transactions on Circuits and Systems I (2), IEEE Transactions on Speech and Audio Processing (1), IEEE Transactions on Wireless Communications (1), IEEE Communications Letters (1), Elsevier's Signal Processing (8), IEE Proceedings - Communications (1), IEE Proceedings - Vision, Image and Signal Processing (2), Electronics Letters (8), International Journal of Adaptive Control and Signal Processing (4), EURASIP Journal of Applied Signal Processing (2), EURASIP Journal on Advances in Signal Processing (1), Neurocomputing (4), Medical & Biomedical Engineering & Computing (1).

Since 2000, I have reviewed 68 journal manuscripts and 39 conference submissions.

My reviewing activities were awarded an *IEEE Reviewer Appreciation for significant commitment to the IEEE Transactions on Signal Processing review process* in 2008 (by Prof. Alle-Jan van der Veen, IEEE TSP Editor-in-Chief in 2006–2008).

I have *chaired* talk sessions at the following conferences:

DSP-2002, 14th International Conference on Digital Signal Processing, Santorini, Greece, July 1–3, 2002

ICA Research Network International Workshop, Liverpool, UK, Sept. 18–19, 2006

Medical Physics and Biomedical Engineering World Congress, Sept. 7–12, 2009 (Focus Session: PCA/ICA in Biomedical Signal Processing, co-chaired with Luca Mainardi, Politecnico di Milano, Italy).

1.3.9 PhD Thesis Jury Participation

Raúl Llinares-Llopis, "Applications of semi-blind source separation in astrophysics and biomedical engineering", supervised by Jorge Igual, Universidad Politécnica de Valencia, Spain (examination: Jan. 19, 2009).

Reza Sameni, "Extraction of fetal cardiac signals from an array of maternal abdominal recordings", supervised by Christian Jutten and Mohammad B. Shamsollahi, Institut Polytechnique de Grenoble, GIPSA-Lab (July 7, 2008).

Ahmed R. Borsali, "Compression paramétrique du signal électrocardiographique : application aux arythmies cardiaques", supervised by Jacques Lemoine and Amine

Naït-Ali, Laboratoire Images, Signaux et Systèmes Intelligents (LISSI), Université Paris XII - Val de Marne (May 31, 2007).

José J. Rieta-Ibáñez, "Estimación de la actividad auricular en episodios de fibrilación auricular mediante separación ciega de fuentes", supervised by José Millet-Roig, Universidad Politécnica de Valencia, Spain (July 21, 2003).

1.3.10 Research Funding Proposals

I have coordinated the following proposals submitted to the French National Research Agency (*Agence nationale de la recherche, ANR*) Young Investigators' Program:

> "Signal Extraction for the Analysis of Supraventricular Arrhythmias in the Surface Electrocardiogram" (Feb. 2008).
>
> "Characterization of Complex Fractionated Electrograms for Improving the Success of Radiofrequency Catheter Ablation in Atrial Fibrillation Patients" (Nov. 2008).

These proposals were defined in the framework of a close collaboration between I3S' BIOMED group and the Cardiology Department, Pasteur University Hospital (CHU), Nice; the second proposal (briefly outlined in Sec. 5.2, pp. 76–77) also involved the Cardiology Department, Princess Grace Hospital, Monaco. After being approved by the Emerging Pathologies and Orphan Diseases (ORPHEME, now EuroBioMed) research pole, both proposals were finally rejected by the ANR.

During my postdoc at the University of Liverpool, I also submitted a standard research grant proposal to the Engineering and Physical Sciences Research Council (EPSRC) of the UK:

> "Blind equalization of multiuser wireless communication channels".

Unfortunately, the proposal was rejected too.

1.4 Teaching Activities

As summed up in Table 1.2, p. 13, my teaching activities after my PhD amount to over 1200 hours of lectures, tutorials and lab sessions, or nearly 1000 equivalent tutorial hours. Most of these have been carried out as a lecturer at the GEII Department, IUT Nice - Côte d'Azur (since 2005).

In particular, I have created and been responsible for the "Digital filtering" (*Filtrage numérique*) optional subject at the GEII Department. This module gives an overview of the basic concepts of digital signal processing and digital filtering. Apart from lecture and tutorial preparation, the module has also involved the design of lab sessions with Matlab/Simulink and Spectrum Digital's C6713 DSP Starter Kit board based on Texas Instruments' TMS320C6713 DSP. These lab sessions introduce the students to elementary computer-aided digital filter analysis and design as well as DSP implementations for real-time filtering of audio signals. Since the creation

of the subject, several demos running on this DSP platform have attracted the attention of numerous visitors on the IUT's annual open day.

During my PhD, I was a teaching assistant at the Department of Electrical & Electronic Engineering, University of Strathclyde, Glasgow (1996–1998). I taught Microprocessor Applications; DSP Lab of the MSc in Communications, Control and Digital Signal Processing; Analog Circuits; Circuit Analysis; and Signal Processing.

1.5 Other Activities

1.5.1 Research-Related Responsibilities

2008– Elected deputy member of I3S Lab Council (*Conseil du laboratoire*).

2007–2008 External member of *Commission de spécialistes, section 61*, Université du Sud Toulon-Var.

2006–2008 Deputy member of *Commission de spécialistes, section 61*, Université de Nice - Sophia Antipolis.

1.5.2 Consultancy

In March 2008, I worked as a consultant for "Sensor Products Inc.", NJ, USA (CEO: Jeffrey Stark) on a project involving sensor-array data analysis.

1.6 Awards and Other Distinctions

Erasmus grant (1995)
I received one of the few Erasmus grants available at the ETSIT to spend the final year of my MEng at the University of Strathclyde, Glasgow, UK.

Award for meritorious final-year project poster presentation (1996)
Department of Electrical & Electronic Engineering, University of Strathclyde, Glasgow.

MEng graduation with the highest distinction (1996)
I ranked first at the MEng in Telecommunications Engineering from ETSIT (class 1991-1996).

Robert Legget Prize (2000)
For an especially distinguished PhD thesis submitted to the Faculty of Engineering, University of Liverpool, UK.

Royal Academy of Engineering Research Fellowship (2000–2005)
Open to young researchers from all branches of engineering, the Fellowships aim to help them develop their research careers at British universities. I was awarded one of the first four Research Fellowships on offer in the UK. This allowed me to enjoy a 5-year postdoctoral position at the University of Liverpool.

Institution	Subject title	Level	Year 2004–2005	2005–2006	2006–2007	2007–2008	2008–2009
ESINSA	Traitement numérique du signal	L4	–/–/50	—	—	—	—
ESIEE	Linear Predictive Coding of Speech	M2	7/–/14	—	—	—	—
IUT Nice GEII	Électronique analogique	L1	—	–/–/66	–/–/66	–/–/66	—
	Électronique numérique et synthèse logique	L1	—	–/42/90	–/48/74	–/24/98	–/24/126
	Mathématiques	L1	—	—	—	—	–/74/–
	Programmation Java et web	L1	—	–/15/24	–/15/24	–/15/27	—
	Études et réalisations	L1	—	–/–/56	—	–/–/25	—
	Filtrage numérique	L2	—	—	12/24/27	12/24/18	6/12/18
Polytech' Nice-Sophia	Traitement numérique du signal biomédical	L5, M2	—	–/–/6	–/–/6	–/–/6	–/–/6
	Total number of hours		7/–/64	–/57/242	12/87/197	12/63/240	6/110/150
	Total number of equivalent tutorial hours		53	218	236	241	219

Table 1.2: Summary of teaching activities after my PhD. A triplet X/Y/Z stands for X lecture hours, Y tutorial hours, Z lab hours. ESINSA: École Supérieur d'Ingénieurs de Nice - Sophia Antipolis; ESIEE: École Supérieur d'Ingénieurs en Électronique et Électrotechnique, antenne Sophia Antipolis; Polytech'Nice-Sophia: École Polytechnique Universitaire de Nice - Sophia Antipolis, Dépt. Électronique.

Bonus for Research and Doctoral Supervision (2007–2011)
This 4-year bonus (known as PEDR) is granted by the French Ministry of Education to university lecturers with a good track record in research, so that they can continue to commit themselves to their research activities.

IEEE Reviewer Appreciation (2008)
For significant commitment to the IEEE Transactions on Signal Processing review process.

Chapter 2

Introduction to Research Activities

2.1 Motivation

The estimation of signals from observations corrupted by noise and interference is a fundamental signal processing problem arising in a wide variety of real-life applications. In telecommunications, limited bandwidth and multipath propagation make the transmitted signal arrive at the receiving end with different delays. This phenomenon, known as intersymbol interference (ISI), can be modeled as a mixture of the desired signal and time-delayed replicas of itself, and worsens as the data rate increases. The problem of recovering the original data from ISI-corrupted measurements is referred to as *time equalization* or *channel deconvolution*. Even in time non-dispersive channels, signals from other users transmitting at the same time/frequency/code slot can corrupt the signal of interest, generating co-channel interference (CCI) at the receive sensor. Since these interfering signals typically originate from sources transmitting at different positions in space, such mixtures are called spatial, and the problem of resolving them is known as *source separation*, *spatial filtering* or *beamforming*. Signal processing techniques for the mitigation of transmission impairments such as ISI and CCI are crucial in meeting the requirements for higher data rates and improved quality of service of future wireless communication systems [79, 104].

Source separation problems are also common in biomedical engineering. Time dispersion effects are often negligible due to the bandwidth of physiological signals and their propagation characteristics across the body tissues. During pregnancy, the fetal heartbeat signal is masked by the stronger maternal heartbeat at the output of surface electrodes placed on the mother's skin. In patients suffering from atrial fibrillation, the most common cardiac arrhythmia encountered in clinical practice, the bioelectrical activity from the atria appears mixed to that from the ventricles on surface recordings. An accurate estimation of the signal of interest (fetal heartbeat, atrial activity) from the observed mixtures is capital for its subsequent clinical analysis and may also provide further insights into the pathophysiological mechanisms of the medical condition under study. Other applications of signal estimation

from observed linear mixtures include seismic exploration, radar and sonar, image processing, and circuit testing and diagnosis, to name but a few.

In the remaining of this introductory chapter, Sec. 2.2 provides a common mathematical model and recalls some standard nomenclature for the different signal scenarios studied in this work. A brief historical survey of techniques for signal estimation in linear mixtures is given in Sec. 2.3. My research activities during my PhD are summarized in Sec. 2.4, while the main research objectives after my PhD are outlined in Sec. 2.5.

2.2 Mathematical Formulation and Problem Taxonomy

The channel equalization and source separation problems can jointly be cast in mathematical form as follows. In a generic setting, let us assume that K zero-mean source signals $\mathbf{s}(t) = [s_1(t), s_2(t), \ldots, s_K(t)]^{\mathrm{T}}$ propagate through a linear but possibly time-dispersive medium. Symbol t denotes the continuous-time index and $(\cdot)^{\mathrm{T}}$ the transpose operator. Mixtures of the sources are observed at the output of an array of L sensors, $\mathbf{x}(t) = [x_1(t), x_2(t), \ldots, x_L(t)]^{\mathrm{T}}$. If $h_{\ell k}(t)$ represents the impulse response of the propagation channel between the kth source and the ℓth sensor, the ℓth sensor output is given by $x_\ell(t) = \sum_{k=1}^{K} h_{\ell k}(t) * s_k(t) + v_\ell(t)$, where symbol $*$ stands for the convolution operator and $v_\ell(t)$ is the additive noise that may further corrupt the measured signal. Denoting $\mathbf{v}(t) = [v_1(t), v_2(t), \ldots, v_L(t)]^{\mathrm{T}}$, the discrete-time vector observation can be expressed in matrix form as:

$$\mathbf{x}_n = \sum_m \mathbf{H}_m \mathbf{s}_{n-m} + \mathbf{v}_n \tag{2.1}$$

where $\mathbf{x}_n = \mathbf{x}(nT_s)$, $\mathbf{s}_n = \mathbf{s}(nT_s)$, $\mathbf{v}_n = \mathbf{v}(nT_s)$, $[\mathbf{H}_m]_{\ell k} = h_{\ell k}(mT_s)$, $1 \le k \le K$, $1 \le \ell \le L$, and T_s is the sampling period. Notation $[\mathbf{A}]_{ij}$ represents the (i,j)-entry of matrix $\mathbf{A}$. The objective of channel equalization and source separation is to recover the source signals $\mathbf{s}_n$ from the observed corrupted measurements $\mathbf{x}_n$.

In communications, each source signal may be generated by a different user, or the same user may generate different sources by transmitting through multiple antennas. Equation (2.1) also models a communication channel with a single sensor output $x(t)$ sampled at L times the baud rate (fractional sampling or oversampling) excited by K inputs transmitting baud-spaced symbols $\mathbf{s}_n = [s_{1,n}, s_{2,n}, \ldots, s_{K,n}]^{\mathrm{T}}$. The channel impulse response between the kth source and the sensor may be denoted as $h_k(t)$. In the resulting multi-channel scenario, the ℓth sensor output $x_{\ell,n} \stackrel{\text{def}}{=} [\mathbf{x}_n]_\ell$ and its associated channels are virtual, and are given by the polyphase representations $x_{\ell,n} = x\big(nT_s + (\ell-1)T_s/L\big)$ and $[\mathbf{H}_m]_{\ell k} = h_k\big(mT_s + (\ell-1)T_s/L\big)$, $1 \le \ell \le L$, respectively [77, 96]. This signal model is easily generalized to the combined use of spatially separated sensors and temporal oversampling.

To recover the source signals, a set of scalar equalizers can be employed. Let $w_{k\ell}(t)$ denote the impulse response of the filter linking the ℓth sensor signal and the kth equalizer output $y_k(t)$, so that $y_k(t) = \sum_{\ell=1}^{L} w_{k\ell}^*(t) * x_\ell(t)$, where $(\cdot)^*$ denotes complex conjugation. In discrete-time matrix notation, we can write:

$$\mathbf{y}_n = \sum_m \mathbf{W}_m^{\mathrm{H}} \mathbf{x}_{n-m} \tag{2.2}$$

where $\mathbf{y}_n = [y_1(nT_s), y_2(nT_s), \ldots, y_K(nT_s)]^{\mathrm{T}}$ and $[\mathbf{W}_m]_{\ell k} = w_{k\ell}(mT_s)$, $1 \leq k \leq K$, $1 \leq \ell \leq L$. Symbol $(\cdot)^{\mathrm{H}}$ stands for the conjugate-transpose (Hermitian) operator. If the equalizers are causal length-N finite impulse response (FIR) filters, eqn. (2.2) accepts the compact matrix formulation:

$$\mathbf{y}_n = \mathbf{W}^{\mathrm{H}}\tilde{\mathbf{x}}_n \tag{2.3}$$

where $\mathbf{W} = [\mathbf{W}_0^{\mathrm{T}}, \mathbf{W}_1^{\mathrm{T}}, \ldots, \mathbf{W}_{N-1}^{\mathrm{T}}]^{\mathrm{T}}$ and

$$\tilde{\mathbf{x}}_n = [\mathbf{x}_n^{\mathrm{T}}, \mathbf{x}_{n-1}^{\mathrm{T}}, \ldots, \mathbf{x}_{n-N+1}^{\mathrm{T}}]^{\mathrm{T}} \tag{2.4}$$

is the stacked observation vector. Keeping this notation in mind, the kth component of the output $\mathbf{y}_n$ in (2.3), denoted $y_{k,n} \stackrel{\text{def}}{=} [\mathbf{y}_n]_k$, is given by

$$y_{k,n} = \mathbf{w}_k^{\mathrm{H}}\tilde{\mathbf{x}}_n \tag{2.5}$$

where $\mathbf{w}_k$ represents the kth column of $\mathbf{W}$. Depending on the values of L and N, and whether time oversampling is performed or not, vector $\mathbf{w}_k$ in eqn. (2.5) can act as a *spatial*, *temporal* or *spatio-temporal filter* for the linear extraction of a source component; in general, it can simply be called *linear extractor*. The goal of channel equalization and source separation is then equivalent to the estimation of suitable extraction filters, represented by the columns of matrix $\mathbf{W}$ in eqn. (2.3), from the observed data. For simplicity, we will sometimes refer to a generic component of $\mathbf{y}_n$ and the corresponding column of $\mathbf{W}$ with the shorthand notation

$$y_n = \mathbf{w}^{\mathrm{H}}\tilde{\mathbf{x}}_n. \tag{2.6}$$

Similarly, time index n will be omitted when convenient.

A case of particular interest occurs when the channel effects can be approximated by FIR filters with maximum order M. Under this assumption, and according to eqn. (2.1), we can further express the stacked observation vector (2.4) as

$$\tilde{\mathbf{x}}_n = \mathbf{H}\tilde{\mathbf{s}}_n + \tilde{\mathbf{v}}_n \tag{2.7}$$

where

$$\tilde{\mathbf{s}}_n = [\mathbf{s}_n^{\mathrm{T}}, \mathbf{s}_{n-1}^{\mathrm{T}}, \ldots, \mathbf{s}_{n-M-N+1}^{\mathrm{T}}]^{\mathrm{T}} \tag{2.8}$$

denotes the stacked source vector and $\mathbf{H}$ is the block Toeplitz matrix

$$\mathbf{H} = \begin{bmatrix} \mathbf{H}_0 & \mathbf{H}_1 & \ldots & \mathbf{H}_M & \mathbf{0}_{L\times K} & \ldots & \mathbf{0}_{L\times K} \\ \mathbf{0}_{L\times K} & \mathbf{H}_0 & \mathbf{H}_1 & \ldots & \mathbf{H}_M & \ldots & \mathbf{0}_{L\times K} \\ \vdots & \ddots & \ddots & \ddots & \ddots & \ddots & \vdots \\ \mathbf{0}_{L\times K} & \ldots & \mathbf{0}_{L\times K} & \mathbf{H}_0 & \mathbf{H}_1 & \ldots & \mathbf{H}_M \end{bmatrix}$$

with dimensions $LN \times K(M+N)$; symbol $\mathbf{0}_{L\times K}$ represents the matrix of $(L \times K)$ zeros. Depending on L, N and the oversampling factor, a column $\mathbf{h}_k$ of the channel (or mixing) matrix $\mathbf{H}$ can be considered as the *spatial*, *temporal* or *spatio-temporal signature* whereby the corresponding source component contributes to the observed vector $\tilde{\mathbf{x}}_n$. The mixing matrix columns are also known as *source directions* or *transfer*

K	L	M	System	Problem
1	1	>0	SISO	SISO time equalization
1	>1	>0	SIMO	SIMO time equalization
>1	>1	0	instantaneous or static MIMO	source separation in instantaneous linear mixtures
		>0	convolutive or dynamic MIMO	source separation in convolutive linear mixtures

Table 2.1: Typical system and problem nomenclature employed in channel equalization and source separation, as a function of the model parameters. SISO: single input, single output; SIMO: single input, multiple output; MIMO: multiple input, multiple output.

vectors. In the case of time (or space-time) mixtures, the observation window of model (2.7) spans $(M+N)$ different delays for each source signal. As a consequence, each source can be recovered with $(M+N)$ different equalization delays. This feature will be revisited in Sec. 3.2, pp. 28–30.

As summarized in Table 2.1, specific nomenclature is employed as a function of the number of sources and observations (K and L, respectively) involved in the above observation model. Multiple channel outputs (SIMO, MIMO) are typically achieved by means of spatially separated sensors or, in communication systems with excess bandwidth, fractional sampling. If $M = 0$, the channel does not introduce time dispersion (flat-fading or frequency non-selective channel); the observed mixtures are then called *static* or *instantaneous*, and spatial filters ($N = 0$) suffice to recover the sources if sufficient spatial diversity is available. In that scenario, model (2.7) can be simplified into:

$$\mathbf{x}_n = \mathbf{H}\mathbf{s}_n + \mathbf{v}_n \tag{2.9}$$

where $\mathbf{H} = \mathbf{H}_0$ due to the system parameters. In the noiseless case, this is the standard model in *blind source separation (BSS)* and *independent component analysis (ICA)*. An example of a popular static MIMO system in digital communications is *vertical Bell Labs layered space-time (V-BLAST)* architecture [44, 49], designed to increase system capacity through the exploitation of the multipath diversity provided by multiple transmit and receive antennas. If $M > 0$ (frequency-selective or time-dispersive channel), one deals with *convolutive* observations and generally requires temporal processing ($N > 0$) in addition to spatial processing if diversity is available [79]. The observed mixtures are referred to as *overdetermined* if $LN \geq K(M + N)$; *underdetermined* otherwise. An overdetermined system can be linearly inverted if the channel matrix is full column rank, whereas an underdetermined system cannot be inverted using linear techniques. The *multiple-input single-output (MISO)* channel, not mentioned in Table 2.1, defines a particularly challenging underdetermined scenario without receive diversity ($L = 1$). Using particular transmission strategies such as *space-time coding* [1, 93], the MISO channel transforms into a MIMO model with sufficient diversity and can thus be linearly inverted, at least in flat-fading environments ($M = 0$); see, e.g., Sec. 3.6.2, pp. 48–49.

2.3 Brief Historical Survey

In communications, classical channel equalization and source separation techniques rely on the transmission of *training* or *pilot sequences* known to the receiver. Pilot data enable the application of optimal Wiener filtering techniques based on second-order statistics (SOS), such as the *minimum mean square error (MMSE)* equalizer. The MMSE equalizer for the extraction of source k at equalization delay δ_k minimizes the cost function:

$$\Upsilon_{\mathrm{MMSE}}(y) = \mathrm{E}\{|y_n - \breve{s}_{k,n-\delta_k}|^2\} \tag{2.10}$$

where $\breve{s}_{k,n}$ denotes the kth-source training sequence and y_n is the equalizer output given by eqn. (2.6). Function (2.10) is minimized in closed-form by the well-known Wiener-Hopf solution, which simply reads:

$$\mathbf{w}_{\mathrm{MMSE}}^{(\delta_k)} = \mathbf{R}_{\tilde{\mathbf{x}}}^{-1}\mathbf{p}_{\delta_k} \qquad \text{with } \mathbf{p}_{\delta_k} = \mathrm{E}\{\tilde{\mathbf{x}}_n \breve{s}_{k,n-\delta_k}^*\} \tag{2.11}$$

and $\mathbf{R}_{\tilde{\mathbf{x}}} = \mathrm{E}\{\tilde{\mathbf{x}}_n\tilde{\mathbf{x}}_n^{\mathrm{H}}\}$ is the stacked observation covariance matrix. For uncorrelated unit-variance source components, we have $\mathbf{p}_{\delta_k} = \mathbf{h}_{\delta_k}$, where $\mathbf{h}_{\delta_k}$ is the column of the channel matrix $\mathbf{H}$ associated with $s_{k,n-\delta_k}$ in (2.7). In practice, expectations are replaced by sample averaging over indices associated with the training data, as in the *least squares (LS)* implementation (which will be recalled in Sec. 3.3.1, p. 31) The price to pay for conceptual simplicity and computational convenience in supervised equalization is a poor utilization of the available bandwidth and power: up to 20% of the data rate is used for training in the GSM mobile telephony system [90]. Also, the pilot sequence must be of sufficient length to compensate a channel of a given order. In addition, training-based operation requires synchronization, which is not always available or feasible in multiuser or non-cooperative (e.g., military) scenarios [100, 104].

In the late 70's, these limitations spurred the first researches into the so-called *blind equalization* techniques [48, 85, 97], sparing the need for training sequences and easing the synchronization requirements. Originally developed in the SISO case, blind techniques essentially rely on the idea of *property restoration*: the unknown waveform is estimated by recovering at the equalizer output a known property of the transmitted signal. A cost, objective or *contrast function* quantifies the deviation from the desired property, and its optimization thus leads to equalizer filters recovering the source signal. Among the properties originally exploited are specific features of digital modulations like their *constant modulus (CM)* [63, 97]. This popular criterion — which can be considered as a particular member of the more general family of Godard's methods [48] — is arguably the most widespread blind equalization principle. It aims at the minimization of the cost function:

$$\Upsilon_{\mathrm{CM}}(y) = \mathrm{E}\{(|y|^2 - \gamma)^2\} \tag{2.12}$$

where γ is a constellation-dependent parameter. Although specifically designed for CM-type modulations like phase-shift keying (PSK), the CM criterion is also able to recover non-CM modulations at the expense of an increased misadjustment due to constellation mismatch. In parallel, measures based on *higher-order statistics (HOS)* such as the *kurtosis* began to draw the attention of the seismic exploration

community [43, 106], and were later taken up for the blind equalization of digital communication channels as well [87]. The rationale behind the use of HOS lies in the Central Limit Theorem: since mixing increases Gausssianity, one should proceed in the opposite direction, i.e., increasing non-Gaussianity by maximizing HOS, to achieve the separation. The *kurtosis maximization* criterion maximizes the contrast:

$$\Upsilon_{\mathrm{KM}}(y) = \frac{|\kappa_4^y|}{(\sigma_y^2)^2} \tag{2.13}$$

where $\kappa_4^y = \mathrm{cum}(y, y^*, y, y^*)$ is the marginal fourth-order cumulant of the equalizer output and σ_y^2 represents its variance. Cumulant definitions can be found in classical references such as [157, 159].

In the mid 90's, the multi-channel (SIMO) scenario enabled by the use of time oversampling or multiple sensors aroused great interest in the blind equalization community. Indeed, while only non-minimum phase channels can be blindly identified by means of circular SOS in the SISO case, SIMO channels can be blindly identified regardless of their phase (minimal or otherwise) using such statistics. Moreover, FIR SIMO channels can be perfectly equalized by FIR filters in the absence of noise [77, 88, 96]. However, the channel must verify strict diversity conditions, and a good number of these methods do not work when the channel length is overestimated [16].

Concerning the MIMO case, traditional array processing or *beamforming* was built upon the *array manifold* concept, whereby the mixing matrix is parameterized according to the sensor array geometry and the signal propagation model (e.g., far-field hypothesis) [86]. As a consequence, deviations from the model assumptions, the so-called *calibration errors*, can have a dramatic impact on the performance of these early techniques. A classical approach sparing the knowledge of the array manifold is Widrow's multi-reference *adaptive noise cancellation (ANC)* framework based on Wiener's optimal filtering [154] and closely connected to the MMSE receiver (2.10). The ANC approach, however, requires reference sensors sufficiently isolated from the physical phenomenon of interest, so as to capture components correlated with the interference but uncorrelated with the desired signal.

The mid 80's witnessed a rapidly increasing interest in the problem of BSS [56], in which spatial mixtures of the source signals are resolved without training data or mixing-matrix parameterization. The assumed signal model can also be considered as a generalization of Widrow's ANC model whereby, under mild spatial diversity conditions, all sources are allowed to contribute to all sensors simultaneously. A first step towards rendering the classical Widrow's ANC scheme suitable in this more general setup was taken in [2]; the blind approach was also formulated independently in [5, 39]. As in the closely related blind equalization problem, the main idea allowing the separation is the exploitation of an assumed property of the sources, such as their probability density function (pdf), statistical independence or, in digital communications, discrete alphabet. The first algorithms for BSS were mainly based on heuristic ideas borrowed from neuro-mimetic information processing [21, 22, 26, 38, 56, 64, 65, 73, 89]. Other early methods solved the two-source two-mixture case in closed form by relating the higher-order cumulants of the sources

and the observations after a prewhitening step involving *principal component analysis (PCA)* [24, 29]. The (2×2)-solution was then applied to all signal pairs until convergence, as in the *Jacobi algorithm* for matrix diagonalization [155].

Prompted by these encouraging early efforts, the mathematical cornerstone was laid down by Comon in his pioneering contribution [25, 27]. He coined the notion of *contrast function* in the context of instantaneous BSS and developed the concept of ICA, already suggested by Jutten and Hérault in [65] as a generalization of the well-known PCA technique. Contrasts can be defined as follows.

Definition* 1 *(contrast function for BSS). A function $\Upsilon(\cdot)$ of the separator output distribution is a contrast for BSS if it verifies:

Invariance:	$\Upsilon(\mathbf{Gs}) = \Upsilon(\mathbf{s})$ for any $(K \times K)$ matrix $\mathbf{G} = \mathbf{PD}$, where $\mathbf{P}$ is a permutation and $\mathbf{D}$ an invertible diagonal matrix.
Domination:	$\Upsilon(\mathbf{Gs}) \leq \Upsilon(\mathbf{s})$ for any $(K \times K)$ matrix $\mathbf{G}$.
Discrimination:	$\Upsilon(\mathbf{Gs}) = \Upsilon(\mathbf{s})$ if and only if $\mathbf{G} = \mathbf{PD}$.

By virtue of the above characteristic properties, the *global* maximization of a contrast function guarantees source separation. Contrasts requiring minimization can be defined likewise. By assuming the sources to be statistically independent, information theoretical measures such as mutual information and negentropy were shown to perform the ICA of the observations and to constitute valid contrasts for the blind separation of independent sources. Mathematical tractability could be improved by approximating the source pdf's via Gram-Charlier or Edgeworth expansions, leading to operational algorithms based on HOS (higher-order cumulants) and the Jacobi iteration [24, 25, 27, 55]. One such algorithm is the so-called *contrast maximization (CoM2)* method of [25, 27], relying on the sum of square kurtoses of the separator outputs:

$$\Upsilon_{\mathrm{CoM2}}(\mathbf{y}) = \sum_{k=1}^{K} \left(\kappa_4^{y_k}\right)^2. \tag{2.14}$$

Likewise, the *CoM1* function

$$\Upsilon_{\mathrm{CoM1}}(\mathbf{y}) = \sum_{k=1}^{K} \left|\kappa_4^{y_k}\right| \tag{2.15}$$

was later shown to be another valid contrast for the separation of independent sources [74]. When all the sources have the same sign of kurtosis, say ε, contrast (2.15) becomes [13, 74]:

$$\Upsilon_{\varepsilon}(\mathbf{y}) = \varepsilon \sum_{k=1}^{K} \kappa_4^{y_k}. \tag{2.16}$$

This expression can be optimized using a closed-form solution at each pairwise iteration of the Jacobi algorithm [29].

Building on these fundamental ideas, iterative ICA algorithms based on gradient or Newton updates were also developed [54, 74]. Methods derived from the *relative*

or *natural gradient* were shown to provide uniform performance, whereby the separation quality is independent of the mixing matrix structure [4, 13]. Extracting one source after another, i.e., performing *deflation*, emerged as another widespread approach to BSS. In this approach, the contribution of the latest source estimate can be computed via linear regression and subtracted from the observations before performing a new extraction, as in [98]; the process is then repeated until all sources have been obtained. The main advantage of deflation lies in the fact that extraction contrasts such as the KM principle (2.13) are free of spurious solutions in the absence of noise and estimation errors (infinite sample size) if the data model is perfectly fulfilled [37, 58, 87, 98]. Due to its simplicity and satisfactory performance in numerous applications, the deflationary FastICA algorithm [58, 60, 61] quickly gained popularity among ICA practitioners. Deflation (or symbol cancellation) has also been employed in the popular V-BLAST detection algorithm [44, 49] (Sec. 2.2, p. 18). V-BLAST, however, requires an accurate channel matrix estimate based on training data.

In parallel, another important line of research began to explore the eigenstructure of matrices and tensors made up of second- and higher-order cumulants of the observed data [10]. This approach led to the widespread *joint approximate diagonalization of eigenmatrices (JADE)* method of [11] for blind separation of independent sources. The use of HOS precludes the treatment of Gaussian sources, which is not a limiting constraint in most applications. The source second-order temporal structure, if available, can likewise be exploited by the diagonalization approach, allowing the separation of Gaussian signals as well [7, 95]. The *algorithm for multiple signal extraction (AMUSE)* of [95] is strongly reminiscent of the technique proposed in [96] for blind equalization of fractionally-spaced digital communication channels. This algorithm, in turn, was later generalized by the *second-order blind identification (SOBI)* method of [7]. Through the joint approximate diagonalization of the input correlation matrices at several time lags, SOBI is more robust to the lag choice and is particularly well suited to the separation of narrowband sources, with long correlation functions.

2.4 PhD Research

My PhD research focused on the problem of blind separation of independent sources in instantaneous linear mixtures (ICA), whose signal model is given by eqn. (2.9), p. 18. The so-called *prewhitening* process restores the source second-order covariance structure, yielding whitened observations $\mathbf{z}_n$ linked to the sources through an unknown $(K \times K)$ unitary matrix $\mathbf{Q}$. In the noiseless case, this relationship reads:

$$\mathbf{z}_n = \mathbf{Q}\mathbf{s}_n. \tag{2.17}$$

If the time coherence of the sources is ignored or just cannot be exploited (as in the i.i.d. case), the estimation of matrix $\mathbf{Q}$ requires the use of HOS. In the real-valued two-signal case ($K = 2$), matrix $\mathbf{Q}$ is a Givens rotation characterized by a single parameter θ:

$$\mathbf{Q} = \begin{bmatrix} \cos\theta & -\sin\theta \\ \sin\theta & \cos\theta \end{bmatrix}.$$

Different analytic methods for the estimation of θ had been proposed in the literature [24,29,55]. My doctoral investigation provided the first unified comprehensive vision of closed-form estimators for BSS based on higher-order cumulants, as summarized next.

An approximate maximum likelihood (AML) estimator was proposed by Harroy and Lacoume in [55]. Its derivation assumed that both sources have symmetric distributions and their kurtoses lie in a limited interval. In my PhD, a new estimator — named *extended ML (EML)* — was built as a complex-valued linear combination of the whitened-data fourth-order statistics:

$$\hat{\theta}_{\text{EML}} = \frac{1}{4}\angle(\gamma\xi_\gamma) \tag{2.18}$$

with $\xi_\gamma = (\kappa^z_{40} - 6\kappa^z_{22} + \kappa^z_{04}) + j4(\kappa^z_{31} - \kappa^z_{13})$ and $\gamma = \kappa^z_{40} + 2\kappa^z_{22} + \kappa^z_{04}$. Function $\angle(\cdot)$ yields the phase of its complex variable relative to the positive real axis, and $j = \sqrt{-1}$ is the imaginary unit. The real-valued parameter γ is an estimate of the source kurtosis sum $(\kappa^s_{40} + \kappa^s_{04})$. In these equations, the pairwise $(p+q)$th-order cumulants are defined as in [159]:

$$\kappa^z_{pq} = \text{cum}(\underbrace{z_1, \ldots, z_1}_{p}, \underbrace{z_2, \ldots, z_2}_{q}).$$

The idea behind the EML estimator is that, under model (2.17) and no estimation errors (infinite sample length), we have that $\xi_\gamma = (\kappa^s_{40} + \kappa^s_{04})e^{j4\theta}$, from which eqn. (2.18) readily follows. This estimator can also be expressed in term of a scatter-plot *centroid*, $\xi_\gamma = \text{E}\{(z_1 + jz_2)^4\}$, and accepts an intuitive geometric interpretation inspired by the work of Bogner and Clarke [23]. More importantly, the EML was shown to generalize the AML to virtually any source probability distribution as long as the source kurtosis sum is different from zero [P75, P86, P90]. The asymptotic performance analysis of the estimator revealed closed-form expressions for its large-sample pdf and variance [P75, P81]. These expressions are able to predict the estimator's behavior given the source statistics. The same analysis tools evidenced the limitations of an earlier closed-form formula by Comon (CF) [P81, 24].

The EML estimator was also shown to be the closed-form solution to the optimization of a contrast function [P81,P90]. Such a function resembles contrast (2.16), proposed by Moreau and Macchi in [74], which required all sources to have the same known sign of kurtosis. Yet the EML contrast shows that only the sign of source kurtosis sum is pertinent for $K = 2$. In turn, this connection allowed the simplification of the associated analytic solution derived by Comon and Moreau in [29].

These fourth-order estimators (AML, EML and CF) were shown to suffer a severe performance degradation when the source kurtosis sum approaches zero. To overcome this drawback, a hybrid estimation strategy was adopted, based on another fourth-order estimator, the so-called *alternative EML (AEML)*:

$$\hat{\theta}_{\text{AEML}} = \frac{1}{2}\angle\xi_\eta \tag{2.19}$$

with $\xi_\eta = (\kappa^z_{40} - \kappa^z_{04}) + j2(\kappa^z_{31} + \kappa^z_{13})$. The hybrid estimator consisted of a simple decision rule to select the EML or the AEML depending on the whitened-observation

statistics [P73]. This way of combining the two estimators avoids their respective shortcomings.

Extensions to scenarios of more than two signals were implemented by means of the Jacobi-like iteration strategy originally proposed by Comon [24, 25, 27]. To illustrate their performance on real data, the resulting methods were successfully applied in the biomedical problem of non-invasive fetal electrocardiogram extraction from maternal cutaneous potential recordings [P72, P77, P79, P82, P85, P88, P89].

The compact centroid-based formulation of the EML and AEML estimators allowed the derivation of simple adaptive (on-line, stochastic, recursive) versions, operating on a sample-by-sample basis. As shown by eqn. (2.18), the pertinent parameter is the orientation rather than the exact position of centroid ξ_γ, which is usually estimated in a few iterations if the centroid is initialized at the origin. As a result, in the two-signal case these adaptive methods present a remarkable convergence speed and global convergence under mild conditions [P74, P84].

The thesis concluded by generalizing some of the above results to other cumulant orders and the complex case. A closed-form estimation family based on the data rth-order statistics was derived, of which the EML turned out to be a particular case for $r = 4$. For $r = 3$, a novel third-order estimator was also obtained and analyzed [P70, P81]. Through the so-called *bicomplex numbers*, some of the previous results were extended to complex-valued mixtures, evidencing an interesting connection between the real and the complex case [P71, P80].

Numerical experiments supported the theoretical results, compared the techniques considered and contrasted them with other non-analytic procedures. The computational complexity of the different methods was also discussed.

2.4.1 Other PhD-Related Research

The direct continuation of my PhD research addressed the direct combination of the EML and AEML estimators [eqns. (2.18)–(2.19)] by using the centroid:

$$\xi_\lambda = \lambda\gamma\xi_\gamma + (1-\lambda)\xi_\eta^2.$$

An asymptotic performance analysis yielded the closed-form expression for the optimal weight coefficient λ as a function of the source statistics. Depending on the source combination to be separated, this generalized weighted fourth-order estimator is able to provide significant performance gains relative to the two estimators from which it is derived, and mitigates their performance degradation when the source kurtosis sum and difference, respectively, are close to zero [P18, P44, P49, P65, P66].[1] When $\lambda = 0.5$ the above estimator is equivalent to JADE [11] in the case of $K = 2$ sources. In the complex case, Cramér-Rao bounds for the estimation of the relevant parameters were derived in [P65].

(p. 137) (p. 281) (p. 281)

Another line of work was an attempt to solve in closed-form the BSS problem in the three-signal case, where the unknown unitary mixing matrix after prewhitening can be considered as a three-dimensional rotation. *Quaternions*, discovered by

[1] Marginal notes show the pages where the attached publications can be found at the end of this document.

the Irish mathematician Sir William R. Hamilton in the 19th century, can be considered as a natural extension of complex numbers and are characterized by their ability to perform rotations in the three-dimensional space. Exploiting this ability, a quaternion-based closed-form solution for the three-source BSS scenario was found for the first time in [P64]. This solution relies on the previous knowledge of certain source cumulants and remains to be extended to the fully blind case. (p. 277)

Publications [P69, P76, P78, P87] are also related to my PhD work.

2.5 Research Goals After my PhD

The research I have carried out after my PhD has aimed at the design of novel signal estimation techniques with improved performance. The guiding principle has been to capitalize on the available prior information in order to derive techniques more adapted to the problems under study. Contributions of this kind have been made in two specific applications of telecommunications and biomedical engineering: the equalization of digital communication channels and the extraction of atrial activity in atrial fibrillation episodes. These contributions are summarized in Chapter 3, pp. 27–51, and Chapter 4, pp. 53–72, respectively. Some possible avenues for the continuation of this work are enumerated in Chapter 5, pp. 73–77.

For the sake of conciseness, in what follows we only elaborate on a few contributions to highlight certain aspects of theoretical interest, whereas the remaining contributions are only briefly sketched. For further details, including experimental results, the reader is referred to the relevant publications, some of which are attached to this report.

Chapter 3

Robust Equalization and Source Separation

3.1 Motivation

As introduced in Sec. 2.3, pp. 19–22, blind techniques have aroused an enormous research interest on account of their improved bandwidth utilization, robustness to calibration errors and reduced synchronization requirements. However, these benefits come at the expense of some practical *drawbacks*, which are briefly summarized below:

D1) Blind methods cannot resolve the indeterminacy of the amplitude and/or the phase of the estimated signal [see eqns. (2.12)–(2.13)], in addition to ordering indeterminacy in the case of multiple sources (multiple-input case). In cases where only a few of the source components are of interest (as in time-dispersive channels, where recovering a single delay per source typically suffices), the permutation ambiguity causes particular problems: the whole mixture needs to be separated before the desired component can be selected, with the subsequent increase in computational complexity. Performing a full separation also worsens estimation errors in algorithms based on sequential extraction (deflation). This shortcoming is inherent to the blind approach and cannot be relieved without resorting to further information about the signal(s) of interest.

D2) Blind cost functions involve HOS, explicitly or implicitly. Their mathematical complexity means that they are often notoriously multi-modal, presenting spurious local extrema [40, 41, 63]. These are are stable equilibria associated with filter tap settings that cannot sufficiently open the eye pattern of the equalizer output signal, so that the detecting device is then unable to extract the transmitted symbols with a reasonably low probability of error. When the model assumptions are violated or short sample blocks are processed, local extrema can also appear in contrasts that otherwise offer theoretical global convergence, like the KM (2.13) [94]. Clearly, spurious extrema hinder the convergence of iterative search techniques used to optimize blind contrasts. In particular, their existence can render the performance of gradient- and Newton-based im-

plementations, such as the widespread CMA [97] or the popular kurtosis-based FastICA [58,60,61], very dependent on the initial value of the extracting filter. These undesired effects have also been evidenced in [P9, P12, P17, P19, P41].

(p. 133) (p. 153) (p. 253)

D3) An increased sample size is necessary to estimate HOS with an accuracy comparable to SOS. Larger data volumes (block sizes) than supervised methods are thus required for the same signal estimation quality. In turn, this drawback leads to increased computational demands and slow convergence, compromising the tracking ability of blind techniques when system parameters vary rapidly.

As discussed in [40, 41, 94], among other works, the misconvergence problems of iterative blind techniques calls for the design of suitable initialization schemes and additional strategies to keep the filter tap trajectories away from undesired local equilibria.

An important part of my research has been devoted to proposing and analyzing a number of strategies to surmount the above limitations and lead to more robust equalization and source separation techniques. My focus has been on digital-modulation based contrasts like the constant modulus and constant power principles, as well as constellation-independent criteria such as kurtosis. Three main strategies have been developed, that can all be combined together: equalizer initialization by means of algebraic solutions, semi-blind operation, and iterative search based on an optimal step size. First, equalizers can be judiciously initialized with algebraic solutions enabled by the use of training symbols known by the receiver (Sec. 3.2, pp. 28–30) or the finite-alphabet property of digital modulations (Sec. 3.3, pp. 30–39). Pilot information and blind contrasts can be used together, giving rise to semi-blind criteria (Sec. 3.4, pp. 39–42) whose optimization can outperform traditional training-based techniques at a fraction of the bandwidth utilization and with just a moderate increase in computational cost. The cost-effectiveness and robustness to initialization of semi-blind techniques can be further improved by an iterative search technique based on an algebraic optimal step size (Sec. 3.5, pp. 42–46), which is also effective in fully blind mode. The combination of these three strategies (algebraic initialization, semi-blind criteria and optimal step-size iterative search) is able to mitigate the impact of local extrema and slow convergence typical of blind methods, leading to signal extractors with increased robustness, high convergence speed and modest complexity. The chapter concludes by reporting other results related to the processing of telecommunication signals (Sec. 3.6, pp. 46–50).

3.2 ICA-Based MIMO Channel Equalization

My first efforts towards alleviating drawbacks D1–D3 above concern the convolutive MIMO channel. If sufficiently spatio-temporal diversity is available at the receive end so that matrix $\mathbf{H}$ in eqn. (2.7), p. 17, is full column rank, the channel can be linearly inverted; a necessary condition is that $LN \geq K(M+N)$, which imposes lower bounds for the receive diversity L and equalizer length N as a function of the source number K and channel order M. If the sources are i.i.d. (or, more generally, temporally

white), the components of vector $\tilde{\mathbf{s}}(t)$ in eqn. (2.8) are statistically independent. The convolutive MIMO model (2.7) can then be resolved by ICA techniques, as pointed out in [20, 108, 110]. An ICA method can be applied directly on the observed signal in (2.7), followed by a simple algorithm (e.g., based on cross-correlations) to identify and group each source's delays. Despite the conceptual simplicity of this approach, the computational complexity of separating $K(M+N)$ independent components can become prohibitive in systems with long delay spreads as a result of high data rates, even for a moderate number of sources.

To overcome this difficulty, the classical blind channel identification methods of [77, 96], originally designed for the single-input case, are generalized to the multiple-input case in [P53, P60]. After the application of these extensions, the spatio-temporal equalization is shown to reduce to a problem of source separation in instantaneous linear mixtures characterized by model (2.9), p. 18. ICA can then be used to separate the remaining spatial mixture, involving only K independent components. Computational complexity is thus considerably reduced [P24, P54, P55]. (p. 223)

To further improve performance, the ICA stage can be initialized by the Wiener receiver, which is feasible in systems where channel state information or training data are available [see eqns.(2.10)–(2.11), p. 19]. Conversely, this approach can be seen as the ICA-based refinement of the Wiener receiver. Indeed, the performance of conventional linear equalizers, such as the MMSE (2.11) based on previous channel identification, is shown to deteriorate in MIMO systems with many source components due to large delay spreads and/or number of inputs, even if the channel matrix is perfectly estimated. A typical effect is the severe performance flooring observed when the finite-sample noise level (estimation error due to finite data length) surpasses the additive noise present at the sensor output. As noted in [83], the ICA stage has the potential to palliate this performance degradation by exploiting HOS.

Inspired by this idea, an ICA-based detection scheme originally put forward in a rather restrictive DS-CDMA signal model [83] is adapted in [P23] to the more general time-dispersive MIMO signal scenario (2.7), p. 17, with $M > 0$. Instead of performing the full separation of all time delays associated with each source, computational complexity can be reduced while improving estimation quality by aiming at the simultaneous extraction of the optimum MMSE equalization delay of each source. The optimum delay for the extraction of the kth source, δ_k^{opt}, is found by minimizing the equalizer output MSE over all possible extraction delays, $1 \leq \delta_k \leq (M+N)$, for which closed-form solutions exist as a function of the observation covariance matrix and the channel matrix. Assuming that the source signal is normalized (i.e., it has zero mean and unit variance), the MSE of the MMSE solution with delay δ_k is given by: (p. 203)

$$\text{MSE}_{\delta_k} = 1 - \mathbf{p}_{\delta_k}^{\text{H}} \mathbf{R}_{\tilde{\mathbf{x}}}^{-1} \mathbf{p}_{\delta_k}. \tag{3.1}$$

where $\mathbf{p}_{\delta_k}$ is defined as in eqn. (2.11), p. 19. Hence:

$$\delta_k^{\text{opt}} = \arg\min_{\delta_k} \text{MSE}_{\delta_k} = \arg\max_{\delta_k} \mathbf{p}_{\delta_k}^{\text{H}} \mathbf{R}_{\tilde{\mathbf{x}}}^{-1} \mathbf{p}_{\delta_k}. \tag{3.2}$$

The resulting ICA-based detection scheme with optimum-delay MMSE initialization is able to yield significant performance gains relative to conventional linear detectors [P23, P50, P55], tolerating higher co-channel interference and additive Gaussian (p. 203)

noise levels, and thus improving system capacity [P47], at only a moderate increase in computational cost. The ICA approach presents the benefit of constellation-independent symbol recovery, which makes it very attractive in next-generation ad-hoc networks as well as in non-cooperative military scenarios.

3.3 Algebraic Equalizers

As explained in the previous section, generic methods for BSS based on statistical independence (ICA) used in other applications can also be employed to perform digital channel equalization if the sources present no time coherence. However, digital commmunication channels present particular features that can be capitalized on to improve source recovery. Among them, digital modulations have finite support or, in other words, they contain only a small number of possible complex amplitudes. Criteria such as the *constant modulus (CM)* or the *constant power (CP)* are specifically adapted to the blind estimation of signals with such modulations and, as shown in [35], constitute valid contrasts for the separation and extraction of these signals in linear mixtures, either instantaneous or convolutive. The CM has long been used in blind equalization [48, 85, 97], whereas the CP criterion has more recently been proposed for inputs with q-ary phase shift keying (q-PSK) modulation, for an arbitrary integer $q \geq 2$. An interesting benefit of these criteria is that they spare the input statistical independence assumption [34].

Furthermore, these constellation-adapted principles can be considered as *quasi-deterministic* rather than statistical criteria, in the sense that signals with adapted modulations cancel exactly (in the absence of noise and if the data model holds perfectly) the sample version of the contrasts for any data length. As a result, these contrasts offer the potential of achieving good performance even for short sample size. More interestingly, the optimization of these criteria accepts *algebraic solutions*, another approach to improving the shortcomings of blind techniques. Algebraic methods (sometimes called *analytic*) provide an equalization or separation solution in a finite number of operations, and are associated with challenging matrix and tensor decomposition problems. Despite their fundamental theoretical interest, algebraic solutions are only approximate in the presence of noise, too short sample size or when linear recovery solutions do not exist for lack of sufficient diversity. Hence, they generally require a refinement based on iterative optimization, and can indeed be always employed as judicious initializations to iterative equalizers (Secs. 3.4–3.5).

Perfect *zero-forcing (ZF)* equalization of a SISO channel is possible when both of the following conditions are verified:

C1) The channel admits a noiseless Mth-order auto-regressive (AR) model.

C2) The FIR equalizer length is sufficient, $N \geq N_0$, with $N_0 = (M+1)$.

Indeed, a channel satisfying C1 can be equalized by an FIR filter $\mathbf{w}_0$ with minimum length N_0. If the equalizer filter is over-parameterized, $N > N_0$, there exist $P = (N - N_0 + 1)$ exact ZF solutions, each one corresponding to a different equalization delay:

$$\mathbf{w}_p = [\mathbf{0}_{p-1}^{\mathrm{T}},\, \mathbf{w}_0^{\mathrm{T}},\, \mathbf{0}_{P-p}^{\mathrm{T}}]^{\mathrm{T}}, \qquad 1 \leq p \leq P. \tag{3.3}$$

As will be seen in the following, under these conditions the MMSE, CM and CP criteria can be perfectly minimized (even canceled if the sources verify the conditions of each criterion), and the global minimum can be computed algebraically, that is, without iterative optimization. A variety of algorithms aiming to estimate algebraically the best SISO equalizer, or to identify the SISO channel, when the input belongs to a known alphabet have been proposed in [6, 42, 45, 51, 53, 70, 91, 102, 103, 105, 109], among other works.

For their theoretical interest and potential use in practical systems, I have focused on the algebraic solutions to the CM contrast [42, 103, 105] and the variants derived from the CP criterion. The algebraic solution that we detail in Sec. 3.3.3 can be considered as a extension of the *analytic constant modulus algorithm (ACMA)* [103] to the CP principle. Algebraic solutions to supervised and blind criteria can also be combined together (Sec. 3.4.1), giving rise to algebraic semi-blind equalizers. These contributions are developed at length in [P9, P12, P19]. We start our exposition in (p. 153) Secs. 3.3.1–3.3.2 by recalling the algebraic solutions to the supervised MMSE and blind CM criteria, respectively.

3.3.1 Algebraic Solutions to the MMSE Criterion

As recalled in Sec. 2.3, the MMSE criterion (2.10), p. 19, is minimized by the Wiener-Hopf solution (2.11); its reconstruction error is given by eqn. (3.1), p. 29. Let the T_t pilot symbols be stored in vector

$$\breve{\mathbf{s}} = [\breve{s}_0, \breve{s}_1, \ldots, \breve{s}_{T_t-1}]^{\mathrm{H}}.$$

Canceling the criterion (2.10) is tantamount to solving the linear system:

$$\breve{\mathbf{X}}_\delta^{\mathrm{H}} \mathbf{w} = \breve{\mathbf{s}} \tag{3.4}$$

where

$$\breve{\mathbf{X}}_\delta = [\tilde{\mathbf{x}}_\delta, \tilde{\mathbf{x}}_{\delta+1}, \ldots \tilde{\mathbf{x}}_{\delta+T_t-1}] \in \mathbb{C}^{N \times T_t} \tag{3.5}$$

and δ represents the equalization delay. If $T_t \geq N$, the above system does not generally have an exact solution, as it consists of more equations than unknowns. It can still be solved in the LS sense, yielding:

$$\mathbf{w}_{\mathrm{LS}}^{(\delta)} = (\breve{\mathbf{X}}_\delta \breve{\mathbf{X}}_\delta^{\mathrm{H}})^{-1} \breve{\mathbf{X}}_\delta \breve{\mathbf{s}}$$

that we consider here as the algebraic solution to the MMSE criterion (2.10). This solution exists and is unique as long as matrix $\breve{\mathbf{X}}_\delta$ is full rank, which is the case in the presence of noise. In the noiseless case and under conditions C1–C2, matrix $\breve{\mathbf{X}}_\delta$ in eqn. (3.5) has rank N_0, so that it exists an infinite number of solutions to system (3.4) as soon as $N > N_0$. The minimum-norm solution is given by $\mathbf{w}_{\mathrm{LS}}^{(\delta)} = \breve{\mathbf{X}}_\delta^{\dagger} \breve{\mathbf{s}}$, where $(\cdot)^{\dagger}$ denotes the Moore-Penrose pseudo-inverse [155]. This solution corresponds to one of the exact ZF equalizers (3.3), which are identical up to a delay. When noise is present, the impact of delay on equalization performance may become important. The term $\frac{1}{T_t} \breve{\mathbf{X}}_\delta \breve{\mathbf{s}}$ can be regarded as a sample estimate of $\mathbf{p}_\delta$ whereas $\frac{1}{T_t} \breve{\mathbf{X}}_\delta \breve{\mathbf{X}}_\delta^{\mathrm{H}}$ approximates the covariance matrix $\mathbf{R}_{\tilde{\mathbf{x}}}$ in eqn. (2.11), p. 19. The optimal delay in the MMSE sense, δ^{opt}, can be determined according to (3.2), p. 29, using these approximations.

3.3.2 Algebraic Solutions to the CM Criterion

Algebraic solutions to the CM contrast (2.12), p. 19, were originally developed in [103] and [42] in the context of blind separation and channel equalization, respectively. These methods concern the case where multiple exact solutions exist, as the static MIMO case with $L \geq K$ or a SISO channel accepting FIR equalizers with perfect recovery (ZF) solutions (e.g., under conditions C1–C2 above). To describe these methods mathematically, we disregard the equalizer index k in eqn. (2.5), p. 17, and consider a single equalizer output, denoted by y_n, as in eqn. (2.6). Let symbol T_d represent the number of observed baud periods, from which $T = (T_d - N + 1)$ full observed vectors $\tilde{\mathbf{x}}_n$ can be constructed in model (2.7), p. 17. The exact solutions to the CM criterion verify $|y_n|^2 = 1$, up to an irrelevant scale factor [constant γ in (2.12), p. 19], for all $0 \leq n \leq (T-1)$. Denote as $\tilde{\mathbf{x}}_n^{\circledast 2}$ the Kronecker product $\tilde{\mathbf{x}}_n^* \otimes \tilde{\mathbf{x}}_n$, which can also be expressed as $\mathbf{vec}\{\tilde{\mathbf{x}}_n \tilde{\mathbf{x}}_n^{\mathrm{H}}\}$, where $\mathbf{vec}\{\mathbf{A}\}$ is the vector obtained by stacking the columns of matrix $\mathbf{A}$; accordingly, $\mathbf{unvec}\{\cdot\}$ performs the inverse operation. Using this notation, we can write $|y_n|^2 = \mathbf{w}^{\mathrm{H}} \tilde{\mathbf{x}}_n \tilde{\mathbf{x}}_n^{\mathrm{H}} \mathbf{w} = (\tilde{\mathbf{x}}_n^{\circledast 2})^{\mathrm{H}} \mathbf{w}^{\circledast 2}$, and the problem is equivalent to the solution of the linearized system:

$$[\tilde{\mathbf{x}}_{N-1}^{\circledast 2}, \tilde{\mathbf{x}}_N^{\circledast 2}, \ldots, \tilde{\mathbf{x}}_{T_d-1}^{\circledast 2}]^{\mathrm{H}} \mathbf{f} = [1,\, 1,\, \ldots,\, 1]^{\mathrm{T}} \tag{3.6}$$

under the structural constraint $\mathbf{f} = \mathbf{w}^{\circledast 2}$. When P equalizers $\{\mathbf{w}_p\}_{p=1}^P$ exist, system (3.6) without constraint accepts P solutions $\{\mathbf{f}_k\}_{k=1}^P$ such that

$$\mathbf{f}_k = \sum_{p=1}^{P} \alpha_{kp} \mathbf{w}_p^{\circledast 2} \tag{3.7}$$

for certain unknown but linearly independent coefficients $\{\alpha_{kp}\}_{k,p=1}^P$. In terms of the associated matrices, $\mathbf{F}_k = \mathbf{unvec}\{\mathbf{f}_k\}$, this relationship can be expressed in the form:

$$\mathbf{F}_k = \sum_{p=1}^{P} \alpha_{kp} \mathbf{w}_p \mathbf{w}_p^{\mathrm{H}} = \mathbf{W} \mathbf{A}_k \mathbf{W}^{\mathrm{H}} \tag{3.8}$$

with $\mathbf{W} = [\mathbf{w}_1, \ldots, \mathbf{w}_P]$ and $\mathbf{A}_k = \mathrm{diag}([\alpha_{k1}, \ldots, \alpha_{kP}])$. It follows that the recovery of the extracting filters $\{\mathbf{w}_p\}_{p=1}^P$ from a basis of the solution space is tantamount to the problem below [103]:

Problem 1 (joint diagonalization). Given the set of matrices $\{\mathbf{F}_k\}_{k=1}^P$ associated with the non-structured solutions to the linearized problem (3.6), find matrices $\mathbf{W}$ and $\{\mathbf{A}_k\}_{k=1}^P$ verifying eqn. (3.8).

As opposed to other joint diagonalization algorithms such as SOBI [7] or JADE [11] (see also Sec. 2.3), the diagonalizing transformation in Problem 1, i.e., matrix $\mathbf{W}$, is in general not unitary. This matrix is composed of the valid equalizer vectors.

From another perspective, the above equality can be considered as the search for coefficients $\{\beta_{pk}\}_{p,k=1}^P$ such that the linear combination $\sum_{k=1}^P \beta_{pk} \mathbf{F}_k$ approximates the rank-1 matrix $\mathbf{w}_p \mathbf{w}_p^{\mathrm{H}}$. This naturally leads to the following problem [33]:

Problem 2 (rank-1 matrix linear combination). Given matrices $\{\mathbf{F}_k\}_{k=1}^P$, find all solutions to

$$\min_{\{\beta_1,\ldots,\beta_P\},\mathbf{w}} \left\| \sum_{k=1}^{P} \beta_k \mathbf{F}_k - \mathbf{w}\mathbf{w}^{\mathrm{H}} \right\|.$$

In the general case, the ACMA of [103] tries to solve the joint diagonalization problem (3.8) by using the generalized Schur decomposition [155] of several (more than two) matrices, a costly iterative method for which a convergence proof has not yet been found. Simplifications are possible [42] when the valid extracting filters are delayed versions of each other, as under conditions C1–C2, where the P different solutions are given by eqn. (3.3), p. 30.

Once a non-structured solution has been obtained via, e.g., pseudo-inversion of the coefficient matrix in (3.6), the minimum-length equalizer can be extracted by a subspace-based approach or other simple procedures for structure restoration exploiting the presence of zero elements in $\mathbf{w}_p^{\circledast 2}$ [see eqns. (3.3) and (3.7)]. In the real case, nearly half the elements of $\tilde{\mathbf{x}}_n^{\circledast 2}$ are redundant, so that ACMA requires special modifications to process signals with one-dimensional alphabets (e.g., BPSK) [42, 103]; such modifications give rise to the *real ACMA (RACMA)* method of [105].

3.3.3 Algebraic Solutions to the CP Criterion

In close collaboration with Pierre Comon, I have explored in [P19] the algebraic solutions to a novel property restoral principle for the blind equalization of q-PSK signals, the so-called *constant power (CP)* criterion. This is a particular case of the *alphabet polynomial fitting (APF)* principle of [32, 34, 50] that aims to match the equalizer output constellation to that of the source, characterized by the complex roots of a specific polynomial $Q(z)$ [34, 84]. Thus, APF criteria rely on the minimization of function (p. 153)

$$\Upsilon_{\mathrm{APF}}(y) = \mathrm{E}\{|Q(y)|^2\}$$

As opposed to independence-based criteria, APF contrasts have the ability to separate spatially correlated and spectrally colored sources. As opposed to the CM criterion, APF can target sources with matching modulation (cf. drawback D1, p. 27).

In particular, the q-PSK modulation can be represented by the roots of the qth degree polynomial $Q(z) = z^q - d$, or by the solutions to $z^q = d$, hence the name *constant power*. The values of q and d depend on the particular constellation; for instance, $(q,\, d) = (2,\, 1)$ for BPSK, $(q,\, d) = (4,\, 1)$ for QPSK, etc. By allowing a time-varying d, the above definitions are directly extended to modulations other than PSK, such as minimum shift keying (MSK) [51], which can be described by $(q,\, d_n) = \big(2,\, (-1)^n\big)$. Accordingly, the CP criterion reads:

$$\Upsilon_{\mathrm{CP}}(y) = \mathrm{E}\{|y_n^q - d_n|^2\}. \tag{3.9}$$

The CP principle can be considered as an extension of the Godard family of criteria [48] that takes into account the particular properties of the q-PSK modulation. This principle is asymptotically insensitive to a large class of circularly distributed (at order q) interference and noise. In the context of BSS, minimizing (3.9) is equivalent, for a sufficiently low noise level, to *maximum a posteriori (MAP)* estimation [30, 50].

The development of analytic solutions to criterion (3.9) follows closely the CM case. Hence, by analogy with the ACMA of [104], we refer to these solutions as *analytic constant power algorithm (ACPA)*. From a linear algebra perspective, finding the analytic solutions to the CP contrast optimization leads to tensorial generalizations of the matrix problems set out in the previous section. To cast these tensor problems mathematically, a few extra definitions are first required.

3.3.3.1 Some definitions

Let $[\mathcal{A}]_{i_1 i_2 \ldots i_q}$ denote the $(i_1, i_2, \ldots, i_q)$-element of qth-order tensor $\mathcal{A} \in \mathbb{C}^{M_1 \times \cdots \times M_q}$, $1 \leq i_p \leq M_p$, $p = 1, \ldots, q$. The Frobenius product of two tensors $\mathcal{A}$ and $\mathcal{B}$ with the same order and dimensions is defined as $\langle \mathcal{A}, \mathcal{B} \rangle = \sum_{i_1 \ldots i_q} [\mathcal{A}]_{i_1 \ldots i_q} [\mathcal{B}]_{i_1 \ldots i_q}$; hence the Frobenius norm $\|\mathcal{A}\|^2 = \langle \mathcal{A}, \mathcal{A} \rangle$. The outer product of two tensors of orders p and q, $\mathcal{C} = \mathcal{A} \circ \mathcal{B}$ is given by the $(p+q)$th-order tensor $[\mathcal{C}]_{i_1 \ldots i_p j_1 \ldots j_q} = [\mathcal{A}]_{i_1 \ldots i_p} [\mathcal{B}]_{j_1 \ldots j_q}$. Given a vector $\mathbf{a} \in \mathbb{C}^L$, we denote $\mathbf{a}^{\circ q} = \underbrace{\mathbf{a} \circ \cdots \circ \mathbf{a}}_{q}$ (for instance, $\mathbf{a}^{\circ 2} = \mathbf{a} \circ \mathbf{a} = \mathbf{a}\mathbf{a}^{\mathrm{T}}$).

A symmetric tensor of order q and dimension N can be stored in a vector $\mathbf{vecs}\{\mathcal{A}\}$, which contains the $N_q = \binom{N+q-1}{q}$ different entries of $\mathcal{A}$. These entries are normalized so as to preserve the Frobenius norm, and we write $\mathbf{a}^{\oslash q} = \mathbf{vecs}\{\mathbf{a}^{\circ q}\}$. Similarly, from a vector $\mathbf{b}$ of dimension N_q, $\mathbf{unvecs}_q\{\mathbf{b}\}$ represents the associated qth-order symmetric tensor.

3.3.3.2 Problem formulation

Recall that a total of $T = (T_d - N + 1)$ full observed vectors $\tilde{\mathbf{x}}_n$ can be constructed from the T_d observed baud periods in model (2.7), p. 17. Given such vectors, we look for the exact minimizers of the CP criterion, verifying

$$y_n^q = d_n \qquad n = 0, 1, \ldots, T-1. \tag{3.10}$$

(p. 153) Proofs of the claims that follow can be found in [P19], and can be considered as extensions to the tensor case of those developed for ACMA in [103]. With the above definitions, we have that $y_n^q = (\tilde{\mathbf{x}}_n^{\oslash q})^{\mathrm{H}} \mathbf{w}^{\oslash q}$. As a result, the cancellation of the CP criterion is equivalent to the solution of the linearized system

$$\mathbf{X}^{q\mathrm{H}} \mathbf{f} = \mathbf{d} \tag{3.11}$$

where $\mathbf{X}^q = [\mathbf{x}_{N-1}^{\oslash q}, \mathbf{x}_N^{\oslash q}, \ldots, \mathbf{x}_{T_d-1}^{\oslash q}]$ and $\mathbf{d} = [d_0, d_1, \ldots, d_{T-1}]^{\mathrm{H}}$. Equation (3.11) must be solved under the following structural constraint: $\mathbf{f} \in \mathbb{C}^{N_q}$ must be of the form form $\mathbf{f} = \mathbf{w}^{\oslash q}$, for certain vector $\mathbf{w} \in \mathbb{C}^N$.

3.3.3.3 Determining a basis of the solution space

When P extracting filters exist (as occurs under conditions C1–C2, p. 30), system (3.11) without constraint accepts P linearly independent solutions $\{\mathbf{f}_k\}_{k=1}^P$. Consequently, the dimension of the null space of $\mathbf{X}^{q\mathrm{H}}$, denoted $\ker(\mathbf{X}^{q\mathrm{H}})$, is $(P-1)$, and the solutions of (3.11) can be expressed as an affine space of the form $\mathbf{f} =$

$\mathbf{f}_0 + \sum_{p=1}^{P-1} \alpha_p \mathbf{f}_p$, where $\mathbf{f}_0$ is a particular solution to the non-homogeneous system (3.11) and $\mathbf{f}_p \in \ker(\mathbf{X}^{q\mathrm{H}})$, for $1 \leq p \leq (P-1)$.

As in [103], we find it more convenient to work in a vector space, obtained through a unitary transformation $\mathbf{Q}$ with dimensions $(T \times T)$, such that $\mathbf{Qd} = [\sqrt{T}, \mathbf{0}_{T-1}^{\mathrm{T}}]^{\mathrm{T}}$, where symbol $\mathbf{0}_{T-1}$ stands for the vector of $(T-1)$ zeros. For instance, $\mathbf{Q}$ can be a Householder transformation [155] or, if $\mathbf{d}$ is composed of T equal values (as is the case for q-PSK modulations), a T-point DFT matrix. Then, denoting:

$$\mathbf{QX}^{q\mathrm{H}} = \begin{bmatrix} \mathbf{r}^{\mathrm{H}} \\ \mathbf{R} \end{bmatrix}$$

system (3.11) reduces to:

$$\begin{cases} \mathbf{r}^{\mathrm{H}}\mathbf{f} = \sqrt{T} \\ \mathbf{Rf} = \mathbf{0}_{T-1}. \end{cases}$$

under the constraint $\mathbf{f} = \mathbf{w}^{\oslash q}$. Similarly to [103, Lemma 4], it is possible to prove that this problem is equivalent to the solution of:

$$\begin{cases} \mathbf{Rf} = \mathbf{0}_{T-1} \\ \mathbf{f} = \mathbf{w}^{\oslash q} \end{cases}$$

followed by a scaling factor to enforce:

$$\mathbf{c}^{\mathrm{H}}\mathbf{f} = 1, \qquad \text{with} \quad \mathbf{c} = \frac{1}{\|\mathbf{d}\|^2} \sum_{n=0}^{T-1} d_n \mathbf{x}_n^{\oslash q} \tag{3.12}$$

or, equivalently:

$$\frac{1}{\|\mathbf{d}\|^2} \sum_{n=0}^{T-1} d_n (\mathbf{w}^{\mathrm{H}}\mathbf{x}_n)^q = 1. \tag{3.13}$$

If $\dim\ker(\mathbf{X}^{q\mathrm{H}}) = (P-1)$ and

$$T_d \geq N_q + N_0 - 1 \tag{3.14}$$

(or $T > N_q - P$), then $\dim\ker(\mathbf{R}) = P$. Hence, all the solutions of $\mathbf{Rf} = \mathbf{0}$ are linearly spanned by a basis $\{\mathbf{f}_k\}_{k=1}^{P}$ of $\ker(\mathbf{R})$. Such a basis can be computed from the *singular value decomposition (SVD)* of matrix $\mathbf{R}$ by taking its P least significant right singular vectors.

3.3.3.4 Matrix and tensor algebra problems

The structured solutions $\{\mathbf{w}_p^{\oslash q}\}_{p=1}^{P}$ are also a basis of the solution space so that:

$$\mathbf{f}_k = \sum_{p=1}^{P} \alpha_{kp} \mathbf{w}_p^{\oslash q} \qquad 1 \leq k \leq P \tag{3.15}$$

for certain unknown coefficients $\{\alpha_{kp}\}_{k,p=1}^{P}$ forming a full-rank matrix $[\mathbf{A}]_{kp} = \alpha_{pk}$. The problem of finding structured solutions to the linearized system (3.11) is hence a particular *subspace fitting* problem with structural constraints.

Problem 3 (subspace fitting with structural constraints). Given a set of vector $\{\mathbf{f}_k\}_{k=1}^P$, find coefficients $\{\alpha_{kp}\}_{k,p=1}^P$ and vectors $\{\mathbf{w}_p\}_{p=1}^P$ verifying relationship (3.15). Equivalently, given the qth-order tensors $\mathcal{F}_k = \mathbf{unvecs}\{\mathbf{f}_k\}$, find the solutions to

$$\mathcal{F}_k = \sum_{p=1}^{P} \alpha_{kp} \mathcal{W}_p$$

where $\mathcal{W}_p = \mathbf{w}_p^{\circ q} = \mathbf{unvecs}_q\{\mathbf{w}_p^{\oslash q}\}$.

As a result, the equalizer filter recovery can be considered as the following *tensorial generalization of the rank-1 linear combination problem* [33]:

Problem 4 (rank-1 tensor linear combination). Given the set of tensors $\{\mathcal{F}_k\}_{k=1}^P$, find all solutions of

$$\min_{\{\beta_1,\ldots,\beta_P\},\mathbf{w}} \left\| \sum_{k=1}^{P} \beta_k \mathcal{F}_k - \mathbf{w}^{\circ q} \right\|.$$

This tensor decomposition is generally a non-trivial task [28, 33].

3.3.3.5 Solution structuring methods

According to Problem 4, finding a structured solution to the linearized system (3.11) consists in enforcing the rank-1 symmetric Kronecker structure to the basis $\{\mathbf{f}_k\}_{k=1}^P$. In the context of the CM criterion (Problem 2, p. 33), a subspace method was proposed in [42, section III.C], operating on a single non-structured (LS) solution. According to Problem 1, p. 32, this structure forcing procedure can be interpreted as the diagonalization of the matrix associated with the non-structured solution.

The method of [52] and [42, section III.B] is based on the observation that, according to eqns. (3.3), p. 30, and (3.15), the first N components of a solution $\mathbf{f}_k$ are equal to

$$\alpha_{k1} w_1^{q-1} [w_1,\ \sqrt{q}\, w_2,\ \ldots,\ \sqrt{q}\, w_{N_0-1},\ \sqrt{q}\, w_{N_0},\ \mathbf{0}_{P-1}^{\mathrm{T}}]^{\mathrm{T}}$$

from which the minimum-length equalizer $\mathbf{w}_0 = [w_1, w_2, \ldots, w_{N_0}]^{\mathrm{T}}$ can easily be deduced. This method is simple and ingenious, but inaccurate when coefficient α_{k1} or the first term w_1 of the equalizer are small relative to the noise level.

To surmount this limitation, one can also note from eqns. (3.3) and (3.15) that the last components of $\mathbf{f}_k$ are equal to [42, section III.B]:

$$\alpha_{kP} w_{N_0}^{q-1} [\mathbf{0}_{P-1}^{\mathrm{T}},\ \ldots,\ \sqrt{q}\, w_1,\ \sqrt{q}\, w_2,\ \ldots,\ \sqrt{q}\, w_{N_0-1},\ w_{N_0}]^{\mathrm{T}}$$

Appropriately combined with the estimation carried out from the first N components, this second option can provide an improved estimation of $\mathbf{w}_0$. To this end, we may employ the following heuristic (suboptimal) linear combination. Let us suppose that the filters estimated from the first and the last non-overlapping components of a non-structure solution are, respectively, $\hat{\mathbf{w}}_1 = \beta_1 \tilde{\mathbf{w}}_0$ and $\hat{\mathbf{w}}_2 = \beta_2 \tilde{\mathbf{w}}_0$, with $\tilde{\mathbf{w}}_0 = \mathbf{w}_0 / \|\mathbf{w}_0\|$. Then, the unit-norm minimum-length equalizer LS estimate

is given by $\hat{\tilde{\mathbf{w}}}_0 = [\hat{\mathbf{w}}_1, \hat{\mathbf{w}}_2]\boldsymbol{\gamma}$, with $\boldsymbol{\gamma} = \boldsymbol{\beta}^*/\|\boldsymbol{\beta}\|^2$, $\boldsymbol{\beta} = [\beta_1, \beta_2]^{\mathrm{T}}$. The coefficients of $\boldsymbol{\beta}$ can simply be estimated from the equation $\beta_i = \|\hat{\mathbf{w}}_i\|$, $i = 1, 2$. This type of linear *maximal ratio combining* is reminiscent of the *RAKE* receiver and the matching filter [80]. Robustness can still be improved by exploiting a whole basis of the solution space $\{\mathbf{f}_k\}_{k=1}^P$ instead of a single solution.

3.3.3.6 A subspace approach to solution structuring

When the valid solutions are of the form (3.3), we have proposed a *subspace method* reminiscent of [77] to recover the minimum-length equalizer $\mathbf{w}_0$ from a basis of (generally) unstructured solutions $\{\mathbf{f}_k\}_{k=1}^P$, thus solving the rank-1 linear combination problem (Problem 4) in that particular case. The method can be described as follows [P19]. (p. 153)

The subspace fitting problem (3.15) can be written in compact form as $\mathbf{F} = \mathbf{WA}$, with $\mathbf{F} = [\mathbf{f}_1, \ldots, \mathbf{f}_P]$ and $\mathbf{W} = [\mathbf{w}_1^{\oslash q}, \ldots, \mathbf{w}_P^{\oslash q}]$; the entries of matrix $\mathbf{A}$ are defined after eqn. (3.15). Since $\mathbf{A}$ is full rank, matrices $\mathbf{F}$ and $\mathbf{W}$ span the same column space. In particular, any vector $\mathbf{u}_i$ in the orthogonal complement of $\mathbf{F}$ also verifies $\mathbf{u}_i^{\mathrm{H}}\mathbf{W} = \mathbf{0}_P^{\mathrm{T}}$. There are $\dim\ker(\mathbf{F}^{\mathrm{H}}) = (N_q - P)$ such linearly independent vectors, where $N_q = \binom{N+q-1}{q}$. Since equalization solutions have the form (3.3), p. 30, the corresponding columns of $\mathbf{W}$ have a particular structure whereby the elements not associated with the minimum-length equalizer $\mathbf{w}_0$ are all zero. The remaining $N_{0q} = \binom{N_0+q-1}{q}$ elements form $\mathbf{w}_0^{\oslash q}$. Let σ_p describe the set of N_{0q} positions of $\mathbf{w}_0^{\oslash q}$ in $\mathbf{w}_p^{\oslash q}$, that is, $\sigma_p = \{j_1 + N(j_2 - 1) + \cdots + N^{q-1}(j_q - 1)\}$, with $j_k \in [p, p + N_0 - 1]$, $k = 1, \ldots, q$, and $j_1 \geq j_2 \geq \cdots \geq j_q$. Similarly, $(\mathbf{u}_i)_{\sigma_p} \in \mathbb{C}^{N_{0q}}$ is the sub-vector composed of the elements of $\mathbf{u}_i$ in positions σ_p. Let $\mathbf{U}_i = [(\mathbf{u}_i)_{\sigma_1}, \ldots, (\mathbf{u}_i)_{\sigma_P}] \in \mathbb{C}^{N_{0q}\times P}$. Hence:

$$\mathbf{u}_i^{\mathrm{H}}\mathbf{W} = \mathbf{0}_P^{\mathrm{T}} \quad \Leftrightarrow \quad \mathbf{U}_i^{\mathrm{H}}\mathbf{w}_0^{\oslash q} = \mathbf{0}_P.$$

The above equalities define a set of $P(N_q - P)$ linear equations, characterized by matrix $\mathbf{U} = [\mathbf{U}_1, \ldots, \mathbf{U}_{N_q-P}] \in \mathbb{C}^{N_{0q}\times P(N_q-P)}$, where the unknowns are the components of $\mathbf{w}_0^{\oslash q}$. As long as $N > N_0$, this linear system determines, up to scale, the well-structured vector $\mathbf{w}_0^{\oslash q}$. In practice, we minimize the quadratic form $\|\mathbf{U}^{\mathrm{H}}\mathbf{w}_0^{\oslash q}\|^2 = \mathbf{w}_0^{\oslash q\mathrm{H}}\mathbf{U}\mathbf{U}^{\mathrm{H}}\mathbf{w}_0^{\oslash q}$, which leads to the estimation of $\mathbf{w}_0^{\oslash q}$ as the least significant left singular vector of matrix $\mathbf{U}$. Once matrix $\mathbf{W}$ has been reconstructed, an LS estimate of coefficients $\{\alpha_{kp}\}_{k,p=1}^P$ can be obtained as $\hat{\mathbf{A}}_{\mathrm{LS}} = (\mathbf{W}^{\mathrm{H}}\mathbf{W})^{-1}\mathbf{W}^{\mathrm{H}}\mathbf{F} = \mathbf{W}^{\dagger}\mathbf{F}$. The elements of $\hat{\mathbf{A}}_{\mathrm{LS}}$ provide a solution to the rank-1 tensor linear combination problem (Problem 4, p. 36).

Unlike the ACMA methods of [42, 103], the proposed blind algebraic solution deals naturally with binary inputs (BPSK, MSK) without any modifications.

3.3.3.7 Recovering the equalizer vector from its symmetric tensor vectorization

Another important issue concerning algebraic equalizers is the recovery of the equalizer impulse response $\mathbf{w}_0$ from its symmetric vectorization $\hat{\mathbf{w}}_0^{\oslash q}$ estimated by the

above method. Denoting $\mathcal{W}_0 = \mathbf{unvecs}_q\{\hat{\mathbf{w}}_0^{\oslash q}\}$, one is actually facing another challenging tensor algebra problem:

Problem 5 (rank-1 symmetric tensor approximation). Given a symmetric tensor $\mathcal{W}_0$, find the solution to

$$\min_{\mathbf{w}} \left\| \mathcal{W}_0 - \mathbf{w}^{\circ q} \right\|.$$

Contrary to the matrix case, this rank-1 tensor approximation is a notoriously non-trivial task. A simple solution is based on a matrix unfolding of $\mathcal{W}_0$ [32, 52]. Let us denote by $\mathbf{W}_0 \in \mathbb{C}^{N_0 \times N_0^{q-1}}$ the matrix with elements

$$[\mathbf{W}_0]_{i_1, i_2 + N_0(i_3-1) + \ldots N_0^{q-2}(i_q-1)} = [\mathcal{W}_0]_{i_1 i_2 i_3 \ldots i_q}.$$

In the ideal case, $\mathcal{W}_0 = \mathbf{w}_0^{\circ q}$, and then $\mathbf{W}_0 = \mathbf{w}_0 \bar{\mathbf{w}}_0^{\mathrm{T}}$, with

$$[\bar{\mathbf{w}}_0]_{i_2 + N_0(i_3-1) + \ldots N_0^{q-2}(i_q-1)} = [\mathbf{w}_0]_{i_2} [\mathbf{w}_0]_{i_3} \ldots [\mathbf{w}_0]_{i_q}.$$

Hence, matrix $\mathbf{W}_0$ has rank one and $\mathbf{w}_0$ can be estimated (up to a scale factor) as its dominant left singular vector.

In the presence of noise or estimation errors, however, it is generally no longer possible to express the estimated vector $\hat{\mathbf{w}}_0^{\oslash q}$ as the symmetric vectorization of a rank-1 tensor; in other words, no vector $\mathbf{w}_0$ exists such that $\hat{\mathbf{w}}_0^{\oslash q} = \mathbf{vecs}_q\{\mathbf{w}_0^{\circ q}\}$ is verified exactly. Consequently, the matrix unfolding will not be of rank one, and the SVD-based solution will only be approximate. To date, only iterative solutions, e.g., inspired on the *iterative power method* [66, 69], have been proposed to solve
(p. 153) Problem 5. Still, our experiments [P9,P12,P19] indicate that the solution previously described for the noiseless case, though suboptimal, yields encouraging performance.

3.3.3.8 Approximate solution in the presence of noise

In the presence of additive noise at the sensor output, conditions C1–C2 are no longer satisfied, and an exact solution of (3.10), p. 34, may no longer exist. An approximate solution in the LS sense can be obtained by minimizing $\|\mathbf{X}^{q\mathrm{H}}\mathbf{f} - \mathbf{d}\|^2$, under the structural constraint $\mathbf{f} = \mathbf{w}^{\oslash q}$. This minimization generally requires an iterative method (Secs. 3.4–3.5). Nevertheless, the guidelines for determining an exact solution in the noiseless case can still provide a sensible initialization to an iterative equalizer in the noisy case.

After applying the transformation $\mathbf{Q}$ (as in Sec. 3.3.3.3, p. 35), the LS problem proves equivalent to the minimization of the quadratic form:

$$|\mathbf{c}^{\mathrm{H}}\mathbf{f} - 1|^2 + \|\mathbf{R}\mathbf{f}\|^2. \tag{3.16}$$

To find a basis of the solution space, we seek a set of vectors minimizing $\|\mathbf{R}\mathbf{f}\|^2$ (for instance, the least significant P right singular vectors of $\mathbf{R}$), then structure them as in Sec. 3.3.3.6, pp. 37–37, and finally normalize the solution to satisfy $\mathbf{c}^{\mathrm{H}}\mathbf{f} = 1$ [eqns. (3.12)–(3.13)].

A more accurate solution can be determined by realizing that expression (3.16) represents a non-negative quadratic form in vector $[\mathbf{f}^{\mathrm{T}}, 1]^{\mathrm{T}}$. Formulating the problem in the projective space, we can look for the least significant eigenvector $\mathbf{v}_{\mathrm{m}}$ of matrix:

$$\begin{bmatrix} \mathbf{R}\mathbf{R}^{\mathrm{H}} + \mathbf{c}\mathbf{c}^{\mathrm{H}} & -\mathbf{c} \\ -\mathbf{c}^{\mathrm{H}} & 1 \end{bmatrix}$$

and take as an approximate estimation of $\mathbf{f}$ the first $\dim(\mathbf{f})$ components of $\mathbf{v}_{\mathrm{m}}$ normalized by the last one.

3.3.3.9 Experimental analysis

The numerical study of [P9, P12, P19] reveals the following results: (p. 153)

- Satisfactory algebraic CP equalization can be obtained with data length below the bound (3.14), p. 35, particularly for the subspace based solution (Sec. 3.3.3.6). Concerning the methods based on a single LS solution (see Sec. 3.3.3.5), performance improvement is observed once the bound is respected.
- As opposed to the ACMA method of [42], the proposed subspace method takes into account a complete basis of the solution space. As a result, it shows an improved robustness to noise and to the structure of the minimum-length equalizer, e.g., the presence of leading or trailing coefficients with small values.
- In the presence of noise, an algebraic solution can always benefit from an iterative optimization procedure such as those described in Secs. 3.4–3.5. Algebraic solutions can thus be considered as sensible initializations to iterative equalizers.

3.4 Semi-Blind Criteria

The hybrid detection method described at the end of Sec. 3.2, pp. 28–30, can be considered as a semi-blind approach whereby the iterative ICA extractor is initialized by the Wiener receiver but otherwise operates freely. This notion can be extended by combining a blind and a supervised contrast into a *semi-blind criterion* in which both parts are to be optimized jointly. The combination of the blind CM and supervised MMSE contrasts leads to the following *semi-blind CM-MMSE* criterion:

$$\Upsilon_{\mathrm{SBCM}}(y) = \lambda\Upsilon_{\mathrm{MMSE}}(y) + (1-\lambda)\Upsilon_{\mathrm{CM}}(y). \tag{3.17}$$

Parameter λ is a real-valued constant in the interval $[0, 1]$ that can be considered as the relative degree of confidence in the blind and pilot-based parts of the criterion. The MMSE part of the cost function aims at the extraction of a suitable equalization delay. Totally analogous semi-blind criteria can be defined if another blind criterion, e.g., the CP, is used instead of the CM in (3.17). The combination of a training-based and a blind criterion has the potential of preventing their respective drawbacks while preserving their advantages. In the context of channel

identification, it was shown that any channel (SISO or SIMO) is identifiable from a small number of known symbols. Thanks to the use of a blind criterion, the pilot sequence necessary to estimate a channel of given length can become shorter relative to the training-only solution; spectral efficiency can thus be increased for a fixed estimation quality. Hence, the semi-blind approach can be interpreted as the regularization of the conventional supervised approach, avoiding the performance degradation for insufficient pilot length. As a result, semi-blind techniques often outperform supervised and blind techniques; when these fail, their semi-blind association can succeed [16].

(p. 153) (p. 269) Works [P9, P12, P19, P46] evaluate the performance of semi-blind criteria of the form (3.17) for *direct equalization*, i.e., without previous channel identification, in the SISO and SIMO cases. As sketched next, both algebraic and iterative solutions can be derived for the optimization of these criteria.

3.4.1 Algebraic Semi-Blind Equalizers

By extending the ideas of Sec. 3.3, we can also develop algebraic solutions to the semi-blind criterion CP-MMSE based on eqn. (2.10), p. 19, and eqn. (3.9), p. 33. The solutions to criterion CM-MMSE (3.17) can be obtained in an analogous manner. To minimize algebraically the CP-MMSE criterion, we seek the simultaneous solution of systems (3.4), p. 31, and (3.11), p. 34:

$$\breve{\mathbf{X}}_{\delta}^{\mathrm{H}}\mathbf{w} = \breve{\mathbf{s}} \tag{3.18}$$

$$\mathbf{X}^{q\mathrm{H}}\mathbf{f} = \mathbf{d} \tag{3.19}$$

under the structural constraint $\mathbf{f} = \mathbf{w}^{\oslash q}$.

The case where conditions C1–C2 are verified is trivial, since both solutions of the composite system are exact and identical. Hence, let us first consider the case of a noisy AR channel with a sufficiently long equalizer. A suboptimal solution can be obtained by combining the solutions computed separately for the two subsystems [32, 52]. Let $\hat{\mathbf{w}}_{\mathrm{MMSE}}$ denote the solution of (3.18) and $\hat{\mathbf{w}}_{\mathrm{CP}}^{\oslash q}$ that of (3.19) associated with the same equalization delay; these solutions can be computed as explained in Sec. 3.3.1, pp. 31–31, and Sec. 3.3.3, pp. 33–39, respectively. Let us unfold $\mathbf{unvecs}_q\{\hat{\mathbf{w}}_{\mathrm{CP}}^{\oslash q}\}$ into a matrix $\mathbf{W}_{\mathrm{CP}}$ with dimensions$(N \times N^{q-1})$, as described in Sec. 3.3.3.7. Then, the joint solution to (3.18)–(3.19) can be approximated by the dominant left singular vector of matrix

$$\mathbf{W}_{\mathrm{SB}} = [\lambda\hat{\mathbf{w}}_{\mathrm{MMSE}},\, (1-\lambda)\mathbf{W}_{\mathrm{CP}}].$$

In the noiseless case, it is obvious that solutions $\hat{\mathbf{w}}_{\mathrm{MMSE}}$ and $\hat{\mathbf{w}}_{\mathrm{CP}}$ coincide with the dominant left singular vector of the rank-1 matrix $\mathbf{W}_{\mathrm{SB}}$.

In the case of an FIR channel, no exact solution to system (3.18)–(3.19) exists, even in the absence of noise. However, the two sub-systems can be solved separately in the LS sense and the respective solutions can then be combined according to the above SVD-based procedure.

3.4.2 Iterative Semi-Blind Equalizers

The derivation of iterative gradient-based equalizers is straightforward, since the gradient of a semi-blind criterion is obtained from the same linear combination of the gradients of its blind and supervised parts. This leads to classical gradient-descent update rules with constant step size:

$$\mathbf{w}^{+} = \mathbf{w} - \mu\big[\lambda\nabla\Upsilon_{\mathrm{MMSE}}(\mathbf{w}) + (1-\lambda)\nabla\Upsilon_{\mathrm{CM}}(\mathbf{w})\big] \tag{3.20}$$

where, with some abuse notation, the contrasts are expressed in terms of the equalizer vector instead of the equalizer output.

Let us define the complex gradient of a generic real-valued function $\Upsilon(\mathbf{w})$ with respect to complex variable $\mathbf{w}$ as:

$$\nabla\Upsilon(\mathbf{w}) = \nabla_{\mathbf{w}_r}\Upsilon(\mathbf{w}) + j\nabla_{\mathbf{w}_i}\Upsilon(\mathbf{w})$$

where $\mathbf{w}_r = \mathbb{R}\mathrm{e}(\mathbf{w})$ and $\mathbf{w}_i = \mathbb{I}\mathrm{m}(\mathbf{w})$ represent the real and imaginary parts, respectively, of vector $\mathbf{w}$. Up to an inconsequential scale factor, this definition corresponds to Brandwood's conjugate gradient [9]. Accordingly, the gradients of the MMSE (2.10), CM (2.12), KM (2.13) and CP (3.9) criteria can be expressed as [P9, P12, P4, P17, P19]: (p. 133) (p. 153)

$$\nabla\Upsilon_{\mathrm{MMSE}}(\mathbf{w}) = 2\mathrm{E}\big\{\big[(\mathbf{w}^{\mathrm{H}}\tilde{\mathbf{x}}) - \breve{s}\big]^{*}\mathbf{x}\big\} \tag{3.21}$$

$$\nabla\Upsilon_{\mathrm{CM}}(\mathbf{w}) = 4\mathrm{E}\big\{(\mathbf{w}^{\mathrm{H}}\tilde{\mathbf{x}})^{*}\big[|\mathbf{w}^{\mathrm{H}}\tilde{\mathbf{x}}|^2 - \gamma\big]\tilde{\mathbf{x}}\big\} \tag{3.22}$$

$$\nabla\Upsilon_{\mathrm{KM}}(\mathbf{w}) = \frac{4}{\mathrm{E}^2\{|y|^2\}}\Bigg\{\mathrm{E}\{|y|^2 y^{*}\tilde{\mathbf{x}}\} - \mathrm{E}\{y\tilde{\mathbf{x}}\}\mathrm{E}\{y^{*2}\} - \frac{\big(\mathrm{E}\{|y|^4\} - |\mathrm{E}\{y^2\}|^2\big)\mathrm{E}\{y^{*}\tilde{\mathbf{x}}\}}{\mathrm{E}\{|y|^2\}}\Bigg\} \tag{3.23}$$

$$\nabla\Upsilon_{\mathrm{CP}}(\mathbf{w}) = 2q\mathrm{E}\big\{(\mathbf{w}^{\mathrm{H}}\tilde{\mathbf{x}})^{q-1}\big[(\mathbf{w}^{\mathrm{H}}\tilde{\mathbf{x}})^{q} - d\big]^{*}\tilde{\mathbf{x}}\big\}. \tag{3.24}$$

In expression (3.23), the dependence on $\mathbf{w}$ is made explicit by relationship (2.6), p. 17, which has been directly incorporated into eqns. (3.21), (3.22) and (3.24). The multiplicative factor $\mathrm{sign}(\kappa_4^y)$ is missing in the KM gradient, but becomes irrelevant with the optimal step-size iterative search technique described later in this chapter.

As shown by the experimental analysis of [P9, P12, P19, P46], the benefits of these semi-blind iterative equalizers include: (p. 153) (p. 269)

- The incorporation of a few pilot symbols 'smoothens' the cost function, suppressing local minima and eliminating the indeterminacies of fully blind criteria (drawback D1, p. 27).
- Equalization performance is more robust to initialization than in the fully-blind case (drawback D2, p. 27).
- Thanks to the incorporation of the blind part of the criterion, source estimation quality is improved relative to the conventional MMSE equalizer with the same pilot-sequence length. Conversely, the same estimation quality can be achieved with reduced pilot length relative to the conventional receiver, thus improving spectral efficiency.

- Equalization performance is robust to confidence parameter λ.

The flattening of the cost function when incorporating training data can slightly slow down convergence relative to the blind case, so that drawback D3, p. 28, is not mitigated by the semi-blind approach if used in conjunction with conventional fixed step-size iterative search methods. However, this adverse effect is prevented by the use of the optimal step-size technique described in Sec. 3.5.2, pp. 43–45.

The performance and robustness of the semi-blind approach justify by themselves the interest in this kind of techniques. The fact that many of the current as well as future communication systems include pilot sequences in their definition standards (in particular to assist in synchronization) provides a strong additional motivation for semi-blind equalization techniques. Nevertheless, their use in currently available commercial products is rather limited.

3.5 Optimal Step-Size Iterative Search

3.5.1 Approaches to Step-Size Selection

The convergence properties of iterative equalization and source separation techniques of the form (3.20) are to a large extent determined by the step size or learning rate, i.e., parameter μ, employed in their update rules. Classical asymptotic results for stochastic algorithms assume a sufficiently small adaption coefficient. Yet small step-size values may slow down convergence and thus restrain the tracking capabilities of the algorithm. Speed can be improved by increasing the step size, at the expense of larger oscillations around the optimal solution after convergence (misadjustment) or even the risk of not converging at all. Although convergence is often faster, similar problems are still encountered in *block* or *batch* implementations. This difficult trade-off between convergence speed and accuracy has urged the development of iterative techniques based on some form of step-size optimization. Such research efforts are not exclusive to blind methods, but include a variety of iterative techniques such as the ubiquitous LMS algorithm [46, 57, 67, 68].

Amari [3, 4] puts forward adaptive rules for learning the step size in the context of neural algorithms. The idea is to make the step size depend on the gradient norm, in order to obtain a fast evolution at the beginning of the iterations and then a decreasing misadjustment as a stationary point is reached. These step-size learning rules, in turn, include other learning coefficients which must be set appropriately. Although the resulting algorithms are said to be robust to the choice of these coefficients, their optimal selection remains application dependent. Other guidelines for choosing the step size in natural gradient algorithms are given in [36], but are merely based on local stability conditions.

In the context of batch algorithms, Regalia [81] finds bounds for the step size guaranteeing monotonic convergence of the normalized fourth-order moment of the extractor output, a contrast function related to the CM and KM criteria. These results are later extended in [82] to a more general class of functions valid for real-valued sources under prewhitening. Determining these step-size bounds for monotonic convergence involves the eigenspectrum of a Hessian matrix on a convex subset containing the unit sphere and is thus a computationally expensive task.

While still ensuring monotonic convergence, another optimal step-size approach is feasible when the contrast can be expressed as a rational function of the learning rate at each iteration, as suggested in [32, 34, 50]. This approach consists of computing at each iteration the step size leading to the absolute optimum of the criterion along the search direction (typically the gradient). In close collaboration with P. Comon, I have developed this optimal step-size technique in the context of the CM, CP and KM contrasts, in both blind and semi-blind operation modes, and evaluated its performance in a variety of experimental scenarios, as summarized next.

3.5.2 An Algebraically Computed Optimal Step Size

Given a point $\mathbf{w}$, exact line search aims at the optimal step size leading to the *global maximum* of the objective function along the search direction $\mathbf{g}$:

$$\mu_{\text{opt}} = \arg\max_{\mu} \Upsilon(\mathbf{w} + \mu\mathbf{g}).$$

Note that if the contrast is to be minimized, as is the case for the CM and CP criteria in eqns. (2.12), p. 19, and (3.9), p. 33, one just needs to use $-\Upsilon(\cdot)$ in the above equation. In this one-dimensional optimization problem, vectors $\mathbf{w}$ and $\mathbf{g}$ are fixed, so that $\Upsilon(\mathbf{w}+\mu\mathbf{g})$ becomes a function of the step size μ only and can thus be denoted (with some abuse of notation) as $\Upsilon(\mu)$. The exact line search technique is in general computationally intensive and presents other disadvantages [158], which explains why, despite being a well-known optimization method, it is very rarely used in practice. However, for a variety of blind criteria such as the CM, KM and CP contrasts, $\Upsilon(\mu)$ is a rational function in μ [P4, P17, P41, P43, P46]. As a result, the numerator of $\partial\Upsilon(\mu)/\partial\mu$ is a low-degree polynomial in μ, and its roots can easily be computed by algebraic techniques. (p. 133) (p. 253) (p. 259) (p. 269)

Iterative algorithms based on this optimal step-size technique repeat the following steps until convergence:

S1) Compute the search direction $\mathbf{g}$ at current point $\mathbf{w}$.

This direction is typically, but not necessarily, the gradient, $\mathbf{g} = \nabla\Upsilon(\mathbf{w})$. Gradient expressions for the MMSE, CM, KM and CP criteria are given in eqns. (3.21)–(3.24), p. 41. Newton directions can also be used at the expense of increased computational cost. To improve numerical conditioning, the search direction should be normalized to unit norm before passing to the next step.

S2) Compute the optimal step-size polynomial coefficients.

The optimal step size is found among the roots of the polynomial in the numerator of $\partial\Upsilon(\mu)/\partial\mu$. This polynomial presents the general form:

$$p(\mu) = \sum_{k=1}^{D} p_k \mu^k.$$

Coefficients $\{p_k\}_{k=1}^{D}$ depend on the observed data statistics as well as the extracting vector $\mathbf{w}$ and the search direction $\mathbf{g}$ at the current iteration. For the

MMSE, CM, KM and CP criteria, one obtains optimal step-size polynomials of degrees $D = 1$, $D = 3$, $D = 4$ and $D = (2q-1)$, respectively. Exact expressions of their optimal step-size polynomial coefficients are derived in [P4, P19, P41, P43], and are reproduced below for easy reference. In the following equations, we define $g = \mathbf{g}^{\mathrm{H}}\tilde{\mathbf{x}}$.

(p. 153) – Optimal step-size polynomial for the MMSE criterion [P19]:

$$p_1 = \mathrm{E}\{|g|^2\} \qquad p_0 = \mathrm{E}\big\{\mathbb{R}\mathrm{e}\big(g^*(y-\breve{s})\big)\big\}.$$

(p. 259) – Optimal step-size polynomial for the CM criterion [P43]:

$$\begin{array}{ll} p_3 = 2\mathrm{E}\{a^2\} & p_2 = 3\mathrm{E}\{ab\} \\ p_1 = \mathrm{E}\{2ac + b^2\} & p_0 = \mathrm{E}\{bc\} \end{array}$$

where $a = |g|^2$, $b = 2\mathbb{R}\mathrm{e}(yg^*)$, and $c = (|y|^2 - \gamma)$.

(p. 253) – Optimal step-size polynomial for the KM criterion [P4, P41]:

$$\begin{array}{ll} p_0 = -2h_0 i_1 + h_1 i_0 & p_1 = -4h_0 i_2 - h_1 i_1 + 2h_2 i_0 \\ p_2 = -3h_1 i_2 + 3h_3 i_0 & p_3 = -2h_2 i_2 + h_3 i_1 + 4h_4 i_0 \\ p_4 = -h_3 i_2 + 2h_4 i_1 & \end{array} \tag{3.25}$$

with

$$\begin{array}{rcl} h_0 & = & \mathrm{E}\{|a|^2\} - |\mathrm{E}\{a\}|^2 \quad h_1 = 4\mathrm{E}\{|a|d\} - 4\mathbb{R}\mathrm{e}(\mathrm{E}\{a\}\mathrm{E}\{c^*\}) \\ h_2 & = & 4\mathrm{E}\{d^2\} + 2\mathrm{E}\{|a||b|\} - 4|\mathrm{E}\{c\}|^2 - 2\mathbb{R}\mathrm{e}(\mathrm{E}\{a\}\mathrm{E}\{b^*\}) \\ h_3 & = & 4\mathrm{E}\{|b|d\} - 4\mathbb{R}\mathrm{e}(\mathrm{E}\{b\}\mathrm{E}\{c^*\}) \quad h_4 = \mathrm{E}\{|b|^2\} - |\mathrm{E}\{b\}|^2 \\ i_0 & = & \mathrm{E}\{|a|\} \qquad i_1 = 2\mathrm{E}\{d\} \qquad i_2 = \mathrm{E}\{|b|\} \\ a & = & y^2 \qquad b = g^2 \qquad c = yg \qquad d = \mathbb{R}\mathrm{e}(yg^*). \end{array}$$

(p. 153) – Optimal step-size polynomial for the qth-order CP criterion [P19]:

$$p_k = \begin{cases} \sum_{p=0}^{k}(k+1-p)\mathrm{E}\{\mathbb{R}\mathrm{e}(a_{k+1-p}^* a_p)\} & \\ -(k+1)\mathrm{E}\{\mathbb{R}\mathrm{e}(a_{k+1}^* d)\}, & 0 \le k \le q-1 \\ \sum_{p=k+1-q}^{q}(k+1-p)\mathrm{E}\{\mathbb{R}\mathrm{e}(a_{k+1-p}^* a_p)\}, & q \le k \le 2q-1 \end{cases}$$

with $a_p = \binom{q}{p} g^p y^{q-p}$, $0 \le p \le q$. Recall that d denotes here the constellation-dependent parameter used in the CP criterion (3.9), p. 33.

S3) Extract the optimal step-size polynomial roots $\{\mu_k\}_{k=1}^{d}$.

The step-size candidates are the real parts of the roots of the polynomial whose coefficients have been calculated in step S2. The roots of polynomials of degree three (cubic) and four (quartic) can be found at practically no cost using standard algebraic procedures such as Cardano's and Ferrari's formula, respectively, known since the 16th century [158]. The computational complexity of this step is negligible compared with the calculation of the statistics required in the previous step.

S4) Select the root leading to the *global maximum* of the contrast along the search direction:

$$\mu_{\text{opt}} = \arg\max_{k} \Upsilon(\mathbf{w} + \mu_k \mathbf{g}).$$

To do so, we only need to plug back the step-size candidates into the contrast expression. Again, this step is performed at a marginal cost from the coefficients computed in step S2.

S5) Update $\mathbf{w}^+ = \mathbf{w} + \mu_{\text{opt}}\mathbf{g}$.

In the context of blind equalization based on the CM and CP criteria, this approach gives rise to the so-called *optimal step-size constant modulus algorithm (OS-CMA)* and *optimal step-size constant power algorithm (OS-CPA)*, respectively; semi-blind optimal step-size algorithms are easily derived by combining supervised (MMSE) and blind criteria, as explained in Sec. 3.4, pp. 39–42. A thorough experimental study evidences the following benefits of the optimal step-size approach [P9, P12, P17, P19, P43, P46]: (p. 133) (p. 153) (p. 259) (p. 253)

- In fully-blind mode, the optimal step size effectively increases the probability of finding the global optimum of the contrast function (e.g., optimum-delay MMSE equalizer), thus improving signal estimation quality and, in turn, providing certain robustness to initialization (cf. drawback D2, p. 27).
- The blind OS-CMA offers a performance-complexity trade-off comparable to more elaborate techniques like the RLS-CMA of [19].
- In semi-blind operation, the optimal step-size iterative search proves practically independent of initialization from just a few pilot symbols (cf. drawback D2), and yields a performance very close to the MMSE bound (where *all* symbols in the transmitted burst are used for training) at only a fraction of the bandwidth utilization of the conventional MMSE receiver.
- Convergence is remarkably accelerated relative to the classical fixed step-size, in both blind and semi-blind modes (cf. drawback D3, p. 28).

3.5.3 The RobustICA Algorithm

Although it can also be applied to blind equalization, we have mainly developed and evaluated the optimal step-size technique operating on the KM contrast in the context of BSS. The resulting method, based on gradient (3.23), p. 41, and optimal step-size polynomial (3.25), p. 44, is called *RobustICA* [P4, P37, P41]; a (p. 253) Matlab implementation is freely available in [P68]. Compared with related classical techniques, such as the popular kurtosis-based FastICA algorithm [58, 60, 61], the advantages of RobustICA are many-fold:

- The generality of the KM contrast guarantees that real- and complex-valued signals can be treated by exactly the same algorithm without any modification. Both type of source signals can be present simultaneously in a given mixture, and complex sources need not be circular.

- Prewhitening is not required, so that the performance limitations it imposes [12] can be avoided. Indeed, the absence of prewhitening improves asymptotic performance. This feature may prove especially beneficial in ill-conditioned scenarios, the convolutive case and underdetermined mixtures. Sequential extraction (deflation) can be carried out via linear regression.

- The algorithm can target sub-Gaussian or super-Gaussian sources in the order defined by the user (cf. drawback D1, p. 27). This property enables the extraction of sources of interest when their Gaussianity character is known in advance, thus sparing a full separation of the observed mixture as well as the consequent unnecessary complexity and increased estimation error.

- The optimal step-size technique provides some robustness to the presence of saddle points and spurious local extrema in the contrast function, which tend to appear when short data blocks are processed [94] (drawback D2, p. 27).

- The method shows a very high convergence speed, that we objectively measure in terms of source extraction quality versus number of operations. In the real-valued two-signal case, the algorithm converges in a single iteration, even without prewhitening (cf. drawback D3, p. 28).

RobustICA's cost-efficiency and robustness are particularly remarkable for short sample length in the absence of prewhitening, where the method offers a superior quality-cost performance compared to other kurtosis-based algorithms such as FastICA [58, 60, 61] in the real case and some of its variants like [72, 78] in the complex non-circular case [P4, P37, P41]. In [P4, P26] (see also Sec. 4.6.2, p. 62), the algorithm is successfully applied to the extraction of atrial activity in atrial fibrillation episodes.

(p. 253)

In summary, this contribution to optimal step-size iterative search, though based on simple theoretical tools, has remarkable operational implications which are not limited to signal estimation in linear mixtures but extend to the general field of numerical optimization.

3.6 Additional results

Some additional lines of research related to telecommunications are sketched next. They include novel source extraction algorithms based on the finite alphabet of digital modulations (Sec. 3.6.1), blind channel identification in Alamouti's space-time coded systems (Sec. 3.6.2) and the application of BSS/ICA techniques to optical transmission monitoring (Sec. 3.6.3).

3.6.1 Source Extraction Using Alphabet-Based Criteria

Despite its appealing simplicity, the deflation approach to BSS presents two main drawbacks. Firstly, estimation errors caused in each extraction-deflation stage accumulate through successive stages. As a result, the source estimation quality deteriorates progressively as more sources are obtained. Secondly, since a linear extractor

is usually employed, the maximum number of sources that can be separated is limited by the available spatial diversity, i.e., it is generally impossible to extract more sources than sensors (Sec. 2.2). This limits the applicability of deflation in the interesting scenario of underdetermined mixtures.

As part of Ludwig Rota's PhD thesis, a novel approach to blind source extraction in MIMO digital communication channels has been put forward in [P42, P45]. (p. 263) This approach exploits the discrete character (finite alphabet property) of digital modulations in the case where sources with different alphabet are present in the mixture, as specified by the following hypothesis.

> The source vector can be divided into R groups:
>
> $$\mathbf{s}_n = [(\mathbf{s}_n^{(1)})^{\mathrm{T}}, (\mathbf{s}_n^{(2)})^{\mathrm{T}}, \ldots, (\mathbf{s}_n^{(R)})^{\mathrm{T}}]^{\mathrm{T}}.$$
>
> The rth group is composed of K_r sources $\mathbf{s}_n^{(r)} = [s_{1,n}^{(r)}, s_{2,n}^{(r)} \ldots, s_{K_r,n}^{(r)}]^{\mathrm{T}}$ that belong to a finite alphabet characterized by d_r complex distinct roots of polynomial $Q_r(z)$, where d_r is the total number of possible symbols in the modulation (constellation size), $1 \leq r \leq R$. The total number of emitted signals is thus $K = \sum_{r=1}^{R} K_r$.

Accordingly, the appropriate APF criterion can be employed to extract, through deflation, the sources with the same matching modulation in each group. Combining appropriate APF criteria, sources with different modulations can be extracted in parallel from the same sensor data. This novel concept, referred to as *parallel deflation*, presents the potential of reducing both the signal estimation errors that typically accumulate in the conventional deflationary approach and the spatio-temporal diversity required for an adequate source extraction. In addition, APF criteria can be optimized through a cost-effective optimal step-size technique (see Sec. 3.5.2, pp. 43–45) with the ability to escape local extrema.

In [P40], we analyze the use of APF criteria in the challenging scenario of under- (p. 249) determined mixtures, where the available spatio-temporal diversity is insufficient to guarantee a successful source estimation by linear extractors. An alphabet-matched linear extraction criterion (APF) followed by projection on the signal alphabet is shown to considerably improve the performance of classical regression-based deflation in extracting all sources from an underdetermined mixture with a reasonably low probability of error. It is also demonstrated that APF criteria outperform the CM principle, even for CM-type sources. More interestingly, classical deflation can improve on parallel deflation, but requires a refinement to render its performance robust to the extraction ordering. Such a refinement can be briefly justified on the following grounds. The amount of interference reduction at each stage of classical deflation depends on the quality of the source estimate. To minimize error accumulation, the 'strongest' or best estimated sources should be extracted and deflated first. In supervised scenarios, the prior knowledge of the channel matrix simplifies the optimal ordering in terms of the output SNR, as in the V-BLAST detection algorithm [44, 49]. For the blind scenario, we propose an ordering method based on a preliminary estimation of the channel matrix, the linear extractors and the additive noise power, which are combined to provide an estimate of the probability of erroneous detection for the given modulation. Deflation is then repeated in

ascending order of detection probability, until the ordering converges, or just for a fixed number of deflation iterations. As opposed to the popular V-BLAST technique of [44, 49], the proposed method for optimizing the extraction order requires no training data and can handle scenarios of less sensors that sources with possibly different modulations.

3.6.2 Blind Channel Estimation in Space-Time Coded Systems

During the last decade, a large number of space-time coding techniques have been proposed to exploit the spatial diversity in MIMO wireless communication systems employing multiple antennas at both transmission and reception [47,62]. A remarkable example is *orthogonal space time block coding (OSTBC)* because it is able to provide full transmit diversity without any channel state information at transmission and with very simple encoding and decoding procedures [1,93]. The basic premise of OSTBC is the encoding of the transmitted symbols into an orthogonal matrix which reduces the optimum *maximum likelihood (ML)* decoder to a matrix-matched filter followed by a symbol-by-symbol detector. The OSTBC scheme for MIMO systems with two transmit antennas is known as the Alamouti code [1] and is the only OSTBC capable of achieving full spatial rate for complex constellations. The Alamouti code can be used in systems with one or multiple antennas at the receiver. The (2×1) Alamouti coded system is the simplest of its kind and provides maximum diversity gain while achieving the full available channel capacity. Because of these advantages, the Alamouti code has been incorporated in the IEEE 802.11 and IEEE 802.16 standards.

Alamouti's (2×1) OSTBC is based on two transmit antennas and only one receive antenna, yet it accepts a MIMO model as described next. At the transmit end, a complex-modulation data stream s_n is separated in two substreams, s_{2n} and s_{2n+1}, for $n = 0, 1, \ldots$. Each symbol pair $\{s_{2n}, s_{2n+1}\}$ is transmitted in two adjacent periods using a simple strategy: s_{2n} and s_{2n+1} are transmitted from the first and the second antenna, respectively, during period $2n$; then $-s^*_{2n+1}$ and s^*_{2n} are transmitted from the first and the second antenna, respectively, during period $2n + 1$. The symbols transmitted through the ith antenna arrive at the receive antenna through fading paths h_i, $i = 1, 2$. Hence, the signal received during the first symbol period has the form:

$$x_{2n} = h_1 s_{2n} + h_2 s_{2n+1} + v_{2n} \tag{3.26}$$

where v_{2n} represents the additive white Gaussian noise that may be corrupt the channel output at instant $2n$. Similarly, if the channel remains constant during two consecutive symbol periods, the signal received in the second period is given by:

$$x_{2n+1} = -h_1 s^*_{2n+1} + h_2 s^*_{2n} + v_{2n+1}. \tag{3.27}$$

Now, let us define the source and observation vectors as $\mathbf{s}_n = [s_{2n}, s_{2n+1}]^{\mathrm{T}}$ and $\mathbf{x}_n = [x_{2n}, x^*_{2n+1}]^{\mathrm{T}}$, respectively. Expressions (3.26)–(3.27) show that these vectors are related through the static MIMO model (2.9), p. 18, with

$$\mathbf{H} = \begin{bmatrix} h_1 & h_2 \\ h_2^* & -h_1^* \end{bmatrix}$$

and additive noise $\mathbf{v}_n = [v_{2n}, v_{2n+1}^*]^{\mathrm{T}}$. Channel matrix $\mathbf{H}$ is unitary up to a scalar factor, that is,

$$\mathbf{H}^{\mathrm{H}}\mathbf{H} = \mathbf{H}\mathbf{H}^{\mathrm{H}} = \lambda \mathbf{I}_2 \tag{3.28}$$

where $\lambda = |h_1|^2 + |h_2|^2$ and $\mathbf{I}_2$ is the (2×2) identity matrix. It follows that the transmitted symbols can be recovered, up to scale, as $\hat{\mathbf{s}} = \hat{\mathbf{H}}^{\mathrm{H}}\mathbf{x}$, where $\hat{\mathbf{H}}$ is a suitable estimate of the channel matrix. As a result, this scheme supports ML detection based only on linear processing at the receiver. However, the standard approach to estimating the (2×2) channel matrix is through the transmission of pilot symbols, with the subsequent reduction in spectral and power efficiency.

In collaboration with Héctor J. Pérez-Iglesias and Adriana Dapena, from the Universidad de la Coruña, Spain, I have investigated the *blind* estimation of Alamouti's channel matrix through the eigendecomposition of matrices made up of the SOS or HOS of the received signal [P7, P16, P27, P39]. If the symbol substreams (p. 123)
transmitted through each antenna are uncorrelated and have the same power, the channel matrix cannot be uniquely identified from the channel output covariance matrix, due to property (3.28). To overcome this limitation, we propose in [P39] to unbalance the power of the substreams, so that the received signal covariance matrix is guaranteed to have different eigenvalues. As a result, the channel matrix is uniquely identifiable from the *eigenvalue decomposition (EVD)* of the received signal covariance matrix. A second method is based on HOS and thus assumes that the symbol substreams have non-Gaussian distributions and are statistically independent, although their exact pdf's may otherwise be unknown. This alternative approach constructs a matrix from the fourth-order cumulants of the received signal. The EVD of this matrix is shown to be more robust than similar previous techniques, e.g., [8], to the relative values of the channel coefficients.

In [P16], we evaluate the performance of these blind channel estimation tech- (p. 123)
niques over both computer simulated flat fading channels and realistic indoor scenarios. For the latter, we have used a MIMO hardware demonstrator developed at the Universidad de la Coruña operating at the 2.4 GHz Industrial, Scientific and Medical (ISM) band. Results show the superior performance of the SOS-based method and its ability to approach the MMSE bound while saving spectral efficiency. Moreover, the SOS-based method is also the least computationally demanding of all compared techniques.

The eigenvalue spread of these HOS matrices is shown to be linked to Alamouti's channel estimation and symbol detection performance. Inspired by this idea, we explore in [P7,P27] the optimal selection of fourth-order cumulant matrices in the eigendecomposition approach. The resulting algorithms provide a performance comparable other methods using exhaustively the fourth-order information contained in the sensor output (e.g., JADE [11]) at a fraction of the computational cost.

3.6.3 Optical Transmission Monitoring

Wavelength division multiplexing (WDM) is arising as the preferred transmission technology for future ultra-high bandwidth multichannel systems. Indeed, it is anticipated that high data-rate WDM-based optical networks will become the backbone of the next generation Internet. In WDM, several baseband-modulated channels

are transmitted along a single fibre, with each channel located at a different wavelength. To guarantee an adequate quality of service, WDM optical network management requires monitoring a variety of transmission performance parameters such as wavelength, power, SNR, etc., without compromising transparency. Traditional monitoring techniques are based on expensive optical components such as tunable optical filters, phased-array demultiplexers or photo-diode arrays with diffraction gratings. In a bid to reduce complexity, alternative monitoring solutions aim to perform most of the processing electronically, with the subsequent benefits in cost.

As part of Yumang Feng's PhD, the statistical independence between the WDM
(p. 189) channels has been exploited in [P22, P58, P59, P61] to simultaneously extract their respective waveforms, from which appropriate performance parameters can then be easily measured. Direct photodetection of the WDM signal mixes the individual constituent baseband channels. A wavelength dependent attenuator (WDA) can be employed to alter the relative weights of each channel in the detected photocurrent. Following this procedure with different WDA attenuation patterns, an equivalent static MIMO signal model can be obtained with sufficient diversity for a suitable BSS method to recover the original WDM channel waveforms [P59, P61]. Contrary to the SOS-based technique used in [92], HOS-based BSS allows the extraction of spectrally white sources, thus allowing potential beneficial reductions in the photocurrent sampling rates. A more optimized optical-loop structure composed of a
(p. 189) single WDA-photodetector pair has been introduced in [P22, P58], providing equivalent separation performance with reduced hardware requirements. It is interesting to observe that the BSS approach is not only useful in monitoring, but is effectively demultiplexing the WDM composite signal. This features anticipates a vast potential for blind techniques in optical transmission systems.

3.7 Summary

The limitations of classical HOS-based channel equalization and source separation techniques, namely, estimation ambiguities, existence of spurious extrema and computational complexity (Sec. 3.1) can be overcome by exploiting the particularities of digital communication systems. The investigation summarized in this chapter has laid particular emphasis on two kinds of prior information: the pilot symbols known by the receiver and the discrete character of digital sources. Pilot sequences can be used to initialize blind iterative equalizers with the MMSE receiver (as in Sec. 3.2). Alternatively, purely blind contrasts can be combined with the supervised MMSE receiver, naturally giving rise to semi-blind criteria (Sec. 3.4). The finite alphabet property of digital modulations allows the derivation of algebraic equalizers (Sec. 3.3) that, by construction, are insensitive to spurious extrema. Algebraic solutions are linked to challenging tensor algebra problems, such as the rank-1 linear combination. Partial solutions to such problems have been proposed under simplifying assumptions related to a particular SISO setup.

Despite their undeniable theoretical interest, algebraic solutions are only approximate in generic equalization scenarios, and iterative techniques are necessary to find the global minimum of the criterion. Blind criteria such as the CM, KM and CP

contrasts admit an iterative exact line search technique whereby the step size leading to the *global* optimum of the criterion along the search direction can be adapted *algebraically* at each iteration (Sec. 3.5). This adaptation only involves the roots of a polynomial that can often be solved by radicals. The optimal step-size iterative algorithm offers a very fast convergence and, in semi-blind mode, yields equalization results very close to the MMSE bound while increasing the useful transmission rate and the robustness to the equalizer vector initialization. In the static MIMO case, the RobustICA technique derived from this idea shows a remarkable trade-off between extraction quality and computational cost compared to alternative ICA algorithms.

Other contributions relying on the finite alphabet property include the possibility of extracting in parallel sources with different modulations (Sec. 3.6.1). We have also shown that the channel can be blindly identified in Alamouti's space-time coded wireless systems using BSS/ICA-based techniques (Sec. 3.6.2). These prove useful as well in cost-effectively demodulating WDM signals in optical transmission networks (Sec. 3.6.3).

Chapter 4

Atrial Activity Extraction in Atrial Fibrillation Episodes

4.1 Motivation

Atrial fibrillation (AF) is the most common sustained cardiac arrhythmia encountered in clinical practice, as it affects approximately 4.5 million people in the European Union and 2.3 million people in North America [121]. Its prevalence increases with age, and up to 10% of the population older than 75 years has been diagnosed with the condition. Over the last two decades, hospital admissions due to AF have more than doubled owing to the aging of the population, a rising prevalence of chronic heart disease and improved diagnostic methods. As a result, the disease accounts for nearly one third of hospitalizations related to cardiac-rhythm disturbances. Although most of its symptoms are not life-threatening, AF is also associated with an increased long-term risk of thromboembolic events, as nearly 20% of strokes are thought to be caused by the condition. The mortality rate of AF sufferers almost doubles that of patients with *normal sinus rhythm (NSR)*. Consequently, this cardiac trouble is an expensive public health problem, with a cost per patient per year of around 3000 € and an overall annual cost rising to 13.5 billion € in the EU alone [121]. Given its potential complications and self-perpetuating character as well as the expected growth of the elderly population, AF is becoming a major health concern for Western society. While practically all other cardiac arrhythmias are well understood and effectively managed, the understanding of the generation and self-perpetuation mechanisms of this disease is still unsatisfactory, despite its incidence, prevalence and risks of serious complications. Indeed, AF is often referred to as the "last great frontier" in cardiac electrophysiology [153].

In physiological conditions, i.e., NSR, the sinoatrial node is the natural pacemaker of the heart, generating 60 to 100 depolarization (activation) impulses per minute that are conducted towards the rest of the myocardium in a well-organized manner [145]. AF is caused by disorders in impulse generation (automaticity) and propagation (reentry), two mechanisms that are likely to coexist [111, 121, 153]. Rapidly-firing ectopic foci, often located near the pulmonary veins or vena cava junctions [125, 131], can supersede the sinoatrial node and are held responsible for

triggering the arrhythmia. A substrate composed of anatomic boundaries and/or tissues with different electrophysiologic properties (functional obstacles) may give rise to reentrant wavelets sustaining the arrhythmia. The result is an uncoordinated atrial activation and a consequent deterioration of atrial mechanical function. In turn, impaired hemodynamic ability increases the risk of thrombus formation and subsequent stroke. An electrophysiologic remodeling phenomenon progressively shortens the atrial myocytes' effective refractory period, i.e., the shortest time interval between two consecutive stimuli capable of exciting the cell, increasing the number of simultaneous wavelets and the episode duration; thus the adage "AF begets AF": the disease self-perpetuates and shows a natural tendency to become chronic, so that spontaneous cardioversion is less likely as AF evolves. On the surface *electrocardiogram (ECG)*, the *atrial activity (AA)* signal associated with the well-organized atrial activation in NSR is represented by the P-wave. During AF, however, the P-wave is replaced by rapid oscillations known as f-waves. By way of illustration, Fig. 4.1(a)(top) shows a 5-second segment of precordial lead V1 from the first patient of an AF ECG database, kindly made available by the Hemodynamics Service, Valencia University Hospital, Spain. Lead V1 contains an important part of the AA observed externally, as this electrode lies close to the atria. As a result, the AA can clearly be perceived as rapid low-amplitude fluctuations between strong negative-amplitude peaks representing consecutive ventricular activations.

Over recent years, signal processing has helped cardiologists in shedding some light over AF. In particular, certain features of the AA signal recorded on the surface ECG provide information about the arrhythmia while avoiding the cost and risks of endocardial electrogram recordings. The externally recorded AA signal has the potential of aiding the physician to diagnose the condition, predict its evolution and select the best treatment option. The dominant frequency of the AA signal, typically located between 5 and 9 Hz, is closely related to the atrial cycle length and the refractory period of atrial myocardium cells. In turn, these parameters are linked to the stage of evolution of the disease, its degree of organization and the probability of cardioversion (return to NSR) [114–116]. More specifically, a decreasing trend in the main frequency is associated with a higher probability of spontaneous cardioversion of the fibrillatory episode. As observed in Fig. 4.1(a)(top), the AA is easily measured during the TQ intervals (time segments between two consecutive heartbeats). But, unfortunately, this signal is masked by the *ventricular activity (VA)*, or QRST complex, precisely when the AA could provide crucial information about physiological phenomena such as the ectopic activation of the atrio-ventricular (AV) node increasing the heart rate (tachycardia) during AF. As a result, the analysis and characterization of AA from the ECG requires (explicitly or otherwise) the previous suppression of interference such as VA, artifacts and noise.

4.2 Approaches to Atrial Signal Extraction in AF

Isolating the ECG segments outside the QRST intervals, i.e., the TQ segments, is probably the simplest possible option for AF analysis [146], but is not suitable when a continuous monitoring is required or in patients with high ventricular rates. Fig-

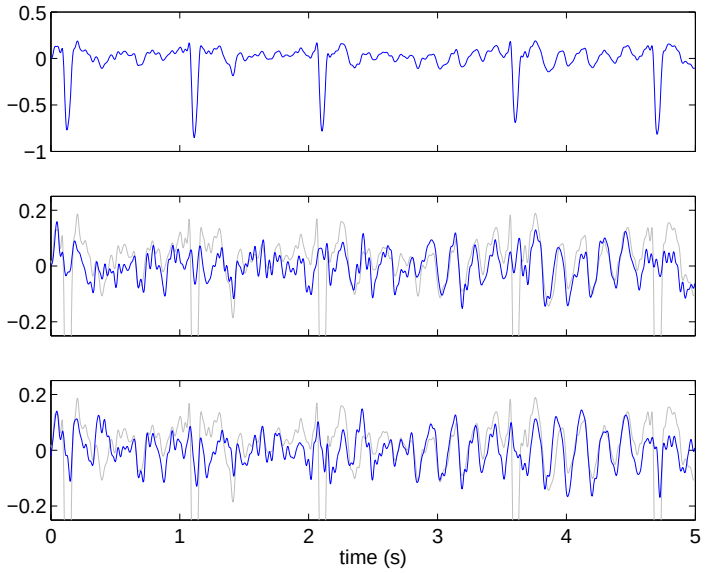

(a)

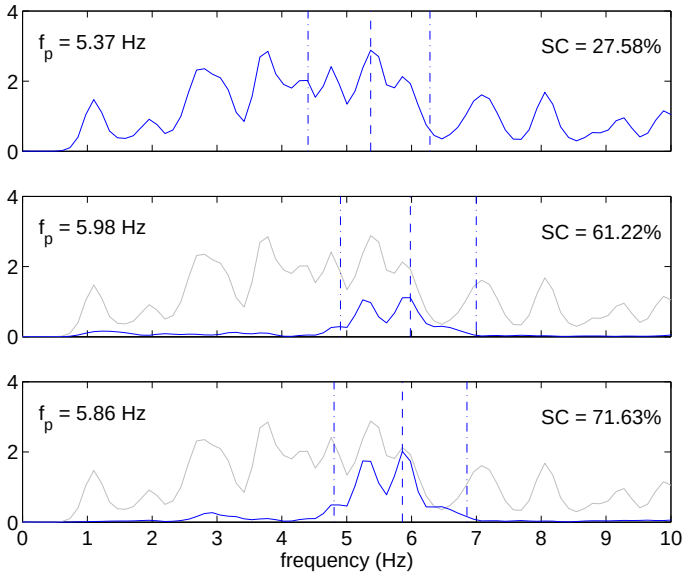

(b)

Figure 4.1: Atrial activity extraction in atrial fibrillation ECGs [P4, P26]. (a) Time courses. (b) Power spectral densities with dominant frequency (f_p) and spectral concentration (SC) estimates. Top plots: a 5-second segment of lead V1 from the first patient of the AF ECG database. Middle plots: AA contribution to lead V1 estimated by ICA-SOBI (Sec. 4.5) from the 12-lead ECG. Bottom plots: AA contribution to lead V1 estimated by RobustICA (Sec. 4.6.2) from the 12-lead ECG. Power spectral densities are estimated by Welch's averaged periodogram method as in [P20]. Vertical dashed lines: estimated dominant frequency locations. Vertical dash-dotted lines: bounds used in the computation of spectral concentration. Vertical axes are normalized, so that only relative amplitudes are important.

ure 4.1(b)(top) shows the power spectral density of the V1-lead waveform displayed in Fig. 4.1(a)(top): the AA frequency components are buried under the VA stronger wider spectrum. This can be appreciated by looking at the middle and bottom plots in Fig. 4.1(b), corresponding to the spectra of two AA estimates (described in Secs. 4.5 and 4.6.2, respectively). Hence, classical frequency filters are also ineffective in this context. More successful techniques focus on the explicit cancellation of the most significant features of the interfering cardiac waveform, that is, the patient's QRST complex. The *average beat subtraction (ABS)* method [114, 129, 149] computes a template of the interfering complex by synchronized averaging and then subtracts it, after appropriate scaling, from the lead output. The technique relies on the assumptions that the interference and the signal of interest are uncoupled, and that the former presents a repetitive regular waveform. The ABS approach requires beat detection and classification before averaging, is thus sensitive to the morphology of the ventricular beats, and cannot suppress noise and artifacts uncoupled with the interfering signal (e.g., noise from electronic equipment). To mitigate the sensitivity to local QRST morphological variations caused by minor changes in the electrical axis of the heart (due, e.g., to respiration), the *spatiotemporal QRST cancellation (STC)* technique [150] and related methods [140] take into account the average beats from adjacent leads via weighted LS fitting before subtraction. Like ABS, STC requires a sufficient number of beats with similar morphology in order to obtain a significant QRST average and ensure the proper cancellation of AA in the averaged beat. Alternative methods extract the VA using artificial neural networks [152], or are based on the decomposition of the ECG using discrete packet wavelet transforms [147].

All the above techniques are unable to fully take advantage of the diversity provided by the spatially-separated electrodes. Indeed, the standard ECG employed in clinical practice is composed of 12 leads, of which at least 8 provide linearly independent measurements, while more sophisticated recording equipment used for body surface potential mapping (BSPM) may include up to hundreds of leads. Each lead captures a different mixture of bioelectrical phenomena of interest, artifacts, interference and noise. This spatial diversity can be efficiently exploited by processing, in a suitable manner, all leads simultaneously [P11]. The spatial information that can be derived by exploiting this kind of diversity may provide new insights into how the physiological mechanisms of interest (e.g., the atrial activation) and clinically relevant aspects (e.g., the degree of evolution of the disease) reflect on the surface ECG, and may help assess the prognostic features of external recordings, currently not fully understood. A classical approach attempting to exploit this diversity is Widrow's multi-reference ANC method (see Sec. 2.3, p. 20), based on Wiener's optimal spatial filtering theory [154]. However, the availability of reference leads linked to the interference but free from the desired signal is a crucial assumption for the success of this method, and introduces strong constraints on the electrode location, as we have evidenced in the context of non-invasive fetal ECG extraction from maternal surface electrodes [P10, P11, P72].

To overcome the limitations of classical methods, a significant part of my research has been devoted to the design of novel spatial filtering techniques for AA extraction in AF. The first such techniques are fully blind in that they mainly exploit

the statistical independence between the different cardiac signals during AF. Other methods have also been put forward by taking into account additional properties of the biomedical problem under study. Due to the incorporation of extra prior information, the resulting techniques can be considered as *semi-blind*. Here, the term is used in a wider sense than in communications, where it implies the existence of a known time segment of the source signal(s), i.e., the availability of training data. After developing in more detail the concept of semi-blind signal processing in biomedical applications (Sec. 4.3), the remaining of this chapter summarizes the results obtained in the context of AA extraction in AF episodes.

4.3 Blind and Semi-Blind Biomedical Signal Processing

As briefly recalled in Sec. 2.3, pp. 19–22, BSS is more robust to calibration errors than more parametric techniques, thanks to the reduced number of model assumptions. As a result, this methodology proves particularly interesting in biomedical problems, where parametric approaches may be cumbersome. Indeed, the use of parameters would require time-consuming calibration protocols and may easily be subjected to a large patient-to-patient variability; parameters for the same patient may also be expected to evolve with time. In addition, it is important that signal processing methods be capable of providing adequate performance in a number of potential pathophysiological conditions. Hence, the blind approach arises as a judicious option in this uncertain environment [135, 136]. In the context of ECG processing, another valuable advantage of the fully-blind approach is that it does not require a preliminary heartbeat detection and classification stage and, as a result, is essentially unaffected by wave morphology variations. Examples illustrating this robustness to ectopic beats in pregnancy and AF ECG episodes are reported in [136] and [118], respectively.

Despite the success achieved by fully-blind techniques over the last years, their performance may be inadequate in certain applications. Indeed, blindness is an attractive feature in the uncertainty of clinical environments, yet a single property like statistical independence alone is sometimes unable to produce physiologically meaningful results in biomedical signal processing applications, as noted in [127, 128]; another example is the direct application of ICA to AA extraction, as will be detailed in the next section. In these conditions, source extraction performance can be improved by taking into account additional assumptions about the signals of interest or the mixing structure other than independence. Furthermore, the exploitation of prior knowledge may enable the resulting algorithms to focus on the extraction of the signal(s) of interest only, thus avoiding the unnecessary complexity of a full separation and the permutation ambiguity of blind methods (drawback D1, p. 27).

In a semi-blind setup, a Bayesian formulation is theoretically optimal but usually impractical, as it involves the specification of probability distributions for the parameters associated with the prior information. Determining such distributions may be difficult or simply not feasible in certain scenarios. Moreover, the convergence of Bayesian model estimation methods (e.g., the expectation-maximization algorithm) is often very slow. These shortcomings have motivated the search for suboptimal

but more practical alternatives for exploiting prior knowledge in BSS. These include the use of signals correlated with the source of interest [113, 133, 138, 139, 148] and spatial patterns (mixing-matrix columns) related to the physiological activity under examination [127,128]. This information can be incorporated into separation criteria to improve source separation performance.

In cooperation with José J. Rieta, Francisco Castells and José Millet, from UPV, Spain, my colleagues Olivier Meste and Pierre Comon, and my PhD students Ronald Phlypo and Pietro Bonizzi, I have investigated some of these practical alternatives to the exploitation of prior information in AA signal extraction from the surface ECG. In particular, our researches have focused on the use of partial information about the
(p. 167) atrial source statistics and spectral features [P20,P30,P33,P34,P36,P38] (Secs. 4.5–
(p. 237) 4.7, pp. 59–68) as well as constraints on the structure of the spatial topographies
(p. 245) [P1, P29, P31] (Sec. 4.8, pp. 69–70). Working on the spatial dimension of multi-
(p. 231) lead ECG recordings has yielded results with potential clinical and physiological impact related to AF classification [P2, P25] and the AV junction behavior during
(p. 241) AF [P35] (Sec. 4.9, pp. 70–71). Although originally aimed at solving a specific real-life problem, this research has also produced a number of theoretical results of much wider scope, such as novel contrast functions for signal separation and extraction incorporating prior information about the sources. Some of these contrasts are based
(p. 117) on HOS [P5, P14] (Sec. 4.6.1, pp. 60–62), while others rely on SOS only [P6, P13]
(p. 105) (Sec. 4.7.2, pp. 64–68). These contributions are explained next, after introducing the BSS/ICA approach to AA extraction.

4.4 BSS/ICA Approach to Atrial Signal Extraction

In collaboration with J. J. Rieta and J. Millet, from UPV, Spain, I was part of the research team who first approached the AA signal extraction in ECG recordings as
(p. 177) a BSS problem in instantaneous linear mixtures [P21, P67]. The adequacy of the static MIMO model (2.9), p. 18, finds strong theoretical support in electrophysiological considerations regarding the generation of cardiac electrical signals and their propagation across the human body. In the AA extraction context, vector $\mathbf{s}_n$ is composed of atrial and ventricular activity sources, as well as other sources of interference and artifacts. Vector $\mathbf{x}_n$ contains the signal mixtures observed at the electrode array output. The mixing matrix coefficient $h_{\ell k} = [\mathbf{H}]_{\ell k}$ represents the contribution or projection of source k onto observation ℓ. The entries of the mixing matrix columns $\{\mathbf{h}_k\}$ reflect the spatial pattern or *topography* of the relative power contribution described by the associated sources $\{s_{k,n}\}$ onto the spatially-separated sensors, and correspond to potential field spatial distributions in the case of bioelectrical signals. The mixing matrix coefficients associated with the cardiac sources are defined by the propagation of physiological signals from the heart to the electrodes through the body tissues. Due to the distance between heart and electrodes, the speed of propagation of electrical signals across the body and the bandwidth of the phenomena of interest, the transfer between sources and sensors can reasonably be considered as linear and instantaneous. These facts support the suitability of eqn. (2.9) to describe the signal generation model in this biomedical problem. By

estimating the sources of AA and the corresponding columns of the mixing matrix, and then isolating them from the remaining components, the AA signal can easily be reconstructed in all leads free from VA and other interference.

Cardiac electrophysiology during AF leads to the assumption that AA and VA can approximately be considered as statistically independent phenomena. This hypothesis enables the application of separation techniques exploiting the independence property like PCA and ICA. Compared to alternative methods such as multi-reference Wiener filtering, ABS or STC, the BSS approach does not assume any particular pattern for the contribution of the sources onto the electrodes (i.e., existence of reference signals), nor a specific morphology or repetitive pattern for the interfering waveforms. The results by PCA are unreliable since, by construction, this approach assumes a particular structure for the mixing matrix whereby its columns are mutually orthogonal. Such a structure is difficult to enforce in the problem in hand, due to the spatial proximity between the atria and the ventricles. By contrast, ICA methods are generally more successful, as they allow a large degree of freedom in electrode placement relative to the source positions. A first validation of these results has been obtained in [P56, P63] by regarding the spectral signatures of the (p. 273)
estimated sources. These signatures allow an automatic identification of the atrial source among the separated components and are able to discriminate between NSR, AF and *atrial flutter (AFL)* [P57]. Despite the interest of these encouraging initial results, AA can often present a near-Gaussian probability distribution, particularly in more disorganized states of AF occurring as the disease evolves. This property compromises the separation of the atrial source from Gaussian noise and interference when relying on HOS only.

4.5 Combining non-Gaussianity and Spectral Features

To improve the performance of conventional ICA in AA extraction, we have proposed a hybrid approach in [P20, P48]. The idea is to exploit a well-known feature of the (p. 167)
AA signal: its time coherence, reflected on a quasi-periodic autocorrelation function and a narrowband spectrum typically concentrated around a dominant frequency in the 3–9 Hz band. HOS-based ICA, e.g., the FastICA algorithm, is first applied on the full ECG recording in order to estimate the strongly non-Gaussian VA components. The remaining sources contain mixtures of AA and Gaussian noise, with low kurtosis values. A kurtosis threshold experimentally set at 1.5 allows the detection of these remaining sources, which are then passed on as inputs to the SOBI method of [7]. As explained at the end of Sec. 2.3, p. 22, SOBI is particularly well suited to the separation of narrowband sources. In this application, the time lags of the correlation matrices to be diagonalized are selected in accordance with typical AF cycle length values: the lag set spans a whole atrial period for the lowest expected dominant atrial frequency.

On the other hand, we have defined the *spectral concentration (SC)* as the percentage of the estimated atrial signal power around its dominant frequency f_p [P20, P48]: (p. 167)

$$\mathrm{SC}(y) = \frac{\int_{f_1}^{f_2} |Y(f)|^2 df}{\sigma_y^2} \tag{4.1}$$

where $Y(f)$ is the Fourier transform of the extractor output and symbol σ_y^2 denotes its variance. The frequency bounds are empirically chosen as $f_1 = 0.82 f_p$ and $f_2 = 1.17 f_p$. In synthetic recordings, the SC is shown to correlate with AA extraction quality, and hence naturally emerges as an objective measure of performance. Results on an AF ECG recording database show that the proposed ICA-SOBI method achieves a substantial increase in SC of up to 40% relative to the ICA-only method
(p. 167) in patients where the atrial signal is close to Gaussian [P20, P48]. In more organized states of the disease, like AFL, the performance improvement brought about by the proposed hybrid technique is less significant, as the AA source is sufficiently non-Gaussian for the ICA-only method to perform a good extraction without further refinement. Fig. 4.1(a)(middle), p. 55, shows a 5-second segment of the AA signal reconstructed by the ICA-SOBI method in lead V1 from the first patient of the AF ECG database. The kurtosis-based FastICA algorithm has been used in the ICA part of the method. Frequency spectra, together with the estimated dominant peak position and the associated SC values, are shown in Fig. 4.1(b)(middle).

4.6 Exploiting Prior Information on Source Kurtoses

Although the AA signal becomes near-Gaussian in longstanding forms of AF, its waveform typically shows a sawtooth shape that can be characterized as a sub-Gaussian distribution, especially in AFL episodes. This prior information can also be capitalized on in several fashions to enhance atrial signal extraction performance. On the other hand, ICA and ICA-SOBI perform a full source separation. When only a few sources are of interest, separating the whole mixture incurs an unnecessary computational cost and, in the case of sequential extraction, an increased source estimation inaccuracy due to error accumulation through successive deflation stages (drawback D1, p. 27). A more judicious alternative is extracting the desired type of sources exclusively. The following AA estimation methods can be considered as contributions in this direction.

4.6.1 Novel HOS-Based Contrasts Using Prior Information

This avenue of research has been explored in collaboration with my PhD student Ronald Phlypo, and has benefited from invaluable theoretical input by my colleague Pierre Comon. Inspired by the existence of prior knowledge on the source kurtosis
(p. 117) signs, we have shown in [P14] that the following function is a valid contrast for BSS after prewhitening (i.e., an *orthogonal contrast*) under the source independence assumption:

$$\Upsilon_{\mathrm{KSP}}^{(K^+)}(\mathbf{y}) = \sum_{k=1}^{K} \varepsilon_k \kappa_4^{y_k} \tag{4.2}$$

where $\varepsilon_k = \mathrm{sign}(\kappa_4^{s_k})$ represents the kth source kurtosis sign, $\kappa_4^{y_k}$ is the kth separator-output kurtosis, and $K^+ \leq K$ denotes the number of sources with positive kurtosis.

This *kurtosis sign priors (KSP)* contrast can be considered as a generalization of Moreau-Macchi's criterion (2.16), p. 21, to the case of sources with possibly different kurtosis signs. The maximization of the KSP contrast arranges the estimated sources in two groups of K^+ and $(K - K^+)$ signals according to their kurtosis sign, thus partially resolving the permutation ambiguity of ICA (drawback D1, p. 27). The contrast can easily be optimized through a Jacobi-like procedure involving the solutions to the contrast maximization in the two-signal case, as originally proposed for ICA in [25, 27]. Incidentally, depending on whether the kurtosis signs of the signals involved are equal or not, these pairwise solutions correspond, respectively, to the EML and AEML closed-form estimators investigated in my PhD thesis [P18, P73, P75, P90] [see eqns. (2.18)–(2.19), p. 23]. Although originally designed for joint separation, the contrast can easily be adapted to perform sequential separation or single-source extraction by keeping fixed one of the signals and sweeping over the rest in the pairwise iterative algorithm. If the kurtosis sign of the source of interest is different from the others and ε_1 is chosen accordingly, the desired signal will appear in the first position of the separator output. With straightforward redefinitions, function (4.2) is shown to be a contrast for any cumulant order $r \geq 3$ and the permutation ambiguity to be partially resolved for even orders $r \geq 4$ [P14]. (p. 137) (p. 117)

The criterion has been applied to AA extraction in [P36, P38] by assuming that the desired signal has a sub-Gaussian amplitude distribution, whose kurtosis is negative. Since in practice there is no guarantee that the AA signal is the only source with negative kurtosis in the mixture, spectral information is also exploited: the Givens rotation estimated by maximizing (4.2) in the two-signal case is performed only if the SC in the AF band of either output signal is increased as a result. The process is terminated when no SC increase has been obtained during a full sweep over the pertinent signal pairs. Results on an AF ECG database [P36, P38] show that the spectrally-constrained KSP method provides comparable atrial central frequency estimates than the ICA-SOBI method of [P20] (Sec. 4.5). Moreover, the proposed technique offers increased SC figures at a reduced computational cost [P36]. (p. 245)

In [P5], this line of research has led to additional theoretical results extending contrast (4.2). Function

$$\Upsilon_{\mathrm{KVP}}(\mathbf{y}) = \sum_{k=1}^{K} \alpha_k \kappa_4^{y_k} \tag{4.3}$$

is shown to be an orthogonal contrast for the separation of independent sources after prewhitening if the weights $\{\alpha_k\}_{k=1}^K$ have the same sign as the source kurtoses. Now, it was shown in [15] that, for independent sources and prewhitened observations, a fourth-order cumulant approximation to the ML function results in expression (4.3) with $\alpha_k = \kappa_4^{s_k}$, $1 \leq k \leq K$. This cumulant-based approximation, however, was never shown to be a contrast. The proof presented in [75] for a similar cumulant-matching approach requires the sources to have the same cumulant sign. We prove in [P5] that not only the approximate ML criterion of [15] is indeed a contrast whatever the source kurtosis signs, but is also a contrast for all values of $\{\alpha_k\}_{k=1}^K$ verifying the source kurtosis sign matching condition. If, in addition, the source kurtoses are different and so are the linear combination weights, the contrast eliminates the permutation ambiguity typical of ICA, as the estimated sources are

sorted at the separator output according to their kurtosis values in the same order as the weights. Our experimental analysis demonstrates that only rough guesses on the source kurtosis values suffice for the new contrast to avoid the permutation ambiguity. As occurs for the KSP criterion (4.2) and other orthogonal contrasts, the *kurtosis value priors (KVP)* contrast (4.3) can be maximized by means of the cost-efficient Jacobi-type pairwise iteration.

The KVP contrast is reminiscent of the nonsymmetrical contrasts presented in [75] and the closely related family of blind extraction contrasts later proposed in [36]. However, these nonsymmetrical contrasts are based on the absolute value of higher-order cumulants. As a result, the permutation ambiguity cannot be resolved if the source cumulants are different but have the same absolute values. Moreover, the gradient-based algorithms used for the maximization of such contrasts may get trapped in spurious local extrema. The maximization of contrast (4.3) through the Jacobi iteration has yielded permutation-free source separation in all our experiments, even if two sources have the same absolute kurtoses [P5].

In the two-signal case, we have also determined the asymptotic (large sample) variance of the resulting Givens angle estimator in closed form [P5]. In turn, this analysis yields the weight coefficients with optimal asymptotic performance. If the source statistics are totally unknown a priori, a simple procedure using the weights with optimal pairwise asymptotic performance can refine a conventional fully blind ICA method. On the other hand, the CoM2 contrast (2.14) arose from an approximate mutual information principle, as recalled in Sec. 2.3, p. 21. Interestingly, the experimental analysis in [P5] confirms that CoM2 presents ML-optimality features, since it achieves, up to permutation, the same asymptotic performance as KVP with weights matched to the source kurtoses.

4.6.2 Atrial Signal Extraction by Kurtosis Maximization with RobustICA

As explained above, AA is a narrowband signal, so that its frequency-domain representation is *sparse*: the spectrum is different from zero at a few frequencies only. Hence, it can be considered to stem from an impulsive distribution with high kurtosis value. Indeed, when mapping certain signals from the time domain to the frequency or the wavelet domains, the statistics of the sources tend to become less Gaussian, as observed in the context of another biomedical problem [130] and later verified in AA extraction from the surface ECG [P34]. Relying on this simple observation, a kurtosis maximization technique can be applied on the ECG recording after transformation into the frequency domain. Due to the ability of the optimal step-size technique used in RobustICA to avoid local extrema and operate on complex-valued possibly non-circular sources (Sec. 3.5.3, pp. 45–46), it is expected that the f-domain AA source be found among the first extracted components (typically those with higher kurtosis values); its time course can then be recovered by transforming back into the time domain.

This idea has been tested in [P4, P26] on a database of over thirty different AF patients. The AA source is automatically selected as the extracted component with the highest SC [eqn. (4.1)] among the sources with dominant peak in the typical AF

frequency band of [3, 9] Hz. As an illustration, the bottom plots in Figs. 4.1(a)–(b), p. 55, show the AA reconstructed by the frequency-domain RobustICA methods in lead V1 from the first patient of the AF ECG database. As can be observed in the intervals between successive heartbeats, RobustICA obtains a more accurate estimate of the AA taking place in lead V1 than ICA-SOBI [middle plots in Figs. 4.1(a)–(b)], as quantified by a higher SC value, requiring half the iterations of the other method for that particular patient. Results over the whole AF patient database [P4, P26] confirm that RobustICA achieves an improved AA signal extraction quality with virtually identical dominant frequency estimate at a comparable complexity relative to the two-stage ICA-SOBI technique of [P20] (Sec. 4.5, pp. 59–60).

The use of kurtosis as a general contrast function has been discouraged in [59] on the basis of poor asymptotic efficiency in the presence of super-Gaussian sources and lack of robustness to outliers. However, the frequency-domain sources extracted by RobustICA in the above experiment are strongly super-Gaussian signals. Hence, these experiments demonstrate that the kurtosis contrast, optimized with the RobustICA technique, can in fact also provide positive results on sources with super-Gaussian distributions.

4.7 Exploiting Spectral Concentration with SOS Only

4.7.1 Atrial Signal Extraction by Spectral Concentration Maximization

All the above AA estimation methods are based on HOS and thus implicitly assume that the atrial signal and all other sources of electrophysiological activity and noise are statistically independent. As part of Ronald Phlypo's PhD thesis, we show in [P33] that this assumption can be relaxed. We propose to maximize directly the (p. 237)
SC function (4.1), p. 60, which leads to a simple yet effective solution based on SOS only and, as a result, on the weaker decorrelation assumption. This maximization can be accomplished in a computationally efficient manner by finding the dominant eigenvector of the frequency-constrained spectral covariance matrix

$$\Phi_{\mathbf{z}}^{(f_1,f_2)} = \int_{f_1}^{f_2} \mathbb{R}\mathrm{e}\big\{\mathbf{Z}(f)\mathbf{Z}^{\mathrm{H}}(f)\big\}df \tag{4.4}$$

where $\mathbf{Z}(f)$ represents the Fourier transform of the whitened observations $\mathbf{z}_n$ [see eqn. (2.17), p. 22]. This procedure requires a previous estimation of the modal frequency f_p, which is not known a priori. One could maximize the SC of the extractor output over the typical AF band [3, 9] Hz. Unfortunately, SC maximization over this interval does not guarantee AA extraction, since the T-wave spectrum partly overlaps with the lower part of this band, although with smaller SC around its dominant frequency. To surmount this difficulty, we choose to maximize the SC in the bands [3, 6] Hz and [5, 9] Hz, respectively, and then estimate the atrial dominant frequency f_p as the modal frequency of the resulting component with the highest SC. In a second stage, SC is maximized in a narrow band around the estimated atrial frequency f_p, as in (4.1). When evaluated on an AF ECG dataset, this cost-effective method

outperforms the original spatio-temporal ICA-SOBI algorithm of [P20] (Sec. 4.5, pp. 59–60) in terms of SC while providing comparable atrial frequency estimates.

The search for the atrial modal frequency is further refined in [P6] by partitioning the typical AF band into more than two different subbands. Each subband is used as a initial guess of the actual AF band present in the recording, from which an AA estimate can be obtained by the above SC maximization procedure. The actual AF band is recomputed as the set of frequencies associated with a fixed high percentile of the AA estimate's amplitude spectrum. Using the new AF band estimate, a new AA signal is estimated and so on, until convergence. One atrial estimate per initial subband is thus obtained and, among them, we retain that with the highest SC. This iterative method for the simultaneous estimation of the AA extraction filter and the significant AF band usually converges in a few iterations and, as quantified by SC, improves on the ICA-SOBI method of [P20] (Sec. 4.5).

4.7.2 A Novel Contrast for Source Extraction Based on Conditional Second-Order Moments

(p. 105) Generalizing these results, a novel criterion for source extraction is developed in [P13], based on the prior knowledge of the *significant support* of the source of interest s_i, i.e., the set of time indices n over which $|s_{i,n}| > C$, for a given positive real constant C. Hence, the required prior information amounts to a presence indicator of the desired source. This presence indicator can also be specified in the frequency domain. For simplicity, in what follows we will assume real-valued sources and mixtures. The criterion relies on the following additional assumptions on the sources:

H1) The source of interest, s_i, is independent of the other sources, $\{s_j\}_{j\neq i}$. These latter are stored in vector $\bar{\mathbf{s}}$. Up to some irrelevant permutation of indices, we can write $\mathbf{s} = [s_i, \bar{\mathbf{s}}^{\mathrm{T}}]^{\mathrm{T}}$.

H2) The sources $\{s_k\}_{k=1}^{K}$ have unit-variance continuous distributions with non-null pdf in a finite interval of $\overline{\mathbb{B}} = [-C, C]$.

It will be seen later that hypothesis H1 is too restrictive and can actually be reduced to second-order decorrelation. First of all, we need the following definition of contrast function for blind source extraction [76], which can be considered as a direct extension of Definition 1, p. 21.

Definition 2 (contrast function for blind extraction). A function $\Upsilon(\cdot)$ of the extractor output distribution is a contrast for the blind extraction of the source of interest s_i if it verifies:

Invariance:	$\Upsilon(\lambda s_i) = \Upsilon(s_i)$ for any scalar $\lambda \neq 0$.
Domination:	$\Upsilon(\mathbf{g}^{\mathrm{T}}\mathbf{s}) \leq \Upsilon(s_i)$ for any length-K vector $\mathbf{g}$.
Discrimination:	$\Upsilon(\mathbf{g}^{\mathrm{T}}\mathbf{s}) = \Upsilon(\mathbf{s})$ if and only if $\mathbf{g} = \lambda\mathbf{e}_i$, where $\lambda \neq 0$ and $\mathbf{e}_i$ denotes the canonical basis vector in $\mathbb{R}^K$ such that $\mathbf{e}_i^{\mathrm{T}}\mathbf{s} = s_i$.

The starting point of the new extraction criterion is the expected log-likelihood of the observed vector $\mathbf{x}$ under the ICA model (2.9), p. 18, which in the noiseless

case reads [14, 15]:

$$\mathcal{L}(\mathbf{H} \,|\, \mathbf{x}) = \mathrm{E}\{\log p_{\mathbf{x}}(\mathbf{x} \,|\, \mathbf{H})\} = \mathrm{E}\{\log p_{\mathbf{s}}(\mathbf{H}^{-1}\mathbf{x})\} - \log|\det \mathbf{H}|.$$

This function can also be expressed in terms of the separating matrix $\mathbf{W}$ as:

$$\mathcal{L}(\mathbf{W} \,|\, \mathbf{x}) = \mathrm{E}\{\log p_{\mathbf{s}}(\mathbf{W}^{\mathrm{T}}\mathbf{x})\} + \log|\det \mathbf{W}| \tag{4.5}$$

since $\mathbf{y} = \mathbf{W}^{\mathrm{T}}\mathbf{x}$ [eqn. (2.3), p. 17] so that $\mathbf{W}^{\mathrm{T}}$ is an estimate of $\mathbf{H}^{-1}$. According to hypothesis H1, the source joint pdf can be decomposed as $p_{\mathbf{s}}(\mathbf{s}) = p_{s_i}(s_i)p_{\bar{\mathbf{s}}}(\bar{\mathbf{s}})$. Likewise, the determinant in (4.5) can be written as the scalar product: $\det \mathbf{W} = \mathbf{w}^{\mathrm{T}}\bar{\mathbf{w}}$, where $[\bar{\mathbf{w}}]_i$ contains the cofactor of element $[\mathbf{w}]_i$ in matrix $\mathbf{W}$. Hence, the log-likelihood becomes:

$$\mathcal{L}(\mathbf{W} \,|\, \mathbf{x}) = \mathrm{E}\{\log p_{s_i}(\mathbf{w}^{\mathrm{T}}\mathbf{x})\} + \mathrm{E}\{\log p_{\bar{\mathbf{s}}}(\bar{\mathbf{W}}^{\mathrm{T}}\mathbf{x})\} + \log(\mathbf{w}^{\mathrm{T}}\bar{\mathbf{w}})$$

where matrix $\bar{\mathbf{W}}$ contains all columns of matrix $\mathbf{W}$ except $\mathbf{w}$. Since we are only interested in extracting s_i, the estimation of $\bar{\mathbf{s}}$, and thus $\bar{\mathbf{W}}$, is irrelevant. Also, any variations in $\det \mathbf{W}$ due to $\mathbf{w}$ can be absorbed by $\bar{\mathbf{W}}$. It follows that function

$$\mathcal{L}(\mathbf{w} \,|\, \mathbf{x}) = \mathrm{E}\{\log p_{s_i}(\mathbf{w}^{\mathrm{T}}\mathbf{x})\}$$

can be considered as the expected log-likelihood for the extraction of the desired source. Expressing the expectation in terms of the extractor output pdf, we arrive at:

$$\mathcal{L}(\mathbf{w} \,|\, \mathbf{x}) = \int_{\mathbb{R}} p_y(u) \log p_{s_i}(u) du.$$

Recall that the dependence of the likelihood on the extraction filter $\mathbf{w}$ is made explicit in the extractor output pdf, $p_y(\cdot)$, by relationship (2.6), p. 17.

Now, according to the above result, we can consider the following function as the expected *conditional log-likelihood* of the extractor output for the estimation of the desired source [P13]: (p. 105)

$$\begin{aligned}\Upsilon_C(y) \stackrel{\mathrm{def}}{=} \mathcal{L}(\mathbf{w} \,|\, \mathbf{x}, \mathbb{I}) &= \int_{\mathbb{R}} p_{y|\mathbb{I}}(u) \log p_{s_i|\mathbb{I}}(u) du \\ &= \int_{\mathbb{B}} p_{y|\mathbb{I}}(u) \log p_{s_i|\mathbb{I}}(u) du + \int_{\overline{\mathbb{B}}} p_{y|\mathbb{I}}(u) \log p_{s_i|\mathbb{I}}(u) du \end{aligned} \tag{4.6}$$

where $\mathbb{I}$ denotes the event $|s_i| > C$, and $p_{y|\mathbb{I}}(\cdot)$ and $p_{s_i|\mathbb{I}}(\cdot)$ represent the pdf's of the extractor output and the source of interest, respectively, conditioned on $\mathbb{I}$. Set $\mathbb{B}$ is defined as $\mathbb{B} = \mathbb{R}\backslash\overline{\mathbb{B}}$, where $\overline{\mathbb{B}}$ is given in hypothesis H2. If we define $P(\mathbb{I}) = \int_{\mathbb{B}} p_{s_i}(u)du$, the conditional pdf of the source of interest reads:

$$p_{s_i|\mathbb{I}}(u) = \begin{cases} p_{s_i}(u)/P(\mathbb{I}), & u \in \mathbb{B} \\ 0, & u \in \overline{\mathbb{B}}. \end{cases}$$

Hence, the conditional likelihood (4.6) is heavily penalized by its last term as soon as $p_{y|\mathbb{I}}(u) \neq 0$ for any $u \in \overline{\mathbb{B}}$, that is, if the extractor output does not verify the condition $|y| > C$ when the desired source does. Indeed, function (4.6) turns out to be an extraction contrast.

***Proposition* 1.** *Under hypotheses H1–H2, $\Upsilon_C(y)$ is a contrast function for the extraction of source s_i in the noiseless model (2.9), p. 18, for any $C > 0$.*

Proof. Under the conventional unit-variance source assumption, the invariance property is readily verified. Domination and discrimination are deduced from the fact that function (4.6) is ruled by its penalizing term $\int_{\overline{\mathbb{B}}} p_{y|\mathbb{I}}(u) \log p_{s_i|\mathbb{I}}(u) du$. If $y = s_i$, function $\Upsilon_C(y)$ becomes the entropy of s_i conditioned on $\mathbb{I}$, which is a finite number. If a contribution from another source is present at the extractor output, we will have $y = g_i s_i + \bar{s}$, with $\bar{s} = \sum_{j \neq i} g_j s_j$. Since s_i is independent of $\bar{s}$ (hypothesis H1), the distribution $p_{y|\mathbb{I}}(u)$ can be written as the convolution of the distributions $p_{s_i|\mathbb{I}}(u)$ and $p_{\bar{s}|\mathbb{I}}(u)$:

$$p_{y|\mathbb{I}}(u) = \int_{\mathbb{R}} p_{s_i|\mathbb{I}}(\tau - u) p_{\bar{s}|\mathbb{I}}(\tau) d\tau.$$

From hypotheses H1–H2, $p_{\bar{s}|\mathbb{I}}(u) \neq 0$ over an interval of $\overline{\mathbb{B}}$ with non-zero Lebesgue measure and, from the above convolution product, $\exists u \in \overline{\mathbb{B}}$ such that $p_{y|\mathbb{I}}(u) \neq 0$. As a result, $\Upsilon_C(y) \leq \Upsilon_C(s_i)$, and the equality can hold only if $\bar{s} = 0$, that is, $g_j = 0$ for $j \neq i$. □

Due to the penalty term in eqn. (4.6), the maximization of $\Upsilon_C(y)$ is not tractable, as it requires an exhaustive search over all possible extraction filters $\mathbf{w}$. This requirement can be relaxed by considering the following weighted integral of the conditional probability of the extractor output:

$$\Upsilon'_C(y) = \int_{\overline{\mathbb{B}}} p_{y|\mathbb{I}}(u) \gamma(u) du$$

where function $\gamma(u)$ is positive except possibly at the origin. The following result shows that

***Lemma* 2.** *Minimizing $\Upsilon'_C(y)$ cancels the penalty term of $\Upsilon_C(y)$ in (4.6).*

Proof. Clearly, $\Upsilon'_C(y) \geq 0$. The function is thus minimized at $\Upsilon'_C(y) = 0$. Since $\gamma(u)$ is positive and can only be null at $u = 0$, at the minimum we can have at most $p_{y|\mathbb{I}}(u) = \alpha \delta_u$, where α is an arbitrary scalar and δ_u represents Dirac's delta function. In particular, $p_{y|\mathbb{I}}(u) = 0$ elsewhere in $\overline{\mathbb{B}} \backslash \{0\}$. Under hypothesis H2, we must have $\alpha = 0$, and thus $p_{y|\mathbb{I}}(u) = 0$ over $\overline{\mathbb{B}}$. □

Still, the minimization of $\Upsilon'_C(y)$ with respect to $\mathbf{w}$ remains generally intractable. However, with the choice $\gamma(u) = u^2$, minimizing $\Upsilon'_C(y)$ is intuitively equivalent to maximizing

$$\frac{\int_{\mathbb{R}} p_{y|\mathbb{I}}(u) u^2 du}{\sigma_y^2} \tag{4.7}$$

where $\sigma_y^2 = \int_{\mathbb{R}} p_y(u) u^2 du$ appears in the denominator to guarantee the invariance property. To see this, let us consider the equality:

$$\frac{\int_{\mathbb{R}} p_{y|\mathbb{I}}(u) u^2 du}{\sigma_y^2} = \frac{\int_{\mathbb{B}} p_{y|\mathbb{I}}(u) u^2 du + \int_{\overline{\mathbb{B}}} p_{y|\mathbb{I}}(u) u^2 du}{\sigma_y^2}.$$

Due to the chosen weighting function, the term $\int_{\mathbb{B}} p_{y|\mathbb{I}}(u) u^2 du$ dominates the nominator on the right-hand side. As a result, maximizing the left-hand side of the equality would tend to shift the probability mass of $p_{y|\mathbb{I}}(u)$ towards large values of

y ($|y| > C$, but bounded by the variance normalization). In turn, this is equivalent to the minimization of $\Upsilon'_C(u)$, and thus (by virtue of Lemma 2) of $\int_{\overline{\mathbb{B}}} p_{y|\mathbb{I}}(u)du$, as required.

Criterion (4.7) seeks for the extractor output with *maximum variance in the tails (MaxViT)* of its distribution, and can be expressed as the maximization of the Rayleigh quotient:

$$\Upsilon_{\mathrm{MaxViT}}(y) = \frac{\Phi_y^{s_i}}{\Phi_y} = \frac{\mathbf{w}^{\mathrm{T}}\Phi_{\mathbf{x}}^{s_i}\mathbf{w}}{\mathbf{w}^{\mathrm{T}}\Phi_{\mathbf{x}}\mathbf{w}} \tag{4.8}$$

where $\Phi_y = \mathrm{E}\{y^2\}$ and $\Phi_y^{s_i} = \mathrm{E}\{y^2 \,|\, \mathbb{I}\}$; the observation covariance and constrained covariance matrices are defined as $\Phi_{\mathbf{x}} = \mathrm{E}\{\mathbf{x}\mathbf{x}^{\mathrm{T}}\}$ and $\Phi_{\mathbf{x}}^{s_i} = \mathrm{E}\{\mathbf{x}\mathbf{x}^{\mathrm{T}} \,|\, \mathbb{I}\}$, respectively.

Proposition 3. *Function $\Upsilon_{\mathrm{MaxViT}}(y)$ is a contrast function for the extraction of source s_i in the noiseless model (2.9), p. 18, under the following sufficient conditions:*

C1) $\mathrm{E}\{s_j s_k\} = 0, \quad \forall j \neq k$

C2) $\mathrm{E}\{s_j s_k \,|\, \mathbb{I}\} = 0, \quad \forall j \neq k$

C3) $\mathrm{E}\{s_i^2 \,|\, \mathbb{I}\} > \mathrm{E}\{s_j^2 \,|\, \mathbb{I}\}, \quad \forall j \neq i.$

Proof. The denominator in eqn. (4.8) ensures the scale invariance property in Definition 2, p. 64. Now, under conditions C1–C2, we can write

$$\Upsilon_{\mathrm{MaxViT}}(y) = \frac{\mathbf{w}^{\mathrm{T}}\Phi_{\mathbf{x}}^{s_i}\mathbf{w}}{\mathbf{w}^{\mathrm{T}}\Phi_{\mathbf{x}}\mathbf{w}} = \frac{\mathbf{g}^{\mathrm{T}}\Phi_{\mathbf{s}}^{s_i}\mathbf{g}}{\mathbf{g}^{\mathrm{T}}\Phi_{\mathbf{s}}\mathbf{g}} = \frac{\sum_j g_j^2 \Phi_{s_j}^{s_i}}{\sum_j g_j^2} \tag{4.9}$$

where $\mathbf{g} = \mathbf{H}^{\mathrm{H}}\mathbf{w}$ and $g_i = [\mathbf{g}]_i$. Accordingly, maximizing $\Upsilon_{\mathrm{MaxViT}}(y)$ is equivalent to maximizing its numerator subject to $\|\mathbf{g}\| = 1$. Splitting the numerator in the different contributions yields

$$g_i^2 \Phi_{s_i}^{s_i} + \sum_{j \neq i} g_j^2 \Phi_{s_j}^{s_i} + \Phi_{s_i}^{s_i}\Big(\sum_{j \neq i} g_j^2 - \sum_{j \neq i} g_j^2\Big)$$

which can be rewritten as

$$\Phi_{s_i}^{s_i} + \sum_{j \neq i} g_j^2 (\Phi_{s_j}^{s_i} - \Phi_{s_i}^{s_i}) \leq \Phi_{s_i}^{s_i}$$

where the inequality follows from $(\Phi_{s_j}^{s_i} - \Phi_{s_i}^{s_i}) < 0$, $\forall j \neq i$, due to condition C3. This proofs the domination. Moreover, we have

$$\Phi_y^{s_i} = \Phi_{s_i}^{s_i} \quad \Leftrightarrow \quad \sum_{j \neq i} g_j^2 (\Phi_{s_j}^{s_i} - \Phi_{s_i}^{s_i}) = 0.$$

Now, since $(\Phi_{s_j}^{s_i} - \Phi_{s_i}^{s_i}) < 0$, $\forall j \neq i$, the above equality holds if and only if $g_j^2 = 0$, $\forall j \neq i$. This proves the discrimination.

Equation (4.9) has taken into account that the conditioned source covariance matrix $\Phi_{\mathbf{s}}^{s_i}$ is diagonal, as expressed by condition C2 above. This can actually be relaxed to conditional decorrelation with the source of interest only:

C2') $\mathrm{E}\{s_i s_j \,|\, \mathbb{I}\} = 0, \quad \forall j \neq i.$

In such a case, condition C3 becomes $\Phi_{s_i}^{s_i} > \lambda_{\max}$, where $\lambda_{\max}$ represents the dominant eigenvalue of $\Phi_{\tilde{\mathbf{s}}}^{s_i}$ [P13]. □ (p. 105)

Condition C1 is a classical second-order decorrelation constraint, and is indeed weaker than the starting assumption H1, p. 64, employed to derive the conditional ML criterion (4.6), p. 65. Condition C2 (or C2') imposes decorrelation over the significant support of s_i. Although full decorrelation can rarely hold in practice, a theoretical analysis and experimental results on simulated data show that MaxViT's
(p. 105) source extraction quality is quite robust to violations of this hypothesis [P13]. Condition C3 ensures the domination property of the contrast when the desired source is recovered at the extractor output.

The maximization of contrast (4.8) reduces to the computation of the dominant eigenvalue of matrix $\Phi_{\mathbf{x}}^{s_i}$ after prewhitening [P13]. The contrast can thus be optimized in a computationally efficient manner.

The method of conditional moments, proposed for BSS in [107] without a direct link with the theory of contrast functions, bears close resemblance to MaxViT. However, as opposed to [107], our method is linked to ML estimation, is designed to target a specific source, is not limited to symmetric distributions, can handle the extraction of Gaussian sources and does not require post-processing manipulations such as correcting rotations for super-Gaussian sources. Connections with other
(p. 105) reference-based BSS techniques, including [18,148], are discussed at length in [P13].

When computed in the frequency domain, the conditional covariance matrix $\Phi_{\mathbf{x}}^{s_i}$ after prewhitening becomes the spectral covariance matrix shown in eqn. (4.4), p. 63, if the assumed significant spectral support lies in the interval $[f_1, f_2]$ Hz. Indeed,
(p. 237) the AA extraction methods proposed in [P6, P33] (see also Sec. 4.7.1, p. 63) are essentially the MaxViT algorithm in the frequency domain, where intervals of the typical AF band serve as initial estimates of the significant support of the desired source.

4.7.3 Blind Source Extraction Based on Second-Order Statistics

A novel technique for blind source extraction relying on SOS has recently been presented in [71]. The technique is based on the instantaneous linear mixing model (2.9), p. 18. The sources are assumed to be uncorrelated and colored with distinct spectra. Let $\mathbf{R}_{\mathbf{x},\tau} = \mathrm{E}\{\mathbf{x}_n \mathbf{x}_{n-\tau}^{\mathrm{T}}\}$ denote the sensor-output autocorrelation matrix at time lag τ. It is claimed in [71] that a valid extracting vector $\mathbf{w}$ can be obtained from the minimization of function

$$\Upsilon_{\mathrm{LZ}}(\mathbf{w}, \mathbf{t}, \mathbf{d}) = \sum_{k=0}^{D} \|\mathbf{R}_{\mathbf{x},\tau_k}\mathbf{w} - d_{\tau_k}\mathbf{t}\|^2 \tag{4.10}$$

with respect to vectors $\mathbf{w}, \mathbf{t} \in \mathbb{R}^K$ and $\mathbf{d} = [d_{\tau_0}, d_{\tau_1}, \ldots, d_{\tau_D}]^{\mathrm{T}} \in \mathbb{R}^{D+1}$. In [71], this claim is given a geometrical interpretation in terms of oblique projection operators and demonstrated through numerical experiments.

(p. 121) Work [P15] provides alternative justifications for this approach and proves that, under the given assumptions and with an appropriate choice of time lags $\{\tau_k\}_{k=0}^{P}$, the minimization of (4.10) is achieved if and only if $\mathbf{w}$ is indeed a valid extracting vector. Asymptotically, as the number of lags tends to infinity, the necessary condition for source identifiability using this method becomes that of the popular SOBI algorithm

[7] (Sec. 2.3, p. 22), i.e., that no pair of source spectra be equal up to scale. This algorithm can thus be seen as an extension of SOBI to blind extraction. Nevertheless, the global convergence of the alternating LS algorithm proposed in [71] to minimize criterion (4.10) is not guaranteed and remains to be proven theoretically.

4.8 Exploiting the Spatial Topographies

As explained earlier, the AA signal can often present a near-Gaussian statistical behavior, which renders HOS-based estimates suboptimal and points out the need for further or alternative information to enhance AA estimation performance. The use of spectral features, through the application of time-coherence based separation methods (e.g., SOBI) or the maximization of spectral concentration, allows the use of SOS only. Another approach of this kind explored in Pietro Bonizzi's PhD thesis is the exploitation of the *spatial signatures* or *topographies* (i.e., the mixing-matrix columns or source directions) associated with the different cardiac complexes in the multi-lead recording. The key idea underlying this approach is the decomposition of the observed ECG signal into non-overlapping time segments associated with the most significant features of the cardiac period, namely, the QRS complex, the T wave and the TQ interval:

$$\mathbf{x} = \mathbf{x}_{\mathrm{QRS}} + \mathbf{x}_{\mathrm{T}} + \mathbf{x}_{\mathrm{TQ}}.$$

In each of these segments, one or both of the most important component interfering with the AA, i.e., the QRS complex and the T wave, are missing. This leads to a more accurate description of the remaining activity, which can later be capitalized on to enhance AA estimation. An obvious disadvantage of this approach is that, just like STC methods [140,150], it requires a previous wave detection and segmentation stage.

The first algorithm of this type, developed in [P31], can be divided in three steps. First, a rough estimate of the AA source topography is obtained by the ICA of the whole observation $\mathbf{x}$. The VA source directions, including the QRS complex and the T wave, are then computed from the PCA of $\mathbf{x}_{\mathrm{QRS}}$ and $\mathbf{x}_{\mathrm{T}}$ (via, e.g., the SVD of the respective data matrices). Finally, a refined spatial filter for AA extraction is obtained by projecting the initial AA topography estimate onto the orthogonal complement of the VA subspace using Gram-Schmidt orthogonalization. This spatial filter is applied on $\mathbf{x}$ to obtain the atrial signal estimate over the whole recording. On an AF ECG database, this simple procedure provides a performance up to the mark of more elaborate techniques such as the STC method of [140] and the ICA-SOBI algorithm of [P20] (Sec. 4.5, pp. 59–60).

The method put forward in [P29] builds upon the absence of QRST contribution (p. 231)
in the TQ segment $\mathbf{x}_{\mathrm{TQ}}$ to refine the AA estimate obtained from the ICA of the whole observation $\mathbf{x}$. Let $\mathbf{h}_1$ denote the atrial topography estimated by ICA applied on $\mathbf{x}$. An additional atrial topography estimate, say $\mathbf{h}_2$, is obtained from the PCA of $\mathbf{x}_{\mathrm{TQ}}$. A refined atrial extractor is sought in the plane spanned by the linear extractors associated with $\mathbf{h}_1$ and $\mathbf{h}_2$. Its optimal orientation is determined by maximizing the SC of the resulting AA signal estimate, a process that, very much along the lines of Sec. 4.7, pp. 63–68, can be carried out algebraically. This method offers a

similar performance to that of [P31] summarized in the above paragraph. Using ICA instead of PCA when computing the reference topography $\mathbf{h}_2$ can slightly enhance AA extraction quality.

4.9 Clinical and Physiological Information from Surface Recordings

As introduced in Sec. 4.1, p. 54, the surface ECG has already reported to be useful in the analysis of AF [114–116], and has the advantage over atrial electrograms of being a non-invasive technique. An important part of Pietro Bonizzi's PhD has been devoted to analyzing whether useful additional clinical and physiological information can be gathered from surface recordings alone, with particular focus on two particular aspects: the ventricular response during AF (Sec. 4.9.1) and AF classification (Sec. 4.9.2).

4.9.1 Atrio-ventricular junction behavior during AF

Although it is generally acknowledged that heart rate variability is enhanced during AF [119], several studies reveal that the prevailing ventricular rate during high atrial rate seems to obey complex dynamics and no unifying mechanism has yet been found. To help shed light on this issue, several quantitative models of the ventricular response during AF have been developed [119,137]. The activation model by Cohen [119] introduced the hypothesis that the AV node can be treated as a lumped structure with well-defined electrical properties, including the refractory period, the automaticity and a certain depolarization threshold. According to this model, the AV conduction would be triggered, thus inducing a heartbeat, when the energy of AA impulses impinging on the node exceeds the depolarization threshold.

(p. 241) In [P35], we attempt to confirm this hypothesis by analyzing the existence of a possible correlation between the occurrence of a heartbeat and the power of the AA observable in the ECG during the preceding TQ interval. A weighted average of the power contained in all leads over the TQ segment is plotted against the duration of the corresponding RR segment. Interestingly, the shape of the scatter plot so obtained from a healthy subject differs considerably from that of a pathological subject. In the latter, an inverse relationship can be clearly perceived that seems to support the hypotheses of [119,137]. The scatter plot, however, shows an important variance for short RR periods, obscuring the relationship between RR interval duration and the observed AA power. Such variance could be explained by the fact that the ECG is unable to capture all the AA actually contributing to the activation of the AV node, but could also be due to an increased noise variance when averaging over shorter TQ segments as the heart rate increases.

4.9.2 AF classification

Motivated by their potential relevance in clinical decision making, a number of previous studies have attempted to distinguish between organized and disorganized states

of AF by analyzing atrial electrograms [120, 134]. Using PCA, single-lead electrograms of more organized AF were shown to be represented by a reduced number of principal components [120]. More recent works have demonstrated the possibility of visually evaluating different activation patterns in AF patients by exploiting the high spatial resolution of BSPM recordings [123].

In collaboration with Francisco Castells, Maria Guillem, Andreu Climent and José Millet, from UPV, Spain, we continue to explore the spatial information provided by surface recordings. In [P2, P25], we aim at an automated non-invasive classification of AF in 56-lead BSPM signals recorded from two groups of patients. These patients have been classified beforehand as AF type I (single wavefront propagating across the body surface) and type II/III (no observable clear wavefront or multiple wavefronts that do not propagate across the body surface observed simultaneously), according to Koning's criteria [134].

To quantify the degree of spatio-temporal organization of the AA in AF, we analyze the structure of the mixing matrix derived by the PCA of the TQ segments in the BSPM recording. For a given patient, the PCA of the cth segment yields an estimate of the noiseless BSS model (2.9), p. 18:

$$\mathbf{x}^{(c)} = \mathbf{H}^{(c)}\mathbf{s}^{(c)}$$

Our first study reveals that the average number of dominant components required to explain 95% of the variance of type-I segments (4 components) is half that of type-II/III segments (9 components), with a p-value of $p < 0.05$. Hence, the number of significant principal components give a first indication of AF organization in external recordings. These findings are consistent with those obtained from endocardial recordings in [120].

To increase the discriminative power of our analysis, the data in the cth TQ segment are projected on the spatial topographies associated with the most significant principal components of the initial segment. Let k denote the number of dominant topographies, and let these k topographies be stored in matrix $\bar{\mathbf{H}}_k^{(1)}$. The projection can then be expressed as:

$$\hat{\mathbf{x}}^{(c)} = \bar{\mathbf{H}}_k^{(1)}\big[(\bar{\mathbf{H}}_k^{(1)})^{\mathrm{T}}\bar{\mathbf{H}}_k^{(1)}\big]^{-1}(\bar{\mathbf{H}}_k^{(1)})^{\mathrm{T}}\mathbf{x}^{(c)}.$$

From this relationship, the normalized reconstruction error between the data present in the cth segment and their projection on the dominant principal topographies of the initial segment is easily computed. This error is a measure of the spatio-temporal stationarity or repetitiveness of the AA observed in the BSPM recording. By selecting the $k = 3$ most significant topographies of the initial segment, the average reconstruction error across the remaining segments is shown to be significantly lower in type-I patients than in type-II/III patients, with $p < 10^{-4}$. This result reveals that more organized states of AF are reflected on an increased repetitiveness of the principal spatial topographies across the surface recording.

This investigation shows that the automated classification of AF in surface recordings is indeed possible and strongly supports the appropriateness of signal processing approaches exploiting spatial diversity, such as BSS/ICA, in AF analysis.

4.10 Summary

Atrial signal extraction in surface ECG recordings of AF can be modeled as a BSS problem of instantaneous linear mixtures (Sec. 4.4). The pertinence of this approach is supported by considerations regarding the generation and propagation of electrophysiological signals across the body. Compared to alternative approaches such as ANC, ABS or STC, BSS does not assume any particular structure for the contribution of the sources onto the electrodes, nor a specific morphology or repetitive pattern for the interfering waveforms. The independence between the sources of interest and the artifacts is a realistic assumption during AF.

Prior knowledge about the spectral content of the AA signal, its statistical behavior or its spatial topographies can also be incorporated into the separation criteria to improve source extraction performance and reduce computational complexity. A variety of such semi-blind methods have been presented throughout this chapter (Secs. 4.5–4.8). As a valuable by-product, our attempt to design AA extraction methods with improved performance has yielded new theoretical results in the area of BSS/ICA, such as novel contrasts based on HOS (Sec. 4.6.1) and conditional SOS (Sec. 4.7.2). In addition, the exploitation of the spatial diversity of multi-lead surface recordings has been shown to reveal useful information of clinical and physiological relevance (Sec. 4.9). These positive results encourage further research efforts into AF analysis approaches exploiting spatial diversity.

Chapter 5

Research Perspectives

Numerous possible avenues remain open for the continuation of the research summarized in the previous chapters of this report. Some of the most promising are briefly pointed out in the following paragraphs.

5.1 Algorithms for Robust Equalization and Source Separation

- The performance of algebraic equalizers (Sec. 3.3, pp. 30–39) depends on an accurate estimation of the number of valid solutions, as well as their optimal equalization delays. Algorithms for the *robust automatic detection* of these parameters need to be developed and assessed.
- The matrix and tensor problems associated with algebraic solutions (Sec. 3.3, pp. 30–39) would be considerably more involved in more elaborate scenarios such as the convolutive MIMO case. Fresh researches would thus be necessary to tackle them.
- Algebraically, the subspace method proposed to find the ACPA equalizer provides a particular solution to the challenging rank-1 tensor linear combination problem (Sec. 3.3.3, pp. 33–39). In our numerical study, the proposed subspace approach proves more robust than other structuring methods, but the blind algebraic solutions offer a low tolerance to noise, particularly for long equalizers. The key point limiting performance is probably the SVD-based rank-1 tensor approximation employed to extract the equalizer vector from the estimated symmetric tensor (Sec. 3.3.3.7, p. 37). A *refinement of the SVD-based rank-1 tensor approximation*, such as that obtained by the power method [66,69] and other algorithms to be developed, could alleviate this limitation.
- Similarly, the *semi-blind algebraic solution* of Sec. 3.4.1, pp. 40–40, is only approximate, and new more effective ways to combine analytic supervised and blind equalizers need to be explored.
- Iterative semi-blind criteria have proven rather robust to the confidence parameter λ (Sec. 3.4.2, pp. 41–42), yet its appropriate choice could bring important

performance gains in specific scenarios. Determining its *optimal value* would require the asymptotic variance analysis of semi-blind contrasts.

- The convergence of the optimal step-size iterative technique (Sec. 3.5, pp. 42–46) has always proven satisfactory in our experiments. However, analyzing the *theoretical convergence* properties of this technique is a challenging open issue, especially in scenarios where spurious local extrema exist (finite data length, additive noise, violation of model assumptions). In general, the convergence of source extraction algorithms based on HOS remains to be investigated in this context.

- The use of cumulant-based criteria such as kurtosis has been objected in [59] on the grounds of its suboptimal asymptotic performance for super-Gaussian sources and lack of robustness to outliers. *Robust cumulant estimators* (see, e.g., [156] and references therein) could alleviate these potential difficulties. Whether the iterative optimization of criteria based on robust estimators could still benefit from the numerical convenience of the optimal step-size approach (Sec. 3.5.2–3.5.3, pp. 43–46) should also be ascertained.

- In conjunction with the optimal step-size technique, we have developed sequential source separation algorithms based on linear regression; an example is RobustICA (Sec. 3.5.3, pp. 45–46). The performance of the regression approach is shown to degrade as more components are extracted. More *robust regression* strategies, inspired by those in [17, 99], need to be developed and thoroughly assessed.

- Although alphabet-based criteria such as the APF and CP principles are shown to be valid contrasts for source separation and extraction [34], the presence of *local extrema* should be clarified and their detrimental impact on source estimation performance evaluated. This study would be particularly relevant in scenarios where the lack of training data precludes the use of semi-blind methods.

- The main drawback of APF criteria relative to alternative properties like CM or kurtosis is their sensitiveness to carrier residual [31, 32]. *Carrier-residual effects* on APF-based equalizers need to be evaluated in detail and reduced through suitable compensation techniques. The inclusion of pilot information in semi-blind criteria may already play a substantial role as a compensation mechanism.

- As most orthogonal contrasts for source separation, the KSP and KVP criteria (Sec. 4.6.1, pp. 60–62) can be maximized by the Jacobi pairwise iteration originally put forward for ICA in [24, 25, 27]. To date, this iterative technique has always yielded positive results, but its convergence has yet to be proven theoretically. Extending the Jacobi technique to single-source extraction and sequential source separation is another interesting open problem.

- The analysis of the *alternating LS algorithm* to optimize the blind source extraction contrast (4.10), p. 68, should be addressed in future investigations, as well as the incorporation of prior information into the contrast.

- A more *exhaustive comparison*, both theoretical and experimental, of other equalization and source separation principles with those studied in the present work remains to be made.

- Further research should also analyze the integration of the proposed techniques in forthcoming commercial communications standards.

5.2 Atrial Fibrillation Analysis

Although the BSS/ICA approach has proven its potential in a variety of biomedical signal processing problems beyond ECG analysis, further research is necessary to answer some important open questions regarding its application in biomedical contexts and, particularly, AF analysis:

- A fundamental issue is the *relationship between the signals estimated by source separation techniques and the actual internal sources of electrophysiological activity*. The simultaneous recording of intracardiac and surface recordings during electrophysiological studies could play a crucial role in answering this question.

- Another important point concerns the *measure of atrial signal estimation quality*, which, as typically occurs in inverse problems, is hampered by the lack of access to the actual physiological activity sources. Experiments on synthetic data support the adequacy of SC as an objective performance index (Sec. 4.5, pp. 59–60). However, its suitability should be further validated by correlation with endocardial signals. Alternative measures such as those based on the *compressed spectrum* could prove more appropriate in more organized forms of atrial arrhythmia like AFL [P28].

- The application of the blind source extraction contrast (4.10), p. 68, to AA extraction should be explored, and compared to the other techniques described in Chapter 4.

- The AA is known in TQ segments, which can help obtain initial estimates of the atrial topography (Sec. 4.8, pp. 69–70). This information could be exploited to derive *optimal spatial beamformers* along the lines of [101] for the estimation of the AA in the whole recording, thus refining the topography-based atrial signal extraction algorithms.

- In fetal ECG extraction during pregnancy, the fetal source typically contributes more strongly to abdominal electrodes. Likewise, the atrial source is expected to appear predominantly in the V1 lead in AA extraction during AF. The mathematical formulation of these *fuzzy constraints* and their incorporation into signal estimation criteria are other interesting problems to be tackled.

- A related issue is how to best exploit and *combine various kinds of available prior information* (second- and higher-order statistics, time coherence, spatial topographies, etc.) to improve separation performance while maintaining the robustness to modeling errors of the BSS/ICA approach.

- The optimal use of the variety of information provided by simultaneous recordings in *different modalities* (e.g., ECG in combination with Doppler ultrasound) constitutes a major research challenge in the field of biomedical signal extraction. For instance, topography-based source extraction techniques could benefit from the improved spatial resolution of recording modalities such as magnetic resonance imaging.

- Encouraging initial results on the ventricular response during AF and AF classification have been obtained from the analysis of surface recordings alone (Sec. 4.9, pp. 70–71). Shedding light on the links between estimated sources and actual sources of cardiac electrical activity (see the first point above) should in turn help discern the additional *clinical and physiological knowledge* to be gained from the analysis of the estimated signals.

To keep this work in the track of clinically relevant results, the continuation of this line of research is taking place in close collaboration with cardiologists from Prof. Jean-Pierre Camous' Cardiology Department, Nice Pasteur University Hospital (CHU), and Prof. Nadir Saoudi's Cardiology Department, Monaco Princess Grace Hospital. Funding has been requested in the form of two joint project proposals submitted to the French National Research Agency (ANR) over the last two years (Sec. 1.3.10, p. 11). Both Cardiology Departments feature state-of-the-art electrophysiological exploration laboratories, and specialize in the treatment of AF by radiofrequency (RF) catheter ablation. The proposed project aims at the analysis and classification of atrial sites for successful catheter ablation, and is briefly summarized below.

Although initially advocated as a second-line choice to pharmacological therapy, ablation of suitably chosen endocardial atrial areas with RF energy applied by means of catheters is becoming an increasing popular treatment, due to its proven arrhythmia termination efficacy and low recurrence rate compared with antiarrhythmic drug therapy. Since Haïsaguerre and co-workers' seminal work [124,125,131,132], conventional ablation procedures have mainly targeted sites of ectopic activity such as the pulmonary veins, which are held responsible for paroxysmal, usually more organized, forms of the disease [144]. Advances in RF-power delivery, catheter and endocardial mapping technology [122] as well as improved medical understanding of the potential pathophysiological mechanisms of the disease and their relationship with the signals observed in electrophysiological studies [112, 117, 126, 141, 142, 144, 151] are all contributing to the development of RF catheter ablation as a first-line clinical option for the treatment of AF. Recent studies have shown that the so-called *complex fractionated atrial electrograms (CFAEs)*, a special type of signals that can sometimes be observed at different points of the atrial endocardium during electrophysiological studies, play a prominent role in the identification of candidate points for successful ablation in chronic, often more disorganized forms of AF [142, 151]. CFAEs are

defined as atrial electrograms displaying waveforms with many deflections, often including baseline perturbation and a prolonged activation complex, or atrial electrograms with very short cycle length. However, electrogram-based ablation requires the visual inspection of electrical activity recorded in numerous manually chosen atrial locations, and is therefore a tedious and time consuming procedure, usually taking several hours [142]. Due to its subjective character, incoherent success rates have been reported by different experts applying the therapy [143].

To bridge this gap, the present joint project intends to develop novel signal processing techniques for a more detailed characterization of CFAEs allowing an automated localization of candidate sites for successful ablation. In particular, we aim to answer the following open questions with potential clinical impact:

- Can the ablation outcome be predicted from certain features of external recordings during AF? Appropriate non-invasive prediction methods would enable the cardiologist to cost-effectively select patients for whom the ablation therapy is more likely to succeed.
- Can CFAEs be characterized externally? In particular, can active foci be detected, classified and localized by relying only on the ECG or alternative surface recordings with improved spatial resolution such as BSPM?
- If the information gathered externally proves insufficient, what features of endocardial electrograms characterize active CFAE foci?

The proposed research aims to take advantage of the spatial diversity provided by the simultaneous recording of bioelectrical activity from multiple surface and intracardiac electrodes. The developed signal processing methods will give rise to novel space-time-frequency characterizations of CFAEs both in external and intracardiac recordings. Such quantitative characterizations are expected to lead not only to improved success rates, but also to significant reductions of the duration, cost and risks associated with the RF catheter ablation therapy for AF. To this end, spatial processing methods such as BSS/ICA could play an important role, but feature extraction, feature selection and data classification techniques will certainly also prove necessary. In turn, this clinically-oriented project could help shed some light on the other open topics enumerated earlier in this section.

Bibliography

Equalization and Source Separation

[1] S. M. Alamouti, "A simple transmit diversity technique for wireless communications," *IEEE Journal on Selected Areas in Communications*, vol. 16, no. 8, pp. 1451–1458, Oct. 1998.

[2] M. J. Al-Kindi and J. Dunlop, "Improved adaptive noise cancellation in the presence of signal leakage on the noise reference channel," *Signal Processing*, vol. 17, no. 3, pp. 241–250, July 1989.

[3] S. Amari, "Natural gradient works efficiently in learning," *Neural Computation*, vol. 10, no. 2, pp. 251–276, Feb. 1998.

[4] S. Amari and A. Cichocki, "Adaptive blind signal processing — neural network approaches," *Proceedings of the IEEE*, vol. 86, no. 10, pp. 2026–2048, Oct. 1998.

[5] Y. Bar-Ness, J. W. Carlin, and M. L. Steinberger, "Bootstrapping adaptive cross pol cancelers for satellite communications," in *Proc. IEEE International Conference on Communications*, vol. 2, Philadelphia, PA, June 13–17, 1982, pp. 4F.5.1–4F.5.5.

[6] A. Belouchrani and J. F. Cardoso, "Maximum likelihood source separation for discrete sources," in *Proc. EUSIPCO-94, VII European Signal Processing Conference*, Edinburgh, UK, Sept. 13–16, 1994, pp. 768–771.

[7] A. Belouchrani, K. Abed-Meraim, J.-F. Cardoso, and E. Moulines, "A blind source separation technique using second-order statistics," *IEEE Transactions on Signal Processing*, vol. 45, no. 2, pp. 434–444, Feb. 1997.

[8] E. Beres and R. B. Adve, "Blind channel estimation for orthogonal STBC in MISO systems," in *Proc. Global Telecommunications Conference*, vol. 4, Nov. 2004, pp. 2323–2328.

[9] D. H. Brandwood, "A complex gradient operator and its application in adaptive array theory," *IEE Proceedings F: Communications Radar and Signal Processing*, vol. 130, no. 1, pp. 11–16, Feb. 1983.

[10] J.-F. Cardoso, "Source separation using higher-order moments," in *Proc. ICASSP-89, 14th IEEE International Conference on Acoustics, Speech and Signal Processing*, Glasgow, Scotland, May 22–25, 1989, pp. 2109–2112.

[11] J.-F. Cardoso and A. Souloumiac, "Blind beamforming for non-Gaussian signals," *IEE Proceedings-F*, vol. 140, no. 6, pp. 362–370, Dec. 1993.

[12] J.-F. Cardoso, "On the performance of orthogonal source separation algorithms," in *Proc. EUSIPCO-94, VII European Signal Processing Conference*, Edinburgh, UK, Sept. 13–16, 1994, pp. 776–779.

[13] J.-F. Cardoso and B. H. Laheld, "Equivariant adaptive source separation," *IEEE Transactions on Signal Processing*, vol. 44, no. 12, pp. 3017–3030, Dec. 1996.

[14] J.-F. Cardoso, "Blind signal separation: statistical principles," *Proceedings of the IEEE*, vol. 86, no. 10, pp. 2009–2025, Oct. 1998.

[15] J.-F. Cardoso, "Higher-order contrasts for independent component analysis," *Neural Computation*, vol. 11, pp. 157–192, 1999.

[16] E. De Carvalho and D. Slock, "Semi-blind methods for FIR multichannel estimation," in *Signal Processing Advances in Wireless and Mobile Communications. Vol. 1: Trends in Channel Estimation and Equalization*, G. B. Giannakis, Y. Hua, P. Stoica, and L. Tong, Eds. Upper Saddle River, NJ: Prentice Hall, 2001, ch. 7, pp. 211–254.

[17] M. Castella, P. Bianchi, A. Chevreuil, and J.-C. Pesquet, "A blind source separation framework for detecting CPM sources mixed by a convolutive MIMO filter," *Signal Processing*, vol. 86, no. 8, pp. 1950–1967, Aug. 2006.

[18] M. Castella, S. Rhioui, E. Moreau, and J.-C. Pesquet, "Quadratic higher order criteria for iterative blind separation of a MIMO convolutive mixture of sources," *IEEE Transactions on Signal Processing*, vol. 55, no. 1, pp. 218–232, Jan. 2007.

[19] Y. Chen, T. Le-Ngoc, B. Champagne, and C. Xu, "Recursive least squares constant modulus algorithm for blind adaptive array," *IEEE Transactions on Signal Processing*, vol. 52, no. 5, pp. 1452–1456, May 2004.

[20] S. Choi and A. Cichocki, "Blind equalisation using approximate maximum likelihood source separation," *Electronics Letters*, vol. 37, no. 1, pp. 61–62, Jan. 2001.

[21] A. Cichocki, R. Ubehauen, L. Moszczyński, and E. Rummert, "A new online adaptive learning algorithm for blind separation of source signals," in *Proc. International Symposium on Artificial Neural Networks*, Taiwan, Dec. 1994, pp. 406–411.

[22] A. Cichocki, W. Kasprzak, and S. Amari, "Multi-layer neural networks with a local adaptive learning rule for blind separation of source signals," in *Proc. NOLTA-95, International Symposium on Nonlinear Theory and its Applications*, Tokyo, Japan, 1995, pp. 61–65.

[23] I. J. Clarke, "Direct exploitation of non-Gaussianity as a discriminant," in *Proc. EUSIPCO-98, IX European Signal Processing Conference*, vol. IV, Rhodes, Greece, Sept. 8–11, 1998, pp. 2057–2060.

[24] P. Comon, "Separation of stochastic processes," in *Proc. Workshop on Higher-Order Spectral Analysis*, Vail, CO, June 28–30, 1989, pp. 174–179.

[25] P. Comon, "Analyse en composantes indépendantes et identification aveugle," *Traitement du signal*, vol. 7, no. 3, pp. 435–450, déc. 1990, numéro spécial non linéaire et non gaussien.

[26] P. Comon, C. Jutten, and J. Hérault, "Blind separation of sources, part II: problems statement," *Signal Processing*, vol. 24, no. 1, pp. 11–20, July 1991.

[27] P .Comon, "Independent component analysis, a new concept?" *Signal Processing*, vol. 36, no. 3, pp. 287–314, Apr. 1994, Special Issue on Higher-Order Statistics.

[28] P. Comon and B. Mourrain, "Decomposition of quantics in sums of powers of linear forms," *Signal Processing (Special Issue on Higher-Order Statistics)*, vol. 53, no. 2, pp. 93–107, Sept. 1996.

[29] P. Comon and E. Moreau, "Improved contrast dedicated to blind separation in communications," in *Proc. ICASSP-97, 22nd IEEE International Conference on Acoustics, Speech and Signal Processing*, Munich, Germany, Apr. 21–24, 1997, pp. 3453–3456.

[30] P. Comon, "Block methods for channel identification and source separation," in *Proc. IEEE Symposium on Adaptive Systems for Signal Processing, Communications and Control*, Alberta, Canada, Oct. 1–4, 2000, pp. 87–92.

[31] P. Comon, "Independent component analysis, contrasts, and convolutive mixtures," in *Proc. 2nd IMA International Conference on Mathematics in Communications*, Lancaster, UK, Dec. 16–18, 2002, pp. 10–17.

[32] P. Comon, "Blind equalization with discrete inputs in the presence of carrier residual," in *Proc. ISSPIT-2002, 2nd IEEE International Symposium on Signal Processing and Information Technology*, Marrakech, Morocco, Dec. 18–21, 2002.

[33] P. Comon, "Tensor decompositions: state of the art and applications," in *Mathematics in Signal Processing V*, J. G. McWhirter and I. K. Proudler, Eds. Oxford, UK: Clarendon Press, 2002, pp. 1–24.

[34] P. Comon, "Contrasts, independent component analysis, and blind deconvolution," *International Journal of Adaptive Control and Signal Processing (Special Issue on Blind Signal Separation)*, vol. 18, no. 3, pp. 225–243, Apr. 2004.

[35] P. Comon and C. Jutten, Eds., *Handbook of Blind Source Separation, Independent Component Analysis and Applications*. Academic Press, in press.

[36] S. Cruces-Alvarez, A. Cichocki, and S. Amari, "From blind signal extraction to blind instantaneous signal separation: criteria, algorithms, and stability," *IEEE Transactions on Neural Networks*, vol. 15, no. 4, pp. 859–873, July 2004.

[37] N. Delfosse and P. Loubaton, "Adaptive blind separation of independent sources: a deflation approach," *Signal Processing*, vol. 45, no. 1, pp. 59–83, July 1995.

[38] Y. Deville, "A unified stability analysis of the hérault-jutten source separation neural network," *Signal Processing*, vol. 51, no. 3, pp. 229–233, June 1996.

[39] A. Dinç and Y. Bar-Ness, "Bootstrap: a fast blind adaptive signal separator," in *Proc. ICASSP-92, 17th IEEE International Conference on Acoustics, Speech and Signal Processing*, vol. II, San Francisco, CA, Mar. 23–26, 1992, pp. 325–328.

[40] Z. Ding, R. A. Kennedy, B. D. O. Anderson, and C. R. Johnson, "Ill-convergence of Godard blind equalizers in data communication systems," *IEEE Transactions on Communications*, vol. 39, no. 9, pp. 1313–1327, Sept. 1991.

[41] Z. Ding, C. R. Johnson, and R. A. Kennedy, "On the (non)existence of undesirable equilibria of Godard blind equalizers," *IEEE Transactions on Signal Processing*, vol. 40, no. 10, pp. 2425–2432, Oct. 1992.

[42] K. Doğançay and R. A. Kennedy, "Least squares approach to blind channel equalization," *IEEE Transactions on Signal Processing*, vol. 47, no. 11, pp. 1678–1687, Nov. 1999.

[43] D. Donoho, "On minimum entropy deconvolution," in *Proc. 2nd Applied Time Series Analysis Symposium*, Tulsa, OK, 1980, pp. 565–608.

[44] G. J. Foschini, "Layered space-time architecture for wireless communication in a fading environment when using multiple antennas," *Bell Laboratories Technical Journal*, vol. 1, no. 2, pp. 41–59, 1996.

[45] E. Gassiat and F. Gamboa, "Source separation when the input sources are discrete or have constant modulus," *IEEE Transactions on Signal Processing*, vol. 45, no. 12, pp. 3062–3072, Dec. 1997.

[46] N. D. Gaubitch, M. Kamrul Hasan, and P. A. Naylor, "Generalized optimal step-size for blind multichannel LMS system identification," *IEEE Signal Processing Letters*, vol. 13, no. 10, pp. 624–627, Oct. 2006.

[47] D. Gesbert, M. Shafi, D. Shan-Shiu, P. J. Smith, and A. Naguib, "From theory to practice: an overview of MIMO space-time coded wireless systems," *IEEE Journal on Selected Areas in Communications*, vol. 21, no. 3, pp. 281–302, Apr. 2003.

[48] D. N. Godard, "Self-recovering equalization and carrier tracking in two-dimensional data communication systems," *IEEE Transactions on Communications*, vol. 28, no. 11, pp. 1867–1875, Nov. 1980.

[49] G. D. Golden, G. J. Foschini, R. A. Valenzuela, and P. Wolniansky, "Detection algorithm and initial laboratory results using V-BLAST space-time communication architecture," *Electronics Letters*, vol. 35, no. 1, pp. 14–15, Jan. 1999.

[50] O. Grellier and P. Comon, "Blind separation of discrete sources," *IEEE Signal Processing Letters*, vol. 5, no. 8, pp. 212–214, Aug. 1998.

[51] O. Grellier and P. Comon, "Blind equalization and source separation with MSK inputs," in *Proc. SPIE Conference on Advances in Signal Processing.*, San Diego, CA, July 19–24, 1998, pp. 26–34.

[52] O. Grellier and P. Comon, "Closed-form equalization," in *Proc. SPAWC-99, 2nd IEEE Workshop on Signal Processing Advances in Wireless Communications*, Annapolis, MD, May 9–12, 1999, pp. 219–222.

[53] O. Grellier, P. Comon, B. Mourrain, and P. Trébuchet, "Analytical blind channel identification," *IEEE Transactions on Signal Processing*, vol. 50, no. 9, pp. 2196–2207, Sept. 2002.

[54] F. Harroy, J.-L. Lacoume, and M. A. Lagunas, "A general adaptive algorithm for nonGaussian source separation without any constraint," in *Proc. EUSIPCO-94, VII European Signal Processing Conference*, Edinburgh, UK, Sept. 13–16, 1994, pp. 1161–1164.

[55] F. Harroy and J.-L. Lacoume, "Maximum likelihood estimators and Cramer-Rao bounds in source separation," *Signal Processing*, vol. 55, no. 2, pp. 167–177, Dec. 1996.

[56] J. Hérault, C. Jutten, et B. Ans, "Détection de grandeurs primitives dans un message composite par une architecture neuromimétique en apprentissage non supervisé," in *Actes 10ème Colloque GRETSI*, Nice, France, 20–24 mai 1985, pp. 1017–1022.

[57] Y. Huang, J. Benesty, and J. Chen, "Optimal step size of the adaptive multichannel LMS algorithm for blind SIMO identification," *IEEE Signal Processing Letters*, vol. 12, no. 3, pp. 173–176, Mar. 2005.

[58] A. Hyvärinen and E. Oja, "A fast fixed-point algorithm for independent component analysis," *Neural Computation*, vol. 9, no. 7, pp. 1483–1492, Oct. 1997.

[59] A. Hyvärinen, "One-unit contrast functions for independent component analysis: a statistical analysis," in *Proc. IEEE Neural Networks for Signal Processing Workshop*, Amelia Island, FL, 1997, pp. 388–397.

[60] A. Hyvärinen, "Fast and robust fixed-point algorithms for independent component analysis," *IEEE Transactions on Neural Networks*, vol. 10, no. 3, pp. 626–634, May 1999.

[61] A. Hyvärinen, J. Karhunen, and E. Oja, *Independent Component Analysis*. New York: John Wiley & Sons, 2001.

[62] H. Jafarkhani, *Space-Time Coding*. Cambridge, UK: Cambridge University Press, 2005.

[63] C. R. Johnson, P. Schniter, I. Fijalkow, L. Tong, J. D. Behm, *et al.*, "The core of FSE-CMA behavior theory," in *Unsupervised Adaptive Filtering, Vol. II: Blind Deconvolution*, S. S. Haykin, Ed. New York: John Wiley & Sons, 2000, ch. 2, pp. 13–112.

[64] C. Jutten et J. Hérault, "Une solution neuromimétique au problème de séparation de sources," *Traitement du signal*, vol. 5, no. 6, pp. 389–403, juin 1988.

[65] C. Jutten and J. Hérault, "Blind separation of sources, part I: an adaptive algorithm based on neuromimetic architecture," *Signal Processing*, vol. 24, no. 1, pp. 1–10, July 1991.

[66] E. Kofidis and P. Regalia, "On the best rank-1 approximation of higher-order supersymmetric tensors," *SIAM Journal on Matrix Analysis*, vol. 23, no. 3, pp. 863–884, July 2002.

[67] A. M. Kuzminskiy, "Automatic choice of the adaption coefficient under nonstationary conditions," *Radioelectronics and Communications Systems*, vol. 25, no. 4, pp. 72–74, Apr. 1982.

[68] A. M. Kuzminskiy, "A robust step size adaptation scheme for LMS adaptive filters," in *Proc. DSP'97, 13th International Conference on Digital Signal Processing*, vol. 1, Santorini, Greece, July 2–4, 1997.

[69] L. De Lathauwer, P. Comon, B. De Moor, and J. Vandewalle, "Higher-order power method - application in independent component analysis," in *Proc. NOLTA-95, International Symposium on Nonlinear Theory and its Applications*, vol. 1, Las Vegas, NV, Dec. 10–14, 1995, pp. 91–96.

[70] T. H. Li and K. Mbarek, "A blind equalizer for nonstationary discrete-valued signals," *IEEE Transactions on Signal Processing*, vol. 45, no. 1, pp. 247–254, Jan. 1997, Special Issue on Communications.

[71] X.-L. Li and X.-D. Zhang, "Sequential blind extraction adopting second-order statistics," *IEEE Signal Processing Letters*, vol. 14, no. 1, pp. 58–61, Jan. 2007.

[72] H. Li and T. Adali, "A class of complex ICA algorithms based on the kurtosis cost function," *IEEE Transactions on Neural Networks*, vol. 19, no. 3, pp. 408–420, Mar. 2008.

[73] O. Macchi and E. Moreau, "Self-adaptive source separation, part I: convergence analysis of a direct linear network controled by the Hérault-Jutten algorithm," *IEEE Transactions on Signal Processing*, vol. 45, no. 4, pp. 918–926, Apr. 1997.

[74] E. Moreau and O. Macchi, "High-order contrasts for self-adaptive source separation," *International Journal of Adaptive Control and Signal Processing*, vol. 10, no. 1, pp. 19–46, Jan. 1996.

[75] E. Moreau and N. Thirion-Moreau, "Nonsymmetrical contrasts for sources separation," *IEEE Transactions on Signal Processing*, vol. 47, no. 8, pp. 2241–2252, Aug. 1999.

[76] E. Moreau et P. Comon, "Contrastes," in *Séparation de sources 1 : concepts de base et analyse en composantes indépendantes*, P. Comon et C. Jutten, Eds. Paris: Hermes, 2007, ch. 3.

[77] E. Moulines, P. Duhamel, J.-F. Cardoso, and S. Mayrargue, "Subspace methods for the blind identification of multichannel FIR filters," *IEEE Transactions on Signal Processing*, vol. 43, no. 2, pp. 516–525, Feb. 1995.

[78] M. Novey and T. Adali, "On extending the complex FastICA algorithm to noncircular sources," *IEEE Transactions on Signal Processing*, vol. 56, no. 5, pp. 2148–2154, May 2008.

[79] H. V. Poor and G. W. Wornell, Eds., *Wireless Communications: Signal Processing Perspectives*. Upper Saddle River, NJ: Prentice Hall, 1998.

[80] J. G. Proakis, *Digital Communications*, 4th ed. New York: McGraw-Hill, 2000.

[81] P. A. Regalia, "A finite-interval constant modulus algorithm," in *Proc. ICASSP-2002, 27th International Conference on Acoustics, Speech and Signal Processing*, vol. III, Orlando, FL, May 13–17, 2002, pp. 2285–2288.

[82] P. A. Regalia and E. Kofidis, "Monotonic convergence of fixed-point algorithms for ICA," *IEEE Transactions on Neural Networks*, vol. 14, no. 4, pp. 943–949, July 2003.

[83] T. Ristaniemi and J. Joutsensalo, "Advanced ICA-based receivers for block fading DS-CDMA channels," *Signal Processing*, vol. 82, no. 3, pp. 417–431, Mar. 2002.

[84] L. Rota and P. Comon, "Blind equalizers based on polynomial criteria," in *Proc. ICASSP-2004, 29th International Conference on Acoustics, Speech and Signal Processing*, vol. IV, Montreal, Canada, May 17–21, 2004, pp. 441–444.

[85] Y. Sato, "A method of self-recovering equalization for multi-level amplitude modulation," *IEEE Transactions on Communications*, vol. 23, pp. 679–682, June 1975.

[86] R. O. Schmidt, "Multiple emitter location and signal parameter estimation," *IEEE Transactions on Antennas and Propagation*, vol. AP-34, no. 3, pp. 276–280, Mar. 1986.

[87] O. Shalvi and E. Weinstein, "New criteria for blind deconvolution of nonminimum phase systems (channels)," *IEEE Transactions on Information Theory*, vol. 36, no. 2, pp. 312–321, Mar. 1990.

[88] D. T. M. Slock, "Blind fractionally-spaced equalization, perfect-reconstruction filter banks and multichannel linear prediction," in *Proc. ICASSP-94, 19th International Conference on Acoustics, Speech and Signal Processing*, vol. IV, Adelaide, Australia, Apr. 19–22, 1994, pp. 585–588.

[89] E. Sorouchyari, "Blind separation of sources, part III: stability analysis," *Signal Processing*, vol. 24, no. 1, pp. 21–29, July 1991.

[90] R. Steele and L. Hanzo, Eds., *Mobile Radio Communications*, 2nd ed. New York: John Wiley & Sons, 1999.

[91] S. Talwar, M. Viberg, and A. Paulraj, "Blind separation of synchronous cochannel digital signals using an antenna array. Part I: Algorithms," *IEEE Transactions on Signal Processing*, vol. 44, no. 5, pp. 1184–1197, May 1996.

[92] E. Tangdiongga, N. Calabretta, P. C. W. Sommen, and H. J. S. Dorren, "WDM monitoring technique using adaptive blind signal separation," *IEEE Photonics Technology Letters*, vol. 13, no. 3, pp. 248–250, Mar. 2001.

[93] V. Tarokh, H. Jafarkhani, and A. R. Calderbank, "Space-time block codes from orthogonal designs," *IEEE Transactions on Information Theory*, vol. 45, no. 5, pp. 1456–1467, July 1999.

[94] P. Tichavský, Z. Koldovský, and E. Oja, "Performance analysis of the FastICA algorithm and Cramér-Rao bounds for linear independent component analysis," *IEEE Transactions on Signal Processing*, vol. 54, no. 4, pp. 1189–1203, Apr. 2006.

[95] L. Tong, R. Liu, V. C. Soon, and Y.-F. Huang, "Indeterminacy and identifiability of blind identification," *IEEE Transactions on Circuits and Systems*, vol. 38, no. 5, pp. 499–509, May 1991.

[96] L. Tong, G. Xu, and T. Kailath, "Blind identification and equalization based on second-order statistics: a time domain approach," *IEEE Transactions on Information Theory*, vol. 40, no. 2, pp. 340–349, Mar. 1994.

[97] J. R. Treichler and B. G. Agee, "A new approach to multipath correction of constant modulus signals," *IEEE Transactions on Acoustics, Speech and Signal Processing*, vol. 31, no. 2, pp. 459–472, Apr. 1983.

[98] J. K. Tugnait, "Identification and deconvolution of multichannel linear non-Gaussian processes using higher order statistics and inverse filter criteria," *IEEE Transactions on Signal Processing*, vol. 45, no. 3, pp. 658–672, Mar. 1997.

[99] J. K. Tugnait, "Adaptive blind separation of convolutive mixtures of independent linear signals," *Signal Processing*, vol. 73, no. 1-2, pp. 139–152, Jan. 1999.

[100] J. K. Tugnait, L. Tong, and Z. Ding, "Single-user channel estimation and equalization," *IEEE Signal Processing Magazine*, vol. 17, no. 3, pp. 16–28, May 2000.

[101] H. L. Van Trees, *Detection, Estimation, and Modulation Theory, Part IV: Optimum Array Processing.* New York: John Wiley & Sons, 2002.

[102] A.-J. van der Veen, S. Talwar, and A. Paulraj, "Blind estimation of multiple digital signals transmitted over FIR channels," *IEEE Signal Processing Letters*, vol. 2, no. 5, pp. 99–102, May 1995.

[103] A.-J. van der Veen and A. Paulraj, "An analytical constant modulus algorithm," *IEEE Transactions on Signal Processing*, vol. 44, no. 5, pp. 1136–1155, May 1996.

[104] A.-J. van der Veen, S. Talwar, and A. Paulraj, "A subspace approach to blind space-time signal processing for wireless communication systems," *IEEE Transactions on Signal Processing*, vol. 45, no. 1, pp. 173–190, Jan. 1997.

[105] A.-J. van der Veen, "Analytical method for blind binary signal separation," *IEEE Transactions on Signal Processing*, vol. 45, no. 4, pp. 1078–1082, Apr. 1997.

[106] R. A. Wiggins, "Minimum entropy deconvolution," *Geoexploration*, vol. 16, pp. 21–35, 1978.

[107] B. Xerri and B. Borloz, "An iterative method using conditional second-order statistics applied to the blind source separation problem," *IEEE Transactions on Signal Processing*, vol. 52, no. 2, pp. 313–328, Feb. 2004.

[108] H. Yang, "On-line blind equalization via on-line blind separation," *Signal Processing*, vol. 68, no. 3, pp. 271–281, Aug. 1998.

[109] D. Yellin and B. Porat, "Blind identification of FIR systems excited by discrete-alphabet inputs," *IEEE Transactions on Signal Processing*, vol. 41, no. 3, pp. 1331–1339, Mar. 1993.

[110] Y. Zhang and S. A. Kassam, "Blind separation and equalization using fractional sampling of digital communications signals," *Signal Processing*, vol. 81, no. 12, pp. 2591–2608, Dec. 2001.

Atrial Fibrillation Analysis and Biomedical

[111] M. A. Allesie, P. A. Boyden, A. J. Camm, A. G. Kléber, M. J. Lab, *et al.*, "Pathophysiology and prevention of atrial fibrillation," *Circulation*, vol. 103, no. 5, pp. 769–777, 2001.

[112] V. Barbaro, P. Bartolini, G. Calcagnini, F. Censi, S. Morelli, and A. Michelucci, "Mapping the organization of atrial fibrillation with basket catheters Part I: validation of a real-time algorithm," *PACE*, vol. 24, pp. 1082–1088, 2001.

[113] A. K. Barros, R. Vigário, V. Jousmäki, and N. Ohnishi, "Extraction of event-related signals from multichannel bioelectrical measurements," *IEEE Transactions on Biomedical Engineering*, vol. 47, no. 5, pp. 583–588, May 2000.

[114] A. Bollmann, N. K. Kanuru, K. K. McTeague, P. F. Walter, D. B. DeLurgio, and J. J. Langberg, "Frequency analysis of human atrial fibrillation using the surface electrocardiogram and its response to Ibutilide," *American Journal of Cardiology*, vol. 81, no. 12, pp. 1439–1445, June 1998.

[115] A. Bollmann and F. Lombardi, "Electrocardiology of atrial fibrillation," *IEEE Engineering in Medicine and Biology Magazine*, vol. 25, no. 6, pp. 15–23, Nov./Dec. 2006.

[116] A. Bollmann, D. Husser, L. Mainardi, F. Lombardi, P. Langley, *et al.*, "Analysis of surface electrocardiograms in atrial fibrillation: techniques, research, and clinical applications," *Europace*, vol. 8, no. 11, pp. 911–926, 2006.

[117] G. Calcagnini, F. Censi, A. Michelucci, and P. Bartolini, "Descriptors of wavefront propagation," *IEEE Engineering in Medicine and Biology Magazine*, vol. 25, no. 6, pp. 71–78, Nov./Dec. 2006.

[118] F. Castells, J. Igual, J. J. Millet, and J. J. Rieta, "Atrial activity extraction from atrial fibrillation episodes based on maximum likelihood source separation," *Signal Processing*, vol. 85, no. 3, pp. 523–535, Mar. 2005.

[119] R. J. Cohen, R. D. Berger, and T. E. Dushane, "A quantitative model for the ventricular response during atrial fibrillation," *IEEE Transactions on Biomedical Engineering*, vol. 30, no. 12, pp. 781–796, Dec. 1983.

[120] L. Faes, G. Nollo, M. Kirchner, E. Olivetti, F. Gaita, R. Riccardi, and R. Antolini, "Principal component analysis and cluster analysis for measuring the local organisation of human atrial fibrillation," *Medical and Biological Engineering and Computing*, vol. 39, no. 6, pp. 656–636, Nov. 2006.

[121] V. Fuster, L. E. Rydén, D. S. Cannom, H. J. Crijns, A. B. Curtis, *et al.*, "ACC/AHA/ESC guidelines for the management of patients with atrial fibrillation – executive summary," *Circulation*, vol. 114, no. 7, pp. 700–752, 2006.

[122] A. J. Greenspon, "Advances in catheter ablation for the treatment of cardiac arrhythmias," *IEEE Transactions on Microwave Theory and Techniques*, vol. 48, no. 12, pp. 2670–2675, Dec. 2000.

[123] M. Guillem, A. Climent, F. Castells, D. Husser, J. Millet, A. Arya, C. Piorkowski, and A. Bollmann, "Noninvasive mapping of human atrial fibrillation," *Journal of Cardiovascular Electrophysiology*, vol. 20, no. 5, pp. 507–513, May 2009.

[124] M. Haïssaguerre, L. Gencel, B. Fischer, *et al.*, "Successful catheter ablation of atrial fibrillation," *Journal of Cardiovascular Electrophysiology*, vol. 5, no. 12, pp. 1045–1052, 1994.

[125] M. Haïssaguerre, P. Jaïs, D. C. Shah, A. Takahashi, M. Hocini, *et al.*, "Spontaneous initiation of atrial fibrillation by ectopic beats originating in the pulmonary veins," *New England Journal of Medicine*, vol. 339, no. 10, pp. 659–666, 1998.

[126] M. Haïssaguerre, P. Sanders, M. Hocini, L.-F. Hsu, D. C. Shah, *et al.*, "Changes in atrial fibrillation cycle length and inducibility during catheter ablation and their relation to outcome," *Circulation*, vol. 109, no. 24, pp. 3007–3013, 2004.

[127] C. W. Hesse and C. J. James, "The FastICA algorithm with spatial constraints," *IEEE Signal Processing Letters*, vol. 12, no. 11, pp. 792–795, Nov. 2005.

[128] C. W. Hesse and C. J. James, "On semi-blind source separation using spatial constraints with applications in EEG analysis," *IEEE Transactions on Biomedical Engineering*, vol. 53, no. 12, pp. 2525–2534, Dec. 2006.

[129] M. Holm, S. Pehrson, M. Ingemansson, L. Sörnmo, R. Johansson, *et al.*, "Noninvasive assessment of the atrial cycle length during atrial fibrillation in man: introducing, validating and illustrating a new ECG method," *Cardiovascular Research*, vol. 38, no. 1, pp. 69–81, Apr. 1998.

[130] M. G. Jafari and J. A. Chambers, "Fetal electrocardiogram extraction by sequential source separation in the wavelet domain," *IEEE Transactions on Biomedical Engineering*, vol. 52, no. 3, pp. 390–400, Mar. 2005.

[131] P. Jaïs, M. Haïssaguerre, D. C. Shah, S. Chouairi, L. Gencel, *et al.*, "A focal source of atrial fibrillation treated by discrete radiofrequency ablation," *Circulation*, vol. 95, pp. 572–576, 1997.

[132] P. Jaïs, D. C. Shah, M. Hocini, L. Macle, K.-J. Choi, *et al.*, "Radiofrequency ablation for atrial fibrillation," *European Heart Journal Supplements*, vol. 5, no. Supplement H, pp. H34–H39, 2003.

[133] C. J. James and O. J. Gibson, "Temporally constrained ICA: an application to artifact rejection in electromagnetic brain signal analysis," *IEEE Transactions on Biomedical Engineering*, vol. 50, no. 9, pp. 1108–1116, Sept. 2003.

[134] K. T. Konings, C. J. Kirchhof, J. R. Smeets, H. J. Wellens, O. C. Penn, and M. A. Allessie, "High-density mapping of electrically induced atrial fibrillation in humans," *Circulation*, vol. 89, no. 4, pp. 1665–1680, Apr. 1994.

[135] L. De Lathauwer, D. Callaerts, B. De Moor, and J. Vandewalle, "Fetal electrocardiogram extraction by source subspace separation," in *Proc. IEEE/ATHOS Signal Processing Conference on Higher-Order Statistics*, Girona, Spain, June 12–14, 1995, pp. 134–138.

[136] L. De Lathauwer, B. De Moor, and J. Vandewalle, "Fetal electrocardiogram extraction by blind source subspace separation," *IEEE Transactions on Biomedical Engineering*, vol. 47, no. 5, pp. 567–572, May 2000, special Topic Section on Advances in Statistical Signal Processing for Biomedicine.

[137] J. Lian, D. Mussig, and V. Lang, "Computer modelling of ventricular rhythm during atrial fibrillation and ventricular pacing," *IEEE Transactions on Biomedical Engineering*, vol. 53, no. 8, pp. 1512–1520, Aug. 2006.

[138] W. Lu and J. C. Rajapakse, "Approach and applications of constrained ICA," *IEEE Transactions on Neural Networks*, vol. 16, no. 1, pp. 203–212, Jan. 2005.

[139] W. Lu and J. C. Rajapakse, "ICA with reference," *Neurocomputing*, vol. 69, pp. 2244–2257, Oct. 2006.

[140] O. Meste and N. Serfaty, "QRST cancellation using bayesian estimation for the auricular fibrillation analysis," in *Proc. 27th Annual International Conference of the IEEE Engineering in Medicine and Biology Society*, Shanghai, China, Sept. 1–4, 2005, pp. 7083–7086.

[141] A. Michelucci, P. Bartolini, G. Calcagnini, F. Censi, A. Colella, *et al.*, "Mapping the organization of atrial fibrillation with basket catheters Part II: regional patterns in chronic patients," *PACE*, vol. 24, pp. 1089–1096, 2001.

[142] K. Nademanee, J. McKenzie, E. Kosar, M. Schwab, B. Sunsaneewitayakul, *et al.*, "A new approach for catheter ablation of atrial fibrillation: mapping of the electrophysiologic substrate," *Journal of the American College of Cardiology*, vol. 43, no. 11, pp. 2044–2053, 2004.

[143] H. Oral, A. Chug, G. E., A. Wimmer, S. Dey, N. Gadeela, *et al.*, "Radiofrequency catheter ablation of chronic atrial fibrillation guided by complex electrograms," *Circulation*, vol. 115, no. 20, pp. 2606–2612, 2007.

[144] C. Pappone, G. Oreto, F. Lamberti, G. Vicedomini, M. L. Loricchio, *et al.*, "Catheter ablation of paroxysmal atrial fibrillation using a 3D mapping system," *Circulation*, vol. 100, no. 11, pp. 1203–1208, 1999.

[145] R. M. Rangayyan, *Biomedical Signal Analysis. A Case-Study Approach.* John Wiley & Sons, Inc., 2002.

[146] D. S. Rosenbaum and R. J. Cohen, "Frequency based measures of atrial fibrillation in man," in *Proc. 12th Annual International Conference of the IEEE Engineering in Medicine and Biology Society*, 1990.

[147] C. Sánchez, J. Millet, and J. J. Rieta, "Packet wavelet decomposition: an approach for atrial activity extraction," in *Computers in Cardiology*, vol. 29, Rotterdam, The Netherlands, Sept. 2001, pp. 33–36.

[148] M. Sato, Y. Kimura, S. Chida, T. Ito, N. Katayama, K. Okamura, and M. Nakao, "A novel extraction method of fetal electrocadiogram from the composite abdominal signal," *IEEE Transactions on Biomedical Engineering*, vol. 54, no. 1, pp. 49–58, Jan. 2007.

[149] J. Slocum, E. Byrom, L. McCarthy, A. Sahakian, and S. Swiryn, "Computer detection of atrioventricular dissociation from surface electrocardiogram during wide QRS complex tachycardia," *Circulation*, vol. 72, pp. 1028–1036, Nov. 1985.

[150] M. Stridh and L. Sörnmo, "Spatiotemporal QRST cancellation techniques for analysis of atrial fibrillation," *IEEE Transactions on Biomedical Engineering*, vol. 48, no. 1, pp. 105–111, Jan. 2001.

[151] Y. Takahashi, M. D. O'Neill, M. Hocini, R. Dubois, S. Matsuo, *et al.*, "Characterization of electrograms associated with termination of chronic atrial fibrillation by catheter ablation," *Journal of the American College of Cardiology*, vol. 51, no. 10, pp. 1003–1010, 2008.

[152] C. Vásquez, A. Hernández, F. Mora, G. Carrault, and G. Passariello, "Atrial activity enhancement by Wiener filtering using an artificial neural network," *IEEE Transactions on Biomedical Engineering*, vol. 48, no. 8, pp. 940–944, Aug. 2001.

[153] G. D. Veenhuyzen, C. S. Simpson, and H. Abdollah, "Atrial fibrillation," *Canadian Medical Association Journal*, vol. 171, no. 7, pp. 755–760, 2004.

[154] B. Widrow, J. R. Glover, J. M. McCool, and *et al.*, "Adaptive noise cancelling: principles and applications," *Proceedings of the IEEE*, vol. 63, no. 12, pp. 1692–1716, Dec. 1975.

Other Topics

[155] G. H. Golub and C. F. Van Loan, *Matrix Computations*, 3rd ed. Baltimore, MD: The John Hopkins University Press, 1996.

[156] D. Mampel and A. K. Nandi, "Robust cumulant estimation," in *Blind Estimation Using Higher-Order Statistics*, A. K. Nandi, Ed. Boston, MA: Kluwer Academic Publishers, 1999, ch. 5.

[157] P. McCullagh, *Tensor Methods in Statistics*, Monographs on Statistics and Applied Probability. London: Chapman and Hall, 1987.

[158] W. H. Press, S. A. Teukolsky, W. T. Vetterling, and B. P. Flannery, *Numerical Recipes in C. The Art of Scientific Computing*, 2nd ed. Cambridge, UK: Cambridge University Press, 1992.

[159] A. Stuart and K. Ord, *Kendall's Advanced Theory of Statistics*, 6th ed. Hodder Arnold, 1994, vol. 1.

List of Publications

Most of these publications, as well as additional documents not listed here (e.g., internal reports), are available on-line at the address:

`http://www.i3s.unice.fr/~zarzoso/research.html`.

Underlined references are attached to this report on the pages shown in the margins.

Submissions in Preparation or Under Review

Book chapter in preparation:

[P1] R. Phlypo, P. Bonizzi, O. Meste, and V. Zarzoso, "Estimation of atrial fibrillatory activity in the electrocardiogram," in *Recent Advances in Biomedical Signal Processing*, J. M. Górriz and E. Lang, Eds. Bentham Publishers, in preparation.

Refereed journal submissions under review:

[P2] P. Bonizzi, M. S. Guillem, A. M. Climent, J. Millet, V. Zarzoso, F. Castells, and O. Meste, "Noninvasive assessment of the complexity and stationarity of the atrial wavefront patterns during atrial fibrillation," *IEEE Transactions on Biomedical Engineering*, submitted (`http://www.i3s.unice.fr/~mh/RR/2009/RR-09.15-P.BONIZZI.pdf`).

[P3] R. Phlypo, V. Zarzoso, and I. Lemahieu, "Spatial filtering and least squares spline approximation for ECG baseline wander removal," *Electronics Letters*, submitted.

[P4] V. Zarzoso and P. Comon, "Robust independent component analysis," *IEEE Transactions on Neural Networks*, submitted (`http://www.i3s.unice.fr/~mh/RR/2009/RR-09.02-V.ZARZOSO.pdf`).

[P5] V. Zarzoso, P. Comon, and R. Phlypo, "A contrast function for independent component analysis without permutation ambiguity," *IEEE Transactions on Neural Networks*, submitted (`http://www.i3s.unice.fr/~mh/RR/2009/RR-09.04-V.ZARZOSO.pdf`).

[P6] R. Phlypo, V. Zarzoso, and I. Lemahieu, "Blind source extraction based on conditional maximum likelihood approach and its application to atrial activity estimation in atrial fibrillation ECGs," *Signal Processing*, submitted.

[P7] A. Dapena, H. J. Pérez-Iglesias, and V. Zarzoso, "Blind channel estimation based on maximizing the eigenvalue spread of cumulant matrices in (2×1) Alamouti's coding schemes," *Wireless Communications and Mobile Computing*, submitted.

Published or in Press

Book chapters:

[P8] V. Zarzoso and A. Hyvärinen, "Iterative algorithms," in *Handbook of Blind Source Separation, Independent Component Analysis and Applications*, P. Comon and C. Jutten, Eds. Academic Press, ch. 6, in press.

[P9] V. Zarzoso, P. Comon, and D. Slock, "Semi-blind methods for communications," in *Handbook of Blind Source Separation, Independent Component Analysis and Applications*, P. Comon and C. Jutten, Eds. Academic Press, ch. 15, in press.

[P10] V. Zarzoso, "Extraction of ECG characteristics using source separation techniques: exploiting statistical independence and beyond," in *Advanced Biosignal Processing*, A. Naït-Ali, Ed. Berlin: Springer, 2009, ch. 2, pp. 15–48.

[P11] V. Zarzoso, R. Phlypo, O. Meste, and P. Comon, "Signal extraction in multisensor biomedical recordings," in *Advances in Biomedical Engineering*, P. Verdonck, Ed. Amsterdam: Elsevier, 2008, ch. 3, pp. 95–143.

[P12] V. Zarzoso and P. Comon, "Méthodes semi-aveugles pour les télécommunications," in *Séparation de sources 2 : au delà de l'aveugle et applications*, C. Jutten and P. Comon, Eds. Paris: Hermes, 2007, ch. 8, pp. 303–353.

Refereed journal papers:

[P13] R. Phlypo, V. Zarzoso, and I. Lemahieu, "Source extraction by maximizing the variance in the conditional distribution tails," *IEEE Transactions on Signal Processing*, accepted for publication. (p. 105)

[P14] V. Zarzoso, R. Phlypo, and P. Comon, "A contrast for independent component analysis with priors on the source kurtosis signs," *IEEE Signal Processing Letters*, vol. 15, pp. 501–504, 2008. (p. 117)

[P15] V. Zarzoso, "Second-order criterion for blind source extraction," *Electronics Letters*, vol. 44, no. 22, pp. 1327–1328, Oct. 2008. (p. 121)

[P16] H. J. Pérez-Iglesias, J. A. García-Naya, A. Dapena, L. Castedo, and V. Zarzoso, "Blind channel identification in Alamouti coded systems: a comparative study of eigendecomposition methods in indoor transmissions at 2.4 GHz," *European Transactions on Telecommunications*, vol. 19, no. 7, pp. 751–759, Sept. 2008. (p. 123)

[P17] V. Zarzoso and P. Comon, "Optimal step-size constant modulus algorithm," *IEEE Transactions on Communications*, vol. 56, no. 1, pp. 10–13, Jan. 2008. (p. 133)

[P18] V. Zarzoso, J. J. Murillo-Fuentes, R. Boloix-Tortosa, and A. K. Nandi, "Optimal pairwise fourth-order independent component analysis," *IEEE Transactions on Signal Processing*, vol. 54, no. 8, pp. 3049–3063, Nov. 2006. (p. 137)

[P19] V. Zarzoso and P. Comon, "Blind and semi-blind equalization based on the constant power criterion," *IEEE Transactions on Signal Processing*, vol. 53, no. 11, pp. 4363–4375, Nov. 2005. (p. 153)

[P20] F. Castells, J. J. Rieta, J. Millet, and V. Zarzoso, "Spatiotemporal blind source separation approach to atrial activity estimation in atrial tachyarrhythmias," *IEEE Transactions on Biomedical Engineering*, vol. 52, no. 2, pp. 258–267, Feb. 2005. (p. 167)

[P21] J. J. Rieta, F. Castells, C. Sánchez, V. Zarzoso, and J. Millet, "Atrial activity extraction for atrial fibrillation analysis using blind source separation," *IEEE Transactions on Biomedical Engineering*, vol. 51, no. 7, pp. 1176–1186, July 2004. (p. 177)

[P22] Y. Feng, V. Zarzoso, and A. K. Nandi, "Quality monitoring of WDM channels with blind signal separation methods," *Journal of Optical Networking (Feature Issue on Optical Performance Monitoring)*, vol. 3, no. 7, pp. 477–489, July 2004. (p. 189)

[P23] V. Zarzoso and A. K. Nandi, "Blind MIMO equalization with optimum delay using independent component analysis," *International Journal of Adaptive Control and Signal Processing (Special Issue on Blind Signal Separation)*, vol. 18, no. 3, pp. 245–263, Apr. 2004. (p. 203)

[P24] V. Zarzoso and A. K. Nandi,"Exploiting non-Gaussianity in blind identification and equalization of MIMO FIR channels," *IEE Proceedings — Vision, Image and Signal Processing (Special Issue on non-Linear and non-Gaussian Signal Processing)*, vol. 151, no. 1, pp. 69–75, Feb. 2004. (p. 223)

Conference papers:

[P25] P. Bonizzi, M. S. Guillem, F. Castells, A. M. Climent, V. Zarzoso, and O. Meste, "Significance of mixing matrix structure on principal component-based analysis of atrial fibrillation body surface potential maps," in *Proc. Computers in Cardiology*, Park City, UT, Sept. 13–16, 2009.

[P26] V. Zarzoso and P. Comon, "Automated extraction of atrial fibrillation activity from the surface ECG using independent component analysis in the frequency domain," in *Proc. Medical Physics and Biomedical Engineering World Congress*, Sept. 7–12, 2009, invited.

[P27] H. Pérez-Iglesias, D. Iglesia, A. Dapena, and V. Zarzoso, "Blind channel identification in (2×1) Alamouti coded systems based on maximinizing the eigenvalue spread of cumulant matrices," in *Proc. ICA-2009, 8th International Conference on Independent Component Analysis and Signal Separation*, Paraty, Brazil, Mar. 15–18, 2009.

[P28] P. Bonizzi, O. Meste, and V. Zarzoso, "Spectral analysis of atrial signals directly from surface ECG exploiting compressed spectrum," in *Proc. Computers in Cardiology*, vol. 35, Bologna, Italy, Sep. 14–17, 2008, pp. 221–224.

[P29] P. Bonizzi, R. Phlypo, V. Zarzoso, O. Meste, and A. Fred, "Atrial signal extraction in atrial fibrillation ECGs exploiting spatial constraints," in *Proc. EUSIPCO-2008, 16th European Signal Processing Conference*, Lausanne, Switzerland, Aug. 25–29, 2008. (p. 231)

[P30] V. Zarzoso and P. Comon, "Robust independent component analysis for blind source separation and extraction with application in electrocardiography," in *Proc. EMBC-2008, 30th Annual International Conference of the IEEE Engineering in Medicine and Biology Society*, Vancouver, BC, Canada, Aug. 20–24, 2008, pp. 3344–3347, invited.

[P31] P. Bonizzi, R. Phlypo, V. Zarzoso, and O. Meste, "The exploitation of spatial topographies for atrial signal extraction in atrial fibrillation ECGs," in *Proc. EMBC-2008, 30th Annual International Conference of the IEEE Engineering in Medicine and Biology Society*, Vancouver, BC, Canada, Aug. 20–24, 2008, pp. 1867–1870.

[P32] R. Phlypo, V. Zarzoso, P. Comon, and I. Lemahieu, "Cumulant matching for independent source extraction," in *Proc. EMBC-2008, 30th Annual International Conference of the IEEE Engineering in Medicine and Biology Society*, Vancouver, BC, Canada, Aug. 20–24, 2008, pp. 3340–3343.

[P33] R. Phlypo, V. Zarzoso, and I. Lemahieu, "Eigenvector analysis for separation of a spectrally concentrated source from a mixture," in *Proc. EMBC-2008, 30th Annual International Conference of the IEEE Engineering in Medicine and Biology Society*, Vancouver, BC, Canada, Aug. 20–24, 2008, pp. 1863–1866. (p. 237)

[P34] R. Phlypo, V. Zarzoso, and I. Lemahieu, "Exploiting independence measures in dual spaces with application to atrial f-wave extraction in the ECG," in *Proc. MEDSIP-2008, 4th International Conference on Advances in Medical, Signal and Information Processing*, Santa Margherita Ligure, Italy, July 14–16, 2008.

[P35] P. Bonizzi, O. Meste, and V. Zarzoso, "Atrio-ventricular junction behaviour during atrial fibrillation," in *Proc. Computers in Cardiology*, vol. 34, Durham, North Carolina, USA, Sep. 30–Oct. 3, 2007, pp. 561–564. (p. 241)

[P36] R. Phlypo, Y. D'Asseler, I. Lemahieu, and V. Zarzoso, "Extraction of the atrial activity from the ECG based on independent component analysis with prior knowledge of the source kurtosis signs," in *Proc. EMBC-2007, 29th Annual International Conference of the IEEE Engineering in Medicine and Biology Society*, Lyon, France, Aug. 23–26, 2007, pp. 6499–6502. (p. 245)

[P37] V. Zarzoso and P. Comon, "Comparative speed analysis of FastICA," in *Proc. ICA-2007, 7th International Conference on Independent Component Analysis and Signal Separation*, London, UK, Sept. 9–12, 2007, pp. 293–300.

[P38] R. Phlypo, V. Zarzoso, P. Comon, Y. D'Asseler, and I. Lemahieu, "Extraction of atrial activity from the ECG by spectrally constrained kurtosis sign based ICA," in *Proc. ICA-2007, 7th International Conference on Independent Component Analysis and Signal Separation*, London, UK, Sept. 9–12, 2007, pp. 641–648.

[P39] H. J. Pérez-Iglesias, A. Dapena, L. Castedo, and V. Zarzoso, "Blind channel identification for Alamouti's coding systems based on eigenvector decomposition," in *Proc. 13th European Wireless Conference*, Paris, France, Apr. 1–4 2007, invited.

[P40] V. Zarzoso and P. Comon, "Alphabet-based deflation for blind source extraction in underdetermined mixtures," in *Proc. ICA Research Network International Workshop*, Liverpool, UK, Sept. 18–19, 2006, pp. 21–24. (p. 249)

[P41] V. Zarzoso, P. Comon, and M. Kallel, "How fast is FastICA?" in *Proc. EUSIPCO-2006, XIV European Signal Processing Conference*, Florence, Italy, Sept. 4–8, 2006. (p. 253)

[P42] V. Zarzoso, L. Rota, and P. Comon, "Déflation parallèle avec des contrastes APF pour l'extraction aveugle de sources," in *Actes du 20ème Colloque GRETSI : Traitement du signal et des images*, vol. 2, Louvain-la-Neuve, Belgique, 6–9 sept. 2005, pp. 1069–1072.

[P43] V. Zarzoso and P. Comon, "Blind channel equalization with algebraic optimal step size," in *Proc. EUSIPCO-2005, XIII European Signal Processing Conference*, Antalya, Turkey, Sept. 4–8, 2005. (p. 259)

[P44] V. Zarzoso, J. J. Murillo-Fuentes, R. Boloix-Tortosa, and A. K. Nandi, "Independent component analysis with optimized pairwise processing," in *Proc. EUSIPCO-2005, XIII European Signal Processing Conference*, Antalya, Turkey, Sept. 4–8, 2005.

[P45] L. Rota, V. Zarzoso, and P. Comon, "Parallel deflation with alphabet-based criteria for blind source extraction," in *Proc. SSP-2005, IEEE Workshop on Statistical Signal Processing*, Bordeaux, France, July 17–20, 2005. (p. 263)

[P46] V. Zarzoso and P. Comon, "Semi-blind constant modulus equalization with optimal step size," in *Proc. ICASSP-2005, 30th International Conference on Acoustics, Speech and Signal Processing*, vol. III, Philadelphia, PA, Mar. 18–23, 2005, pp. 577–580. (p. 269)

[P47] V. Zarzoso and A. K. Nandi, "Improving MIMO channel equalization with independent component analysis," in *Proc. 6th IMA International Conference on Mathematics in Signal Processing*, Cirencester, UK, Dec. 14–16, 2004, pp. 223–226.

[P48] F. Castells, J. Igual, V. Zarzoso, J. J. Rieta, and J. Millet, "Exploiting spatiotemporal information for blind atrial activity extraction in atrial arrhythmias," in *Proc. ICA-2004, 5th International Conference on Independent Component Analysis and Blind Signal Separation*, Granada, Spain, Sept. 22–24, 2004, pp. 18–25.

[P49] J. J. Murillo-Fuentes, R. Boloix-Tortosa, S. Hornillo-Mellado, and V. Zarzoso, "Independent component analysis based on marginal entropy approximations," in *Proc. ISIAC-2004, 5th International Symposium on Intelligent Automation and Control*, Seville, Spain, June 28–July 1, 2004.

[P50] V. Zarzoso, "Exploiting independence for co-channel interference cancellation and symbol detection in multiuser digital communications," in *Proc. ISSPA-2003, 7th International Symposium on Signal Processing and its Applications*, Paris, France, July 1–4, 2003.

[P51] K. Kokkinakis, V. Zarzoso, and A. K. Nandi, "Blind separation of acoustic mixtures based on linear prediction analysis," in *Proc. ICA-2003, 4th International Symposium on Independent Component Analysis and Blind Signal Separation*, Nara, Japan, Apr. 1–4, 2003, pp. 343–348.

[P52] L. P. G. Sarperi, V. Zarzoso, and A. K. Nandi, "Blind equalization of fractionally-spaced channels," in *Proc. ICA-2003, 4th International Symposium on Independent Component Analysis and Blind Signal Separation*, Nara, Japan, Apr. 1–4, 2003, pp. 1035–1040.

[P53] V. Zarzoso, A. K. Nandi, J. Igual-García, and L. Vergara-Domínguez, "Blind identification and equalization of MIMO FIR channels based on subspace decomposition and independent component analysis," in *Proc. 2nd IMA International Conference on Mathematics in Communications*, Lancaster, UK, Dec. 16–18, 2002.

[P54] A. K. Nandi and V. Zarzoso, "Novel air interface solutions based on alternative system properties," in *Proc. Wireless World Research Forum, 7th Meeting*, vol. II, Eindhoven, The Netherlands, Dec. 3–4, 2002.

[P55] A. K. Nandi and V. Zarzoso, "On the use of statistical independence for blind equalization of wireless digital communication channels," in *Proc. Wireless World Research Forum, 7th Meeting*, vol. II, Eindhoven, The Netherlands, Dec. 3–4, 2002.

[P56] J. Millet-Roig, J. J. Rieta, V. Zarzoso, A. Cebrián, F. Castells, C. Sánchez, and R. García-Civera, "Surface-ECG atrial activity extraction via blind source separation: spectral validation," in *Proc. Computers in Cardiology*, vol. 29, Memphis, TN, Sept. 23–25, 2002, pp. 605–608. (p. 273)

[P57] J. J. Rieta, J. Millet-Roig, V. Zarzoso, F. Castells, C. Sánchez, R. García-Civera, and S. Morell, "Atrial fibrillation, atrial flutter and normal sinus rhythm discrimination by means of blind source separation and spectral parameters extraction," in *Proc. Computers in Cardiology*, vol. 29, Memphis, TN, Sept. 23–25, 2002, pp. 25–28.

[P58] Y. Feng, V. Zarzoso, and A. K. Nandi, "Application of blind signal separation to WDM optical transmission monitoring," in *Proc. EUSIPCO-2002, XI European Signal Processing Conference*, vol. III, Toulouse, France, Sept. 3–6, 2002, pp. 383–386.

[P59] Y. Feng, V. Zarzoso, and A. K. Nandi, "WDM monitoring using blind signal separation based on higher-order statistics," in *Proc. DSP-2002, 14th International Conference on Digital Signal Processing*, vol. I, Santorini, Greece, July 1–3, 2002, pp. 155–158.

[P60] V. Zarzoso, A. K. Nandi, J. I. García, and L. V. Domínguez, "Blind identification and equalization of MIMO FIR channels based on second-order statistics and blind source separation," in *Proc. DSP-2002, 14th International Conference on Digital Signal Processing*, vol. I, Santorini, Greece, July 1–3, 2002, pp. 135–138.

[P61] Y. Feng, V. Zarzoso, and A. K. Nandi, "WDM monitoring through blind signal separation," in *Proc. OFC-2002, Optical Fiber Communication Conference*, Anaheim, CA, Mar. 17–22, 2002, pp. 746–748.

[P62] V. Zarzoso and A. K. Nandi, "A general theory of closed-form estimators for blind source separation," in *Proc. ICA-2001, 3rd International Conference on Independent Component Analysis and Blind Signal Separation*, San Diego, CA, Dec. 9–12, 2001, pp. 25–30.

[P63] J. J. Rieta, J. Millet, V. Zarzoso, P. Misa, C. Sánchez, R. Ruiz, S. Morell, and R. García-Civera, "Extracción e identificación de la actividad auricular en episodios de fibrilación auricular mediante separación ciega de fuentes y análisis espectral," in *Actas CASEIB-2001, XIX Congreso Anual de la Sociedad Española de Ingeniería Biomédica*, Madrid, Spain, Nov. 29–30, 2001, pp. 185–188.

[P64] V. Zarzoso and A. K. Nandi, "Closed-form semi-blind separation of three sources from three real-valued instantaneous linear mixtures via quaternions," in *Proc. ISSPA-2001, 6th International Symposium on Signal Processing and its Applications*, vol. I, Kuala Lumpur, Malaysia, Aug. 13–16, 2001, pp. 1–4. (p. 277)

[P65] V. Zarzoso, F. Herrmann, and A. K. Nandi, "Weighted closed-form estimators (p. 281)

for blind source separation," in *Proc. SSP-2001, 11th IEEE Workshop on Statistical Signal Processing*, Singapore, Aug. 6–8, 2001, pp. 456–459.

[P66] V. Zarzoso and A. K. Nandi, "Blind source separation using closed-form estimators with optimal finite-sample performance," in *Proc. DERA/IEE Workshop on Intelligent Sensor Processing*, ser. no. 01/050, Birmingham, UK, Feb. 14, 2001, pp. 15/1–15/6.

[P67] J. J. Rieta, V. Zarzoso, J. Millet-Roig, R. García-Civera, and R. Ruiz-Granell, "Atrial activity extraction based on blind source separation as an alternative to QRST cancellation for atrial fibrillation analysis," in *Proc. Computers in Cardiology*, vol. 27, Boston, MA, Sept. 24–27, 2000, pp. 69–72.

Software package:

[P68] "RobustICA package," [Online].
Available: `http://www.i3s.unice.fr/~zarzoso/robustica.html`

Publications Related to PhD Research

Book chapter:

[P69] V. Zarzoso and A. K. Nandi, "Blind source separation," in *Blind Estimation Using Higher-Order Statistics*, A. K. Nandi, Ed. Boston, MA: Kluwer Academic Publishers, 1999, ch. 4, pp. 167–252.

Refereed journal papers:

[P70] V. Zarzoso and A. K. Nandi, "Closed-form estimators for blind separation of sources — part I: real mixtures," *Wireless Personal Communications*, vol. 21, no. 1, pp. 5–28, Apr. 2002.

[P71] V. Zarzoso and A. K. Nandi, "Closed-form estimators for blind separation of sources — part II: complex mixtures," *Wireless Personal Communications*, vol. 21, no. 1, pp. 29–48, Apr. 2002.

[P72] V. Zarzoso and A. K. Nandi, "Noninvasive fetal electrocardiogram extraction: blind separation versus adaptive noise cancellation," *IEEE Transactions on Biomedical Engineering*, vol. 48, no. 1, pp. 12–18, Jan. 2001.

[P73] V. Zarzoso, A. K. Nandi, F. Herrmann, and J. Millet-Roig, "Combined estimation scheme for blind source separation with arbitrary source PDFs," *Electronics Letters*, vol. 37, no. 2, pp. 132–133, Jan. 2001.

[P74] V. Zarzoso and A. K. Nandi, "Adaptive blind source separation for virtually any source probability density function," *IEEE Transactions on Signal Processing*, vol. 48, no. 2, pp. 477–488, Feb. 2000.

[P75] V. Zarzoso and A. K. Nandi, "Blind separation of independent sources for virtually any source probability density function," *IEEE Transactions on Signal Processing*, vol. 47, no. 9, pp. 2419–2432, Sept. 1999.

[P76] V. Zarzoso and A. K. Nandi, "Modelling signals of arbitrary kurtosis for testing BSS methods," *Electronics Letters*, vol. 34, no. 1, pp. 29–30, Jan. 1998, (Errata: vol. 34, no. 7, Apr. 1998, p. 703).

[P77] V. Zarzoso, A. K. Nandi, and E. Bacharakis, "Maternal and foetal ECG separation using blind source separation methods," *IMA Journal of Mathematics Applied in Medicine & Biology*, vol. 14, no. 3, pp. 207–225, 1997.

[P78] A. K. Nandi and V. Zarzoso, "Fourth-order cumulant based blind source separation," *IEEE Signal Processing Letters*, vol. 3, no. 12, pp. 312–314, Dec. 1996.

Conference papers:

[P79] V. Zarzoso, J. Millet-Roig, and A. K. Nandi, "Fetal ECG extraction from maternal skin electrodes using blind source separation and adaptive noise cancellation techniques," in *Proc. Computers in Cardiology*, vol. 27, Boston, MA, Sept. 24–27, 2000, pp. 431–434.

[P80] V. Zarzoso and A. K. Nandi, "Unified formulation of closed-form estimators for blind source separation in complex instantaneous linear mixtures," in *Proc. EUSIPCO-2000, X European Signal Processing Conference*, vol. I, Tampere, Finland, Sept. 5–8, 2000, pp. 597–600.

[P81] V. Zarzoso and A. K. Nandi, "Unified formulation of closed-form estimators for blind source separation in real instantaneous linear mixtures," in *Proc. ICASSP-2000, 25th International Conference on Acoustics, Speech and Signal Processing*, vol. V, Istanbul, Turkey, June 5–9, 2000, pp. 3160–3163.

[P82] V. Zarzoso and A. K. Nandi, "Comparison between blind separation and adaptive noise cancellation techniques for fetal electrocardiogram extraction," in *Proc. IEE Colloquium on Medical Applications of Signal Processing*, ser. no. 107, Savoy Place, London, UK, Oct. 6, 1999, pp. 1/1–1/6.

[P83] V. Zarzoso and A. K. Nandi, "Blind source separation without optimization criteria?" in *Proc. ICASSP-99, 24th International Conference on Acoustics, Speech and Signal Processing*, vol. III, Phoenix, AZ, Mar. 15–19, 1999, pp. 1453–1456.

[P84] V. Zarzoso and A. K. Nandi, "Source distribution independent adaptive blind signal separation," in *Proc. ICA-99, 1st International Workshop on Independent Component Analysis and Signal Separation*, Aussois, France, Jan. 11-15, 1999, pp. 65–70.

[P85] V. Zarzoso and A. K. Nandi, "Extracción del ECG fetal mediante técnicas de separación ciega de fuentes," in *Actas CASEIB-98, XVI Congreso Anual de la Sociedad Española de Ingeniería Biomédica*, Valencia, Spain, Sept. 21–23, 1998, pp. 89–92.

[P86] V. Zarzoso and A. K. Nandi, "Generalization of a maximum-likelihood approach to blind source separation," in *Proc. EUSIPCO-98, IX European Signal Processing Conference*, vol. IV, Rhodes, Greece, Sept. 8–11, 1998, pp. 2069–2072.

[P87] V. Zarzoso and A. K. Nandi, "The potential of decorrelation in blind separation of sources based on cumulants," in *Proc. ECSAP-97, 1st European Conference on Signal Analysis and Prediction*, Prague, Czech Republic, June 24–27, 1997, pp. 293–296.

[P88] A. K. Nandi and V. Zarzoso, "Foetal ECG separation," in *Proc. IEE Colloquium on the Use of Model Based Digital Signal Processing Techniques in the Analysis of Biomedical Signals*, Savoy Place, London, UK, Apr. 16, 1997, pp. 8/1–8/6.

[P89] E. Bacharakis, A. K. Nandi, and V. Zarzoso, "Foetal ECG extraction using blind source separation methods," in *Proc. EUSIPCO-96, VIII European Signal Processing Conference*, Trieste, Italy, Sept. 10–13, 1996, pp. 395–398.

PhD Thesis:

[P90] V. Zarzoso, "Closed-form higher-order estimators for blind separation of independent source signals in instantaneous linear mixtures," Ph.D. dissertation, The University of Liverpool, UK, Oct. 1999.

Selected Publications

Journal Papers

Conference Papers

Source Extraction by Maximizing the Variance in the Conditional Distribution Tails

Ronald Phlypo*, *Student Member, IEEE,* Vicente Zarzoso, *Member, IEEE* and Ignace Lemahieu, *Senior Member, IEEE*

***Abstract*—This work presents a method for signal extraction based on conditional second-order moments of the output of the extraction filter. The estimator of the filter is derived from an approximate maximum likelihood criterion conditioned on a presence indicator of the source of interest. The conditional moment is shown to be a contrast function under the conditions that (1) all cross-moments of the same order between the source signal of interest and the other source signals are null and (2) that the source of interest has the largest conditional moment among all sources. For the two-source two-observation case, this allows us to derive the theoretical recovery bounds of the contrast when the conditional cross-moment does not vanish. A comparison with empirical results confirms these bounds. Simulations show that the estimator is quite robust to additive Gaussian distributed noise. Also through simulations, we show that the error level induced by a rough approximation of the presence indicator shows a strong similarity with that of additive noise. The robustness, both with respect to noise and to inaccuracies in the prior information about the source presence, guarantees a wide applicability of the proposed method.**

***Index Terms*—Source Extraction, Estimation, Contrast Functions, Conditional Likelihood.**

I. Introduction

Signal extraction methods focus on the estimation of a specific source when only a linear combination of source signals is available on a sensor array. A classical approach to the estimation of a specific source from the observations is based on a complete separation of the observations into its sources, followed by a posterior selection of the source of interest. The first step is solved for with the class of Blind source separation (BSS) algorithms. Their aim is to recover source signals when only a mixture of them is observed on a sensor array. This implicitly involves the inversion of an estimate of the linear mixture. This inverse of the estimate applied to the observations then yields outputs that are estimates of the source signals.

In the past two decades, the topic of blind separation has received growing interest, specially since the introduction of the quite natural model of independent sources, which seems to be an appropriate model for communications and biomedical signal analysis, to give a few examples. BSS under the aforementioned model can be achieved by the tool of Independent Component Analysis (ICA) [1], [2]. The algorithms for ICA are based on the optimisation of a contrast function, imposing a measure for independence on the separator outputs. It has been shown that the optimisation of any a such measure based on the independence of the outputs is sufficient to solve the separation of the observations into the independent sources, up to the inherent ambiguities of scaling, source permutation (order) and phase [3]. Since these ambiguities are waveform preserving, they are generally admissible. However, the above divide-and-conquer strategy presents a significant computational overload for the estimation of a single component, especially when large datasets are considered.

Recently, specific contrast functions for source extraction have been proposed in literature, e.g., in [4], [5], and valuable objective functions are known to depend (implicitly) on the marginal negentropy of the extractor output. Theoretically, the extraction order of the sources can be fixed, based upon their stochastic properties [6], allowing for the more informative sources (higher negentropy) to be extracted first. However, when the source of interest is not the source with highest negentropy, the extraction has to be pursuit, estimating source by source until the source of interest has been found. To prevent having twice an estimate of the same source, the observation space is deflated by the current source space before a next source has to be estimated [7], [8]. Unfortunately, this iterative estimation-deflation scheme engenders a propagating error which accumulates over the iterations [7], [9]. Since the source of interest is not always the source with highest entropy, and since the extraction order of the sources can not always be fixed in practice, the source of interest accumulates an error in its estimate whenever it does not appear in the first extraction.

It is clear from the above that we can not resolve for the permutation ambiguity without adding some discriminating information about the source of interest - other than negentropy - into the source extraction objective function. However, the prior information used to discriminate our source of interest from the other sources, should be kept to a minimum if we want to keep the source extraction maximally blind. This is the aim of the class of constrained ICA (cICA) algorithms proposed in [10], [11]. cICA introduces a constraint on the solution space of the (approximated) negentropy objective function, by means of a penalising term, generally based on a maximally admissible distance measure between the output and a reference signal. In contrast to the solution obtained by minimising the squared error between the filter output and the reference signal (the basis to the Wiener filter [12]), the solution to cICA is the output that has maximal negentropy

R. Phlypo and I. Lemahieu are with MEDISIP/IBBT, UGent - Heymans Institute Block B, 185 De Pintelaan, 9000 Ghent, Belgium. E-mail: {ronald.phlypo,ignace.lemahieu}@ugent.be

V. Zarzoso is with UNSA/CNRS, Les Algorithmes - Euclide B, B.P. 121, 2000 Route des Lucioles, 06903 Sophia Antipolis Cedex, France. E-mail: zarzoso@i3s.unice.fr

among the solutions meeting the constraint on the distance measure. A closely related algorithm is BSS with a reference (BSSR) [13], based on the higher order dependencies between the output signal and a reference. The BSSR algorithm differs from the Wiener filter mainly in the distance measure used. Because higher order moments are considered, BSSR offers a better performance when the reference signal has relatively few non-zero values [13]. The Quadratic Higher Order Criteria (QHOC) [14], [15] can be considered as a generalisation of the BSSR approach. QHOC have been proven to be contrasts for source separation, but they have not been derived in a maximum likelihood sense, so that they do not inherit the estimation optimality of maximum likelihood estimators in the sense of Fisher's information. Since the reference signal is chosen arbitrary, there is no explicit control over the extractor output. The best one could do if a specific source of interest has to be estimated, is the use of the QHOC with an estimation-deflation scheme until the source of interest has been found. But this estimation-deflation scheme suffers from error propagation and accumulation as mentioned above.

The Method of Conditional Moments (MCM) has also been used for source separation [16], where a possible link with the theory of contrast functions has been evoked. In this paper we will show that the use of well-chosen conditional moments indeed results in a contrast function for source extraction. But contrary to the method of Xerri *et al.*, our method is not limited to symmetrical distributions, does handle the extraction of Gaussian sources and does not require a posteriori manipulations, such as correcting rotations for super Gaussian distributed sources. Remark also that the method in [16] does not envisage the estimation of a specific source, but focusses solely on the full separation problem. On the other hand, although the approach of conditional moments differs from that of reference based filtering, we will show that for certain well defined cases, the above algorithms, namely, BSSR, QHOC and Wiener filtering, can be related to the theory presented in this paper.

The paper begins with an introduction on the signal model and the notational conventions in Section II. We then provide the theoretical aspects of the framework and present our method in Section III. Section IV places the presented method in perspective with respect to some competing models and algorithms found in literature and we show that under certain conditions, some explicit or implicit relations exist between these methods and the proposed method. Because of their similarities, these algorithms and models will be used in comparison studies in Section V after the performance bounds and some properties/characteristics of our model have been examined. This will be followed by a discussion in Section VI to conclude with a summary in Section VII.

II. Signal Model and Notation

A. Notational Conventions

Scalar variables, column vectors and matrices are respectively given by lowercase lightface (u), lowercase boldface ($\mathbf{u}$) and uppercase boldface ($\mathbf{U}$) characters. Consistency of the notations then requires the j-th entry of $\mathbf{u}$ to be denoted by u_j and the j-th column of $\mathbf{U}$ by $\mathbf{u}_j$. The probability density function (pdf) associated to the random variable a will be denoted by p_a for continuous sample domains and P_a for discrete sample domains. The association is denoted as $a \sim p_a$ and $p_a(u) \equiv p(a = u)$. Realizations of random variables or vectors are respectively given as scalars or vectors with an (arbitrary) indexing to identify the samples, e.g., $\mathbf{u}[k]$ stands for a sample of $\mathbf{u}$, referenced to by the index k. Also, let constants be given as uppercase lightface characters (U), the set of real numbers as $\mathbb{R}$ and sets by calligraphic uppercase characters, such as $\mathcal{U}$, whose cardinal number is $\#(\mathcal{U})$. A set of K realisations from the random vector $\mathbf{u}$ (a population) is then defined as $\mathcal{U} = \{\mathbf{u}[k] \mid \mathbf{u} \sim p_{\mathbf{u}}, k = 1, 2 \dots K\}$ and will be referred to by the short-hand notation $\{\mathbf{u}\}_K$, although with some abuse of notation we will commonly drop K as well as the accolades.

Furthermore, the mathematical expectation of a function f with respect to $\mathbf{u}$ defined as $\int p_{\mathbf{u}}(\mathbf{x}) f(\mathbf{x})\, d\mathbf{x}$ will be denoted by $\mathbb{E}\{f(\mathbf{u})\}$. Finally, the transpose of a column vector $\mathbf{u}$ is written as $\mathbf{u}^T$.

B. Signal Model and Contrast Functions

In this work, we assume the generative linear model where an M-dimensional random observation vector $\mathbf{y}$ can be linked to the underlying N-dimensional random source vector $\mathbf{s}$, through the instantaneous linear relation

$$\mathbf{y} = \mathbf{A}\mathbf{s} \tag{1}$$

with $M \geq N$. Contrary to classical algorithms, we assume that s_j is independently distributed with respect to $\tilde{\mathbf{s}} = [s_1, s_2, \dots, s_{j-1}, s_{j+1}, \dots, s_N]^T$, while mutual dependencies may exist between the entries of $\tilde{\mathbf{s}}$. We further assume that all random variables are zero-mean, without loss of generality. We denote by $x = \mathbf{h}^T\mathbf{y}$ an output of the filter $\mathbf{h}$ acting on $\mathbf{y}$.

Our goal is to estimate s_j from the observations $\mathbf{y}$. An appropriate strategy is to use the notion of a contrast function for the extraction of s_j.

Definition 1: A function $\Psi(x)$ is a contrast function for the extraction of the source s_j from the observations under the model (1) if it fulfils the following three properties:

(P1) Scaling Invariance
$\Psi(x) = \Psi(\lambda x), \forall \lambda \in \mathbb{R}\backslash\{0\}$

(P2) Domination
$\Psi(s_j) \geq \Psi(\mathbf{g}^T\mathbf{s}), \forall \mathbf{g} \in \mathbb{R}^N$

(P3) Discrimination
$\Psi(s_j) = \Psi(\mathbf{g}^T\mathbf{s}) \Leftrightarrow \mathbf{g} = \boldsymbol{\lambda}_j$

where $\boldsymbol{\lambda}_j$ is the j-th column of a non-singular diagonal scaling matrix $\boldsymbol{\Lambda} \in \mathbb{R}^{N \times N}$.

It follows that, if $\Psi(x)$ is a contrast function for the extraction of s_j from the observations, we have that $\hat{\mathbf{h}} = \arg\max_{\mathbf{h}} \Psi(\mathbf{h}^T\mathbf{y})$ is an extraction filter and $x = \hat{\mathbf{h}}^T\mathbf{y} = \hat{s}_j$. We also observe that, by fixing the index j, no permutation ambiguity exists with the above definition of contrast functions for source extraction, contrary to the definition of contrast functions for source separation [2] and the previous definitions of contrasts functions for source extraction [4], [5], [15]. This follows from the fact that previous definitions of contrast

functions for source extraction are based on a source by source extraction scheme to solve the full separation problem and do not consecrate more importance to s_j than to any other source.

III. Methods

A. A Likelihood Based Contrast

If we start from the distribution of $\mathbf{s}$ and we suppose $M = N$ we obtain the expected likelihood of the observations $\mathbf{y}$ as

$$\mathcal{L}_{\text{BSS}}(\mathbf{A} \,|\, \mathbf{y}) = \int_{\mathbb{R}^N} p_{\mathbf{A}^{-1}\mathbf{y}}(\mathbf{u}) \log p_{\mathbf{s}}(\mathbf{u})\, d\mathbf{u} - \log[\det(\mathbf{A})]$$

where $\boldsymbol{\vartheta}_{\mathbf{s}}$ is a possible parametrisation of the source densities and $\mathbf{A}$ has been supposed non-singular. This is the maximum likelihood approach to BSS proposed in [17], [18]. By factorising $p_{\mathbf{s}|\vartheta_{\mathbf{s}}}$ as $p_{s_j|\boldsymbol{\vartheta}_{s_j}} p_{\tilde{\mathbf{s}}|\boldsymbol{\vartheta}_{\tilde{\mathbf{s}}}}$ and retaining only the terms depending on the j-th column of $\mathbf{H} = (\mathbf{A}^{-1})^T$, which we denote by $\mathbf{h}$, we obtain

$$\mathcal{L}_{\text{E}}(\mathbf{h} \,|\, \mathbf{y}) \propto \int_{\mathbb{R}} p_{\mathbf{h}^T\mathbf{y}}(u) \log p_{s_j}(u)\, du \tag{2}$$

where we have discarded the last term of $\mathcal{L}_{\text{BSS}}$, since $\log[\det(\mathbf{H})] = -\log[\det(\mathbf{A})]$ can be considered constant if we absorb any changes in $\det(\mathbf{H})$ due to $\mathbf{h}$ in the remaining columns of $\mathbf{H}$. If we want to consider the above likelihood function as a contrast function for the extraction of the source s_j, it should satisfy properties **(P1)-(P3)** of Def. 1, which is not straightforward. It is obvious from Eq. (2) that two sources s_i and s_j for which $p_{s_i} = p_{s_j}$ cannot be distinguished with the above likelihood function.

Our goal is to find some adaptation of the likelihood $\mathcal{L}_{\text{E}}(\mathbf{h}|\mathbf{y})$ such that it can be used as a contrast function for the extraction of s_j, but without having p_{s_j} (neither a parametrisation) at its disposition. In what follows, we illustrate first the basis of the conditional expected log-likelihood as a contrast function for source extraction under the general model (1). Since the maximisation of the proposed estimator will be shown to be combinatorial in nature, we next derive a practical algorithm based on conditional second-order statistics.

B. The Conditional Likelihood

We assume that we have a presence indicator $\mathbb{I}_{s_j}$ for s_j with respect to a threshold C, which is defined as

$$\begin{cases} \mathbb{I}_{s_j} & \text{if } |s_j/\sigma_{s_j}| \geq C \\ \overline{\mathbb{I}}_{s_j} & \text{otherwise} \end{cases}. \tag{3}$$

If we define furthermore $\mathbb{B} = \mathbb{R}\backslash(-C, C)$ and $\overline{\mathbb{B}} = (-C, C)$, then we may rewrite the log-likelihood of Eq. (2) conditioned on $\mathbb{I}_{s_j}$ as

$$\begin{aligned} \mathcal{L}_{\text{E}}(\mathbf{h} \,|\, \mathbf{y}, \mathbb{I}_{s_j}) \quad \propto \quad & \int_{\mathbb{B}} p_{x|\mathbb{I}_{s_j}}(u) \log p_{s_j|\mathbb{I}_{s_j}}(u)\, du \\ & + \int_{\overline{\mathbb{B}}} p_{x|\mathbb{I}_{s_j}}(u) \log p_{s_j|\mathbb{I}_{s_j}}(u)\, du \end{aligned} \tag{4}$$

With the definition $P(\mathbb{I}_{s_j}) = \int_{\mathbb{B}} p_{s_j}(u)\, du$, we have

$$p_{s_j|\mathbb{I}_{s_j}}(u) = \begin{cases} p_{s_j}(u)/P(\mathbb{I}_{s_j}), & \forall u \in \mathbb{B} \\ 0, & \forall u \in \overline{\mathbb{B}} \end{cases}$$

Let us admit the commonly accepted definition $0 \log 0 \triangleq 0$. The conditional log-likelihood of Eq. (4) is heavily penalised by the term $\int_{\overline{\mathbb{B}}} p_{x|\mathbb{I}_{s_j}}(u) \log p_{s_j|\mathbb{I}_{s_j}}(u)\, du$, which is 0 if and only if $\mathbf{h}$ is such that $p_{x|\mathbb{I}_{s_j}}(u) = 0, \forall u \in \overline{\mathbb{B}}$.

Proposition 1: $\mathcal{L}(x) = \mathcal{L}_{\text{E}}(\mathbf{h} \,|\, \mathbf{y}, \mathbb{I}_{s_j})$ is a contrast for the source model (1) and this for any $C > 0$.

For a proof, we refer the reader to the appendix.

We can follow an analogous reasoning for the conditional log-likelihood $\mathcal{L}_{\text{C}}(\mathbf{h} \,|\, \mathbf{y}, \overline{\mathbb{I}}_{s_j})$, from which we see that our goal is to obtain $p_{x|\overline{\mathbb{I}}_{s_j}}(u) = 0, \forall u \in \mathbb{B}$.

Since $\mathcal{L}(x)$ is a contrast under the above condition, $\hat{\mathbf{h}}$ (and thus $\hat{s}_j$) can be found through its maximisation. However, the heavy penalisation term makes the solution not tractable and the maximisation of $\mathcal{L}(x)$ is equivalent to an exhaustive search over all possible filters $\mathbf{h}$. This is an NP hard problem.

C. Relaxation of the Conditional Likelihood Function

We have seen that a numerical optimisation of the conditional log-likelihood in Eq. (4) is NP hard. In this paragraph we try to relax the condition $p_{x|\mathbb{I}_{s_j}}(u) = 0, \forall u \in \overline{\mathbb{B}}$ such that a numerically tractable solution exists. Consider the following relaxation:

$$\min_{\mathbf{h}} \int_{\overline{\mathbb{B}}} p_{x|\mathbb{I}_{s_j}}(u) \gamma(u)\, du \tag{5}$$

where $\gamma(u)$ is any positive function. It is straightforward that $p_{x|\mathbb{I}_{s_j}}(u) = 0, \forall u \in \overline{\mathbb{B}} \Rightarrow \int_{\overline{\mathbb{B}}} p_{x|\mathbb{I}_{s_j}}(u)\gamma(u) = 0$. The inverse holds equally true for all (general) distributions (proof in appendix). We thus have that $\min_{\mathbf{h}} \int_{\overline{\mathbb{B}}} p_{x|\mathbb{I}_{s_j}}(u)\gamma(u)\, du = 0$, which is equivalent to the minimisation of $p_{x|\mathbb{I}_{s_j}}$. However, the above minimisation remains NP hard due to the integration over the posterior $\overline{\mathbb{B}}$.

To make the minimisation in Eq. (5) numerically tractable, we take $\gamma(u) = u^2$ as a possible weighting function. The minimisation reads

$$\min_{\mathbf{h}} \int_{\overline{\mathbb{B}}} p_{x|\mathbb{I}_{s_j}}(u) u^2\, du$$

and would then intuitively be equivalent to a maximisation problem

$$\max_{\mathbf{h}} \frac{\int_{\mathbb{R}} p_{x|\mathbb{I}_{s_j}}(u) u^2\, du}{\sigma_x^2} \tag{6}$$

where we used $\sigma_x^2 = \int_{\mathbb{R}} p_x(u) u^2\, du$ in the denominator to satisfy the scale invariance **(P1)**. The equivalence can be seen from the equality

$$\frac{\int_{\mathbb{R}} p_{x|\mathbb{I}_{s_j}}(u) u^2\, du}{\sigma_x^2} = \frac{\int_{\mathbb{B}} p_{x|\mathbb{I}_{s_j}}(u) u^2\, du + \int_{\overline{\mathbb{B}}} p_{x|\mathbb{I}_{s_j}}(u) u^2\, du}{\sigma_x^2}$$

where $\int_{\mathbb{B}} p_{x|\mathbb{I}_{s_j}}(u) u^2\, du$ dominates the nominator due to the chosen weighting function. Maximising the former means that the probability mass of $p_{x|\mathbb{I}_{s_j}}(u)$ would shift towards large values of x ($|x| \gg C$, bounded by the variance normalisation), which can be regarded as a minimisation of $p_{x|\mathbb{I}_{s_j}}(u), \forall u \in \overline{B}$, as required.

D. A Contrast with an Algebraic Optimum

The maximisation in Eq. (6) is thus equivalent to the maximisation of $\Psi(x) = \mathbb{E}_{s_j}\{x^2\}/\mathbb{E}\{x^2\}$, with $\mathbb{E}_{s_j}\{x^2\} = \int_{\mathbb{R}} p_{x|\mathbb{I}_{s_j}}(u)u^2\,du$. Introducing the shorthand notations $\Phi_{\mathbf{u}}^{s_j} = \mathbb{E}_{s_j}\{\mathbf{u}\mathbf{u}^T\}$ and $\Phi_{\mathbf{u}} = \mathbb{E}\{\mathbf{u}\mathbf{u}^T\}$, we write

$$\Psi(x) = \frac{\Phi_x^{s_j}}{\Phi_x} = \frac{\mathbf{h}^T\Phi_{\mathbf{y}}^{s_j}\mathbf{h}}{\mathbf{h}^T\Phi_{\mathbf{y}}\mathbf{h}} \ . \tag{7}$$

This is a generalised Rayleigh quotient, and its maximisation has as an algebraic solution; see e.g., [19, Sec. 8.7.1].

The maximisation of Eq. (7) can be done through the eigenvalue decomposition of $\Phi_{\mathbf{y}}^{-1}\Phi_{\mathbf{y}}^{s_j}$ (whenever $\Phi_{\mathbf{y}}$ is invertible) and choosing the major eigenvector/eigenvalue pair $\mathbf{q}, \lambda$ for which

$$\Phi_{\mathbf{y}}^{-1}\Phi_{\mathbf{y}}^{s_j}\mathbf{q} = \mathbf{q}\lambda \ . \tag{8}$$

Taking $\hat{\mathbf{h}} = \mathbf{q}$, we obtain $x = \hat{s}_j = \hat{\mathbf{h}}^T\mathbf{y}$ and $\Psi(x) = \lambda$.

We have already seen that the log-likelihood as defined in Eq. (4) is a contrast function for the extraction of a source s_j independently distributed with respect to $\tilde{\mathbf{s}}$. However, since $\Psi(x)$ in Eq. (7) is an approximation thereof, we need to investigate under what conditions the above approximate likelihood is indeed a contrast function.

Proposition 2:

$$\Psi(x) = \frac{\Phi_x^{s_j}}{\Phi_x} \text{ subject to } x = \mathbf{h}^T\mathbf{y} \tag{9}$$

is a contrast for the extraction of s_j under the following sufficient conditions $\forall i \neq j$:

(C1) $\mathbb{E}\{s_j s_i\} = 0$;
(C2) $\mathbb{E}_{s_j}\{s_j s_i\} = 0$;
(C3) $\mathbb{E}_{s_j}\{s_j^2\}/\mathbb{E}\{s_j^2\} > \mathbb{E}_{s_j}\{s_i^2\}/\mathbb{E}\{s_i^2\}$.

For the proof, we refer the reader to the appendix.

Remark that the statistical independence of s_j with respect to $\tilde{\mathbf{s}}$ is no longer a necessary condition, and that this condition has been relaxed to second-order independence (decorrelation) only. Since the conditioning on $|s_j| \geq C$ is used for the calculation of the conditional variance, we refer to our method as the method of *Maximum Variance in the Tails* of the conditional distribution (*MaxViT*).

Remark that we can formulate a slightly adapted version for the MaxViT contrast function as

$$\Psi'(x) = \frac{\mathbb{E}_{s_j}\{x^2\} - \mathbb{E}\{x^2\}}{\mathbb{E}\{x^2\}} = \Psi(x) - 1 \ .$$

This equation has the same maximiser $\hat{\mathbf{h}}$, but we now have that all eigenvalues - other than the major eigenvalue - equal 0 under model (1).

IV. Connection to Other Methods

While the starting point of our method is quite different than that of most of the methods that will be discussed below, certain connections exist with these methods. We insist on clarifying possible connections before the presentation of the results as to motivate our choice of algorithms used in later section V.

A. ICA

In most practical cases, the mutual independence of the sources is an acceptable prior, which makes ICA one of the most popular source separation algorithms nowadays [20], [21], [22], [2]. We prove next that the independence of the source s_j with respect to $\tilde{\mathbf{s}}$ is a sufficient condition to be recovered by the approximate maximum likelihood estimator of MaxViT, under the assumption that the conditional covariance can be calculated, i.e., the set $\mathcal{C}_{s_j}$ should be available. As such we show also that our assumptions are more general than the assumptions made to derive Eq. (4).

Since the independence of the entries already assures that (**C1**) and (**C2**) are met, we are only left to show the plausibility of (**C3**) under the independence assumption. Independence means that $p_{z|s_j}(u) = p_z(u), \forall z \neq f(s_j)$ and where $f(\cdot)$ can be any function. We thus have $\mathbb{E}_{s_j}\{s_i^2\} = \mathbb{E}\{s_i^2\}, \forall i \neq j$ and $\mathbb{E}_{s_j}\{s_j^2\} > \mathbb{E}\{s_i^2\}$, where the last inequality is proven in the appendix. In addition, the results obtained in the appendix, allow us to alter the condition in Eq. (5) to $\int_{(-C,C)} p_{s_j}(u)g(u)du \rightarrow 0$, which is a condition on the function $g(u) = \log\hat{p}_{s_j|\mathbb{I}_{s_j}}(u)$, but now directly in relation to $p_{s_j}(u)$.

B. Reference-based Filtering

When a reference signal is available for the extraction of a source, one can use extraction filters such as obtained, amongst others, via the optimal Wiener filter estimate [12] or via Blind Source Separation with a Reference (BSSR) [13]. In this section we show that by choosing the right reference for the Wiener filter or the BSSR method, we obtain the same result as with the approximate maximum likelihood estimator of MaxViT under certain conditions.

Consider first the Wiener filter $\mathbf{h}_W = \mathbb{E}\{\mathbf{y}\mathbf{y}^T\}^{-1}\mathbb{E}\{\mathbf{y}r\}$, where r is the reference signal. Taking as a reference $r = s_j$, we have $\mathbf{h}_W = \Phi_{\mathbf{y}}^{-1}\mathbb{E}\{\mathbf{y}s_j\}$ and the variance of the output $x_W = \mathbf{h}_W^T\mathbf{y}$ is

$$\begin{aligned}\Phi_{x_W} &= \mathbb{E}\{s_j\mathbf{y}^T\}\Phi_{\mathbf{y}}^{-1}\mathbb{E}\{\mathbf{y}s_j\} \\ &= \mathbb{E}\{s_j\mathbf{s}^T\}\mathbf{A}^T(\mathbf{A}\Phi_{\mathbf{s}}\mathbf{A}^T)^{-1}\mathbf{A}\mathbb{E}\{\mathbf{s}s_j\} \\ &= \mathbb{E}\{s_j^2\}^2[\Phi_{\mathbf{s}}^{-1}]_{jj} \ ,\end{aligned} \tag{10}$$

where the last equality follows from (**C1**), from which follows that $[\Phi_{\mathbf{s}}^{-1}]_{jj} = (\det\Phi_{\mathbf{s}})^{-1}(\det\Phi_{\tilde{\mathbf{s}}}) = (\det\Phi_{\tilde{s}})^{-1}[\Phi_{\mathbf{s}}]_{jj}^{-1}(\det\Phi_{\tilde{\mathbf{s}}}) = [\Phi_{\mathbf{s}}]_{jj}^{-1} = \mathbb{E}\{s_j^2\}^{-1}$. The conditional variance is analogously given by

$$\Phi_{x_W}^{s_j} = \mathbb{E}\{s_j^2\}^2[(\Phi_{\mathbf{s}}^{s_j})^{-1}]_{jj} \ , \tag{11}$$

where $[(\Phi_{\mathbf{s}}^{s_j})^{-1}]_{jj} = [(\Phi_{\mathbf{s}}^{s_j})]_{jj}^{-1} = \mathbb{E}_{s_j}\{s_j^2\}^{-1}$ if (**C2**) is fulfilled.

The value of the solution to the Wiener filter in the contrast function can be given by combining Eqs (10) and (11) and putting them into Eq. (7), yielding

$$\Psi(x_W) = \frac{\Phi_{x_W}^{s_j}}{\Phi_{x_W}} = \frac{\Phi_{s_j}}{\Phi_{s_j}^{s_j}} \leq 1 \leq \frac{\Phi_{s_j}^{s_j}}{\Phi_{s_j}} \ , \tag{12}$$

with equalities if and only if $\Phi_{s_j} = \Phi_{s_j}^{s_j}$, or $P_{s_j}(\overline{\mathcal{B}}) = 0$. Unfortunately, we then no longer have the dominance of the

source s_j in the contrast function since all sources now satisfy $\Phi_{s_i}^{s_j}/\Phi_{s_i} = 1$.

For the BSSR method we have the more general objective function (defined for real variables):

$$\phi_{BSSR}^{(p)}(x) = \frac{1}{2n}\mathbb{E}\{(xr)^{2p}\} - \frac{\lambda}{2}(\mathbf{h}^T\mathbf{h} - 1) \ , \qquad (13)$$

where r is an *a priori* defined reference signal and $2p$ the order. An iterative fixed-point algorithm has been proposed in [13] to maximise this function, but, algebraic solutions exist at orders $p = 1/2$ and $p = 1$. At $p = 1/2$ the BSSR cost function accepts the closed-form solution $\hat{\mathbf{h}} = \mathbb{E}\{\mathbf{y}r\}$ and is equivalent to the optimal Wiener filter associated with reference signal r if the observations $\mathbf{y}$ are spatially white ($\Phi_{\mathbf{y}} = \mathbf{I}_m$). At order $p = 1$, the cost function can also be solved algebraically; indeed, $\hat{\mathbf{h}}$ is then given by the dominant eigenvector of the reference-weighted covariance matrix $\mathbb{E}\{\mathbf{y}\mathbf{y}^T r^2\}$.

A similar approach can be found in the QHOC as developed in [14], [15], where we have in the real, instantaneous case

$$\Psi_{QHOC}^{(R)}(x, \mathbf{r}) = \kappa_{R,\mathbf{r}}\{x\}, \text{ subject to } \Phi_x = 1 \ , \qquad (14)$$

with $\kappa_{R,\mathbf{r}}\{x\} = \text{Cum}\{x, x, r_1, r_2 \ldots r_{R-2}\}$. In practice, most often a single reference signal r is used, which is arbitrarily chosen (e.g., as an arbitrary linear combination of the observations). By the multilinearity of cumulants, one may then write $\kappa_{R,r}\{x\} = \mathbf{h}^T\Phi_{\mathbf{y},r}\mathbf{h}$, where $(\Phi_{\mathbf{y},r})_{i,j} = \text{Cum}\{y_i, y_j, \underbrace{r, r \ldots r}_{\times(R-2)}\}$. Alternating between updates of $\mathbf{h} = \arg\max_{\mathbf{h}} \mathbf{h}^T\Phi_{\mathbf{y},r}\mathbf{h}$ (subjected to $\mathbf{h}^T\Phi_{\mathbf{y}}\mathbf{h} = 1$) and recalculating the reference as $r = \mathbf{h}^T\mathbf{y}$, one then obtains a source estimate $\hat{s}_i$. Contrary to the BSSR method, QHOC aim at estimating the full separation and thus no source order has been fixed for the successive extractions (with possible deflation). Evidently, the reference could be chosen with respect to a specific source, similarly to the BSSR method. If the observations are prewhitened, the BSSR objective [Eq. (13)] for $p = 1$ and the QHOC objective [Eq. (14)] for $R = 2$ are then essentially the same.

The BSSR and QHOC methods are closely related in the sense that their objective differs mainly in their choice of reference. Moreover, the BSSR at order $2p = 2$ and QHOC method for any pair order R are similar to the MaxViT method when using the following specific reference

$$r[k] = \begin{cases} \text{sign}(s_j[k]) & \text{if } |s_j[k]| \geq C \\ 0 & \text{otherwise} \end{cases} \ , \qquad (15)$$

and for a spatially white observation vector $\mathbf{y}$. The latter is not explicitly required by MaxViT, which renders MaxViT less susceptible to the performance bounds imposed by a prewhitening stage [23], [9]. In addition, the choice of a conditional probability (resulting in the reference signal of Eq. (15) for QHOC or BSSR) guarantees an algebraic solution for MaxViT and no cumulating errors due to successive estimation-deflation procedures as with a random reference in [15].

It should also be noted that the BSSR method in [13] has been proposed with a specific application in mind, and little research has been done on its convergence and robustness. In this paper, we make use of the connection between BSSR and our method to show the robustness with respect to arbitrary binary references, which we prefer to address as a conditional indicator function. Remark that, whenever we will refer to BSSR in what follows, we refer explicitly to the original iterative implementation as can be found in [13].

C. ICA with a reference

As we have shown above (Section IV-A), the independent source model, which is the basis for ICA, is also a suitable MaxViT model under a not too restrictive condition (i.e., the conditions (**C1**)-(**C3**) are generally satisfied under the ICA model). Within this perspective, MaxViT may be seen as a direct competitor to cICA [11]. While the methods of cICA are generally based on an augmented Lagrangian in the framework of constrained programming using iterative updating methods, the contrast function in MaxViT offers a closed-form estimator for the extraction filter. Contrary to the family of cICA algorithms, we can now guarantee a global optimiser in low-noise conditions. Moreover, in the noiseless case and for independent sources, MaxViT will provide a filter estimate from which we can obtain the independent source, under the condition that we can approximate the conditional set $\mathcal{C}_{s_j}$ sufficiently well. A simple indicator function $\mathbb{I}_{s_j}$, can be used to construct a simple binary reference signal as in (15) (see also [24], [11]), where we have now shown its relation to a maximum likelihood approach. It should be investigated whether another choice for the conditional probability function $\hat{p}_{s_j|\mathbb{I}_{s_j}}$ with an appropriate updating rule would yield better results.

D. Sparse Decompositions

Also interesting is the similarity between our method and the sparsity pursuit methods (e.g. [25]), where the objective is to have a low approximation error of the observations (with respect to some measure, generally ℓ_2) with as few representative basis functions as possible. This is similar to the objective in our MaxViT model, aiming at minimising the approximation error (through a maximisation of the explained variance of the observations) on a limited amount of samples (the basis functions being Dirac functions). While MaxViT needs a prior knowledge about the presence of s_j, which is reflected in the condition $\mathbb{I}_{s_j}$, sparsity pursuit for multidimensional signals aims at searching a combination of a minimum number of dictionary elements to approximate the observations [26], when the mixing matrix $\mathbf{A}$ is supposed known. Combining these two strategies would give a weighted conditional covariance $\mathbb{E}_{s_j}\{\mathbf{y}\mathbf{y}^T\} = \mathbb{E}\{\mathbf{y}\mathbf{D}(\mathbb{I}_{s_j})\mathbf{D}(\mathbb{I}_{s_j})^T\mathbf{y}^T\}$, where $\mathbf{D}$ can be any linear basis and $\mathbb{I}_{s_j}$ acts as an indicator function for those elements in that dictionary on which s_j has a significant presence. Maximising the MaxViT contrast under a maximum sparsity constraint could then be done jointly over $\mathbf{h}$ and $\mathbb{I}_{s_j}$, but this problem will be tackled in future research.

Within the framework of sparse component analysis, MaxViT - calculating the variance dominance on a subset of the observations - can also be seen in the category of algorithms based on piecewise linear source separation [26],

[27]. The latter has the basic assumption that outside the support of the source of interest, its amplitude is zero or is captured in the background noise with a predefined (low) noise variance (our σ_ε). MaxViT has an equivalent assumption on the source presence, as may be seen from Section III-C.

E. The Method of Conditional Moments

At first glance, our approach seems similar to the MCM of [16]. MCM is based on a generalised eigenvalue decomposition of second order moments conditioned on the halfspace $x_i > 0$ of the current estimates $\mathbf{x} = \mathbf{H}^T\mathbf{y}$. As is the case for QHOC, an estimate is obtained by iterating over alternating updates, this time between $\mathbf{H} = \arg\max \mathbf{H}^T(\Phi_{\mathbf{x}}^{x_i})^{-1}\tilde{\Phi}_{\mathbf{x}}^{x_i}\mathbf{H}$ and $\mathbf{x} \leftarrow \mathbf{H}^T\mathbf{x}$, with $\Phi_{\mathbf{x}}^{x_i} = \mathbb{E}\{\mathbf{x}\mathbf{x}^T \mid x_i > 0\}$ and $\tilde{\Phi}_{\mathbf{x}}^{x_i} = \Phi_{\mathbf{x}}^{x_i} - \mathbb{E}\{\mathbf{x} \mid x_i > 0\}\mathbb{E}\{\mathbf{x} \mid x_i > 0\}^T$. As opposed to MCM, our method does not limit itself to Laplace or Uniformly distributed sources, and does not impose a correction on the estimation of Laplace (super Gaussian) sources. In addition, contrary to MCM, MaxViT does not limit its application to symmetrically distributed sources and can deal with Gaussian sources. Of course, these advantages go at the expense of the extra additional information of the presence indicator $\mathbb{I}_{s_j}$.

In this paper we have also shown that methods based on conditional moments are derived from a conditional likelihood function and that a specific class of these conditional likelihood functions for which $\int_{(-C,C)} p_{s_j}(u) \log \hat{p}_{s_j|\mathbb{I}_{s_j}}(u)du \to 0$ (see Sec. IV-A) result in a contrast under model (1).

V. Performance Analysis

A. Theoretical Estimation Bounds of MaxViT

In this section we establish the error bounds on the estimation of s_j in the model $x = \mathbf{h}^T\mathbf{A}\mathbf{s} = \mathbf{g}^T\mathbf{s}$. This error can be measured through the interference to signal ratio (ISR) defined as

$$\text{ISR} = \frac{\sum_{i\neq j}|g_i|^2}{(n-1)|g_j|^2} \ , \tag{16}$$

which is a measure for the average interference, and takes the value zero if and only if the extraction filter is the j-th canonical vector.

The filter $\mathbf{g}$ is the product of the dominant generalised eigenvector $\mathbf{h}$ associated to $\mathbf{A}\Phi_{\mathbf{s}}^{s_j}\mathbf{A}^T/\mathbf{A}\Phi_{\mathbf{s}}\mathbf{A}^T$ and $\mathbf{A}$. Here, we only consider the bias in the estimate of $\mathbf{h}$ as a consequence of the non-vanishing conditional covariance between s_j and $s_i, i \neq j$. The ISR as a function of this covariance can be calculated for $\mathbf{s} \in \mathbb{R}^2$ as:

$$\text{ISR}(\rho,\delta) = \frac{\sqrt{\delta^2+|\rho|^2}-\delta}{\sqrt{\delta^2+|\rho|^2}+\delta} \overset{\delta\neq 0}{=} \frac{\sqrt{1+(|\rho|/\delta)^2}-1}{\sqrt{1+(|\rho|/\delta)^2}+1} \ , \tag{17}$$

where

$$\delta = \left(\Phi_{s_j}^{s_j} - \Phi_{s_i}^{s_j}\right)/2 \tag{18}$$

$$\rho = \mathbb{E}_{s_j}\{s_j s_i\} \ . \tag{19}$$

The calculations for the value of ISR are given in appendices D and E and the relation between $|\rho|/\delta$ and the theoretical ISR value is given in Fig. 1. We can give an impression of the accuracy of this theoretical measure by comparing it with the obtained ISR as obtained through the relation of Eq. (16)). We did this for 1000 Monte Carlo realisations of 2 i.i.d. (respectively Laplacian, Gaussian and uniformly distributed) unit variance, zero-mean source signals of $K = 1000$ samples each observed through an orthonormal mixing matrix $\mathbf{A}$. With this simulations, we obtained a maximum absolute error of 9.4410^{-16} confirming the accuracy of Eq. (17).

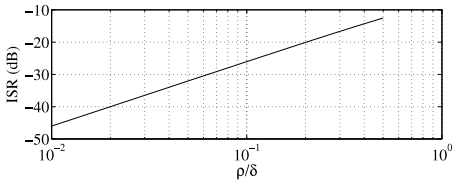

Fig. 1. The theoretical bounds for the value of ISR as a function of the conditional covariance ρ and the conditional variance domination δ.

From both Eq. (17) and Fig. 1, we see that $x = \hat{s}_j \approx s_j$ if $|\rho| \ll \delta$ and a good estimation of the source s_j is guaranteed even if $|\rho|$ tends to δ (we still have a theoretical -7.7dB if $|\rho| = \delta$), which is a reasonable assumption in many practical situations. It can be seen that the smaller the discrimination in the conditional variance becomes in (**C3**), the more stringent the condition (**C2**) on $|\rho|$ becomes (and thus automatically also (**C1**)). Under the condition $|\rho| = 0$, we have already shown that Eq. (9) is a contrast for the separation of s_j from a mixture in Section III-D and, indeed, we obtain ISR$= 0$ from Eq. (17), as long as $\delta \neq 0$ (for $\delta = 0$, we have that ISR=1, since no discrimination is possible with the current contrast).

Table I gives the mean fraction of $|\rho|/\delta$ for three different distributions (Uniform, Laplacian and Normal) and for different values of C. Note that the number of sample indices in the set $\mathcal{C}_{s_j}$ differs according to the chosen distribution, and consequently has a considerable influence on the variance of the statistics $\hat{\mathbb{E}}_{s_j}\{f(x)\} = \sum_{k\in\mathcal{C}_{s_j}} f(x[k])/\#\mathcal{C}_{s_j}$. Therefore, we decided to use K samples on a basis of K_b, where $K = K_b/P_{s_j}(\mathcal{B})$. This brings the number of sample indices in $\mathcal{C}_{s_j}$ from which $\mathbb{E}_{s_j}\{f(u)\}$ is estimated to an almost equal number, independent of the distribution used. The ISR or the fraction $|\rho|/\delta$ can now directly be compared for a given K_b.

TABLE I
THE FRACTION $|\hat{\rho}|/\hat{\delta}$ FOR DIFFERENT DISTRIBUTIONS AND DIFFERENT VALUES FOR c BASED ON UNIT VARIANCE, ZERO MEAN I.I.D. REALISATIONS AND A BASIS OF $K_b = 10^3$ SAMPLES (SEE TEXT). THE VALUES ARE GIVEN AS MEAN $\pm$ STANDARD DEVIATION.

	Uniform	Normal	Laplace
$C = 1$	0.12 ± 0.09	0.09 ± 0.07	0.07 ± 0.06
$C = \sqrt{2}$	0.12 ± 0.10	0.09 ± 0.07	0.07 ± 0.06
$C = \sqrt{3}$	N/A[1]	0.10 ± 0.06	0.09 ± 0.06

The above Eq. (17) is a compact expression for the case $\mathbf{s} \in \mathbb{R}^2$, but for $\mathbf{s} \in \mathbb{R}^n, n > 2$ the calculations become more cumbersome. For $n = 3$ we turn to simulations on a synthetic dataset, for which we give the results below.

[1]For $c = \sqrt{3}$, we have $P_{s_j}(\mathcal{B}) = 0$ and our method is not applicable (N/A).

B. Experimental Performance Comparison

To compare the performance of our algorithm with respect to the related algorithms discussed in Section IV, a dataset has been created based on realisations of a source vector $\mathbf{s} \in \mathbb{R}^3$, for which we have $K = 1000$ realizations. The entries in $\{\mathbf{s}\}_{10^3}$ are samples from an i.i.d. unit-variance, zero-mean Laplacian distribution. The so-obtained source signals are then transformed through a unitary matrix $\mathbf{A}$ to the observation space $\mathbf{y} = \mathbf{A}\mathbf{s}$. Without further specifications, we have set $C = 1$ to determine the conditional probabilities and let s_1 be the source of interest.

The algorithms of the Wiener filter and our MaxViT algorithm both have a closed form solution, whilst the ICA algorithm (COM2 [2], without pre-whitening, since we have a unitary mixture) and the BSSR algorithm (taken at higher order $2p = 4$ for the evident reason of avoiding similarity with our MaxViT contrast, see section IV-B) are iterative. The COM2 algorithm has been run over the classical $\lfloor 1 + \sqrt{n} \rfloor$ sweeps over all the signal pairs, which guarantees (although heuristically) its convergence. The BSSR algorithm has either been run until convergence or over 10^3 iterations, whatever has been reached first. Since COM2 provides a separation rather than an extraction, we only retained the output x_i that had the highest correlation with s_1, the source of interest.

Both BSSR and the Wiener filter can be used with different reference signals. To restrict the wide scope of possibilities, we retain only those references that have a close resemblance with the conditional used for MaxViT, i.e., through the indicator function $\mathbb{I}_{s_1}$. The so obtained reference signal r is then defined as

$$r[k] = \begin{cases} s_j[k] & \text{if } |s_j[k]| > C \\ 0 & \text{otherwise} \end{cases} . \qquad (20)$$

Derivations of this reference function defined as $b = \text{sign}(r)$ [see also Eq. (15)] or $|b| = |\text{sign}(r)|$ are also used, where we define $\text{sign}(0) = 0$. Similar reference functions have also been proposed, e.g., in [24], [11]. All experiments are evaluated over 1000 Monte Carlo realisations of $\{\mathbf{s}\}_{10^3}$ and $\mathbf{A}$.

In Table II, we show the mean ISR value as defined in Eq. (16). The ISR is a measure that quantitatively measures the estimation of the filter $\mathbf{h}$, through an evaluation of $\mathbf{g} = \mathbf{A}^T\mathbf{h}$. Contrary to measures such as Pearson's correlation coefficient, it is an asymptotic evaluation of the interference to signal ratio, and does not make any assumption on the distribution of the error. Table II is organised in such a way, that, reading it from left to right, the information content in the reference signal decreases. The values between brackets are obtained after a rotation of the i.i.d. vector $\mathbf{s}$ by a unitary matrix. This results in decorrelated entries of $\mathbf{s}$ that are no longer guaranteed independent.

TABLE II
ISR AS A MEASURE FOR THE ASYMPTOTIC ACCURACY OF THE SOURCE ESTIMATE FROM A SYNTHETIC DATASET OF 3 I.I.D. LAPLACIAN SOURCES OF $K = 10^3$ SAMPLES FOR DIFFERENT ALGORITHMS AND DIFFERENT INFORMATION FEEDS. VALUES BETWEEN BRACKETS ARE OBTAINED FROM UNCORRELATED SOURCES WHICH ARE NOT INDEPENDENT.

	r	b	$\lvert b\rvert$	no ref.
MaxViT(1)	.	.	-36.01	.
	.	.	(-28.62)	.
MaxViT($\sqrt{3}$)	.	.	-34.19	.
	.	.	(-28.58)	.
Wiener	-36.61	-35.80	17.31	.
	(-29.37)	(-28.91)	(17.08)	.
BSSR$_{p=2}$	-26.13	-31.91	-31.91	.
	(-25.37)	(-29.30)	(-29.30)	.
COM2	.	.	.	-33.80
	.	.	.	(-24.26)

C. Influence of Additive Noise

We start from the same observations and source signals as defined above. To discard the influence of the parameter quotient $|\rho|/\delta$ on the ISR - see Eq. (17) - we assure that we have $p_{s_i}(|u| > C \mid \mathbb{I}_{s_j}) = p_{s_j}(|u| > C \mid \mathbb{I}_{s_i}) = 0, \forall i \neq j$ by permuting the samples of $\{s_j\}_K$ appropriately. To test the performance of the algorithm under noisy conditions, centred Gaussian noise $\eta \sim \mathcal{N}(\mathbf{0}, \sigma_\eta^2 \mathbf{I}_3)$ has been added to the observations $\mathbf{y}$. Since the observations are standardized and the noise is isotropic, the signal to noise ratio (SNR) can be given by the simple expression SNR $= \sigma_\eta^{-2}$. The model reads $\mathbf{y} = \mathbf{A}\mathbf{s} + \eta$ and the estimate of s_j is $x = \mathbf{g}^T\mathbf{s} + \mathbf{g}^T\eta$.

The influence of the SNR on the performance parameter ISR is shown In Fig. 2. Since in the case of additive noise, an accurate estimate of the filter does not guarantee an accurate estimate of the source, we also give the value of $1 - |\hat{\rho}|$, with $\hat{\rho}$ the sample estimate of $\mathbb{E}\{xs_j\}/(\mathbb{E}\{x^2\}^{1/2}\mathbb{E}\{s_j^2\}^{1/2})$. This direct comparison between the source estimate x and the source s_1 can be found in Fig. 3. The comparison of MaxViT has been carried out with respect to the algorithms used in Table II, however, making a selection of reference signals which we judged most useful for comparison. This includes the performance of a Wiener filter and the BSSR method with an unsigned reference $|b|$, adding exactly the same amount of information as is used in MaxViT.

To complete the performance picture, we also add MaxViT with $c = \sqrt{3}$ for comparison. Note that in Fig. 3, the Wiener solution has all of its performance values out of the range used for plotting (ISR($Wiener(|b|)$)$\in [10, 50]$dB).

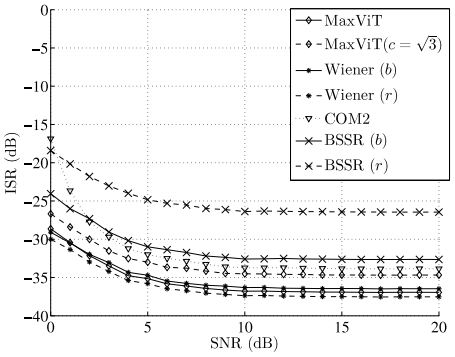

Fig. 2. The source interference ISR (dB) as a function of the signal to noise ratio SNR (dB). The noise is normally distributed additive noise (see text for details). The method is compared with a classical ICA method, the BSSR solution and the solution by a Wiener filter.

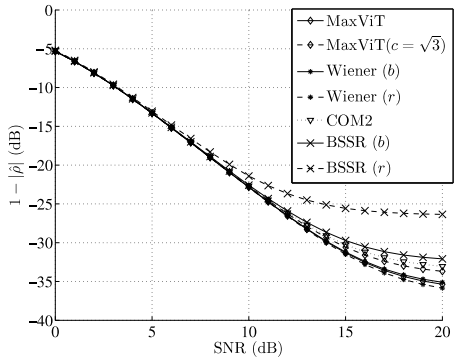

Fig. 3. The 'correlation' $1 - \hat{\rho}(x, s_j)$ (dB) as a function of the signal to noise ratio SNR (dB). The noise is normally distributed zero-mean additive isotropic noise (see text for details). The method is compared with a classical ICA method, the BSSR solution and the solution by a Wiener filter.

D. Robustness with Respect to the Conditional Set

Assume we no longer have $p(\cdot \mid |s_j| > C\sigma_{s_j})$ but rather $p(\cdot \mid |s_j| + \eta > C\sigma_{s_j})$, where η is a nuisance parameter expressing the uncertainty we have about our initial condition. As before, let us denote by $\mathcal{C}_{s_j} = \{k \mid |s_j[k]| > C\sigma_{s_j}\}$ the conditional set of sample indices. We can now suppose that the condition $|s_j| + \eta > C\sigma_{s_j}$ gives rise to an indicator $\hat{\mathbb{I}}_{s_j}$ which results in a mismatch in the conditional set $\mathcal{C}_{s_j}$. In what follows we experimentally analyse the robustness of the algorithm with respect to a mismatch of the conditional set $\mathcal{C}_{s_j}$.

As above, we have $K = 1000$ realisations of three i.i.d. standardised Laplacian sources $\mathbf{s}$ observed in $\mathbf{y}$ through a unitary mixture $\mathbf{A}$. The samples of s_j have been permuted such that $\forall i \neq j, \mathcal{C}_{s_j} \bigcap (\bigcup_i \mathcal{C}_{s_i}) = \emptyset$ and thus the source s_j can be estimated since we have $\mathbb{E}\{s_i s_j\} \approx 0$, $\mathbb{E}_{s_j}\{s_i s_j\} \approx 0$ (i.i.d. variables) and $\Phi^{s_j}_{s_j}/\Phi_{s_j} > 1$ (see Sections IV-A and V-A). Remark that we artificially lowered the theoretical ISR estimation bound by permuting the samples and thus augmenting δ. Also, define the following sets of sample indices:

- $\mathcal{K} = \{k \mid k \in \mathbb{N}, 1 \leq k \leq K\}$
- $\overline{\mathcal{C}}_{s_i} = \mathcal{K} \backslash \mathcal{C}_{s_i}$
- $\mathcal{C}_{ne} = \bigcap_i \overline{\mathcal{C}}_{s_i}$
- $\mathcal{C}_{co,j} = (\bigcup_{i \neq j} \mathcal{C}_{s_i}) \backslash \mathcal{C}_{s_j}$

The latter two sets are respectively the neutral and the conflicting set with respect to s_j.

Consider also the following three set operations:

- $\mathcal{P}_2 = \text{Shrinkage}(\mathcal{P}_1, \alpha)$:
  $\mathcal{P}_2 \subseteq \mathcal{P}_1$ with $\#(\mathcal{P}_2) = (1 - \alpha) \times \#(\mathcal{P}_1)$
- $\mathcal{P}_3 = \text{Inflation}(\mathcal{P}_1, \mathcal{P}_2, \alpha)$:
  $\mathcal{P}_3 = \mathcal{P}_1 \cup \mathcal{Z}$ with $\#(\mathcal{P}_3) = (1+\alpha) \times \#(\mathcal{P}_1)$ and $\mathcal{Z} \subseteq \mathcal{P}_2$
- $\mathcal{P}_3 = \text{Interchange}(\mathcal{P}_1, \mathcal{P}_2, \alpha)$:
  $\mathcal{P}_3 = \text{Inflation}\left(\text{Shrinkage}(\mathcal{P}_1, \alpha), \mathcal{P}_2, \frac{\alpha}{1-\alpha}\right)$

where $\#$ is the cardinal number of the set and $0 \leq \alpha \leq 1$.

By applying set operations to $\mathcal{C}_{s_j}$, we obtain an estimate of the perturbation of the conditional probability $p(\cdot \mid |s_j| + \eta > C\sigma_{s_j})$ as has been explained above. The results of this perturbation study can be found in Fig. 4, where we present the results of the above defined set operations with $\mathcal{C}_{s_j}$ as the basis set. The set ($\mathcal{P}_2$) is chosen as $\mathcal{C}_{ne}$ or $\mathcal{C}_{co,j}$ for a neutral, respectively a conflicting operation with respect to s_j. The influence of the set perturbation is expressed in terms of the source interference ratio ISR (16).

The following scenarios can now be investigated to observe the behaviour in the most optimistic, a random or respectively the most pessimistic scenario:

- The smart set choice, see Fig. 4(c), has a shrinkage operator for which $\forall k_1 \in \mathcal{P}_2, k_2 \in \mathcal{P}_1 \backslash \mathcal{P}_2 : |s_j[k_1]| \geq |s_j[k_2]|$ and an inflation operator for which $\forall k_1 \in \mathcal{Z}, k_2 \in \mathcal{P}_2 \backslash \mathcal{Z} : |s_j[k_1]| \leq |s_j[k_2]|$;
- The random set choices, see Fig. 4(b), does not make any assumption about a possible order and apply the rules naïvely.
- The worst case scenario (wcs), see Fig. 4(a), has a shrinkage operator for which $\forall k_1 \in \mathcal{P}_2, k_2 \in \mathcal{P}_1 \backslash \mathcal{P}_2 : |s_j[k_1]| \leq |s_j[k_2]|$ and an inflation operator for which $\forall k_1 \in \mathcal{Z}, k_2 \in \mathcal{P}_2 \backslash \mathcal{Z} : |s_j[k_1]| \geq |s_j[k_2]|$.

VI. Discussion

The performance of MaxViT in the noiseless case has shown competitive results with respect to the algorithms used in the comparison Table II. MaxViT even outperforms the reference based algorithms BSSR ($2p = 4$) and the limited support Wiener filter that have access to a larger amount of information (b instead of $|b|$ makes a 1 bit per sample information gain). We also outperform a completely blind algorithm based on higher order statistics (COM2), showing the advantage of using a probability conditioned on the source of interest only. Moreover, the little performance gain that can be obtained by the Wiener filter is at the expense of a highly informative prior, using the waveform r from Eq. (20), which is generally not available. In an observation environment contaminated by additive isotropic Gaussian distributed zero-mean i.i.d. noise, the MaxViT estimator shows to be robust, being competitive with the methods used in the comparison, with a slight estimation gain over almost the whole SNR range used in the simulations (Figs 2, 3). The only competitor that outperforms MaxViT when additive noise is present is the Wiener estimate with reference r from Eq. (20).

We also observe from Table II that the performance of BSSR remains equal, whether a signed or unsigned binary reference is used. This is an immediate consequence of the limitation of the BSSR algorithm to use even powers of the reference signal ($2p$) [13]. Surprisingly, as can be seen from the same Table II, the BSSR algorithm (and we may assume that the same would hold for the QHOC algorithm) does not yield a significant increase in estimation accuracy with an increase in available information, i.e., changing the reference signal from b to r. This points out that the conditional relative variance may be seen as a sufficient statistic to extract the source s_j from the mixture.

The MaxViT estimator also has been shown to be quite robust to mismatches with respect to the conditional set $\mathcal{C}_{s_j}$, see Fig. 4(b). This distinguishes our method from other works such as [10], [28], [13], where the estimator is reported to be susceptible to mismatches between the used reference and $s[k]_j$, especially with respect to its phase. Empirically, BSSR

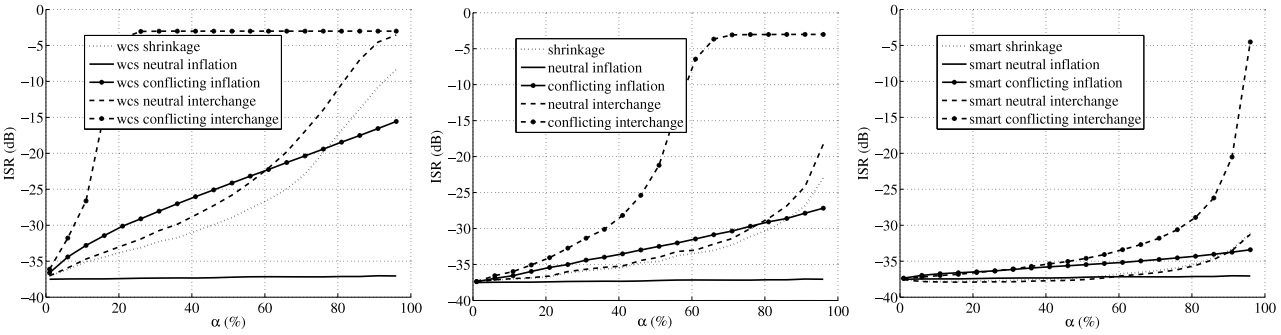

Fig. 4. The effect of a perturbation of the conditional set $\mathcal{C}_{s_j}$. The effect of the mismatch is measured through the source interference ISR (16) as a function of the relative number of samples α that are affected by the set operations. See text for more details.

has been shown robust to reference mismatches including time shift and sample omission (i.e., the equivalent of an interchange, respectively a shrinkage operator acting on the set $\mathcal{C}_{s_j}$) [29]. By placing BSSR in the framework of MaxViT, this can now partly be explained by the robustness of MaxViT to the conditional set $\mathcal{C}_{s_j}$. This follows from the assumption that BSSR with a binary reference inherits certain properties of MaxViT, whilst being equivalent to MaxViT for $p = 1$ and reference signal b defined in Section V-B.

The errors induced by the mismatch between the conditional set $\mathcal{C}_{s_j}$ and $\hat{\mathcal{C}}_{s_j}$ feeded as a prior to the algorithm are comparable to those induced by additive noise, as has been suggested in Sec. V-D. However, notice that small errors in the filter estimate do induce a smaller error in the filter output than does the additive noise. This can be deduced from the fact that our filter output can be written as a function of the optimal filter $\mathbf{h}^\star$ and a perturbation $\varepsilon_{\mathbf{h}}$ as $x^\star + \varepsilon_x = (\mathbf{h}^\star + \varepsilon_{\mathbf{h}})^T\mathbf{y}$, whereas in the case of additive noise, the same error in the filter estimate results in $x^\star + \varepsilon_{x,2} = (\mathbf{h}^\star + \varepsilon_{\mathbf{h}})^T(\mathbf{y} + \eta) = x^\star + \varepsilon_x + (\mathbf{h}^\star + \varepsilon_{\mathbf{h}})^T\eta$. Thus for the same error in the filter estimate, we logically obtain a better estimate of the source if the error is due to the set mismatch only.

Note that despite the use of specially designed simulations to reduce the fraction $|\rho|/\delta$ and thus to minimise the ISR (by choosing $\mathcal{C}_{s_j} \bigcap (\bigcup_{i\neq j} \mathcal{C}_{s_i}) = \emptyset$), we may generalise our results to independently distributed sources that have not been corrected. This is because, from Table I, we have that the fraction $|\rho|/\delta$ generally remains acceptably small for i.i.d. Laplacian, Gaussian and uniform sources.

A quick overview of the performance of the MaxViT algorithm can be given by evaluating under what conditions we obtain an acceptable ISR of -30dB. It follows from Figs 2 and 3 that we accept a signal to noise level no lower than 4dB and [from Figs 4(a)-(c)] a worst case interchange of indices of $\mathcal{C}_{s_j}$ with $\mathcal{C}_{s_i}$ of up to 7% of $\#\mathcal{C}_{s_j}$. However, in practical situations, an estimation of the set $\mathcal{C}_{s_j}$ is usually done with more care and even when unfortunately chosen, we would interchange samples between sets randomly rather than creating a worst case scenario. This random interchange can be done for up to some 30% to 70% of the samples of $\mathcal{C}_{s_j}$, depending on whether conflicting, respectively neutral sample indices have been involved. In practical situations, a set estimate $\hat{\mathcal{C}}_{s_j}$ offering a considerable performance should thus often be available, e.g., by using a threshold on the amplitude of the observations (as in [28]) or based upon prior knowledge of the support in the frequency domain (see e.g., [30]).

The estimation of a source s_j from a set of observations $\mathbf{y}$ can be done for every source in the mixture (approximately) satisfying the sufficient conditions (**C1**)-(**C3**) and this whenever an approximation of its conditional set is available. When more than one source is of interest, we propose an iterative estimation without deflation, especially when $\#(\mathcal{C}_{s_i} \bigcap \mathcal{C}_{s_j})$ is relatively small. Avoiding the subtraction of the projection of $\mathbf{y}$ onto s_j from $\mathbf{y}$ prior to estimating s_i, reduces the possible error propagation from which these deflation approaches suffer.

As explained in Section III, the only constant in MaxViT that has to be set, is C, and its influence on different source distributions can be found in Table I. We see that its value is not critical, at least for large sample populations. In practical situations, where only a limited population sample is available, it should neither be taken too large, nor too small, because the conditional covariance with respect to $\mathbb{I}_{s_j}$, respectively (implictly) with respect to $\overline{\mathbb{I}}_{s_j}$, would be calculated on too small a sample set and its estimation would suffer from an increase in variance.

VII. Conclusion

We have shown that maximising the likelihood criterion conditioned on a presence indicator gives rise to a contrast function for the extraction of a source of interest. The filter corresponding to the optimum of the contrast function can be found algebraically, provided that the conditional second moment can be estimated from the observations. The MaxViT estimator has interesting properties, such as robustness to noise or perturbations of the conditional set, making it a valuable alternative to constrained ICA algorithms.

Appendix

A. Proof of Proposition 1

(**P1**) holds if we consider unit variance variables only. This can be done without loss of generality. Since the log-likelihood $\mathcal{L}(x)$ of Eq. (4) is either 0 or tends to $-\infty$, and $\mathcal{L}(x) = 0$

holds if and only if we have $p_{x|\mathbb{I}_{s_j}}(u) = 0, \forall u \in \overline{\mathbb{B}}$ and $p_{x|\bar{\mathbb{I}}_{s_j}}(u) = 0, \forall u \in \mathbb{B}$ **(P2)**, it remains to prove that the latter two conditions imply the equality $x = \lambda_j s_j$ of **(P3)**.

Proof: Suppose that we have $x \neq \lambda_j s_j$, and thus $x = \mathbf{g}^T\mathbf{s} = g_j s_j + \sum_{i\neq j} g_i s_i = g_j s_j + \breve{s}$, where at least one g_i has a non-zero value and for which $p_{x|\mathbb{I}_{s_j}}(u) = 0, \forall u \in \overline{\mathbb{B}}$.

Since s_j is independently distributed with respect to $\tilde{\mathbf{s}}$ and thus with respect to all $s_i (i \neq j)$, we have that s_j is independently distributed with respect to $\breve{s}$. As a consequence, the distribution $p_{x|\mathbb{I}_{s_j}}(u)$ can be written as the convolution of the distributions $p_{s_j|\mathbb{I}_{s_j}}(u)$ and $p_{\breve{s}}(u)$, or

$$p_{x|\mathbb{I}_{s_j}}(u) = \int_{\mathbb{R}} p_{s_j|\mathbb{I}_{s_j}}(\tau - u) p_{\breve{s}}(\tau) d\tau \ . \tag{21}$$

A necessary condition for x to yield $\mathcal{L}(x) = 0$, is that $p_{x|\mathbb{I}_{s_j}}(u) = 0, \forall u \in \overline{\mathbb{B}}$. However, if $\exists\ \varepsilon$ with non-zero Lebesgue measure for which the support set $\mathcal{S}$ of $p_{\breve{s}}$ has a measure $|\mathcal{S}| \geq \varepsilon$ and for which $p_{s_j|\mathbb{I}_{s_j}}(u) > 0, \forall u : |u| \in [C,\ C + |\varepsilon|]$, then, by Eq. (21), $\exists\ u : |u| < C, p_{x|\mathbb{I}_{s_j}}(u) > 0$. As a consequence, our initial supposition was wrong and we must have $g_i = 0, \forall i \neq j$, i.e. $\mathcal{L}(x) = 0 \Rightarrow x = \lambda_j s_j$. ■

An analogous reasoning can be used to proof that $p_{x|\bar{\mathbb{I}}_{s_j}}(u) = 0, \forall u \in \mathbb{B}$ implies $x = \lambda s_j$.

B. Proof of $\int_{\overline{\mathbb{B}}} p_{x|\mathbb{I}_{s_j}}(u)\gamma(u) = 0 \Rightarrow p_{x|\mathbb{I}_{s_j}}(u) = 0, \forall u \in \overline{\mathbb{B}}$

Proof: If $\int_{\overline{\mathbb{B}}} p_{x|\mathbb{I}}(u)\gamma(u)\, du = 0$, with $\gamma(u)$ a positive function taking $\gamma(u) = 0$ for $u = 0$ only. We must have

$$\begin{cases} p_{x|\mathbb{I}}(u) = 0, & \forall u \in \overline{\mathbb{B}} \backslash \{0\} \\ p_{x|\mathbb{I}}(0) = \alpha_k \delta_{u,0}, \end{cases}$$

where $\delta_{u,0} = 1$ is Dirac's delta at the origin. Assuming sources with continuous distributions, the second option is not possible, unless $\mathbf{h} = \mathbf{0}$. This trivial case is avoided by the constraints introduced later in the construction of the algorithm.

The assumption of continuous distributions can be relaxed if C is chosen such that $\overline{\mathbb{B}}$ and $\mathbb{B}$ both have a non-zero Lebesgue measure (for discrete distributions, we have respectively $\#\overline{\mathbb{B}} > 1$ and $\#\mathbb{B} > 1$).

■

C. The objective function of Eq. (9) is a contrast for the extraction of s_j.

To proof that Ψ_x is a contrast under the conditions **(C1)**-**(C3)** from Section III-D, we need to show that it has the properties **(P1')**-**(P3')** from Section II-B.

Proof: The indeterminacy of the source scaling has been taken care of by the denominator in Eq. (9), and thus **(P1')** holds.

Furthermore we have

$$\frac{\mathbf{h}^T\Phi_{\mathbf{y}}^{s_j}\mathbf{h}}{\mathbf{h}^T\Phi_{\mathbf{y}}\mathbf{h}} = \frac{\mathbf{g}^T\Phi_{\mathbf{s}}^{s_j}\mathbf{g}}{\mathbf{g}^T\Phi_{\mathbf{s}}\mathbf{g}} = \frac{\sum_i |g_i|^2\Phi_{s_i}^{s_j}}{\sum_i |g_i|^2} \ ,$$

since our sources are uncorrelated, both conditionally and unconditionally. Splitting up the sum in the different contributions gives us (up to a multiplicative positive constant)

$$|g_{jj}|^2\Phi_{s_j}^{s_j} + \sum_{i\neq j} |g_i|^2\Phi_{s_i}^{s_j} + \sum_{i\neq j} |g_i|^2\Phi_{s_j}^{s_j} - \sum_{i\neq j} |g_i|^2\Phi_{s_j}^{s_j}$$

which can be rewritten as

$$\Phi_{s_j}^{s_j} + \sum_{i\neq j} |g_i|^2(\Phi_{s_i}^{s_j} - \Phi_{s_j}^{s_j}) \leq \Phi_{s_j}^{s_j} \ ,$$

where the inequality follows from $(\Phi_{s_i}^{s_j} - \Phi_{s_j}^{s_j}) < 0, \forall i \neq j$. This proofs the domination.

We also have

$$\Phi_x^{s_j} = \Phi_{s_j}^{s_j} \Leftrightarrow \sum_{i\geq 2} |g_i|^2(\Phi_{s_i}^{s_j} - \Phi_{s_1}^{s_j}) = 0 \ .$$

Now, since $(\Phi_{s_i}^{s_j} - \Phi_{s_1}^{s_j}) < 0, \forall i \neq j$, we have the above equality if and only if $|g_i|^2 = 0, \forall i \geq 2$. And thus

$$\frac{\mathbf{g}^H\Phi_{\mathbf{s}}^{s_j}\mathbf{g}}{\mathbf{g}^H\Phi_{\mathbf{s}}^{\mathbb{R}}\mathbf{g}} = \frac{\Phi_{s_j}^{s_j}}{\Phi_{s_1}}$$

This proofs the discrimination and thus, together with the domination, **(P2')** and **(P3')** are fulfilled.

Since any objective function fulfilling **(P1')**-**(P3')** is a contrast function for source extraction, our function $\Psi(x)$ in Eq. (9) is a contrast under the conditions **(C1)**-**(C3)**. ■

Note that this could be extended to the case where the covariance $\mathbb{E}_{s_j}\{s_i s_k\} \neq 0, \forall i,k \neq j\, i \neq k$, as long as $\mathbb{E}_{s_j}\{s_j s_i\} = 0, \forall i \neq j$. For the proof, define $\tilde{\mathbf{s}} = [s_1, s_2 \ldots s_{j-1}, s_{j+1} \ldots s_N]^T$. Now take the eigenvalue decomposition of $\Phi_{\tilde{\mathbf{s}}}^{s_j}$ as $\mathbf{V}^T\Phi_{\tilde{\mathbf{s}}}^{s_j}\mathbf{V} = \Delta$, where Δ is a diagonal matrix with the eigenvalues λ_i on its diagonal and extend $\mathbf{V}$ to

$$\tilde{\mathbf{V}} = \begin{pmatrix} 1 & \mathbf{0}_{n-1}^T \\ \mathbf{0}_{n-1} & \mathbf{V} \end{pmatrix} \ ,$$

where $\mathbf{0}_{n-1}$ is a vector of zeros in $\mathbb{R}^{n-1}$. The proof then continues similarly as above but replacing $\Phi_{\tilde{\mathbf{s}}}^{s_j}$ by Δ and $\mathbf{g}$ by $\tilde{\mathbf{V}}\mathbf{g}$. As a consequence, condition **(C3)** in Section III-D becomes $\Phi_{s_j}^{s_j} > \max \lambda_i$.

D. Algebraic Solution for the 2×2 Case

Suppose that $\mathbf{y}$ has uncorrelated, unit-variance and zero mean entries, without loss of generalisation, since $\mathbf{y}$ can always be rendered so through whitening. Since $\Phi_{\mathbf{y}} = \mathbf{I}_2$, the eigenvector that would separate our source as $x = \mathbf{e}_1^T\mathbf{y}$ is the dominant eigenvector of the covariance matrix $\Phi_{\mathbf{y}}^{s_1}$, which has a general symmetric form

$$\Phi_{\mathbf{y}}^{s_1} = \begin{bmatrix} a & b \\ b & c \end{bmatrix} \ . \tag{22}$$

The above matrix has eigenvalues

$$\lambda_{1,2} = \frac{a+c}{2} \pm \sqrt{\left(\frac{a-c}{2}\right)^2 + |b|^2} \ , \tag{23}$$

and thus, if $a \neq c$, has a largest eigenvector

$$\mathbf{e}_1 = \pm \begin{bmatrix} \frac{1}{\sqrt{2}}\sqrt{1 + \frac{\xi}{\xi^2 + |b|^2}} \\ \frac{1}{\sqrt{2}}\sqrt{1 - \frac{\xi}{\xi^2 + |b|^2}} \end{bmatrix} \ , \tag{24}$$

with $\xi = \frac{a-c}{2}$.

E. Calculation of ISR

We induce the estimation bound in case the sources are not perfectly conditionally uncorrelated. Since we only consider unitary transformations $\mathbf{A} = \mathbf{Q}$ (for our $\mathbf{y}$ is or has been rendered spatially *white*), we know that the eigenvalues of $\Phi_{\mathbf{s}}^{s_j}$ and $\Phi_{\mathbf{y}}^{s_j}$ are equal. Moreover, the i-th eigenvector $\mathbf{q}_i$ of $\Phi_{\mathbf{y}}^{s_j}$ equals $\mathbf{Q}\mathbf{e}_i$, where $\mathbf{e}_i$ is the i-th eigenvector of $\Phi_{\mathbf{s}}^{s_j}$ (see also the equivariance property [9]). As a consequence, we only need to consider the simpler case where $\mathbf{Q} = \mathbf{I}_m$, without loss of generality.

Limiting $\mathbf{s}$ to belong to $\mathbb{R}^2$, the matrix $\Phi_{\mathbf{s}}^{s_1}$ takes the form

$$\Phi_{\mathbf{s}}^{s_1} = \begin{bmatrix} \Phi_{s_1}^{s_1} & \mathbb{E}_{s_1}\{s_1 s_2\} \\ \mathbb{E}_{s_1}\{s_1 s_2\} & \Phi_{s_2}^{s_1} \end{bmatrix} . \tag{25}$$

From Eq. (24), one can explicitly calculate the separation filter $\mathbf{h}$ associated to $\Phi_{\mathbf{s}}^{s_1}$ by the above Eq. (24). As such we obtain for the ISR ($|g_2|^2/|g_1|^2 = |h_2|^2/|h_1|^2$):

$$\text{ISR} = \frac{\sqrt{\delta^2 + |\rho|^2} - \delta^2}{\sqrt{\delta^2 + |\rho|^2} + \delta^2} , \tag{26}$$

with $\delta = \frac{\Phi_{s_1}^{s_1} - \Phi_{s_2}^{s_1}}{2}$ and $\rho = \mathbb{E}_{s_1}\{s_1 s_2\}$.

F. Proof of the inequality $\mathbb{E}_{s_j}\{s_j^2\} \geq \mathbb{E}\{s_j^2\}$

Proof: To proof the inequality, we proof the more general form $\mathbb{E}_{s_j}\{\gamma(s_j)\} \geq \mathbb{E}\{\gamma(s_j)\}$ for any positive valued function γ. We have

$$\begin{aligned} \mathbb{E}_{s_j}\{\gamma(s_j)\} &= \int p_{s_j|\mathbb{I}_{s_j}}(u)\gamma(u)du \\ &= \frac{\int_{\mathbb{B}} p_{s_j}(u)\gamma(u)du}{\int_{\mathbb{B}} p_{s_j}(u)\,du} \\ &= \frac{\int p_{s_j}(u)\gamma(u)du - \int_{\overline{\mathbb{B}}} p_{s_j}(u)\gamma(u)du}{\int_{\mathbb{B}} p_{s_j}(u)\,du} \\ &> \int p_{s_j}(u)\gamma(u)du = \mathbb{E}\{\gamma(s_j)\} , \end{aligned}$$

These results hold if we impose the condition of Eq. (5), since we have from Hölders inequality that $\int_{\overline{\mathbb{B}}} p_{s_j}(u)du \int_{\overline{\mathbb{B}}} \gamma(u)du \geq \int_{\overline{\mathcal{B}}} p_{s_j}(u)\gamma(u)du$ and thus $\int_{\overline{\mathbb{B}}} p_{s_j}(u)du \to 0 \Rightarrow \int_{\overline{\mathcal{B}}} p_{s_j}(u)\gamma(u)du \to 0$ for all positive valued functions γ. As a consequence, we have $\mathbb{E}_{s_j}\{\gamma(s_j)\} \geq \mathbb{E}\{\gamma(s_j)\}$ with equality if and only if $\int_{\mathbb{B}} p_{s_j}(u)\,du = 1$, i.e., $C < \min|s_j|$. Since u^2 is a non-negative valued function, $C > 0$ and we generally have $\min|s_j[k]| = 0$ (continuous distributions defined on the whole real line), we have $\mathbb{E}_{s_j}\{s_j^2\} > \mathbb{E}\{s_j^2\}$. ■

REFERENCES

[1] C. Jutten and J. Herault, "Blind separation of sources, part i: An adaptive algorithm based on neuromimetic architecture," *Signal Processing*, vol. 24, no. 1, pp. 1–10, 1991.

[2] P. Comon, "Independent component analysis, a new concept?" *Signal Processing*, vol. 36, pp. 287–314, 1994.

[3] L. Tong, R.-W. Liu, V. C. Soon, and Y.-F. Huang, "Indeterminacy and identifiability of blind identification," *IEEE Trans on Circuits and Systems*, vol. 38, no. 5, pp. 499–509, 1991.

[4] S. A. Cruces-Alvarez, A. Cichocki, and S.-i. Amari, "From blind signal extraction to blind instantaneous signal separation: Criteria, algorithms and stability," *IEEE Transactions on Neural Networks*, vol. 15, no. 4, pp. 859–873, 2004.

[5] E. Moreau and P. Comon, *Séparation de sources*. Hermès-Lavoisier, 2007, vol. 1, ch. Fonctions de Contraste, pp. 75–115, in french.

[6] A. Cichocki, R. Thawonmas, and S. ichi Amari, "Sequential blind signal extraction in order specified by stochastic properties," *Electronics Letters*, vol. 33, no. 1, pp. 64–65, 1997.

[7] N. Delfosse and P. Loubaton, "Adaptive blind separation of independent sources: A deflation approach," *Signal Processing*, vol. 45, pp. 59–83, 1995.

[8] A. Hyvärinen and E. Oja, "Independent Component Analysis: Algorithms and Applications," *Neural Networks*, vol. 13, no. 4-5, pp. 411–430, 2000.

[9] J.-F. Cardoso and B. H. Laheld, "Equivariant adaptive source separation," *IEEE Trans. on Signal Processing*, vol. 44, no. 12, pp. 3017–3030, 1996.

[10] W. Lu and J. C. Rajapakse, "ICA with reference," in *Proc. Int. Conf. on ICA and BSS*, 2001, pp. 120 – 125.

[11] ——, "Approach and applications of constrained ica," *IEEE Trans on Neural Networks*, vol. 16, no. 1, pp. 203–212, 2005.

[12] B. Widrow, J. R. Glover, J. M. McCool, J. Kaunitz, C. S. Williams, R. H. Hearn, J. R. Zeidler, E. Dong, and R. C. Goodlin, "Adaptive noise cancelling: Principles and applications," *Proceedings of the IEEE*, vol. 63, no. 12, pp. 1692–1716, 1975.

[13] M. Sato, Y. Kimura, S. Chida, T. Ito, N. Katayama, K. Okamura, and M. Nakao, "A novel extraction method of fetal electrocardiogram from the composite abdominal signal," *IEEE Trans on Biom Eng*, vol. 54, no. 1, pp. 49–58, 2007.

[14] A. Adib, E. Moreau, and D. Aboutajdine, "Source separation contrasts using a reference signal," *IEEE Signal Processing Letters*, vol. 11, no. 3, pp. 312–315, 2004.

[15] M. Castella, S. Rhioui, E. Moreau, and J. C. Pesquet, "Quadratic higher order criteria for iterative blind separation of a mimo convolutive mixture of sources," *IEEE Trans. Signal Process.*, vol. 55, no. 1, pp. 218–232, Jan. 2007.

[16] B. Xerri and B. Borloz, "An iterative method using conditional second-order statistics applied to the blind source separation problem," *IEEE Trans. Signal Process.*, vol. 52, no. 2, pp. 313–328, Feb. 2004.

[17] D.-T. Pham and P. Garat, "Blind separation of mixture of independent sources through a quasi-maximum likelihood approach," *IEEE Transactions on Signal Processing*, vol. 45, no. 7, pp. 1712–1725, 1997.

[18] J.-F. Cardoso, "Infomax and maximum likelihood for blind source separation," *IEEE Signal Processing Letters*, vol. 4, no. 4, pp. 112–114, 1997.

[19] G. H. Golub and C. F. Van Loan, *Matrix Computations*, 3rd ed. The Johns Hopkins University Press, 1996.

[20] A. Hyvärinen, J. Karhunen, and E. Oja, *Independent Component Analysis*. Wiley Interscience, 2001.

[21] A. Cichocki and S.-I. Amari, *Adaptive Blind Signal and Image Processing: Learning Algorithms and Applications*, 2005th ed. Wiley, 2002.

[22] S. Roberts and R. Everson, Eds., *Independent Component Analysis: Principles and Practice*. Cambridge University Press, 2001.

[23] J.-F. Cardoso, "On the performance of orthogonal source separation algorithms," in *Proc. EUSIPCO*, Edinburgh, 1994, pp. 776–779.

[24] C. J. James and O. Gibson, "ICA with a reference: extracting desired electromagnetic brain signals," *Medical Applications of Signal Processing*, 2002.

[25] S. Mallat and Z. Zhang, "Matching pursuits with time-frequency dictionaries," *IEEE Trans on Signal Processing*, vol. 41, no. 12, pp. 3397–3415, Dec. 1993.

[26] R. Gribonval, "Piecewise linear source separation," in *Proc. SPIE'03*, ser. Wavelets: Applications in Signal and Image Processing, vol. 5207, San Diego, California, USA, 2003.

[27] M. Aharon, M. Elad, and A. Bruckstein, "K-SVD: An algorithm for designing overcomplete dictionaries for sparse representation," *IEEE Trans. Signal Process.*, vol. 54, no. 11, pp. 4311–4322, Nov. 2006.

[28] C. J. James and O. J. Gibson, "Temporally constrained ICA: an application to artifact rejection in electromagnetic brain signal analysis," *IEEE Trans on Biomed Eng*, vol. 30, no. 9, pp. 1108–1115, 2003.

[29] T. Netabayashi, Y. Kimura, S. Chida, T. Ito, K. Ohwada, N. Katayama, K. Okamura, and M. Nakao, "Robustness of the blind source separation with reference against uncertainties of the reference signals," in *30th Annual International IEEE EMBS Conference*, vol. 30, Vancouver, British Columbia, Canada, 2008, pp. 1875–1878.

[30] R. Phlypo, V. Zarzoso, and I. Lemahieu, "Eigenvector analysis for separation of a spectrally concentrated source from a mixture," in *30th Annual International IEEE EMBS Conference*, Vancouver, British Columbia, Canada, 2008, pp. 1863–1866.

Ronald Phlypo was born in Ostend, Belgium, in 1981. He graduated in industrial engineering from the KHBO, Ostend, Belgium in 2003 and obtained a Master in Artificial Intelligence from the KULeuven, Leuven, Belgium in 2004. From 2004 on, he is pursuing his Ph.D. in engineering sciences at the University of Ghent, Belgium within the Medical Image and Signal Processing (MEDISIP) Research Group. He has been a visitor of the Laboratoire d'Informatique, Signaux et Systèmes de Sophia Antipolis, France since 2006. His research interests include blind statistical signal and array processing and its application to biomedical problems.

Vicente Zarzoso (S'94–M'03) was born in Valencia, Spain, in 1973. He graduated (with highest distinction) in telecommunications engineering from the Universidad Politécnica de Valencia in 1996. The beginning of his Ph.D. studies were partly funded by a scholarship from the University of Strathclyde, Glasgow, U.K., and the Defence Evaluation and Research Agency (DERA) of the United Kingdom. He received the Ph.D. degree from the University of Liverpool, U.K., in 1999. He spent five years with the University of Liverpool under a Research Fellowship from the Royal Academy of Engineering, U.K. Since September 2005, he has been a Lecturer with the Universit de Nice - Sophia Antipolis and a Researcher with the Laboratoire d'Informatique, Signaux et Systèmes de Sophia Antipolis, France. His research interests include blind statistical signal and array processing and its application to biomedical problems and communications.

Ignace Lemahieu (M'92–SM'00) was born in Belgium in 1961. He graduated in physics from Ghent University, Ghent, Belgium, in 1983, and received the doctoral degree in physics in 1988 from the same university. He joined the Department of Electronics and Information Systems (ELIS), Ghent University, in 1989 as a Research Associate with the Fund for Scientific Research (F.W.O.-Flanders), Belgium. He is now a Professor of medical image and signal processing and head of the MEDISIP Research Group. His research interests comprise all aspects of image processing and biomedical signal processing, including image reconstruction from projections, pattern recognition, image fusion, and compression. He is the co-author of more than 200 papers. Dr. Lemahieu is a member of SPIE, the European Society for Engineering and Medicine, and the European Association of Nuclear Medicine.

IEEE SIGNAL PROCESSING LETTERS, VOL. 15, 2008 501

A Contrast for Independent Component Analysis With Priors on the Source Kurtosis Signs

Vicente Zarzoso, *Member, IEEE*, Ronald Phlypo, *Student Member, IEEE*, and Pierre Comon, *Fellow, IEEE*

***Abstract*—A contrast function for independent component analysis (ICA) is presented incorporating the prior knowledge on the sub-Gaussian or super-Gaussian character of the sources as described by their kurtosis signs. The contrast is related to the maximum likelihood principle, reduces the permutation indeterminacy typical of ICA, and proves particularly useful in the direct extraction of a source signal with distinct kurtosis sign. In addition, its numerical maximization can be performed cost-effectively by a Jacobi-like pairwise iteration. Extensions to standardized cumulants of orders other than four are also given.**

***Index Terms*—Blind source separation, contrast functions, higher-order statistics, independent component analysis, kurtosis, performance analysis, standardized cumulants.**

I. Introduction

INDEPENDENT component analysis (ICA) aims at maximizing the statistical independence between the entries of multivariate data. ICA is the fundamental technique for blind source separation (BSS) in linear mixtures when the sources are assumed mutually independent [1]. The plausibility of the assumption in a wide variety of applications has rapidly made of ICA a reference tool in biomedical engineering, communications, and image processing, among many other domains [2]–[4].

In the real-valued noiseless case, ICA assumes the following linear model for the observed data vector $\mathbf{x} \in \mathbb{R}^m$:

$$\mathbf{x} = \mathbf{H}\mathbf{s} \tag{1}$$

where $\mathbf{s} \in \mathbb{R}^n$ contains the independent components or sources and $\mathbf{H} \in \mathbb{R}^{m \times n}$ represents the mixing matrix, with $m \geq n$. The sources are recovered by maximizing a so-called contrast function measuring the statistical independence between the separator output components [1]. Seminal contrasts such as "COM1" and "COM2" originated from cumulant-based approximations (usually at order four) of information-theoretical principles such as maximum likelihood (ML), mutual information, and marginal entropy [1], [5]. The hypothesis that the kurtosis (normalized fourth-order marginal cumulant) of all the sources has the same sign allows the definition of computationally simpler contrasts [5], [6] but is unable to reduce the ambiguity in the ordering of the recovered sources, or permutation indeterminacy, typical in BSS.

The power of the blind approach lies in its robustness to modeling errors, a feature achieved by making as few assumptions about the problem as possible. However, additional information is often available in practice such as the non-Gaussian character of the sources: that of a digital modulation signal depends on the relative probability of its symbols; the atrial activity signal of an atrial fibrillation electrocardiogram is usually sub-Gaussian or quasi-Gaussian; etc. Separation performance can be considerably improved by capitalizing on this information.

The present contribution puts forward a contrast function that takes into account the prior knowledge about the non-Gaussian character of the sources. The new contrast has optimality properties in the ML sense, is efficiently maximized by Jacobi-like iterations, and alleviates (indeed, may totally resolve) the permutation indeterminacy left by blind processing. This latter feature, illustrated in Section IV through simulations, has been successfully put into practice, without mathematical proof, on real signals issued from electrocardiography [7], [8].

II. Contrast Based on Source Kurtosis Signs

Let us first recall the concept of contrast function. The standardization or whitening (second-order processing) of observation (1) yields another vector $\mathbf{z} = \mathbf{Q}\mathbf{s}$, where $\mathbf{Q}$ is a unitary matrix. The sources can then be recovered by applying a unitary transform $\hat{\mathbf{Q}}$, resulting in the separator output $\mathbf{y} = \hat{\mathbf{Q}}^T\mathbf{z} = \mathbf{G}\mathbf{s}$, where $\mathbf{G} = \hat{\mathbf{Q}}^T\mathbf{Q}$. A function $\Psi(\mathbf{y})$ of the separator-output distribution is an orthogonal contrast for ICA if $\Psi(\mathbf{s}) \geq \Psi(\mathbf{G}\mathbf{s})$, for any orthogonal matrix $\mathbf{G}$ (domination), with equality if and only if $\mathbf{G}$ is a trivial filter

$$\mathbf{G} = \mathbf{P}\mathbf{D} \tag{2}$$

where $\mathbf{P}$ is a permutation and $\mathbf{D}$ a non-singular diagonal matrix (discrimination). Consequently, contrast maximization restores the independent sources at the separator output up to a possible permutation and scaling.

Let κ_i denote the ith-source kurtosis and ε_i its sign, $\varepsilon_i = \operatorname{sign}(\kappa_i)$, $1 \leq i \leq n$. We assume in the sequel that p sources have positive kurtosis, $\varepsilon_i = 1$, $1 \leq i \leq p$, and $(n-p)$ sources have negative kurtosis, $\varepsilon_i = -1$, $p < i \leq n$. Symbol μ_i represents the kurtosis of the separator's ith output. Proofs for the mathematical results that follow can be found in the Appendix .

Proposition 1: Criterion

$$\Psi_p(\mathbf{y}) = \sum_{i=1}^{n} \varepsilon_i \mu_i \tag{3}$$

Manuscript received September 25, 2007; revised December 20, 2007. The associate editor coordinating the review of this manuscript and approving it for publication was Prof. Yimin Zhang.

V. Zarzoso and P. Comon are with the Laboratoire I3S, Université de Nice-Sophia Antipolis, CNRS, 06903 Sophia Antipolis Cedex, France (e-mail: zarzoso@i3s.unice.fr; pcomon@i3s.unice.fr).

R. Phlypo is with the Department of Electrical and Information Systems (ELIS), Ghent University, Institute for Broadband Technology (IBBT), IBiTech Block Heymans, B-9000 Ghent, Belgium (e-mail: ronald.phlypo@ugent.be).

Digital Object Identifier 10.1109/LSP.2008.919845

is a contrast function under the above assumptions.

Remark: The maximum likelihood recovery of the source signals under the whitening constraint is achieved by maximizing the following function:

$$\Psi_{\mathrm{ML}}(\mathbf{y}) = \sum_{i=1}^{n} \kappa_i \mu_i. \tag{4}$$

This contrast is obtained from an approximation of the Kullback–Leibler divergence based on the Edgeworth expansion of the separator-output probability density function (pdf) truncated at fourth order [6]. If only the source kurtosis signs are known, contrast (4) naturally reduces to (3). Hence, the latter is expected to inherit the optimality features of the approximate ML estimate while reducing the prior information required. The reduced amount of information helps to keep the desirable features of a blind formulation and is capable of partially solving the permutation ambiguity, as shown by Proposition 2 below.

Remark: Reference [9] addresses the so-called one-bit matching conjecture, whereby the sources can be separated if there exists a one-to-one correspondence between the kurtosis signs of the sources and those resulting from the truncated Gram–Charlier expansion of their pdf's. A function obtained in [9] bears certain resemblance to contrast (3), but the proof of the conjecture is cumbersome and valid only when the source skewness (standardized third-order cumulant) is null. We prove in the Appendix that function (3) is a contrast for all orders $r \geq 3$, of which Proposition 1 is just a particular case for $r = 4$.

Proposition 2: Trivial filters associated with contrast (3) are of the form (2), where

$$\mathbf{P} = \begin{pmatrix} \mathbf{P}_1 & \mathbf{0} \\ \mathbf{0} & \mathbf{P}_2 \end{pmatrix} \tag{5}$$

with $\mathbf{P}_1$ and $\mathbf{P}_2$ being permutation matrices of size $p \times p$ and $(n-p) \times (n-p)$, respectively, and $\mathbf{D}$ made up of unit-norm diagonal entries.

Remark: Sources with positive kurtosis are extracted separately from sources with negative kurtosis by contrast (3), provided that parameter p is known. In particular, a source of interest can be recovered without permutation ambiguity if its kurtosis sign is different from all the others'. The Appendix shows that contrast (3) enjoys this source ordering property for standardized cumulants of even order $r \geq 4$.

III. Contrast Optimization

The Jacobi-like pairwise iteration technique originally proposed in [1] can also be used to optimize contrast function (3). The function is maximized for each signal pair in turn over several sweeps until convergence. Let us assume that we are processing pair $\mathbf{z}_{12} = [z_1, z_2]^T$, the result being readily adapted to other pairs by a simple change of indices. The corresponding two-signal separator output is given by $\mathbf{y}_{12} = \hat{\mathbf{Q}}^T \mathbf{z}_{12}$, where $\hat{\mathbf{Q}}$ is a Givens rotation that can be parameterized as

$$\hat{\mathbf{Q}}(\theta) = \frac{1}{\sqrt{1+t^2}} \begin{pmatrix} 1 & -t \\ t & 1 \end{pmatrix} \tag{6}$$

with $t = \tan\theta$. The associated pairwise contrast is $\Psi(\mathbf{y}_{12}) = \varepsilon_1 \mu_1 + \varepsilon_2 \mu_2$. By virtue of the multilinearity property of cumulants, this function can easily be expressed in terms of the unknown t and the fourth-order cumulants of $\mathbf{z}_{12}$, denoted as $c_{ij} = \mathrm{Cum}_{ij}(z_1, z_2)$, with $(i+j) = 4$ (using Kendall's notation). The stationary points of $\Psi(\mathbf{y}_{12})$ are then found to be the solutions to the quartic equation as follows:

$$a_3 t^4 + 2(a_2 - 2a_4) t^3 + 3(a_1 - a_3) t^2 + 2(2a_0 - a_2) t - a_1 = 0 \tag{7}$$

where $a_0 = (\varepsilon_1 c_{40} + \varepsilon_2 c_{04})$, $a_1 = 4(\varepsilon_1 c_{31} - \varepsilon_2 c_{13})$, $a_2 = 6(\varepsilon_1 + \varepsilon_2) c_{22}$, $a_3 = 4(\varepsilon_1 c_{13} - \varepsilon_2 c_{31})$, and $a_4 = (\varepsilon_1 c_{04} + \varepsilon_2 c_{40})$. The above quartic can be solved by radicals (Ferrari's formula) at a cost that can be considered negligible compared to the cumulant computation. The solutions can also be simply expressed in terms of the extended ML (EML) estimator of [10] if $\varepsilon_1 = \varepsilon_2$ or the alternative EML (AEML) estimator of [11] if $\varepsilon_1 \neq \varepsilon_2$. Typically, about $O(\sqrt{n})$ sweeps over all signal pairs are required for convergence, as suggested in [1]. However, as a by-product of Proposition 2, the extraction of a source of interest with distinct (e.g., positive) kurtosis sign can be carried out by sweeping the contrast over pairs $\mathbf{z}_{1j}$ only, with $\varepsilon_1 = 1, \varepsilon_j = -1$, for $2 \leq j \leq n$. After convergence, the desired source will appear at the first entry of the separator output vector.

IV. Numerical Experiments

The contrast is tested on synthetic random unitary mixtures of $n = 10$ binary signals composed of 1000 samples. Sources kurtosis values of either $\kappa = 2$ (super-Gaussian) or $\kappa = -2$ (sub-Gaussian) are obtained by setting the probability of the two states in the binary distribution accordingly [12]. The error

$$E = \frac{1}{2n(n-1)} \left[\sum_{i=1}^{n} \left(\sum_{j=1}^{n} \frac{|G_{ij}|}{\max_k |G_{ik}|} - 1 \right) + \sum_{j=1}^{n} \left(\sum_{i=1}^{n} \frac{|G_{ij}|}{\max_k |G_{kj}|} - 1 \right) \right] \tag{8}$$

is used as a separation performance criterion [4], [13]. The error is always positive, and zero if and only if matrix $\mathbf{G}$ is a trivial filter of the form (2). Error values are averaged over 250 independent realizations of the sources and the mixing matrix. Three contrasts are considered: "COM2" [1] ($\triangle$ marker); "COM1+"; and "COM1−"; which correspond to the contrast of [5], assuming that all sources have positive and negative kurtosis, respectively ($+$ and $\times$ markers, resp.); and function (3), which we refer to as "*kurtosis sign priors (KSP)*" contrast ($\circ$ marker). For each tested contrast, we carry out $5(1 + \lfloor\sqrt{n}\rfloor)$ sweeps over all signal pairs.

Fig. 1 shows the performance variation as a function of the number p of sources with positive kurtosis, where p is assumed to be perfectly known *a priori*. As expected, COM1+ and COM1− fail to perform the separation, except when all sources have the same kurtosis sign. KSP outperforms the other contrasts.

The robustness of contrast (3) to a mismatch in the prior information is analyzed in Fig. 2, where $\hat{p}$ sources are assumed to

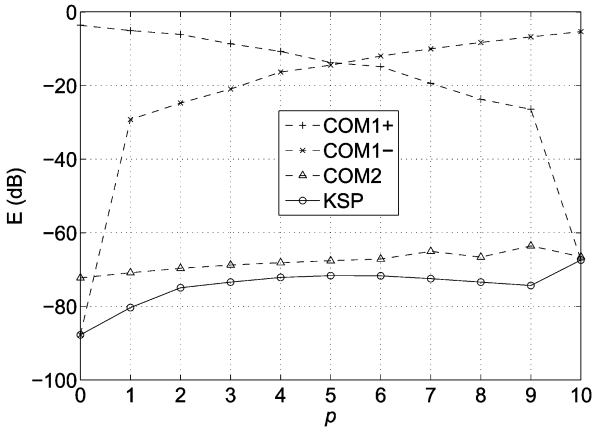

Fig. 1. Source separation performance of ICA contrasts as a function of the number of positive-kurtosis sources p. The KSP method employs the correct value of p.

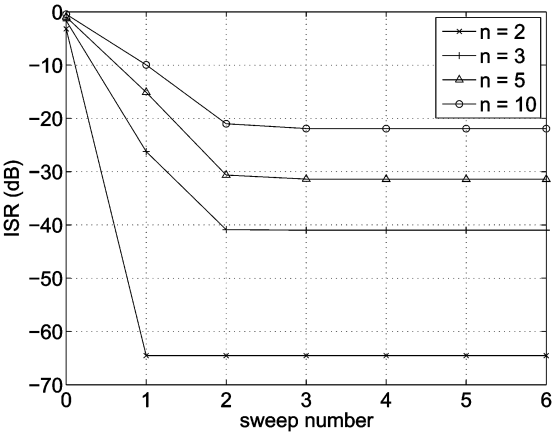

Fig. 3. Source extraction performance of the KSP contrast (3) for different mixture sizes.

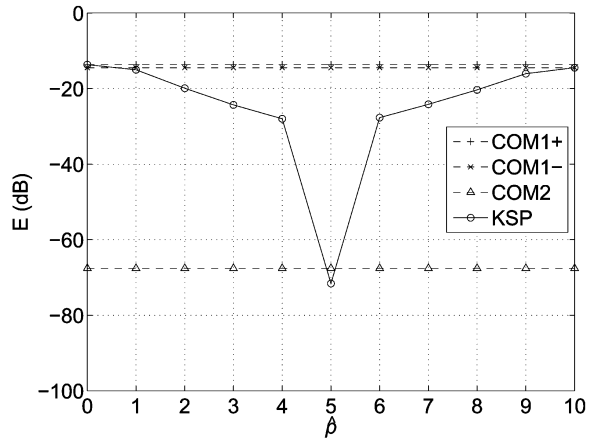

Fig. 2. Source separation performance of ICA contrasts as a function of the estimated number of positive-kurtosis sources $\hat{p}$. The correct value is $p = 5$.

have positive kurtosis while, actually, $p = 5$. KSP's separation performance degrades as the available knowledge becomes less accurate.

Finally, we set $p = 1$ and aim at the single source with positive kurtosis through the extraction procedure described at the end of Section III. Fig. 3 plots the average interference-to-signal ratio (ISR) for the estimation of the first source, defined as

$$ISR = 1 - \frac{|G_{11}|^2}{\sum_{j=1}^{n} |G_{1j}|^2}$$

as a function of the sweep number. This result illustrates the ability of the KSP contrast (3) to extract a source of known kurtosis sign from a mixture where all other sources have the opposite sign, without having to separate the whole mixture and resolve the permutation ambiguity after separation.

V. Conclusions

An orthogonal contrast for ICA has been proposed which takes into account the non-Gaussian character of the source signals as measured by the sign of their fourth-order marginal cumulants (kurtosis). The contrast is linked to an approximate ML principle and is able to separate the independent sources into two groups, depending on their kurtosis sign, thus partially solving the permutation ambiguity usually associated with ICA. The iterative pairwise maximization of the proposed contrast can be carried out at low complexity by closed-form solutions. As opposed to alternative fully blind techniques, the new contrast is particularly suited to the direct extraction of a source with known kurtosis sign distinct from the others'. The principle extends to higher-order cumulants other than kurtosis, as proved in the Appendix.

Appendix

Proof of Proposition 1: The following proof generalizes the result of Proposition 1 to rth-order cumulants, with $r \geq 3$. Accordingly, in the sequel, κ_i and μ_i denote the standardized rth-order cumulant of source s_i and output y_i, respectively, whereas $\varepsilon_i = \mathrm{sign}(\kappa_i)$.

By the multilinearity property of cumulants, we have $\mu_i = \sum_{j=1}^{n} G_{ij}^r \kappa_j$, where $G_{ij} = [\mathbf{G}]_{ij}$. Hence

$$\Psi_p(\mathbf{y}) = \sum_{i=1}^{n} \varepsilon_i \sum_{j=1}^{n} G_{ij}^r \kappa_j.$$

The triangular inequality yields

$$\Psi_p(\mathbf{y}) \leq \sum_{i=1}^{n} \sum_{j=1}^{n} |G_{ij}|^r |\kappa_j| \leq \sum_{i=1}^{n} \sum_{j=1}^{n} |G_{ij}|^2 |\kappa_j|$$

where the right-hand side term stems from the fact that $r \geq 3$ and the orthonormality of matrix $\mathbf{G}$, which can be expressed as $\sum_i |G_{ij}|^2 = 1$. Invoking again this property, we obtain

$$\Psi_p(\mathbf{y}) \leq \sum_{j=1}^{n} |\kappa_j| = \sum_{j=1}^{n} \varepsilon_j \kappa_j = \Psi_p(\mathbf{s}).$$

This proves the domination. Now if the equality $\Psi_p(\mathbf{y}) = \Psi_p(\mathbf{s})$ holds, we must have

$$\sum_{i=1}^{n} \sum_{j=1}^{n} \left[|G_{ij}|^2 - |G_{ij}|^r \right] |\kappa_j| = 0.$$

Yet all the terms in the sums are positive, and thus, they must all vanish. In other words, $|G_{ij}|^2 - |G_{ij}|^r = 0, \forall\, i,j$, with $r \geq 3$, which can occur only if $|G_{ij}| \in \{0,1\}$. Because $\mathbf{G}$ is orthonormal, it must then have only one nonzero element in every row and column. Hence, $\mathbf{G}$ is of the form (2), with $D_i = [\mathbf{D}]_{ii} = \pm 1$. This proves the discrimination property. Function $\Psi_p(\mathbf{y})$ is thus a contrast for ICA. ■

Proof of Proposition 2: This proof extends the validity of Proposition 2 to any even order $r \geq 4$. As seen above, equality $\Psi_p(\mathbf{y}) = \Psi_p(\mathbf{s})$ holds if and only if

$$\sum_{i=1}^{n} \varepsilon_i \sum_{j=1}^{n} G_{ij}^r \kappa_j = \sum_{j=1}^{n} \varepsilon_j \kappa_j.$$

Because $D_j = \pm 1$ and $\mathbf{P}$ is a permutation, we have that $G_{ij}^r = P_{ij}$, with $P_{ij} = [\mathbf{P}]_{ij}$, as r is even. Also, $\varepsilon_i^2 = 1$ and $\varepsilon_j \kappa_j = |\kappa_j|$, so that

$$\sum_{j=1}^{n} \left[1 - \sum_{i=1}^{n} \varepsilon_i P_{ij} \varepsilon_j \right] |\kappa_j| = 0.$$

Yet, since all the terms in the sum are positive, they must individually vanish, yielding the relation

$$\sum_{i=1}^{n} \varepsilon_i P_{ij} \epsilon_j = 1, \quad \forall\, j.$$

Now, by splitting the sum into two parts, we are able to replace ε_i by its value, yielding $\sum_{i=1}^{p} P_{ij}\varepsilon_j - \sum_{i=p+1}^{n} P_{ij}\varepsilon_j = 1$. Let us distinguish between the cases $j \leq p$ and $j > p$, and take into account the fact that, for any permutation, $\sum_{i=1}^{n} P_{ij} = 1$. Then

$$\begin{cases} 1 - 2 \sum\limits_{i=p+1}^{n} P_{ij} = 1, & \forall\, j \leq p \\ 1 - 2 \sum\limits_{i=1}^{p} P_{ij} = 1, & \forall\, j > p. \end{cases}$$

The first equality yields, for any $j \leq p$, $\sum_{i=p+1}^{n} P_{ij} = 0$. That is, by positivity, $P_{ij} = 0$. Thus, the $(n-p) \times p$ bottom left block of $\mathbf{P}$ is null. Analogously, we see that for any $j > p$, $\sum_{i=1}^{p} P_{ij} = 0$, and thus, the $p \times (n-p)$ top right block of $\mathbf{P}$ must also be null. Consequently, the permutation matrix takes indeed the form (5). ■

REFERENCES

[1] P. Comon, "Independent component analysis, a new concept?," *Signal Process.*, vol. 36, no. 3, pp. 287–314, Apr. 1994.

[2] S. Haykin, Ed., *Unsupervised Adaptive Filtering*, ser. Adaptive and Learning Systems for Communications, Signal Processing, and Control. New York: Wiley, 2000.

[3] A. Hyvärinen, J. Karhunen, and E. Oja, *Independent Component Analysis*. New York: Wiley, 2001.

[4] A. Cichocki and S.-I. Amari, *Adaptive Blind Signal and Image Processing: Learning Algorithms and Applications*. New York: Wiley, 2002.

[5] P. Comon and E. Moreau, "Improved contrast dedicated to blind separation in communications," in *Proc. ICASSP-97, 22nd IEEE Int. Conf. Acoustics, Speech and Signal Processing*, Munich, Germany, Apr. 20–24, 1997, pp. 3453–3456.

[6] J.-F. Cardoso, "Higher-order contrasts for independent component analysis," *Neural Comput.*, vol. 11, pp. 157–192, 1999.

[7] R. Phlypo, Y. D'Asseler, I. Lemahieu, and V. Zarzoso, "Extraction of the atrial activity from the ECG based on independent component analysis with prior knowledge of the source kurtosis signs," in *Proc. EMBC-2007, 29th Annu. Int. Conf. IEEE Engineering in Medicine and Biology Society*, Lyon, France, Aug. 23–26, 2007.

[8] R. Phlypo, V. Zarzoso, P. Comon, Y. D'Asseler, and I. Lemahieu, "Extraction of atrial activity from the ECG by spectrally constrained kurtosis sign based ICA," in *Proc. ICA-2007, 7th Int. Conf. Independent Component Analysis and Signal Separation*, London, U.K., Sep. 9–12, 2007.

[9] Z.-Y. Liu, K.-C. Chiu, and L. Xu, "One-bit-matching conjecture for independent component analysis," *Neural Comput.*, vol. 16, no. 2, pp. 383–399, Feb. 2004.

[10] V. Zarzoso and A. K. Nandi, "Blind separation of independent sources for virtually any source probability density function," *IEEE Trans. Signal Process.*, vol. 47, no. 9, pp. 2419–2432, Sep. 1999.

[11] V. Zarzoso, A. K. Nandi, F. Herrmann, and J. Millet-Roig, "Combined estimation scheme for blind source separation with arbitrary source PDFs," *Electron. Lett.*, vol. 37, no. 2, pp. 132–133, Jan. 2001.

[12] V. Zarzoso and A. K. Nandi, "Modelling signals of arbitrary kurtosis for testing BSS methods," *Electron. Lett.*, vol. 34, no. 1, pp. 29–30, Jan. 1998.

[13] E. Moreau and O. Macchi, "A one stage self-adaptive algorithm for source separation," in *Proc. ICASSP-94, 19th IEEE Int. Conf. Acoustics, Speech and Signal Processing*, Apr. 1994, vol. 3, pp. 49–52.

Second-order criterion for blind source extraction

V. Zarzoso

A second-order criterion for blind signal extraction in instantaneous linear mixtures has recently been proposed. It is proved that, with an adequate choice of autocorrelation time lags, the criterion leads indeed to a successful source extraction in the noiseless case. Using this criterion, the source identifiability conditions turn out to be the same as in the popular second-order blind identification method for blind source separation.

Introduction: Recently, a novel technique for blind source extraction (BSE), relying on second-order statistics (SOS), has been presented [1]. The technique is based on the instantaneous linear mixing model for the observed signals $\boldsymbol{x}(t) = [x_1(t), \ldots, x_N(t)]^{\mathrm{T}} \in \mathbb{R}^N$:

$$\boldsymbol{x}(t) = \boldsymbol{M}\boldsymbol{s}(t) \tag{1}$$

where $s(t) = [s_1(t), \ldots, s_N(t)]^{\mathrm{T}} \in \mathbb{R}^N$ is the source vector and $\boldsymbol{M} = [\boldsymbol{m}_1, \ldots, \boldsymbol{m}_N] \in \mathbb{R}^{N\times N}$ represents the full column rank mixing matrix. BSE aims at estimating one of the sources at the extractor output:

$$y(t) = \boldsymbol{n}^{\mathrm{T}}\boldsymbol{x}(t) \tag{2}$$

through an appropriately designed extracting vector $\boldsymbol{n} \in \mathbb{R}^N$. Let $\boldsymbol{R}_\tau = \mathrm{E}\{\boldsymbol{x}(t)\boldsymbol{x}^{\mathrm{T}}(t-\tau)\}$ denote the sensor-output autocorrelation matrix at time lag τ. It is claimed in [1] that a valid extracting vector $\boldsymbol{n}$ can be obtained from the minimisation of functional

$$J(\boldsymbol{n}, \boldsymbol{t}, \boldsymbol{d}) = \sum_{k=0}^{K} \|\boldsymbol{R}_{\tau_k}\boldsymbol{n} - d_{\tau_k}\boldsymbol{t}\|^2 \tag{3}$$

with respect to vectors $\boldsymbol{n}, \boldsymbol{t} \in \mathbb{R}^N$ and $\boldsymbol{d} = [d_{\tau_0}, d_{\tau_1}, \ldots, d_{\tau_K}]^{\mathrm{T}} \in \mathbb{R}^{K+1}$. In that work, this claim is given a geometrical interpretation in terms of oblique projection operators and demonstrated through numerical experiments. The sources are assumed to be uncorrelated and coloured, but no evidence is presented as to why their spectra should be distinct. This Letter provides a more thorough justification for this approach and proves that, under the assumptions of model (1) and with an appropriate choice of time lags $\{\tau_k\}_{k=0}^K$, the minimisation of (3) is indeed achieved if and only if $\boldsymbol{n}$ is a valid extracting vector. In addition, the source identifiability conditions are found to be the same as in the well-known second-order blind identification (SOBI) method [2] for blind source separation (BSS).

Any valid extracting vector minimises the criterion: Let us assume that $\boldsymbol{n}$ is a valid extraction vector for source $s_i(t)$. Then, by definition:

$$\boldsymbol{n}^{\mathrm{T}}\boldsymbol{x}(t) = \alpha s_i(t) \tag{4}$$

for an admissible (but otherwise irrelevant) non-zero scale factor $\alpha \in \mathbb{R}$. Left-multiplying both sides of (4) by $\boldsymbol{x}^{\mathrm{T}}(t-\tau)$, taking mathematical expectations and exploiting the source uncorrelation assumption, one arrives at $\boldsymbol{R}_\tau\boldsymbol{n} = \alpha r_i(\tau)\boldsymbol{m}_i$, where $r_i(\tau)$ stands for the ith source autocorrelation function at time lag τ. Hence, all valid extracting vectors $\boldsymbol{n}$ for source $s_i(t)$ exactly minimise function (3) for any τ with $d_\tau\boldsymbol{t} = \alpha r_i(\tau)\boldsymbol{m}_i$. This result provides supporting evidence for the validity of BSE criterion (3). Next, we see that, under some additional conditions, all minimisers of (3) are indeed valid extracting vectors.

Any minimiser of the criterion is a valid extracting vector: Let $\boldsymbol{R}_\tau^s = \mathrm{E}\{s(t)s^{\mathrm{T}}(t-\tau)\} = \mathrm{diag}(r_1(\tau), r_2(\tau), \ldots, r_N(\tau))$ denote the source autocorrelation matrix at time lag τ. Assume that vectors $\boldsymbol{n}$, $\boldsymbol{t}$ and $\boldsymbol{d}$ are non-trivial exact minimisers of (3) for a time-lag set $\mathrm{T} = \{\tau_k\}_{k=0}^K$. By virtue of model (1), we have

$$\boldsymbol{R}_{\tau_k}\boldsymbol{n} = \boldsymbol{M}\boldsymbol{R}_{\tau_k}^s\boldsymbol{M}^{\mathrm{T}}\boldsymbol{n} = \boldsymbol{M}\boldsymbol{R}_{\tau_k}^s a, \quad 0 \le k \le K \tag{5}$$

where

$$\boldsymbol{a} = \boldsymbol{M}^{\mathrm{T}}\boldsymbol{n}, \quad [\boldsymbol{a}]_i = a_i = \boldsymbol{m}_i^{\mathrm{T}}\boldsymbol{n} \tag{6}$$

Extractor output (2) can then be written as

$$y(t) = \sum_{i=1}^{N} a_i s_i(t) \tag{7}$$

Hence, a successful source extraction requires that at most one entry of $\boldsymbol{a}$ be different from zero.

Since the triplet $(\boldsymbol{n}, \boldsymbol{t}, \boldsymbol{d})$ is a perfect minimiser of criterion (3), the last term in (5) can be expressed as

$$\boldsymbol{M}\boldsymbol{R}_{\tau_k}^s\boldsymbol{a} = d_{\tau_k}\boldsymbol{t} \quad 0 \le k \le K \tag{8}$$

As $\boldsymbol{M}$ is full column rank, its columns span $\mathbb{R}^N$ and there is a unique linear combination, with coefficients stacked in vector $\boldsymbol{b} \in \mathbb{R}^N$, yielding $\boldsymbol{t}$:

$$\boldsymbol{M}\boldsymbol{b} = \boldsymbol{t} \tag{9}$$

Combining (8) and (9), we must have that $\boldsymbol{R}_{\tau_k}{}^s\,\boldsymbol{a} = d_{\tau_k}\,\boldsymbol{b}$, which implies that

$$a_i r_i(\tau_k) = d_{\tau_k} b_i, \quad 1 \le i \le N, \quad 0 \le k \le K \tag{10}$$

Define the ith-source autocorrelation vector as $\boldsymbol{r}_i(\mathrm{T}) = [r_i(\tau_0), r_i(\tau_1), \ldots, r_i(\tau_K)]^{\mathrm{T}}$. Then, relationship (10) can be compactly expressed as $\boldsymbol{r}_i(\mathrm{T})a_i = \boldsymbol{d}b_i$, $1 \le i \le N$. Since $\boldsymbol{r}_i(\mathrm{T})$ and $\boldsymbol{d}$ are non-null vectors, we can only have either $a_i = b_i = 0$ or $\boldsymbol{r}_i(\mathrm{T}) = \boldsymbol{d}b_i/a_i$. If vector $\boldsymbol{a}$ had another element different from zero, say its jth entry, $j \ne i$, then we would also have $\boldsymbol{r}_j(\mathrm{T}) = \boldsymbol{d}b_j/a_j$, and the autocorrelation functions of $s_i(t)$ and $s_j(t)$ would be proportional to each other at the selected lags, $\boldsymbol{r}_i(\mathrm{T}) = c_{ij}\boldsymbol{r}_j(\mathrm{T})$, with $c_{ij} = b_i a_j/(b_j a_i)$. To prevent this possibility, which leads to a non-extracting solution [recall (7)], it is necessary to choose a time-lag set T such that $\boldsymbol{r}_i(\mathrm{T})$ and $\boldsymbol{r}_j(\mathrm{T})$ are not parallel, $1 \le i < j \le N$. If this condition is met, there can be at most one coefficient $a_i \ne 0$. From (6), it follows that $\boldsymbol{m}_j^{\mathrm{T}}\boldsymbol{n} = 0$, $j \ne i$, and, according to (2) and (7), the application of vector $\boldsymbol{n}$ verifying such constraints yields $\boldsymbol{n}^{\mathrm{T}}\boldsymbol{x}(t) = \alpha s_i(t)$, with $\alpha = a_i = \boldsymbol{m}_i^{\mathrm{T}}\boldsymbol{n}$. Therefore, vector $\boldsymbol{n}$ obtained from the exact minimisation of criterion (3) is a valid extracting vector as long as the time-lag set T fulfils the above condition.

In general, the finite sample size or the presence of noise will prevent functional (3) from being cancelled exactly. Nevertheless, its minimisation constitutes a somewhat natural least squares (LS) criterion, the solutions of which are thus expected to lie near valid extractors.

Source identifiability conditions: According to the above proof, a time-lag set for which a pair of source autocorrelation vectors are parallel does not guarantee source identifiability through the minimisation of criterion (3), even if the source spectra are different. At first sight, this condition may seem slightly more stringent than the uniqueness condition of the SOBI algorithm for BSS [2]: $\forall 1 \le i < j \le N$, $\exists k$, $0 \le k \le K$, such that $r_i(\tau_k) \ne r_j(\tau_k)$, which in our notation can be expressed as $\boldsymbol{r}_i(\mathrm{T}) \ne \boldsymbol{r}_j(\mathrm{T})$, $1 \le i < j \le N$. However, the data whitening step in SOBI enforces $r_i(0) = 1$, $1 \le i \le N$, so that two source autocorrelation vectors can only be parallel if they are identical. Hence, the necessary conditions for source identifiability are actually the same in both techniques. As in SOBI, increasing the number of lags will also reduce the probability of degeneracy in the BSE criterion (3). Asymptotically, as the number of lags tends to infinity, the condition becomes that no pair of source spectra be equal up to scale. Again, owing to the amplitude constraints imposed by prewhitening, this asymptotic condition is identical to SOBI's.

Conclusions: This Letter has proven that the minimisation of function (3) is a valid criterion for BSE under the same conditions as the well-known SOBI technique for BSS. It should be noted, however, that the global convergence of the alternating LS algorithm proposed in [1] to minimise the criterion is not guaranteed. The analysis of this iterative algorithm should be addressed in future investigations.

Acknowledgment: The author thanks A. Yeredor for his interesting comments on a preliminary version of this Letter.

4 September 2008
Electronics Letters online no: 20082581
doi: 10.1049/el:20082581

V. Zarzoso (*I3S Laboratory, University of Nice - Sophia Antipolis, CNRS, Les Algorithmes, Euclide-B, BP 121, 2000 route des Lucioles, Sophia Antipolis Cedex 06903, France*)

E-mail: zarzoso@i3s.unice.fr

References

1 Li, X.-L., and Zhang, X.-D.: 'Sequential blind extraction adopting second-order statistics', *IEEE Signal Process. Lett.*, 2007, **14**, (1), pp. 58–61

2 Belouchrani, A., Abed-Meraim, K., Cardoso, J.-F., and Moulines, E.: 'A blind source separation technique using second-order statistics', *IEEE Trans. Signal Process.*, 1997, **45**, (2), pp. 434–444

EUROPEAN TRANSACTIONS ON TELECOMMUNICATIONS
Eur. Trans. Telecomms. 2008; **19**:751–759
Published online 29 September 2008 in Wiley InterScience
(www.interscience.wiley.com) DOI: 10.1002/ett.1321

Blind channel identification in Alamouti coded systems: a comparative study of eigendecomposition methods in indoor transmissions at 2.4 GHz†

Héctor J. Pérez-Iglesias[1], José A. García-Naya[1], Adriana Dapena[1]*, Luis Castedo[1] and Vicente Zarzoso[2]

[1]*Departamento de Electrónica y Sistemas, Universidade da Coruña, Facultad de Informática, Campus de Elviña, no. 5, 15071 A Coruña, Spain*
[2]*Laboratoire I3S, Université de Nice-Sophia Antipolis, Les Algorithmes, Euclide-B, BP 121 06903 Sophia Antipolis, France*

SUMMARY

This paper focuses on blind channel estimation in Alamouti coded systems with one receiving antenna working in indoor scenarios where the flat fading assumption is reasonable. A comparative study of several channel estimation techniques in both simulated and realistic scenarios is presented. The tested methods exploit the orthogonality property of the Alamouti coded channel matrix, and are based on the eigendecomposition of a square matrix made up of second-order statistics (SOS) or higher order statistics (HOS) of the observed signals. An experimental evaluation is carried out on a testbed developed at the University of A Coruña (UDC) and operating at 2.4 GHz. The results show the superior performance of the SOS-based blind channel estimation technique in both line of sight (LOS) and non-LOS (NLOS) channels.

1. INTRODUCTION

During the last decade, a large number of space-time coding (STC) techniques have been proposed to exploit the spatial diversity in multiple input multiple output (MIMO) wireless communication systems that employ multiple antennas at both transmission and reception (see, for instance, References [1, 2] and references therein). A remarkable example is orthogonal space time block coding (OSTBC) because it is able to provide full transmit diversity without any channel state information (CSI) at transmission and with very simple encoding and decoding procedures [3, 4]. The basic premise of OSTBC is the encoding of the transmitted symbols into an orthogonal matrix which reduces the optimum maximum likelihood (ML) decoder to a matrix-matched filter followed by a symbol-by-symbol detector.

The OSTBC scheme for MIMO systems with two transmit antennas is known as the Alamouti code [3] and it is the only OSTBC capable of achieving full spatial rate for complex constellations. Other OSTBCs have been proposed for more than two transmit antennas but they suffer from severe spatial rate loss [4, 5]. The Alamouti code can be used in systems with one or multiple antennas at the receiver. Here, (2×1) Alamouti coded systems are used due to their simplicity and their ability to provide maximum diversity gain while achieving the full available channel capacity. It should be noted that Alamouti schemes do not achieve the full potential capacity with more than one receive antenna [6], although the difference is small and of course both diversity and capacity are significantly increased with more than one receive antenna. Because of these advantages, the Alamouti code has been incorporated in the IEEE 802.11 and IEEE 802.16 standards [7].

Coherent detection in (2×1) Alamouti coded systems requires the identification of a (2×2) unitary channel matrix. The standard way to estimate this channel matrix is through the transmission of pilot symbols, also referred to as training sequences. However, the inclusion of pilot symbols reduces the system throughput (equivalently, it reduces the

* Correspondence to: Adriana Dapena, Departamento de Electrónica y Sistemas, Universidade da Coruña, Facultad de Informática, Campus de Elviña, no. 5, 15071 A Coruña, Spain. E-mail: adriana@udc.es
† A previous version of this paper was presented in the 13th European Wireless Conference (EW 2007), Paris, France.

 Accepted 16 June 2008

system spectral efficiency) and wastes transmission energy because training sequences do not convey information. One way to avoid this limitation is the utilisation of differential STBC (DSTBC) [8], a generalisation of differential modulations to the transmission over MIMO channels. Indeed, DSTBCs can be incoherently decoded without the aid of channel estimates but at the cost of a 3-dB performance penalty when compared to coherent detection.

Alternatively, training sequences can be avoided by the use of blind channel identification methods. Although a lot of techniques exist in the literature, in this paper we focus on blind channel estimation methods that are based on the eigenvector decomposition of a (2×2) matrix because of their good trade-off between complexity and performance. In particular, we propose novel methods based on diagonalising matrices containing second-order statistics (SOS) and higher order statistics (HOS) of the receiving signals. These methods, originally proposed in Reference [9], are particularly suitable for the application at hand for three reasons: they exploit the orthogonal property of the channel matrix to be identified; their complexity is very low and they provide an adequate channel estimation for small data blocks. We also consider the method proposed by Beres and Adve [10] for OSTBC which has similar complexity load. As a benchmark, we compare the results with the joint approximate diagonalisation of eigenmatrices (JADE) algorithm [11] although its feasibility in real-time systems is very limited due to its high complexity.

In this paper, we evaluate the performance of the blind channel estimation techniques over both computer simulated flat fading channels and realistic indoor scenarios. For this latter performance evaluation, we have used a MIMO hardware demonstrator developed at the University of A Coruña (UDC), Spain, that operates at the 2.4 GHz Industrial, Scientific and Medical (ISM) band. The evaluation results show the superior performance of the SOS-based method and its ability to approach the same performance as if the channel were least squares (LS) estimated with long training sequences. The SOS-based method is also the least computationally demanding of all compared techniques.

This paper is structured as follows. Section 2 presents the signal model of a (2×1) Alamouti coded system. Section 3 explains the blind methods used to estimate the channel matrix. Section 4 presents the performance results obtained by means of computer simulations. Section 5 describes the MIMO testbed and presents the obtained experimental results. Finally, Section 6 is devoted to the conclusions.

Notations. Throughout this work, boldface uppercase letters are used to denote matrices, for example $\mathbf{X}$, with elements $x_{i,j}$; boldface lowercase letters for column vectors, for example $\mathbf{x}$, and lightface lowercase letters for scalar quantities. Superscripts $(\cdot)^*$, $(\cdot)^{\mathrm{T}}$ and $(\cdot)^{\mathrm{H}}$ represent the conjugate, transpose and Hermitian operators, respectively. The identity matrix of dimensions $(p \times p)$ will be denoted as $\mathbf{I}_p$ and E[·] stands for the expectation operator.

2. ALAMOUTI CODED SYSTEMS

Figure 1 depicts the baseband representation of an Alamouti coded system with one receiving antenna. Each pair of symbols $\{s_1, s_2\}$ is transmitted in two adjacent periods using a simple strategy: in the first period s_1 and s_2 are transmitted

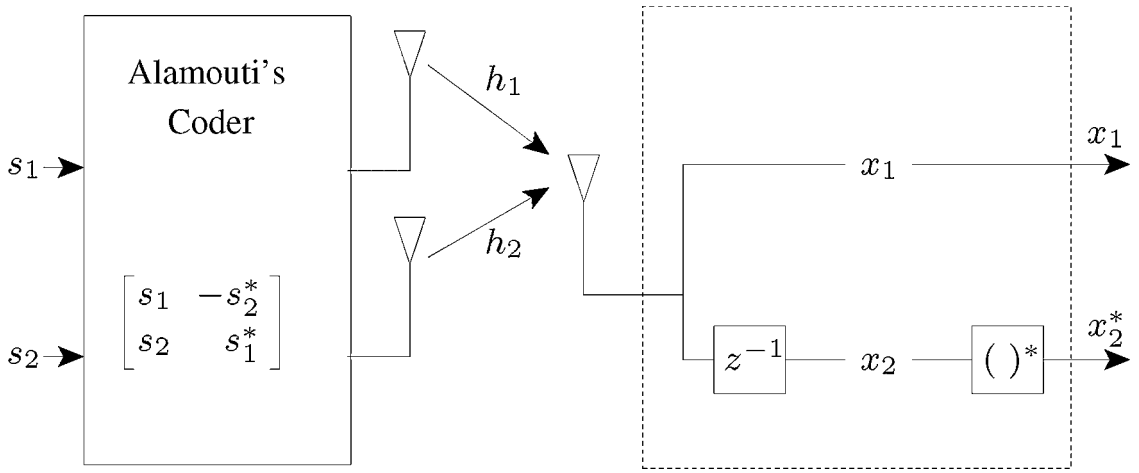

Figure 1. Block diagram of the 2×1 Alamouti coded system.

Eur. Trans. Telecomms. 2008; **19**:751–759
DOI: 10.1002/ett

through the first and second antennas, respectively, and in the second period $-s_2^*$ is transmitted through the first antenna and s_1^* from the second one. We assume that the exact probability density function of s_i is unknown although they take values from the alphabet of a typical complex modulation such as QAM or PSK. The data sequence is assumed to be composed of independent and identically distributed symbols, so that s_1 and s_2 are statistically independent.

In indoor scenarios, the delay spread of the different multipaths is rather small so it is natural to model the wireless channel as flat fading: the transmitted symbols arrive at the receiving antenna through the fading paths h_1 and h_2. Thus, the signal received during the first period is $x_1 = s_1 h_1 + s_2 h_2 + n_1$. Assuming that the channel remains unchanged, the observation in the second period is given by $x_2 = s_1^* h_2 - s_2^* h_1 + n_2$. Defining the observation vector as $\mathbf{x} = [x_1 \;\; x_2^*]^{\mathrm{T}}$, we obtain that the relationship between the observation vector $\mathbf{x}$ and the source vector $\mathbf{s} = [s_1 \;\; s_2]^{\mathrm{T}}$ is given by

$$\mathbf{x} = \mathbf{H}\mathbf{s} + \mathbf{n} \tag{1}$$

where $\mathbf{H}$ is the (2×2) effective channel matrix,

$$\mathbf{H} = \begin{bmatrix} h_1 & h_2 \\ h_2^* & -h_1^* \end{bmatrix} \tag{2}$$

and where $\mathbf{n} = [n_1 \;\; n_2^*]^{\mathrm{T}}$ is the AWGN modelled as a vector of two uncorrelated zero-mean, complex-valued, circularly symmetric, Gaussian distributed random processes. It is interesting to note that $\mathbf{H}$ is an orthogonal matrix, that is $\mathbf{H}\mathbf{H}^{\mathrm{H}} = \mathbf{H}^{\mathrm{H}}\mathbf{H} = \|\mathbf{h}\|^2 \mathbf{I}_2$ where $\|\mathbf{h}\|^2 = |h_1|^2 + |h_2|^2$ is the squared Euclidean norm of $\mathbf{h}$.

Filtering $\mathbf{x}$ with the matrix-matched filter yields the following decision statistics

$$\mathbf{y} = \mathbf{H}^{\mathrm{H}}\mathbf{x} = \|\mathbf{h}\|^2 \mathbf{s} + \tilde{\mathbf{n}} \tag{3}$$

where $\tilde{\mathbf{n}} = \mathbf{H}^{\mathrm{H}}\mathbf{n}$ is the output noise vector, with the same statistical properties as the input noise. It is apparent from Equation (3) that ML detection of s_1 and s_2 can be calculated by applying $\mathbf{y}$ to a pair of independent scalar slicers. Consequently, the correct detection of the transmitted symbols $\mathbf{s}$ requires the accurate estimation of the channel matrix $\mathbf{H}$ from the received data $\mathbf{x}$.

3. MIMO CHANNEL ESTIMATION

This section describes the channel estimation techniques that will be tested in Sections 4 and 5. The methods are based on computing a (2×2) squared matrix, $\mathbf{C}$, containing SOS or HOS of the received signals. The basic premise of the considered methods is that $\mathbf{C}$ has an algebraic structure of the form $\mathbf{H}\boldsymbol{\Delta}\mathbf{H}^{\mathrm{H}}$ where $\boldsymbol{\Delta}$ is a diagonal matrix. Due to the orthogonal structure of $\mathbf{H}$, if the diagonal entries of $\boldsymbol{\Delta}$ are different, the channel matrix can be identified from the eigenvectors of $\mathbf{C}$ with a possible change of scale and permutation.

3.1. SOS-based approach

We will start by describing a method that estimates the channel from the eigenvectors of the observations autocorrelation matrix. Unlike other SOS-based algorithms [12, 13], this method does not require the use of an additional outer encoder.

According to the signal model in Equation (1), the observations autocorrelation matrix can be written as

$$\mathbf{C}_{\mathrm{SOS}} = \mathrm{E}[\mathbf{x}\mathbf{x}^{\mathrm{H}}] = \mathbf{H}\mathbf{R}_{\mathbf{s}}\mathbf{H}^{\mathrm{H}} + \sigma_n^2 \mathbf{I}_2 \tag{4}$$

where σ_n^2 is the noise power and $\mathbf{R}_{\mathbf{s}} = \mathrm{E}[\mathbf{s}\mathbf{s}^{\mathrm{H}}]$ is the correlation matrix of the transmitted signals. Since $\mathbf{H}$ is orthogonal, Equation (4) can be rewritten as the following eigenvalue decomposition:

$$\mathbf{C}_{\mathrm{SOS}} = \mathbf{H}\left(\mathbf{R}_{\mathbf{s}} + \frac{\sigma_n^2}{\|\mathbf{h}\|^2}\mathbf{I}_2\right)\mathbf{H}^{\mathrm{H}} \tag{5}$$

Notice that if the two transmitted sources have the same power $\mathbf{C}_{\mathrm{SOS}}$ is diagonal and, as a consequence, $\mathbf{H}$ is not identifiable from an eigenvalue decomposition.

For the system to be identifiable, we propose to unbalance the power of the transmitted sources as follows:

$$\mathrm{E}[|s_1'|^2] = \frac{2\sigma_s^2}{1+\gamma^2}, \quad \mathrm{E}[|s_2'|^2] = \frac{2\gamma^2\sigma_s^2}{1+\gamma^2} \tag{6}$$

where $0 < \gamma^2 < 1$ and s_1', s_2' are the new unbalanced sources. In spite of the power unbalancing, notice that the total mean power remains unchanged (i.e. σ_s^2). Now, the eigenvalue decomposition of $\mathbf{C}_{\mathrm{SOS}}$ is

$$\mathbf{C}_{\mathrm{SOS}} = \sigma_s^2 \mathbf{H}\boldsymbol{\Delta}_{\mathrm{SOS}}\mathbf{H}^{\mathrm{H}} \tag{7}$$

where

$$\mathbf{\Delta}_{\mathrm{SOS}} = \begin{bmatrix} 1+\sigma_h^2 & 0 \\ 0 & \gamma^2+\sigma_h^2 \end{bmatrix} \tag{8}$$

contains the eigenvalues of $\mathbf{C}_{\mathrm{SOS}}$ and $\sigma_h^2 = \frac{\sigma_n^2}{\sigma_s^2\|\mathbf{h}\|^2}$. Thanks to the source power imbalance, now matrix $\mathbf{H}$ is identifiable from $\mathbf{C}_{\mathrm{SOS}}$, as $\mathbf{\Delta}_{\mathrm{SOS}}$ contains different eigenvalues.

Obviously, if the power of the two sources is unbalanced, the total channel capacity is lower than that of equally balanced sources. This is the price to be paid for making the SOS-based method applicable and taking advantage of its extremely low computational requirements. However, in Sections 4 and 5, we will show that the best choice is $\gamma^2 \approx 0.6$ and that in this case the total channel capacity is quite close to the balanced case.

3.2. HOS-based approaches

The orthogonal MIMO channel matrix $\mathbf{H}$ can also be estimated from the eigendecomposition of matrices made up of HOS of the received signals without the need of unbalancing the source powers. Indeed, for a (2×1) observation vector, $\mathbf{x}$, the fourth-order cumulant matrix $\mathbf{C}_{\mathrm{HOS}}(\mathbf{M})$ is a (2×2) matrix with components

$$[\mathbf{C}_{\mathrm{HOS}}(\mathbf{M})]_{ij} = \sum_{k,\ell=1}^{2} \mathrm{cum}(x_i, x_j^*, x_k, x_\ell^*) m_{lk} \tag{9}$$

where m_{lk} $k, l = 1, 2$, denote the entries of a (2×2) matrix $\mathbf{M}$ and the fourth-order cumulant is defined by

$$\begin{aligned}\mathrm{cum}(x_1, x_2, x_3, x_4) = {} & E[x_1x_2x_3x_4] - E[x_1x_2]E[x_3x_4] \\ & - E[x_1x_3]E[x_2x_4] - E[x_1x_4]E[x_2x_3]\end{aligned} \tag{10}$$

It has been proved in Reference [11] that, for the particular case of zero-mean signals, the cumulant matrix admits the following decomposition

$$\mathbf{C}_{\mathrm{HOS}}(\mathbf{M}) = \mathbf{H}\mathbf{\Delta}_{\mathrm{HOS}}(\mathbf{M})\mathbf{H}^{\mathrm{H}} \tag{11}$$

where $\rho_{4i} = \mathrm{cum}(s_i, s_i^*, s_i, s_i^*)$ is the kurtosis of the ith source and $\mathbf{\Delta}(\mathbf{M})$ is a diagonal matrix given by

$$\mathbf{\Delta}_{\mathrm{HOS}}(\mathbf{M}) = \mathrm{diag}(\rho_{41}\mathbf{h}_1^{\mathrm{H}}\mathbf{M}\mathbf{h}_1, \rho_{42}\mathbf{h}_2^{\mathrm{H}}\mathbf{M}\mathbf{h}_2) \tag{12}$$

Here, $\mathbf{h}_i$ is the ith column of $\mathbf{H}$, that is $\mathbf{h}_1 = [h_1 \;\; h_2^*]^{\mathrm{T}}$ and $\mathbf{h}_2 = [h_2 \;\; -h_1^*]^{\mathrm{T}}$. Since for the Alamouti coded scheme the channel matrix is orthogonal, $\mathbf{H}^{\mathrm{H}}$ diagonalises $\mathbf{C}_{\mathrm{HOS}}(\mathbf{M})$ for any $\mathbf{M}$ provided that $\mathbf{\Delta}(\mathbf{M})$ contains different entries, that is

$$L = \left|\rho_{41}\mathbf{h}_1^{\mathrm{H}}\mathbf{M}\mathbf{h}_1 - \rho_{42}\mathbf{h}_2^{\mathrm{H}}\mathbf{M}\mathbf{h}_2\right| \neq 0 \tag{13}$$

In particular, the approach proposed by Beres and Adve in Reference [10] considers the cases $m_{11} = 1$, $m_{12} = m_{21} = m_{22} = 0$; and $m_{11} = m_{12} = m_{21} = 0$ and $m_{22} = 1$. Assuming that the transmitted signals have the same kurtosis, we obtain from Equation (13) that the channel matrix is identifiable as long as $|h_1|^2 \neq |h_2|^2$.

As an extension of this approach, we propose to identify $\mathbf{H}$ by computing the eigenvectors of a linear combination of fourth-order cross-cumulant matrices. This can be obtained by using a matrix $\mathbf{M}$ with entries $m_{11} = 1$, $m_{12} = m_{21} = 0$ and $m_{22} = \lambda$, being λ a real valued parameter. From Equation (13), we conclude that this method allows to estimate $\mathbf{H}$ as long as

$$L = (1-\lambda)(|h_1|^2 - |h_2|^2) \neq 0 \tag{14}$$

Thus, the channel is identifiable if $\lambda \neq 1$ and $|h_1|^2 \neq |h_2|^2$. In particular, we propose the utilisation of $\lambda = -1$ since this choice provides a significant performance improvement with respect to the Beres and Adve approach in Reference [10], as will be shown in the following sections.

Another way to estimate the mixing matrix consists in performing a simultaneous diagonalisation of several fourth-order cumulant matrices, as the JADE algorithm [11]. This algorithm provides an excellent performance but, unfortunately, its computational load is very high. In Sections 4 and 5, the JADE algorithm will be used only as a benchmark.

4. COMPUTER SIMULATIONS

This section presents the results of several computer simulations carried out to evaluate the performance of the estimation algorithms proposed in Section 3. The experiments have been carried out by simulating the transmission of QPSK signals in Rayleigh-distributed randomly generated flat fading channels affected by additive white Gaussian noise (AWGN). We assume block fading where the channel remains constant during the transmission of a block of K symbols. The statistics in Equations (4) and (9) have been calculated by sample averaging over each

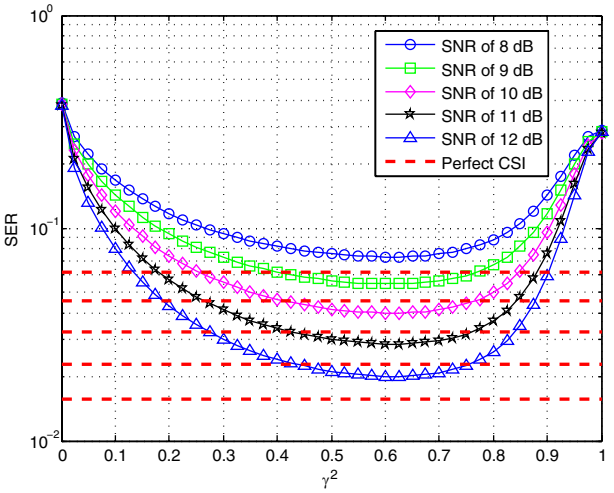

Figure 2. Computer simulations: SER *versus* γ^2 obtained with the SOS-based approach for QPSK signals and different values of SNR $= \sigma_s^2/N_0$. The horizontal dashed lines represent the SER obtained with perfect CSI.

block of symbols and the performance has been measured in terms of the symbol error rate (SER).

We have evaluated the performance of the SOS-based approach for several values of γ^2. Figure 2 shows the SER *versus* γ^2 for signal to noise ratio (SNR) values of 8, 9, 10, 11 and 12 dB. The autocorrelation matrix has been estimated with $K = 500$ symbols. This figure also plots the SER obtained with perfect CSI (horizontal dashed lines). It is apparent that the SOS-based channel estimation approach fails for $\gamma^2 = 1$ because this case corresponds to signals with the same power. The same occurs when $\gamma^2 = 0$ which corresponds to the limiting case where only s_1 is transmitted. Note also that the best performance is obtained with $\gamma^2 \approx 0.6$.

Figure 3 shows the SER *versus* SNR curves of a (2×1) Alamouti coded QPSK system using different methods for the channel estimation: Beres *et al.*, JADE, the novel SOS approach with $\gamma^2 = 0.6$ and the novel HOS approach with $\lambda = -1$. The system performance with perfect CSI is also plotted as a benchmark. The SER curves were obtained by simulating data blocks of $K = 500$ symbols and by averaging the results for 10 000 different realisations. Note that the method proposed by Beres *et al.* is outperformed by the novel HOS approach. However, notice the poor performance of HOS-based methods in the high SNR regime when compared with the novel SOS approach. It is apparent from Figure 3 the superior performance of the SOS approach since it only incurs in a 0.5 dB penalty with respect to the perfect CSI case.

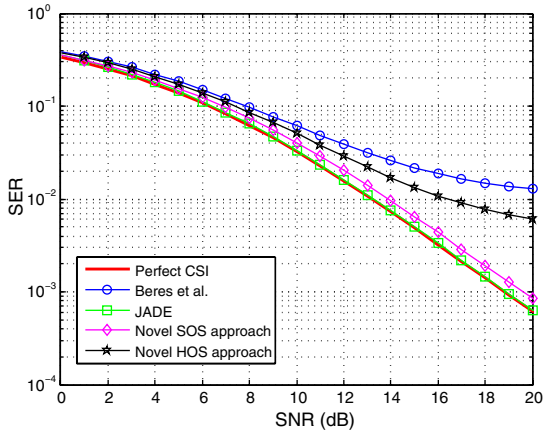

Figure 3. Computer simulations: SER *versus* SNR obtained with the different channel estimation methods.

It is still possible to obtain an even better performance, almost reaching the optimum curve, by using the JADE algorithm (see Figure 3). However, notice the high complexity of the JADE algorithm illustrated in Figure 4 that shows the execution time required to compute 10^4 channel estimates, as a function of the block size. On the other hand, the SOS method exhibits the lowest complexity, which remains almost constant with the block size. Figure 4 also shows the higher complexity of the proposed HOS method with respect to that of Beres *et al.* Thus, we can conclude that the SOS approach exhibits an excellent trade-off between performance and complexity.

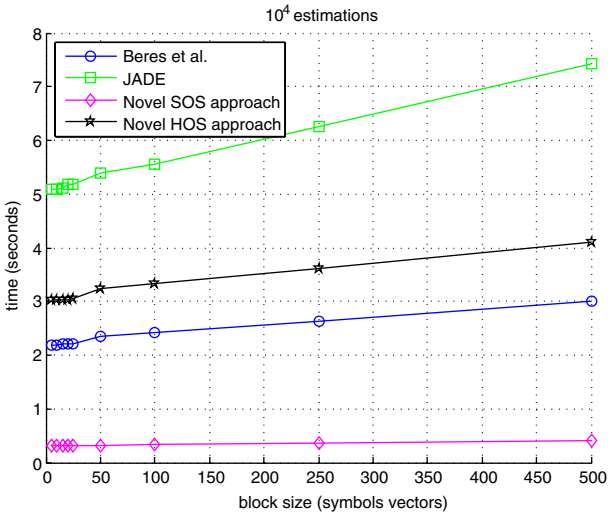

Figure 4. Time required to process 10^4 blocks.

Eur. Trans. Telecomms. 2008; **19**:751–759
DOI: 10.1002/ett

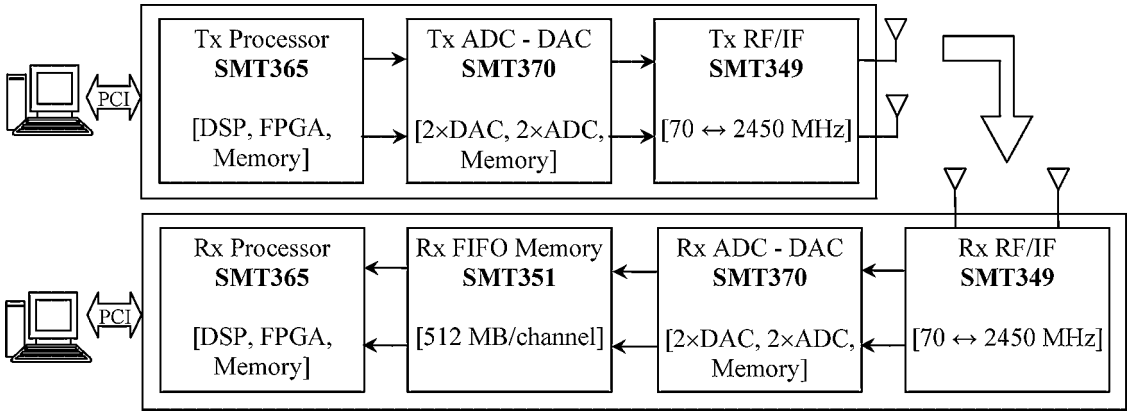

Figure 5. Schematic diagram of the MIMO testbed employed in the experiments.

5. TESTBED RESULTS

5.1. *Description of the* (2 × 2) *MIMO testbed*

Figure 5 shows a diagram of the Testbed PCs. The hardware testbed is based on a PCI carrier board SMT310Q and a basic processing module: the SMT365 equipped with a Xilinx Virtex-II FPGA and a Texas Instruments C6416 DSP at 600 MHz. The processing module has two buses that can transfer 32-bit words up to 400 MB/s, allowing the connection with the SMT370 module, that contains a dual AD9777 D/A converter and two AD6645 A/D converters. The SMT370 module also has a 2 MB per-channel memory that is used to load the frames to be transmitted. At the receiver side, the data acquired by the A/D converters is stored in real time in a 1 GB FIFO memory SMT351 module and, in an off-line task, passed to the middleware through the PCI bus. Finally, the testbed contains two SMT349 RF front-end modules. They perform the up and down conversion operations from an 70 MHz Intermediate Frequency (IF) to a 2.45 GHz carrier RF, with 16 MHz of maximum bandwith.

In order to synchronise both the transmitter and the receiver, a simple synchronisation protocol is implemented over a common Ethernet connection. When the transmitter sends data over the channel, it also sends a control signal to the receiver in order to start the signal acquisition process.

5.2. *Experiments setup*

The MIMO testbed described before has been used to test the estimation methods described in Section 3. Figure 6 shows the block diagram of the (2 × 1) Alamouti coded system with QPSK modulation implemented on the testbed. During the experiments, we generated 1000 QPSK symbols of each source (s_1 and s_2). The first subframe of (2 × 500) symbols is used to test the HOS-based methods. The second subframe, also composed by (2 × 500) symbols, is employed to test the SOS-based method. The power of the second subframe is unbalanced before the Alamouti encoder according to Equation (6).

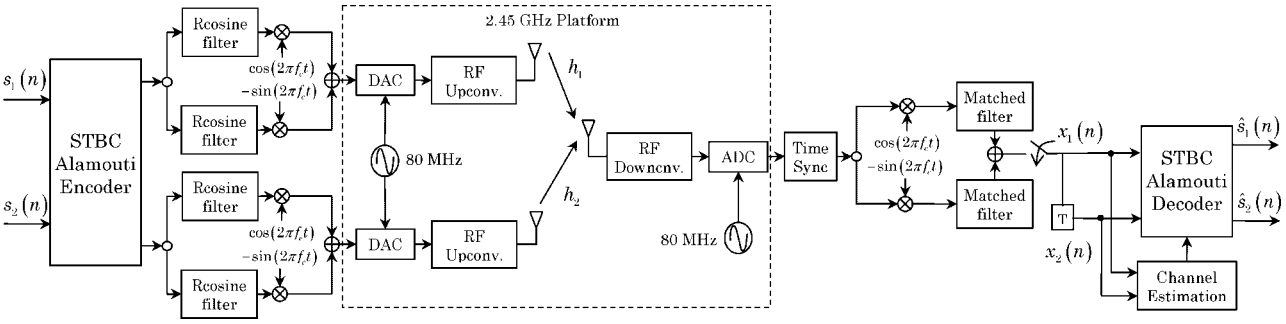

Figure 6. Block diagram of the implemented 2 × 1 Alamouti coded QPSK system.

As a performance bound, we have also evaluated the system performance when using LS channel estimation [15] considering that all symbols of the first subframe are used for training. Subsequently, LS estimation has been used to decode only this subframe. Therefore, its performance is very close to the case where perfect CSI is available at reception.

After the Alamouti encoder, symbols were IQ modulated using 16 samples per symbol, a square root raised cosine pulse shaping with a roll-off factor of 40 per cent and a discrete-time IF of 0.125. Passing this signal through a D/A converter configured with a clock frequency of 80 MHz yields to a QPSK analogue signal of 5 MBauds symbol rate, 7 MHz bandwidth and 10 MHz carrier frequency. Finally, the replica at 70 MHz is filtered out and up converted to a carrier RF frequency of 2.45 GHz.

With the aim of achieving a correct time synchronisation, a 50 pseudo-random symbol sequence is added at the beginning of the frame obtained after the Alamouti encoder. The preamble sequence is only transmitted by one of the two antennas while the other is idle. The resulting frame is thus composed of a 50 symbol preamble 4000 data symbols (2000 information symbols). Since we are using 16 samples per symbol, the frame contains 65 600 16-bit signal samples which results in a frame size equal to 128 125 Kbytes. At the receiver, the known preamble is correlated with the acquired signal to determine the first frame sample. Also a carrier recovery step must be incorporated after the time synchronisation to correct signal frequency impairments due to reference oscillator misadjustments. After IQ demodulation, a root raised cosine-matched filter is used in each demodulator branch followed by a down sampler to produce the I and the Q components of the baseband signal.

In order to experimentally obtain SER *versus* SNR curves for each estimation method, every frame is sent several times with different transmitting power. Different channel realisations and distinct signal strength values are obtained in this manner. In a later step, the SNR is estimated for each received frame jointly with the SER obtained by the estimation method. Finally, the pairs formed by the SNR with its corresponding SER are sorted by SNR value and plotted to obtain a performance curve.

5.3. *Scenario 1: line of sight (LOS)*

Figure 7 shows a schematic diagram of the room layout and the antenna locations where we carried out the experiments. The transmitter and the receiver were approximately 5 m away from each other with a clear LOS between them.

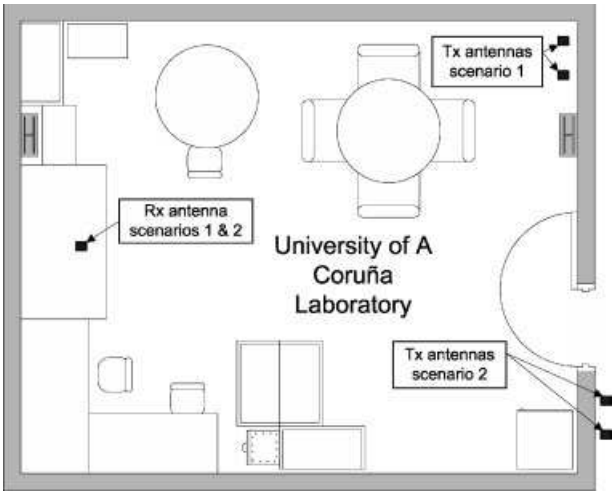

Figure 7. Experimental setup, showing the room layout and the antenna locations.

The transmitting antennas were separated about 30 cm from each other, in order to provide a good spatial diversity.

In order to apply the SOS-based approach proposed in Subsection 3.1, the optimum value of the source power unbalance parameter γ^2 must be found. To this end, the SER was evaluated for different values of γ^2. The results are plotted in Figure 8 for the LOS scenario and show that the optimal value is around $\gamma^2 = 0.64$. This value is in accordance with that obtained by simulations over an uncorrelated Rayleigh channel. In the experiments that follow, we set $\gamma^2_{\text{opt}} = 0.64$.

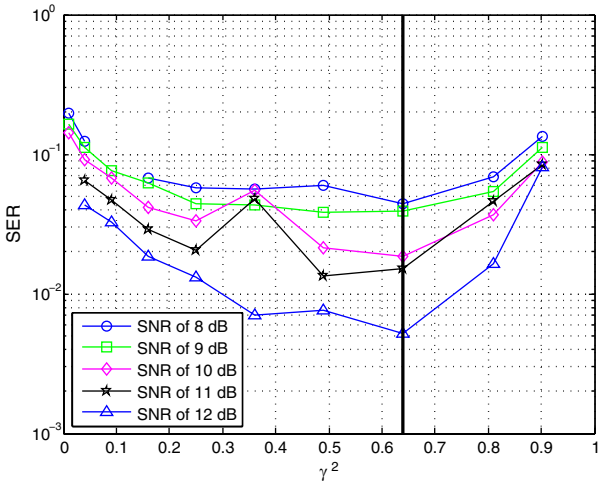

Figure 8. LOS scenario: performance of the SOS-based method as a function of parameter γ^2.

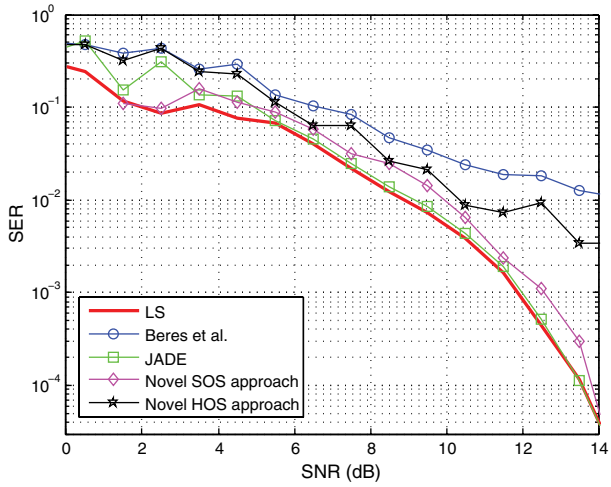

Figure 9. LOS scenario: SER performance *versus* SNR.

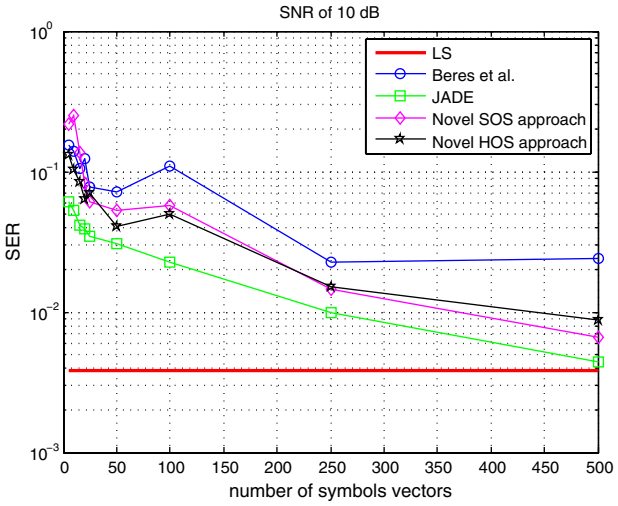

Figure 10. LOS scenario: computational efficiency of the channel estimation methods in terms of SER as a function of the number of used symbols.

Figure 9 shows the obtained SER *versus* SNR curves for a block size $K = 500$ and different methods for channel estimation: JADE, Beres *et al.*, the novel SOS approach with $\gamma^2 = 0.64$ and the novel HOS approach with $\lambda = -1$. Notice that, similarly to the results obtained with computer simulations, the JADE algorithm achieves the same performance as with LS estimation while the SOS-based approach differs in just about 0.5 dB. Figure 9 also shows the poorer performance of HOS methods since they present a flooring effect for SNR values greater than 10 dB. Nevertheless, the performance of the HOS-based method proposed by the authors is better than that of the one proposed by Beres and Adve [10].

In order to evaluate the convergence speed of the channel estimation methods, we calculated the SER for different number of symbols employed to estimate the statistics in Equations (4) and (9), at an SNR of 10 dB. The results are plotted in Figure 10. Notice, again, the superior performance of the SOS-based approach with respect to those based on HOS and its proximity to JADE.

5.4. Scenario 2: non-line of sight

We implemented a second scenario without LOS, where the transmitter was placed about 9 m away from the receiver (see Figure 7). The transmitting antennas were still separated about 30 cm from each other.

Figure 11 illustrates the SER in the non-LOS (NLOS) scenario as a function of the received SNR for a block size $K = 500$ and the different channel estimation methods. Contrarily to the LOS scenario, both the novel SOS and HOS methods perform adequately showing a penalty with

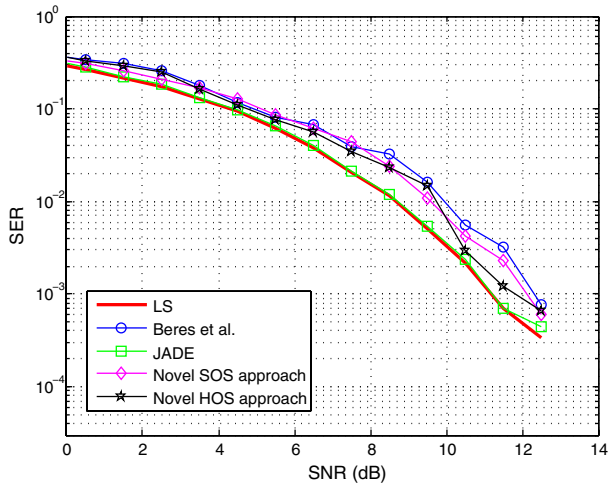

Figure 11. NLOS scenario: SER performance *versus* SNR.

respect to the LS case lower than 1 dB. Again, JADE is the method that exhibits better performance whereas the HOS-method proposed by Beres and Adve [10] shows the worst.

6. CONCLUSIONS

The experimental performance of several blind channel estimation techniques for Alamouti coded systems with one receiving antenna has been evaluated in this paper. The considered techniques exploit the orthogonality property

of the effective MIMO channel matrix through the eigendecomposition of matrices made up of SOS or HOS of the received signals. The algorithms were tested *via* computer simulations and on real data obtained from indoor scenarios using a MIMO hardware platform working at 2.4 GHz. Both simulations and realistic experiments in LOS and NLOS scenarios show that the proposed SOS-based method exhibit a performance penalty of less than 1 dB when compared with the case of perfect CSI. Thus, we can conclude that the SOS approach exhibits an excellent compromise quality between channel estimation and computational complexity.

ACKNOWLEDGEMENTS

This work has been partially supported by Xunta de Galicia, Ministerio de Educación y Ciencia of Spain and FEDER funds of the European Union under grants number PGIDT06TIC10501PR and TEC2007-68020-C04-01.

REFERENCES

1. Gesbert D, Shafi M, Shan-Shiu D, Smith PJ, Naguib A. From theory to practice: an overview of MIMO space-time coded wireless systems. *IEEE Journal on Selected Areas in Communications* 2003; **21**:281–302.
2. Jafarkhani H. *Space Time Coding*. Cambridge University Press: Cambridge, UK, 2005.
3. Alamouti SM. A simple transmit diversity technique for wireless communications. *IEEE Journal on Selected Areas in Communications* 1998; **16**:1451–1458.
4. Tarokh V, Jafarkhani H, Calderbank AR. Space-time block codes from orthogonal designs. *IEEE Transactions on Information Theory* 1999; **45**(5):1456–1467.
5. Larsson EG, Stoica P. *Space-Time Block Coding for Wireless Communications*. Cambridge University Press: Cambridge, UK, 2003.
6. Sandhu S, Paulraj A. Space-time block codes: a capacity perspective. *IEEE Communications Letter* 2000; **4**(12):384–386.
7. Andrews JG, Ghosh A, Muhamed R. *Fundamentals of WiMAX: Understanding Broadband Wireless Networking*. Prentice Hall Communications Engineering and Emerging Technologies Series, 2007.
8. Hughes BL. Differential space-time modulation. *IEEE Transactions on Information Theory* 2000; **46**(7):2567–2578.
9. Pérez-Iglesias HJ, Dapena A, Castedo L, Zarzoso V. Blind channel identification for Alamouti's coding systems based on eigenvector decomposition. In *Proceedings of 13th European Wireless Conference*, Paris, France. April 2007.
10. Beres E, Adve R. Blind channel estimation for orthogonal STBC in MISO systems. In *Proceedings of Global Telecommunications Conference, 2004*, Vol. 4, November 2004; pp. 2323–2328.
11. Cardoso J-F, Souloumiac A. Blind beamforming for non-Gaussian signals. In *IEE Proceedings-F*, Vol. 140, no. 6, December 1993; pp. 362–370.
12. Shahbazpanah S, Gershman AB, Manton J. Closed-form blind MIMO channel estimation for orthogonal space-time block codes. *IEEE Transactions on Signal Processing* 2005; **53**(12): 4506–4516.
13. Vía J, Santamaría I, Pérez J, Ramírez D. Blind decoding of MISO-OSTBC systems based on principal component analysis. In *Proceedings of International Conference on Acoustic, Speech and Signal Processing*, Vol. IV, 2006; pp. 545–549.
14. García-Naya JA, Fernández-Caramés T, Pérez-Iglesias H, *et al*. Performance of STBC transmissions with real data. In *Proceedings of 16th IST Mobile and Wireless Communications Summit*, Budapest, Hungary, July 2007.
15. Naguib AF, Tarokh V, Seshadri N, Calderbank AR. A space-time coding modem for high-data-rate wireless communications. *IEEE Journal on Selected Areas in Communications* 1998; **16**(8):1459–1478.

Optimal Step-Size Constant Modulus Algorithm

Vicente Zarzoso, *Member, IEEE*, and Pierre Comon, *Fellow, IEEE*

***Abstract*— The step size leading to the absolute minimum of the constant modulus (CM) criterion along the search direction can be obtained algebraically at each iteration among the roots of a third-degree polynomial. The resulting optimal step-size CMA (OS-CMA) is compared with other CM-based iterative techniques in terms of performance-versus-complexity trade-off.**

***Index Terms*— Adaption coefficient, blind equalization, CMA, exact line search, SIMO and SISO channels.**

I. Introduction

An important problem in digital communications is the recovery of the data symbols transmitted through a distorting medium. The constant modulus (CM) criterion is arguably the most widespread blind channel equalization principle [1], [2]. The CM criterion generally presents local extrema — often associated with different equalization delays — in the equalizer parameter space [3]. This shortcoming renders the performance of gradient-based implementations, such as the well-known constant modulus algorithm (CMA), very dependent on the equalizer impulse response initialization. Even when the absolute minimum is found, convergence can be severely slowed down for initial equalizer settings with trajectories in the vicinity of saddle points [4], [5]. The constant value of the step-size parameter (or adaption coefficient) must be carefully selected to ensure a stable operation while balancing convergence rate and final accuracy (misadjustment or excess mean square error). The stochastic gradient CMA drops the expectation operator and approximates the gradient of the criterion by a one-sample estimate, as in LMS-based algorithms. This rough approximation generally leads to slow convergence and poor misadjustment, even if the step size is carefully chosen.

As opposed to recursive (or sample-by-sample) algorithms, block (or fixed-window) methods obtain a more precise gradient estimate from a batch of channel output samples, improving convergence speed and accuracy [6]. Tracking capabilities are preserved as long as the channel remains stationary over the observation window. Moreover, sample-by-sample versions are easily obtained from block implementations by considering signal blocks of one data vector and iterating over consecutive received vectors. The block-gradient CMA (simply denoted as CMA hereafter) is particularly suited to burst-mode transmission systems. Unfortunately, the multimodal nature of the CM criterion sustains the negative impact of local extrema on block implementations. Asymptotically (for sufficient block size), the least-squares CMA (LSCMA) [7] guarantees global convergence to a cost function stationary point, for any initial weight setting, with a cost per iteration similar to CMA's. This is achieved at the expense of an increased computational overhead due to the calculation of the data matrix pseudoinverse or its QR factorization, needed to solve the LS step at each iteration. In the QR-CMA method of [6], data prewhitening through the QR decomposition of the sensor-output matrix simplifies the block-CMA iteration, so that bounds on its step size can be found to ensure monotonic convergence. The recently proposed recursive least squares CMA (RLS-CMA) [8], which operates on a sample-by-sample basis, also proves notably faster and more robust than the classical CMA. The derivation of the RLS-CMA relies on an approximation to the CM cost function in stationary or slowly varying environments, where block implementations may actually prove more efficient in exploiting the available information (the received signal burst). Interestingly, the RLS-CMA turns out to be equivalent to the recursive CMA (RCMA), put forward over a decade earlier in [9]; it also bears close resemblance to the orthogonalized CMA (O-CMA) of [10].

Analytical solutions to the minimization of the CM criterion are developed in [11], [12]. After solving a linearized LS problem, these methods require to recover the right structure of the solution space when multiple equalization solutions exist. In the general case, this can be achieved through a costly QZ matrix iteration. In addition, special modifications are required for input signals with a one-dimensional (i.e., binary) alphabet [11]–[13]. More importantly, these analytic methods aim at exact solutions to the CM criterion, which may yield suboptimal equalizers in the presence of noise.

A judicious alternative to existing techniques consists of performing consecutive one-dimensional absolute minimizations of the CM cost function. This technique, known as exact line search, is generally considered computationally inefficient [14]. However, it was first observed in [15] that the value of the adaption coefficient that leads to the absolute minimum of most blind cost functions along a given search direction can be computed algebraically. It was conjectured that the use of this algebraic optimal step size could not only accelerate convergence but also avoid local extrema in some cases. The present Letter carries out a more detailed (yet concise) theoretical development and experimental evaluation of the optimal step-size CMA (OS-CMA) derived from this idea, which was briefly presented in [16] under a different name.

Paper approved by V. A. Aalo, the Editor for Diversity and Fading Channel Theory of the IEEE Communications Society. Manuscript received November 2, 2005; revised November 3, 2006. Supported through a Research Fellowship awarded to V. Zarzoso by the Royal Academy of Engineering of the UK.

V. Zarzoso was with the Department of Electrical Engineering and Electronics, The University of Liverpool, Liverpool L69 3GJ, UK. He is now with the Laboratoire I3S, Université de Nice – Sophia Antipolis, France (e-mail: zarzoso@i3s.unice.fr).

P. Comon is with the Laboratoire I3S, CNRS/UNSA, 2000 route des Lucioles, BP 121, 06903 Sophia Antipolis Cedex, France (e-mail: pcomon@i3s.unice.fr).

Digital Object Identifier 10.1109/TCOMM.2008.050484.

II. Constant Modulus Equalization

Zero-mean data symbols $\{s_n\}$ are transmitted at a known baud-rate $1/T$ through a time dispersive channel with impulse response $h(t)$. The channel is assumed linear and time-invariant (at least over the observation window), with a stable, causal and possibly non-minimum phase transfer function, and comprises the transmitter pulse-shaping and receiver front-end filters. The channel order is M baud periods. Assuming perfect synchronization and carrier-residual elimination, fractionally-spaced sampling by a factor of P yields the discrete-time channel output

$$\mathbf{x}_n = \sum_{k=0}^{M} \mathbf{h}_k s_{n-k} + \mathbf{v}_n \tag{1}$$

in which $\mathbf{x}_n = [x(nT),\, x(nT+T/P),\, \ldots,\, x(nT+T(P-1)/P)]^{\mathrm{T}} \in \mathbb{C}^P$, $x(t)$ denoting the continuous-time baseband received signal. Similar definitions hold for $\mathbf{h}_k$ and the additive noise $\mathbf{v}_n$. Eqn. (1) represents the so-called single-input multiple-output (SIMO) signal model, and reduces to the single-input single-output (SISO) model for $P = 1$. The SIMO model is also obtained if spatial diversity (e.g., an antenna array) is available at the receiver end, with or without time oversampling, and can easily be extended to the multiple-input (MIMO) case.

To recover the original data symbols from the received signal, a linear equalizer is employed with finite impulse response spanning L baud periods $\mathbf{f} = [\mathbf{f}_1^{\mathrm{T}},\, \mathbf{f}_2^{\mathrm{T}},\, \ldots,\, \mathbf{f}_L^{\mathrm{T}}]^{\mathrm{T}} \in \mathbb{C}^D$, $D = PL$, $\mathbf{f}_l = [f_{l,1},\, f_{l,2},\, \ldots,\, f_{l,P}]^{\mathrm{T}} \in \mathbb{C}^P$, $l = 1, \ldots, L$. This filter produces the output signal $y_n = \mathbf{f}^{\mathrm{H}} \tilde{\mathbf{x}}_n$, where $\tilde{\mathbf{x}}_n = [\mathbf{x}_n^{\mathrm{T}},\, \mathbf{x}_{n-1}^{\mathrm{T}},\, \ldots,\, \mathbf{x}_{n-L+1}^{\mathrm{T}}]^{\mathrm{T}} \in \mathbb{C}^D$. In these conditions, the channel effects can be represented by a block Toeplitz convolution matrix with dimensions $D \times (L+M)$ [3], [17].

The equalizer vector can be blindly estimated by minimizing the CM cost function [1], [2]:

$$J_{\mathrm{CM}}(\mathbf{f}) = \mathrm{E}\big\{ \big(|y_n|^2 - \gamma \big)^2 \big\} \tag{2}$$

where $\gamma = \mathrm{E}\{|s_n|^4\} / \mathrm{E}\{|s_n|^2\}$ is a constellation-dependent parameter. The CMA is a gradient-descent iterative procedure to minimize the CM cost. Its update rule reads

$$\mathbf{f}(k+1) = \mathbf{f}(k) - \mu \mathbf{g}(k) \tag{3}$$

where $\mathbf{g} \stackrel{\mathrm{def}}{=} \nabla J_{\mathrm{CM}}(\mathbf{f}) = 4\mathrm{E}\big\{ (|y_n|^2 - \gamma) y_n^* \tilde{\mathbf{x}}_n \big\}$ is the gradient vector at $\mathbf{f}$, symbol μ represents the step-size parameter and k denotes the iteration number. In the sequel, we assume that a block of length N_d baud periods $\mathbf{x}_n$ is observed at the channel output, from which $N = (N_d - L + 1)$ received data vectors $\tilde{\mathbf{x}}_n$ can be constructed.

III. Optimal Step-Size CMA

A. Exact Line Search

Exact line search consists of finding the absolute minimum of the cost function along the line defined by the search direction (typically the gradient) [14]:

$$\mu_{\mathrm{opt}} = \arg\min_{\mu} J_{\mathrm{CM}}(\mathbf{f} - \mu \mathbf{g}). \tag{4}$$

In general, exact line search algorithms are unattractive because of their relatively high complexity. Even in the one-dimensional case, function minimization must usually be performed using costly numerical methods. However, as originally observed in [15] and later also remarked in [16], the CM cost $J_{\mathrm{CM}}(\mathbf{f} - \mu \mathbf{g})$ is a polynomial in the step size μ. Consequently, it is possible to find the optimal step size μ_{opt} in closed form among the roots of a polynomial in μ. Exact line minimization of function (2) can thus be performed at relatively low complexity.

B. Algebraic Optimal Step Size: the OS-CMA

In effect, some algebraic manipulations show that the derivative of $J_{\mathrm{CM}}(\mathbf{f} - \mu \mathbf{g})$ with respect to μ is the 3rd-degree polynomial with real-valued coefficients:

$$\begin{aligned} p(\mu) &= d\mu^3 + d_2\mu^2 + d_1\mu + d_0 \\ d_3 = 2\mathrm{E}\{a_n^2\} \qquad & d_2 = 3\mathrm{E}\{a_n b_n\} \\ d_1 = \mathrm{E}\{2a_n c_n + b_n^2\} \qquad & d_0 = \mathrm{E}\{b_n c_n\} \end{aligned} \tag{5}$$

where $a_n = |g_n|^2$, $b_n = -2\mathbb{R}\mathrm{e}(y_n g_n^*)$, and $c_n = (|y_n|^2 - \gamma)$, with $g = \mathbf{g}^{\mathrm{H}} \tilde{\mathbf{x}}_n$. Alternatively, the coefficients of the OS-CMA polynomial can be obtained as a function of the sensor-output statistics, calculated before starting the iterative search. These two equivalent forms of the OS-CMA coefficients are derived in [18], [19].

Having obtained its coefficients, the roots of 3rd-degree polynomial (5) can be extracted with standard algebraic procedures such as Cardano's formula, or other efficient iterative methods [20], [21].[1] The optimal step size corresponds to the root attaining the lowest value of the cost function, thus accomplishing the *global* minimization of J_{CM} in the gradient direction. When complex conjugate roots appear, the real root typically provides the lowest equalizer output mean square error (MSE). Once μ_{opt} has been determined, the filter taps are updated as in (3), and the process is repeated with the new filter and gradient vectors, until convergence. This algorithm is referred to as *optimal step-size CMA (OS-CMA)*.

To improve numerical conditioning in the determination of μ_{opt}, gradient vector $\mathbf{g}$ should be normalized. This normalization does not cause any adverse effects since the relevant parameter in the optimal step-size technique is the search direction $\tilde{\mathbf{g}} = \mathbf{g} / \|\mathbf{g}\|$.

C. Computational Complexity

Table I summarizes the OS-CMA's computational cost in terms of the number of real-valued floating point operations or *flops* (a flop represents a multiplication followed by an addition; multiplies and divisions are counted as flops as well). Also shown is the cost for other CM-based algorithms such as the CMA, the LSCMA [7], the QR-CMA [6] and the RLS-CMA [8], [9]. Complex-valued signals and filters are assumed; rough estimates of complexity for the real-valued signal scenario can be obtained by dividing the flop figures by 4. For typical values of (D, N), the OS-CMA is more costly per iteration over the observed signal block than the other

[1] The MATLAB code of a general algorithm for extracting the roots of a 3rd-degree polynomial is given in [18] (see also [14]).

TABLE I

COMPUTATIONAL COST IN NUMBER OF REAL-VALUED FLOPS FOR SEVERAL CM-BASED ALGORITHMS. D: NUMBER OF TAPS IN EQUALIZER VECTOR; N: NUMBER OF DATA VECTORS IN OBSERVED SIGNAL BURST. THE BOTTOM HALF OF THE TABLE CORRESPONDS TO THE EXPERIMENTAL SET-UP OF SECTION IV AND FIGS. 1–2.

	Flops	CMA	LSCMA	QR-CMA	RLS-CMA	OS-CMA
(D, N)	initialization	—	$4D^2N$	$4D^2N$	—	—
	per block iteration	$4(2D+1)N$	$(8D+5)N$	$(8D+5)N$	$2D(7D+10)N$	$2(6D+7)N$
$(4, 199)$	initialization	0	12736	12736	0	0
	per block iteration	7164	7363	7363	60496	12338

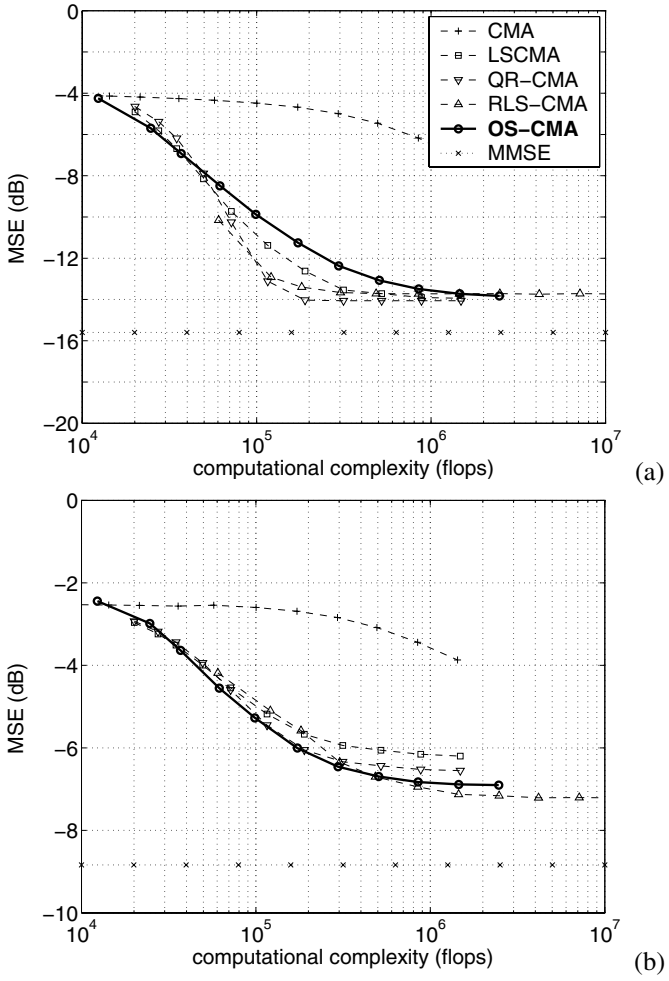

Fig. 1. Performance vs. complexity trade-off of CM-based algorithms with QPSK source, signal bursts of $N_d = 200$ symbols, equalizer length $L = 2$ baud periods, oversampling factor $P = 2$, SNR = 20 dB, 1000 Monte Carlo runs. (a)Linearly invertible 4×4 channel convolution matrix (channel order $M = 2$). (b) Lack of linear invertibility of the channel, with a 4×6 channel convolution matrix (channel order $M = 4$)

CM-based algorithms except the RLS-CMA. The initial cost and the cost per iteration are of order $\mathrm{O}(D^4N)$ and $\mathrm{O}(D^4)$, respectively, with the second form of the OS-CMA polynomial [18], [19].

IV. EXPERIMENTAL RESULTS

We evaluate and compare the equalization quality as a function of computational cost (performance vs. complexity trade-off) achieved by the CM-based methods considered in this Letter. Bursts of $N_d = 200$ baud periods are observed at the output of a $T/2$-spaced channel ($P = 2$) excited by a QPSK source ($\gamma = 1$) and corrupted by complex circular additive white Gaussian noise with 20-dB SNR. For $L = 2$, these parameters result in an equalizer vector $\mathbf{f}$ composed of $D = 4$ taps. The channel impulse response coefficients are randomly drawn from a normalized complex Gaussian distribution. After a given number of iterations, performance is measured as the MSE between the equalizer output and the original channel input. Results are averaged over 1000 channel, source and noise realizations. For each plot in the figures, markers are placed at block iterations $[1, 2, 3, 5, 8, 14, 24, 41, 69, 118, 200]$. We set $\mu = 10^{-3}$ for the conventional fixed step-size CMA (a value found empirically to provide fastest performance while preventing divergence in our simulation set-up), and the typical forgetting factor $\lambda = 0.99$ and inverse covariance matrix initialized at the identity for the RLS-CMA [8]. Double first-tap initializations are chosen for the equalizer vectors. Two scenarios are considered, depending on the linear invertibility of the channel matrix.

Scenario 1: linearly invertible channel. A channel order $M = 2$ yields an equivalent 4×4 channel convolution matrix that can be perfectly inverted in the absence of noise, thus guaranteeing the global convergence of the fractionally-spaced CMA [17]. Fig. 1(a) shows that the OS-CMA dramatically outperforms the conventional fixed step-size CMA and slightly improves on the other CM-based methods at low complexity.

Scenario 2: lack of linear invertibility. A channel order $M = 4$ results in a 4×6 channel convolution matrix. Despite the lack of linear invertibility of the channel, a linear equalizer may still attempt to estimate the channel input at an extraction delay with reasonably low MSE. As shown in Fig. 1(b), the OS-CMA's quality-cost trade-off is only surpassed by the RLS-CMA's for sufficient complexity. In both scenarios, results at the reported 20-dB SNR level are quite representative of the methods' relative performance under the same fixed complexity over a wider $[0, 40]$-dB SNR range.

Optimal step-size trajectory. The average evolution of the OS-CMA's optimal step size in the above experiments is represented in Fig. 2. Depending on the cost function shape (which is determined by the actual channel, source and noise realizations), the optimal step size may take negative values at a given iteration. This fact may explain the peaks observed in the curves. Nevertheless, the optimal step size shows a monotonically decreasing trend.

V. CONCLUSIONS

Global line minimization of the CM cost function can be carried out algebraically by finding the roots of a 3rd-degree

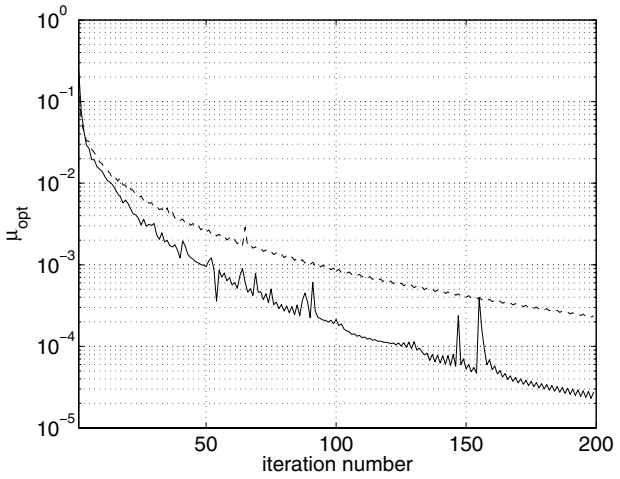

Fig. 2. Optimal step-size average trajectory in the simulation scenarios of Fig. 1(a) (dashed line) and Fig. 1(b) (solid line).

polynomial with real coefficients. The resulting OS-CMA presents a performance versus complexity trade-off similar to the LSCMA [7], the QR-CMA [6] and the RLS-CMA [8], [9], slightly improving on those methods when perfect equalization conditions are not met. Due to space constraints, the numerical study presented in this Letter is of rather limited scope, and thus needs to be completed with a more thorough theoretical and experimental analysis of the OS-CMA technique evaluating its performance against a variety of system parameters such as block size, SNR, equalizer length, channel conditioning, etc. Indeed, additional experimental results reported in [18], [19] seem to point out that the optimal step-size strategy arises as a promising practical approach to improving the performance of blind equalizers in burst-mode transmission systems. The continuation of this work should also include the incorporation of the optimum step-size scheme in alternative blind and semi-blind criteria for equalization and beamforming. A first step in this direction has already been taken in [22], [23].

REFERENCES

[1] D. N. Godard, "Self-recovering equalization and carrier tracking in two-dimensional data communication systems," *IEEE Trans. Commun.*, vol. 28, no. 11, pp. 1867–1875, Nov. 1980.

[2] J. R. Treichler and B. G. Agee, "A new approach to multipath correction of constant modulus signals," *IEEE Trans. Acoust., Speech, Signal Processing*, vol. 31, no. 2, pp. 459–472, Apr. 1983.

[3] Z. Ding, C. R. Johnson, and R. A. Kennedy, "On the (non)existence of undesirable equilibria of Godard blind equalizers," *IEEE Trans. Signal Processing*, vol. 40, no. 10, pp. 2425–2432, Oct. 1992.

[4] S. Lambotharan, J. Chambers, and C. R. Johnson, "Attraction of saddles and slow convergence in CMA adaptation," *Signal Processing*, vol. 59, no. 3, pp. 335–340, June 1997.

[5] C. R. Johnson, P. Schniter, I. Fijalkow, L. Tong, et al., "The core of FSE-CMA behavior theory," in *Unsupervised Adaptive Filtering, Vol. II: Blind Deconvolution*, S. S. Haykin, ed. New York: John Wiley & Sons, 2000, ch. 2, pp. 13–112.

[6] P. A. Regalia, "A finite-interval constant modulus algorithm," in *Proc. ICASSP, 27th International Conf. Acoust., Speech, Signal Processing*, May 13–17, 2002, vol. III, pp. 2285–2288.

[7] B. G. Agee, "The least-squares CMA: A new technique for rapid correction of constant modulus signals," in *Proc. 11th, IEEE-ICASSP, Intl. Conf. Acoustics, Speech, Signal Processing*, Apr. 7–11, 1986, pp. 953–956.

[8] Y. Chen, T. Le-Ngoc, B. Champagne, and C. Xu, "Recursive least squares constant modulus algorithm for blind adaptive array," *IEEE Trans. Signal Processing*, vol. 52, no. 5, pp. 1452–1456, May 2004.

[9] R. Pickholtz and K. Elbarbary, "The recursive constant modulus algorithm: A new approach for real-time array processing," in *Proc. 27th Asilomar Conf. Signals, Syst. Computers*, Nov. 1–3, 1993, pp. 627–632.

[10] R. Gooch and J. Lundell, "The CM array: An adaptive beamformer for constant modulus signals," in *Proc. ICASSP, 11th IEEE Intl. Conf. Acoust., Speech, Signal Processing*, Apr. 7–11, 1986, pp. 2523–2526.

[11] A.-J. van der Veen and A. Paulraj, "An analytical constant modulus algorithm," *IEEE Trans. Signal Processing*, vol. 44, no. 5, pp. 1136–1155, May 1996.

[12] K. Doğançay and R. A. Kennedy, "Least squares approach to blind channel equalization," *IEEE Trans. Signal Processing*, vol. 47, no. 11, pp. 1678–1687, Nov. 1999.

[13] A.-J. van der Veen, "Analytical method for blind binary signal separation," *IEEE Trans. Signal Processing*, vol. 45, no. 4, pp. 1078–1082, Apr. 1997.

[14] W. H. Press, S. A. Teukolsky, W. T. Vetterling, and B. P. Flannery, *Numerical Recipes in C. The Art of Scientific Computing*, 2nd ed. Cambridge, UK: Cambridge University Press, 1992.

[15] P. Comon, "Blind equalization with discrete inputs in the presence of carrier residual," in *Proc. ISSPIT, 2nd IEEE International Symp. Signal Processing Inform. Technol.*, Dec. 18–21, 2002, [CD-ROM].

[16] C. Xu and J. Li, "A batch processing constant modulus algorithm," *IEEE Commun. Lett.*, vol. 8, no. 9, pp. 582–584, Sep. 2004.

[17] Y. Li and Z. Ding, "Global convergence of fractionally spaced Godard (CMA) adaptive equalizers," *IEEE Trans. Signal Processing*, vol. 44, no. 4, pp. 818–826, Apr. 1996.

[18] V. Zarzoso and P. Comon, "Optimal step-size constant modulus algorithm," Laboratoire I3S, Sophia Antipolis, France, Tech. Rep. I3S/RR-2004-23-FR, Sep. 2004. Available: `http://www.i3s.unice.fr/~zarzoso/biblio/RR-04.23-V.ZARZOSO.pdf.gz`

[19] ——, "Blind channel equalization with algebraic optimal step size," in *Proc. EUSIPCO, XIII European Signal Processing Conf.*, Sep. 4–8, 2005, [CD-ROM].

[20] E. Durand, *Solutions numériques des équations algébriques*, vol. I. Paris: Masson, 1960.

[21] C. Lanczos, *Applied Analysis*. New York: Dover, 1988.

[22] V. Zarzoso and P. Comon, "Semi-blind constant modulus equalization with optimal step size," in *Proc. ICASSP, 30th Intl. Conf. Acoust., Speech, Signal Processing*, Mar. 18–23, 2005, vol. III, pp. 577–580.

[23] ——, "How fast is FastICA?" in *Proc. EUSIPCO, XIV European Signal Processing Conf.*, Sep. 4–8, 2006, [CD-ROM].

IEEE TRANSACTIONS ON SIGNAL PROCESSING, VOL. 54, NO. 8, AUGUST 2006

Optimal Pairwise Fourth-Order Independent Component Analysis

Vicente Zarzoso, *Member, IEEE*, Juan José Murillo-Fuentes, *Member, IEEE*, Rafael Boloix-Tortosa, and Asoke K. Nandi, *Senior Member, IEEE*

***Abstract*—Blind source separation (BSS) aims at the reconstruction of unknown mutually independent signals, so-called sources, from their mixtures observed at the output of a sensor array. The BSS of instantaneous linear mixtures, which finds application in numerous fields, can be solved through the statistical tool of independent component analysis (ICA). This paper concentrates on the analytic solutions for the fundamental two-signal ICA scenario. A novel estimation class, so-called general weighted fourth-order estimator (GWFOE), is put forward, which is based on the fourth-order statistics of the whitened sensor output. By means of a weight parameter, the GWFOE is able to unify a variety of apparently disparate estimation expressions previously scattered throughout the literature, including the well-known JADE method in the two-signal case. A theoretical asymptotic performance analysis is carried out, resulting in the GWFOE large-sample mean square error and the source-dependent weight value of the most efficient estimator in the class. To extend the pairwise estimators to the general scenario of more than two sources, an improved Jacobi-like optimization technique is proposed. The approach consists of calculating the necessary sensor-output fourth-order statistics at the initialization stage of the algorithm, which can lead to significant computational savings when large sample blocks are processed. Based on this idea, adaptive algorithms are also devised, showing very satisfactory convergence characteristics. Experiments illustrate the good performance of these optimal pairwise ICA strategies, in both off- and on-line processing modes.**

***Index Terms*—Array signal processing, blind source separation, higher order statistics, independent component analysis, performance analysis, unsupervised learning.**

I. Introduction

A. Problem and Motivation

The problem of blind source separation (BSS) consists of recovering a set of unobserved signals, so-called sources, from another set of observed signals which are mixtures of the sources [1]–[3]. The term "blind" signifies that (typically) very few assumptions are made about the sources and the mixing process. By contrast, conventional array processing techniques (e.g., for direction-of-arrival estimation) assume a certain structure for the mixing matrix in terms of the array manifold, or the array response as a function of the arrival angle. Deviations of the assumed structure from reality (calibration errors) can have a significant negative impact on the algorithms' performance. The relative freedom given by BSS methods to the mixing structure makes them very robust to calibration errors [4]. This flexibility and robustness have spurred the interest in the BSS problem over the last decade. Another important motivation has been the vast number of application areas where BSS proves useful [2], [3], [5], ranging from communications [6] to biomedical signal processing (electrocardiogram and electroencephalogram analysis, fMRI, brain imaging) [7]–[9], condition monitoring, image processing [10], financial data analysis, seismic exploration, classification, or data compression and coding [11], among others. Instantaneous linear mixtures, where no time delays occur in the propagation from sources to sensors, is a very accurate signal model in many of those applications. The solution of the more elaborate convolutive-mixture model can often be decoupled into a stage resolving the effects caused by the multipath channel (time equalization) followed by the separation of the remaining instantaneous mixture. The separation of nonlinear mixtures is more involved, and is also receiving attention by some authors (see, e.g., [2], [3], and references therein).

When the time structure cannot be exploited or is simply ignored, the basic approach to instantaneous linear source separation consists of projecting the observation vectors into some basis where the resulting components are statistically independent. This is the independent component analysis (ICA) of the observed data [12], and in its more general form it relies (explictly or not) on higher order statistics. A previous spatial whitening process (entailing second-order decorrelation and power normalization) helps to reduce the number of unknowns, resulting in a set of normalized uncorrelated components (whitened signals) related with the sources through a unitary transformation. ICA is then tantamount to the identification of this unitary matrix.

B. Closed-Form Solutions in the Two-Signal Case

In the fundamental real-valued two-signal case, the problem reduces to the identification of a single parameter, the unknown angle characterizing the Givens-rotation mixing matrix. A variety of closed-form methods for the estimation of this angle have been proposed in the literature. These methods arise from approximations of certain optimality criteria (contrast functions) and provide direct solutions with no iterative search involved. Most of these share the common feature

Manuscript received November 30, 2004; revised September 4, 2005. The associate editor coordinating the review of this manuscript and approving it for publication was Dr. Peter Handel. The work of V. Zarzoso was supported by the Royal Academy of Engineering, U.K., under a Research Fellowship. The work of J. J. Murillo-Fuentes and R. Boloix-Tortosa was supported by the Spanish Government under Grant MCYT TIC2003-03781.

V. Zarzoso was with the Department of Electrical Engineering and Electronics, The University of Liverpool, U.K. He is now with Laboratoire I3S, Université de Nice - Sophia Antipolis, 06903 Sophia Antipolis Cedex, France (e-mail: zarzoso@i3s.unice.fr).

J. J. Murillo-Fuentes and R. Boloix-Tortosa are with the Departamento de Teoría de la Señal y Comunicaciones, Escuela Superior de Ingenieros, Universidad de Sevilla, 41092 Sevilla, Spain (e-mail: murillo@us.es; rboloix@us.es).

A. K. Nandi is with the Department of Electrical Engineering and Electronics, University of Liverpool, Liverpool L69 3GJ, U.K. (e-mail: aknandi@liv.ac.uk).

Digital Object Identifier 10.1109/TSP.2006.875391

of being based on the fourth-order statistics of the sensor output. The first expression was obtained in [13] by relating the fourth-order statistics of sources and sensors. Its performance was later shown to depend on the actual value of the unknown parameter [14], [15], thus losing the desirable uniform performance property [16]. A good number of early methods were derived from the maximum likelihood (ML) approach. The truncated Gram–Charlier expansion of the source probability density function (pdf) yielded the solution of [17], restricted to symmetric sources with normalized kurtosis in certain positive range. These validity conditions were broadened through the extended ML (EML) and the alternative EML (AEML) estimators [14], [18], [19]. The EML also generalized the maximum kurtosis (MK) cost function of [20], [21], initially thought to be valid only for sources with same kurtosis sign [14], to source pairs with nonzero source kurtosis sum (sks). The EML and the AEML remain consistent providing the sks and source kurtosis difference (skd) are not null, respectively. This deficiency was overcome in [14], [19], and [22]. In [14] and [19], the choice between the EML or the AEML was made with a simple decision rule as a function of the sensor-output fourth-order statistics. In [22], adopting the ML framework of [17], the two estimators were unified into a single analytic expression, the approximate ML (AML).

The contrast function of [12], which had earlier been reached from the ML principle [23], is itself an approximation of a negentropy maximization principle measuring the deviation of the separator output from Gaussianity. Negentropy can also be readily connected to alternative information-theoretical criteria such as the mutual information (MI) between the separator outputs or the sum of their marginal entropies (ME) [4], [5]. Another major group of two-dimensional closed-form solutions arises from the trigonometric expansion and approximate minimization of the ME contrast criteria developed in [12]. The MaSSFOC (maximum of sum squared fourth-order cumulant) estimator [24] and the recently proposed sinusoidal ICA (SICA) [25], which resemble the AML, are approximate minimizers of the fourth-order contrast function. Further simplifications of this contrast function when the source kurtoses have the same modulus lead to the so-called source kurtosis sum and source kurtosis difference estimators (SKSE, SKDE) [24], very similar to the EML and AEML estimators [14], [18], [19], respectively. The simultaneous exploitation of orders three and four is shown to improve the separation performance when some of the sources present nonsymmetric distributions [26].

The original solution to Comon's fourth-order contrast involved finding the roots of a fourth-degree polynomial (a biquadratic or quartic equation). An analytic procedure for rooting quartics is well known since the sixteenth century (Ferrari's formula), but its calculation can be cumbersome; approximate numerical methods are usually preferred instead. The closed-form estimators that we are concerned with are considerably less elaborate: they consist of simple formulas involving straightforward operations on certain statistics of the whitened sensor output.

The notion of linearly combining estimators was originally put forward in [22]. Through a weight parameter, the EML and AEML are combined together into a single expression, the so-called weighted AML (WAML) estimator. It was suggested that the weight parameter could be adjusted by taking advantage of a priori information on the source pdfs, although no specific guidelines were given on how the actual choice should be made.

C. Scenario of More Than Two Signals

In the n-dimensional case, $n > 2$, ICA can be carried out by applying the two-signal estimators to each whitened signal pair over several sweeps until convergence [12]. This iterative approach is reminiscent of the Jacobi optimization (JO) technique for matrix diagonalization [27], [28], and can indeed be seen as its extension to higher dimensional tensors [12]. Although no theoretical proof of global convergence has yet been obtained for the pairwise iterations in the tensor case [12], [29], the method remains valid in practice since no experimental or theoretical counterexample of misconvergence has been encountered to date, provided that the validity conditions of the two-dimensional criteria are fulfilled for every signal pair. In the standard JO iteration, the fourth-order statistics used by the closed-form estimators need to be computed for each signal pair at every sweep until convergence. Typically, the statistics are estimated from the signal samples, which may involve extensive computations especially when processing long signal blocks. Adaptive algorithms, such as the so-called adaptive rotation (AROT) [13] and the adaptive EML (adEML) [30], are easily derived from this strategy. However, they sometimes show poor convergence, especially for a large number of sources.

D. Contributions and Outline

Many successful methods are available to perform ICA in the general scenario of more than two sources (see, e.g., [2], [3], and references therein). Nevertheless, the two-signal case remains a scenario of fundamental importance, since it is the most basic and can be considered as the elementary unit for the solution of the general $n > 2$ in the JO approach. Despite this relevance, the relationships between the different analytic solutions have only been explored to a limited extent. The purpose of this paper is to fill the gap in these connections. By means of the complex-centroid notation used in the EML and the AEML [14], [18], [19], [31], we arrive at a compact formulation for the WAML estimator of [22]. It is seen that through different values of the weight parameter, many of the existing fourth-order estimators are obtained, including the well-known JADE method [4] for $n = 2$; hence the more suitable name of *general weighted fourth-order estimator* (GWFOE). The centroid formalism allows a simple derivation of the estimator's large-sample mean square error (MSE), from which the weight parameter of the optimal estimator is determined as a function of the source statistics. Here, "optimal" refers to the asymptotically most efficient estimator in the GWFOE class.

In the general case of more than two signals, we aim to optimize the computational cost of the JO technique. An alternative moment-calculation procedure is proposed, which is less costly in scenarios where the sample size is large relative to the number of sources. The relevant statistics are computed from the sensor-output samples before starting the JO iterations and then modified according to the pairwise rotations. We refer to this

method as *initialized JO* (IJO). By comparing the complexity of the proposed and the conventional moment-estimation procedure, a decision rule is derived to select the most computationally efficient option. This results in the *optimal JO* (OJO). Adaptive algorithms based on IJO can also be designed to improve the convergence properties of previous online approaches. In short, the results presented in this paper unify, generalize, and enhance ICA techniques based on two-dimensional fourth-order contrasts.

This paper encompasses substantially extended as well as thoroughly revised versions of conference publications [32]–[36]. The material is organized as follows. After reviewing the BSS signal model and ICA contrast functions in Section II, Section III derives the GWFOE, highlights its connections with other analytic solutions, performs its asymptotic analysis, and obtains the best estimator of the class. Section IV is devoted to the scenarios of more than two signals, featuring the computationally efficient IJO and OJO procedures. Adaptive implementations are the focus of Section V. Experimental results are reported in Section VI. Section VII concludes herein. The Appendices contain some proofs and other mathematical derivations.

E. Notations

Throughout this paper, vectors and matrices are represented as lowercase and uppercase boldface letters, respectively. Symbols $(\cdot)^{\mathrm{T}}$ and $(\cdot)^{-1}$ indicate the transpose and inverse matrix operators, respectively. $\mathbb{R}$ and $\mathbb{C}$ are the sets of real and complex numbers, respectively; symbol $j = \sqrt{-1}$ is the imaginary unit; $\mathbb{Re}(\cdot)$ and $\mathbb{Im}(\cdot)$ denote the real and imaginary part of its complex argument, respectively, whereas function $\angle(\cdot)$ supplies its principal value (i.e., its argument in the interval $]-\pi,\pi]$). $\mathrm{E}[\cdot]$ represents the mathematical expectation. Given a set of signals $\{s_i\}_{i=1}^n$, $\mathrm{M}^s_{i_1\cdots i_r} \stackrel{\mathrm{def}}{=} \mathrm{E}[s_{i_1}\cdots s_{i_r}]$ and $\mathrm{C}^s_{i_1\cdots i_r} \stackrel{\mathrm{def}}{=} \mathrm{Cum}[s_{i_1},\ldots,s_{i_r}]$, $1 \leqslant i_k \leqslant n$, $1 \leqslant k \leqslant r$, denote their rth-order moments and cumulants, respectively, whose mathematical definitions can be found in [37] and [38]. For the pairwise case, we prefer Kendall's notation [37]: $\mu^s_{r-p,p} \stackrel{\mathrm{def}}{=} \mathrm{M}^s_{\underbrace{1\ldots1}_{r-p}\,\underbrace{2\ldots2}_{p}} = \mathrm{E}[s_1^{r-p}s_2^p]$ and $\kappa^s_{r-p,p} \stackrel{\mathrm{def}}{=} \mathrm{C}^s_{\underbrace{1\ldots1}_{r-p}\,\underbrace{2\ldots2}_{p}}$ stand for the rth-order moment and cumulant of the signal pair $\mathbf{s} = [s_1, s_2]^{\mathrm{T}}$.

II. BSS and ICA

A. Matrix Model

In its simplest form, the BSS problem accepts the following matrix model. The entries of sensor-output vector $\mathbf{x}(t) = [x_1(t),\ldots,x_m(t)]^{\mathrm{T}}$ are instantaneous linear combinations of a set of unobserved source signals $\mathbf{s}(t) = [s_1(t),\ldots,s_n(t)]^{\mathrm{T}}$

$$\mathbf{x}(t) = \mathbf{A}\mathbf{s}(t) \tag{1}$$

where $\mathbf{A}$ represents the *mixing matrix,* with dimensions $(m\times n)$, $m \geqslant n$. In this paper all signals and mixtures are assumed to be real valued. If the mixing matrix is full column rank, the sources are mutually independent, and at most one of them is Gaussian, it is possible to obtain a separation matrix $\mathbf{B}$ and estimate the sources [12], [39] as

$$\mathbf{y}(t) = \mathbf{B}\mathbf{x}(t) = \mathbf{B}\mathbf{A}\mathbf{s}(t) = \mathbf{C}\mathbf{s}(t). \tag{2}$$

Since the scale and order of the components of $\mathbf{s}(t)$ do not affect their statistical independence, a satisfactory separation is characterized by a global matrix $\mathbf{C}$ with a nonmixing structure, that is, with a single nonnull element per row and per column (the product of a invertible diagonal matrix and a permutation matrix). As the source amplitudes are not important, it can be assumed, without loss of generality, that the source variance is unity $\mathrm{E}[\mathbf{s}(t)\mathbf{s}(t)^{\mathrm{T}}] = \mathbf{I}_n$.

Source separation is typically carried out in two steps. First, whitening or standardization [principal component analysis (PCA)] projects the observed vector on the signal subspace and yields a set of second-order decorrelated, normalized signals $\mathbf{z}(t) = [z_1(t),\ldots,z_n(t)]^{\mathrm{T}}$ such that $\mathrm{E}[\mathbf{z}\mathbf{z}^{\mathrm{T}}] = \mathbf{I}_n$. As a result, the source and whitened vectors must be related through a unitary transformation

$$\mathbf{z}(t) = \mathbf{Q}\mathbf{s}(t). \tag{3}$$

The separation problem thus reduces to the computation of unitary matrix $\mathbf{Q}$, which is accomplished in a second step. The ICA approach to BSS consists of computing $\mathbf{Q}$ such that the entries of the separator output $\mathbf{y}(t) = \mathbf{Q}^{\mathrm{T}}\mathbf{z}(t)$ are as independent as possible.[1] Since we consider methods that do not exploit the temporal structure of the source process $\mathbf{s}(t)$, in the sequel, the time index t will be dropped when convenient.

B. Contrast Functions

A contrast function [12] is a mapping $\psi(\mathbf{y})$ from the set of densities $\{p_{\mathbf{y}}, \mathbf{y} \in \mathbb{R}^n\}$ to $\mathbb{R}$ satisfying the following requirements. If $\mathbf{y}$ has independent components, then $\psi(\mathbf{y}) \geqslant \psi(\mathbf{A}\mathbf{y})$, $\forall\mathbf{A}$ nonsingular (domination), with equality if and only if $\mathbf{A}$ is nonmixing (discrimination); also, $\psi(\mathbf{y})$ is unaltered by permutations or scaling of the components of $\mathbf{y}$ (invariance). Thus, the maximization of a contrast function yields the ICA solution. Contrasts are attractive because they allow an optimal processing in the presence of unknown noise and interference, adding robustness to the separation performance.

The ML principle provides the contrast [23]

$$\psi^{\mathrm{ML}}(\mathbf{y}) = \log p_x(\mathbf{x}|\mathbf{A})\Big|_{\mathbf{x}=\mathbf{A}\mathbf{y}} = \sum_{i=1}^{n}\log p_{s_i}(y_i) - \log|\det\mathbf{A}|. \tag{4}$$

[1]This two-step process corresponds to the "hard whitening" approach. Recently, the "soft whitening" concept has been introduced [40], in which the second- and higher order processing is carried out simultaneously.

If this function is maximized for all possible distributions under the whitening constraint, we arrive at the ME contrast [41]

$$\psi^{\mathrm{ME}}(\mathbf{y}) = -\sum_{i=1}^{n} \mathrm{H}[y_i] \tag{5}$$

where $\mathrm{H}[\cdot]$ represents the differential entropy. Using the Edgeworth expansion of the source pdf [37], after second-order whitening, the ME contrast can be approximated as a function of the fourth-order cumulants [12], [41]

$$\psi_{24}^{\mathrm{ME}}(\mathbf{y}) = \sum_{i=1}^{n} (\mathrm{C}_{iiii}^{y})^2 \tag{6}$$

where C_{iiii}^{y} is the fourth-order marginal cumulant (kurtosis) of y_i, which, in the zero-mean unit-variance case, reduces to $(\mathrm{E}[y_i^4] - 3)$. This contrast is discriminating over the set of random vectors $\mathbf{y}$ having at most one non-kurtic component [12]. Alternatively, instead of maximizing the ML for all possible distributions, we can also exploit some available information on the source pdf to maximize the ML contrast. In the fourth-order case, if all sources have the same sign of kurtosis, (6) simplifies to [20]

$$\psi_{24}^{\mathrm{ML}}(\mathbf{y}) = \pm \sum_{i=1}^{n} \mathrm{E}\left[y_i^4\right]. \tag{7}$$

Finally, the JADE method [4] is based on the criterion

$$\psi^{\mathrm{JADE}} = \sum_{i,k,l=1}^{n} (\mathrm{C}_{iikl}^{y})^2 \tag{8}$$

whose maximization can be efficiently carried out as the joint approximate diagonalization of a set of matrix slices of the whitened cumulant tensor. In the two-signal scenario, approximations to these optimality criteria can be solved in closed form as explained in the next section. In the case of JADE, the associated closed-form estimator that we develop is an exact minimizer of criterion (8).

III. Optimal Analytic Solution in the Two-Signal Case

A. Complex Centroids

In the two-signal case, $\mathbf{Q}$ is a Givens rotation matrix, characterized by an unknown angle $\theta \in]-\pi, \pi]$

$$\mathbf{Q}(\theta) = \begin{bmatrix} \cos\theta & -\sin\theta \\ \sin\theta & \cos\theta \end{bmatrix}. \tag{9}$$

ICA then reduces to the estimation of θ from the whitened sensor outputs. Relation (3) accepts a compact complex-valued formulation

$$z_1 + jz_2 = \mathrm{e}^{j\theta}(s_1 + js_2) \tag{10}$$

or $\phi = \phi' + \theta$, where $(z_1 + jz_2) = \rho \mathrm{e}^{j\phi}$ and $(s_1 + js_2) = \rho \mathrm{e}^{j\phi'}$. Geometrically, (10) signifies that the whitened-signal pdf is a rotated version of the source pdf.

Centroids are defined as particular nonlinear averages of the complex points (10) [14], [18], [31]. The following centroids are useful in deriving closed-form expressions for the estimation of θ

$$\xi_\gamma \stackrel{\mathrm{def}}{=} \mathrm{E}[\rho^4 \mathrm{e}^{j4\phi}] = (\kappa_{40}^z - 6\kappa_{22}^z + \kappa_{04}^z) + j4(\kappa_{31}^z - \kappa_{13}^z) \tag{11}$$

$$\xi_\eta \stackrel{\mathrm{def}}{=} \mathrm{E}[\rho^4 \mathrm{e}^{j2\phi}] = (\kappa_{40}^z - \kappa_{04}^z) + j2(\kappa_{31}^z + \kappa_{13}^z) \tag{12}$$

$$\beta \stackrel{\mathrm{def}}{=} \mathrm{E}[\rho^4] - 8 = \kappa_{40}^z + 2\kappa_{22}^z + \kappa_{04}^z. \tag{13}$$

When written as a function of the source statistics, the above centroids yield

$$\xi_\gamma = \gamma \mathrm{e}^{j4\theta}, \quad \xi_\eta = \eta \mathrm{e}^{j2\theta}, \quad \beta = \gamma \tag{14}$$

where symbols $\gamma \stackrel{\mathrm{def}}{=} (\kappa_{40}^s + \kappa_{04}^s)$ and $\eta \stackrel{\mathrm{def}}{=} (\kappa_{40}^s - \kappa_{04}^s)$ represent the sks and the skd, respectively.[2]

B. General Weighted Fourth-Order Estimator (GWFOE)

The EML estimator [18] can be expressed as

$$\hat{\theta}_{\mathrm{EML}} = \frac{1}{4}\angle(\beta\xi_\gamma) \tag{15}$$

Similarly, the AEML [19] reads

$$\hat{\theta}_{\mathrm{AEML}} = \frac{1}{2}\angle\xi_\eta. \tag{16}$$

Under mild conditions, the sample versions of centroids ξ_γ, ξ_η, and β are consistent estimators of $\gamma \mathrm{e}^{j4\theta}$, $\eta \mathrm{e}^{j2\theta}$, and γ, respectively, so that $\hat{\theta}_{\mathrm{EML}}$ and $\hat{\theta}_{\mathrm{AEML}}$ consistently estimate θ as long as $\gamma \neq 0$ and $\eta \neq 0$, respectively [14], [18]. The lack of consistency for certain values of source kurtosis is precisely the main drawback of these two estimators.

In order to circumvent this deficiency, let us form the compound centroid

$$\xi_{\mathrm{GWFOE}} = w\beta\xi_\gamma + (1-w)\xi_\eta^2, \quad 0 < w < 1. \tag{17}$$

Then, parameter θ can also be estimated through

$$\hat{\theta}_{\mathrm{GWFOE}} = \frac{1}{4}\angle\xi_{\mathrm{GWFOE}} \tag{18}$$

which we call the GWFOE. The relevance of the GWFOE lies in the fact that it is a consistent estimator of θ for *any* source distribution, since the GWFOE centroid consistently estimates the complex number $[w\gamma^2 + (1-w)\eta^2]\mathrm{e}^{j4\theta}$. More importantly, the GWFOE unifies many of the analytic solutions already proposed in the literature, which are simply obtained for different values of the weight parameter w:

i) $w = 0$: AEML estimator of [14], [19];
ii) $w = 1/3$: AML estimator of [22];
iii) $w = 3/7$: SICA estimator of [25], [33];

[2]Note that β is an estimate of γ from the whitened sensor output. Hence, the equality expressed in (14) only holds for the ensemble averages.

iv) $w = 1/2$: MaSSFOC estimator of [24];
v) $w = 1$: EML estimator of [14], [18].

In addition, Appendix I proves that the solution provided by JADE [4] for $n = 2$ sources is equivalent to the GWFOE with $w = 1/2$. Similarly, the fourth-order part of the recently proposed CuBICA method [26] corresponds to the GWFOE with $w = 3/7$. On the other hand, by substituting β with ± 1 in (17)–(18), we also obtain the ML, MK, and SKSE/SKDE estimators of [17], [20], [21], [24], and [41]. These latter methods require advance knowledge of the source kurtosis sign.

Some of the above estimators arise from the ML criterion when the source pdf is approximated by its Gram–Charlier expansion truncated at fourth-order, and the sources are symmetrically distributed. Different solutions are then obtained under additional conditions:

EML estimator: $\eta = 0, \gamma \neq 0$;
AEML estimator: $\gamma = 0, \eta \neq 0$;
AML estimator: $\gamma \neq 0, \eta \neq 0$.

The GWFOE does not directly arise from the ML criterion, but it can be considered as the combination of two solutions (EML and AEML) which are approximate ML estimators under specific assumptions. Even if the validity conditions of an approximate ML solution hold, the use of a different weight w will divert the GWFOE from such a solution. However, the GWFOE variance can be fine-tuned by appropriately selecting w. In this manner the GWFOE can be made more efficient than any of the pairwise ML methods, especially in scenarios where their validity conditions do not hold. This improved efficiency is possible because the other estimators are only *approximate* ML solutions. This interesting feature will be developed in the next section and illustrated by the experiments of Section VI.

The use of the complex-centroid formalism allows us to bring out the connections with other existing closed-form solutions and facilitates the theoretical performance analysis of the estimator (as carried out next). Since some of these solutions (such as MaSSFOC or SICA) were originally obtained as approximations to optimality criteria other than ML, we prefer to adhere to the more generic denomination of GWFOE.

C. Performance Analysis: Optimal GWFOE

In this section, we intend to provide specific guidelines for the choice of GWFOE's weight parameter. We search for the value of w that minimizes the asymptotic (large-sample) MSE of the GWFOE class.

The asymptotic MSE of the GWFOE (18) is determined in Appendix II and is given by

$$\mathrm{MSE}_{\mathrm{GWFOE}} = \frac{\mathrm{E}\left\{\left[w\gamma\left(s_1^3 s_2 - s_1 s_2^3\right) + (1-w)\eta\left(s_1^3 s_2 + s_1 s_2^3\right)\right]^2\right\}}{T\left[w\gamma^2 + (1-w)\eta^2\right]^2} \quad (19)$$

where T is the number of samples per signal. It is interesting to note the following.

i) $\mathrm{MSE}_{\mathrm{GWFOE}}$ reduces to the asymptotic MSE of the AEML and EML estimators [14], [15] for $w = 0$ and $w = 1$, respectively. This is not surprising, since the GWFOE becomes such estimators at those weight values (see the previous section).
ii) When $\gamma = 0$ (respectively, $\eta = 0$), GWFOE performance reduces to that of the AEML (respectively, EML) estimator, for any $0 < w < 1$.

If $|\kappa_{40}^s| \neq |\kappa_{04}^s|$, the global minimum of $\mathrm{MSE}_{\mathrm{GWFOE}}$ (19) is obtained at (see Appendix II)

$$w_{\mathrm{opt}} = \frac{1}{2} + \frac{\mu_{40}^s \mu_{04}^s \left[\left(\kappa_{40}^s\right)^2 - \left(\kappa_{04}^s\right)^2\right] + \kappa_{40}^s \kappa_{04}^s \left(\mu_{60}^s - \mu_{06}^s\right)}{2\left[\left(\kappa_{40}^s\right)^2 \mu_{06}^s - \left(\kappa_{04}^s\right)^2 \mu_{60}^s\right]}. \quad (20)$$

If $w_{\mathrm{opt}} \notin [0, 1]$, the derivative of $\mathrm{MSE}_{\mathrm{GWFOE}}$ with respect to w does not change sign and thus $\mathrm{MSE}_{\mathrm{GWFOE}}$ is monotonic in such an interval. In that case, we choose between $w_{\mathrm{opt}} = 0$ (AEML) and $w_{\mathrm{opt}} = 1$ (EML) the value that provides the lowest $\mathrm{MSE}_{\mathrm{GWFOE}}$ in (19). If $|\kappa_{40}^s| = |\kappa_{04}^s|$, case ii) holds. Hence, given the source statistics, one can select the estimator of the GWFOE family with minimum asymptotic MSE. The experiments of Section VI will illustrate the validity of the asymptotic approximation (19) and the performance improvements that can be derived from the use of the optimal weight coefficient.

In the event that nothing is known in advance about the source statistics, a possible simple strategy is to perform an initial separation with any $w \in]0, 1[$. The optimal value of w can then be estimated from the obtained sources, and the separation can be repeated until w_{opt} converges. This iterative estimation of w_{opt} converges very fast (typically within one to two iterations), as will be demonstrated in the experiments of Section VI. Depending on the actual source statistics and the application in hand, the performance gain may compensate the increased cost of performing several separations.

IV. More Than Two Signals Case

A. Standard Jacobi Optimization

Jacobi optimization (JO) techniques have favorable rounding-error properties and high computational parallelism, allowing for numerically stable efficient implementations [28]. In the ICA context, Comon applied a JO-like procedure to extend a two-dimensional contrast $\phi(\theta)$ to the n-dimensional scenario, with $n > 2$. Thanks to its flexibility, the JO approach can easily integrate any valid two-signal solution, such as the GWFOE.

Algorithm (JO-GWFOE)

n-dimensional GWFOE using conventional Jacobi optimization.

1) *Whitening*. Compute the whitened signals as $\mathbf{z} = \mathbf{W}\mathbf{x}$ from a whitening matrix $\mathbf{W}$. Set $\mathbf{y} = \mathbf{z}$ and sweep number $c = 1$.
2) *Sweep* c. For all $g = n(n-1)/2$ pairs, $1 \leq p < q \leq n$, do
   a) Set $[z_p, z_q]^{\mathrm{T}} = [y_p, y_q]^{\mathrm{T}}$ and compute the Givens angle $\theta_{pq} = \hat{\theta}_{\mathrm{GWFOE}}$ from (18).
   b) If $|\theta_{pq}| > \theta_{\min}$, rotate the pair $[y_p, y_q]^{\mathrm{T}}$ by θ_{pq}.
3) *End*? If the number of sweeps c reaches a maximum value $c = K$ or no angle θ_{pq} has been updated, terminate. Otherwise go to Step 2) for another sweep, with $c = c+1$.

In [41], the algorithm only stops when the whole set of g Givens rotations have been updated by a value under a threshold $\theta_{\min}$, but no limit is set on the number of sweeps c. The value $\theta_{\min}$ is chosen in such a way that rotations by a smaller angle are not statistically significant; typically, $\theta_{\min} = 10^{-2}/\sqrt{T}$, where T is the sample size. In [12], the algorithm stops after $K = 1 + \sqrt{n}$ sweeps. This limit is also appropriate in our implementation, due to the existing connection between the contrast of [12] in the basic two-dimensional case and the GWFOE solutions. In a bid to avoid useless computations, we also set a fixed threshold $\theta_{\min} = \pi/360$ rad (0.5°).

B. Initialized Jacobi Optimization

Step 2a) of the JO-GWFOE computes the Givens angle θ_{pq} by using (18). The centroids (11)–(13) are calculated by averaging over the whole set of samples of signal pair $[z_p, z_q]^{\mathrm{T}}$. Since the sample averaging is repeated over several sweeps, this procedure may be computationally very costly for large sample sizes.

A more efficient alternative may be obtained as follows. Centroids (11)–(13) may be written as a function of the moments of the current output pair $\{\mu^y_{4-i,i}\}_{i=0}^4$. The idea is to compute the whole set of whitened-signal moments just once at an initial stage and later "rotate" them at each step of the algorithm without reusing the observed signal samples. The relationship between the moments of the whitened sensor output and their rotated counterparts is established below (Appendix III).

Proposition 1: Let $\mathbf{y} = \mathbf{V}\mathbf{z}(t)$, where $\mathbf{V}$ is an arbitrary $(n \times n)$ matrix. Then, there exists a symmetric $(r \times r)$ matrix $\mathbf{M}^z$, with $r = n(n+1)/2$, such that

$$\mathbf{M}^z\left(a(i,j), a(k,l)\right) = \mathrm{M}^z_{ijkl} \tag{21}$$

where

$$a(i,j) = (i-1)\left(n - \frac{i}{2}\right) + j, \qquad 1 \leqslant i \leqslant j \leqslant n. \tag{22}$$

Moreover, there exist vectors $\mathbf{v}_{pp}$, $\mathbf{v}_{pq}$, and $\mathbf{v}_{qq}$ of length r, such that the fourth-order moments of the outputs $[y_p, y_q]^{\mathrm{T}}$ are given by

$$\begin{aligned} \mu^y_{40} &= \mathbf{v}_{pp}^{\mathrm{T}}\mathbf{M}^z\mathbf{v}_{pp}, \quad \mu^y_{31} = \mathbf{v}_{pp}^{\mathrm{T}}\mathbf{M}^z\mathbf{v}_{pq}, \\ \mu^y_{22} &= \mathbf{v}_{pp}^{\mathrm{T}}\mathbf{M}^z\mathbf{v}_{qq}, \quad \mu^y_{13} = \mathbf{v}_{pq}^{\mathrm{T}}\mathbf{M}^z\mathbf{v}_{qq}, \\ \mu^z_{04} &= \mathbf{v}_{qq}^{\mathrm{T}}\mathbf{M}^z\mathbf{v}_{qq}. \end{aligned} \tag{23}$$

The formulation introduced above allows an easy computation of the output statistics for a given rotation matrix, as the entries of $\mathbf{V}$ are easily arranged into the three "rotation vectors" $\mathbf{v}_{pp}$, $\mathbf{v}_{pq}$, and $\mathbf{v}_{qq}$ used in (23). Since only the subset $1 \leqslant i \leqslant j \leqslant k \leqslant l \leqslant n$ is needed in matrix $\mathbf{M}^z$, the number of computed moments reduces to $\binom{n+3}{4} = (n+3)!/((n-1)!4!)$. The resulting ICA algorithm based on this algebraic structure is outlined below.

Algorithm (IJO-GWFOE)

---

n-dimensional GWFOE using *initialized* Jacobi optimization.

1) *Whitening*. Compute a whitening matrix $\mathbf{W}$ and set $\mathbf{z} = \mathbf{W}\mathbf{x}$.
2) *Moments Initialization*. Compute matrix $\mathbf{M}^z$ in (21) from the sample estimates of M^z_{ijkl}, $1 \leqslant i, j, k, l \leqslant n$. Initialize the accumulated rotation matrix as $\mathbf{V} = \mathbf{I}_n$.
3) *Sweep* c. For all $g = n(n-1)/2$ pairs, $1 \leq p < q \leq n$, do
   a) Compute the moments of current signal pair from (23) and $\mathbf{V}$. Compute the Givens angle $\theta_{pq} = \hat{\theta}_{\mathrm{GWFOE}}$ from (18).
   b) if $|\theta_{pq}| > \theta_{\min}$, update the rotation matrix $\mathbf{V}$ by rotating an angle θ_{pq} the proper coordinates.
4) *End*? If the number of sweeps c satisfies $c = K$ or no angle θ_{pq} has been updated, terminate. Otherwise return to Step 3) for another sweep, with $c = c + 1$.

At convergence, matrix $\mathbf{V}$ is an estimate of $\mathbf{Q}^{\mathrm{T}}$ in (3). The main advantage of the alternative formulation presented in this section is that the whitened sensor samples are directly used only once, for computing matrix $\mathbf{M}^z$ before starting the iterations. The moments of each signal pair at each step of Algorithm IJO-GWFOE are computed as quadratic forms involving simple vector-matrix products. The main drawback of this alternative procedure is that at a large number of components, the number of entries of the moment matrix is of order $\mathrm{O}(n^4)$. However, we will show later in this section that the complexity of the standard JO can be improved if the number of sources is low. Hence, memory problems will not appear. By "initialization" we mean a previous computation of the whitened-signal statistics to simplify subsequent calculations.

The IJO algorithm described above is reminiscent of JADE [4]. Indeed, the GWFOE with $w = 1/2$ is equivalent to JADE in the scenario of $n = 2$ sources, as seen in Section III-B and Appendix I. Moreover, JADE also calculates the cumulant matrix in advance and performs planar rotations in a JO-like fashion. Nevertheless, the equivalence between JADE and GWFOE-based algorithms vanishes in the presence of more than two sources, for JADE's cost function involves cumulants from more than two signals at each Jacobi iteration. On the other hand, JADE updates the cumulant matrix with the Givens angles after each iteration, whereas the IJO algorithm calculates the pertinent signal-pair cumulants from the moment matrix as in Proposition 1, without updating the moment matrix.

C. Computational Complexity: Optimal Jacobi Optimization

This section compares the computational complexity of the initialized and standard JO methods. As in [30], and for the sake of comparison, a floating-point operation (flop) will be considered as a real multiplication followed by an addition. The following values are used: $g = n(n-1)/2$ is the number of signal pairs, $K = 1 + \sqrt{n}$ denotes the maximum number of sweeps in the JO, and $r = n(n+1)/2$ represents the dimension of the moment matrix $\mathbf{M}^z$ in (21).

The computational burden of a fourth-order moment sample estimate is $3T$ flops. The number of flops for the JO-GWFOE algorithm is

$$f_{\mathrm{JO}} = 15gKT + 4gKT = 19gKT. \tag{24}$$

The first term is the computational cost related to the calculation of the moments, whereas the second accounts for the data

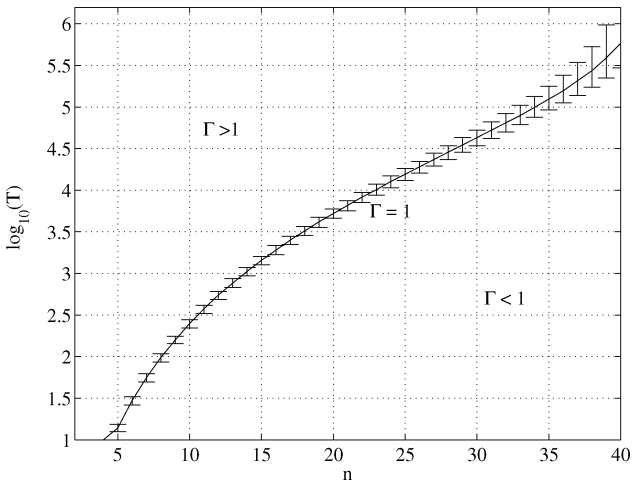

Fig. 1. Computational burden ratio between the JO and the IJO approaches. The vertical lines represent the range of (n, T) with Γ between 0.9 and 1.1.

rotation performed at Step 2b) of Algorithm JO-GWFOE. The number of operations of the IJO-GWFOE algorithm is given by

$$f_{\mathrm{IJO}} = 3T\binom{n+3}{4} + gKr(r+1) \tag{25}$$

where the first term is the number of operations needed to compute the entries of the moment matrix (21). Since some multiplications are repeated in the calculation of the moments (e.g., the product $x_i x_j$ appears in any term of the form $x_i x_j x_k x_l$), this number could be further reduced to $T(\binom{n+3}{4} + \binom{n+1}{2})$. The second term in (25) is the number of operations in computing (23) at each Givens angle. Hence, the relation between f_{JO} and f_{IJO} is

$$\Gamma(n,T) = \frac{19gKT}{T\left(\binom{n+3}{4} + \binom{n+1}{2}\right) + gKr(r+1)}. \tag{26}$$

Fig. 1 plots the loci of $\Gamma(n,T) = 1$. We can draw the following conclusions. Since usually $T > 10^2$, IJO is to be used for a low number of sources, $n \leqslant 5$. As $n \to \infty$, the number of moments μ^z_{ijkl} becomes of the order $\mathrm{O}(n^4)$, making $\Gamma(n,T) < 1$ for any sample size. This outcome takes place at $n \approx 40$. Since the IJO is not to be used for large numbers of components, potential memory problems associated with the storage of matrix $\mathbf{M}^z$ are avoided. As a result of the above decision rule, the following computationally optimal JO algorithm can be devised.

Algorithm (OJO-GWFOE)

n-dimensional GWFOE using computationally *optimal* Jacobi optimization.

1) Compute the condition $\Gamma(n,T)$ in (26), and decide:
   a) If $\Gamma(n,T) < 1$ then use JO-GWFOE.
   b) Else, use IJO-GWFOE.

V. Adaptive Algorithms

A. Adaptive Jacobi Optimization

The JO procedure is easily extended to operate online, resulting in the adaptive Jacobi optimization (AJO). The AROT [13] and the adEML [30] are methods of this type. This section derives the AJO implementation of the GWFOE pairwise solution. This implementation is referred to as AJO-GWFOE.

The JO computes the two-dimensional estimate $\hat{\theta}_{\mathrm{GWFOE}}$ for each signal pair over several sweeps. Accordingly, centroids (11)–(13) must be calculated for every sweep c and signal pair (p,q). In the design of an adaptive version, such statistics can be updated with a new sample arriving at instant t as

$$\xi_\gamma^{(c,pq)}(t+1) = (1-\lambda)\xi_\gamma^{(c,pq)}(t) + \lambda\rho_{c,pq}^4(t)\mathrm{e}^{j4\phi_{c,pq}(t)} \tag{27}$$

$$\xi_\eta^{(c,pq)}(t+1) = (1-\lambda)\xi_\eta^{(c,pq)}(t) + \lambda\rho_{c,pq}^4(t)\mathrm{e}^{j2\phi_{c,pq}(t)} \tag{28}$$

$$\beta^{(c,pq)}(t+1) = (1-\lambda)\beta^{(c,pq)}(t) + \lambda\left(\rho_{c,pq}^4(t) - 8\right) \tag{29}$$

where λ is the learning or adaption coefficient. Since we estimate the rotation matrix $\mathbf{V}$ under the whitening constraint, we must first update the whitening matrix $\mathbf{W}(t)$. In the following, we will use the relative gradient based whitening algorithm [16]

$$\mathbf{W}(t+1) = \mathbf{W}(t) + \alpha\frac{\mathbf{I}_n - \mathbf{z}(t)\mathbf{z}(t)^{\mathrm{T}}}{1 + \alpha\left|\mathbf{z}(t)^{\mathrm{T}}\mathbf{z}(t)\right|}\mathbf{W}(t) \tag{30}$$

where α is the associated learning rate, which may be different from λ. The adaptive algorithm is then:

Algorithm (AJO-GWFOE)

Adaptive n-dimensional GWFOE using standard Jacobi optimization.

Initial setting. Set $\mathbf{W}(0) = \mathbf{I}_{n\times m}$.

At each sample instant: run Algorithm JO-GWFOE replacing the following steps:

Step 1) Use (30) to update the whitening matrix $\mathbf{W}(t)$. Compute $\mathbf{z}(t) = \mathbf{W}(t)\mathbf{x}(t)$. Set $\mathbf{y}(t) = \mathbf{z}(t)$ and $c = 1$.

Step 2)
   a) Set $[z_p(t), z_q(t)]^{\mathrm{T}} = [y_p(t), y_q(t)]^{\mathrm{T}}$ to update centroid estimates $\xi_\gamma^{(c,pq)}(t)$, $\xi_\eta^{(c,pq)}(t)$ and $\beta^{(c,pq)}(t)$ in (27)–(29). Compute the Givens angle $\hat{\theta}^{(pq)}_{\mathrm{GWFOE}}$ in (18) from those estimates.

Algorithm AJO-GWFOE is the adaptive version of Algorithm JO-GWFOE. From the connections established in Section III-B, it turns out that adEML of [30] is equivalent to the AJO-GWFOE with $w = 1$.

B. Adaptive Initialized Jacobi Optimization

In this section, we develop the adaptive version of the IJO-GWFOE—consequently called *AIJO-GWFOE*—aiming to alleviate the computational burden and covergence problems of

the previous algorithm. The main idea is to adaptively update matrix $\mathbf{M}^z$ of Proposition 1 as

$$\mathbf{M}^z(t+1) = (1-\lambda)\mathbf{M}^z(t) + \lambda\mathcal{M}^z(t) \tag{31}$$

where matrix $\mathcal{M}^z(t)$ is computed as $\mathbf{M}^z$ in (21) but using only $\mathbf{z}(t)$, the whitened-output sample at time instant t. The corresponding adaptive algorithm takes the form:

Algorithm (AIJO-GWFOE)

Adaptive n-dimensional GWFOE using *initialized* Jacobi optimization.

Initial setting. Set $\mathbf{W}(0) = \mathbf{I}_{n\times m}$ and $\mathbf{V}(0) = \mathbf{I}_n$.

- At each sample instant:
  1) *Whitening*. Update the whitening matrix $\mathbf{W}(t)$ as in (30) and obtain the whitened output sample $\mathbf{z}(t) = \mathbf{W}(t)\mathbf{x}(t)$.
  2) *Moment matrix updating*. Adaptively compute matrix $\mathbf{M}^z(t)$ as in (31) using the current whitened output $\mathbf{z}(t)$ to form matrix $\mathcal{M}(t)$.
- Each N samples: set sweep number $c = 1$ and run Steps 3)–4) of Algorithm IJO-GWFOE.

In the conventional AJO-GWFOE algorithm, centroids are updated from samples of the last estimated outputs $[y_p(t), y_q(t)]^{\mathrm{T}}$. However, these outputs depend on the updated statistics of previous pairs of outputs and sweeps, and, in consequence, the statistics of latest sweeps cannot converge until the previous statistics do. Furthermore, fluctuations around the convergence point of the statistics in the first sweeps make those in the final stages fluctuate as well, in a manner difficult to predict, compromising the stability of the algorithm. Since the number of sweeps grows with the dimension of the problem, the AJO method typically shows convergence problems for a high number of components.

By contrast, in the AIJO-GWFOE, the learning of the separation system and the computation of the solution are decoupled. In the first stage, the output moments are updated with the last output sample. In the second stage, a current separating matrix $\mathbf{B}(t)$ is computed. The right solution for $\mathbf{B}(t)$ is obtained if the learning of $\mathbf{M}^z$ has converged. Classical results of adaptive-algorithm analysis [42] show that, if the whitened-output moments are well defined, the equilibrium point of moment matrix update (31) is locally asymptotically stable and corresponds to the ensemble average $\mathbf{M}^z$. Consequently, this two-stage design improves the stability and convergence rate of the conventional AJO. To reduce complexity, the computation of $\mathbf{V}(t)$ can be carried out every N samples, with $N > 1$. In such a case, the algorithm could better be regarded as *semi-online*.

C. Computational Complexity of the Adaptive Algorithms

We now estimate the computational cost of the AIJO-GWFOE and compare it to that of the AJO-GWFOE, AROT [13] and EASI [16]. The authors of [30] estimate the number of flops per iteration for the adEML (an AJO method) and the AROT as $C_{\mathrm{AJO}} = C_{\mathrm{adEML}} = g(18+f)(1+\sqrt{n})$ and $C_{\mathrm{AROT}} = g(14+f)(1+\sqrt{n})$, respectively, where $f = 26$. They also compute it for the EASI as $C_{\mathrm{EASI}} = n^3 + 3n^2 + hn$, where each nonlinearity elements assumed to require h flops (e.g., for cubic nonlinearities $h = 2$). An extra number of flops would have to be added in the normalized version of EASI [16]. Note also that the figures for C_{AJO} and C_{AROT} in [30] do not include the whitening stage, so $n^2(n+1)$ flops must be added.

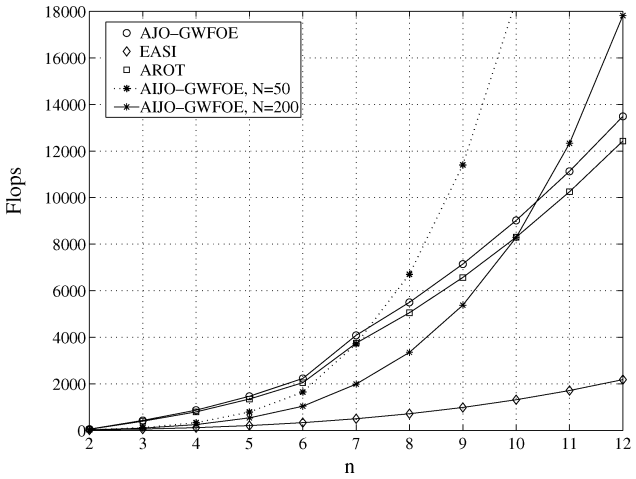

Fig. 2. Computational complexity as a function of the number of sources for AJO-GWFOE, AROT, EASI, and AIJO-GWFOE with $N = 50$ and $N = 200$.

Regarding the AIJO-GWFOE algorithm, at each sample instant this algorithm must perform the following tasks.

1) *Whitening:* The whitening algorithm (30) takes $n^2(n+1)$ flops.
2) *Moment matrix calculation:* As described before, the number of flops necessary to compute $\mathcal{M}^z(t)$ can be reduced to $\binom{n+3}{4} + \binom{n+1}{2}$.
3) *Moment matrix updating:* Adaptively computing matrix $\mathbf{M}(t)$ in (31) takes $r^2 = \binom{n+1}{2}^2$ flops.

On the other hand, each N samples, for each signal pair, we have the following.

Compute the moments: As described before, the number of flops needed to compute (23) is approximately $gKr(r+1)$.
Compute $\hat{\theta}^{(pq)}_{\mathrm{GWFOE}}$*:* Using (18), this task takes about $f = 26$ flops.
Rotate: 4 flops.

This makes $\binom{n+3}{4} + \binom{n+1}{2}[\binom{n+1}{2} + 1] + n^3 + n^2$ flops per iteration plus no more than $(1+\sqrt{n})(n(n-1)/2)[\binom{n+1}{2}^3 + \binom{n+1}{2} + 30]$ flops every N iterations.

Hence, the computational burden of AIJO is always higher than that of AJO, AROT, and EASI when $N = 1$. However, as N increases and for a reduced number of sources, we can force the complexity of AIJO below that of AJO and AROT, and of the order of EASI's. This result is illustrated in Fig. 2, which displays the number of flops per iteration as a function of the number of sources for these four adaptive methods, with $N = 50$ and $N = 200$. When the number of independent sources is $n \leqslant 7$ and $N = 50$ is selected, the complexity of AIJO is lower than AJO and AROT, as evidenced by the dotted line of Fig. 2. Also, when N is increased to 200, AIJO is less costly than AJO and AROT if the number of independent sources is $n \leqslant 10$, as

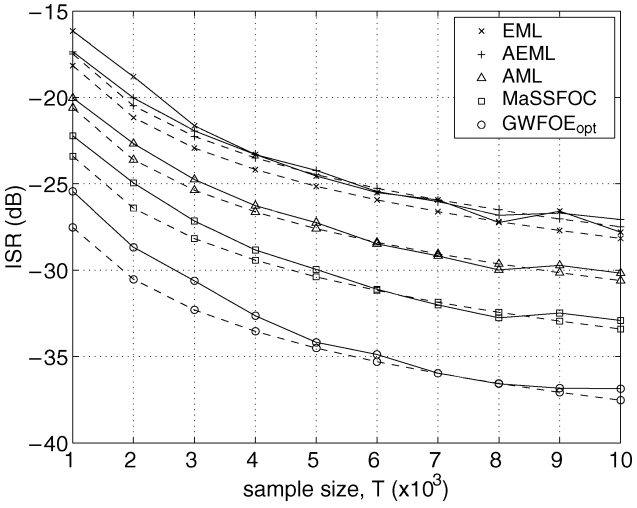

Fig. 3. ISR performance of the GWFOE versus sample size, for different weight coefficients. Uniform-Rayleigh sources, $\theta = 15^\circ$, ν independent Monte Carlo runs, with $\nu T = 5 \cdot 10^6$. Solid lines: average experimental values. Dashed lines: asymptotic MSE (19).

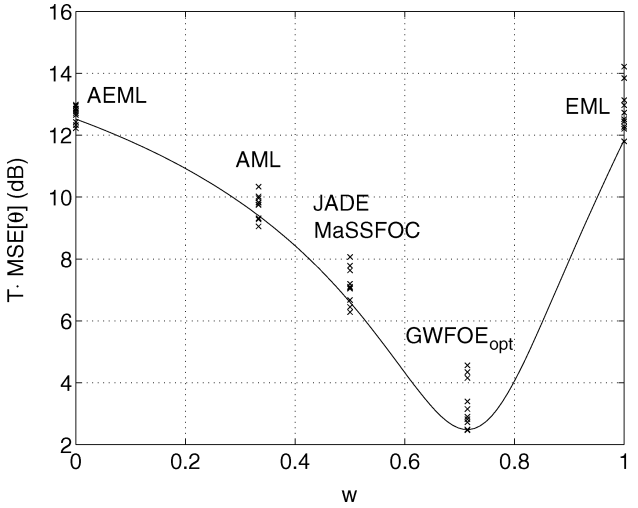

Fig. 4. Performance of the GWFOE as a function of the weight coefficient in the experiment of Fig. 3. Solid line: theoretical MSE (19). "×": experimental values from Fig. 3.

observed in Fig. 2. In such a case ($N = 200$ and $n \leqslant 7$), the computational burden of AIJO is still heavier than EASI's, but they become of the same order of magnitude.

VI. Experimental Results

The interference-to-signal power ratio (ISR) will be used as an objective separation index [1] to illustrate the main results presented in this paper. This performance index reads

$$\text{ISR} = \sum_{i=1}^{n} \left(\frac{\sum_{j=1}^{n} |c_{ij}|^2}{\max_j |c_{ij}|^2} - 1 \right) \tag{32}$$

where c_{ij} represents the element (i, j) of the global mixing–unmixing matrix $\mathbf{C}$. The ISR is an objective measure of separation performance, for it is method independent. In the two-signal case, the ISR approximates the MSE of the angle estimates around any valid separation solution (as shown at the end of Appendix II).

A. Performance of the GWFOE

We first demonstrate the potential benefits of the GWFOE and test the goodness of asymptotic approximation (19). Two source signals with independent identically distributed (i.i.d.) uniform and Rayleigh distribution are mixed through a unitary transformation with $\theta = 15^\circ$. According to (20), this source combination provides an optimal weight value of $w_{\text{opt}} = 0.7141$. Centroids are computed from their polar forms (11)–(13). ISR values are averaged over ν independent signal realizations, with $\nu T = 5 \cdot 10^6$. Fig. 3 shows the ISR performance obtained by the EML, AEML, AML, MaSSFOC, and optimal GWFOE, together with the expected asymptotic MSE, for varying sample size. The optimal GWFOE substantially outperforms the other estimators; e.g., it proves five and ten times more efficient than the AML and the AEML, respectively. The fitness of asymptotic approximation (19) is very precise in all cases and improves as T increases, as expected. Fig. 4 shows the variation in the MSE of the GWFOE angle estimates as a function of the weight coefficient. The solid line plots the theoretical values of $T \cdot \text{MSE}_{\text{GWFOE}}$ from (19), whereas the crosses represent the empirical values of $T \cdot \text{ISR}$ obtained in Fig. 3. Remark that a 10-dB gap appears between the maximum and the minimum performance achievable by the GWFOE family in this scenario. These results highlight the substantial impact that the choice of w can have on the separation performance.

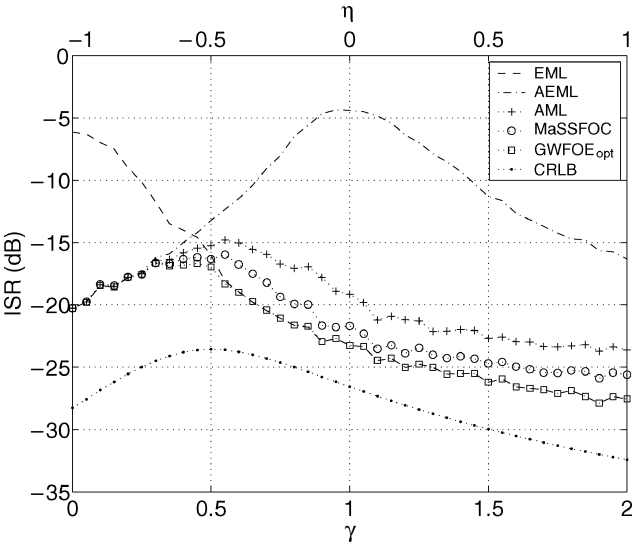

Fig. 5. ISR performance versus sks γ and skd η. GGD sources, $\kappa_{04}^s = 0.5$, $\theta = 15^\circ$, $T = 5 \cdot 10^3$ samples, 10^3 Monte Carlo runs.

The generalized Gaussian distribution (GGD) with shape parameter α, $p(s) \propto \exp(-|s|^\alpha)$, is used as source pdf in the simulation of Fig. 5. We fix $\kappa_{04}^s = 0.5$ and smoothly vary κ_{40}^s to generate a range of sks and skd values. The optimal GWFOE, with w_{opt} calculated as in (20) and shown in Fig. 6, is compared with other analytic solutions and the Cramer–Rao lower bound (CRLB) obtained in [22] for the real case. The optimal

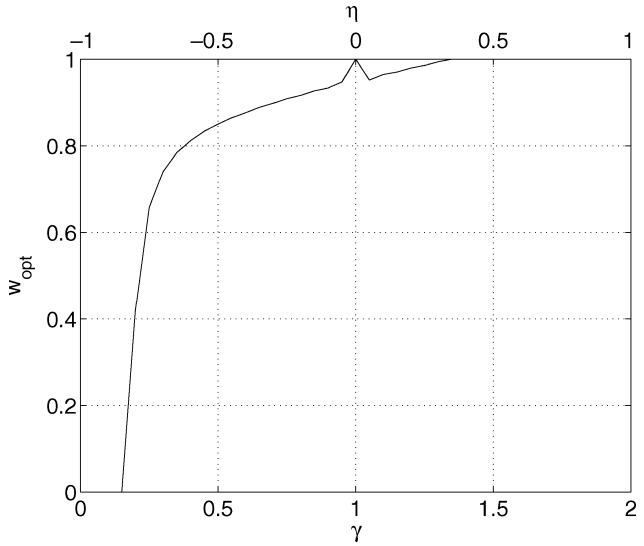

Fig. 6. Optimal value of the GWFOE weight parameter in the separation scenario of Fig. 5.

GWFOE avoids EML's and AEML's performance degradation around $\gamma = 0$ and $\eta = 0$ (respectively) and, though closely followed by MaSSFOC and AML, approaches the CRLB more tightly than any of the other methods.

When the source distribution is unknown, the iterative procedure presented at the end of Section III-C can be used to estimate GWFOE's optimal weight. To illustrate the performance of this iterative method, uniform-Rayleigh source realizations are mixed by a (2×2) mixing matrix with elements drawn from a zero-mean unit-variance Gaussian distribution. The mixture is first whitened via PCA based on the singular value decomposition of the observed data matrix. The GWFOE with initial weight uniformly distributed in [0, 1] is then applied to the whitened signals, resulting in a set of estimated sources. From the sample estimate of the source statistics, $w_{\rm opt}$ is obtained as in (20); then the GWFOE with the new weight is applied to the whitened observations, and so forth. Fig. 7 displays the trajectories of the $w_{\rm opt}$ estimate as a function of the iteration number, for several sample sizes T. The curves have been averaged over ν independent Monte Carlo runs, with $\nu T = 5 \cdot 10^6$. The method typically converges to the theoretical value of the optimal weight within just one to two iterations, the final bias decreasing as the sample size increases.

B. Performance of the OJO-GWFOE

The performance of the n-dimensional OJO-GWFOE using SICA [25] $(w = 3/7)$ is compared to JADE [4], the fourth-order-based ME method by Comon [12], and the FastICA algorithm [43].[3] The same whitening method is used in all algorithms, as the focus is on the computation of the unitary matrix $\mathbf{Q}$. A few changes are introduced in the code by Comon to save up some operations, while FastICA is executed with the parameters by default, including stabilization. In the OJO-GWFOE,

[3]MATLAB code for these methods is available at ftp://sig.enst.fr/pub/jfc/Algo/Jade/jadeR.m, http://www.i3s.unice.fr/~comon/matlab.html, and http://www.cis.hut.fi/projects/ica/fastica/index.shtml.

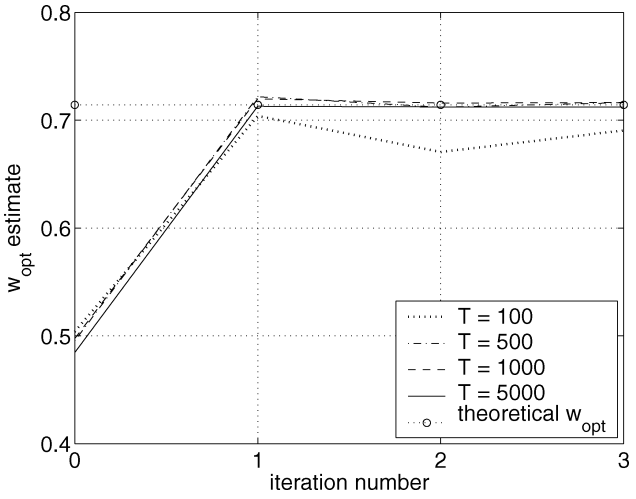

Fig. 7. Iterative estimation of GWFOE's optimal weight from the observed sensor output. Uniform-Rayleigh sources, mixing matrix with normalized Gaussian random elements, initial $w_{\rm opt}$ with uniform random distribution in [0, 1], ν independent Monte Carlo runs, with $\nu T = 5 \cdot 10^6$.

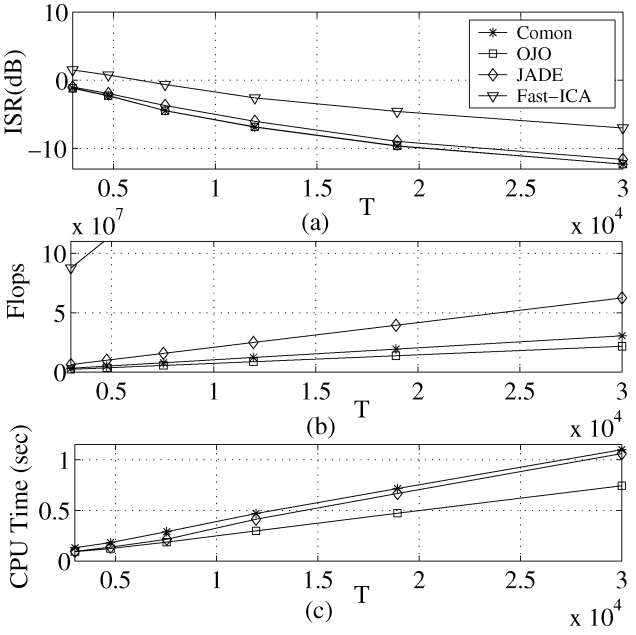

Fig. 8. Comparison of Comon's ME, OJO-GWFOE, JADE, and FastICA in the $n = 6$ dimensional case: (a) mean ISR, (b) flops, and (c) CPU time.

JADE, and ME by Comon, the Jacobi optimization stops whenever no angle has been updated more than $\pi/360$ rad (0.5°) or it has iterated more than $K = 1 + \sqrt{n}$ times. The flop count and CPU time are used as indices of computational complexity. The mixing matrix entries a_{ij} are random numbers in the range $[-1,1]$. The experiments have been performed using MATLAB on an Intel Pentium 4 2.40-GHz processor and 512 MB RAM.

In this experiment, $n = 6$ zero-mean unit-variance signals with different distributions are mixed: uniform, Laplacian $(p(s) \propto \mathrm{e}^{-|s|})$, Rayleigh $(p(s) \propto s\mathrm{e}^{-s^2/2})$, exponential $(p(s) \propto \mathrm{e}^{-s}, s \geqslant 0)$, Gaussian $(p(s) \propto \mathrm{e}^{-s^2/2})$, and log-normal $(p(s) \propto \mathrm{e}^{-(\log s)^2/2})$. We study the performance in the sample-size range $3 \cdot 10^3 \leqslant T \leqslant 3 \cdot 10^4$. Each point corresponds to the average of 1000 independent Monte Carlo runs in

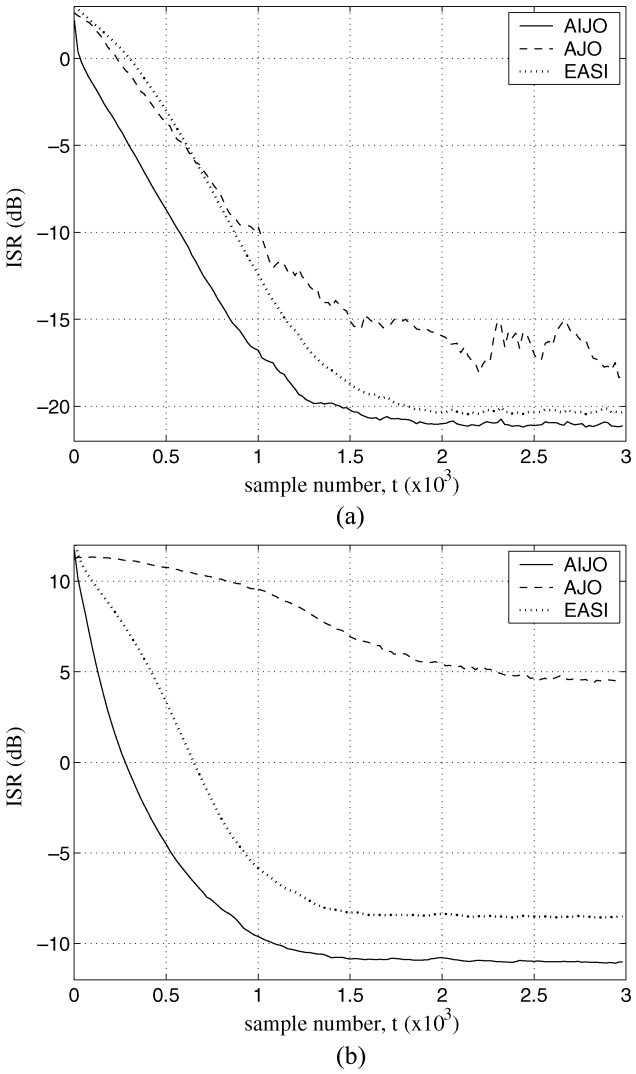

Fig. 9. Performance of the AIJO-GWFOE, AJO-GWFOE, and EASI methods for (a) $n = 3$ (uniform, binary, and sinusoid) and (b) $n = 8$ (six uniform, one binary, and one sinusoid).

which the mixing matrix is randomly chosen. Fig. 8(a) shows that OJO-SICA and ME have nearly identical performance, as expected. JADE also shows a good performance, close to that of the OJO-SICA. The FastICA method exhibits the worst behavior. Regarding the computational cost [Fig. 8(b) and (c)], the OJO-GWFOE method presented in this paper clearly outperforms the other methods. Although JADE takes a larger number of flops than the ME, its CPU time is lower. Similar results may be expected for other mixtures, except for FastICA. Although this latter method usually presents good performance at a low complexity, it may exhibit poor convergence and a high computational burden if its parameters are not properly chosen, as discussed in [25] and [44]. This is evidenced in this experiment, where the parameters by default yield a poor ISR, and a number of flops and CPU time out of the plotted range.

C. Performance of the AIJO-GWFOE

The AIJO-GWFOE method with weight parameter $w = 1$ is compared to other adaptive procedures: AJO-GWFOE with the same value of w (adEML) [30] and EASI [16]. The adaptation coefficient for both the whitening stage and the EASI method is selected as $\alpha = 5 \cdot 10^{-3}$, whereas the learning rate is set to $\lambda = 10^{-3}$ for the two other methods. For all methods, the separating matrix is initialized at the identity $\mathbf{B}(0) = \mathbf{I}_n$. Performance curves are averaged over 1000 independent Monte Carlo runs. By default, the solution of the AIJO-GWFOE method is calculated at each sample, $N = 1$. Results for any other N may be easily deduced from the plots for $N = 1$ by holding the value obtained for sample kN until sample $(k+1)N$. The first experiment considers a mixture of three independent sources: a binary sequence, a uniformly distributed process, and a sinusoid with random frequency and phase. Fig. 9(a) shows that AIJO-GWFOE converges to a lower ISR than AJO-GWFOE and EASI. In addition, the stationary state is reached faster than in the two other methods.

To compare the performance of the three algorithms in a more complex separation system, a mixture of eight independent sources is observed in a second setup. All but two of these are uniformly distributed processes; the other two are a binary sequence and a sinusoid with random frequency and phase. The evolution of the performance curves in Fig. 9(b) demonstrates again that the AIJO-GWFOE provides the best final ISR in the lowest number of iterations. By contrast, the AJO-GWFOE algorithm shows a slow poor convergence.

VII. Conclusion

This paper has investigated the approximate closed-form solutions to ICA contrasts in the two-dimensional case. The GWFOE gathers under the same expression many existing analytic solutions based on fourth-order statistics. In particular, for $w = 1/2$ the GWFOE is equivalent to JADE in the two-source scenario. The weight parameter of the most efficient estimator in the GWFOE class has been obtained as a function of the source statistics. Even if these are unknown, a simple iterative procedure allows a fast accurate estimation of the optimal weight. The optimal GWFOE can considerably outperform other analytic solutions, as demonstrated by experimental results.

Analytic solutions can be extended to the general scenario of more than two sources by means of the pairwise JO technique. The algebraic structure of the problem has been exploited through the multilinearity property of moments and cumulants in a bid to optimize the computational complexity of the conventional JO procedure. The resulting IJO computes the necessary statistics before the iteration process, so that the observed signal samples are employed only once. A detailed discussion has concluded that the decision on which method to use (JO or IJO) depends on the relative values of source number and sample size. In our experiments, IJO-GWFOE using SICA has achieved a similar performance than Comon's ME and FastICA, with a reduced complexity.

In the adaptive implementation of IJO, the learning of the system and the computation of the ICA solution are decoupled. This feature enhances the convergence properties (particularly the stability) of the algorithm. With a complexity that can be reduced to the order of EASI's, AIJO presents the advantage of an increased robustness to the source distributions. Experimental

results have shown that the convergence of AIJO is faster than EASI's and adEML's (indeed, its ISR evolution is always below that of the other methods), reaching the best final performance for any number of sources and different source distributions.

Further work includes the development of GWFOE's optimal weight coefficient as a function of the array-output statistics in order to enable a fully blind operation and the incorporation of the optimal GWFOE in the multidimensional JO-based algorithms. The separation performance and convergence characteristics in the presence of additive noise and interference needs to be explored, for both offline and online implementations. Extensions to statistics of orders other than four also deserves to be investigated. The use of characteristic functions [45] might prove helpful in that line of inquiry.

Appendix I
Equivalence Between GWFOE With $w = 1/2$ and JADE for $n = 2$

The maximization of contrast function (8) is associated with the joint approximate diagonalization of the so-called parallel set of cumulant matrices $\{\mathbf{N}_r\}$, whose entries are defined as $(\mathbf{N}_r)_{ij} = \mathrm{C}^z_{ijkl}$ [4]. In this Appendix we prove that, in the two-source scenario, the solution provided by the conventional version of JADE based on the parallel set provides the GWFOE solution (18) with $w = 1/2$.

For $n = 2$, the cumulant matrices of the parallel have the form $\mathbf{N}_r = \begin{bmatrix} a_r & b_r \\ c_r & d_r \end{bmatrix}$

$$\mathbf{N}_1 = \begin{bmatrix} \kappa^z_{40} & \kappa^s_{31} \\ \kappa^z_{31} & \kappa^z_{22} \end{bmatrix}, \quad \mathbf{N}_2 = \mathbf{N}_3 = \begin{bmatrix} \kappa^z_{31} & \kappa^z_{22} \\ \kappa^z_{22} & \kappa^z_{13} \end{bmatrix}$$
$$\mathbf{N}_4 = \begin{bmatrix} \kappa^z_{22} & \kappa^s_{13} \\ \kappa^z_{13} & \kappa^z_{04} \end{bmatrix}. \tag{33}$$

As shown in [4, Sec. 8.1], the joint diagonalization criterion is equivalent to maximizing $\psi = \sum_r |a'_r - d'_r|^2$, where (a'_r, d'_r) are the diagonal elements of $\mathbf{Q}^{\mathrm{T}}\mathbf{N}_r\mathbf{Q}$, matrix $\mathbf{Q}$ denoting the sought Givens rotation of angle θ in (9). Following [4, Sec. 8.1], the criterion can be expressed as $\psi = \mathbf{v}^{\mathrm{T}}\mathbf{H}\mathbf{v}$, with $\mathbf{v} = [\cos 2\theta, \sin 2\theta]^{\mathrm{T}}$ and $\mathbf{H} \stackrel{\mathrm{def}}{=} \mathbf{G}\mathbf{G}^{\mathrm{T}}$, $\mathbf{G} = [\mathbf{g}_1, \ldots, \mathbf{g}_4]$, $\mathbf{g}_r = [a_r - d_r, b_r + c_r]^{\mathrm{T}}$, where (a_r, d_r) and (b_r, c_r) represent the diagonal and off-diagonal entries, respectively, of $\mathbf{N}_r$. Hence, $\mathbf{v}$ is the dominant eigenvector of the symmetric matrix $\mathbf{H} = \begin{bmatrix} a & b \\ b & d \end{bmatrix}$, whose elements are given by

$$\begin{aligned} a &= \sum_{r=1}^{4}(a_r - d_r)^2 \\ &= (\kappa^z_{40} - \kappa^z_{22})^2 + 2(\kappa^z_{31} - \kappa^z_{13})^2 + (\kappa^z_{22} - \kappa^z_{04})^2 \end{aligned} \tag{34}$$

$$\begin{aligned} b &= \sum_{r=1}^{4}(a_r - d_r)(b_r + c_r) \\ &= 2\kappa^z_{31}(\kappa^z_{40} - \kappa^z_{22}) + 4\kappa^z_{22}(\kappa^z_{31} - \kappa^z_{13}) \\ &\quad + 2\kappa^z_{13}(\kappa^z_{22} - \kappa^z_{04}) \end{aligned} \tag{35}$$

$$\begin{aligned} d &= \sum_{r=1}^{4}(b_r + c_r)^2 \\ &= 4(\kappa^z_{31})^2 + 8(\kappa^z_{22})^2 + 4(\kappa^z_{13})^2. \end{aligned} \tag{36}$$

Now, to find the dominant eigenvector of $\mathbf{H}$, we take into account that its eigenvector matrix must be of the form $\tilde{\mathbf{V}} = [\mathbf{v}, \tilde{\mathbf{v}}]$, with $\tilde{\mathbf{v}} = \pm[-\sin 2\theta, \cos 2\theta]^{\mathrm{T}}$. Also, matrix $\tilde{\mathbf{V}}$ must diagonalize $\mathbf{H}$. Thus, we force a diagonal structure for matrix $\tilde{\mathbf{V}}^{\mathrm{T}}\mathbf{H}\tilde{\mathbf{V}}$, which leads to two constraints on the resulting off-diagonal elements reducing to $\mathbf{v}^{\mathrm{T}}\mathbf{H}\tilde{\mathbf{v}} = b(\cos^2 2\theta - \sin^2 2\theta) - (a-d)\cos 2\theta \sin 2\theta = 0$. We thus obtain $\tan 4\theta = 2b/(a-d)$. By means of some straightforward algebraic manipulations on (34)-(36), this solution is readily shown to coincide with the GWFOE solution (18) for $w = 1/2$. □

Appendix II
Asymptotic Analysis of the GWFOE

In this Appendix, we analyze the asymptotic performance of the GWFOE estimator (18) for i.i.d. sources. Our main objective is an analytic expression for its large-sample MSE. The estimator reads

$$\tilde{\theta} = \frac{1}{4}\angle\left\{w\hat{\beta}\hat{\xi}_\gamma + (1-w)\hat{\xi}^2\right\} \tag{37}$$

where

$$\hat{\xi} = \frac{1}{T}\sum_{k=1}^{T}\rho_k^4 \mathrm{e}^{j4\phi_k}, \quad \hat{\xi}_\eta = \frac{1}{T}\sum_{k=1}^{T}\rho_k^4 \mathrm{e}^{j2\phi_k}, \quad \hat{\beta} = \frac{1}{T}\sum_{k=1}^{T}\rho_k^4 - 8 \tag{38}$$

are the sample estimates of centroids (11)-(13). Note that

$$\hat{\xi}_\gamma = \hat{\xi}'_\gamma \mathrm{e}^{j4\theta}, \quad \hat{\xi}_\eta = \hat{\xi}'_\eta \mathrm{e}^{j2\theta} \tag{39}$$

with

$$\hat{\xi}'_\gamma = \frac{1}{T}\sum_{k=1}^{T}\rho_k^4 \mathrm{e}^{j4\phi'_k}, \quad \hat{\xi}'_\eta = \frac{1}{T}\sum_{k=1}^{T}\rho_k^4 \mathrm{e}^{j2\phi'_k}. \tag{40}$$

Hence, $\Delta\hat{\theta} \stackrel{\mathrm{def}}{=} (\hat{\theta} - \theta) = (1/4)\angle\hat{\xi}'$, where $\hat{\xi}' = w\hat{\beta}\hat{\xi}'_\gamma + (1-w)\hat{\xi}'^2_\eta$. By virtue of the law of large numbers, the combined source centroid $\hat{\xi}'$ is a consistent estimator of a positive real number

$$\mathrm{E}[\hat{\xi}'] \xrightarrow[T\to\infty]{} w\gamma^2 + (1-w)\eta^2. \tag{41}$$

It follows that the GWFOE is also consistent and, in particular

$$\mathrm{E}[\Delta\tilde{\theta}] \xrightarrow[T\to\infty]{} 0. \tag{42}$$

Now, $\mathrm{MSE}_{\mathrm{GWFOE}} \stackrel{\mathrm{def}}{=} \mathrm{MSE}[\hat{\theta}] = \mathrm{E}[\Delta\hat{\theta}^2]$. At large T, and since the estimator is consistent, $\Delta\hat{\theta}$ will be close to zero; thus $4\Delta\hat{\theta} \approx \tan(4\Delta\hat{\theta})$. Also, since $\Delta\hat{\theta}$ is small and, according to (41), typically $\mathrm{E}[\mathbb{R}\mathrm{e}(\hat{\xi}')] \gg \mathrm{E}[\mathbb{I}\mathrm{m}(\hat{\xi}')]$, the variations of $\hat{\theta}$ will

be mainly due to fluctuations in the imaginary part of ξ'. As a result, we can approximate

$$16\mathrm{E}[\Delta\tilde{\theta}^2] \approx \frac{\mathrm{E}\left[\mathbb{I}\mathrm{m}^2(\hat{\xi}')\right]}{\mathrm{E}^2\left[\mathbb{R}\mathrm{e}(\hat{\xi}')\right]}. \tag{43}$$

Being real valued, $\hat{\beta}$ does not alter the argument of $\hat{\xi}'_\gamma$. Moreover, on the grounds of consistency, it can be further assumed that $\hat{\beta} \approx \gamma$. Then

$$\begin{aligned}\mathbb{R}\mathrm{e}(\hat{\xi}') \approx & w\gamma\mathbb{R}\mathrm{e}^2\left(\hat{\xi}'_\gamma\right) \\ & + (1-w)\left\{\mathbb{R}\mathrm{e}^2\left(\hat{\xi}'_\eta\right) - \mathbb{I}\mathrm{m}^2\left(\hat{\xi}'_\eta\right)\right\} \qquad (44)\\ \mathbb{I}\mathrm{m}(\hat{\xi}') \approx & w\gamma\mathbb{I}\mathrm{m}^2\left(\hat{\xi}'_\gamma\right) \\ & + 2(1-w)\mathbb{R}\mathrm{e}\left(\hat{\xi}'_\eta\right)\mathbb{I}\mathrm{m}\left(\hat{\eta}'_\gamma\right) \qquad (45)\end{aligned}$$

with

$$\begin{aligned}\hat{\xi}'_\gamma = & \frac{1}{T}\sum_{k=1}^{T}\left(s_{1k}^4 - 6s_{1k}^2 s_{2k}^2 + s_{2k}^4\right) \\ & + j\frac{4}{T}\sum_{k=1}^{T}\left(s_{1k}^3 s_{2k} - s_{1k}s_{2k}^3\right) \qquad (46)\\ \hat{\xi}'_\eta = & \frac{1}{T}\sum_{k=1}^{T}\left(s_{1k}^4 - s_{2k}^4\right) + j\frac{2}{T}\sum_{k=1}^{T}\left(s_{1k}^3 s_{2k} + s_{1k}s_{2k}^3\right) \qquad (47)\end{aligned}$$

where, to ease the notation, we have written $s_{pk} = s_p(k)$, $p = 1, 2$. The denominator of (43) can be easily obtained by invoking the consistency of the real part of $\hat{\xi}'$ in (41). The calculation of the numerator is slightly more involved. From (45)–(47), we have (48) as shown at the bottom of the page. Taking into account the i.i.d. assumption, the most significant parts of terms A–C turn out to be

$$\begin{aligned}\mathrm{A} = & T\mathrm{E}\left[\left(s_1^3 s_2 - s_1 s_2^3\right)^2\right] \\ \mathrm{B} = & T(T-1)(T-2)\eta^2\mathrm{E}\left[\left(s_1^3 s_2 + s_1 s_2^3\right)^2\right] \\ \mathrm{C} = & T(T-1)\eta\mathrm{E}\left[\left(s_1^3 s_2 - s_1 s_2^3\right)\left(s_1^3 s_2 + s_1 s_2^3\right)\right]. \qquad (49)\end{aligned}$$

Gathering and rearranging terms, we arrive at

$$\begin{aligned}\mathrm{E}\left[\mathbb{I}\mathrm{m}^2(\hat{\xi}')\right] \xrightarrow[T\to\infty]{} & \frac{16}{T}\mathrm{E}\left\{\left[w\gamma\left(s_1^3 s_2 - s_1 s_2^3\right)\right.\right. \\ & \left.\left. + (1-w)\eta\left(s_1^3 s_2 + s_1 s_2^3\right)\right]^2\right\}. \qquad (50)\end{aligned}$$

Finally, the combination of (41), (43), and (50) yields the asymptotic MSE of the GWFOE shown in (19).

The derivation of w_{opt} is simplified with the substitutions $\tilde{\gamma} = \gamma(s_1^3 s_2 - s_1 s_2^3)$ and $\tilde{\eta} = \eta(s_1^3 s_2 + s_1 s_2^3)$, in which case $\mathrm{MSE}_{\mathrm{GWFOE}}$ can be written as

$$\mathrm{MSE}_{\mathrm{GWFOE}} = \frac{\mathrm{E}\left\{\left[w(\tilde{\gamma}-\tilde{\eta})+\tilde{\eta}\right]^2\right\}}{T\left[w(\gamma^2-\eta^2)+\eta^2\right]^2}. \tag{51}$$

This function of w becomes constant if $\gamma\eta = 0$, i.e., $|\kappa_{40}^s| = |\kappa_{04}^s|$. Performance then reduces to that of the EML (when $\eta = 0$) or AEML (when $\gamma = 0$) estimators for any w. Otherwise, in the interval of interest, $0 \leqslant w \leqslant 1$, we have that $w(\gamma^2-\eta^2)+\eta^2 \neq 0$. The derivative of (51) then cancels at

$$w_{\mathrm{opt}} = \frac{\mathrm{E}\left\{\tilde{\eta}(\gamma^2\tilde{\eta} - \eta^2\tilde{\gamma})\right\}}{\mathrm{E}\left\{\gamma^2\tilde{\eta}^2 + \eta^2\tilde{\gamma}^2 - (\gamma^2+\eta^2)\tilde{\gamma}\tilde{\eta}\right\}}. \tag{52}$$

Some tedious but straightforward algebraic simplifications then show that the above expression reduces to (20). In addition, it is simple to check that $\partial^2\mathrm{MSE}_{\mathrm{GWFOE}}/\partial w^2|_{w_{\mathrm{opt}}} > 0$, so that w_{opt} defines a minimum.

To conclude this asymptotic study, it is interesting to realize the connection between $\mathrm{MSE}[\hat{\theta}]$ and the ISR performance parameter (32). Assuming a unitary mixture in the two-signal case, the global transformation $\mathbf{C} = \mathbf{V}\mathbf{Q} = \hat{\mathbf{Q}}^{\mathrm{T}}\mathbf{Q}$ is a rotation of angle $(\theta - \hat{\theta})$. Any angle estimate of the form $(\hat{\theta} - \theta) = \Delta\tilde{\theta} + k\pi/2$, with small $\Delta\tilde{\theta}$ and integer k, provides a valid separation solution up to the inherent separation indeterminacies mentioned in Section II. This angle estimate produces $\mathrm{ISR} = \tan^2\Delta\tilde{\theta} \approx \Delta\tilde{\theta}^2$. As a result, in the vicinity of a valid separation solution, the average ISR approximates $\mathrm{MSE}[\hat{\theta}]$ without the potential bias introduced by the admissible $(k\pi/2)$-rad rotations.

$$\begin{aligned}\mathrm{E}\left[\mathbb{I}\mathrm{m}^2(\hat{\xi}')\right] = & \frac{16w^2\gamma^2}{T^2}\underbrace{\sum_i\sum_j \mathrm{E}\left[\left(s_{1i}^3 s_{2i} - s_{1i}s_{2i}^3\right)\left(s_{1j}^3 s_{2j} - s_{1j}s_{2j}^3\right)\right]}_{\mathrm{A}} \\ & + \frac{16(1-w)^2}{T^4}\underbrace{\sum_i\sum_j\sum_k\sum_l \mathrm{E}\left[\left(s_{1i}^4 - s_{2i}^4\right)\left(s_{1j}^4 - s_{2j}^4\right)\left(s_{1k}^3 s_{2k} + s_{1k}s_{2k}^3\right)\left(s_{1l}^3 s_{2l} + s_{1l}s_{2l}^3\right)\right]}_{\mathrm{B}} \\ & + \frac{32w(1-w)\gamma}{T^3}\underbrace{\sum_i\sum_j\sum_k \mathrm{E}\left[\left(s_{1i}^3 s_{2i} - s_{1i}s_{2i}^3\right)\left(s_{1j}^4 - s_{2j}^4\right)\left(s_{1k}^3 s_{2k} + s_{1k}s_{2k}^3\right)\right]}_{\mathrm{C}} \qquad (48)\end{aligned}$$

APPENDIX III
PROOF OF PROPOSITION 1

Expression (23) is a particular case of

$$\mu^y_{pqrs} = \sum_{ij} \mathbf{V}(p,i)\mathbf{V}(q,j) \sum_{kl} \mathbf{V}(r,k)\mathbf{V}(s,l)\mu^z_{ijkl}. \quad (53)$$

Let us denote $\mathbf{M}^z$ the $(r \times r), r = n(n+1)/2$, symmetric matrix containing the fourth-order moments $\{\mu^z_{ijkl}\}^n_{i,j,k,l=1}$. Moment μ^z_{ijkl} is stored in the entry $\mathbf{M}^z(a(i,j), a(k,l))$, where a is given by (22). In order to exploit the symmetry of the whitened-output moment tensor, only the moments with $i \leqslant j$ and $k \leqslant l$ are kept. The computation of (53) can be expressed as a quadratic form involving matrix $\mathbf{M}^z$ and a pair of column vectors related to matrix $\mathbf{V}$

$$\mu^y_{pqrs} = \mathbf{v}^{\mathrm{T}}_{pq} \mathbf{M}^z \mathbf{v}_{rs}. \quad (54)$$

To guarantee the equivalence between this quadratic form and (53), vectors $\mathbf{v}_{pq}$ and $\mathbf{v}_{rs}$ must be constructed by arranging the entries of $\mathbf{V}$ in accordance with the structure of $\mathbf{M}^z$

$$\mathbf{v}_{pq}\left(a(i,j)\right) = \begin{cases} \mathbf{V}(p,i)\mathbf{V}(q,j) + \mathbf{V}(p,j)\mathbf{V}(q,i), & i < j \\ \mathbf{V}(p,i)\mathbf{V}(q,i), & i = j \end{cases} \quad (55)$$

where indexes (i,j) and a are related through (22). □

ACKNOWLEDGMENT

V. Zarzoso wishes to thank P. Comon for his kind hospitality.

REFERENCES

[1] V. Zarzoso and A. K. Nandi, "Blind source separation," in *Blind Estimation Using Higher-Order Statistics*, A. K. Nandi, Ed. Boston, MA: Kluwer Academic, 1999, ch. 4, pp. 167–252.

[2] A. Hyvärinen, J. Karhunen, and E. Oja, *Independent Component Analysis*. New York: Wiley, 2001.

[3] A. Cichocki and S. Amari, *Adaptive Blind Signal and Image Processing*. Chichester, U.K.: Wiley, 2002.

[4] J. F. Cardoso and A. Souloumiac, "Blind beamforming for non-Gaussian signals," *Proc. Inst. Elect. Eng. F*, vol. 140, no. 6, pp. 362–370, Dec. 1993.

[5] J. F. Cardoso, "Blind signal separation: Statistical principles," *Proc. IEEE*, vol. 86, pp. 2009–2025, Oct. 1998.

[6] A. Caamaño-Fernandez, R. Boloix-Tortosa, J. Ramos, and J. J. Murillo-Fuentes, "Hybrid higher-order statistics learning in multiuser detection," *IEEE Trans. Syst., Man, Cybern. C, Appl. Rev.*, vol. 34, no. 4, pp. 417–424, Nov. 2004.

[7] S. Makeig, T.-P. Jung, D. Ghahremani, A. Bell, and T. Sejnowski, "Blind separation of auditory event-related brain responses into independent components," in *Proc. Nat. Acad. Sci.*, 1997, pp. 10979–10984.

[8] L. De Lathauwer, B. De Moor, and J. Vandewalle, "Fetal electrocardiogram extraction by blind source subspace separation," *IEEE Trans. Biomed. Eng. (Special Topic Section Advances in Statistical Signal Processing for Medicine)*, vol. 47, pp. 567–572, May 2000.

[9] V. Zarzoso and A. K. Nandi, "Noninvasive fetal electrocardiogram extraction: Blind separation versus adaptive noise cancellation," *IEEE Trans. Biomed. Eng.*, vol. 48, pp. 12–18, Jan. 2001.

[10] J. Murillo-Fuentes, H. Molina-Bulla, and F. González-Serrano, "Independent component analysis applied to digital image watermarking," in *Proc. ICASSP'01*, Salt Lake City, UT, May 2001, vol. III, pp. 1997–2000.

[11] T. Lee, M. Lewicki, and T. Sejnowski, "Unsupervised classification with non-Gaussian mixture models using ICA," in *Advances in Neural Information Processing Systems*. Cambridge, MA: MIT Press, 1999, vol. 11, pp. 58–64.

[12] P. Comon, "Independent component analysis, a new concept?," *Signal Process.*, vol. 36, no. 3, pp. 287–314, Apr. 1994.

[13] ——, "Separation of stochastic processes," in *Proc. Workshop Higher-Order Spectral Anal.*, Vail, CO, Jun. 28–30, 1989, pp. 174–179.

[14] V. Zarzoso, "Closed-form higher-order estimators for blind separation of independent source signals in instantaneous linear mixtures," Ph.D. dissertation, Univ. of Liverpool, Liverpool, U.K., Oct. 1999.

[15] V. Zarzoso and A. K. Nandi, "Unified formulation of closed-form estimators for blind source separation in real instantaneous linear mixtures," in *Proc. ICASSP'00*, Istanbul, Turkey, Jun. 5–9, 2000, vol. V, pp. 3160–3163.

[16] J. F. Cardoso and B. H. Laheld, "Equivariant adaptive source separation," *IEEE Trans. Signal Process.*, vol. 44, no. 12, pp. 3017–3030, Dec. 1996.

[17] F. Harroy and J.-L. Lacoume, "Maximum likelihood estimators and Cramer-Rao bounds in source separation," *Signal Process.*, vol. 55, no. 2, pp. 167–177, 1996.

[18] V. Zarzoso and A. K. Nandi, "Blind separation of independent sources for virtually any source probability density function," *IEEE Trans. Signal Process.*, vol. 47, no. 9, pp. 2419–2432, Sep. 1999.

[19] V. Zarzoso, A. K. Nandi, F. Herrmann, and J. Millet-Roig, "Combined estimation scheme for blind source separation with arbitrary source PDFs," *Electron. Lett.*, vol. 37, no. 2, pp. 132–133, Jan. 2001.

[20] E. Moreau and O. Macchi, "Higher order contrast for self-adaptive source separation," *Int. J. Adapt. Contr. Signal Process.*, vol. 10, no. 1, pp. 19–46, Jan 1996.

[21] P. Comon and E. Moreau, "Improved contrast dedicated to blind separation in communications," in *Proc. ICASSP'97*, Munich, Germany, 1997, vol. V, pp. 3453–3456.

[22] M. Ghogho, A. Swami, and T. Durrani, "Approximate maximum likelihood blind source separation with arbitrary source pdfs," in *Proc. SSAP'00*, Pocono Manor, PA, Aug. 14–16, 2000, pp. 368–372.

[23] M. Gaeta and J.-L. Lacoume, "Source separation without a priori knowledge: the maximum likelihood solution," in *Proc. EUSIPCO'90*, Barcelona, Spain, 1990, vol. V, pp. 621–624.

[24] F. Herrmann and A. Nandi, "Blind separation of linear instantaneous mixture using close forms estimators," *Signal Process.*, vol. 81, no. 7, pp. 1537–1556, Jul. 2001.

[25] J. J. Murillo-Fuentes and F. J. González-Serrano, "A sinusoidal contrast function for the blind separation of statistically independent sources," *IEEE Trans. Signal Process.*, vol. 52, pp. 3459–3463, Dec. 2004.

[26] T. Blaschke and L. Wiskott, "CuBICA: Independent component analysis by simultaneous third- and fourth-order cumulant diagonalization," *IEEE Trans. Signal Process.*, vol. 52, pp. 1250–1256, May 2004.

[27] G. H. Golub and C. F. Van Loan, *Matrix Computations*, 3rd ed. Baltimore, MD: Johns Hopkins Univ. Press, 1996.

[28] A. Bunse-Gerstner, R. Byers, and V. Mehrmann, "Numerical methods for simultaneous diagonalization," *SIAM J. Matrix Anal. Applicat.*, vol. 14, no. 4, pp. 927–949, 1993.

[29] P. Comon, "Remarques sur la diagonalisation tensorielle par la méthode de Jacobi," in *Proc. XIVème Colloque GRETSI*, Juan-les-Pins, France, Sep. 13–16, 1993, pp. 125–128.

[30] V. Zarzoso and A. K. Nandi, "Adaptive blind source separation for virtually any source probability density function," *IEEE Trans. Signal Process.*, vol. 48, pp. 477–488, Feb. 2000.

[31] I. J. Clarke, "Direct exploitation of non-Gaussianity as a discriminant," in *Proc. EUSIPCO'98*, Rhodes, Greece, Sept. 8–11, 1998, vol. IV, pp. 2057–2060.

[32] V. Zarzoso, F. Herrmann, and A. K. Nandi, "Weighted closed-form estimators for blind source separation," in *Proc. SSP-2001, 11th IEEE Workshop Statist. Signal Process.*, Singapore, Aug. 6–8, 2001, pp. 456–459.

[33] J. Murillo-Fuentes and F. González-Serrano, "Independent component analysis with sinusoidal fourth-order contrast," in *Proc. ICASSP'01*, Salt Lake City, UT, May 2001, vol. V, pp. 2785–2788.

[34] J. J. Murillo-Fuentes, R. Boloix-Tortosa, and F. J. González-Serrano, "Initialized Jacobi optimization in independent component analysis," in *Proc. ICA-2003 4th Int. Symp. Indep. Comp. Anal. Blind Signal Separat.*, Nara, Japan, Apr. 1–4, 2003.

[35] ——, "Adaptive initialized Jacobi optimization in independent component analysis," in *Proc. ICA-2003 4th Int. Symp. Indep. Comp. Anal. Blind Signal Separat.*, Nara, Japan, Apr. 1–4, 2003.

[36] J. J. Murillo-Fuentes, R. Boloix-Tortosa, S. Hornillo-Mellado, and V. Zarzoso, "Independent component analysis based on marginal entropy approximations," in *Proc. ISIAC'04 5th Int. Symp. Intell. Autom. Contr.*, Seville, Spain, Jun. 28–Jul. 1, 2004.

[37] A. Stuart and J. K. Ord, *Kendall's Advanced Theory of Statistics*, 6th ed. London, U.K.: Edward Arnold, 1994, vol. I.
[38] P. McCullagh, *Tensor Methods in Statistics*, ser. Monographs on Statistics and Applied Probability. London, U.K.: Chapman & Hall, 1987.
[39] F. J. Theis, "A new concept for separability problems in blind source separation," *Neural Comput.*, vol. 16, pp. 1827–1850, 2004.
[40] A. Yeredor, "Non-orthogonal joint diagonalization in the least-squares sense with application in blind source separation," *IEEE Trans. Signal Process.*, vol. 50, pp. 1545–1553, Jul. 2002.
[41] J. F. Cardoso, "High-order contrasts for independent component analysis," *Neural Comput.*, vol. 11, no. 1, pp. 157–192, Jan 1999.
[42] A. Benveniste, M. Métivier, and P. Priouret, *Adaptive Algorithms and Stochastic Approximations*. Berlin, Germany: Springer-Verlag, 1990.
[43] A. Hyvärinen, "Fast and robust fixed-point algorithms for independent component analysis," *IEEE Trans. Neural Netw.*, vol. 10, no. 3, pp. 626–634, 1999.
[44] X. Giannakopoulos, J. Karhunen, and E. Oja, "An experimental comparison of neural ICA algorithms," in *Proc. ICANN'98*, Skovde, Sweden, Sep 1998, pp. 651–656.
[45] J. Eriksson and V. Koivunen, "Characteristics-function based independent component analysis," *Signal Process.*, vol. 83, pp. 2195–2208, 2003.

Vicente Zarzoso (S'94–M'03) was born in Valencia, Spain, in 1973. He graduated (with highest distinction) in telecommunications engineering from the Universidad Politécnica de Valencia in 1996. The beginning of his Ph.D. studies were partly funded by a scholarship from the University of Strathclyde, Glasgow, U.K., and the Defence Evaluation and Research Agency (DERA) of the United Kingdom. He received the Ph.D. degree from the University of Liverpool, U.K., in 1999.

He spent five years with the University of Liverpool under a Research Fellowship from the Royal Academy of Engineering, U.K. Since September 2005, he has been a Lecturer with the Université de Nice - Sophia Antipolis and a Researcher with the Laboratoire d'Informatique, Signaux et Systèmes de Sophia Antipolis, France. His research interests include blind statistical signal and array processing and its application to biomedical problems and communications.

Juan José Murillo-Fuentes (M'99) was born in Sevilla, Spain, in 1973. He received the telecommunications engineering degree from the Universidad de Sevilla in 1996 and the Ph.D. degree in telecommunication engineering in 2001 from the Universidad Carlos III de Madrid, Spain.

He is currently an Associate Professor in the Department of Signal Theory and Communication, Universidad de Sevilla. His research interests lie in algorithm development for blind source separation and other signal-processing tools and their application to digital communications and image processing.

Rafael Boloix-Tortosa received the M.Eng. degree in telecommunications engineering and the Ph.D. degree from the Universidad de Sevilla, Spain, in 2000 and 2005, respectively.

He joined the School of Engineering there in 1999 as Research Assistant with the Department of Electronic Engineering. Currently, he is an Assistant Professor with the Department of Signal Theory and Communications. His research interests include blind source separation and higher order statistics and their application to digital communications.

Asoke K. Nandi (SM'96) received the Ph.D. degree from Trinity College, University of Cambridge, Cambridge, U.K., in 1979.

He held research positions with Rutherford Appleton Laboratory, U.K.; the European Organisation for Nuclear Research, Switzerland; the Department of Physics, Queen Mary College, London, U.K.; and the Department of Nuclear Physics, Oxford, U.K. In 1987, he joined Imperial College London as the Solartron Lecturer in the Signal Processing Section of the Electrical Engineering Department. In 1991, he jointed the Signal Processing Division of the Electronic and Electrical Engineering Department, University of Strathclyde, Glasgow, U.K., as a Senior Lecturer; subsequently, he became a Reader in 1995 and a Professor in 1998. In 1999, he joined the University of Liverpool, Liverpool, U.K., as the David Jardine Chair of Signal Processing in the Department of Electrical Engineering and Electronics. In 1983, he was a member of the UA1 team at CERN that discovered the three fundamental particles known as W^{+}, W^{-} and Z°, providing the evidence for the unification of the electromagnetic and weak forces, which was recognized by the Nobel Committee for Physics in 1984. Currently, he is Head of the Signal Processing and Communications Research Group, with interests in the areas of nonlinear systems, non-Gaussian signal processing, and communications research. With his group he has been carrying out research in blind source separation, blind deconvolution, machine condition monitoring, signal modelling, system identification, communication signal processing, time-delay estimation, biomedical signals, underwater sonar, and applications and development of machine learning. He has authored or coauthored more than 130 journal papers and more than 300 technical publications, including *Automatic Modulation Recognition of Communications Signals* (Boston, MA: Kluwer Academic, 1996) and *Blind Estimation Using Higher-Order Statistics* (Boston, MA: Kluwer Academic, 1999).

Prof. Nandi is a Fellow of the Cambridge Philosophical Society, the Institution of Engineering and Technology, U.K., the Institute of Mathematics and its Applications, the Institute of Physics, and the Royal Society of Arts. He received the Mounbatten Premium Division Award from the Electronics and Communications Division, the Institution of Electrical Engineers, in 1998 and the Water Arbitration Prize from the Institution of Mechanical Engineers, U.K., in 1999.

IEEE TRANSACTIONS ON SIGNAL PROCESSING, VOL. 53, NO. 11, NOVEMBER 2005 4363

Blind and Semi-Blind Equalization Based on the Constant Power Criterion

Vicente Zarzoso, *Member, IEEE,* and Pierre Comon, *Senior Member, IEEE*

***Abstract*—This paper focuses on the constant power (CP) criterion for blind linear equalization of digital communication channels. This recently proposed criterion is specially designed for the extraction of q-ary phase shift keying (q-PSK) signals using finite impulse response equalizers. When zero-forcing equalizers exist, the CP cost function accepts exact analytic solutions that are unaffected by undesired local extrema and spare costly iterative optimization. A subspace-based method exploiting the Toeplitz-like structure of the solution space is put forward to recover the minimum-length equalizer impulse response from the overestimated-length solutions. The proposed method is more robust to the relative weights of the minimum-length equalizer taps than existing techniques. In less ideal scenarios where the analytic solutions are only approximate minimizers of the criterion, a gradient-descent algorithm is proposed to minimize the cost function. To reduce the detrimental effects of suboptimal equilibria and accelerate convergence, the iterative algorithm is initialized with the approximate closed-form solution, and an optimal step size is incorporated into its updating rule. This optimal step size, which globally minimizes the cost function along the search direction, can be computed algebraically. A semi-blind implementation, which is useful when training data are available, further reduces the impact of undesired local extrema and enhances the convergence characteristics (particularly the robustness to the equalizer initialization) of the iterative algorithm from just a few pilot symbols. All these beneficial features are demonstrated with an experimental study of the proposed CP-based methods in a variety of channels and simulation conditions.**

***Index Terms*—Analytical constant power algorithm, blind equalization, closed-form solutions, iterative algorithms, optimal step size, semi-blind equalization, subspace methods, tensor algebra.**

I. Introduction

A. Background

In digital communications, transmission effects such as multipath propagation and limited bandwidth produce linear distortion in the emitted signal, causing intersymbol interference (ISI) at the receive sensor output. To enable the recovery of the input symbols, channel equalization aims to compensate these distorting effects [1]. Since the late 1970s, the drawbacks of training-based methods [1], [2] have aroused considerable research interest in the so-called *blind* equalization techniques, which spare the use of bandwidth-consuming pilot sequences and prove especially attractive in broadcast and noncooperative scenarios. In the fundamental single-input single-output (SISO) scenario, nonminimum phase (NMP) channels cannot be blindly identified using only second-order statistics (SOS); hence, the need for blind SISO equalizers to rely (explicitly or not) on higher-order statistics (HOS) [3]–[5]. Most blind methods are essentially property restoral techniques: The equalizer filter is updated to produce an output signal that recovers an *a priori* known property of the input signal, such as the finite alphabet or constant modulus of its data symbols.

The constant modulus (CM) criterion [4], [5]—which can be considered as a particular member of the more general family of Godard's methods [4]—is arguably the most widespread blind equalization principle. Although Godard's methods were proven to be globally convergent in the combined channel-equalizer parameter space, they were later shown to generally present suboptimal equilibria in the equalizer parameter space [6], [7]. Suboptimal equilibria are stable local extrema associated with filter tap settings that cannot sufficiently open the equalizer output signal eye pattern so that the detecting device is then unable to extract the transmitted symbols with a reasonably low probability of error.[1] This shortcoming renders the performance of gradient-based implementations of Godard's criterion very dependent on the initial value of the equalizer impulse response. As discussed in [6] and [7], the misconvergence problems of iterative blind SISO equalization methods calls for the design of suitable initialization schemes and, perhaps, additional strategies to keep the equalizer tap trajectories away from undesired local equilibria.

Analytic methods can be used as judicious initializations for iterative equalizers. A closed-form CM solution is obtained in [8], where the CM criterion is posed as a nonlinear least squares (LS) problem. Through an appropriate mapping of the equalizer parameter space, the nonlinear setting is transformed into a linear LS problem subject to a constraint on the solution structure. Recovering the right structure of the solution space is particularly important when multiple zero-forcing (ZF) solutions exist; for instance, in all-pole channels with overparameterized finite impulse response (FIR) equalizers, different ZF equalization delays are possible. From a matrix algebra perspective, imposing this structure can be considered as a matrix diagonalization problem, in which the matrix performing the diagonalization of the unstructured solution matrix is composed of

Manuscript submitted July 23, 2004; revised January 10, 2005. This work was supported by a Research Fellowship awarded to V. Zarzoso by the Royal Academy of Engineering of the U.K. The associate editor coordinating the review of this manuscript and approving it for publication was Dr. Markus Rupp.

V. Zarzoso was with the Department of Electrical Engineering and Electronics, The University of Liverpool, Liverpool L69 3GJ U.K. He is now with the Laboratoire I3S, Les Algorithmes, 06903 Sophia Antipolis, France (e-mail: zarzoso@i3s.unice.fr).

P. Comon is with the Laboratoire I3S, Les Algorithmes, 06903 Sophia Antipolis, France (e-mail: comon@i3s.unice.fr).

Digital Object Identifier 10.1109/TSP.2005.857051

[1]Suboptimal equilibria are sometimes referred to as spurious equilibria in the literature. However, as will be illustrated in Section VII, such solutions often lie near Wiener equalizers, which questions the appropriateness of the term "spurious."

the equalizers' tap vectors. After obtaining a nonstructured LS solution via pseudoinversion, the minimum-length equalizer is extracted by a subspace-based approach or two other simpler structuring procedures. Least mean squares (LMS) and recursive least squares (RLS) algorithms are also designed to solve the linear LS problem; hence, they still require structuring after convergence. Alternatively, the linearized LMS algorithm can be modified to partially impose the appropriate structure. However, the introduction of nonlinear constraints precludes the formulation of a closed-form solution.

The blind equalization method of [8] is strongly related to the analytical CM algorithm (ACMA) of [9] for blind source separation, which is a related but somewhat different problem. ACMA provides, in the noiseless case, exact closed-form solutions for the spatial filters that extract the source signals from their observed instantaneous linear mixtures. Interestingly, recovering the separating spatial filters from a basis of the solution space turns out to be tantamount to the joint diagonalization of the corresponding matrices. This joint diagonalization can be achieved through the generalized Schur decomposition [10] of several (more than two) matrices, for which convergence proof has yet to be found. Whether for source separation or for equalization, ACMA requires special modifications to handle input signals with a one-dimensional (i.e., binary) alphabet [8], [9], [11]. These modifications give rise to the so-called real ACMA (RACMA) method [11].

Multichannel (fractionally spaced) implementations are also able to avoid some of the deficiencies of SISO equalizers. In the first place, single-input multiple-output (SIMO) channels can be blindly identified using only SOS, regardless of their phase characteristics. In addition, FIR SIMO channels can be perfectly equalized, in the absence of noise, by FIR filters. Seminal methods are presented in [12]–[14]. Godard SIMO equalizers do not present suboptimal minima for noiseless channels satisfying length and zero conditions [15]. All minima are global and coincide with the minimum mean square error (MMSE) solutions associated with the attainable equalization delays. In the presence of noise, however, some of the minima become local, their respective equalizers providing different levels of MSE performance [16]. Depending on its performance, a local minimum may also become suboptimal. Hence, the need for techniques to avoid local extrema remains pertinent in the multichannel context. In certain practical scenarios, it may not be possible to achieve the degree of spatio-temporal diversity required by a SIMO formulation, due to lack of excess bandwidth or to hardware constraints limiting the number of receiving sensors (e.g., antennas in a mobile handset). This paper is mainly concerned with, but not restricted to, the basic SISO model.

B. Contribution and Outline

The present contribution studies a novel criterion for the blind equalization of digital channels excited by input signals with q-ary phase shift keying (q-PSK) modulations for arbitrary $q \geqslant 2$. The criterion can be considered as a modification on the original Godard's family of blind equalizers, with a power value q matched to the signal constellation, hence, the suitable name of *constant power (CP)* criterion. It is shown that if multiple ZF solutions exist—e.g., when the noiseless SISO channel follows a pure autoregressive (AR) model and the FIR equalizer filter is of sufficient length—the criterion accepts, much in ACMA's fashion, an exact solution that can be computed analytically, i.e., without iterative optimization. The minimum-length equalizer impulse response can then be obtained from a joint decomposition of qth-order tensors: the so-called rank-1 combination problem [17]. Since no effective tool has yet been developed for this task, an approximate solution is proposed in the form of a subspace-based method, which exploits the particular structure of the tensors associated with satisfactory equalization solutions. As opposed to [8], the subspace method proposed herein takes into account a whole basis of the solution space. This use of extra information is expected to increase the algorithm's robustness to the minimum-length equalizer structure. In addition, our closed-form blind equalization method naturally deals with binary inputs (e.g., BPSK, MSK) without further modification.

In additive noise or less ideal channel-equalizer conditions, the CP cost function can be minimized through a gradient-descent algorithm. The impact of undesired extrema are considerably reduced by initializing the algorithm with the approximate closed-form solution. In computationally limited systems, however, simple initializations may be preferred to more sophisticated, and thus more complex, alternatives. Whatever the option, the value of the step size (adaptation coefficient) that globally minimizes the cost function along the search direction can be computed analytically at each iteration. This optimal step size provides remarkable benefits in convergence speed and avoidance of local extrema, even with conventional (e.g., center-tap) initializations. The CP criterion is easily modified to operate in semi-blind mode, which is relevant in communication scenarios where training sequences are available. The optimal step size can also be algebraically computed in pilot-assisted operation. Using just a few pilot symbols, this semi-blind optimal step-size algorithm shows an outstanding robustness to the equalizer filter initialization.

The material is organized as follows. A brief explanation of the problem and the signal model is given in Section II. After presenting the CP criterion in Section III, its closed-form solutions are found in Section IV with the aid of a subspace-based algorithm for recovering the minimum-length equalizer. Iterative implementations are the focus of Section V, featuring the optimal step-size gradient-descent algorithm. Semi-blind solutions, in block and iterative operation, are put forward in Section VI. An experimental study is reported in Section VII. Finally, the summary and concluding remarks of Section VIII bring the paper to an end. For the sake of clarity, proofs and other mathematical derivations are postponed to the Appendix.

C. Notations

In the following, scalars, vectors, and tensors (of which matrices are assumed a particular case) will usually be denoted by plain lowercase (a), boldface lowercase $(\mathbf{a})$, and boldface uppercase $(\mathbf{A})$ symbols, respectively, the only exceptions being the structures derived from Kronecker tensorial products, as explained below. $\mathbf{I}_n$ refers to the $(n \times n)$ identity matrix, whereas $\mathbf{0}_n$ is the length-n zero vector; $(\cdot)^{\mathrm{T}}$, $(\cdot)^{\mathrm{H}}$, and $(\cdot)^{-1}$ indicate the transpose, Hermitian (conjugate-transpose), and inverse matrix operators, respectively; $\|\cdot\|$ is the conventional 2-norm.

$(\mathbf{A})_{i_1 i_2 \ldots i_q}$ denotes the entry located in position $(i_1, i_2, \ldots, i_q)$ of the qth-order tensor $\mathbf{A}$. $\mathbb{C}$ is the set of complex numbers; $\mathbb{R}\mathrm{e}(\cdot)$ and $\mathbb{I}\mathrm{m}(\cdot)$ denote the real and imaginary part, respectively, of their complex argument; $j = \sqrt{-1}$ is the imaginary unit. $\mathrm{E}\{\cdot\}$ represents the mathematical expectation. Symbol $*$ denotes the convolution operator, whereas $\circ$ and $\odot$ stand for the outer and elementwise products, respectively. Given a vector $\mathbf{a} \in \mathbb{C}^L$, we define its qth-order rank-1 Kronecker tensor product as $\mathbf{a}^{\circ q} = \underbrace{\mathbf{a} \circ \cdots \circ \mathbf{a}}_{q}$ (e.g., $\mathbf{a}^{\circ 2} = \mathbf{a} \circ \mathbf{a} = \mathbf{a}\mathbf{a}^{\mathrm{T}}$). A symmetric tensor $\mathbf{A}$ of order q and dimension L can be stored in a vector $\mathbf{vecs}\{\mathbf{A}\}$, which contains only the $L_q = \binom{L+q-1}{q}$ distinct entries of $\mathbf{A}$, scaled by the square root of the number of times they appear so that the Frobenius norm is preserved [17]. In particular, we denote $\mathbf{a}^{\oslash q} = \mathbf{vecs}\{\mathbf{a}^{\circ q}\}$. Similarly, given a vector $\mathbf{b}$ of dimension L_q, $\mathbf{unvecs}_q\{\mathbf{b}\}$ denotes the symmetric qth-order tensor constructed from its entries.

II. Problem Statement and Signal Model

The problem of channel equalization can simply be posed as follows. A digital signal $s(t) = \sum_n s_n \delta(t - nT)$ is transmitted at a known baud-rate $1/T$ through a time dispersive channel with impulse response $h(t)$. The channel is assumed linear and time-invariant (at least over the observation window) with a stable, causal, and possibly nonminimum phase transfer function. The continuous-time baseband signal at the receive sensor output is given by $x(t) = r(t) + n(t)$, where $r(t) = h(t) * s(t)$ denotes the noiseless observation and $v(t)$ the additive noise. Assuming perfect synchronization and carrier-residual elimination, baud-rate sampling produces the discrete-time output

$$x_n = r_n + v_n = \sum_k h_k s_{n-k} + v_n \tag{1}$$

in which $x_n = x(nT)$, and analogous definitions hold for h_k, s_n, and v_n. Each observed sample consists of a noisy linear mixture of the original data symbols, which is an undesired phenomenon known as intersymbol interference (ISI). Our goal is to recover the original data symbols from the received signal corrupted by ISI and noise. To this end, a baud-spaced linear equalizer with impulse response taps $\mathbf{f} = [f_1, \ldots, f_L]^{\mathrm{T}} \in \mathbb{C}^L$ is sought so that the equalizer output $y_n = \mathbf{f}^{\mathrm{H}} \mathbf{x}_n$ is a close estimate of the source symbols s_n, where $\mathbf{x}_n = [x_n, x_{n-1}, \ldots, x_{n-L+1}]^{\mathrm{T}}$.

In this paper, the data symbols are assumed to belong to a q-ary phase shift keying (q-PSK) constellation $\mathcal{A}_q = \{a_k\}_{k=0}^{q-1}$, with $a_k = a^k$, in which $a^q = d$ depends on the actual constellation; for instance, $(q, d) = (2,\ 1)$ for BPSK, and $(q, d) = (4, -1)$ for QPSK.[2] By allowing a time-varying d, the above definitions are readily extended to encompass other non-PSK modulations such as MSK [18], modeled with $(q, d_n) = (2, (-1)^n)$.

III. Blind Equalization Criterion for PSK Modulations

A. Constant Power Criterion

Since $s_n \in \mathcal{A}_q$, it follows that $s_n^q = d_n$. In particular, the qth power of input symbols drawn from a q-PSK constellation is constant. Thus, a somewhat natural cost function to measure the closeness of the equalizer output to the original data symbols is given by the *constant power (CP)* criterion

$$J_{\mathrm{CP}}(\mathbf{f}) = \mathrm{E}\left\{\left|y_n^q - d_n\right|^2\right\} = \mathrm{E}\left\{\left|(\mathbf{f}^{\mathrm{H}}\mathbf{x}_n)^q - d_n\right|^2\right\}. \tag{2}$$

Cost function (2) is a particular case of the more general class of alphabet polynomial fitting (APF) criteria, where the equalizer output constellation is matched to the source alphabet, characterized by the complex roots of a specific polynomial [19], [20]. In the context of blind source separation, criterion (2) is shown to be equivalent, for sufficiently low noise levels, to the maximum a posteriori (MAP) principle [21], [22]. In addition, it is proved in [19] that, when the total channel-equalizer impulse response is of finite length and the input signal sufficiently exciting, the global minima in the combined noiseless channel and equalizer parameter space of the sample estimate of criterion (2) correspond to ZF equalization solutions. However, this result does not assure that the desired solutions can always be reached or that undesired equilibria do not exist when the cost function is observed from the actual equalizer parameter space, as noted in [6] and [7] for Godard's criterion. The existence of suboptimal extrema in the CP criterion will be illustrated with a few simple experiments in Section VII.

B. Connections With Existing Criteria

CP functional (2) bears close resemblance to Godard's class of cost functions [4], which in the PSK case shows the general form

$$J_{\mathrm{G}}(\mathbf{f}) = \mathrm{E}\left\{\left(|y_n|^q - |s_n|^q\right)^2\right\} = \mathrm{E}\left\{\left(|\mathbf{f}^{\mathrm{H}}\mathbf{x}_n|^q - 1\right)^2\right\}. \tag{3}$$

For $q = 2$, the above function corresponds to the CM criterion [4], [5]. For BPSK sources and a real-valued channel and equalizer, the CP and CM criteria are identical; in such a case, we anticipate that the closed-form treatment of the CP minimization (Section IV) is equivalent to that of the specialized ACMA for binary modulations [8], [11]. This parallelism between the CM and CP cost function points to the existence of local extrema in the latter, even for $q > 2$.

The phase insensitivity of the CM criterion is one of its main advantages, as it allows the decoupled simultaneous operation of the equalization and carrier recovery stages [4], [5]. The CP criterion, in contrast, requires either a previous carrier-residual elimination or the incorporation of appropriate carrier-residual compensation mechanisms. However, all PSK constellations being CM, the CM principle is not discriminant over the set of PSK constellations. Similarly, it is not clear, at least at first glance, how the more general criterion (3) could privilege a particular PSK modulation. By contrast, criterion (2) explicitly takes into account the discrete nature of PSK-type alphabets so that it should exhibit enhanced discriminating properties among the CM constellations.

If d_n is substituted by the available pilot symbols s_n^{t} (where symbol t stands for "training"), the CP cost function (2) reduces, with $q = 1$, to the supervised MMSE equalization principle. This fact will be revisited when designing the semi-blind methods of Section VI.

[2] Defining the QPSK alphabet as $\mathcal{A}_4 = \{1, -1, j, -j\}$, we would have $(q,\ d) = (4,\ 1)$.

IV. Blind Closed-Form Solutions

When the channel accepts a noiseless AR model and the FIR equalizer is sufficiently long, perfect ZF SISO equalization is possible. In particular, the CP criterion (2) can be perfectly minimized (zeroed), and an exact global minimum can be computed in closed-form, that is, without iterative optimization. This analytic solution can be considered as an extension of the ACMA algorithm [9] to the CP principle. Consequently, the method may be called the *analytical constant power algorithm (ACPA)*.

A. Obtaining a Basis of the Solution Space

The perfect minimizers of (2) are given by the solutions to the set of equations:

$$(\mathbf{f}^{\mathrm{H}}\mathbf{x}_n)^q = d_n, \quad n = 0, 1, \ldots, N-1 \tag{4}$$

where $N = (N_d - L + 1)$, and N_d denotes the observation length in number of samples. This nonlinear system can be linearized by taking into account that $(\mathbf{f}^{\mathrm{H}}\mathbf{x}_n)^q = \mathbf{f}^{\otimes q\mathrm{H}}\mathbf{x}_n^{\otimes q}$ (see the Appendix) and can be compactly expressed as

$$\mathbf{X}^{q\mathrm{H}}\mathbf{w} = \mathbf{d} \tag{5}$$

where $\mathbf{X}^q = [\mathbf{x}_0^{\otimes q}, \mathbf{x}_1^{\otimes q}, \ldots, \mathbf{x}_{N-1}^{\otimes q}]$, and $\mathbf{d} = [d_0, d_1, \ldots, d_{N-1}]^{\mathrm{H}}$. Equation (5) is to be solved under the structural constraint that $\mathbf{w}$ be written as $\mathbf{w} = \mathbf{f}^{\otimes q}$ for certain $\mathbf{f} \in \mathbb{C}^L$ (see the Appendix).

Let us assume an all-pole channel with AR-model order of M. Such a channel can be equalized with a minimum-length FIR filter $\mathbf{f}_0$ composed of $L_0 = (M+1)$ taps. Assume the equalizer filter is overparameterized, that is, the equalizer length L has been overestimated, and $L \geqslant L_0$. Then, $P = (L - L_0 + 1)$ ZF solutions exist, each of them corresponding to a different equalization delay

$$\mathbf{f}_p = \left[\mathbf{0}_{p-1}^{\mathrm{T}},\, \mathbf{f}_0^{\mathrm{T}},\, \mathbf{0}_{P-p}^{\mathrm{T}}\right]^{\mathrm{T}}, \quad 1 \leqslant p \leqslant P. \tag{6}$$

Since there are P linearly independent solutions, the dimension of the null space of $\mathbf{X}^{q\mathrm{H}}$ is equal to $(P-1)$. Hence, the solutions to (5) can be written as an affine space of the form $\mathbf{w} = \mathbf{w}_0 + \sum_{p=1}^{P-1} \alpha_p \mathbf{w}_p$, where $\mathbf{w}_0$ is a particular solution to the nonhomogeneous system, and $\mathbf{w}_p \in \ker(\mathbf{X}^{q\mathrm{H}})$, $1 \leqslant p \leqslant (P-1)$.

As in [9], we find it more convenient to work in a fully linear subspace, which is obtained through a $(N \times N)$ unitary transformation $\mathbf{Q}$ such that $\mathbf{Q}\mathbf{d} = [\sqrt{N}, \mathbf{0}_{N-1}^{\mathrm{T}}]^{\mathrm{T}}$. For instance, $\mathbf{Q}$ can be a Householder transformation [10] or, if $\mathbf{d}$ is composed of N equal values, an N-point DFT matrix. Then

$$\mathbf{Q}\mathbf{X}^{q\mathrm{H}} = \begin{bmatrix} \mathbf{r}^{\mathrm{H}} \\ \mathbf{R} \end{bmatrix} \tag{7}$$

and system (5) reduces to

$$\begin{cases} \mathbf{r}^{\mathrm{H}}\mathbf{w} = \sqrt{N} \\ \mathbf{R}\mathbf{w} = \mathbf{0}_{N-1} \end{cases} \tag{8}$$

subject to the constraint $\mathbf{w} = \mathbf{f}^{\otimes q}$. Along the lines of [9, Lemma 4], it can be proved (Appendix A) that this problem is equivalent to solving

$$\begin{cases} \mathbf{R}\mathbf{w} = \mathbf{0}_{N-1} \\ \mathbf{w} = \mathbf{f}^{\otimes q} \end{cases} \tag{9}$$

and then scaling the solution to impose

$$\mathbf{c}^{\mathrm{H}}\mathbf{w} = 1, \quad \text{with} \quad \mathbf{c} = \frac{1}{\|\mathbf{d}\|^2} \sum_{n=0}^{N-1} d_n \mathbf{x}_n^{\otimes q} \tag{10}$$

or, equivalently

$$\frac{1}{\|\mathbf{d}\|^2} \sum_{n=0}^{N-1} d_n (\mathbf{f}^{\mathrm{H}}\mathbf{x}_n)^q = 1. \tag{11}$$

If $\dim \ker(\mathbf{X}^{q\mathrm{H}}) = (P-1)$ and

$$N_d \geqslant L_q + L_0 - 1 \tag{12}$$

(or $N > L_q - P$), then $\dim \ker(\mathbf{R}) = P$ (see the Appendix). Hence, all solutions to $\mathbf{R}\mathbf{w} = \mathbf{0}$ are linearly spanned by a basis $\{\mathbf{w}_k\}_{k=1}^P$ of $\ker(\mathbf{R})$. This basis can be computed from the singular value decomposition (SVD) of $\mathbf{R}$ by taking its P least significant right singular vectors. The structured solutions $\{\mathbf{f}_p^{\otimes q}\}_{p=1}^P$ are also a basis of the same subspace, and therefore, a set of scalars $\{\alpha_{pk}\}_{p,k=1}^P$ exists such that

$$\mathbf{f}_p^{\otimes q} = \sum_{k=1}^{P} \alpha_{pk} \mathbf{w}_k, \quad 1 \leqslant p \leqslant P \tag{13}$$

where matrix $(\mathbf{A})_{kp} = \alpha_{pk}$ is full rank. The problem of structuring the solution to the linearized system (5) consists of imposing the rank-1 symmetric Kronecker structure to the basis $\{\mathbf{w}_k\}_{k=1}^P$, which, in turn, yields $\{\mathbf{f}_p\}_{p=1}^P$. This is a particular subspace-fitting problem with structural constraints. In terms of qth-order tensors, (13) can be expressed as

$$\mathbf{f}_p^{\circ q} = \sum_{k=1}^{P} \alpha_{pk} \mathbf{W}_k, \quad 1 \leqslant p \leqslant P \tag{14}$$

where $\mathbf{W}_k = \mathbf{unvec}_q\{\mathbf{w}_k\}$. This is the rank-1 combination problem: Given the set $\{\mathbf{W}_k\}$, find the scalars producing tensors of rank one. The obtained rank-1 tensors will precisely correspond to $\{\mathbf{f}_p^{\circ q}\}$. Such a tensor decomposition is, in general, a notoriously nontrivial task (see, e.g., [17], [23], and references therein).

Before continuing, it is worth remarking that sample-size bound (12) is too restrictive. In practice, satisfactory closed-form equalization usually requires shorter observation windows, as will be demonstrated in the experiments of Section VII.

B. Solution Structuring: Subspace-Based Approach

A subspace-based method, reminiscent of [14], can be used to recover the minimum-length equalizer impulse response $\mathbf{f}_0$ from a basis of (generally) unstructured solutions $\{\mathbf{w}_k\}_{k=1}^P$. The subspace-fitting problem (13) can be compactly written as $\mathbf{W}\mathbf{A} = \mathbf{F}$, with $\mathbf{W} = [\mathbf{w}_1, \ldots, \mathbf{w}_P]$ and $\mathbf{F} = [\mathbf{f}_1^{\otimes q}, \ldots, \mathbf{f}_P^{\otimes q}]$. Since $\mathbf{A}$ is full rank, matrices $\mathbf{W}$ and $\mathbf{F}$ span the same column space: $\mathrm{range}(\mathbf{W}) = \mathrm{range}(\mathbf{F})$. In particular, $\forall \mathbf{u}_i \in \ker(\mathbf{W}^{\mathrm{H}})$, $\mathbf{u}_i^{\mathrm{H}}\mathbf{F} = \mathbf{0}_P^{\mathrm{T}}$. There are $\dim \ker(\mathbf{W}^{\mathrm{H}}) = (L_q - P)$ such linearly independent vectors.

Now, since equalization solutions are of the form (6), the corresponding columns of $\mathbf{F}$ have a particular structure whereby the elements not associated with the minimum-length equalizer $\mathbf{f}_0$ are all zero. The remaining $L_{0_q} = \binom{L_\circ + q - 1}{q}$ entries form $\mathbf{f}_0^{\otimes q}$. Denote by σ_p the set of L_{0_q} positions of $\mathbf{f}_0^{\otimes q}$ in $\mathbf{f}_p^{\otimes q}$,

that is, $\sigma_p = \{j_1 + L(j_2 - 1) + \cdots + L^{q-1}(j_q - 1)\}$, with $j_k \in [p, p+L_0-1]$, $k = 1, \ldots, q$, and $j_1 \geqslant j_2 \geqslant \ldots \geqslant j_q$. Accordingly, $(\mathbf{u}_i)_{\sigma_p} \in \mathbb{C}^{L_{0_q}}$ is the subvector composed of the elements of $\mathbf{u}_i$ in positions σ_p. Let $\mathbf{U}_i = [(\mathbf{u}_i)_{\sigma_1}, \ldots, (\mathbf{u}_i)_{\sigma_P}] \in \mathbb{C}^{L_{0_q} \times P}$. Hence

$$\mathbf{u}_i^{\mathrm{H}}\mathbf{F} = \mathbf{0}_P^{\mathrm{T}} \quad \Leftrightarrow \quad \mathbf{U}_i^{\mathrm{H}}\mathbf{f}_0^{\oslash q} = \mathbf{0}_P. \tag{15}$$

In total, the above equalities define a set of $P(L_q - P)$ linear equations, characterized by matrix $\mathbf{U} = [\mathbf{U}_1, \ldots, \mathbf{U}_{L_q - P}] \in \mathbb{C}^{L_{0_q} \times P(L_q - P)}$, on the entries of $\mathbf{f}_0^{\oslash q}$. As long as $L > L_0$, this linear system determines, up to a scale, the properly structured $\mathbf{f}_0^{\oslash q}$; its scale can later be set via (11) from a zero-padded version (any $\mathbf{f}_p$) of the estimated $\mathbf{f}_0$. In practice, we minimize the quadratic form $||\mathbf{U}^{\mathrm{H}}\mathbf{f}_0^{\oslash q}||^2 = \mathbf{f}_0^{\oslash q\mathrm{H}}\mathbf{U}\mathbf{U}^{\mathrm{H}}\mathbf{f}_0^{\oslash q}$ so that $\mathbf{f}_0^{\oslash q}$ can be estimated as the least significant left singular vector of matrix $\mathbf{U}$. Once matrix $\mathbf{F}$ has been reconstructed, an LS estimate of coefficients $\{\alpha_{kp}\}$ can be obtained as $\hat{\mathbf{A}}_{\mathrm{LS}} = (\mathbf{W}^{\mathrm{H}}\mathbf{W})^{-1}\mathbf{W}^{\mathrm{H}}\mathbf{F} = \mathbf{W}^{\dagger}\mathbf{F}$. These coefficients relate qth-order tensors $\{\mathbf{W}_k\}$ with their rank-1 symmetric tensor decomposition (14). Hence, the elements of $\hat{\mathbf{A}}_{\mathrm{LS}}$ solve the rank-1 combination problem.

To recover the equalizer impulse response $\mathbf{f}_0$ from its symmetric Kronecker vectorization $\mathbf{f}_0^{\oslash q}$, one can resort to the SVD of a matrix unfolding of $\mathbf{f}_0^{\circ q} = \mathbf{unvecs}_q\{\mathbf{f}_0^{\oslash q}\}$ [24], [25]. Let matrix $\mathbf{F}_0 \in \mathbb{C}^{L_0 \times L_0^{q-1}}$ such that

$$(\mathbf{F}_0)_{i_1, i_2 + L_0(i_3-1) + \ldots L_0^{q-2}(i_q - 1)} = (\mathbf{f}_0^{\circ q})_{i_1 i_2 i_3 \ldots i_q}.$$

Then, $\mathbf{F}_0 = \mathbf{f}_0\bar{\mathbf{f}}_0^{\mathrm{T}}$, with $(\bar{\mathbf{f}})_{i_2 + L_0(i_3-1) + \ldots L_0^{q-2}(i_q-1)} = (\mathbf{f}_0)_{i_2}(\mathbf{f}_0)_{i_3} \ldots (\mathbf{f}_0)_{i_q}$. Therefore, $\mathbf{f}_0$ can be estimated (up to a scale) as the dominant left singular vector of the rank-1 matrix unfolding $\mathbf{F}_0$. In the presence of noise, it will generally be impossible to express the estimated $\hat{\mathbf{f}}_0^{\oslash q}$ as the symmetric vectorization of a rank-1 tensor, that is, a vector $\mathbf{f}_0$ cannot be found such that $\hat{\mathbf{f}}_0^{\oslash q} = \mathbf{vecs}_q\{\mathbf{f}_0^{\circ q}\}$ holds exactly. As a result, the matrix unfolding will not be of rank one, and the above SVD-based procedure will yield inaccuracies that may ultimately limit the equalization performance. Results could be improved with more sophisticated methods for finding the best rank-1 approximation of symmetric tensor $\hat{\mathbf{f}}_0^{\circ q}$ [26].

C. Other Structuring Methods

In the context of the CM criterion, a similar subspace-based structuring method was proposed in [8, Sec. III.C], which operates on a single (LS) unstructured solution (see also [27]). Such structure-forcing procedure can be interpreted as the diagonalization of the matrix associated with the unstructured solution. By contrast, our approach takes advantage of a full basis of the solution subspace, which should lead to a subsequent increase in robustness, especially for large P. The method of [8, Sec. III.B] and [24] is based on the observation that the top L entries of a solution $\mathbf{w}_k$ are equal to $\tilde{\alpha}_{k1} f_1^{q-1}[f_1, \sqrt{q} f_2, \ldots, \sqrt{q} f_{L_\circ - 1}, \sqrt{q} f_{l_\circ}, \mathbf{0}_{P-1}^{\mathrm{T}}]^{\mathrm{T}}$, $\tilde{\alpha}_{kp} = (\mathbf{A}^{-1})_{pk}$ from which $\mathbf{f}_0$ can be extracted. This ingenious simple method is bound to be inaccurate when either the coefficient $\tilde{\alpha}_{k1}$ or the equalizer leading tap f_1 are small relative to the noise level.

To circumvent this drawback, one may notice that the L entries at the bottom of $\mathbf{w}_k$ are equal to $\tilde{\alpha}_{kP} f_{L_\circ^{q-1}}[\mathbf{0}_{P-1}^{\mathrm{T}}, \ldots, \sqrt{q} f_1, \sqrt{q} f_2, \ldots, \sqrt{q} f_{L_\circ - 1}, f_{L_\circ}]^{\mathrm{T}}$ [8, Sec. III.B]. This second option can provide, when properly combined with the estimate from the first L entries, an improved estimate of $\mathbf{f}_0$. In the experiments of Section VII, we use the following (still suboptimal) LS linear combination. Assume that the filter estimate from the top and bottom nonoverlapping entries of an unstructured solution are, respectively, $\hat{\mathbf{f}}_1 = \beta_1 \tilde{\mathbf{f}}_0$ and $\hat{\mathbf{f}}_2 = \beta_2 \tilde{\mathbf{f}}_0$, with $\tilde{\mathbf{f}}_0 = \mathbf{f}_0 / ||\mathbf{f}_0||$. Then, the unit-norm minimum-length equalizer LS estimate is given by $\hat{\tilde{\mathbf{f}}}_0 = [\hat{\mathbf{f}}_1, \hat{\mathbf{f}}_2]\boldsymbol{\gamma}$, with $\boldsymbol{\gamma} = \boldsymbol{\beta}^* / ||\boldsymbol{\beta}||^2$, $\boldsymbol{\beta} = [\beta_1, \beta_2]^{\mathrm{T}}$. The coefficients in $\boldsymbol{\beta}$ are simply estimated as $\beta_i = ||\hat{\mathbf{f}}_i||$, $i = 1, 2$. This kind of maximal-ratio combining (MRC) is reminiscent of the RAKE receiver and the matched filter [28]. Robustness can be further enhanced by exploiting a whole set $\{\mathbf{w}_k\}$ instead of just one solution.

D. Approximate Solution in the Presence of Noise

In the presence of additive noise at the receive sensor output, the exact solution to (4) may no longer exist. An approximate solution in the LS sense can be reached by minimizing $||\mathbf{X}^{q\mathrm{H}}\mathbf{W} - \mathbf{d}||^2$, always subject to the structural constraint $\mathbf{w} = \mathbf{f}^{\oslash q}$. This minimization generally requires an iterative method, as will be detailed in the next section.

Nevertheless, the guidelines to obtain the exact solution in the noiseless case may still provide a sound initialization for the iterative search. After applying transformation $\mathbf{Q}$, the LS problem turns out to be equivalent to the minimization of $|\mathbf{c}^{\mathrm{H}}\mathbf{w} - 1|^2 + ||\mathbf{R}\mathbf{w}||^2$. To find a basis of the (approximate) solution space, we look for a set of vectors that minimize $||\mathbf{R}\mathbf{w}||^2$ (e.g., the P least significant right singular vectors of $\mathbf{R}$), then structure them as in Section IV-B, and finally normalize the solution to fulfil $\mathbf{c}^{\mathrm{H}}\mathbf{w} = 1$ [see (10) and (11)].

V. Blind Iterative Solutions

A. Gradient-Based Algorithm

In practice, exact ZF equalization may not be feasible, due to the presence of noise, the existence of an FIR SISO channel, or just because the equalizer length is insufficient. In such cases, the CP cost function must be iteratively minimized, e.g., via a gradient-descent algorithm. The gradient of function (2) with respect to $\mathbf{f}$ is given by $\nabla J_{\mathrm{CP}}(\mathbf{f}) = \nabla_{\mathbb{R}\mathrm{e}(\mathbf{f})} J_{\mathrm{CP}}(\mathbf{f}) + j\nabla_{\mathbb{I}\mathrm{m}(\mathbf{f})} J_{\mathrm{CP}}(\mathbf{f})$ and can be expressed as

$$\nabla J_{\mathrm{CP}}(\mathbf{f}) = 2q\mathrm{E}\left\{(\mathbf{f}^{\mathrm{H}}\mathbf{x}_n)^{q-1}\left[(\mathbf{f}^{\mathrm{H}}\mathbf{x}_n)^q - d_n\right]^* \mathbf{x}_n\right\}. \tag{16}$$

We refer to the resulting iterative method as the *constant power algorithm (CPA)*. As a sensible initialization, one can use the equalizer vector provided by an ACPA method, such as the approximate structured solution described in Section IV-D or the (generally unstructured) direct LS solution to the linearized problem (5), $\hat{\mathbf{f}}_{\mathrm{LS}} = (\mathbf{X}^{q\mathrm{H}})^{\dagger}\mathbf{d}$. At each iteration, the equalizer vector is updated in the LMS fashion as

$$\mathbf{f}_{k+1} = \mathbf{f}_k - \mu \nabla J_{\mathrm{CP}}(\mathbf{f}_k), \quad k = 0, 1, \ldots. \tag{17}$$

The iterations are terminated when

$$\frac{||\mathbf{f}_{k+1} - \mathbf{f}_k||}{||\mathbf{f}_k||} < \frac{\eta}{N} \tag{18}$$

where η is a small positive constant.

We advocate the use of block (or "windowed") iterative implementations, as opposed to stochastic algorithms. The latter

methods approximate the gradient by using a one-sample estimate, which is tantamount to dropping the expectation operator. This simplification generally leads to a rather slow convergence and poor misadjustment. By contrast, the former methods approximate the gradient by its sample estimate from a block of channel output samples, repeatedly using the received data block at each iteration. This more precise gradient estimate improves convergence speed and accuracy [22], [29]. In addition, tracking capabilities are not necessarily sacrificed since good performance can be obtained from quite small block sizes; it suffices that the channel be stationary over the (short) observation window. Block methods are particularly suited to burst-mode transmission systems.

It is well known that gradient-based optimization algorithms, though simple, are plagued with a number of drawbacks, such as convergence to local extrema, lack of robustness to initialization, and slow convergence [6], [7], [16]. These problems persist in block implementations, although convergence is often faster. When the function to be optimized is quadratic in the unknowns, more elaborate approaches, such as conjugate-direction algorithms, alleviate these shortcomings [30]. However, the fact that function (2) is not quadratic leads us to seek alternative optimization strategies.

B. Closed-Form Steepest Descent

Steepest descent (or exact line search) methods look for the value of the step size that minimizes the cost function along the search direction:

$$\mu_{\text{opt}} = \arg\min_{\mu} J_{\text{CP}}(\mathbf{f} - \mu\mathbf{g}). \tag{19}$$

A sensible search direction is the gradient $\mathbf{g} = \nabla J_{\text{CP}}(\mathbf{f})$. These algorithms are generally unattractive due to their complexity, for the one-dimensional minimization must usually be performed using costly numerical methods. Another drawback is the orthogonality of consecutive gradient vectors, which, depending on the initialization and the shape of the cost-function surface, may slow down convergence [30].

However, it is observed in [19], [25], and [31] that the CP cost $J_{\text{CP}}(\mathbf{f} - \mu\mathbf{g})$ is a rational function in the step size μ, so that μ_{opt} can be found in closed form. This fact allows the *global* line minimization of the cost function while reducing complexity. In effect, μ_{opt} can be found among the roots of the $(2q-1)$th-degree polynomial $p(\mu) = \mathbb{R}\text{e}(\sum_{m=1}^{2q-1} b_m \mu^m)$, where

$$b_m = \begin{cases} \sum_{p=0}^{m}(m+1-p)\mathrm{E}\left\{a_{m+1-p}^* a_p\right\} \\ \quad -(m+1)\mathrm{E}\left\{a_{m+1}^* d_n\right\}, & 0 \leqslant m \leqslant q-1 \\ \sum_{p=m+1-q}^{q}(m+1-p) \\ \quad \times \mathrm{E}\left\{a_{m+1-p}^* a_p\right\}, & q \leqslant m \leqslant 2q-1 \end{cases} \tag{20}$$

with $\alpha_p = (-1)^p\binom{q}{p}(\mathbf{g}^{\text{H}}\mathbf{x}_n)^p(\mathbf{f}^{\text{H}}\mathbf{x}_n)^{q-p}$, $0 \leqslant p \leqslant q$ (see the Appendix). The cost function can then be evaluated at the candidate roots in order to find the global minimum along direction $\mathbf{g}$. Numerical conditioning is improved by normalizing vector $\mathbf{g}$ before evaluating (20) and updating the equalizer taps.

Although undesired equilibria (especially those lying near flat areas) are not avoided in all cases, our experiments indicate that this *optimal step-size CPA (OS-CPA)* converges much faster and more accurately than the CPA with a constant adaptation coefficient. In addition, the frequency of misconvergence to nonequalizing solutions is remarkably diminished. These benefits will be demonstrated in Section VII. An analogous optimal step-size algorithm for the CM criterion (OS-CMA) is developed in [32].

VI. Semi-Blind Equalization

A. Semi-Blind CP-Based Criterion

The previous sections have developed CP-based equalization algorithms in the fully blind case. However, practical communication systems typically feature pilot sequences to aid synchronization and channel equalization. For example, the second-generation GSM wireless system uses 26 out of the 148 bits in its data frame for training. Exploiting this available information can notably improve equalization performance. In order to take advantage of these benefits, the CP criterion can be easily modified to incorporate training symbols, resulting in a semi-blind equalization method. The minimization of the following hybrid cost function constitutes a semi-blind CP-MMSE criterion:

$$J_{\text{SB}}(\mathbf{f}) = \lambda J_{\text{MMSE}}(\mathbf{f}) + (1-\lambda)J_{\text{CP}}(\mathbf{f}) \tag{21}$$

where $J_{\text{MMSE}}(\mathbf{f}) = \mathrm{E}\{|y_n - s_{n-\tau}^{\text{t}}|^2\}$ is the pilot-based MMSE cost function, $\{s_n^{\text{t}}\}$ denote the available training symbols, and τ represents the equalization delay. Parameter λ is a real constant in the interval [0, 1], which can be considered as the relative degree of confidence between the blind- and the training-based parts of the criterion. By looking at expression (2), it turns out that J_{MMSE} can be derived from J_{CP} by setting $q = 1$ and substituting s_n^{t} for d_n. This equivalence will be useful in simplifying some of the following mathematical derivations. As in the blind scenario, closed-form and iterative solutions for this semi-blind CP-based criterion exist and are developed next.

B. Semi-Blind Closed-Form Solutions

Assume N_t training symbols are transmitted and are known to the receiver. We are looking for the simultaneous solution of the compound system

$$\mathbf{X}^{\text{H}}\mathbf{f} = \mathbf{s} \tag{22}$$

$$\mathbf{X}^{q\text{H}}\mathbf{w} = \mathbf{d} \tag{23}$$

subject to $\mathbf{w} = \mathbf{f}^{\oslash q}$, with $\mathbf{X} = [\mathbf{x}_0, \mathbf{x}_1, \ldots, \mathbf{x}_{N_t-1}]$, $\mathbf{X}^q = [\mathbf{x}_{N_t}^{\oslash q}, \mathbf{x}_{N_t+1}^{\oslash q}, \ldots, \mathbf{x}_{N-1}^{\oslash q}]$, $\mathbf{s} = [s_0, s_1, \ldots, s_{N_t-1}]^{\mathbf{H}}$, and $\mathbf{d} = [d_{N_t}, d_{N_t+1}, \ldots, d_{N-1}]^{\mathbf{H}}$.

First, let us consider the case of a possibly noisy AR-channel with a sufficiently long equalizer. An approximate suboptimal solution can be found by combining the solutions computed separately for both systems. Let $\hat{\mathbf{f}}_{\text{MMSE}}$ be the solution to (22), and $\hat{\mathbf{f}}_{\text{CP}}^{\oslash q}$ the same delay solution to (23), computed as in Section IV. Unfold $\mathbf{unvecs}_q\{\hat{\mathbf{f}}_{\text{CP}}^{\oslash q}\}$ into an $(L \times L^{q-1})$ matrix $\mathbf{F}_{\text{CP}}$, as described at the end of Section IV-B. Then, the joint solution to (22) and (23) can be approximated as the most significant left singular vector of matrix $\mathbf{F}_{\text{SB}} = [\lambda\hat{\mathbf{f}}_{\text{MMSE}}, (1-\lambda)\mathbf{F}_{\text{CP}}]$. In the noiseless case, solutions $\hat{\mathbf{f}}_{\text{MMSE}}$ and $\hat{\mathbf{f}}_{\text{CP}}$ are exact, identical, and equal to the dominant left singular vector of rank-1 matrix $\mathbf{F}_{\text{SB}}$; an iterative search is not necessary.

In the case of an FIR channel, no exact solution to (22) and (23) exists, even in the absence of noise. Still, the systems can be solved separately in the LS sense, and their respective solutions combined by the SVD-based procedure just described. The combined solution can initialize an iterative search aiming to refine the approximate closed-form result.

C. Semi-Blind Iterative Solutions

As in the fully blind case, cost function (21) can be iteratively minimized using a steepest-descent gradient-based algorithm in which the optimal step size can be algebraically computed at each iteration. The equalizer impulse response is updated as

$$\mathbf{f}_{k+1} = \mathbf{f}_k - \mu \nabla J_{\mathrm{SB}}(\mathbf{f}_k), \quad k = 0, 1, \ldots \tag{24}$$

where $\nabla J_{\mathrm{SB}}(\mathbf{f}) = \lambda \nabla J_{\mathrm{MMSE}}(\mathbf{f}) + (1-\lambda)\nabla J_{\mathrm{CP}}(\mathbf{f})$. Criterion (18) still remains valid for checking convergence. Due to the relationship between the CP and the MMSE cost functions, gradient ∇J_{MMSE} can readily be computed by setting $q = 1$ and substituting s_n^{t} for d_n in (16). By virtue of the same relationship, the step size that minimizes function J_{SB} along direction $\mathbf{g} = \nabla J_{\mathrm{SB}}(\mathbf{f})$ can be found among the roots of the composite polynomial $\mathbb{R}\mathrm{e}\,(\lambda p_{\mathrm{MMSE}}(\mu) + (1-\lambda) p_{\mathrm{CP}}(\mu))$, where p_{CP} and p_{MMSE} are obtained as in (20) from the appropriate values of q and d_n. Note that for $\lambda = 1$, the above iterative procedure reduces to the algebraic optimal step-size version of the well-known LMS algorithm for supervised MMSE equalization.

VII. Experimental Results

This section reports some computer simulations to evaluate the performance of the CP-based methods elaborated in this paper.

Blind ACPA solutions. The first experiment compares the performance of the closed-form blind equalization methods of Section IV. The methods compared are the unstructured direct LS solution to (5) ("LS, no struct"); the structuring method of [24] from the top nonoverlapping sections of the LS solution ("LS, top"); *idem*, from the bottom sections ("LS, bottom"); the MRC of the top and bottom parts as explained in Section IV-C ("LS, top+bottom"); *idem*, from the whole basis of solutions ("basis, top+bottom"); and the subspace method of Section IV-B ("basis, subspace"). After estimating the symmetric Kronecker vectorizations, the respective equalizer vectors are obtained through the SVD-based rank-1 tensor approximation described at the end of Section IV-B. The performance of the supervised MMSE receiver is also computed as a reference. In the first simulation setup, a QPSK signal $(q = 4)$ excites a simple AR-1 channel

$$H_1(z) = \frac{1}{1 - 0.5 z^{-1}}, \quad |z| > 0.5 \tag{25}$$

with pole at $\rho = 0.5$, well approximated by an order-50 FIR truncation. ISI is perfectly removed by the equalizer $\mathbf{f}_0 = [1, -0.5]^{\mathrm{T}}$, which presents a dominant leading tap. The equalizer minimum length is $L_0 = 2$, but an overestimated length of $L = 5$ is chosen, yielding $P = 4$ possible ZF solutions, which are just delayed versions of each other [as in (6)]. Additive white complex circular Gaussian noise is present at the channel output, with signal-to-noise ratio (SNR) given by $\mathrm{E}\{|r|^2\}/\mathrm{E}\{|v|^2\}$. Blocks of $N_d = 100$ symbol periods are observed, and performance parameters are averaged over ν independent Monte Carlo (MC) runs, with $\nu N_d \geqslant 10^5$. Fig. 1 plots the symbol error rate (SER) obtained by the different analytic methods as a function of the SNR. The performance of direct LS solution makes apparent the need for structuring. Using the bottom part of the LS solution exhibits similarly poor results, with a rather low noise tolerance. By contrast, the other methods present a superior performance, just 2 to 3 dB above the MMSE bound. Interestingly, taking the top part of the LS solution proves best for moderate SNR values in this scenario. This superiority depends, however, on the equalizer tap configuration, as demonstrated in the next example.

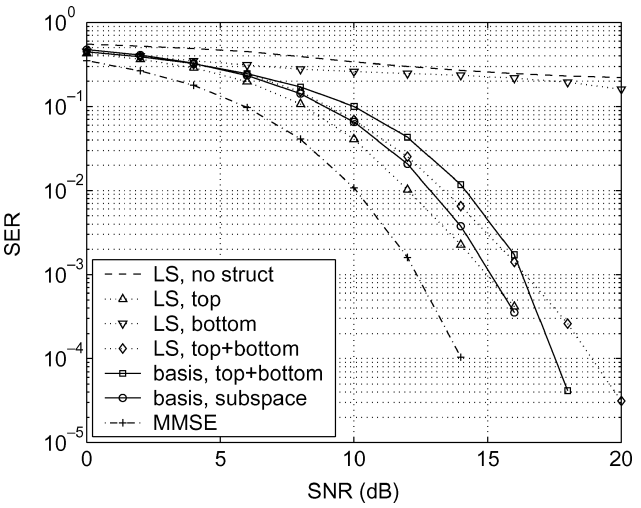

Fig. 1. Closed-form blind equalization based on the CP criterion for several structuring methods. Channel $H_1(z)$, QPSK input $(q = 4)$, $N_d = 100$ symbol periods, 1000 MC runs.

We repeat the above experiment, but moving the AR channel pole to $\rho = 2$, and taking a stable causal implementation of the channel transfer function

$$H_2(z) = \frac{1}{1 - 2 z^{-1}}, \quad |z| < 2 \tag{26}$$

by shifting the truncated impulse response. The minimum-length equalizer now becomes $\mathbf{f}_0 = [1, -2]^{\mathrm{T}}$, with dominant trailing tap. Fig. 2 shows the closed-form blind equalization results. The performance of the LS-top method considerably degrades, being very similar to that of the LS-bottom method in the previous experiment. The performance of the subspace structuring method remains almost the same as in the simulation of Fig. 1, thus showing its robustness to the relative weights of the equalizer coefficients.

Fig. 3 evaluates the sample size requirements of the closed-form solutions under the general conditions of the first experiment and SNR $= 15$ dB. Satisfactory equalization from a basis of the solution space is achieved even below the limit imposed by (12) for this simulation example, $N_d \geqslant 71$. The subspace approach provides the most efficient results for short observation windows.

CPA Solutions—Basins of Attraction. The next experiments assess the CP-based iterative methods, both in blind (Section V) and semi-blind (Section VI-C) operation. We observe a burst of $N_d = 200$ symbols with SNR $= 10$ dB at the output of channel $H_1(z)$ excited by a BPSK input. The contour lines (in the equalizer parameter space) of the logarithm of the blind CP criterion (2) calculated from the data are plotted in Fig. 4(a).

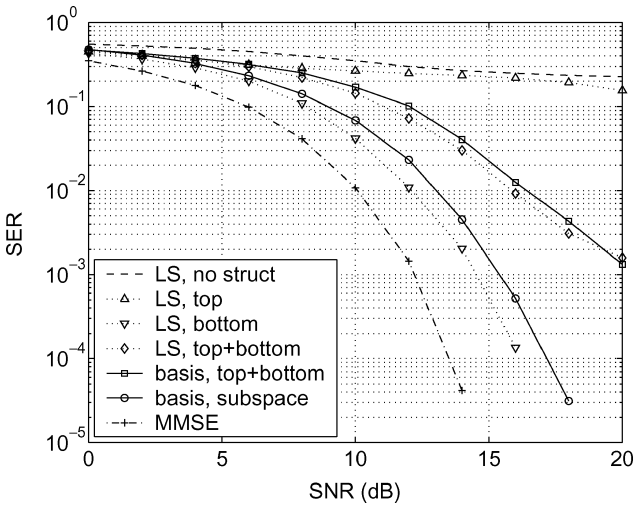

Fig. 2. Closed-form blind equalization based on the CP criterion for several structuring methods. Channel $H_2(z)$, QPSK input ($q = 4$), $N_d = 100$ symbol periods, 1000 MC runs.

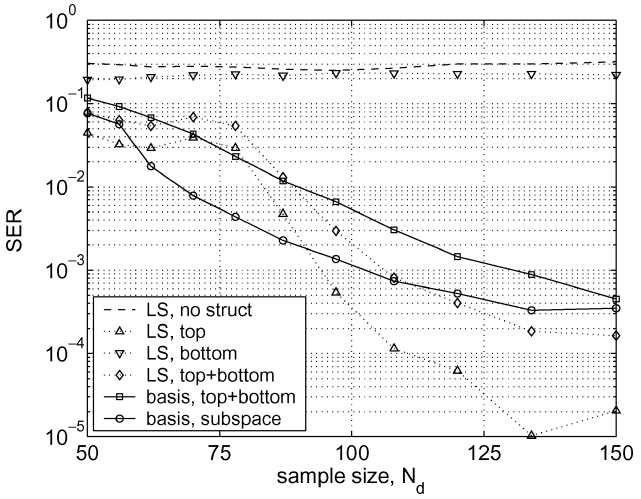

Fig. 3. Closed-form blind equalization based on the CP criterion for several structuring methods. Channel $H_1(z)$, QPSK input ($q = 4$), SNR = 15 dB, ν MC runs, with $\nu N_d \geqslant 10^5$.

The solid lines display the trajectories of the equalizer taps updated with the CPA (17), from 16 different initial configurations (marked with "+") and $\eta = 10^{-5}$ in termination criterion (18); convergence points are marked with "×." A step size $\mu = 10^{-2}$ was chosen for fastest convergence without compromising stability. The plot also represents the delay-zero and delay-one MMSE solutions $\mathbf{f}_{\mathrm{MMSE},0} = [0.85, -0.38]^{\mathrm{T}}$ and $\mathbf{f}_{\mathrm{MMSE},1} = [0, 0.70]^{\mathrm{T}}$, which provide an output MSE of -8.66 and -4.98 dB, respectively. From most of the initial points, the algorithm converges to the desired solutions, close to the optimal-delay MMSE equalizer. However, the algorithm gets sometimes stuck at suboptimal stable extrema located at $\pm$[0.01,0.58], near the suboptimal-delay MMSE equalizer. The basins of attraction of these undesired equilibria are not negligible and may have a significant negative impact on equalization performance. The suboptimal convergence points of the CPA correspond to the theoretical values obtained in [6, Sec. III.D] for the CM criterion $\pm$[0,0.65]. Indeed, as already pointed out

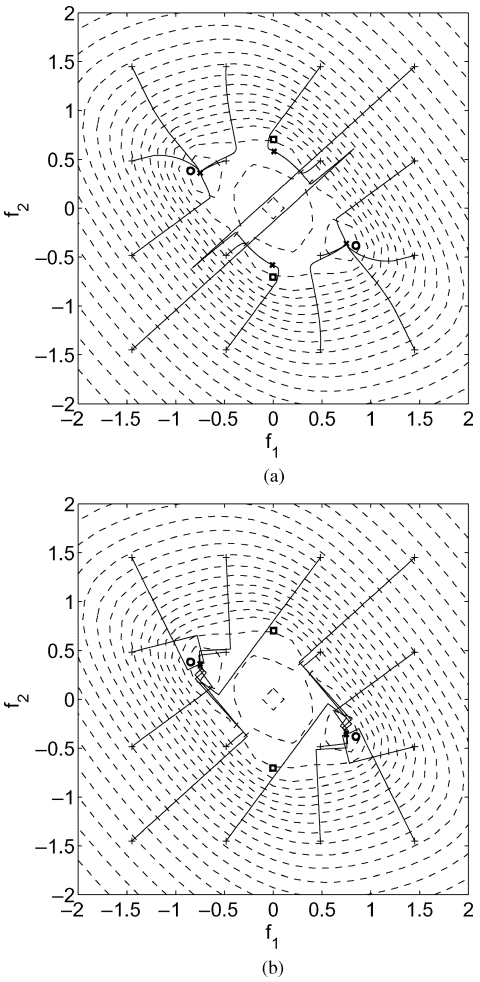

Fig. 4. Blind CP cost function contour lines (dashed) and CPA equalizer tap trajectories (solid lines). (a) Constant step size. (b) Optimal step size. Channel $H_1(z)$, BPSK input ($q = 2$), $N_d = 200$ symbol periods, SNR = 10 dB. "+": initial point; "×": final point; "∘": optimal-delay MMSE solution; "□": suboptimal-delay MMSE solution.

TABLE I
AVERAGE NUMBER OF ITERATIONS FOR CONVERGENCE IN THE EXPERIMENTS OF FIGS. 4 AND 5

Step size	Blind	Semi-blind
constant	422	363
optimal	11	9

in Section III-B, the CM and CP criteria coincide for $q = 2$ and real-valued source and filters. The CPA requires, on average, about 500 iterations to converge (Table I).

Under identical conditions and the same observed data, the tap trajectories for the OS-CPA (Section V-B) are obtained as in Fig. 4(b). Not only are undesired solutions avoided, but convergence is notably accelerated relative to the previous case: Just over ten iterations suffice (Table I).

Using $N_t = 10$ pilot symbols and a confidence parameter $\lambda = 0.5$, the contour lines of the semi-blind CP criterion (21) follow the shape displayed in Fig. 5(a). The introduction of training data alters the CP cost function by emphasizing the minimum near the MMSE solution while naturally vanishing the previously acceptable equilibrium across the origin. The use of

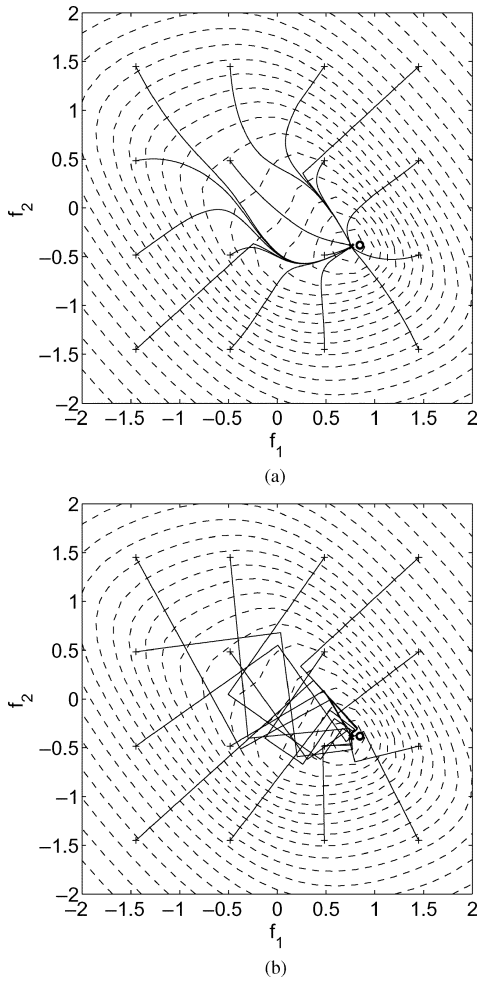

Fig. 5. Semi-blind CP cost function contour lines (dashed) and CPA equalizer tap trajectories (solid line). (a) Constant step size,. (b) Optimal step size. Channel $H_1(z)$, BPSK input ($q = 2$), $N_d = 200$ symbol periods, $N_t = 10$ pilot symbols, SNR $= 10$ dB, $\lambda = 0.5$. "+": initial point; "×": final point; "o": optimum-delay MMSE solution.

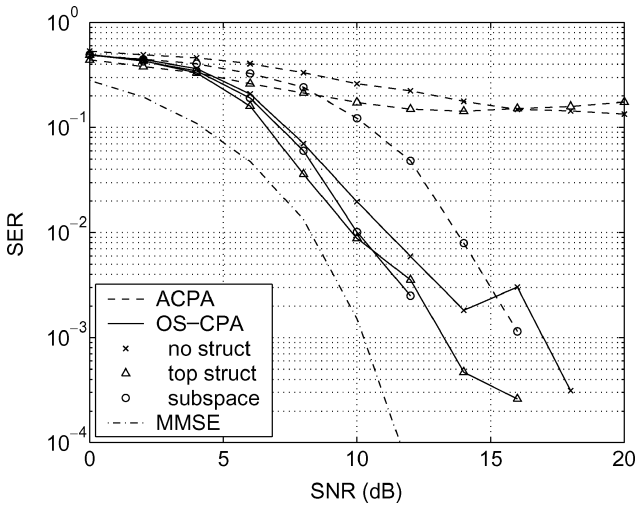

Fig. 6. Blind CP equalization. The OS-CPA is initialized with the corresponding ACPA solution. Channel $H_3(z)$, QPSK input ($q = 4$), $N_d = 100$ symbol periods, 200 MC runs.

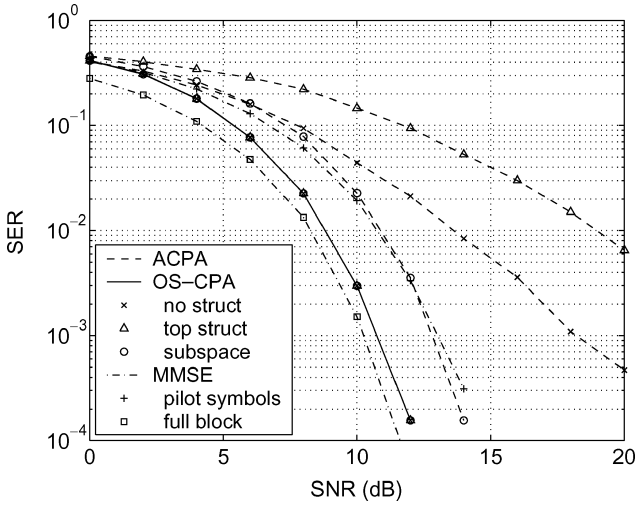

Fig. 7. Semi-blind CP equalization in the simulation of Fig. 6 with $N_t = 10$ pilot symbols and $\lambda = 0.5$. The OS-CPA is initialized with the corresponding ACPA solution.

the optimal step size (Section VI-C) still leads to good equalization solutions [see Fig. 5(b)] and, again, remarkably speeds up convergence (Table I).

Nonminimum Phase Channel. We now evaluate performance on the nonminimum phase channel of [8], which is given by

$$\begin{aligned} H_3(z) = &(-0.033 + 0.014j) + (0.085 - 0.039j)z^{-1} \\ &- (0.232 - 0.136j)z^{-2} + (0.634 - 0.445j)z^{-3} \\ &+ (0.070 - 0.233j)z^{-4} - (0.027 + 0.071j)z^{-5} \\ &- (0.023 + 0.012j)z^{-6}. \end{aligned} \tag{27}$$

This order-6 FIR channel can be well equalized with a length-3 FIR filter ($L_0 = 3$), but we choose $L = 5$. From a data block of $N_d = 100$ symbols and using several structuring procedures, the blind closed-form CP methods display the SER performance shown in the dashed lines of Fig. 6. The closed-form solutions are then used to initialize the OS-CPA described in Section V-B, yielding the solid curves in Fig. 6. The gradient iterations refine the analytical estimates, approaching the MMSE bound.

The performance of the semi-blind CP methods is summarized in Fig. 7 for the same simulation setting with $N_t = 10$ pilot symbols and $\lambda = 0.5$. Analytical estimates are first obtained by combining the blind and pilot-based solutions as in Section VI-B (dashed lines) and then used to initialize the semi-blind OS-CPA of Section VI-C (solid lines). Depending on the window length employed to calculate the MMSE solution, two MMSE curves are obtained as a reference (dash-dotted lines): using just the pilot sequence, as would occur in a conventional receiver, and using the whole data block (MMSE bound). The benefits of the semi-blind approach are noteworthy. First, the performance of the analytic solutions is considerably enhanced compared with blind operation. Second, the semi-blind OS-CPA shows identical performance irrespective of initialization, following quite closely the MMSE bound. The exploitation of "blind symbols" in addition to the training period improves the conventional receiver, and nearly reaches the MMSE bound while considerably increasing the effective data throughput. In addition, the convergence rate is improved

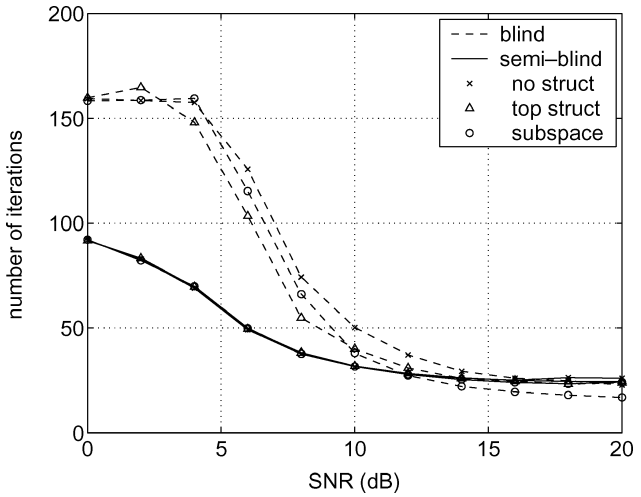

Fig. 8. Average number of iterations for the three initializations of the OS-CPA in the experiments of Figs. 6 and 7.

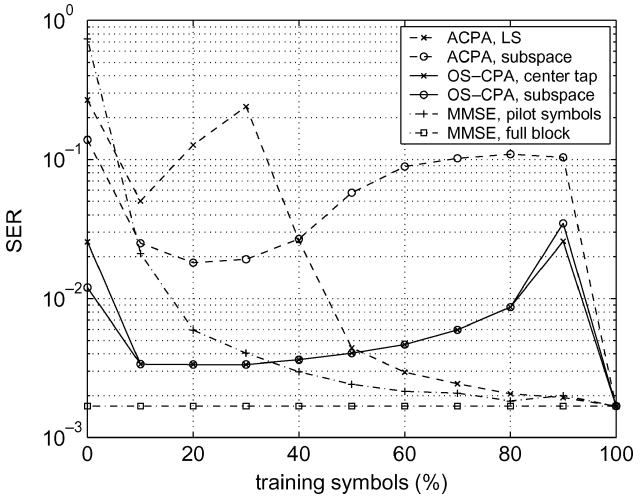

Fig. 9. Impact of the training window length on the performance of the semi-blind CP methods. Channel $H_3(z)$, QPSK input ($q = 4$), $N_d = 100$ symbol periods, SNR $= 10$ dB, $\lambda = 0.5$, 500 MC runs.

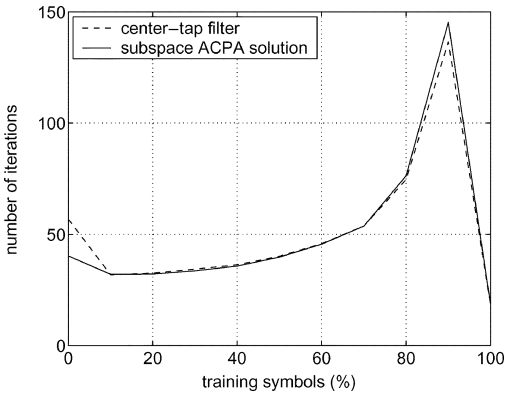

Fig. 10. Average number of iterations for the two initializations of the OS-CPA in the experiment of Fig. 9.

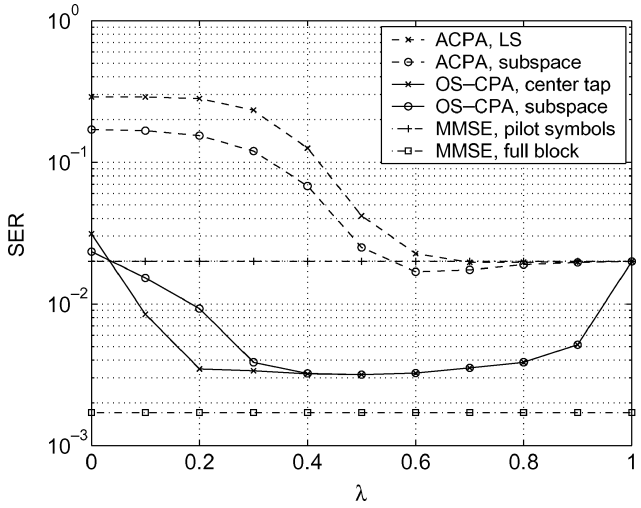

Fig. 11. Impact of confidence parameter λ on the performance of the semi-blind CP methods. Channel $H_3(z)$, QPSK input ($q = 4$), $N_d = 100$ symbol periods, $N_t = 10$ pilot symbols, SNR $= 10$ dB, 500 MC runs.

relative to the fully-blind case, particularly at low SNR, as depicted in Fig. 8.

Influence of Pilot-Sequence Length. Next, we evaluate the CP criterion performance as a function of the proportion of data block symbols used for training. In the previous scenario ($\lambda = 0.5$), two blind ACPA methods are combined with the MMSE solution to generate respective closed-form estimates: the direct LS solution (without structuring) and the subspace-based structuring procedure from a basis of solutions. The OS-CPA is initialized with the center-tap filter and the analytical subspace-based estimate. Results are displayed in Figs. 9 and 10. The MMSE term does not seem to offset the performance degradation of the subspace-based structuring as less data are considered in the blind part of the criterion [cf. (12)]. As a result, the semi-blind method is gradually diverted from a satisfactory equalization solution, reverting to the MMSE bound when all symbols are used for training. Similarly, a peak in SER and convergence time is shown by the iterative methods at around 90% of training, as if the few symbols in the blind part of the criterion hindered the convergence to the MMSE solution imposed by the pilot symbols. Nevertheless, both performance indices naturally drop to the MMSE limit when the whole observed block is employed for training. The performance and convergence speed of the semi-blind OS-CPA seem independent of initialization, although the subspace approach slightly improves the center-tap initial filter for short training sequences. Note that the performance of a given conventional receiver with up to 30% of pilot symbols can be attained by operating in semi-blind mode with a shorter training preamble and, hence, a higher spectral efficiency.

Influence of Parameter λ. The performance of the semi-blind CP methods as a function of confidence parameter λ is illustrated in Figs. 11 and 12, obtained in the above scenario with $N_t = 10$ pilot symbols. Equalization results gradually improve as more weight is laid on the known data. Performance then suffers as the blind part of the criterion is neglected and equalization relies on just a few pilot symbols; thus, we observe an increase in SER up to the conventional MMSE receiver level as λ approaches one. Accordingly, this severe increase is not observed in larger training windows. Over a wide range of λ

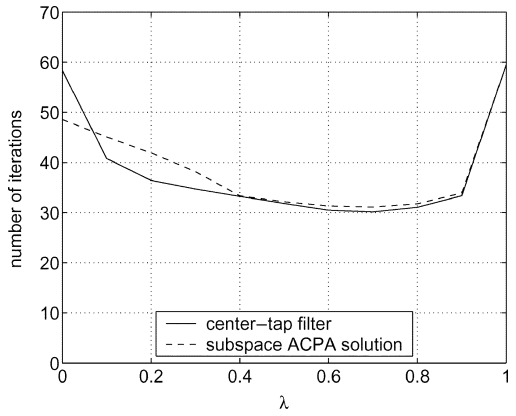

Fig. 12. Average number of iterations for the two initializations of the OS-CPA in the experiment of Fig. 11.

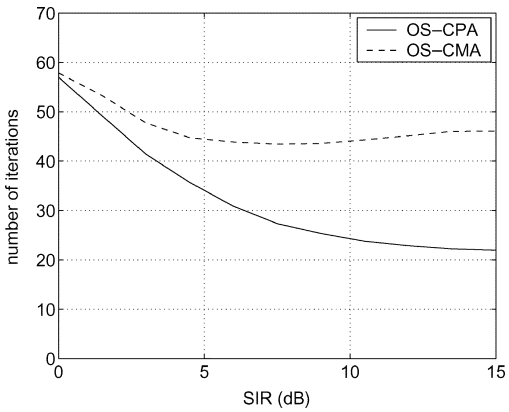

Fig. 14. Average number of iterations in the experiment of Fig. 13.

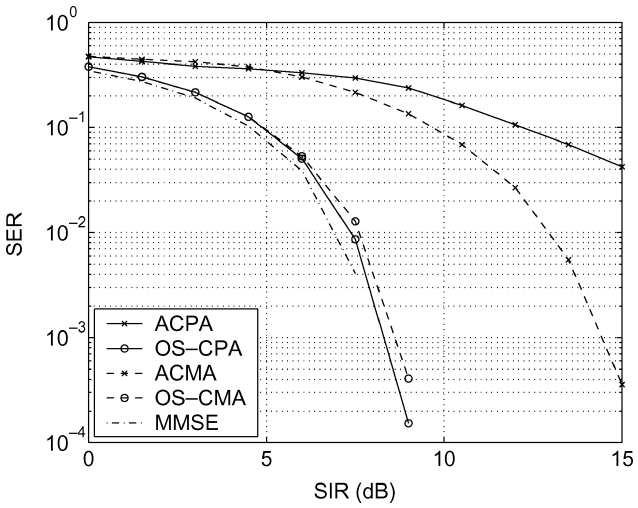

Fig. 13. Semi-blind equalization with the CP and CM criteria. The analytic solutions are obtained using the top structuring method. Channel $H_3(z)$, QPSK input ($q = 4$), QPSK co-channel interferer, $N_d = 200$ symbol periods, $N_t = 20$ pilot symbols, 100 MC runs.

(roughly in the interval [0.3,0.9]), the influence of initialization on the performance and convergence speed of the semi-blind OS-CPA seems unimportant, and for practically any $\lambda \in]0,\ 1[$, the semi-blind iterative methods improve the conventional equalizer. Fig. 12 also shows that a value of the confidence parameter exists ($\lambda \approx 0.7$), for which the cost-function surface is best adapted to the operation of the optimal step-size gradient-descent algorithm; therefore, convergence is achieved in the lowest number of iterations. This optimal value of λ will generally depend on the specific system conditions, sample size, and SNR.

Comparison with CM Criterion. A final experiment makes an brief illustrative comparison between the CP and CM criteria in semi-blind operation (10% training). A co-channel interferer with the same modulation as the desired signal (QPSK) and a given signal-to-interference ratio (SIR) is added at the output of channel $H_3(z)$. The respective top-structuring analytic solutions are first obtained and then used as initial points for the optimal-step size iterations. Figs. 13 and 14 show that although the ACPA solution is poorer than ACMAs in this particular scenario, the OS-CPA improves its CM counterpart with half the number of iterations.

VIII. Summary and Conclusions

The present work has focused on the CP criterion for blind linear equalization of digital communication channels excited by PSK signals. When exact FIR ZF solutions exist (as in all-pole SISO channels), the global minima can be reached in closed form. These noniterative solutions are unaffected by the existence of nonequalizing local extrema in the cost-function surface. Through an appropriate transformation, the nonlinear criterion can be linearized; then, the structure of the solution must be restored. The algebraic treatment is similar to ACMA's, but the analytic solutions to the CP criterion (ACPA) do not need to be specialized to handle binary modulations. Obtaining a basis of the solution space allows the design of more refined structure-forcing methods to recover the minimum-length equalizer from the solutions to the linearized problem. In simulations, the proposed subspace-based approach has effectively proven to be more robust than simpler structuring methods. Algebraically, the subspace method solves a particular instance of the rank-1 tensor combination problem. In simulations, the blind analytic solutions show a restricted tolerance to noise, especially for long equalizers. The key issue limiting performance is probably the SVD-based rank-1 tensor approximation procedure described in Sections IV-B and VI-B for extracting the equalizer vector from the estimated symmetric tensor. The use of more elaborate rank-1 tensor approximation methods (such as those of [26] and references therein) should relieve this limitation.

When the algebraic solution is only an approximation (e.g., when no exact FIR ZF equalizer exists) or when it is too costly to compute, iterative techniques are necessary to seek the global minima of the criterion; an iterative method can also be used to refine a good algebraic guess. An exact line search gradient-descent block algorithm has been proposed in which the optimal step size is computed algebraically at each iteration. This algorithm (OS-CPA) shows a very fast convergence and is able to avoid local extrema.

The CP criterion is easily modified to include training information. Indeed, the conventional supervised MMSE principle

can be seen as a special case of CP equalization. With just a few pilot symbols, the analytic solutions' noise tolerance is ameliorated. The semi-blind OS-CPA performs near the MMSE bound at a fraction of the bandwidth cost and is very robust to the equalizer-filter initialization.

In short, the CP criterion has been endowed with a number of strategies aiming to reduce the impact of local minima and slow convergence in iterative blind equalizers:

1) judicious initialization with analytical solutions;
2) block iterative operation;
3) global line minimization with algebraically-computed optimal step size;
4) incorporation of training data.

These strategies are not exclusive to the CP principle but can also benefit other equalization criteria.

Further lines of inquiry could include the theoretical study of suboptimal extrema in the CP criterion; the robust automatic detection of the number of ZF solutions and extraction of the optimum-delay equalizer [33]; the optimal choice of pilot-confidence parameter λ (e.g., based on an asymptotic analysis of variance); the evaluation and mitigation of the carrier residual effects on CP equalizers [25], [31]; and a thorough theoretical and experimental comparison of the CP principle with other equalization schemes, such as the CM criterion.

APPENDIX
PROOFS OF SECTION IV-A

$(\mathbf{f}^{\mathrm{H}}\mathbf{x}_n)^q = \mathbf{f}^{\oslash q\mathrm{H}}\mathbf{x}_n^{\oslash q}$.

• $(\mathbf{f}^{\mathrm{H}}\mathbf{x}_n)^q = (\sum_i (\mathbf{f})_i^*(\mathbf{x}_n)_i)^q = \sum_{i_1,\ldots i_q} (\mathbf{f})_{i_1}^* \ldots (\mathbf{f})_{i_q}^* (\mathbf{x}_n)_{i_1} \ldots (\mathbf{x}_n)_{i_1}$ can be expressed as the sum of all terms of tensor $\mathbf{f}^{\circ q^*} \odot \mathbf{x}_n^{\circ q}$ or, equivalently, of vector $\mathbf{f}^{\oslash q} \odot \mathbf{x}_n^{\oslash q}$. This sum is the same as $\mathbf{f}^{\oslash q\mathrm{H}}\mathbf{x}_n^{\oslash q}$. □

• Problem (5) is equivalent to problem (4).

We need to prove that the set of solutions $\{\mathbf{w}_k\}_{k=1}^P$ of the form $\mathbf{w}_k = \mathbf{f}_k^{\oslash q}$ is linearly independent if and only if (iff) the set $\{\mathbf{f}_k\}_{k=1}^P$ is linearly independent. This can be done along the lines of [9, Proof of Lemma 3] by considering the matrix unfolding $\mathbf{F}_k \in \mathbb{C}^{L\times L^{q-1}}$ of $\mathbf{f}_k^{\circ q} = \mathbf{unvecs}_q\{\mathbf{f}_k^{\oslash q}\}$, which is defined as $(\mathbf{F}_k)_{i_1,i_2+L(i_3-1)+\ldots L^{q-2}(i_q-1)} = (\mathbf{f}_k^{\circ q})_{i_1 i_2 i_3 \ldots i_q}$. This matrix can be expressed as the rank-1 product $\mathbf{F}_k = \mathbf{f}_k\bar{\mathbf{f}}_k^{\mathrm{T}}$, with $(\bar{\mathbf{f}}_k)_{i_2+L(i_3-1)+\ldots L^{q-2}(i_q-1)} = (\mathbf{f}_k)_{i_2}(\mathbf{f}_k)_{i_3}\ldots(\mathbf{f}_k)_{i_q}$. Now, vectors $\{\mathbf{f}_k^{\oslash q}\}$ are linearly independent iff $\sum_{k=1}^P \alpha_k \mathbf{f}_k^{\oslash q} = \mathbf{0}_{L_q}$ implies $\alpha_k = 0$, for all $k = 1,\ldots,P$. That linear combination vanishes iff $\sum_{k=1}^P \alpha_k \mathbf{f}_k^{\circ q}$ is the null tensor or, equivalently, $\sum_{k=1}^P \alpha_k \mathbf{F}_k$ the zero matrix. Due to the structure of matrices $\{\mathbf{F}_k\}$, this latter condition necessarily implies that $\{\alpha_k\}$ be zero iff $\mathrm{rank}([\mathbf{f}_1,\ldots\mathbf{f}_P]) = P$, i.e., $\{\mathbf{f}_k\}$ form a linearly independent set. □

• Problem (8) is equivalent to problem (9) with scale constraint (10) and (11).

We only need to show that $\mathbf{r}^{\mathrm{H}}\mathbf{w} = \sqrt{N}$ and expressions (10) and (11) are equivalent. Vector $\mathbf{r}^{\mathrm{H}}$ is given by the product of the first row of $\mathbf{Q}$, say $\mathbf{q}^{\mathrm{H}}$, and matrix $\mathbf{X}^{q\mathrm{H}}$. Since $\mathbf{Q}\mathbf{d} = [\sqrt{N}, \mathbf{0}_{N-1}^{\mathrm{T}}]^{\mathrm{T}}$, it follows that the rest of the rows of $\mathbf{Q}$ are orthogonal to vector $\mathbf{d}$. In addition, $\mathbf{Q}$ is unitary, so that $\mathbf{q}$ must be parallel to $\mathbf{d}$; specifically, $\mathbf{q} = \sqrt{N}\mathbf{d}/\|\mathbf{d}\|^2$. Then, $\mathbf{q}^{\mathrm{H}}\mathbf{X}^{q\mathrm{H}} = (\sqrt{N}/\|\mathbf{d}\|^2)\sum_{n=0}^{N-1} d_n^* \mathbf{x}_n^{\oslash q}$. The scale constraint becomes $(\mathbf{w}^{\mathrm{H}}/\|\mathbf{d}\|^2)\sum_{n=0}^{N-1} d_n \mathbf{x}_n^{\oslash q} = 1$, which reduces to $(1/\|\mathbf{d}\|^2)\sum_{n=0}^{N-1} d_n(\mathbf{f}^{\mathrm{H}}\mathbf{x}_n)^q = 1$ when $\mathbf{w} = \mathbf{f}^{\oslash q}$. □

• If $\dim\ker(\mathbf{X}^{q\mathrm{H}}) = (P-1)$ and $N > (L_q - P) \Rightarrow \dim\ker(\mathbf{R}) = P$.

Since $\dim\ker(\mathbf{R}) = (L_q - \mathrm{rank}(\mathbf{R}))$ and $\mathrm{rank}(\mathbf{R}) \leqslant (N-1)$, it follows that $\dim\ker(\mathbf{R}) \geqslant (L_q - N + 1)$. Hence, a necessary condition for $\dim\ker(\mathbf{R}) = P$ is that $N > (L_q - P)$ or, in terms of the observed sample size, $N_d \geqslant L_q + L_0 - 1$. The solutions to (5) can be written as $\mathbf{w} = \mathbf{w}_0 + \sum_{p=1}^{P-1} \alpha_p \mathbf{w}_p$, where $\mathbf{w}_0$ is the minimum-norm solution, and $\{\mathbf{w}_k\}_{k=1}^{P-1}$ is a basis of $\ker(\mathbf{X}^{q\mathrm{H}})$. It is simple to check that $\mathbf{w}_0 \in \ker(\mathbf{X}^{q\mathrm{H}})^{\perp}$, so that $\{\mathbf{w}_k\}_{k=0}^{P-1}$ form a linearly independent set. Since $\mathbf{Q}\mathbf{X}^{q\mathrm{H}} = [\mathbf{r}, \mathbf{R}^{\mathrm{H}}]^{\mathrm{H}}$, we have that $\mathbf{X}^{q\mathrm{H}}\mathbf{w}_k = \mathbf{0}_N$ iff $\mathbf{r}^{\mathrm{H}}\mathbf{w}_k = 0$ and $\mathbf{R}\mathbf{w}_k = \mathbf{0}_{N-1}$. Thus, $\{\mathbf{w}_k\}_{k=1}^{P-1} \in \ker(\mathbf{R})$ and $\dim\ker(\mathbf{R}) \geqslant (P-1)$. Since $\mathbf{w}_0$ is a solution to (5) and (8), in particular, $\mathbf{R}\mathbf{w}_0 = \mathbf{0}_{N-1}$. This adds another linearly independent vector to the null space of $\mathbf{R}$ so that $\dim\ker(\mathbf{R}) \geqslant P$. To prove that the basis of $\ker(\mathbf{R})$ is complete, assume that another linearly independent $\mathbf{w}_P \in \ker(\mathbf{R})$ exists. It follows that $\mathbf{R}\mathbf{w}_P = \mathbf{0}_{N-1}$ and $\mathbf{r}^{\mathrm{H}}\mathbf{w}_P = c$, for certain constant $c \in \mathbb{C}$. If $c = 0$, $\mathbf{w}_P \in \ker(\mathbf{X}^{q\mathrm{H}})$. If $c \neq 0$, vector $\mathbf{w}_P\sqrt{N}/c$ is a solution to (5). In both cases, $\mathbf{w}_P$ lies in the span of the basis of $\ker(\mathbf{R})$ previously found, which contradicts the assumption and proves that $\dim\ker(\mathbf{R}) = P$. □

PROOF OF SECTION V-B

• Optimal step-size polynomial.

$J_{\mathrm{CP}}(\mathbf{f} - \mu\mathbf{g}) = \mathrm{E}\{|\varepsilon_n|^2\}$, with $\varepsilon_n = \xi(\mu) - d_n$, where $\xi(\mu) = \big((\mathbf{f}-\mu\mathbf{g})^{\mathrm{H}}\mathbf{x}_n\big)^q$. This latter polynomial in μ can be expanded as $\xi(\mu) = \sum_{p=0}^q a_p\mu^p$, where $a_p = (-1)^p\binom{q}{p}(\mathbf{g}^{\mathrm{H}}\mathbf{x}_n)^p(\mathbf{f}^{\mathrm{H}}\mathbf{x}_n)^{q-p}$. Since $\partial J_{\mathrm{CP}}(\mathbf{f} - \mu\mathbf{g})/\partial\mu = 2\mathrm{E}\{\mathbb{R}\mathrm{e}(\xi'^*\varepsilon_n)\} \stackrel{\mathrm{def}}{=} 2p(\mu)$, the first-order necessary condition $\partial J_{\mathrm{CP}}/\partial\mu = 0$ reduces to finding the zeros of $p(\mu)$. It remains to prove that such a polynomial accepts the expansion of (20). Now, $p(\mu) = \mathrm{E}\{\mathbb{R}\mathrm{e}(\xi'^*(\xi - d_n)\} = \mathbb{R}\mathrm{e}(\mathrm{E}\{\xi_1 - \xi_2\})$, with $\xi_1(\mu) = \xi'^*\xi$ and $\xi_2(\mu) = \xi'^* d_n$. As $\xi'(\mu) = \sum_{p=1}^q p a_p \mu^{p-1}$, the coefficients of the $(2q-1)$th-degree polynomial $\xi_1(\mu)$ are given by the convolution $[qa_q^*, (q-1)a_{q-1}^*, \ldots, a_1^*] * [a_q, a_{q-1}, \ldots, a_0]$, which produces

$$b_m^{(1)} = \begin{cases} \sum_{p=0}^m (m+1-p)a_{m+1-p}^* a_p, & 0 \leqslant m \leqslant q-1 \\ \sum_{p=m+1-q}^q (m+1-p)a_{m+1-p}^* a_p, & q \leqslant m \leqslant 2q-1. \end{cases} \tag{28}$$

Similarly, the coefficients of the qth-degree polynomial $\xi_2(\mu)$ are simply $b_m^{(2)} = (m+1)a_{m+1}^* d_n, 0 \leqslant m \leqslant (q-1)$. The combination of these two sets of coefficients and the expectation operator leads to expansion (20). □

REFERENCES

[1] J. K. Tugnait, L. Tong, and Z. Ding, "Single-user channel estimation and equalization," *IEEE Signal Process. Mag.*, vol. 17, no. 3, pp. 16–28, May 2000.

[2] A.-J. van der Veen, S. Talwar, and A. Paulraj, "A subspace approach to blind space-time signal processing for wireless communication systems," *IEEE Trans. Signal Process.*, vol. 45, no. 1, pp. 173–190, Jan. 1997.

[3] Y. Sato, "A method of self-recovering equalization for multi-level amplitude modulation," *IEEE Trans. Commun.*, vol. COM-23, no. 6, pp. 679–682, Jun. 1975.

[4] D. N. Godard, "Self-recovering equalization and carrier tracking in two-dimensional data communication systems," *IEEE Trans. Commun.*, vol. COM-28, no. 11, pp. 1867–1875, Nov. 1980.

[5] J. R. Treichler and B. G. Agee, "A new approach to multipath correction of constant modulus signals," *IEEE Trans. Acoust., Speech, Signal Process.*, vol. ASSP-31, no. 2, pp. 459–472, Apr. 1983.

[6] Z. Ding, R. A. Kennedy, B. D. O. Anderson, and C. R. Johnson, "Ill-convergence of Godard blind equalizers in data communication systems," *IEEE Trans. Commun.*, vol. 39, no. 9, pp. 1313–1327, Sep. 1991.

[7] Z. Ding, C. R. Johnson, and R. A. Kennedy, "On the (non)existence of undesirable equilibria of Godard blind equalizers,," *IEEE Trans. Signal Process.*, vol. 40, no. 10, pp. 2425–2432, Oct. 1992.

[8] K. Doğançay and R. A. Kennedy, "Least squares approach to blind channel equalization," *IEEE Trans. Signal Process.*, vol. 47, no. 11, pp. 1678–1687, Nov. 1999.

[9] A.-J. van der Veen and A. Paulraj, "An analytical constant modulus algorithm," *IEEE Trans. Signal Process.*, vol. 44, no. 5, pp. 1136–1155, May 1996.

[10] G. H. Golub and C. F. Van Loan, *Matrix Computations*, Third ed. Baltimore, MD: Johns Hopkins Univ. Press, 1996.

[11] A.-J. van der Veen, "Analytical method for blind binary signal separation," *IEEE Trans. Signal Process.*, vol. 45, no. 4, pp. 1078–1082, Apr. 1997.

[12] D. T. M. Slock, "Blind fractionally-spaced equalization, perfect-reconstruction filter banks and multichannel linear prediction," in *Proc. ICASSP-94, 19th Int. Conf. Acoust., Speech Signal Process.*, vol. IV, Adelaide, Australia, Apr. 19–22, 1994, pp. 585–588.

[13] L. Tong, G. Xu, and T. Kailath, "Blind identification and equalization based on second-order statistics: a time domain approach," *IEEE Trans. Inf. Theory*, vol. 40, no. 2, pp. 340–349, Mar. 1994.

[14] E. Moulines, P. Duhamel, J.-F. Cardoso, and S. Mayrargue, "Subspace methods for the blind identification of multichannel FIR filters," *IEEE Trans. Signal Process.*, vol. 43, no. 2, pp. 516–525, Feb. 1995.

[15] Y. Li and Z. Ding, "Global convergence of fractionally spaced Godard (CMA) adaptive equalizers," *IEEE Trans. Signal Processing*, vol. 44, no. 4, pp. 818–826, Apr. 1996.

[16] C. R. Johnson, P. Schniter, I. Fijalkow, and L. Tong *et al.*, "The core of FSE-CMA behavior theory," in *Unsupervised Adaptive Filtering II: Blind Deconvolution*, S. S. Haykin *et al.*, Ed. New York: Wiley, 2000, ch. 2, pp. 13–112.

[17] P. Comon, "Tensor decompositions: state of the art and applications," in *Mathematics in Signal Processing V*, J. G. McWhirter and I. K. Proudler, Eds. Oxford, U.K.: Clarendon, 2002, pp. 1–24.

[18] O. Grellier and P. Comon, "Blind equalization and source separation with MSK inputs," in *Proc. SPIE Conf. Adv. Signal Process.*, Jul. 19–24, 1998, pp. 26–34.

[19] P. Comon, "Contrasts, independent component analysis, and blind deconvolution," *Int. J. Adaptive Contr. Signal Process. (Special Issue on Blind Signal Separation)*, vol. 18, no. 3, pp. 225–243, Apr. 2004.

[20] L. Rota and P. Comon, "Blind equalizers based on polynomial criteria," in *Proc. ICASSP-2004, 29th Int. Conf. Acoust., Speech, Signal Process.*, vol. IV, Montreal, QC, Canada, May 17–21, 2004, pp. 441–444.

[21] O. Grellier and P. Comon, "Blind separation of discrete sources," *IEEE Signal Process. Lett.*, vol. 5, no. 8, pp. 212–214, Aug. 1998.

[22] P. Comon, "Block methods for channel identification and source separation," in *Proc. IEEE Symp. Adaptive Syst. Signal Process., Commun. Contr.*, Calgary, AB, Canada, Oct. 1–4, 2000, pp. 87–92.

[23] P. Comon and B. Mourrain, "Decomposition of quantics in sums of powers of linear forms," *Signal Process. (Special Issue on Higher Order Statistics)*, vol. 53, no. 2, pp. 93–107, Sept. 1996.

[24] O. Grellier and P. Comon, "Closed-form equalization," in *Proc. SPAWC-99, 2nd IEEE Workshop Signal Process. Adv. Wireless Commun.*, May 9–12, 1999, pp. 219–222.

[25] P. Comon, "Blind equalization with discrete inputs in the presence of carrier residual," in *Proc. 2nd IEEE Int. Symp. Signal Process. Inf. Theory*, Marrakech, Morocco, Dec. 2002.

[26] E. Kofidis and P. A. Regalia, "On the best rank-1 approximation of higher-order supersymmetric tensors," *SIAM J. Matrix Anal. Appl.*, vol. 23, no. 3, pp. 863–884, Jul. 2002.

[27] K. Doğançay, K. Abed-Meraim, and Y. Hua, "Convex optimization for blind equalization," in *Proc. ICOTA-98, 4th Int. Conf. Optimization: Techniques Appl.*, Perth, Australia, July 3–5, 1998, pp. 1017–1023.

[28] J. G. Proakis, *Digital Communications*, Fourth ed. New York: McGraw-Hill, 2000.

[29] P. A. Regalia, "A finite-interval constant modulus algorithm," in *Proc. ICASSP-2002, 27th Int. Conf. Acoust., Speech, Signal Process.*, vol. III, Orlando, FL, May 13–17, 2002, pp. 2285–2288.

[30] W. H. Press, S. A. Teukolsky, W. T. Vetterling, and B. P. Flannery, *Numerical Recipes in C. The Art of Scientific Computing*, Second ed. Cambridge, U.K.: Cambridge Univ. Press, 1992.

[31] P. Comon, "Independent component analysis, contrasts, and convolutive mixtures," in *Proc. 2nd IMA Int. Conf. Math. Commun.*. Lancaster, U.K., Dec. 16–18, 2002.

[32] V. Zarzoso and P. Comon, "Blind channel equalization with algebraic optimal step size," in *Proc. XIII Eur. Signal Process. Conf.*, Antalya, Turkey, Sep. 2005.

[33] V. Zarzoso and A. K. Nandi, "Blind MIMO equalization with optimum delay using independent component analysis," *Int. J. Adaptive Contr. Signal Process. (Special Issue on Blind Signal Separation)*, vol. 18, no. 3, pp. 245–263, Apr. 2004.

Vicente Zarzoso (S'94–M'03) was born in Valencia, Spain, in 1973. He graduated with the highest distinction in telecommunications engineering from the Universidad Politecnica de Valencia in 1996. He was then awarded a scholarship by the University of Strathclyde, Glasgow, U.K., to study with the Department of Electronic and Electrical Engineering toward the Ph.D. degree, which was also partly supported by the Defence Evaluation and Research Agency (DERA) of the U.K. He received the Ph.D. degree from the Department of Electrical Engineering and Electronics, The University of Liverpool, Liverpool, U.K., in 1999, where he subsequently held a five-year Research Fellowship awarded by the Royal Academy of Engineering of the U.K.

Since September 2005, he has been a lecturer with the Université de Nice, Sophia Antipolis, France, and a researcher with the Laboratoire d'Informatique, Signaux et Systèmes de Sophia Antipolis. His research interests include blind statistical signal and array processing and its application to biomedical problems and communications.

Pierre Comon (M'87–SM'95) graduated in 1982, and received the Doctorate degree in 1985, both from the University of Grenoble, Grenoble, France. He later received the Habilitation to Lead Researches in 1995 from the University of Nice, Sophia Antipolis, France.

For nearly 13 years, he has been in industry, first with Crouzet-Sextant, Valence, France, between 1982 and 1985, and then with Thomson Marconi, Sophia-Antipolis, France, between 1988 and 1997. He spent 1987 with the ISL Laboratory, Stanford University, Stanford, CA. He joined the Eurecom Institute, Sophia Antipolis, in 1997 and left during the Fall of 1998. He was an Associate Research Director with CNRS, Sophia-Antipolis, from 1994 to 1998. He has been Research Director at Laboratory I3S, CNRS, since 1998. His research interests include high order statistics, blind deconvolution and equalization, digital communications, and statistical signal and array processing.

Dr. Comon was Associate Editor of the IEEE TRANSACTIONS ON SIGNAL PROCESSING from 1995 to 1998 and a member of the French National Committee of Scientific Research from 1995 to 2000. He was the coordinator of the European Basic Research Working Group ATHOS from 1992 to 1995. Between 1992 and 1998, he was a member of the Technical and Scientific Council of the Thomson Group. Between July 2001 and January 2004, he acted as the launching Associate Editor of the IEEE TRANSACTIONS ON CIRCUITS AND SYSTEMS I in the area of Blind Techniques. He was IEEE Distinguished Lecturer from 2002 to 2003. He is currently a member of the SAM Technical Committee.

Spatiotemporal Blind Source Separation Approach to Atrial Activity Estimation in Atrial Tachyarrhythmias

F. Castells*, J. J. Rieta, J. Millet, and V. Zarzoso, *Associate Member, IEEE*

***Abstract*—The analysis and characterization of atrial tachyarrhythmias requires, in a previous step, the extraction of the atrial activity (AA) free from ventricular activity and other artefacts. This contribution adopts the blind source separation (BSS) approach to AA estimation from multilead electrocardiograms (ECGs). Previously proposed BSS methods for AA extraction—e.g., independent component analysis (ICA)—exploit only the spatial diversity introduced by the multiple spatially-separated electrodes. However, AA typically shows certain degree of temporal correlation, with a narrowband spectrum featuring a main frequency peak around 3.5–9 Hz. Taking advantage of this observation, we put forward a novel two-step BSS-based technique which exploits both spatial and temporal information contained in the recorded ECG signals. The spatiotemporal BSS algorithm is validated on simulated and real ECGs from a significant number of atrial fibrillation (AF) and atrial flutter (AFL) episodes, and proves consistently superior to a spatial-only ICA method. In simulated ECGs, a new methodology for the synthetic generation of realistic AF episodes is proposed, which includes a judicious comparison between the known AA content and the estimated AA sources. Using this methodology, the ICA technique obtains correlation indexes of 0.751, whereas the proposed approach obtains a correlation of 0.830 and an error in the estimated signal reduced by a factor of 40%. In real ECG recordings, we propose to measure performance by the spectral concentration (SC) around the main frequency peak. The spatiotemporal algorithm outperforms the ICA method, obtaining a SC of 58.8% and 44.7%, respectively.**

***Index Terms*—Atrial fibrillation, biomedical signal processing, blind source separation, independent component analysis, QRST cancellation, spatiotemporal signal processing.**

Manuscript received October 6, 2003; revised July 18, 2004. This work was supported in part by the Spanish Ministry of Science and Technology under Grant TIC2002-00957 and in part by the Universidad Politécnica de Valencia through a research incentive program. *Asterisk indicates corresponding author.*

*F. Castells is with the Bioengineering Electronics and Telemedicine Research Group (BeT), Electronics Engineering Department, Universidad Politécncia de Valencia, Escuela Politécnica Superior de Gandía-UPV (EPSG-UPV), Ctra. Nazaret-Oliva s/n 46730, Gandía, Valencia, Spain (e-mail: fcastells@eln.upv.es).

J. J. Rieta is with the Bioengineering Electronics and Telemedicine Research Group (BeT), Electronics Engineering Department, Universidad Politécnica de Valencia, Escuela Politécnica Superior de Gandía-UPV (EPSG-UPV), Ctra. Nazaret-Oliva s/n 46730, Gandía, Valencia, Spain (e-mail: jjrieta@eln.upv.es).

J. Millet is with the Bioengineering Electronics and Telemedicine Research Group (BeT), Electronics Engineering Deparment, Universidad Politécnica de Valencia. ETSIT-UPV, Camí de Vera s/n 46022, Valencia, Spain (e-mail: jmillet@eln.upv.es).

V. Zarzoso is with the Laboratoire de Informatique, Signaux et Systèmes, Université de Nice, F-06903 Sophia-Antipolis, France (e-mail: zarzoso@i3s.unice.fr). He is also with the Department of Electrical Engineering and Electronics, The University of Liverpool, L16 9JD Liverpool, U.K.

Digital Object Identifier 10.1109/TBME.2004.840473

I. Introduction

ATRIAL FIBRILLATION (AF) is the most frequent cardiac arrhythmia, and has a prevalence of 10% in population over 70 years old [11]. The interest in the study and understanding of AF has considerably increased during the last years. Many studies have been carried out to analyze the underlying mechanism on isolated hearts of animals [28] but, unfortunately, these results are not directly applicable to humans. The analysis and characterization of AF and other atrial tachyarrhythmias such as atrial flutter (AFL) from noninvasive techniques requires the previous estimation of the actrial activity (AA) signal from the surface electrocardiogram (ECG). Several approaches have been proposed for this purpose. The explicit QRST cancellation from a matching template has demonstrated its effectiveness, as in Average Beat Subtraction [5], [14] or in the spatiotemporal QRST cancellation [32]. A model based on blind source separation (BSS) [37] introduces an interesting point of view, and two solutions based on principal component analysis (PCA) [21] and independent component analysis (ICA) [29] have been proposed. Recently, a study has been carried out to compare and validate all these techniques [22]. Finally, other approaches based on neural networks allow the introduction of nonlinearities in the estimation model [35]. BSS proves a powerful formulation which has also been successfully applied to other biomedical problems [38].

By exploiting the spatial diversity introduced by the multiple spatially-separated electrodes, previously proposed BSS solutions are able to estimate the independent bioelectric sources—comprising ventricular activity (VA), AA and other bioelectric artefacts—from a statistical analysis of the ECG. However, any temporal information which may be present in the sources is disregarded. Motivated by the observation that AA signal typically exhibits a narrowband spectrum with a main frequency of between 3.5–9 Hz [6], [14], [21], [26], [31], [33], the main goal of this contribution is the design of a new BSS-based algorithm which aims to utilize more fully the spatiotemporal information of the ECG recordings. Experimental results demonstrate that the proposed spatiotemporal algorithm enhances AA estimation relative to a BSS technique exploiting only spatial information (ICA).

Measuring performance is a difficult issue in inverse problems. Objective assessments can be accomplished by means of synthetic recordings in which AF contributions are artificially added to normal sinus rhythm (NSR) signals [30], [32]. Some authors have created simulated signals by adding known activity which is generated from an equivalent current dipole (ECD) with a moment of a determined frequency [18]. The forward problem of this ECD using a volume conductor model of the

torso/head provides the observations. However, in this model the observations of the ECD are mathematically a linear combination of each other. Hence, the generated observations perfectly match the BSS model of instantaneous linear mixtures and, as a result, the performance obtained by ICA would be too satisfactory so as to be considered realistic. Another contribution of the present paper is a novel methodology for the synthetic generation of ECGs with realistic AF episodes. This methodology includes a simple but judicious comparison between the added and the estimated AA.

The paper is structured as follows. Section II briefly reviews the state of the art on atrial tachyarrhythmias and BSS techniques. The methods are put forward in Section III, whereas Section IV describes the signal databases used for validation and comparison. To evaluate the performance of the proposed technique, synthesized ECGs with known AA have been created, but the algorithm has been validated on real signals as well. The results obtained with both databases are reported in Section VI, whose conclusions bring the paper to and end in Section VII.

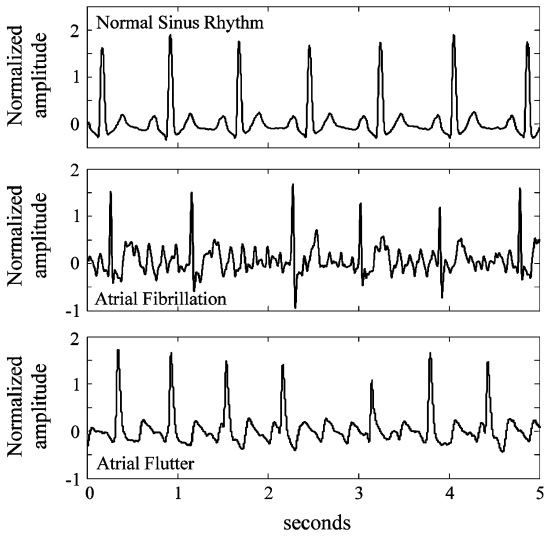

Fig. 1. Typical examples of NSR, AF, and AFL signals.

II. State of the Art

A. Atrial Tachyarrhythmias

Atrial tachyarrhithmias are cardiac arrhythmias in which normal atrial electrical activation is substituted by continuous activation, with multiple wavelets depolarising the atria simultaneously [1], [13]. On the ECG, normal atrial activity (P wave) is no longer visible, being substituted by rapid oscillations or fibrillatory waves that vary in size, shape and timing. The most frequent atrial tachyarrhythmias are AF and AFL, where AF is characterized by apparently chaotic atrial activation with a cycle length typically of around 160 ms, and an irregular and frequently rapid ventricular response (QRS complex) [1], [6], [14], [26], [34]. The ventricular response to AF depends on electrophysiological properties of the atrioventricular node, and the R-R interval becomes more irregular. On the other hand, AFL is characterized by a more regular atrial activation with a cycle length of around 250 ms [1], [25], [34], [36]. Fig. 1 shows an example of NSR, AF, and AFL ECGs.

B. Blind Source Separation

The body-surface potentials as a result of cardiac electrical activity can be modeled as a BSS problem [29]

$$\mathbf{x}(t) = \mathbf{A}\mathbf{s}(t) \tag{1}$$

where $\mathbf{x}(t)$ is a length-m vector which represents the electrode outputs at time instant t, i.e., the standard multilead ECG, $\mathbf{s}(t)$ is a length-n $(\mathrm{n} \leq \mathrm{m})$ random vector that represents the bioelectric sources (AA, VA, respiration, muscular movement, etc.), and $\mathbf{A}$ is the mxn channel-parameter matrix. For the standard ECG, we have $\mathrm{m} = 12$. Neither the original sources nor the transfer coefficients from the epicardial surface toward the body surface are known.

The main advantage of the BSS model lies in its flexibility. Indeed, only two conditions must be fulfilled to recover the original sources from the exclusive knowledge of the observations [12], [37]. Firstly, the sources must be mutually statistically independent. Secondly, the transfer channel must be linear and instantaneous, and must generate linearly independent observations (in the sense that matrix $\mathbf{A}$ be full column rank). Since the AA, the VA, and other sources arise from physically independent bioelectric phenomena, it can also be assumed that they are statistically independent. Furthermore, for the frequency range of the ECG (below 100 Hz), bioelectric theory has modeled the torso as an inhomogeneous volume conductor [23], [27]. Consequently, any signal recorded at the body surface can be assumed to arise as a linear instantaneous transformation of the independent bioelectric sources and, therefore, BSS techniques are appropriate for the estimation of the AA [29].

Depending on the separation problem, several BSS techniques have been developed. For orthogonal mixtures (i.e., when the columns of $\mathbf{A}$ are orthogonal), PCA provides the optimal solution and it only requires the sources to be uncorrelated (second-order independence) [19]. However, the mixing matrix may well have an arbitrary structure, which discards PCA as an appropriate solution. For a more general situation of nonorthogonal mixtures, techniques based on ICA must be employed [17], [20], which typically resort to the higher order statistics (HOS) of the signals. Since the higher-order cumulants of Gaussian signals are zero, ICA is unable to separate Gaussian sources. For nonorthogonal mixtures of Gaussian sources, some additional structure must be exploited. If the sources have different spectra, temporal information may be useful, and an algorithm based on the joint diagonalization of several (second-order) autocorrelation matrices at different lags [4] offers a reliable solution.

III. Methods

A. Statistical Source Analysis

Depending on their nature, the sources contained in an ECG recording can be divided into three types. VA sources are the ECG components with the highest energy. These components have a high amplitude during ventricular depolarization and repolarization (QRS complex and T wave, respectively), but the rest of the time they present values close to zero due to the period

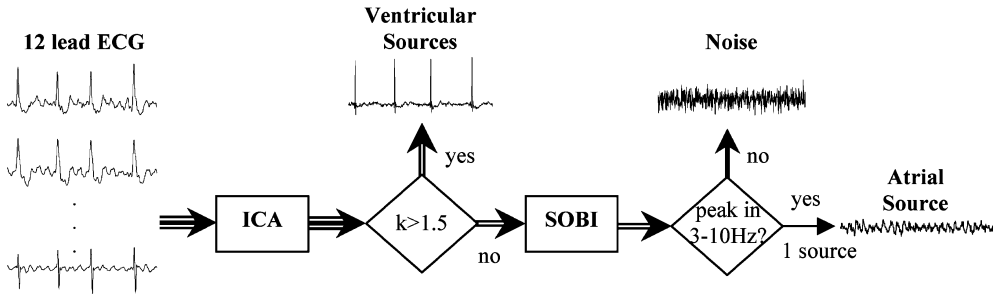

Fig. 2. Diagram block of the proposed spatiotemporal algorithm for AA estimation.

of inactivity of the myocardium cells. Therefore, VA sources possess supergaussian random distributions [8], even with kurtosis values above those of Laplacian distributions, which will be confirmed in Section VI by computing the kurtosis of the estimated VA sources. In AF and AFL episodes, AA consists of small and continuous wavelets with a cycle typically around 160 and 250 ms, respectively. A statistical analysis of the sources shows that AA has quasi-Gaussian distributions [8], with kurtosis values very close to zero (as will be discussed later on). However, AA waves have a characteristic spectrum, with a main peak due to the refractory period, which can be located between 3.5 and 9 Hz depending on the patient. Finally, noise and other artefacts are the contributions with the lowest energy, although in more than a few leads they could show an amplitude of the same order of magnitude as the atrial sources, or even higher. The statistical behavior of the noise may be different for each recording; even several noise sources with different statistical behavior may be found in a single ECG. Hence, no assumption about the noise pdf or correlation is made. The only noise assumption included in the separation model we propose is that the noise has a different spectrum from the AA source, which is verified in practically all cases.

B. Two-Step Strategy

The fact that VA presents supergaussian distributions can be exploited to remove ventricular components in the first stage, which is implemented with ICA. Since ventricular components appear at the ECG recording with higher energy than any other components, this stage eliminates the major source of interference. The nonventricular components (AA, artefacts and noise) are the inputs of the second stage. In this stage, the characteristic spectrum of the AA source is exploited in order to enhance AA estimation. Fig. 2 illustrates a block diagram of the proposed two-step methodology. Using this method, the AA can be estimated in both AF and AFL arrhythmias.

1) First Stage: ICA: As it has been stated above, ICA techniques are most suitable to separate independent non-Gaussian sources. They are able to estimate the independent sources from the analysis of the higher order statistics (HOS) of the multilead signal [17]. Most ICA methods are based on the optimization of a contrast function that maximizes non-Gaussianity. Indeed, from the Central Limit Theorem it follows that maximization of non-Gaussianity is equivalent to the maximization of independence. Several algorithms have been developed for this purpose: some of them are based on information-theoretic concepts, such as entropy and mutual information [3], [12]; a solution based on the joint diagonalization of fourth-order cumulant matrices has also been proposed [7]; etc. All these algorithms employ (explicitly or otherwise) HOS to maximize statistical independence, and provide equivalent solutions under mild assumptions. Considering the model in (1), ICA methods estimate the separation matrix $\mathbf{B}$ such that the estimated sources

$$\hat{\mathbf{s}}(t) = \mathbf{B}\mathbf{x}(t) \tag{2}$$

fulfil certain statistical independence criterion. Among all existing ICA algorithms, in this study we have chosen an algorithm that estimates non-Gaussianity as a function of the following approximation of negentropy $J(\cdot)$ [17]

$$J(y) \propto [\mathrm{E}[G(y)] - \mathrm{E}[G(v)]]$$
$$G(y) = \log\cosh y \tag{3}$$

where y is the output signal and v is a unit variance Gaussian variable. The approximation of the negentropy combines the simplicity of kurtosis with the robustness of negentropy, providing a solution which is both reliable and computationally efficient [17]. Furthermore, the maximization of the contrast function can be carried out by means of a fixed point algorithm that provides very fast convergence [16]. Nevertheless, the aim of this paper is not to emphasize the convenience of a determined ICA algorithm, but to demonstrate the suitability of ICA as a more general concept for this first processing stage.

ICA algorithms are especially equipped to extract all non-Gaussian sources, but are unable to separate Gaussian sources since their HOS are null. Hence, all Gaussian sources will appear mixed at the ICA output. The practical consequence over AF recordings is that VA sources will be correctly extracted, but the AA source can appear combined with other Gaussian-like sources such as thermal noise and other artefacts. Due to the very low energy of the AA signal, the separation of AA from all these additional sources of interference becomes an important necessary task. This task will be carried out in the second stage, which is described in the next section.

The inputs to the second processing stage are the nonventricular source components estimated by the first stage. The decision as to which components belong to the ventricular subspace and which components belong to the nonventricular subspace can be done automatically. Due to the existence of the QRS complex, the ventricular sources show high kurtosis values. On the other hand, AA is quasi-Gaussian and, thus, it usually displays kurtosis values marginally different from zero. Consequently, a kurtosis-based threshold can be employed to distinguish between ventricular and nonventricular sources. Preliminary experiments show that a conservative kurtosis threshold of around 1.5 allows

us to retain the AA information in the nonventricular subspace (the signal subspace which lies orthogonal to that spanned by the mixing-matrix columns associated to the ventricular sources) and reject all other sources that contain QRS complexes.

2) Second Stage: Second-Order Blind Identification (SOBI): The so-called SOBI technique aims at separating a mixture of uncorrelated sources with different spectral content through a second-order statistical analysis which also takes into consideration the source temporal information [4]. For this purpose, SOBI seeks a transformation that simultaneously diagonalizes several correlation matrices at different lags. Since, in general, no transformation may exist that accomplish such a stringent condition, a function that objectively measures the degree of joint (approximate) diagonalization (JD) at different lags is employed instead.

Let us assume that the observations have been previously whitened (which is the case in our problem, since the ICA step involves prewhitening), and let us focus on the elementary case of two sources and two observations. The correlation matrix $\mathbf{C}$ of the whitened observations at a lag τ_i is

$$\mathbf{C}(\tau_i) = \begin{bmatrix} a_i & b_i \\ c_i & d_i \end{bmatrix} \tag{4}$$

with

$$\mathbf{C}(\tau_i) = \mathrm{E}[\mathbf{z}(t)\mathbf{z}^{\mathrm{T}}(t-\tau_i)] \tag{5}$$

where $\mathrm{E}[\cdot]$ represents the expectation operator.

The real sources $\mathbf{s}$ and the whitened observations $\mathbf{z}$ are related through a Givens rotation

$$\mathbf{z} = \mathbf{Q}\mathbf{s}, \quad \mathbf{Q} = \begin{bmatrix} \cos\theta & -\sin\theta \\ \sin\theta & \cos\theta \end{bmatrix} \tag{6}$$

where θ is an unknown rotation angle. The correlation matrix of the sources, $\mathbf{C}'$, at a lag τ_i is

$$\mathbf{C}'(\tau_i) = \begin{bmatrix} a'_i & b'_i \\ c'_i & d'_i \end{bmatrix} \tag{7}$$

where

$$\mathbf{C}'(\tau_i) = \mathrm{E}[\mathbf{s}(t)\mathbf{s}^{\mathrm{T}}(t-\tau_i)]. \tag{8}$$

The goal of separating the AA from other sources of interference is equivalent to finding an orthogonal transformation $\mathbf{Q}$ from the whitened observations $\mathbf{z}$. The source signals being uncorrelated, their covariance matrix at any lag shows a diagonal structure. Hence, for sources with different spectra (i.e., with different autocorrelation function) the goal is shown to be equivalent to finding an orthogonal transformation that diagonalizes $\mathbf{C}'$ for each τ_i, i.e., at all lags simultaneously. Since no solution may exist that satisfies that strict condition, a JD criterion must be defined.

Assuming that N different lags will be employed for JD, N correlation matrices $\mathbf{C}'(\tau_i)$ are evaluated, $i = 1 \ldots N$ **.** The JD criterion proposed in [4] (which is also employed in the ICA method of [7]) is given by:

$$\hat{\mathbf{Q}} = \arg\max_{\mathbf{V}} J(\mathbf{V}), \quad J(\mathbf{V}) = \sum_{i=1}^{N} ||\mathrm{diag}[\mathbf{V}^{\mathrm{T}} C(\tau_i)\mathbf{V}]||^2 \tag{9}$$

and $\mathbf{V}$ is a unitary matrix. Let us define a $Nx2$ matrix $\mathbf{G}$ and a column vector of N elements $\mathbf{u}$

$$\begin{aligned} \mathbf{G} &= [\mathbf{a}-\mathbf{d} \quad \mathbf{b}+\mathbf{c}] \\ \mathbf{u} &= \mathbf{G}[\cos 2\theta \quad \sin 2\theta]^{\mathrm{T}} \end{aligned} \tag{10}$$

where $\mathbf{a}, \mathbf{b}, \mathbf{c}$ and $\mathbf{d}$ are column vectors containing the respectives matrix entries of the ith correlation matrix $\mathbf{C}(\tau_i)$. Then, JD can be measured through the following cost function [4]

$$F(\theta) = \mathbf{u}^{\mathrm{T}}\mathbf{u} \tag{11}$$

which is exclusively a function of the rotation angle θ. Hence, the independence criterion has been transformed into the maximization problem of (11). The rotation angle that maximizes the JD criterion allows the recovery of the original sources. Remark that the maximization of this quadratic form can be efficiently computed in closed-form as the eigenvector corresponding to the largest eigenvalue of the 2×2 matrix $\mathbf{G}^{\mathrm{T}}\mathbf{G}$; also, the calculation of θ does not even require trigonometric functions. For more than two sources and two observations, the problem can be solved by Jacobi-like pairwise iterations until convergence [4].

Since the AA has a narrowband spectrum, the SOBI algorithm is appropriate for estimating the AA. The number of matrices for joint diagonalization and their time lags must be properly selected. Since the autocorrelation of the AA source in AF episodes is quasiperiodic with a period around 160 ms—i.e., 160 samples at a sampling rate of 1 KHz —, correlation matrices with time lags involving two cycles (that is, 320 ms) are chosen. This choice guarantees that even for AF signals with larger AA cycle the lag range spans at least one complete cycle length. This condition is fulfilled even in the case of AFL arrhythmias, with a cycle length between 200 and 300 ms. Choosing correlation matrices at evenly spaced lags of 20 ms (i.e., a total of 17 correlation matrices) guarantees a high proportion of significant (nonzero) autocorrelation values among the selected lags with an affordable computational complexity. Indeed, this choice achieved a good AA extraction performance in preliminary experiments, as confirmed in the more thorough results reported in the following sections.

IV. Databases

The fact that the AA is unknown in real recordings hinders an in-depth experimental comparative study of AA extraction methods. Hence, suitable simulated AF ECGs must be designed in order to evaluate the performance of the proposed approach. With the formulation described in Section IV-B, pseudoreal ECGs are generated with known AA, which allows us to easily compare the estimated and the real AA. Ultimately the method is to be applied over actual AF episodes and, thus, a database of such recordings (Section IV-B) is also employed to demonstrate the suitability of the algorithm in real scenarios.

A. Pseudoreal AF Recordings

Several models for simulated AF signals have been already proposed in previous works [30], [32]. However, the simulated AF recordings created with those models differ considerably from real AF recordings, since the AA which is added to each

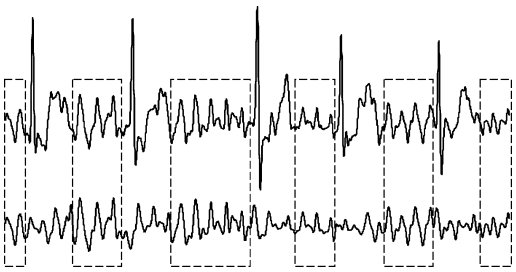

Fig. 3. Generation of synthesized AF ECG. The boxed areas are the regions where the AF contribution dominates. These regions are singled out and then extrapolated to generate the synthetized AA signal.

lead is generated from a single AA waveform. One of the objectives of this work is to develop a new model for synthesized AF recordings that simulate as realistically as possible genuine AF recordings. This new model is described as follows.

Since the AF signals are the superposition of VA and AA, both activities can be obtained separately from real recordings and then added together. VA can be obtained from NSR episodes, after correctly removing P-waves. The acquisition of AA signals is more involved. A first idea would be to record ECGs during ventricular asystole periods of AF patients, but this option is unfortunately nonviable in most practical situations. Another alternative might consist of estimating the AA from the ECG by employing a QRST cancellation technique, like template matching and subtraction [5], [14] or the spatiotemporal cancellation method [32]. However, this alternative has been discarded, since the estimated AA could contain some QRS residual, which could be particularly important in those leads where the AA is hardly appreciable. In addition, the resulting simulation model would not be applicable to evaluate such QRST cancellation techniques since the simulation model would match the AA estimation methodology. Taking into consideration those limitations, we aim to define a simulation model valid for different methodologies, which would allow their fair comparison in a further study. We propose to simulate the atrial wave by isolating the AA from T-Q intervals during AF episodes and carefully extrapolate it between those segments. An example of AA generation is shown in Fig. 3. The AA within T-Q intervals matches the ECG signal, and the AA within Q-T intervals is reconstructed from the extrapolation of two adjacents T-Q segments [8]. A simple extrapolation method is used, where the fibrillatory cycles prior to the QRST complex are replicated within the QRST interval, but linearly weighted such that the weights are one at the beginning of the interval and decrease down to zero at the end of the interval. Analogously, the fibrillatory cycles following the QRST complex are replicated within the QRST interval, and are weighted from zero at the beginning of the interval rising up to one at the end of the interval. The segments to be replicated are selected so as to preserve the phase of the fibrillatory wave observed within the T-Q intervals. Both contributions are combined to build up the extrapolated AA wave within the QRST interval [32]. This process is repeated for each lead, thus obtaining a 12-lead synthesized AA. Although the reconstructed AA samples do not exactly correspond to the true AA signal masked by the QRST complex, this model preserves the general features

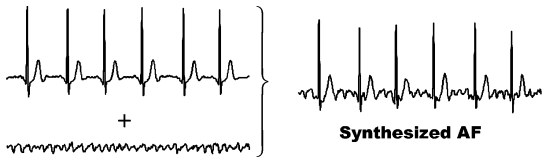

Fig. 4. Generation of AF-episode ECG lead from synthesized VA and AA signals.

of the AA signal observed in the different leads according to a real AF recording. The resulting composite AA signal is more realistic than that obtained by the ECD model [18], which follows ICA's generative pattern and, as a result, would produce too optimistic results.

Following the proposed simulation model, the statistical properties of both VA and AA on which is based the separation algorithm as well as the autocorrelation cycle of AA are preserved. In this sense, the kurtosis of VA and AA is 12.2 ± 5.8 and -0.17 ± 0.68, respectively, for our simulated database. As will be confirmed in Section VI-B, the kurtosis values of the real VA in AF episodes also follow a super-Gaussian distribution. On the other hand, it is known that the heart rate variability in AF episodes is higher than in NSR. However, this observation does not influence our approach, since the degree of Gaussianity is not affected by this temporal oscillation. Also, time information (correlation at different time lags) is only considered in a second processing step where VA is mostly cancelled.

Furthermore, a rigorous model for synthesized AF signals requires an additional constraint: the AF episode for the AA generation and the NSR episode must be acquired from the same patient. If both episodes came from different patients, the mixing matrix for the AA would generally be different from that of the NSR and, hence, the simulation model would not be realistic. However, if both episodes are obtained from the same patient, the synthesized AF signal approximates very accurately the conditions and characteristics of an ECG recording with genuine AF. In addition, it is desirable that both signals be acquired during the same session, in order for the electrode position to remain unaltered. This is only possible during a cardioversion process at an electrophysiology lab. The AF episode is taken at the beginning of the recording, before the cardioversion. The cardioversion restores and stabilizes the NSR, which can then be neatly recorded. The AA is synthetized from the AF episode as described in the previous paragraph, whereas the VA is obtained from the NSR episode after cardioversion. Finally, the synthesized signals are created through the superposition of VA and AA for each lead (Fig. 4). Following this simulation model, 10 pseudoreal ECGs were generated for our analysis, including 6 AF ECGs and 4 AFL ECGs.

B. Real AF Recordings

Twenty-five ECGs digitized during 30 s at 1-KHz sampling rate with 16-bit amplitude resolution were employed for our study. In order to demonstrate that the method is valid for AF as well as AFL arrhythmias, the database included 14 AF ECGs and 11 AFL ECGs. All recordings were obtained at an electrophysiological laboratory from patients suffering from persistent AF or AFL. All patients were under amiodarone treatment in order to increase the refractory period.

V. Performance Measurement

A. Simulated AF ECGs

As explained in the previous section, the fact that the AA is known in simulated AF ECGs enables a more accurate performance analysis. The observations $\mathbf{x}$ are the combination of VA $(\mathbf{x}_{\mathrm{VA}})$ and simulated AA waves $\mathbf{x}_{\mathrm{AA}}$: $\mathbf{x} = \mathbf{x}_{\mathrm{VA}} + \mathbf{x}_{\mathrm{AA}}$. Hence, the estimated sources can be decomposed as

$$\hat{\mathbf{s}}(t) = \mathbf{B}\mathbf{x}(t) = \mathbf{B}\mathbf{x}_{\mathrm{VA}}(t) + \mathbf{B}\mathbf{x}_{\mathrm{AA}}(t) \tag{12}$$

that is, the ith source is recovered from a linear combination of the leads given by the ith-row coefficients of the $\mathbf{B}$ matrix. Accordingly, the AA source is recovered from a row, say $\mathbf{b}_{\mathrm{AA}}$, defining a linear combination which aims to cancel the contribution of the QRS complexes while trying to maximize the contribution of the AA

$$\hat{s}_{\mathrm{AA}}(t) = \mathbf{b}_{\mathrm{AA}}\mathbf{x}(t) = \mathbf{b}_{\mathrm{AA}}\mathbf{x}_{\mathrm{VA}}(t) + \mathbf{b}_{\mathrm{AA}}\mathbf{x}_{\mathrm{AA}}(t). \tag{13}$$

As observed in (13), the estimated AA source $\hat{s}_{\mathrm{AA}}$ presents two components

$$\begin{aligned} e(t) &= \mathbf{b}_{\mathrm{AA}}\mathbf{x}_{\mathrm{VA}}(t) \\ s_{\mathrm{AA}}(t) &= \mathbf{b}_{\mathrm{AA}}\mathbf{x}_{\mathrm{AA}}(t). \end{aligned} \tag{14}$$

Since s_{AA} is reconstructed from the actual AA and is not contaminated by VA, it can be considered as the pure AA source. The term e mainly consists of residual VA, and hence can be considered as an error or nondesired component. Note that this error term is not only due to ventricular contributions, but also to the noise present in $\mathbf{x}_{\mathrm{VA}}$. The noise that may be present in $\mathbf{x}_{\mathrm{AA}}$ is inherent to this problem formulation of the problem and it can neither be measured nor cancelled. However, due to the higher amplitude of VA, the residual VA in the estimated AA will usually be more important than any residual noise or interference caused in the reference AA (s_{AA}) by an erroneous estimation of the separating matrix $\mathbf{B}$. Therefore, in general the noise present in $\mathbf{x}_{\mathrm{AA}}$ will have a negligible effect on the proposed performance measure.

In the light of this model, performance can be objectively measured using a number of indexes. In the first place, the normalized mean square error (NMSE) is defined as

$$\mathrm{NMSE} = \frac{\mathrm{E}[(\hat{s}_{\mathrm{AA}} - s_{\mathrm{AA}})^2]}{\mathrm{E}[s_{\mathrm{AA}}^2]}. \tag{15}$$

Since $\mathrm{E}[(\hat{s}_{\mathrm{AA}} - s_{\mathrm{AA}})^2] = \mathrm{E}[e^2]$, low values of NMSE indicate an effective rejection of VA and associated interference in x_{VA} and, thus, an improved AA estimation performance. Another objective performance parameter is the Pearson cross-correlation coefficient (CC) between s_{AA} and $\hat{s}_{\mathrm{AA}}$. In addition, we propose the spectral concentration (SC) around the main frequency peak f_p as another indicator. This indicator will later be shown to be useful in measuring performance in real AF recordings. The SC in the band of the peak is based on the parameters employed for measuring the SC in ventricular fibrillation arrhythmias [2], [24], and is computed as

$$\mathrm{SC} = \frac{\sum_{0.82f_p}^{1.17f_p} P_{\mathrm{AA}}(f_i)}{\sum_0^{f_s/2} P_{\mathrm{AA}}(f_i)} \tag{16}$$

where P_{AA} is the power spectrum of the AA signal, which is computed using the Welch's method, with a 8192 points FFT, 4096 sample size Hamming window and 50% overlapping; f is the frequencies vector, and f_s is the ECG sample frequency. The bandwidth considered for the SC computation is of 2 Hz for a typical f_{p} of 6 Hz, which is sufficient even for those AF episodes that show a wide-band spectrum with several peaks. In the cases where the bandwidth of the AF signal was wider, this parameter would be no longer valid and should be redefined. For the simulated signals under test, it was verified that the SC of the AA increased according to the error reduction (NMSE), which in turn is associated with an improved AA estimation performance. Hence, the correlation between SC and NMSE points to the validity of the former as performance index of AA estimation quality in real AF recordings, where the NMSE cannot be measured. This outcome was consistent with the results obtained on real signals, as confirmed in Section VI-B.

B. Real AF ECGs

AA extraction performance in real AF ECGs is very difficult to measure objectively, because the signal to be estimated is not known *a priori*. A sensible performance parameter is the degree of SC around the main frequency peak [9]. The rationale for this parameter lies in the fact that the AA spectrum is typically condensed around a single frequency, whereas the spectral content of other components such as VA or noise is more spread out over the frequency range. If the estimated AA signal is contaminated with other nondesired components, the spectral content outside the main frequency peak will become more significant and, thus, the estimated AA will suffer a decrease in the SC around the main peak. Hence, the method that provides an AA signal with higher SC can be considered as the technique with higher performance. The justification of SC as a valid performance index (at least for the proposed method) is further endorsed by the correlation between SC and NMSE found in simulated AF ECGs, as commented at the end of the preceding section.

VI. Results

A. Results With Simulated AF ECGs

The proposed two step approach was applied over a set of 10 simulated recordings with known AA content, and was compared to the results obtained by applying only the first step, i.e., an ICA algorithm. As explained above, the FastICA fixed-point algorithm was chosen as ICA method [16]. Several approaches included in the ICALAB toolbox [10] have also been tested (JADE, AMUSE, etc.), obtaining equivalent solutions. After applying ICA, at least one AA source was identified among the whole set of 12 independent sources. Performance evaluation was then measured in terms of NMSE and CCs. In addition, the spectral concentration (SC) around the main frequency peak was also computed. In those cases where more than one source contained AA, it was selected the source that better matched the known AA according to the performance parameters NMSE and CC. However, after applying SOBI, the AA was present in only one source for the signals under study.

Table I. shows the results obtained. After applying the second stage (i.e., SOBI), the NMSE is reduced up to 40% in average. Correlation indexes also indicate an improvement in the estima-

TABLE I
PERFORMANCE INDEXES OF THE ESTIMATED AA IN SIMULATED ECGS

	Type	Main Frequency	ICA			ICA - SOBI		
			NMSE (%)	CC	SC (%)	NMSE (%)	CC	SC (%)
Patient 1	AF	5.74	128.54	0.656	20.18	68.96	0.752	38.03
Patient 2	AF	4.78	114.02	0.687	32.76	74.04	0.759	42.32
Patient 3	AFL	3.59	42.61	0.825	31.74	31.13	0.861	38.15
Patient 4	AF	6.45	117.32	0.677	28.53	49.7	0.812	49.96
Patient 5	AF	5.38	45.60	0.830	50.70	21.54	0.906	65.55
Patient 6	AF	6.45	109.90	0.688	27.86	98.09	0.722	37.23
Patient 7	AFL	3.35	72.16	0.766	19.53	27.08	0.889	35.37
Patient 8	AF	7.29	148.14	0.640	13.14	59.39	0.787	62.43
Patient 9	AFL	4.42	43.03	0.831	20.76	20.08	0.906	60.88
Patient 10	AFL	3.60	19.55	0.908	55.18	19.77	0.907	60.39
Mean			**74.19**	**0.751**	**30.04**	**46.98**	**0.830**	**49.03**

TABLE II
SPECTRAL ANALYSIS OF ESTIMATED AA IN REAL ECGS

	Main Frequency (Hz)	Spectral concentration	
		ICA	ICA-SOBI
AF Patients	6.19 ± 0.73	37.1 ± 11.8 %	53.7 ± 11.7 %
AFL Patients	4.06 ± 0.65	54.5 ± 19.4 %	65.2 ± 13.9 %

tion of the AA. After applying ICA, there exists a 0.751 correlation between the estimated and the real AA. However, if SOBI is also applied, the correlation indexes arise up to 0.830. Concerning the spectral concentration around the main frequency peak, it can be observed that the AA estimated by using the complete spatiotemporal approach has higher spectral concentration than that estimated by ICA. The validity of this parameter for performance evaluation will be further discussed in the next section.

B. Results With Real AF ECGs

ICA and ICA-SOBI were applied to the database of 14 AF ECGs and 11 AFL ECGs. In all cases, it was possible to estimate the AA source. A spectral analysis was carried out in order to detect the main frequency. The AA source estimated with ICA provides the same frequency as the AA source estimated with ICA-SOBI, being of 6.19 ± 0.73 Hz for AF and 4.06 ± 0.65 Hz for AFL. However, the AA source obtained with ICA-SOBI has a higher spectral concentration around the main frequency peak. In average, ICA obtains a spectral concentration of 37.1% for AF and 54.5% for AFL. The spectral concentration is increased with ICA-SOBI up to 53.7% and 65.2% for AF and AFL, respectively. Table II and Fig. 5 summarize the spectral analysis of the AA. The higher spectral concentration of the AA signal obtained after SOBI processing indicates that part of the noise present in the AA signal after ICA has been removed. Fig. 6 shows the results from patient 3, where the estimated AA obtained by ICA (top) is free from QRS complexes but it still contains noise, giving rise to a smeared frequency distribution with spurious peaks. After the SOBI stage, the estimated AA (bottom) is successfully denoised, its frequency spectrum closely resembling that of a typical AF signal.

Regarding the kurtosis values of the VA and the AA, the results confirm the hypothesis employed in the separation model. Indeed, VA is supergaussian, with a kurtosis value of 16.5 ± 5.9 for the ECGs under test. By contrast, AA cannot be assumed not to be Gaussian, with a kurtosis value of -0.21 ± 0.45 for this database. Table III details the kurtosis values of VA and AA sources for AF and AFL patients. The significance level (p-value) of these results was obtained by means of a kurtosis statistical test about the gaussianity of VA and AA sources. A t-student test where the null hypothesis is that the sources are Gaussian (i.e., the kurtosis distribution have zero-mean value)

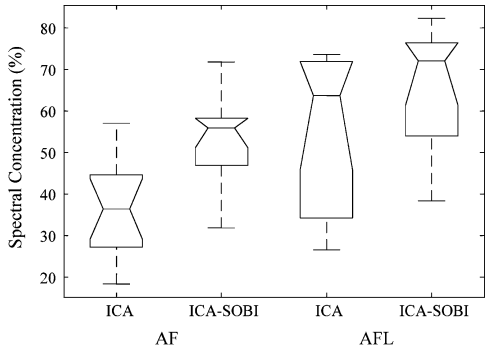

Fig. 5. Spectral concentration of the AA for AF and AFL ('box-and-whiskers' plot).

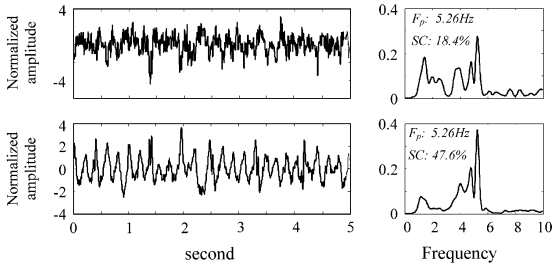

Fig. 6. An example where the proposed ICA-SOBI outperforms ICA.

TABLE III
KURTOSIS VALUES OF VENTRICULAR AND ATRIAL SOURCES

	k_{VA}	k_{AA}
Simulated ECGs	12.2 ± 5.8	-0.17 ± 0.68
AF Patients	14.9 ± 5.6	0.03 ± 0.34
AFL Patients	18.5 ± 5.9	-0.52 ± 0.38

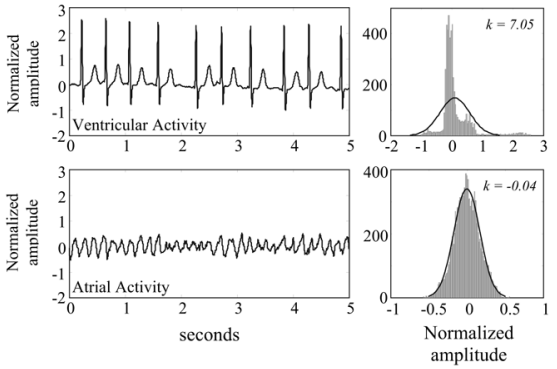

Fig. 7. Histogram and kurtosis values (k) of the estimated VA and AA sources. The continuous solid lines on the right-hand side plots represent the closest Gaussian approximations to the observed distributions.

was performed. For the kurtosis distribution of AA, we obtain $p = 0.236$ (the hypothesis null should not be discarded), and for the kurtosis distribution of VA we obtain $p = 1.22 \cdot 10^{-13}$ (the hypothesis null can be discarded). The histograms of VA and AA sources from patient 10 are shown in Fig. 7, where the normalized Gaussian distribution has been superimposed for comparison. As can be observed, the VA is supergaussian, clearly more 'peaky" and with heavier tails than the Gaussian pdf, whereas the AA exhibits a near-Gaussian distribution. The fact that the estimated ventricular and atrial sources fulfil the hypothesis assumed in the problem formulation regarding their statistical behavior and spectral characteristics validates the proposed approach for the enhanced estimation of AA in patients with AF.

VII. Study Limitations

The BSS-based AA-extraction approach presented in this paper has been validated using a self-constructed database of simulated AF recordings and an own database of real AF ECGs, as previously explained. Although the proposed validation methodology introduces some useful concepts and the results are consistent, this study presents some inherent limitations that are considered next.

Regarding the simulation model for generating AF recordings, the 12-lead synthesized AA contains reconstructed samples within the intervals corresponding to the QRST waves. Therefore, the number of reconstructed points is considerable with respect to the number of true AA samples. This fact could render the extrapolated AA information rather inaccurate, specially near the center of the extrapolation window. This limitation could be addressed, e.g., by employing ventricular asystole periods registered from AF patients. These recordings consist of several seconds length ECG segments without any VA, which can be triggered by blocking the atrioventricular conduction (His bundle) within the heart. This action is highly invasive and, therefore, is not applicable or convenient in most situations.

In addition, the SC parameter may not be sufficiently discriminating in real AF recordings. Indeed, the SOBI algorithm employed in the second separation stage tends to enhance narrow-band components (with high SC) in wide-band noise. Although the SC parameter has been contrasted and shows a high degree of correlation with other objective parameters in simulated recordings, this index could unfairly benefit the proposed approach against other methods. Alternative parameters should also be employed to assess the performance of the estimated AA. In this respect, further research is needed to search for new parameters to determine either numerically or qualitatively (e.g., more clinical indexes) the correct estimation of the desired source.

VIII. Discussion and Conclusions

A typical feature of ICA-based BSS techniques is that they are able to estimate independent sources by exploiting spatial information from multilead signals. Usually, temporal information is not taken into account. This paper has demonstrated that the source temporal information is indeed relevant in the estimation of AA from ECG recordings of AF episodes. A spatiotemporal BSS algorithm adapted to this specific problem has been designed and implemented. The algorithm consists of an initial spatial-HOS based separation stage (ICA) aiming to remove non-Gaussian interference (mainly VA), followed by a time-SOS based separation stage (SOBI) aiming to cancel Gaussian-like noise. Hence, the AA can be separated not only from VA, but also from other independent sources of noise and interference regardless of their distribution. As an important advantage, the BSS-based approach does not require a previous R-peak detection, thus avoiding any subsequent problems such as sensitivity to ectopic beats, false negatives/positives in automated processes, etc. With this new method, results on synthesized AF signals have experienced a significant improvement in AA estimation performance. A study with real AF signals has further validated the suitability of the proposed method.

This work has also tackled the problem of synthesizing pseudoreal signals for ICA. The proposed approach does not take into account the generative model of instantaneous linear mixtures of the bioelectric sources assumed by BSS techniques in this biomedical problem. This detachment from the assumed underlying signal model allows the definition of more significant indexes for objective performance evaluation and comparison.

In addition, the lack of objective parameters to measure performance in real AF recordings has led us to propose a new parameter based on the spectral concentration, which shows a correlation with the AA estimation quality. In the experimental results, AA estimation has always improved with the application of the second separation stage based on the exploitation of temporal information. Even in some ECGs where ICA had already estimated the AA accurately (e.g., because the existing AA was far from Gaussian), the second step has been able to maintain the separation quality. Since the statistical behavior of the AA source is not *a priori* known, it seems sensible to make use of the full two-step approach in all cases.

This contribution improves the existing solutions for AF analysis. Once the AA has been extracted, it can be further analyzed for spectral characterization, pattern recognition, time-

frequency parameter extraction, etc. Some clinical applications derived from the AA analysis could involve, e.g., the prediction of AF recurrence after successful cardioversion. A significant number of patients return to sustained AF in few days after electrical cardioversion. The analysis of the AA could contribute to the prediction of AF recurrence in order to prevent some patients from suffering ineffective electrical discharges. Other interesting application could be based on the analysis of paroxysmal AF (PAF), which appears and terminates spontaneously. It is commonly accepted that PAF is a precursor of persistent AF. Improved knowledge about the mechanisms that cause PAF and its spontaneous termination may introduce improvements in the treatment of AF. The proposed methodology, thus, emerges as a helpful tool in clinical diagnosis.

ACKNOWLEDGMENT

The authors would like to acknowledge the helpful support received from Servicio de Hemodinámica of the Hospital Clínico Universitario the Valencia, and specially from R. Ruiz, S. Morell, and R. García Civera, for providing signals and for the high quality of their clinical advice. V. Zarzoso has carried out part of this research work while on leave at Laboratoire I3S, Universite de Nice—Sophia Antipolis, France. He gratefully acknowledges Dr. P. Comon for his kind hospitality.

REFERENCES

[1] M. Allessie, K. Konings, and M. Wijffels, *Atrial Arrhythmias—State of the Art: Electrophysiological Mechanism of Atrial Fibrillation*, J. P. DiMarco and E. N. Prystowsky, Eds. Armonk, NY: Futura, 1995.

[2] S. Barro, R. Ruiz, D. Cabello, and J. Mira, "Algorithmic sequential decision-making in the frequency domain for life threatening ventricular arrhythmias and imitative artefacts: A diagnostic system," *J. Biomed. Eng.*, vol. 11, pp. 320–328, 1989.

[3] A. J. Bell and T. J. Sejnowsky, "An information maximization approach to blind separation and blind deconvolution," *Neural Computation*, vol. 7, pp. 1129–1159, 1995.

[4] A. Belouchrani, K. Abed-Meraim, J. F. Cardoso, and E. Moulines, "A blind source separation technique using second-order statistics," *IEEE Trans. Signal Process.*, vol. 45, no. 2, pp. 434–444, Feb. 1997.

[5] A. Bollmann, N. K. Kanuru, K. K. McTeague, P. F. Walter, D. B. DeLurgio, and J. J. Langberg, "Frequency analysis of human atrial fibrillation using the surface electrocardiogram and its response to ibutilide," *Am. J. Cardiol.*, vol. 81, pp. 1439–1445, 1998.

[6] A. Bollmann, K. Sonne, H. D. Esperer, I. Toepffer, J. J. Langberg, and H. U. Klein, "Non-invasive assessment of fibrillatory activity in patients with paroxysmal and persistent atrial fibrillation using the Holter ECG," *Cardiovasc Res.*, vol. 44, pp. 60–6, 1999.

[7] J. F. Cardoso and A. Souloumiac, "Blind beamforming for non Gaussian signals," *Inst. Elect. Eng. Proc.-F*, vol. 140, pp. 362–370, 1993.

[8] F. Castells, J. Igual, J. J. Rieta, C. Sánchez, and J. Millet, "Atrial fibrillation análisis based on ICA including statistical and temporal source information," in *Proc ICASSP*, Hong Kong, 2003. V-94-96.

[9] F. Castells, R. Ruiz, J. J. Rieta, and J. Millet, "An integral atrial wave identification based on spatiotemporal source separation: Clinical validation," *Comput. Cardiol.*, pp. 717–720, 2003.

[10] A. Cichocki, S. Amari, and K. Siwek, "ICALAB Toolboxes,", [Online]. Available: http://www.bsp.brain.riken.go.jp/ICALAB, 2003.

[11] S. S. Chugh, J. L. Blackshear, W. K. Shen, S. C. Hammill, and B. J. Gersh, "Epidemiology and natural history of atrial fibrillation: Clinical implications," *J. Am. Coll. Cardiol.*, vol. 37, pp. 371–378, 2001.

[12] P. Comon, "Independent component analysis—A new concept?," in *Signal Process.*, vol. 36, 1994, pp. 287–314.

[13] V. Fuster *et al.*, "ACC/AHA/ESC guidelines for the management of patients with atrial fibrillation," *J. Am. Coll. Cardiol.*, vol. 38, pp. 1231–1265, 2001.

[14] M. Holm, S. Pehrson, M. Ingemansson, L. Sornmo, R. Jahansson, L. Sandhall, M. Sunemark, B. Smideberg, C. Olsson, and S. B. Olsson, "Non-invasive assessment of the atrial cycle length during atrial fibrillation in man: Introducing, validating, and illustrating a new ECG method," *Cardiovasc Res.*, vol. 38, pp. 69–81, 1998.

[15] *The FastICA Package*, [Online]. Available: http://www.cis.hut.fi/projects/ica/fastica/, 1998.

[16] A. Hyvärinen, "Fast and robust fixed-point algorithms for independent component analysis," *IEEE Trans. Neural Networks*, vol. 10, no. 3, pp. 626–634, May 1999.

[17] A. Hyvärinen, J. Karhunen, and E. Oja, *Independent Component Analysis*. New York: Wiley, 2001.

[18] C. James, D. Lowe, and O. Gibson, "An objective study into single vs multiple channel brain signal analysis using realistic ictal EEG," in *Proc. NNESMED*, Sheffield, 2003, pp. 139–144.

[19] I. T. Joliffe, *Principal Component Analysis*. Berlin, Germany: Springer-Verlag, 2002.

[20] C. Jutten and J. Hérault, "Blind separation of sources, part I: An adaptive algorithm based on neuromimetic architecture," *Signal Process.*, vol. 24, pp. 1–10, 1991.

[21] P. Langley, J. P. Bourke, and A. Murray, "Frequency analysis of atrial fibrillation," *Comput. Cardiol.*, pp. 65–68, 2000.

[22] P. Langley, J. J. Rieta, M. Stridh, J. Millet, L. Sornmo, and A. Murray, "Comparison of atrial signals derived from the 12-lead ECG using atrial signal extraction techniques," *Comput. Cardiol.*, pp. 129–132, 2003.

[23] J. Malmivuo and R. Plonsey, *Bioelectromagnetism*. New York: Oxford Univ. Press, 1995.

[24] F. M. Nolle, R. W. Bowser, and F. K. Badura, "Evaluation of a frequency-domain algorithm to detect ventricular fibrillation in the surface electrocardiogram," *Comput. Cardiol.*, pp. 337–340, 1989.

[25] B. Olshansky, K. Okumura, R. W. Henthorn, and A. L. Waldo, "Characterization of double potentials in human atrial flutter: Studies during transient entrainment," *J Am. Coll. Cardiol.*, vol. 15, no. 4, pp. 833–841, Mar. 15, 1990.

[26] S. Pehrson, M. Holm, C. Meurling, M. Ingemansson, B. Smideberg, L. Sornmo, and S. B. Olsson, "Non-invasive assessment of magnitude and dispersion of atrial cycle length during chronic atrial fibrillation in man," *Eur. Heart J.*, vol. 19, pp. 1836–1844, 1998.

[27] R. Plonsey, *Bioelectric Phenomena*. New York: McGraw-Hill, 1969.

[28] P. L. Rensma, M. A. Allessie, W. J. E. P. Lammers, F. I. M. Bonke, and M. J. Schalij, "Length of excitation wave and susceptibility to reentrant atrial arrhythmias in normal conscious dogs," *Circ. Res.*, vol. 62, pp. 395–410, 1988.

[29] J. J. Rieta, F. Castells, C. Sánchez, and V. Zarzoso, "Atrial activity extraction for atrial fibrillation analysis using blind source separation," *IEEE Trans. Biomed. Eng.*, vol. 51, no. 7, pp. 1176–1186, Jul. 2004.

[30] J. J. Rieta, V. Zarzoso, J. Millet-Roig, R. García-Civera, and R. Ruiz-Granell, "Atrial activity extraction based on blind source separation as an alternative to QRST cancellation for atrial fibrillation analysis," *Comput. Cardiol.*, pp. 69–72, Sep. 2000.

[31] J. Slocum, A. Sahakian, and S. Swiryn, "Diagnosis of atrial fibrillation from surface electrocardiograms based on computer-detected atrial activity," *J. Electrocardiol.*, vol. 25, pp. 1–8, 1992.

[32] M. Stridh and L. Sörnmo, "Spatiotemporal QRST cancellation techniques for analysis of atrial fibrillation," *IEEE Trans. Biomed. Eng.*, vol. 48, no. 1, pp. 105–111, Jan. 2001.

[33] M. Stridh, L. Sörnmo, C. Meurling, and B. Olsson, "Characterization of atrial fibrillation using the surface ECG: time-dependent spectral properties," *IEEE Trans. Biomed. Eng.*, vol. 48, no. 1, pp. 19–27, Jan. 2001.

[34] M. Stridh, "Signal Characterization of Atrial Arrhythmias Using the Surface ECG," Ph.D. dissertation, Lund Univ., Lund, Sweden, 2003.

[35] A. Vasquez, A. Hernandez, F. Mora, G. Carrault, and G. Passariello, "Atrial activity enhancement by wiener filtering using an artificial neural network," *IEEE Trans. Biomed. Eng.*, vol. 48, no. 8, pp. 940–944, Aug. 2001.

[36] J. L. Wells Jr., W. A. McLean, T. N. James, and A. L. Waldo, "Characterization of atrial flutter. Studies in man after open heart surgery using fixed atrial electrodes," *Circulation*, vol. 60, no. 3, pp. 665–673, Sep. 1979.

[37] V. Zarzoso and A. K. Nandi, "Blind source separation," in *Blind Estimation Using Higher-Order Statistics*, A. K. Nandi, Ed. Boston, MA: Kluwer, 1999, pp. 167–252.

[38] ——, "Noninvasive fetal electrocardiogram extraction: Blind separation versus adaptive noise cancellation," *IEEE Trans. Biomed. Eng.*, vol. 48, no. 1, pp. 12–18, Jan. 2001.

F. Castells was born in Valencia, Spain in 1976. He received the M.Eng. degree in telecommunications engineering from the Universidad Politécnica de Valencia (UPV), Valencia, Spain, in 2000, where he is currently working toward the Ph.D. degree.

After working in the telecommunications manufacturing industry for Alcatel SEL AG in Germany (2000–2001), he started his PhD. studies at the UPV in 2002. He is currently an Associate Lecturer with the Department of Electronic Engineering, UPV, where he is also a member of the Bioengineering, Electronic and Telemedicine (BeT) research group. His research interests lie in the area of biomedical signal processing, with special emphasis on the application of blind signal processing techniques to atrial fibrillation analysis.

J. J. Rieta received the M. Eng. degree in image and sound from the Polytechnic University of Madrid, Madrid, Spain, in 1991, the M. Sc. degree in telecommunications from the Polytechnic University of Valencia, Valencia, Spain, in 1996 and the Ph.D. degree in Biomedical Signal Processing in 2003 in the same university.

Since 1994, he has been a Lecturer with the Electronic Engineering Department in the Valencia University of Technology, developing his teaching responsibilities at the Gandía Higher School of Technology. As lecturer he has taught several subjects related to electronic and biomedical instrumentation, analog systems, data conversion systems and control engineering, and has been the author of several docent publications in these areas. He belongs to the Bioengineering, Electronic and Telemedicine (BeT) research group where is the responsible for the Advanced Signal Processing research line. His research interests include statistical signal and array processing applied to biomedical signals, specially focused in cardiac signals, blind signal separation techniques, and the develop of clinical applications to study and characterize the atrial activity inside the challenging problem of supraventricular arrhythmias.

J. Millet was born in Valencia, Spain, in 1968. He received the M.S. degree in physics from the University of Valencia (UV), Valencia, Spain, in 1991 and the Ph.D. degree in electrical and electronic engineering from the Universidad Politécnica de Valencia (UPV), Valencia, Spain, in 1997.

Since 1997, he is the coordinator of the Biomedical Engineering branch within the Biomedical Engineering, Electronics, and Telemedicine (BET) research group of UPV. His professional research interests involve biomedical signal processing, biomedical signal acquisition and instrumentation, implantable devices for treatment of cardiac arrhythmias and Cardiac MRI.

V. Zarzoso (S'94–A'99) was born in Valencia, Spain, on September 12, 1973. He received the degree in telecommunications engineering with the highest distinction (Premio Extraordinario de Terminación de Estudios) from the Universidad Politécnica de Valencia, Valencia, Spain, in 1996, and the Ph.D. degree from the University of Liverpool, Liverpool, U.K., in 1999. He was awarded a scholarship by the University of Strathclyde, Glasgow, U.K., to study in the Department of Electronic and Electrical Engineering toward the Ph.D. degree, which was also funded in part by the Defence Evaluation and Research Agency (DERA) of the U.K.

Since September 2000, he is a Postdoctoral Research Fellow (awarded by the Royal Academy of Engineering of the U.K.). His research interests include blind statistical signal and array processing and its application to biomedical problems and communications.

Atrial Activity Extraction for Atrial Fibrillation Analysis Using Blind Source Separation

José Joaquín Rieta*, Francisco Castells, César Sánchez, Vicente Zarzoso, *Associate Member, IEEE*, and José Millet

***Abstract*—This contribution addresses the extraction of atrial activity (AA) from real electrocardiogram (ECG) recordings of atrial fibrillation (AF). We show the appropriateness of independent component analysis (ICA) to tackle this biomedical challenge when regarded as a blind source separation (BSS) problem. ICA is a statistical tool able to reconstruct the unobservable independent sources of bioelectric activity which generate, through instantaneous linear mixing, a measurable set of signals. The three key hypothesis that make ICA applicable in the present scenario are discussed and validated: 1) AA and ventricular activity (VA) are generated by sources of independent bioelectric activity; 2) AA and VA present non-Gaussian distributions; and 3) the generation of the surface ECG potentials from the cardioelectric sources can be regarded as a narrow-band linear propagation process. To empirically endorse these claims, an ICA algorithm is applied to recordings from seven patients with persistent AF. We demonstrate that the AA source can be identified using a kurtosis-based reordering of the separated signals followed by spectral analysis of the sub-Gaussian sources. In contrast to traditional methods, the proposed BSS-based approach is able to obtain a unified AA signal by exploiting the atrial information present in every ECG lead, which results in an increased robustness with respect to electrode selection and placement.**

***Index Terms*—Atrial fibrillation, blind source separation, ECG, forward electrocardiography problem, independent component analysis, QRS cancellation.**

I. Introduction

ATRIAL fibrillation (AF) is the most common sustained arrhythmia encountered by clinicians and occurs in approximately 0.4%–1.0% of the general population. Its prevalence increases with age, and up to 10% of the population older than 80 years has been diagnosed with AF. With the projected growth of the elderly population, the prevalence of AF will certainly increase [1]. There is also increasing awareness that AF is a major cause of embolic events which in 75% of cases are complicated by cerebrovascular accidents [2], [3]. AF is often associated with heart disease but a significant proportion of patients (about 30%) have no detectable heart disease. Symptoms such as occasionally disabling haemo-dynamic impairment and a decrease in life expectancy are among the untoward effects of atrial fibrillation, resulting in an important morbidity, mortality, and an increased cost for the health care provider [1], [2]. In this respect, AF has been the subject of arousing interest and intensive clinical research in recent years.

The proper analysis and characterization of AF from electrocardiogram (ECG) recordings—regardless of the leads considered—requires the extraction or cancellation of the signal components associated with ventricular activity (VA), that is, the QRS complex and the T-wave (QRS-T). Unfortunately, a number of facts hinder this operation. First, atrial activity (AA) presents in the ECG much lower amplitude—in some cases well under the noise level—than its ventricular counterpart. Additionally, both phenomena possess spectral distributions that notably overlap, rendering linear filtering solutions unsuccessful.

Methods reported in the literature to cancel out VA in the ECG involve direct suppression of the QRS complex and T-wave through the subtraction of a fixed template [4]–[6]. Also, the use of an adaptive template in conjunction with the correct spatio-temporal alignment of every QRS complex has proven to be very effective [7]. All of these methods—though different in their performance—share similar limitations such as high sensitivity to QRS morphological changes in [4]–[6] and their inability to eliminate artifacts from electrode movement or ectopic beats in [4]–[7]. More recent methods have focused on extracting the VA using artificial neural networks and subtracting it from the ECG [8] or on the decomposition of the original ECG in a set of coefficients that obtain the AA using discrete packet wavelet transform [9]. A common limitation of all of the previously mentioned methods is their inability to exploit the spatial diversity of an ECG recording.

However, the key observation that AA and VA are decoupled [1], [6] introduces a new interesting perspective which does not rely on direct QRS-T elimination. Under certain assumptions, the AA extraction problem accepts a formulation based on blind source separation (BSS) of instantaneous linear mixtures [10], in which atrial and ventricular source contributions to be appear mixed at the electrode outputs in the ECG. Hence, the separation of AA sources through a suitable BSS method would allow the reconstruction of atrial contribution to each electrode free from VA and other disturbances. The multichannel signal processing standpoint adopted in the BSS approach aims at an effective utilization of the atrial information present in all ECG leads. Two main families of BSS techniques for AA extraction have been proposed, based on principal component analysis (PCA) [11],

Manuscript received February 21, 2003; revised July 28, 2003. This work was supported in part by TIC2002-00957 and the research incentive program of the Polytechnic University of Valencia. *Asterisk indicates corresponding author.*

*J. J. Rieta is with the Bioengineering Electronic and Telemedicine Research Group, Electronic Engineering Department, Polytechnic University of Valencia. EPSG, Carretera Nazaret Oliva s/n, 46730, Gandía, Valencia, Spain (e-mail: jjrieta@eln.upv.es).

F. Castells and J. Millet are with the Bioengineering Electronic and Telemedicine Research Group, Electronic Engineering Department, Polytechnic University of Valencia. EPSG, Carretera Nazaret Oliva s/n, 46730, Gandía, Valencia, Spain.

C. Sánchez is with the Bioengineering Electronic and Telemedicine Research Group, University of Castilla-La Mancha, 16071 Cuenca, Spain.

V. Zarzoso is with the Signal Processing and Communications Group, Department of Electrical Engineering and Electronics, The University of Liverpool, L69 3GJ Liverpool, U.K.

Digital Object Identifier 10.1109/TBME.2004.827272

[12] and independent component analysis (ICA) [13], [14], respectively. PCA methods search for a solution, using second-order statistics (SOSs), that decorrelates the input signals. By contrast, the assumptions that AA and VA are independent at orders higher than two and do not present random Gaussian distributions [6], [7] may be exploited to separate AA from VA by imposing the necessary higher order statistical conditions. If such assumptions are fulfilled, the application of ICA-based methods makes it possible to reconstruct the atrial contribution to each electrode free from VA and other large-amplitude nuisance signals, like respiration artifacts, ectopic beats, or muscular noise.

One of the most important research areas where ICA techniques have proven their success is precisely in biomedical engineering. Today the use of BSS is well known in electroencephalogram and magnetoencephalogram applications [15], [16] or in the extraction of the fetal ECG from maternal cutaneous recordings [17]. Regarding the ECG, examples of the application of BSS-based methods are the separation of breathing artifacts, muscular noise, and other disturbances [18], [19], analysis of ST segments for ischemia detection [20], identification of humans using the ECG [21], and ventricular arrhythmia detection and classification [22].

In the present contribution, a new application of BSS to the multilead ECG is presented. We show the suitability of ICA techniques to extract the AA present in the ECG of patients with persistent AF episodes. It is argued that AA and VA are generated by independent sources of bioelectric activity, that this activity exhibits non-Gaussian character, and that the ECG recordings fulfil the instantaneous linear model. To empirically validate these claims, an ICA method is applied to real recordings obtained from patients suffering from AF. A simple yet effective method for the identification of AA from the estimated sources is put forward, based on higher order statistics (HOS) (more specifically, the fourth-order marginal cumulant or kurtosis) and spectral analysis [14], [23].

The paper is structured as follows. Section II justifies the assumptions that lead to the suitability of the ICA-based BSS approach to the AA extraction problem. Section III develops a method for the identification and reconstruction of AA from the separated sources of cardioelectric activity. Section IV summarizes the results obtained from the application of the ICA-based AA extraction technique on real multilead ECG signals recorded from AF patients, and the results are discussed in Section V. Section VI presents the concluding remarks.

II. AF BSS Model

If BSS methods based on ICA are to be applied to the AA extraction from the 12-lead ECG, the fulfillment of three basic considerations regarding AA, VA and the fashion in which both activities arise on the body surface must first be justified: independence of the sources, non-Gaussianity, and observations generated by instantaneous linear mixing of the bioelectric sources [24]. This section begins with an outline of the basic mathematical principles behind the BSS of instantaneous linear mixtures. Then, physical mechanisms of AF generation give strong support to the independence and non-Gaussianity of AA and VA. Next, the validity of the instantaneous linear mixing model for the ECG is endorsed through the matrix solution for the forward problem of electrocardiography. The corroboration of these conditions make it possible to assume that the ECG of a patient in AF satisfies the BSS instantaneous linear mixture model, thus justifying the application of ICA.

A. BSS Principles

The BSS consists of recovering a set of source signals from the observation of linear mixtures of the sources [10], [25]. The term "blind" emphasizes that nothing is known about the source signals or the mixing structure, the only hypothesis being the source mutual independence [24]. Mathematically, let us denote by $\mathbf{s}(t) = [s_1(t), s_2(t), \ldots, s_N(t)]^T \in \Re^N$ (^{T} stands for the transpose operator) the vector that represents the N source signals and $\mathbf{x}(t) = [x_1(t), x_2(t), \ldots, x_M(t)]^T \in \Re^M$ the M sensor output vector, i.e., the observation vector. It is assumed that $M \geq N$, so that there are at least as many sensors as sources. In the noiseless case, the BSS model for instantaneous linear mixtures reads

$$\mathbf{x}(t) = \mathbf{A}\mathbf{s}(t) \tag{1}$$

where $\mathbf{A} \in \Re^{M \times N}$ is the unknown mixing matrix. The objective of BSS is to estimate $\mathbf{s}(t)$ and $\mathbf{A}$ from the exclusive knowledge of $\mathbf{x}(t)$. To achieve the source separation, a linear transformation $\mathbf{W} \in \Re^{N \times M}$ is sought such that the components of the output signal vector $\mathbf{x}(t)$ become statistically independent, thus representing an estimate of the sources

$$\hat{\mathbf{s}}(t) = \mathbf{W}\mathbf{x}(t) \tag{2}$$

except for (perhaps) scaling and permutation, which are considered admissible indeterminacies.

Some authors have proposed the use of PCA to solve the model of (1) [11]. However, it is important to remark that the success of PCA relies heavily on the orthogonality of the columns of the mixing matrix. However, in general, there is no reason why bioelectrical sources of the heart should be spatially orthogonal to one another in the ECG. This orthogonality condition can only be forced through appropriate electrode placement, as was previously emphasized in the context of the fetal ECG extraction problem [26], [27] and the cancellation of artifacts in the electroencephalogram [16]. As a consequence, PCA is not expected to separate each source from the ECG with a quality similar to that of ICA. Moreover, PCA methods assume sources with a Gaussian distribution, which is not the case for AA and VA in the AF problem (as will be justified in Section II-C). In general, the measurement of independence for non-Gaussian signals can be carried out more accurately using HOS, rather than SOS, like PCA methods do.

By contrast, ICA does not introduce any restriction on the geometrical structure of the mixing matrix (apart from the linear independence of its columns) and, in addition, takes into account the non-Gaussian nature of the source signals. Consequently, ICA arises as a more sensible approach to this problem.

Several ICA techniques have been proposed mainly based on HOS and information theory [28], due to their ability to measure statistical independence. In practice, additive measurement

noise and other disturbances (e.g., mains interference) are unavoidably present in the sensor outputs of (1). It is usually a very plausible assumption to consider the noise signals independent of the bioelectric sources of interest. When the number of electrodes is larger than the number of bioelectric sources, certain degrees of freedom are available for part of the additive noise to be extracted as separate source signals (as will be observed in the experimental results of Section IV). However, in the general case, the effective treatment of noisy observations in BSS [28], as well as in other signal processing problems, remains an open issue, which is beyond the scope of this paper.

B. Mechanisms of AF

One normal cardiac cycle is started at the sinus node with the depolarization of the right atrium and spreads toward the entire atria in a well-ordered manner. Atrial depolarization defines the P-wave in the ECG. Next, the depolarization impulse reaches the ventricles and their fast contraction produces the QRS complex of the ECG. Finally, ventricular repolarization produces the T-wave and concludes the cardiac cycle [29]. The manifestation of AF, a supraventricular arrhythmia, is characterized by uncoordinated atrial activation with consequent deterioration of atrial mechanical function. AF occurs when the electrical impulses in the atria degenerate from their usual organized pattern into a rapid chaotic pattern. This disruption results in an irregular and often rapid heartbeat that is classically described as "irregularly irregular" and is due to the unpredictable conduction of these disordered impulses across the atrioventricular node [1].

On the ECG, AF is described by the replacement of consistent P-waves by rapid oscillations or fibrillatory waves that vary in size, shape, and timing, associated with an irregular, frequently rapid ventricular response. Theories of the AF mechanism involve two processes [1]: enhanced automaticity in one or several foci [see Fig. 1(a)] and reentry involving one or more circuits [Fig. 1(b)].

The focal origin of AF is supported by experimental models and appears to be more important in patients with paroxysmal AF than in those with persistent AF. Nevertheless, the most widely accepted theory of persistent AF mechanisms was proposed by Moe in [30]. He postulated that AF perpetuation is based on the continuous propagation of multiple wavelets wandering throughout the atria. The fractionation of the wavefronts as they propagate results in self-perpetuating independent wavelets [2]. The number of simultaneous wavelets depends on the refractory period, mass, and conduction velocity along the atria, because these parameters present severe inhomogeneities in AF [1]. Therefore, during AF, several independent atrial propagation circuits are involved and the length of the path through which the depolarization wavefronts can travel is influenced by conduction velocity, anisotropies related to the orientation of atrial fibers and refractoriness, producing wave collision and reentry [1], [3]. Moreover, the self-perpetuating propensity of AF is justified by the electrophysiological remodeling, a phenomenon consisting in the progressive shortening of effective refractory periods, thus increasing the number of simultaneous wavelets and, as a consequence, the episode duration [1]. Through the mapping of experimentally induced AF in canine hearts, the multiple wavelet hypothesis has been proved. Similar observations have been reported in humans [1]–[3].

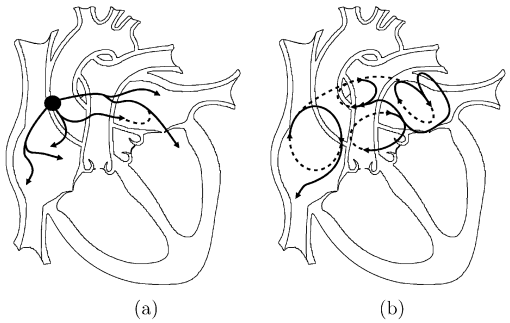

Fig. 1. Main electrophysiological mechanisms of AF. (a) Focal activation: there is an initiating focus and the resulting wavelets represent fibrillatory conduction. (b) Multiple-wavelet reentry: wavelets, indicated by arrows, randomly reenter tissue previously activated by them or by another wavelet.

C. Independence and Non-Gaussianity of AA and VA

During an AF episode several independent wavefronts propagate simultaneously throughout the atria but only a reduced part of them will reach the AV node. Moreover, several properties of the AV node tend to limit strongly the ventricular activation. First, the excitability of cells within the AV node is significantly less than the atrial myocardium, thus meaning that the refractory period is considerably larger than in the atria [1]. Second, the AV node demonstrates decremental conduction properties; that is, the amplitude and rate of rise of cardiac action potentials decrease progressively from cell to cell. Because of this property, impulses may traverse only a portion of the AV node before blocking [2]. One clinical manifestation of this property is the phenomenon of concealed conduction, in which a atrial impulse that itself does not conduct to the ventricles may impair conduction of subsequent impulses, blocking the propagation of other impulses that otherwise would have conducted [2]. As a consequence of the aforementioned AV node properties, most of the atrial wavefronts do not reach conduction and are not able to produce ventricular depolarization.

On the other hand, the physical origin of the atrial wavefront that has been able to produce ventricular depolarization could be very variable. This uncoordinated operation of AA and VA during an AF episode makes it reasonable to regard both activities as physically independent and, in turn, as generated by statistically independent sources of cardioelectric activity. The validity of the atrio-ventricular statistical-independence assumption is in line with the findings reported by other authors in the field [1], [2], [7].

With respect to non-Gaussianity, VA presents high values within the heart beat (QRS complex) and low values in the rest of the cardiac cycle. Hence, the histogram analysis of VA reveals an impulsive, i.e., super-Gaussian, behavior [6] with typical kurtosis values above 15. On the other hand, AA of an AF episode has been accurately modeled as a sawtooth signal consisting of a sinusoid with several harmonics [7], which behaves, statistically speaking, as a sub-Gaussian random process. Moreover, when a QRS complex and T-wave cancellation algorithm, like those described in [4]–[7], is employed to cancel out VA

over one ECG lead, it can be observed that the remaining ECG, mainly the AA, presents a sub-Gaussian behavior with negative kurtosis values. The non-Gaussian assumption of AA and VA is hence justified and will be shown in the results in Section IV.

D. ECG Instantaneous Linear Mixture Model

Electrocardiography involves interpretation of the potentials recorded at the body surface due to electrical activity of the heart. To this end, we use the concept of an electrical representation of the heart's activity: an equivalent source, in conjunction with a specified volume conductor to model the torso [29].

There are several physical models to represent both the cardiac current sources and the enclosing torso shape and conductivity. Source models range from simple current dipoles to complex current surfaces. Torso shape and conductivity models range from infinite homogeneous conductors to finite element models. The combination of torso and source models to calculate the body surface potentials is known as the forward problem [31]. One of the most accepted solutions for the forward problem relys on the calculation, using surface methods, of the outer body surface potentials from the epicardial (external surface of the heart) surface potentials [32]. Surface methods are based on integral equations for the potential derived by applying Green's second identity in a torso model comprising the body surface and the heart surface [33]. The general approach for finding solutions to this kind of integral equations is to discretize the problem and write one equation for each of a number of points on both surfaces and solve these equations simultaneously [31]. For N_B points defined on the body surface, representing the field points (leads), and N_H on the epicardium representing the source positions, it is possible to write the following set of discretized expressions as the observation point sweeps all the body and the heart surface:

$$\sum_{j=1}^{N_B} p_{BB}^{ij}\Phi_B^j + \sum_{j=1}^{N_H} p_{BH}^{ij}\Phi_H^j + \sum_{j=1}^{N_H} g_{BH}^{ij}\Gamma_H^j = 0 \quad (3)$$

$$\sum_{j=1}^{N_B} p_{HB}^{ij}\Phi_B^j + \sum_{j=1}^{N_H} p_{HH}^{ij}\Phi_H^j + \sum_{j=1}^{N_H} g_{HH}^{ij}\Gamma_H^j = 0 \quad (4)$$

where Γ_H^j is the normal component of the potential gradient for point j on the heart surface. In general, the g_{PQ}^{ij} term links the potential at observation point i on surface P to the value of the potential gradient Γ_H^j at point j on surface Q, while p_{PQ}^{ij} is the geometrical coefficient which weights the contribution in the observation point i on surface P of the potential at node j on surface Q. Therefore, the equations can be separated into the product of a potential (Φ_B^j or Φ_H^j) or the gradient of a potential (Γ_H^j) at a specific point j on either one of the surfaces and a second factor (the terms with general form p_{PQ}^{ij} and g_{PQ}^{ij}) based entirely on the geometry of the torso and the heart. Φ_B^j and Φ_H^j are the potential at node j on the body and heart surfaces, respectively. Now expressing the summations in matrix form, we have

$$\mathbf{P}_{BB}\mathbf{\Phi}_B + \mathbf{P}_{BH}\mathbf{\Phi}_H + \mathbf{G}_{BH}\mathbf{\Gamma}_H = 0 \quad (5)$$

$$\mathbf{P}_{HB}\mathbf{\Phi}_B + \mathbf{P}_{HH}\mathbf{\Phi}_H + \mathbf{G}_{HH}\mathbf{\Gamma}_H = 0 \quad (6)$$

where $\mathbf{\Phi}_B$ and $\mathbf{\Phi}_H$ are N_B and N_H potential column vectors, $\mathbf{\Gamma}_H$ is a column vector of N_H epicardial potential gradients, and the various $\mathbf{P}$ and $\mathbf{G}$ coefficient matrices are determined solely by integrations involving the geometry of the epicardial and body surfaces. Here again, the first subscript of $\mathbf{P}$ (or $\mathbf{G}$) represents the surface containing the observation points, having as much rows as points (N_H or N_B), and the second one represents the surface (heart or body) of integration with the number of columns equal to the number of points where the integration is computed (N_H or N_B). Solving (6) for the matrix of epicardial potential gradients $\mathbf{\Gamma}_H$ and substituting the result into (5) yields

$$\mathbf{\Phi_B} = \mathbf{T}_{BH}\mathbf{\Phi}_H \quad (7)$$

with $\mathbf{T}_{BH}$ defined as

$$\mathbf{T}_{BH} = (\mathbf{P}_{BB} - \mathbf{G}_{BH}(\mathbf{G}_{HH})^{-1}\mathbf{P}_{HB})^{-1} \cdot(\mathbf{G}_{BH}(\mathbf{G}_{HH})^{-1}\mathbf{P}_{HH} - \mathbf{P}_{BH}). \quad (8)$$

Equations (7) and (8) define the solution to the forward problem. The elements of matrix $\mathbf{T}_{BH}$ are the *transfer coefficients* relating the potential at a particular point on the epicardial surface to that at a particular point on the body surface, and they depend solely on the geometry of the epicardial and body surfaces and the conductivity of the torso.

Equation (7) shows that the electric potential in one point of the body surface can be obtained by adding the partial contributions of the heart potentials, weighted by a transfer coefficient. Obviously, (7) corresponds to a linear mixing model where a set of observations are obtained by linearly combining a set of sources. In our case, the sources are the set of bioelectric potentials in the epicardium and the observations the set of body-surface potentials.

The transfer (or mixing) matrix of (8) models the conductivity of the human torso and, in a first approximation, may be considered as an isotropic homogeneous volume conductor. A more realistic modeling of the torso can consider inhomogeneities of the volume conductor and the presence of different tissues. One can take such inhomogeneities into account by approximating the volume conductor by a collection of regions, each one of which is homogeneous, resistive, and isotropic but, at the same time retaining the results of (7) [32]. Hence, inhomogeneities and anisotropies in the human torso only modify the transfer coefficients, i.e., the elements of $\mathbf{T}_{BH}$, but do not affect the fulfillment of the model [34].

Finally, in the description of the volume conductor constituted by the human body, the capacitive component of tissue impedance is negligible in the frequency band of internal bioelectric events (0–100 Hz). Hence, the volume conductor currents generated by the heart's bioelectrical activity are essentially conduction currents and require only specification of the tissue resistivity. The electromagnetic propagation effect can also be neglected [29]. As a reinforcement of this assumption, the finite-difference method for solving the forward problem represents the torso geometry by a three-dimensional (3-D) grid of discrete points interconnected using resistive elements [35]. These considerations imply that time-varying bioelectric currents and voltages in the human body can be examined with the

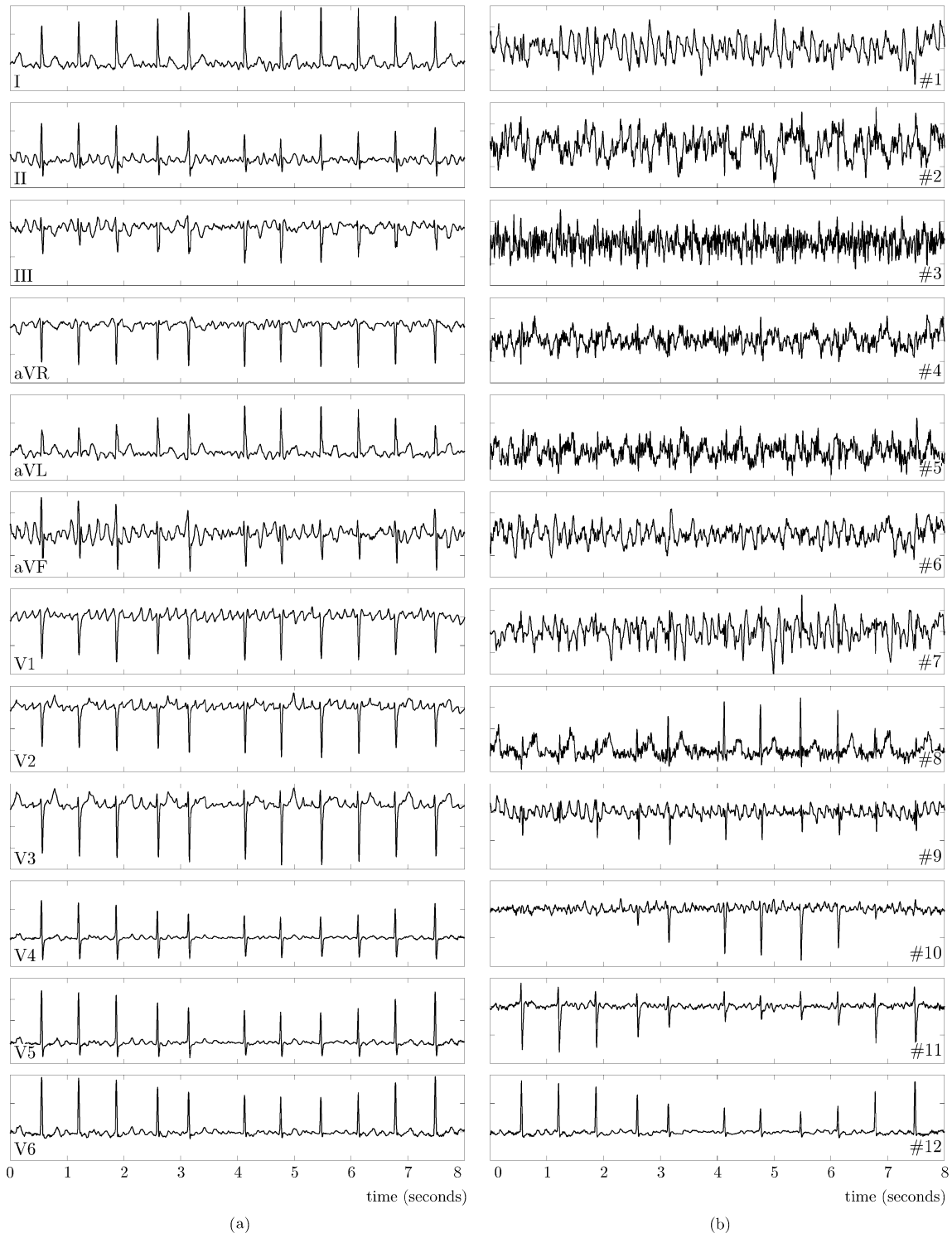

Fig. 2. Input and result of the ICA separation process. (a) A 12-lead ECG segment from a patient in AF. (b) Estimated sources obtained via ICA and reordered from lower to higher kurtosis value. The AA is contained in source #1.

conventional quasi-static approximation [36]. That is, all currents and fields behave, at any instant, as if they were stationary and we can assume the fulfillment of the BSS instantaneous linear mixture model for (7).

The joint activity of the cardiac cells can be observed via the multilead ECG but it is evident that the mathematical operations that define the voltages for the 12-lead ECG are only linear combinations of the body surface potentials and, hence, do not af-

fect at all the aforementioned instantaneous linear mixture BSS model. Then, the application of BSS-based methods on the standard ECG is completely justified and remarked with the duality between (7) and (1). As a consequence of the results from Sections II-C and II-D, the three most important requirements to apply the ICA-based BSS technique, namely, instantaneous linear mixtures, source independence, and non-Gaussianity, do indeed hold for the 12-lead ECG recordings of a patient with AF.

III. Methods

By virtue of the previous discussion, the skin-electrode signal vector of the ECG can be identified with $\mathbf{x}(t)$ and complies with the generative BSS model in (1), where vector $\mathbf{s}(t)$ is composed of the independent sources of atrial and ventricular cardiac activity and other nuisance signals. The mixing matrix entries depend on the body geometry, tissue conductivity, and electrode position similarly as occurs in the BSS formulation of the fetal ECG extraction problem [17]. Consequently, the atrial contribution to the recordings can be recovered by extracting, via ICA, the sources of AA and the corresponding columns of the mixing matrix.

Before applying ICA, all signals were sampled (or upsampled from 500 Hz) at 1 kHz in order to improve frequency resolution when performing the spectral analysis and, at the same time, make use of the most standard sampling rate for ECG studies. The upsampling process consisted of low-pass FIR filtering the ECG segment and inserting new samples obtained via a nearest neighbor interpolation. After amplitude normalization the signals were preprocessed using a 50-Hz notch filter to cancel out mains interference, followed by a band-pass filter with cut-off frequencies of 0.5 and 60 Hz to remove baseline wandering and reduce thermal noise [4].

The authors' own signal database comprised recordings from seven patients suffering from AF. All of the ECGs were composed of 12 leads and were 8 s in length. No dimensionality reduction was performed in the whitening process before ICA computation. The FastICA algorithm [37] was preferred to perform the BSS process, due to its fast convergence and robust performance, previously demonstrated in a variety of different applications [38]. In addition, FastICA can operate in a deflation mode, in which the independent components are estimated one by one. Hence, the algorithm can be stopped as soon as the AA sources have been extracted, with the consequent benefit in computational complexity.

After the application of ICA, the sub-Gaussian statistical character of AA as opposed to the super-Gaussian behavior of VA allows the identification of the estimated AA source using a kurtosis-based source reordering. This reordering process arranges first the sub-Gaussian sources, associated with AA, then the Gaussian ones, associated with noise and other artifacts, and finally the super-Gaussian sources, corresponding to VA. Therefore, according to the predicted statistical behavior of AA, the separated signals with lower kurtosis are considered to be the AA sources.

After the kurtosis-based reordering, in order to validate the AA identification, the power spectral density (PSD) was computed for all of the separated sources with sub-Gaussian kurtosis ($k < 0$). The procedure consisted of obtaining the modified periodogram using the Welch-WOSA method [39] with a Hamming window of 4096 points length, a 50% overlapping between adjacent windowed sections, and an 8192-point fast Fourier transform (FFT). Later, the spectral content above 20 Hz was discarded due to its low contribution. In this manner, it was possible to observe and compare the spectral content of the separated sources with the clinically accepted spectral content of AF [4], [11], [23], [40], [41].

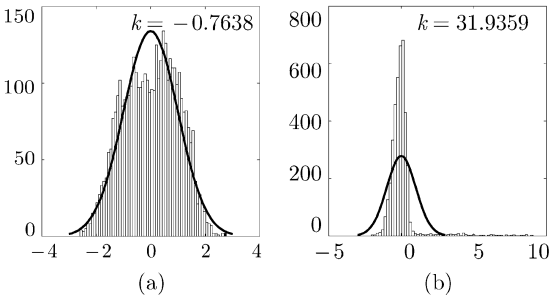

Fig. 3. Histogram of separated sources of Fig. 2, with superimposed Gaussian distribution. (a) Source #1, associated with the AA signal estimate. (b) Source #12, associated with VA.

IV. Results

After the ICA separation process, it was always possible to identify the AA source among the whole set of 12 separated sources. The identification was carried out following the aforementioned steps based on reordering the sources from lower to higher kurtosis, obtaining and analyzing the PSD of the sources with sub-Gaussian kurtosis, and, finally, visually inspecting the fibrillatory waves in the original ECG against the estimated AA source obtained by the ICA separation. Fig. 2(a) plots a 12-lead ECG with an AF episode. Observe the fibrillatory waves that can be clearly identified in several leads. It is generally accepted by the scientific community [1] that leads II, III, aVF, and especially V1 have the largest AA content, as can be seen in the figure.

The result of applying ICA to this AF episode and reordering the estimated sources as a function of its kurtosis generates the sources plot of Fig. 2(b), where source #1 has the lowest kurtosis (-0.76) and source #12 has the largest one ($+31.93$). Due to the kurtosis reordering, the first separated sources (#1–3) have a more sub-Gaussian PDF and hence are the candidates to contain the AA, the central sources are associated with Gaussian noise and signal artifacts (#4–7), and the last sources (#8–12) mainly contain VA. Fig. 3 plots the histogram of sources #1 and #12 with a superimposed normal distribution with the same mean and variance. As can be observed, AA presents a sub-Gaussian character whereas VA exhibits a strong super-Gaussian behavior, as has been previously indicated in the AF BSS model of Section II-C.

Additionally, a spectral analysis is applied over the sources with sub-Gaussian kurtosis ($k < 0$) to determine the AA source. Fig. 4 plots the results of the PSD estimation for all the negative-kurtosis sources. As can be observed, source #1 presents a typical spectral morphology of the AA from a patient with AF.

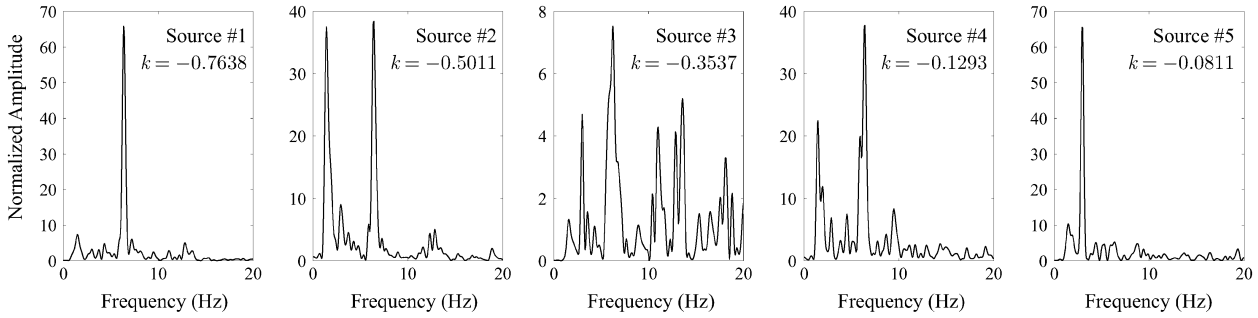

Fig. 4. Power spectral densities from several ICA-estimated sources of Fig. 2. After kurtosis-based reordering only five sources have sub-Gaussian kurtosis, and the one with lowest kurtosis (source #1) presents a PSD typically associated with the AA in AF episodes.

TABLE I
COEFFICIENTS OF THE SIXTH COLUMN OF THE MIXING MATRIX SHOWING THE PROJECTION OF SOURCE #6 (CONSIDEREDTO BE THE AA) ONTO EACH ECG LEAD

Lead	Coeff. $a_{i,6}$	Lead	Coeff. $a_{i,6}$
I	– 0.0113	V1	0.0684
II	– 0.0137	V2	0.0067
III	– 0.0018	V3	0.0034
aVR	0.0130	V4	– 0.0030
aVL	– 0.0047	V5	0.0052
aVF	– 0.0078	V6	– 0.0065

The pattern of this type of episode is characterized by a very pronounced peak in frequencies from 5 to 8 Hz, without harmonics and with insignificant amplitudes above 15 Hz. In the case of source #1, the main peak frequency is $f_p = 6.34$ Hz. It can also be appreciated in Fig. 4 that the only separated source with similar spectral content is source #5. However, the main peak frequency of this signal is f_p =2.93 Hz and, thus, it cannot be considered as AA. This decision is further reinforced by its kurtosis value $(k_5 = -0.081)$, which indicates a closer proximity to Gaussianity.

The application of the proposed BSS-based AA extraction procedure on the rest of the AF patient database consistently provided satisfactory results, as summarized in Fig. 5. These results correspond to patients #2–#7 (the results from patient #1 are presented in Figs. 3, 4, and 6), where each row is associated with one patient. In the first column, lead V1 (in the bottom) can be observed from the 12-lead ECG in AF, along with the ICA-estimated AA for that episode (at the top) for visual comparison. The estimated AA has been scaled by the factor associated with its projection onto lead V1 (as will be shown later in Table II). The visual similarity between the estimated AA and the AA contained inside V1 is remarkable. The second column shows the estimated AA PSD along with the computed main peak frequency (atrial frequency). As can be appreciated, the spectral content associated with the estimated AA source is in agreement with the expected one associated with AF [4], [11], [23], [40], [41]. Finally, the third column shows the histogram of the AA estimated source for each patient with superimposed Gaussian distribution. In general, now we can say that the sub-Gaussian behavior of the estimated AA is not so far from Gaussianity. Hence, the kurtosis values (also indicated in the figure) are close to zero but are still negative.

V. DISCUSSION

After the use of the FastICA [37] approach over the ECG segments, additional ICA algorithms were applied to the signal database in order to compare results in the AA extraction process. The algorithms employed were AMUSE and JADE from ICALAB Toolbox [42] and HOEVD [10]. All cases yielded similar results. Note that the objective of this paper is to justify and show the use of ICA in solving the AA extraction problem in AF episodes rather than find out what ICA approach performs better in this concrete problem; this could be studied in future papers.

The direct visual identification of the AA source, after applying ICA to the ECG, is not always possible. The kurtosis-based source reordering, which takes advantage of the dissimilar statistical properties of AA and VA, has proven its ability to identify the AA component from the set of estimated source signals with the lower kurtosis values. The sub-Gaussian behavior of the estimated AA source in all patients analyzed has not been as pronounced as expected. All of the kurtosis values of the estimated AA sources have been negative, but not so far from zero (Gaussianity). Nevertheless, this result is not considered to be a problem for the separation of AA from Gaussian noise. Though ICA can separate at most one Gaussian source and, hence, Gaussian noise could not be separated from near-Gaussian AAs, the noise power in the ECG is much smaller than AA, as demonstrated in the results. Moreover, it could be possible to separate the AA from Gaussian noise via their very dissimilar spectral contents. In a second step, the AA identification process has been completed with the spectral analysis of the sub-Gaussian sources. The combination of these two steps constitutes a robust AA identification method from the BSS results.

The AA estimates obtained by BSS from these ECGs in AF were considered by cardiologists as very approximate to the real atrial waveforms contained in the episode. This outcome is illustrated in Fig. 6, which shows (in the top) the atrial source #1 of Fig. 2 estimated via BSS scaled by the factor 0.0684, which corresponds to the projection of the estimated AA onto lead V1. V1 is usually accepted as the lead with the largest AA content and is shown in the bottom of Fig. 6 for visual comparison. Shown in the middle of Fig. 6 is the AA estimation result obtained when PCA is applied over the same ECG. As has been pointed out in

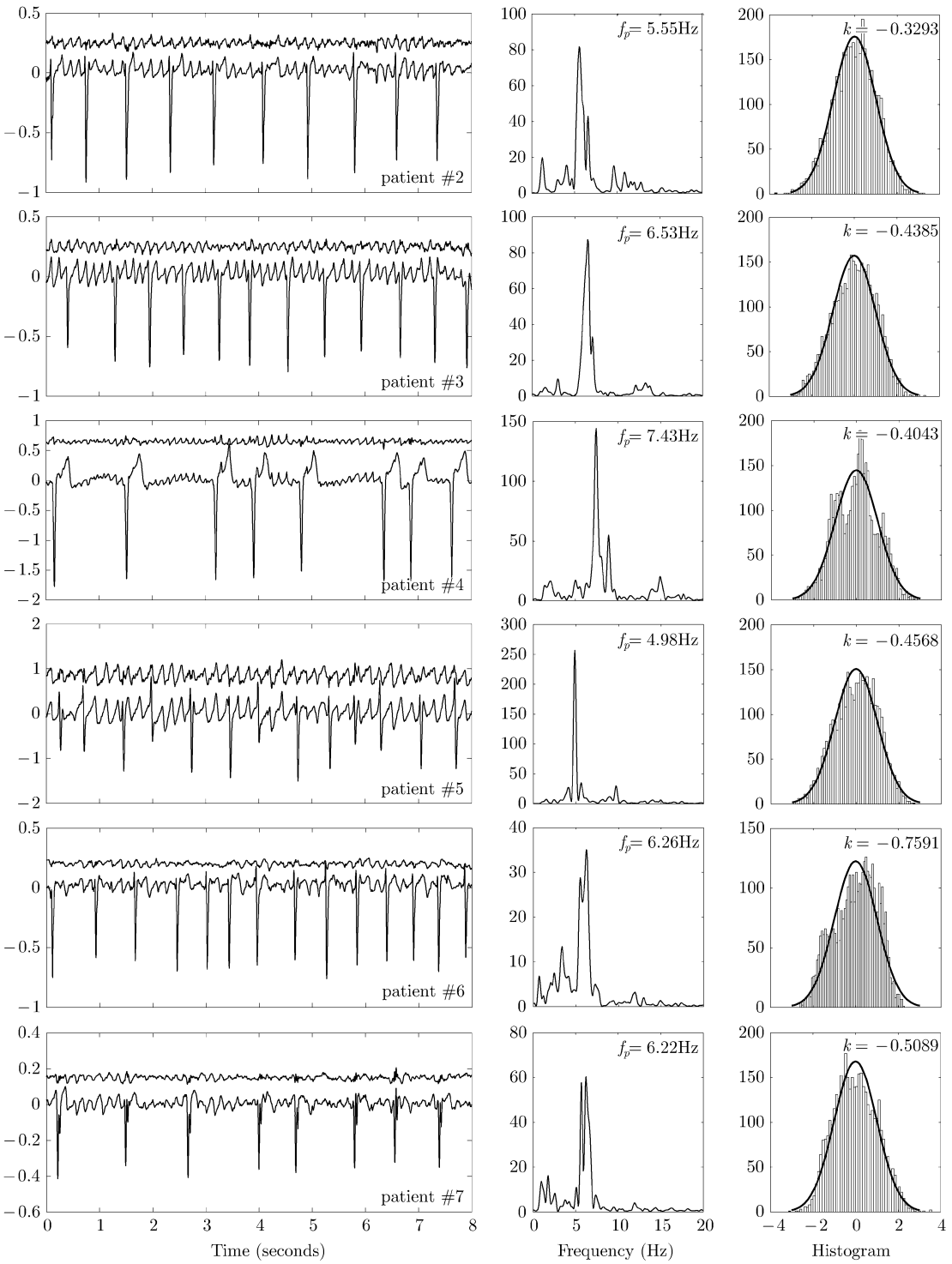

Fig. 5. AA extraction results from patients #2–#7 (one patient per row). The first column shows the estimated AA source (top) and lead V1 (bottom). The second column shows the PSD computed for the estimated AA along with the atrial frequency. The third column shows the histogram of the estimated AA with superimposed Gaussian distribution (of the same mean and variance) and its kurtosis value.

previous sections, the VA cancellation in this case is not as good as that in ICA. This can be especially observed in the R-peaks. Similar results have been reported in [41].

Before applying the kurtosis-based reordering to the estimated sources (as shown in Fig. 2), the AA obtained by the ICA separation process was present in source #6. Hence, the sixth column of the estimated mixing matrix $\mathbf{A}$ indicates how the associated source is projected onto the observations. Table I shows the projection of the AA estimated source (#1 in Figs. 2 and 4) to each observation. Clearly, lead V1 has the largest

TABLE II
PROJECTION COEFFICIENTS OF THE ESTIMATED AA SOURCES ONTO THE ECG LEADS OF PATIENTS #2–#7

Leads	I	II	III	aVR	aVL	aVF	V1	V2	V3	V4	V5	V6
Patient #2	– 0.0103	0.0052	0.0151	0.0029	– 0.0131	0.0099	0.0254	0.0054	– 0.0048	0.0200	0.0205	0.0089
Patient #3	– 0.0067	– 0.0207	– 0.0126	0.0140	0.0025	– 0.0166	– 0.0307	– 0.0273	– 0.0256	– 0.0206	– 0.0164	– 0.0159
Patient #4	0.0094	– 0.0112	– 0.0200	0.0015	0.0147	– 0.0153	0.0365	0.0251	0.0243	0.0268	0.0204	0.0236
Patient #5	– 0.0040	– 0.0074	– 0.0031	0.0051	– 0.0005	– 0.0051	0.0379	0.0194	0.0160	0.0198	0.0103	0.0189
Patient #6	0.0464	– 0.1178	– 0.1288	0.0178	0.0903	0.0631	– 0.6715	– 0.3314	– 0.2515	– 0.0159	– 0.1033	0.0485
Patient #7	0.0084	0.0223	0.0143	– 0.0155	– 0.0029	0.0185	– 0.0313	– 0.0249	– 0.0172	– 0.0280	– 0.0098	– 0.0217

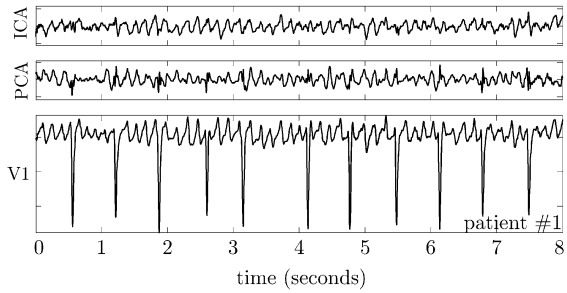

Fig. 6. Visual comparison of the reconstructed AA contribution to lead V1. At the top, separated source #1 of Fig. 2, associated with the AA signal estimate using ICA, is scaled by coefficient 0.0684 which corresponds to the projection of this source on the observation lead V1. In the middle is shown the result of the same process using PCA. The bottom shows lead V1 of the 12-lead ECG in Fig. 2.

contribution from the estimated AA source. This result, which is in close agreement with clinical experience, is an additional indication of the AA extraction quality. In the cases where the absolute amplitude of the extracted AA using BSS could be of clinical interest, it is possible to reconstruct it back to each ECG lead using the aforementioned column coefficients.

Note that we are dealing with an inverse problem, where the true sources are not accessible (noninvasively, at least), and hence the difficulty in evaluating the success of the AA source separation. One is left with estimating the AA contribution to the ECG leads typically containing the largest AA and making a visual comparison of the corresponding fibrillatory waves. Despite the large visual similarity between the fibrillatory waves of the estimated AA source and the AA contained in lead V1 (see Fig. 6), it must be said that this kind of direct visual comparison, strictly speaking, only has to be considered in an illustrative way, because the obtained AA source via BSS combines AA information from all of the ECG leads and not only from V1. Nevertheless, the only way to corroborate if the AA source separation has been satisfactory is to compare it with those ECG leads containing the largest atrial activity. This is a typical consequence of the BSS-based methods where the real sources are latent variables that cannot be directly observed.

Finally, Table II shows the projection coefficients of the estimated AA source corresponding to patients #2–#7. As can be seen (similarly as in Table I), lead V1 contains the largest AA contribution. Nevertheless, it can also be observed that the estimated AA is spread over all of the ECG leads (for a given patient, all of the projection coefficients are nonzero). This observation demonstrates the presence of AA in all of the leads, and, at the same time, the power of this ICA-based AA extraction technique, capable of taking into account the atrial contribution in every lead to generate a unified signal estimate condensing the AA information. The authors also have verified that similarly good results can be obtained in other supraventricular arrhythmias, like atrial flutter [23], and hope that this new methodology will also work in cardiac pathologies where atrial and ventricular activities are unsynchronized or decoupled, like in the AV-block.

Nevertheless, note that BSS techniques are based on statistical analysis of the data, and hence its results will not be satisfactory if the data given to the algorithm are incorrect. Therefore, it will only be possible to derive the spatial filters associated with the mixing matrix entries and the independent sources from the ECG, when the physical sources associated with the heart's bioelectrical activity are spatially stationary in time and the total number of these sources is less than the number of observations (ECG leads), as indicated in [43]. Strictly speaking, movements of the heart, such as contraction of the atria and ventricles, could violate the ICA assumption of spatial stationarity of the physical sources but, in general, the authors consider that these possible variations do not significantly affect the BSS instantaneous linear mixing model for AF episodes. This consideration is reinforced by the fact that results providing the estimation of the main atrial frequency of AA using this ICA-based BSS technique are the same as those obtained through the application of other accepted AA extraction techniques, as proved in [41].

VI. CONCLUSION

This paper has shown that the noninvasive extraction of AA in AF episodes recorded from the surface ECG can be effectively carried out by HOS-based BSS techniques for instantaneous linear mixtures. The applicability of this type of technique in this biomedical problem has been discussed in connection with its three main assumptions. First, in atrial arrhythmia episodes, the cardioelectric sources generating AA and VA can be regarded as statistically independent. Second, both activities present a non-Gaussian character. Finally, AA and VA are manifested on the body surface as an instantaneous linear mixture of the cardiac sources, in which the unknown mixture coefficients depend on the ECG electrode position and the conductivity of the body tissues. The justification of these key assumptions makes feasible the application of HOS-based BSS, and this contribution has indeed demonstrated its usefulness to solve the AA extraction problem. Traditional techniques obtain as many AA signals as leads processed by the cancellation algorithm; in contrast, the BSS-based method estimates a single signal which is able to reconstruct the complete AA present in every ECG lead. On the other hand, the BSS approach can be considered

as an alternative procedure for (indirect) QRST cancellation in atrial arrhythmia analysis.

The positive results reported in this paper mean the advent of novel noninvasive techniques for AF analysis and are the first step in the development and future improvement of new diagnostic strategies, pathology prediction methodologies, and aid tools based on AA-wave analysis in the management of patients with AF. In fact, most of the actual diagnosis and management of patients with AF are judged on the basis of clinical symptoms and ECG recordings. Therefore, the development and availability of suitable techniques allowing the knowledge of AF patterns (paroxysmal, persistent, or permanent) and aiding in the decision making about restoration and maintenance of sinus rhythm or control of the ventricular rate may be a tool of fundamental importance for the treatment of AF, a commonly encountered arrhythmia in permanent expansion.

ACKNOWLEDGMENT

The authors would like to thank cardiologists R. Ruiz Granell, S. Morell, F. J. Chorro, and R. García Civera, from the Electrophysiology Laboratory of the Universitary Clinical Hospital of Valencia, Spain, for their clinical advice and kind help in obtaining the signals.

REFERENCES

[1] V. Fuster, L. E. Ryden, R. W. Asinger, D. S. Cannom, H. J. Crijns, R. L. Frye, J. L. Halperin, G. N. Kay, W. W. Klein, S. Levy, R. L. McNamara, E. N. Prystowsky, L. S. Wann, and D. G. Wyse, "ACC/AHA/ESC guidelines for the management of patients with atrial fibrillation: a report of the American College of Cardiology/American Heart Association Task Force on Practice Guidelines and the European Society of Cardiology Committee for Practice Guidelines and Policy Conferences (Committee to Develop Guidelines for the Management of Patients With Atrial Fibrillation)," *J. Amer. Coll. Cardiol.*, vol. 38, pp. 1266 i–1266 lxx, 2001.

[2] S. Levy *et al.*, "Atrial fibrillation: Current knowledge and recommendations for management," *Eur. Heart J.*, vol. 19, no. 9, pp. 1294–1320, 1998.

[3] R. H. Falk, "Medical progress: Atrial fibrillation," *New Eng. J. Med.*, vol. 344, no. 14, pp. 1067–1078, 2001.

[4] A. Bollmann, N. K. Kanuru, K. K. McTeague, P. F. Walter, D. B. DeLurgio, and J. J. Langberg, "Frequency analysis of human atrial fibrillation using the surface electrocardiogram and its response to ibutilide," *Amer. J. Cardiol.*, vol. 81, no. 12, pp. 1439–1445, 1998.

[5] N. V. Thakor and Y. S. Zhu, "Applications of adaptive filtering to ecganalysis: Noise cancellation and arrhytmia detection," *IEEE Trans. Biomed. Eng.*, vol. 38, pp. 785–794, Aug. 1991.

[6] S. Shkurovich, A. V. Sahakian, and S. Swiryn, "Detection of atrial activity from high-voltage leads of implantable ventricular defibrillators using a cancellation technique," *IEEE Trans. Biomed. Eng.*, vol. 45, pp. 229–234, Feb. 1998.

[7] M. Stridh and L. Sörnmo, "Spatiotemporal QRST cancellation techniques for analysis of atrial fibrillation," *IEEE Trans. Biomed. Eng.*, vol. 48, pp. 105–111, Jan. 2001.

[8] C. Vasquez, A. Hernandez, F. Mora, G. Carrault, and G. Passariello, "Atrial activity enhancement by wiener filtering using an artificial neural network," *IEEE Trans. Biomed. Eng.*, vol. 48, pp. 940–944, Aug. 2001.

[9] C. Sanchez, J. Millet, J. J. Rieta, J. Rodenas, F. Castells, R. Ruiz, and V. Ruiz, "Packet wavelet decomposition: An approach for atrial activity extraction," *IEEE Comput. Cardiol.*, vol. 29, pp. 33–36, Sept. 2001.

[10] V. Zarzoso and A. K. Nandi, "Blind source separation," in *Blind Estimation Using Higher-Order Statistics*, A. K. Nandi, Ed. Boston, MA: Kluwer, 1999, pp. 167–252.

[11] P. Langley, J. P. Bourke, and A. Murray, "Frequency analysis of atrial fibrillation," *IEEE Comput. Cardiol.*, vol. 27, pp. 65–68, Sept. 2000.

[12] L. Faes, G. Nollo, M. Kirchner, E. Olivetti, F. Gaita, R. Riccardi, and R. Antolini, "Principal component analysis and cluster analysis for measuring the local organization of human atrial fibrillation," *Med. Biol. Eng. Comput.*, vol. 39, pp. 656–663, 2001.

[13] J. J. Rieta, V. Zarzoso, J. Millet, R. Garcia, and R. Ruiz, "Atrial activity extraction based on blind source separation as an alternative to QRST cancellation for atrial fibrillation analysis," *IEEE Comput. Cardiol.*, vol. 27, pp. 69–72, Sept. 2000.

[14] J. J. Rieta, F. Castells, C. Sanchez, and J. Igual, "ICA applied to atrial fibrillation analysis," in *Proc. Int. Conf. Independent Component Analysis and Blind Signal Separation (ICA)*, vol. 4, Nara, Japan, 2003, pp. 59–64.

[15] R. Vigario, J. Sarela, V. Jousmaki, M. Hamalainen, and E. Oja, "Independent component approach to the analysis of EEG and MEG recordings," *IEEE Trans. Biomed. Eng.*, vol. 47, pp. 589–593, May 2000.

[16] T. P. Jung, S. Makeig, C. Humphries, T. W. Lee, M. J. McKeown, V. Iragui, and T. J. Sejnowski, "Removing electroencephalographic artifacts by blind source separation," *Psychophysiol.*, vol. 37, no. 2, pp. 163–178, 2000.

[17] V. Zarzoso and A. K. Nandi, "Noninvasive fetal electrocardiogram extraction: Blind separation versus adaptive noise cancellation," *IEEE Trans. Biomed. Eng.*, vol. 48, pp. 12–18, Jan. 2001.

[18] J. O. Wisbeck, A. K. Barros, and R. C. Ojeda, "Application of ica in the separation of breathing artifacts in ECG signals," in *Proc. 5th Int. Conf. Neural Information Processing (ICONIP'98)*, vol. 1, pp. 211–214.

[19] A. K. Barros, A. Mansour, and N. Ohnishi, "Adaptive blind elimination of artifacts in ECG signals," in *Proc. Int. Workshop Independence & Artificial Neural Networks (I&ANN'98)*, pp. 1380–1386.

[20] T. Stamkopoulos, K. Diamantaras, N. Maglaveras, and M. Strintzis, "ECG analysis using nonlinear PCA neural networks for ischemia detection," *IEEE Trans. Signal Processing*, vol. 46, pp. 3058–3067, Nov. 1998.

[21] L. Biel, O. Pettersson, L. Philipson, and P. Wide, "ECG analysis: A new approach in human identification," *IEEE Trans. Instrum. Meas.*, vol. 50, pp. 808–812, June 2001.

[22] M. I. Owis, A. B. M. Youssef, and Y. M. Kadah, "Characterization of electrocardiogram signals based on blind source separation," *Med. Biol. Eng. Comput.*, vol. 40, no. 5, pp. 557–564, 2002.

[23] J. J. Rieta, J. Millet, V. Zarzoso, F. Castells, C. Sanchez, R. Garcia, and S. Morell, "Atrial fibrillation, atrial flutter and normal sinus rhythm discrimination by means of blind source separation and spectral parameters extraction," *IEEE Comput. Cardiol.*, vol. 29, pp. 25–28, 2002.

[24] J. F. Cardoso, "Blind signal separation: Statistical principles," *Proc. IEEE*, vol. 86, pp. 2009–2025, Oct. 1998.

[25] P. Comon, "Independent component analysis, a new concept?," *Signal Processing*, vol. 36, no. 3, pp. 287–314, 1994.

[26] J. Vanderschoot, D. Callaerts, W. Sansen, J. Vandewalle, G. Vantrappen, and J. Janssens, "Two methods for optimal MECG elimination and FECG detection from skin electrode signals," *IEEE Trans. Biomed. Eng.*, vol. 34, pp. 233–243, Mar. 1987.

[27] D. Callaerts, B. Demoor, J. Vandewalle, W. Sansen, G. Vantrappen, and J. Janssens, "Comparison of SVD methods to extract the fetal electrocardiogram from cutaneous electrode signals," *Med. Biol. Eng. Comput.*, vol. 28, no. 3, pp. 217–224, 1990.

[28] A. Hyvarinen, J. Karhunen, and E. Oja, *Independent Component Analysis*. New York: Wiley, 2001.

[29] J. Malmivuo and R. Plonsey, *Bioelectromagnetism: Principles and Applications of Bioelectric and Biomagnetic Fields*. Oxford, U.K.: Oxford Univ. Press, 1995.

[30] G. K. Moe, "On multiple wavelet hypothesis of atrial fibrillation," *Archives Internationales de Pharmacodynamie et de Therapie*, vol. 140, no. 1–2, pp. 183–188, 1962.

[31] R. M. Gulrajani, "The forward and inverse problems of electrocardiography," *IEEE Eng. Med. Biol. Mag.*, vol. 17, pp. 84–101, May 1998.

[32] R. C. Barr, T. C. Pilkington, J. P. Boineau, and M. S. Spach, "Determining surface potentials from current dipoles, with application to electrocardiography," *IEEE Trans. Biomed. Eng.*, vol. BME-13, pp. 88–92, 1966.

[33] R. C. Barr, M. Ramsey, and M. S. Spach, "Relating epicardial to body surface potential distribution by means of transfer coefficients based on geometry measurements," *IEEE Trans. Biomed. Eng.*, vol. BME-24, pp. 1–11, Jan. 1977.

[34] R. N. Klepfer, C. R. Johnson, and R. S. MacLeod, "The effects of inhomogeneities and anisotropies on electrocardiographic fields: A 3-d finite-element study," *IEEE Trans. Biomed. Eng.*, vol. 44, pp. 706–719, Aug. 1997.

[35] S. J. Walker and D. Kilpatrick, "Forward and inverse electrocardiographic calculations using resistor network models of the human torso," *Circ. Res.*, vol. 61, no. 4, pp. 504–513, 1987.

[36] R. Plonsey and D. B. Heppner, "Considerations of quasistationarity in electrophysiological systems," *Bull. Math. Biophys.*, vol. 29, no. 4, pp. 657–664, 1967.

[37] The Fastica Package for Matlab, J. Hurri, J. Gavert, J. Sarela, and A. Hyvarinen. (1998). [Online]. Available: http://www.cis.hut.fi/projects/ica/fastica

[38] A. Hyvarinen, "Fast and robust fixed-point algorithms for independent component analysis,," *IEEE Trans. Neural Networks*, vol. 10, pp. 626–634, May 1999.

[39] P. D. Welch, "Use of fast fourier transform for estimation of power spectra: A method based on time averaging over short modified periodograms," *IEEE Trans. Audio Electroacoust.*, vol. AE-15, no. 2, pp. 70–73, 1967.

[40] M. Stridh, L. Sörnmo, C. J. Meurling, and S. B. Olsson, "Characterization of atrial fibrillation using the surface ECG: Time-dependent spectral properties," *IEEE Trans. Biomed. Eng.*, vol. 48, pp. 19–27, Jan. 2001.

[41] P. Langley, M. Stridh, J. J. Rieta, L. Sörnmo, J. Millet, and A. Murray, "Comparison of atrial rhythm extraction techniques for the detection of the main atrial frequency from the 12-lead ECG in atrial fibrillation," *IEEE Comput. Cardiol.*, vol. 29, pp. 29–32, Sept. 2002.

[42] Icalab Toolboxes, A. Cichocki, S. Amari, K. Siwek, T. Tanaka, and T. Rutkowski. (2003). [Online]. Available: http://www.bsp.brain.riken.go.jp/ICALAB

[43] T. P. Jung, S. Makeig, T. W. Lee, M. J. McKeown, G. Brown, A. J. Bell, and T. J. Sejnowski, "Independent component analysis of biomedical signals," in *Proc. Int. Conf. Independent Component Analysis and Blind Signal Separation (ICA)*, vol. 2, 2000, pp. 633–644.

José Joaquín Rieta received the M. Eng. degree in image and sound from the Polytechnic University of Madrid, Madrid, Spain, in 1991, the M. Sc. degree in telecommunications from the Polytechnic University of Valencia, Valencia, Spain, in 1996 and the Ph.D. degree in Biomedical Signal Processing in 2003 in the same university.

Since 1994, he has been a Lecturer with the Electronic Engineering Department in the Valencia University of Technology, developing his teaching responsibilities at the Gandía Higher School of Technology. As lecturer he has taught several subjects related to electronic and biomedical instrumentation, analog systems, data conversion systems and control engineering, and has been the author of several docent publications in these areas. He belongs to the Bioengineering, Electronic and Telemedicine (BeT) research group where is the responsible for the Advanced Signal Processing research line. His research interests include statistical signal and array processing applied to biomedical signals, specially focused in cardiac signals, blind signal separation techniques, and the develop of clinical applications to study and characterize the atrial activity inside the challenging problem of supraventricular arrhythmias.

Francisco Castells was born in Spain in 1976. He received the M.Eng. degree in telecommunications engineering from the Universidad Politécnica de Valencia (UPV), Valencia, Spain, in 2000, where he is currently working toward the Ph.D. degree.

After working in the telecommunications manufacturing industry for Alcatel SEL AG in Germany (2000–2001), he started his PhD. studies at the UPV in 2002. He is currently an Associate Lecturer with the Department of Electronic Engineering, UPV, where he is also a member of the Bioengineering, Electronic and Telemedicine (BeT) research group. His research interests lie in the area of biomedical signal processing, with special emphasis on the application of blind signal processing techniques to atrial fibrillation analysis.

César Sánchez was born in Albacete, Spain, in 1973. He received the M.Eng. degree in telecommunications engineering from the Universidad Politécnica de Madrid, Madrid, Spain, in 1998 and he is currently working toward the Ph.D. degree at the Universidad Politécnica de Valencia (UPV), Valencia, Spain, in 2000.

He is currently a Lecturer with the Universidad de Castilla—La Mancha (UCLM), Spain, and works as an external member of the Bioengineering, Electronic and Telemedicine (BeT) research group of the UPV. His research interests are centered on the application of advanced signal processing techiques such as the wavelet transform to cardiac signals.

Vicente Zarzoso (S'94–A'99) was born in Valencia, Spain, on September 12, 1973. He received the degree in telecommunications engineering with the highest distinction (Premio Extraordinario de Terminación de Estudios) from the Universidad Politécnica de Valencia, Valencia, Spain, in 1996, and the Ph.D. degree from the University of Liverpool, Liverpool, U.K., in 1999.

He was awarded a scholarship by the University of Strathclyde, Glasgow, U.K., to study in the Department of Electronic and Electrical Engineering toward his Ph.D. degree, which was also funded in part by the Defence Evaluation and Research Agency (DERA) of the U.K. Since September 2000, he is in receipt of a Post-doctoral Research Fellowship awarded by the Royal Academy of Engineering of the U.K. He is currently on leave at the Laboratoire de Informatique, Signaux et Systèmes (I3S), Université de Nice, Sophia-Antipolis, France. His research interests include blind statistical signal and array processing and its application to biomedical problems and communications.

José Millet was born in Valencia, Spain, in 1968. He received the M.S. degree in physics from the University of Valencia (UV), Valencia, Spain, in 1991 and the Ph.D. degree in electrical and electronic engineering from the Universidad Politécnica de Valencia (UPV), Valencia, Spain, in 1997.

He is currently an Associate Professor of Electronics and Biomedical Signal Processing with the Electronic Engineering Department, UPV. From 1991 to 1999, he worked as Assistant Professor in the same department. Since 1997, he has been the coordinator of the Biomedical Engineering branch within the Bioengineering, Electronic and Telemedicine (BeT) research group of UPV. His professional research interests are in biomedical signal processing, biomedical signal acquisition and instrumentation, implantable devices for treatment of cardiac arrhythmias, and cardiac MRI.

Quality monitoring of WDM channels with blind signal separation methods

Yumang Feng, Vicente Zarzoso, and Asoke K. Nandi

Department of Electrical Engineering and Electronics, The University of Liverpool, Brownlow Hill, Liverpool, L69 3GJ, United Kingdom

aknandi@liverpool.ac.uk

RECEIVED 5 SEPTEMBER 2003; REVISED 26 APRIL 2004; ACCEPTED 30 APRIL 2004; PUBLISHED 10 JUNE 2004

An effective technique to monitor the quality of wavelength-division-multiplexed (WDM) channels is presented. This process uses a blind signal separation (BSS) method based on higher-order-statistics (HOS), and an optical-loop structure to extract the baseband channels from the WDM transmission. From the reconstructed baseband waveforms, a series of WDM transmission quality parameters are evaluated. Relative to previously proposed methods for WDM-channel monitoring, the HOS-based optical-loop procedure shows reduced complexity, improved cost efficiency, and better performance. © 2004 Optical Society of America

OCIS codes: 060.4510, 060.4230.

1. Introduction

For the proper management of WDM transmission systems and particularly optical networks that use optical add–drop multiplexing (OADM) and optical cross connect (OXC), it is essential to monitor a variety of channel-performance parameters such as signal-to-noise ratio (SNR), bit-error rate (BER), and Q factor without compromising transparency. Traditional methods for WDM channel monitoring use tunable optical filters, phased-array demultiplexers, or photodiode arrays with diffraction gratings [1].

The disadvantage of these methods is that complex (expensive) optical components are involved.

In an effort to reduce the number of expensive optical components, cost-effective monitoring solutions aim to perform most of the processing electronically. The (spatial) independence between the transmitted WDM channels has been exploited in recent studies [2–4]. The technique presented in Ref. [3] can be used to reconstruct the complete channel waveforms, from which performance parameters can be measured. Along the lines of Ref. [4], wavelength-dependent attenuators (WDAs) are employed to obtain additional observations of the WDM signal, each observation considered as a mixture of the constituent channels. Because the WDA has an adjustable nonlinear relation between the wavelength and the output power, the independent channels contribute with different strengths to each observation, and sufficient spatial diversity is available for a suitable blind signal separation (BSS) method to recover the original transmitted waveforms.

The symmetric adaptive decorrelation (SAD) technique of Ref. [5] was adopted as a separation device. This particular technique, however, has a number of deficiencies. On the one hand, its complexity is of order $O(N!)$ for an N-channel WDM transmission. On the other hand, the method has inherent stability and convergence difficulties—including spurious nonseparating solutions [5]—which may hinder the monitoring process in practical cases. More specifically, the method is based on second-order statistics, which causes problems with identification in the separation of spectrally white sources. In Refs. [6] and

[7], each channel uses a unique set of WDA and photodetector, which makes this technique less efficient with increasing number of channels.

In this paper we overcome these shortcomings with a more cost-effective optical-loop structure to WDM monitoring, but still applying BSS based on higher-order statistics (HOS), and provide a satisfactory solution of WDM quality evaluation through the reconstructed baseband waveforms. In Section 2, the system setup is described in sufficient detail for understanding the computer experiments that follow. Three BSS methods are reviewed in Section 3, and these are subsequently applied in the following experiments. In Section 4 are described quality-monitoring parameters from WDM transmissions. Simulations are described and results are presented in Section 5. Finally, the paper is concluded in Section 6.

2. System Description

Figure 1 shows a system setup of the proposed WDM channel monitoring scheme. A small fraction of each of the N channels' WDM signal is coupled out of the network with an asymmetric power splitter. A predetermined period of time, say, T_1, of this split optical signal is then sent into an optical loop, which contains a delay fiber and an optical pump, to generate a periodic optical signal sequence of repeating signal fraction T_1 for N times, each period of the signal is spaced from the other by a predetermined period of "all-zeros." An adjustable WDA [6] is used to attenuate this sequence. The WDA is synchronized with the optical switch; thus the attenuation factors for each period of signal fraction T_1 are adjusted to be different from one another. This synchronization is implemented by relating the driving voltage of the WDA to the optical switch; the required switching speed of the optical switch and WDA is related to T_1, thus the length of the delay fiber, and the length of the "all-zero" sequences used to space the "T_1" sequences. An optical pump is also applied to compensate the power coupled out of the optical loop. The attenuated optical signal sequence is converted into an electrical signal sequence by a photodetector. The purpose of the loop and WDA structure is to generate several linear mixtures of the WDM channels, which a BSS method can later use for extracting the WDM channels separately. From the reconstructed WDM waveforms, quality parameters such as eye diagrams, Q factor, and BER can be estimated.

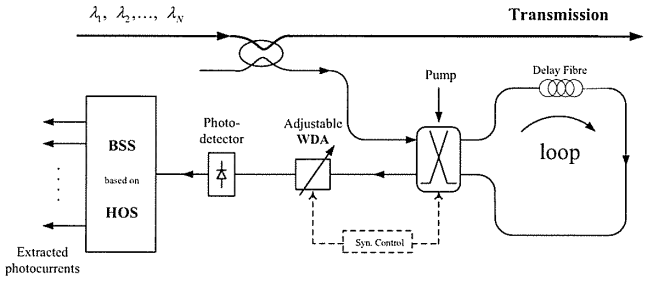

Fig. 1. Experimental setup.

The wavelength-dependent attenuating procedure above is a form of nonlinear optical signal processing, which can compensate the loss of wavelength information caused by the conversion from optical domain to electrical domain [4]. By applying appropriate electrical signal processing methods, up to some extent, we do not need to know the details of this

nonlinear optical signal processing (i.e., the WDA). In Section 3 we show that BSS methods based on HOS can be applied to extract the WDM signals.

3. WDM Signal Extraction Using HOS-Based BSS

Let $y_i(k)$, $1 \leq i \leq M$, denote the M observed photocurrents of the N-channel WDM signal ($M \geq N$), where k represents a discrete time index. Accordingly, let $s_i(k)$, $1 \leq i \leq N$, represent the channel (or source) baseband data, multiplexed within the WDM signal and thus not directly observable.

Direct photodetection of the WDM transmission causes all wavelength information to be lost. As a result, with additive noise terms neglected, the detected signal appears as a weighted linear combination of the baseband data:

$$y_i(k) = \sum_{j=1}^{N} h_{ij} s_j(k), \qquad 1 \leq i \leq M. \tag{1}$$

Coefficients h_{ij} represent the WDA effects over channel j in observed photocurrent i. Hence the observation vector $\mathbf{y} = [y_1, \ldots, y_M]^T$ (symbol T denoting the transpose operator) and the channel vector $\mathbf{s} = [s_1, \ldots, s_N]^T$ fulfill at any time instant the linear model:

$$\mathbf{y} = \mathbf{H}\mathbf{s}, \tag{2}$$

where the elements of the $(M \times N)$ mixing matrix $\mathbf{H}$ are given by $(\mathbf{H})_{ij} = h_{ij}$. Equation (2) corresponds to the BSS model of instantaneous linear mixtures [8].

Separation is generally achievable under two main assumptions:

(A1) the source signals are mutually statistically independent;

(A2) the mixing matrix is full column rank.

Otherwise both entities—$\mathbf{H}$ and $\mathbf{s}$—are unknown in model (2). Note that assumption A2 guarantees considerable freedom in the selection of the WDA attenuation patterns.

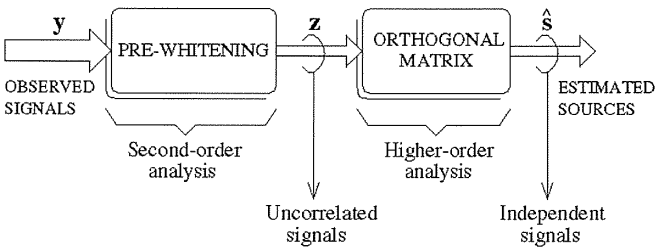

Fig. 2. Two-step approach to BSS.

As in Ref. [4], we aim to perform the monitoring by first extracting the channel waveforms from the photocurrent observations, but here we resort to the BSS methods based on HOS. The use of HOS is restricted to non-Gaussian signals, which is clearly the case in the problem at hand, with sources composed of digital modulations. Most methods operate in two steps (Fig. 2). The first step is so-called (spatial) prewhitening, which seeks to normalize and decorrelate the observations by means of conventional second-order statistical analysis (principal component analysis). This operation results in a signal vector $\mathbf{z}$, which is

linked to the channel components through an unknown $(M \times N)$ orthogonal transformation $\mathbf{Q}$:

$$\mathbf{z} = \mathbf{Q}\mathbf{s}. \tag{3}$$

The second step finds an estimate $\hat{\mathbf{Q}}$ of $\mathbf{Q}$, from which the channel signals can be reconstructed as $\hat{\mathbf{s}} = \hat{\mathbf{Q}}^T\mathbf{z}$. Essentially, a linear transformation approximating the inverse of $\mathbf{Q}$ is sought such that it maximizes the statistical independence between the separator output components. This is the purpose of independent component analysis (ICA) techniques. Independence can be measured, directly or indirectly, through a variety of different criteria such as Kullback–Leibler divergence, negentropy, mutual information, maximum likelihood (ML), and so on, leading to an array of different algorithms. The general rationale behind these techniques as well as more details about them can be found in Ref. [9]. Below are described the three HOS-based BSS methods used in the experiments reported later in this paper.

3.A. JADE

Let us denote the fourth-order cumulant of random variables $\{z_i\}_{i=1}^N$ as

$$\kappa^z_{ikjl} = \mathrm{Cum}\{z_i, z_j, z_k, z_l\}, \tag{4}$$

which is endowed with a tensor structure. The cross cumulants of independent random variables are zero, a property that can be used to measure statistical independence. Gaussian signals have a particular property that all their higher-order (cross and marginal) cumulants are always zero; thus it is impossible to discern whether a set of Gaussian signals is mixed. The cumulant tensor of independent non-Gaussian variables shows a diagonal shape, that is, $\kappa^s_{ikjl} = 0$ unless $i = j = k = l$. Hence the diagonalization of the cumulant tensor would accomplish the source separation. However, as yet no algebraic tools are available to diagonalize a tensor of order higher than two. The JADE (joint approximate diagonalization of eigenmatrices) method [10] tries to circumvent this difficulty by simultaneously diagonalizing a particular set of matrix "slices" of the fourth-order cumulant tensor. This diagonalization can be carried out in a cost-effective manner by means of conventional Jacobi-like iterations [11] based on planar Givens rotations:

$$\mathbf{Q} = \begin{bmatrix} \cos\theta & -\sin\theta \\ \sin\theta & \cos\theta \end{bmatrix}. \tag{5}$$

It has been proven [10] that this joint diagonalization is associated with a particular *contrast* function. Contrast functions [12] are an important concept in BSS / ICA, since they are particularly well suited for signal separation in the presence of noise. The main disadvantage of JADE is its computational complexity. The method requires the calculation of the N^4 elements of the fourth-order cumulant tensor, followed by the diagonalization of N^2 matrices with dimensions $(N \times N)$, each made from such cumulants. This complexity can be restrictive in separation problems with a large number of sources.

3.B. EML

In the two-signal case $(N = 2)$, matrix $\mathbf{Q}$ becomes a Givens rotation defined by a single real-valued parameter θ [Eq. (5)]. The estimation of θ can be accomplished in closed form, i.e., without any sort of iterative optimization. Several analytic expressions exist, but the estimator of Ref. [13] presents the advantage that it approximates (using the Gram–Charlier pdf expansion truncated at fourth order) the maximum-likelihood solution when the source signals have the same statistics. This is the case in the WDM monitoring problem, in which

all transmitted channels are composed of bit streams, possibly contaminated by noise and interference. This estimator expression reads:

$$\hat{\theta}_{\mathrm{EML}} = \frac{1}{4}\angle\left[\xi \operatorname{sign}(\gamma)\right], \tag{6}$$

with

$$\xi = \left(\kappa^z_{1111} - 6\kappa^z_{1122} + \kappa^z_{2222}\right) + j4\left(\kappa^z_{1112} - \kappa^z_{1222}\right), \tag{7}$$

$$\gamma = \kappa^z_{1111} + 2\kappa^z_{1122} + \kappa^z_{2222}, \tag{8}$$

where $j = \sqrt{-1}$ is the imaginary unit. Notation $\angle a$ denotes the principal value of the argument of complex-valued quantity a. Estimator (6) can be considered as an extension of the approximate ML solution of [14], thus its name "extended ML" (EML).

To achieve the source estimation for $N > 2$ channels, the closed-form expression is applied over each pair of whitened signals until convergence is reached. Since there exist $N(N-1)/2$ signal pairs and approximately $\left(1+\sqrt{N}\right)$ sweeps over the signal pairs are usually necessary for convergence, the method's complexity with respect to the number of channels is of order $O\left(N^{5/2}\right)$. This value is lower than the $O(N!)$ of Ref. [2], especially for a large number of channels.

3.C. MaSSFOC

The ICA contrast function of Ref. [12] results from certain approximations of negentropy. Further simplifications show that such contrast admits, in the two-signal case, a closed-form solution, called the maximum sum of squared fourth-order cumulants (MaSSFOC) estimator [15]. It was later discovered [16] that MaSSFOC belongs to a wider family of so-called weighted closed-form estimators (WEs), whose general expression is given by

$$\hat{\theta}_{\mathrm{WE}} = \frac{1}{4}\angle\xi_{\mathrm{WE}}, \tag{9}$$

with

$$\xi_{\mathrm{WE}} = \omega\gamma\xi + (1-\omega)\xi_2^2, \qquad 0 < \omega < 1, \tag{10}$$

where

$$\xi_2 = \left(\kappa^z_{1111} - \kappa^z_{2222}\right) + j2\left(\kappa^z_{1112} + \kappa^z_{1222}\right). \tag{11}$$

The above expression reduces to the EML estimator [Eq. (6)] for $\omega = 1$. Similarly, the MaSSFOC estimator is obtained with $\omega = 1/2$. The approximate ML solution of Ref. [17] (similar to that for MaSSFOC) is also reached for $\omega = 1/3$.

The EML performance degrades when the source kurtosis sum tends to zero [16]. MaSSFOC overcomes this adverse effect, hence proving more robust in the presence of noise and impulsive interference. This method handles more than two signals in the same Jacobi-like fashion as the EML.

Finally, it should be noted that the HOS-based methods described in this section ignore any temporal structure in the processed signals so that spectrally white photocurrents could also be separated. If the data symbols transmitted by a single user are uncorrelated, such spectrally white photocurrents could arise when the photodectector output are sampled at rates as low as the symbol rate. Low sampling frequencies enable us to reduce the speed requirements, and hence the cost, of the digital signal processing used for WDM channel extraction and monitoring without sacrificing performance.

4. Quality Evaluation of WDM Transmissions

Inasmuch as WDM signal waveforms (and thus the eye diagrams) can be reconstructed in electrical domain, it is not always necessary to use optical methods to obtain WDM transmission quality information. Several reports have evaluated amplitude histograms, Q factors, and BER obtained by the electrical technique [18–20]. Reference [18] confirmed that the degradation of an optical signal due to noise, cross talk, and chromatic dispersion can be detected from amplitude histograms. However, it is difficult to evaluate SNR degradation quantitatively because the mark level peak in the histograms is not clear when the chromatic dispersion is large. Reference [19] defined a method to evaluate average Q factor from the eye diagrams and amplitude histograms. This method has sensitivity to both the SNR degradation and pulse distortion of optical signals influenced by chromatic dispersion in transmission fiber. Reference [20] introduced a technique to evaluate BER through the Q factor.

As described in Fig. 3, the average Q factor(Q_{avg}) is expressed by [19]

$$Q_{\text{avg}} = \frac{|\mu_{1,\text{avg}} - \mu_{0,\text{avg}}|}{\sigma_{1,\text{avg}} + \sigma_{0,\text{avg}}}, \tag{12}$$

where $\mu_{i,\text{avg}}$ and $\sigma_{i,\text{avg}}$ are the mean and standard deviation of the mark ($i = 1$) and space ($i = 0$) levels of all sampled data, respectively. μ is set to the difference of the mean of the mark and the space levels. Two thresholds are defined with coefficient α lying between 0 and 0.5:

$$D_{0,1} = \mu_{0,1} \pm \alpha\mu, \qquad 0 < \alpha < 0.5. \tag{13}$$

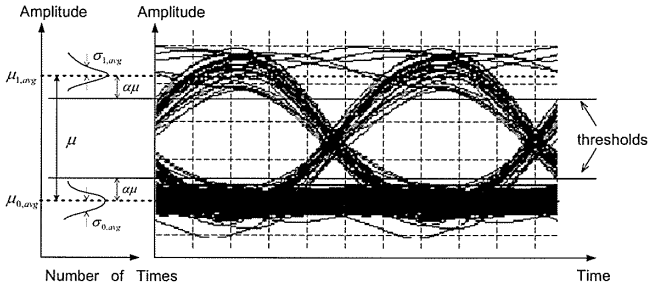

Fig. 3. Definition of averaged Q factor.

Histograms with amplitudes larger than $\mu_1 - \alpha\mu$ are regarded as mark level distributions, whereas histograms with amplitudes smaller than $\mu_0 + \alpha\mu$ are regarded as space level distributions. This masking process removes the cross-point data and improves measurement accuracy [21].

Although the exact probability density function for optical noise is not exactly Gaussian, a Gaussian approximation can lead to good BER estimates [20]:

$$\text{BER}(D) = \frac{1}{2}\left\{\text{erfc}\left(\frac{|\mu_1 - D|}{\sigma_1}\right) + \text{erfc}\left(\frac{|\mu_0 - D|}{\sigma_0}\right)\right\}, \tag{14}$$

where $\mu_{0,1}$ and $\sigma_{0,1}$ are the mean and standard deviation of the mark and space data rails, D is the decision level, and $\text{erfc}(x)$ is a form of the complementary error function given by

$$\text{erfc}(x) = \frac{1}{\sqrt{2\pi}}\int_x^\infty e^{-\beta^2/2}\,d\beta \approx \frac{1}{x\sqrt{2\pi}}e^{-x^2/2}, \tag{15}$$

where the approximation is nearly exact for $x > 3$.

In a high-performance optical transmission system, the BER is very low, traditional quality-monitoring methods need very long time to detect errors in transmission. Equations (12) and (14) provide fast and simple evaluations of WDM optical transmission quality with acceptable accuracy, as demonstrated in Section 5.

5. Simulations and Results

Illustrative experiments are carried out with the aid of the VPI simulation software, with the blind separation part implemented in MATLAB code.

First, we demonstrate the technique in a four-channel WDM setup. Four channels at wavelengths 1551.0, 1554.2, 1557.4, and 1560.6 nm (i.e., 3.2-nm separation), respectively, compose the WDM signal. The laser sources are modulated with Mach–Zehnder modulators by NRZ data from a pseudorandom binary sequence at a 10-Gbit/s bit rate.

As explained in Section 2, a small fraction of the transmitted WDM signal is diverted from the optical link into the monitoring system through an asymmetric splitter, and a fiber span of 50 km is included in front of the monitoring point. A block of this WDM signal fraction is then let into an optical loop. The signal block runs in the loop for four circles, and at the end of each circle the signal is coupled out of the optical loop. This means that the output of the optical loop are four blocks of repeated signals, with blocks spaced from one another by 128-bit all-zeros. These four signal blocks are sent to an optical signal processor, i.e., the adjustable WDA, sequentially. The adjustable WDA is synchronized with the optical loop, and is tuned to have different but unknown attenuation on each of the signal blocks. All these attenuated signal blocks are detected by a p-i-n photodetector, which generates the corresponding observed photocurrents shown in Fig. 4.

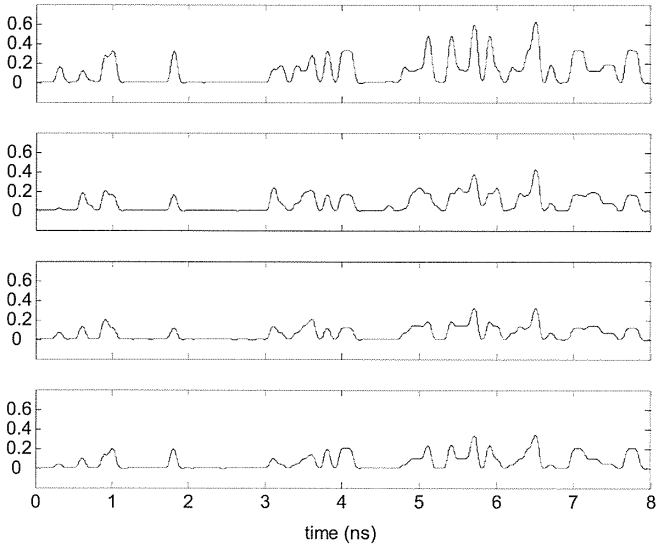

Fig. 4. Observed photocurrents in the four-channel experiment.

These electronic signals are then collected and processed by the HOS-based BSS methods described in Section 3 to obtain the signal separation. The normalized (i.e., zero-mean,

unit-power) channel data estimated by EML method are shown by the solid curves of Fig. 5. A block of 256 bits (32,768 samples) was processed, of which only a short portion is displayed in the figure for the sake of clarity. Observe the accuracy with which the estimated sequences approximate the actual transmitted data (dotted curves).

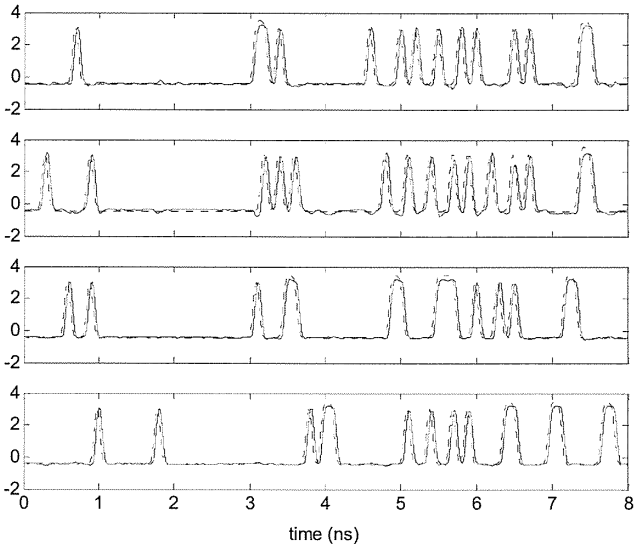

Fig. 5. Normalized data sequences in the four-channel experiment. Dotted curves, transmitted data. Solid curves, channel data estimated by the HOS-based BSS method (EML) from the photocurrents shown in Fig. 4.

Eye diagrams for each channel can be plotted from the separated waveforms, shown in Fig. 6; thus the average Q factors and BERs for each channel can be evaluated with the method introduced in Section 4.

Table 1 gives the average Q factors of all four channels, with the channel waveforms extracted by EML, MaSSFOC, and JADE method, respectively. The input power levels at the Mach–Zehnder modulators are tuned between -38 and -30 dBm, and the coefficient α in Eq. (13) is set to 0.1, 0.2, 0.3, 0.4, respectively. VPI software estimates BER through a Gaussian assumption [22], and the estimated average Q factors are presented in the tables as well. Comparison of the results shows that the EML method provides the best approach of Q_{avg} estimation to the industrial simulation software (VPI) with $\alpha = 0.3$. Figure 7 presents the average BER curves with the channel waveforms extracted by the EML, MaSSFOC, and JADE method, respectively, which shows that the EML method provides the best approach of BER estimation to the industrial simulation software (VPI), with the BER curves for each single channel shown in Fig. 8.

The proposed method is also capable of monitoring a higher number of channels. Figure 9 shows the observed photocurrents and separation results for an eight-channel WDM transmission with 1.6-nm channel spacing, under the general conditions for the four-channel experiment. The estimated BER curves for each channel are shown in Fig. 10(a), with the EML method, compared with the results from VPI software shown in Fig. 10(b).

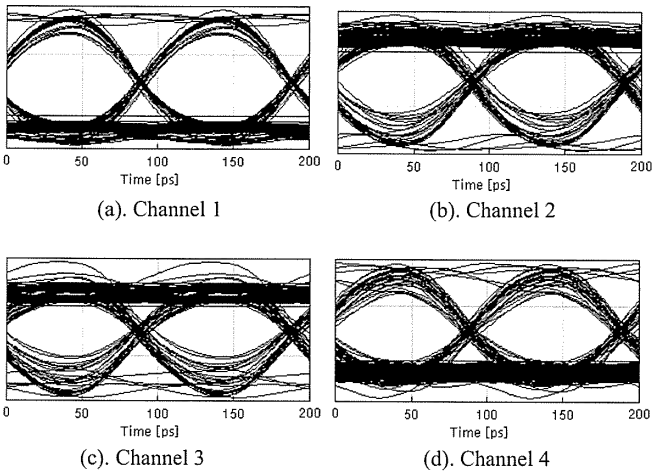

Fig. 6. Eye diagrams for the four-channel experiment.

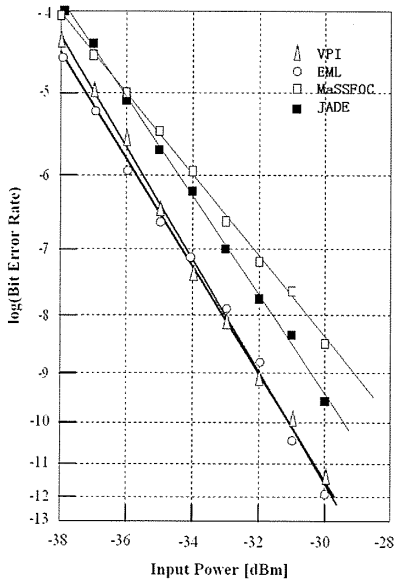

Fig. 7. Comparison of average BER curves from different methods.

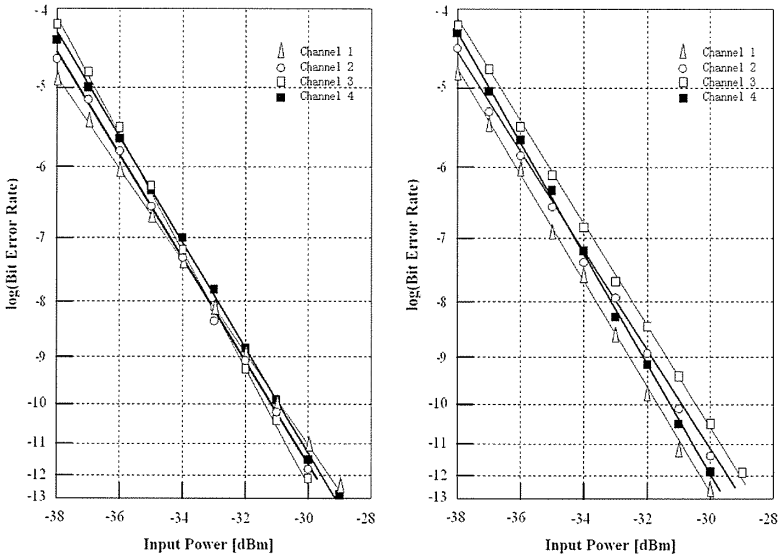

Fig. 8. BER versus input power curves. (a) EML method with the optical loop structure, (b) Gaussian assumption by VPI.

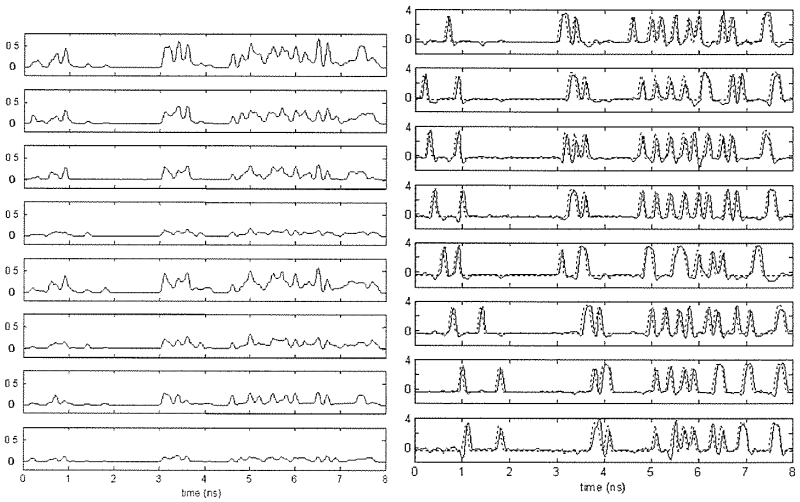

Fig. 9. (a) Observed photocurrents and (b) separation results for an eight-channel WDM transmission.

Table 1. Average Q Factors

Input power (dBm)	Average Q-factor			
	VPI	EML	MaSS	JADE
-38	3.7	4.3	4.1	3.4
-37	4.5	5.0	4.6	4.0
-36	5.2	5.6	5.1	4.5
-35	5.8	6.3	5.5	4.9
-34	6.3	6.9	6.0	5.4
-33	6.7	7.4	6.3	6.0
-32	7.3	8.0	6.4	6.4
-31	7.8	8.5	6.7	6.7
-30	8.5	9.2	6.9	7.1

(a). $\alpha = 0.1$

Input power (dBm)	Average Q-factor			
	VPI	EML	MaSS	JADE
-38	3.7	4.1	3.6	3.3
-37	4.5	4.8	4.1	4.0
-36	5.2	5.5	4.8	4.8
-35	5.8	6.0	5.2	5.2
-34	6.3	6.7	5.5	5.5
-33	6.7	7.2	5.7	5.8
-32	7.3	7.9	6.0	6.3
-31	7.8	8.5	6.2	6.7
-30	8.5	8.9	6.6	7.1

(b). $\alpha = 0.2$

Input power (dBm)	Average Q-factor			
	VPI	EML	MaSS	JADE
-38	3.7	3.9	3.4	3.1
-37	4.5	4.6	4.0	3.7
-36	5.2	5.3	4.5	4.2
-35	5.8	5.9	4.9	4.8
-34	6.3	6.3	5.2	5.2
-33	6.7	6.7	5.5	5.7
-32	7.3	7.2	5.8	6.3
-31	7.8	7.8	6.2	6.8
-30	8.5	8.6	6.6	7.5

(c). $\alpha = 0.3$

Input power (dBm)	Average Q-factor			
	VPI	EML	MaSS	JADE
-38	3.7	3.2	2.9	2.6
-37	4.5	3.8	3.4	3.1
-36	5.2	4.5	4.0	3.7
-35	5.8	5.1	4.4	4.2
-34	6.3	5.6	4.7	4.6
-33	6.7	6.0	5.0	5.1
-32	7.3	6.3	5.2	5.7
-31	7.8	6.9	5.3	6.1
-30	8.5	7.7	5.8	6.6

(d). $\alpha = 0.4$

6. Conclusions

We have proposed and demonstrated an optical transmission monitoring technique that uses blind signal separation (BSS) methods based on higher-order statistics (HOS), and an optical-loop structure. This technique shows reduced complexity, reformative cost efficiency, and improved performance.

The EML method provides an approximate optimal solution (in the maximum-likelihood sense) for the case of two channels, and entails a computational cost of $O\left(N^{5/2}L\right)$ when processing L-sample blocks of an N-channel WDM signal. For the signal distributions typically occurring in WDM monitoring, the method presents no undesired solutions. In addition, the case of spectrally white channels can also be handled, thus allowing beneficial reductions in the rates at which the photocurrents are sampled. Although the suggested procedure operates on signal blocks (batch processing), fast adaptive implementations can easily be designed as well [23].

Relative to previously proposed methods [6, 7], the optical-loop structure presented in this paper has cost-effective features, especially when WDM signals are composed of a large number of channels. We have found that a combination of the BSS method and quality measurement methods with associated thresholds that provide average Q-factor and BER estimates, with most of the processing in the electrical domain, to yield results close to those of traditional methods requiring expensive optical components, which simulated in an industrial simulation package (VPI).

It should be noted that the blind separation approach is not only useful in monitoring but also effectively demultiplexes the WDM signal. It appears that this feature has enormous potential for BSS in optical transmission systems.

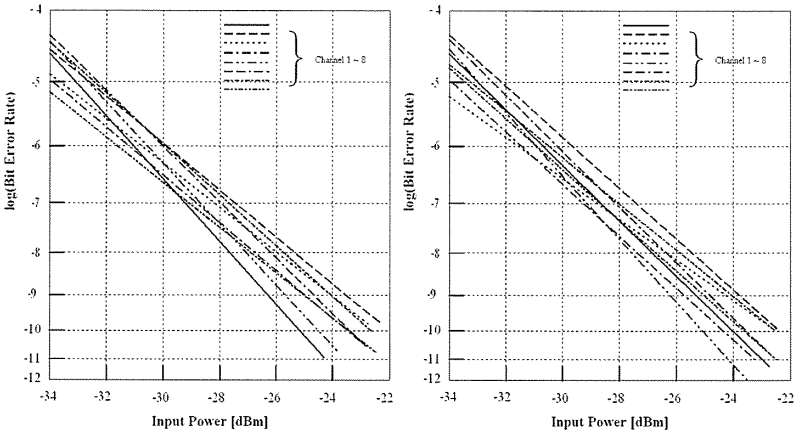

Fig. 10. BER versus input power curves. (a) EML method with the optical loop structure; (b) Gaussian assumption by VPI.

Acknowledgments

Y. Feng acknowledges scholarship awards from the Overseas Research Studentship (ORS) Committee and the University of Liverpool, UK. V. Zarzoso is in receipt of a Postdoctoral Research Fellowship from the Royal Academy of Engineering, UK. The authors acknowledge the assistance of VPIsystem.

References and Links

[1] K. Otsuka, T. Maki, Y. Sampei, Y. Tachikawa, N. Fukushima, and T. Chikama, "A high-performance optical spectrum monitor with high-speed measuring time for WDM optical networks," in *IOOC-ECOC97 IEE Conference Publication* (Edinburgh, UK, 1997), pp. 147–150.

[2] L. E. Nelson, S. T. Cundiff, and C. R. Giles, "Optical monitoring using data correlation for WDM systems," IEEE Photon. Technol. Lett. **7**, 1030–1032 (1998).

[3] M. P. H. van de Bergh, J. J. G. M. van der Tol, and H. J. S. Dorren, "A novel WDM monitoring method," Photon. Netw. Commun, **4**, 323–329 (1999).

[4] E. Tangdiongga, N. Calabretta, P. C. W. Sommen, and H. J. S. Dorren, "WDM monitoring technique using adaptive blind signal separation," IEEE Photon. Technol. Lett. **3**, 248–250 (2001).

[5] S. van Gerven and D. van Compernolle, "Signal separation by symmetric adaptive decorrelation: stability, convergence, and uniqueness," IEEE Trans. Signal Process. **7**, 1602–1612 (1995).

[6] Y. Feng, V. Zarzoso, and A. K. Nandi, "WDM monitoring through blind signal separation," in *Optical Fiber Communication Conference (OFC 2002)*, Vol. 70 of OSA Trends in Optics and Photonics Series (Optical Society of America, Washington, D.C., 2002), pp. 746–748.

[7] Y. Feng, V. Zarzoso, and A. K. Nandi, "WDM monitoring using blind signal separation based on higher-order statistics," in *Proceedings of DSP'02* (IEEE, New York, 2002), pp. 155–158.

[8] V. Zarzoso and A. K. Nandi, "Blind source separation," in *Blind Estimation Using Higher-Order Statistics*, A. K. Nandi, ed. (Kluwer Academic, Boston, 1999), pp. 167–252.

[9] A. Hyvärinen, J. Karhunen, and E. Oja, *Independent Components Analysis* (Wiley, New York, 2001).

[10] J. F. Cardoso and A. Souloumiac, "Blind beamforming for non-Gaussian signals," in IEE Proc. F (1993), pp.362–370.

[11] G. H. Golub and C. F. Van Loan, *Matrix Computations*, 2nd ed. (Johns Hopkins University, Baltimore, 1989).

[12] P. Comon, "Independent component analysis, a new concept?" Signal Process. **3**, 287–314 (1994).

[13] V. Zarzoso and A. K. Nandi, "Blind separation of independent sources for virtually any source probability density function," IEEE Trans. Signal Process., **9**, 2419–2432 (1999).
[14] F. Harroy and J. Lacoume, "Maximum likelihood estimators and Cramer-Rao bounds in source separation," Signal Process. **12**, 167–177 (1996).
[15] F. Hermann and A. K. Nandi, "Blind separation of linear instantaneous mixtures using closed-form estimators," Signal Process. **7**, 1537–1556 (2001).
[16] V. Zarzoso, F. Herrmann, and A. K. Nandi, "Weighted closed-form estimators for blind source separation," in *Proceeding s of 11 th IEEE Workshop on Statistical Signal Processing* (IEEE, New York, 2001), pp. 456–459.
[17] M. Ghogho, A. Swami, and T. Durrani, "Approximate maximum likelihood blind source separation with arbitrary source PDFs," in *Proceedings of 10th IEEE Workshop on Statistical Signal and Array Processing* (IEEE, New York, 2000), pp. 368–372.
[18] N. Hanik, A. Gladisch, C. Caspar, and B. Strebel, "Application of amplitude histograms to monitor performance of optical channels," Electron. Lett. **35**, 403–404 (1999).
[19] I. Shake, H. Takara, K. Uchiyama, and Y. Yamabayashi, "Quality monitoring of optical signals influenced by chromatic dispersion in a transmission fiber using averaged Q-factor evaluation," IEEE Photon. Technol. Lett. **4**, 385–387 (2001).
[20] N. S. Bergano, F. W. Kerfoot, and C. R. Davidson, "Margin measurements in optical amplifier systems," IEEE Photon. Technol. Lett. **3**, 304–306 (1993).
[21] I. Shake, H. Takara, S. Kawanishi, and Y. Yamabayashi, "Optical signal quality monitoring method based on optical sampling," Electro. Lett. **22**, 2152–2154 (1998).
[22] VPI Virtual Photonics, *VPI Photonic Modules Reference Manual* (2001), pp. 45–49.
[23] V. Zarzoso and A. K. Nandi, "Adaptive blind source separation for virtually any source probability density function," IEEE Trans. Signal Proc. **2**, 477–488 (2000).

INTERNATIONAL JOURNAL OF ADAPTIVE CONTROL AND SIGNAL PROCESSING
Int. J. Adapt. Control Signal Process. 2004; **18**:245–263 (DOI: 10.1002/acs.792)

Blind MIMO equalization with optimum delay using independent component analysis

Vicente Zarzoso*,† and Asoke K. Nandi

Department of Electrical Engineering and Electronics, The University of Liverpool, Brownlow Hill, Liverpool L69 3GJ, U.K.

SUMMARY

Blind space–time equalization of multiuser time-dispersive digital communication channels consists of recovering the users' simultaneously transmitted data free from the interference caused by each other and the propagation effects, without using training sequences. In scenarios composed of mutually independent non-Gaussian i.i.d. users' signals, independent component analysis (ICA) techniques based on higher-order statistics can be employed to refine the performance of conventional linear detectors, as recently shown in a code division multiple access environment (*Signal Process* 2002; **82**:417–431). This paper extends these results to the more general multi-input multi-output (MIMO) channel model, with the minimum mean square error (MMSE) as conventional equalization criterion. The time diversity introduced by the wideband multipath channel enables a reduction of the computational complexity of the ICA post-processing stage while further improving performance. In addition, the ICA-based detector can be tuned to extract each user's signal at the delay which provides the best MMSE. Experiments in a variety of simulation conditions demonstrate the benefits of ICA-assisted MIMO equalization. Copyright © 2004 John Wiley & Sons, Ltd.

KEY WORDS: blind source separation; blind space–time equalization; equalization delay; higher-order statistics; independent component analysis; MIMO channel; MMSE detection; multiuser communications; SIMO channel; second-order statistics

1. INTRODUCTION

Blind space–time equalization—motivation. Future wireless communication systems are expected to support a wide variety of high data rate multimedia applications [1, 2]. Increased transmission speeds combined with multipath propagation environments result in highly time-dispersive (or frequency selective) channels, which introduce severe intersymbol interference (ISI) in the received signal [3]. Novel multiple access techniques are currently being investigated whereby simultaneous transmission of different users in the same time–frequency slot is allowed (e.g.

*Correspondence to: Vicente Zarzoso, Department of Electrical Engineering and Electronics, The University of Liverpool, Brownlow Hill, Liverpool L69 3GJ, U.K.
†E-mail: vicente@liv.ac.uk

Contract/grant sponsor: Royal Academy of Engineering, U.K.

Received 11 August 2003
Revised 13 October 2003
Accepted 17 October 2003

spatial division multiple access, SDMA). This overlapped sharing of channel resources enhances bandwidth utilization at the expense of an increased level of co-channel interference (CCI). Signal processing techniques for space–time equalization aim at the cancellation of CCI and ISI at the receive antenna output, and the recovery of the transmitted users' data [4]. Traditionally, equalization is aided with the transmission of training or pilot sequences, which makes a poor use of the available bandwidth and is not feasible or practical in certain scenarios [5, 6]; hence the enormous research interest aroused by blind equalization techniques since the seminal works of References [7–11].

SIMO model. In the single-user case, the use of receivers with spatially separated multiple antenna elements and/or oversampling (i.e. sampling faster than the baud rate) leads to the single-input multiple-output (SIMO) signal model. Compared to the conventional single-output (SISO) case, SIMO systems exhibit two remarkable features [12–14]: first, non-minimum phase channels can be blindly identified using only second-order statistics (SOS); second, finite impulse response (FIR) channels can be perfectly equalized, in the noiseless case, using FIR filters.

MIMO model—ICA-based CCI-cancellation. The multiuser scenario is naturally described by the multiple-input multiple-output (MIMO) signal model. This model also arises in systems with multiple transmitter antennas (using, e.g. spatial multiplexing), even if just a single user is present. The MIMO extensions of SIMO equalization techniques are able to suppress ISI, resulting in a memoryless CCI-only cancellation problem [5, 15–17]. This latter can then be resolved using source separation techniques based on the finite alphabet or constant modulus properties of digital modulations [5,18–20]. Alternatively, the mutual statistical independence between the users' signals can be exploited through the use of independent component analysis (ICA) [21] based on higher-order statistics (HOS) [15, 22–24]. The main advantage of HOS-based ICA techniques is that, under mild conditions (typically, that at most one of the sources be Gaussian [23]), signal recovery is guaranteed regardless of the source constellation and spectral characteristics [24].

Channel identification and optimum-delay estimation. Blind multichannel equalization can be performed with (e.g. References [12, 13, 25]) or without (e.g. References [5, 26, 27]) previous channel identification. Channel identification-based equalization presents the main drawback that inaccuracies in the channel estimate have a detrimental effect on the signal detection stage. However, a channel estimate may prove useful in a variety of tasks such as power control, propagation characterization, or source localization and tracking. More importantly, knowledge of the channel structure makes it possible to select the equalization delay which yields optimum performance. The equalized signal mean square error (MSE) for a given delay depends on the corresponding column of the channel matrix, as shown in the exact MSE expression for the linear minimum mean square error (MMSE) equalizer [28] as well as in the approximated Cramér–Rao lower bound of Reference [29]. Even direct equalization methods require to estimate the channel response from the equalized output in order to perform optimum delay selection [27, 30]. In addition, Reference [27] needs to compute the equalizers for all delays before discerning the optimum solution. The iterative procedure described in Reference [31] avoids channel estimation, but its convergence to the optimum-delay equalizer is only conjectured and is not theoretically guaranteed; the procedure is also computationally expensive.

ICA-based detection. The exploitation of HOS through ICA proves useful in refining conventional linear detection, as recently demonstrated in Reference [1] in a particular code division multiple access (CDMA) model. The ICA refinement alleviates the negative impact of

channel estimation errors on the equalization performance. Similar results are obtained in Reference [32] in the more generic MIMO model, where it is shown that ICA-aided MMSE equalization outperforms the conventional MMSE receiver. Furthermore, the time redundancies of the MIMO model allow certain simplifications which yield considerable performance improvements with significant computational savings.

Contribution. The purpose of this paper is to elaborate on the findings of Reference [32]. We propose the use of ICA for the simultaneous extraction of the users' signals at their respective optimal MMSE equalization delays. The subsequent performance gains are achieved at only a modest increase in computational load relative to the conventional receiver. We also intend to carry out, through simulation, a more rigorous experimental analysis of ICA-assisted blind detection in MIMO digital communication systems.

Outline of the paper. Section 2 summarizes the signal model and mathematical preliminaries. Section 3 presents the theory behind ICA-aided optimum-delay equalization, which is the core of our contribution. An experimental study is reported in Section 4. The concluding remarks of Section 5 bring the paper to an end.

Notations. Vectors and matrices are denoted by boldface lowercase and uppercase symbols, respectively; $\mathbb{C}$ is the set of complex numbers; $\mathbf{I}_n$ refers to the $n \times n$ identity matrix; $(\cdot)^{\mathrm{T}}$, $(\cdot)^{\mathrm{H}}$, $(\cdot)^{-1}$ and $(\cdot)^{\dagger}$ indicate the transpose, Hermitian (conjugate-transpose), inverse and Moore-Penrose pseudoinverse matrix operators, respectively; $(\mathbf{a})_i$ is ith component of vector $\mathbf{a}$; $\|\mathbf{A}\|_{\mathrm{F}}^2 = \mathrm{trace}(\mathbf{A}\mathbf{A}^{\mathrm{H}}) = \mathrm{trace}(\mathbf{A}^{\mathrm{H}}\mathbf{A})$ denotes the Frobenius norm of matrix $\mathbf{A}$; $\mathbb{R}\mathrm{e}(\cdot)$ denotes the real part of its complex argument; $\mathrm{E}\{\cdot\}$ represents the mathematical expectation; $\otimes$ and $\odot$ stand for the Kronecker and elementwise product, respectively.

2. SIGNAL MODEL

Let us consider a multiuser communication system composed of

(A1) K users transmitting, at a known constant baud rate, zero-mean unit-variance mutually independent non-Gaussian i.i.d. data symbols $\mathbf{s}(n) = [s_1(n), \ldots, s_K(n)]^{\mathrm{T}} \in \mathbb{C}^K$,
(A2) a receiver with vector output $\mathbf{x}(n) = [x_1(n), \ldots, x_L(n)]^{\mathrm{T}} \in \mathbb{C}^L$,
(A3) FIR channels (including pulse-shaping and receive filter effects) spanning at most $M+1$ symbols, with matrix coefficients $\mathbf{H}(k) \in \mathbb{C}^{L\times K}$, $k = 0, 1, \ldots, M$, where the channel order M is assumed to be known and the channel taps fixed over the observation window,
(A4) zero-mean additive noise $\mathbf{v}(n) \in \mathbb{C}^L$ independent of the data sources.

Symbols n and k above represent discrete-time indices relative to the baud period. The receiver output components in (A2) are not necessarily associated with spatially separated physical devices. Since digital signals are cyclostationary, oversampling or fractionally spaced sampling (i.e. taking more than a sample per baud period) can induce extra 'virtual' sensors [12, 13]. The virtual channels are given by the phases of the physical channels, a phase corresponding to a baud-sampled sequence of the impulse response with a different time origin. Space–time processing operates on the spatial (physically separated sensors) as well as the temporal dimension [4, 5]. Although time- or space-only processing may suffice in theory, improved ISI-CCI suppression can be achieved by joint space–time processing [4]. Assumptions (A3) model block (or time-non-selective or slowly) fading channels, typical of low mobility systems, with small to moderate Doppler spread values.

Under the above assumptions, the MIMO model can be expressed as

$$\mathbf{x}(n) = \sum_{k=0}^{M} \mathbf{H}(k)\mathbf{s}(n-k) + \mathbf{v}(n) \tag{1}$$

Stacking N consecutive received signal vector samples leads to the matrix model

$$\mathbf{x}_n = \mathbf{H}\mathbf{s}_n + \mathbf{v}_n \tag{2}$$

with $\mathbf{s}_n = [\mathbf{s}(n)^{\mathrm{T}}, \mathbf{s}(n-1)^{\mathrm{T}}, \ldots, \mathbf{s}(n-M-N+1)^{\mathrm{T}}]^{\mathrm{T}} \in \mathbb{C}^{K(M+N)}$

$$\mathbf{H} = \begin{bmatrix} \mathbf{H}(0) & \cdots & \mathbf{H}(M) & 0 & \cdots & 0 \\ 0 & \mathbf{H}(0) & \cdots & \mathbf{H}(M) & \cdots & 0 \\ \vdots & \ddots & \ddots & \ddots & \ddots & \vdots \\ 0 & \ldots & 0 & \mathbf{H}(0) & \cdots & \mathbf{H}(M) \end{bmatrix} \tag{3}$$

$\mathbf{x}_n = [\mathbf{x}(n)^{\mathrm{T}}, \mathbf{x}(n-1)^{\mathrm{T}}, \ldots, \mathbf{x}(n-N+1)^{\mathrm{T}}]^{\mathrm{T}} \in \mathbb{C}^{LN}$, and analogous definition for $\mathbf{v}_n$. For convenience, we call $P = LN$, $C = M + N$, and $D = KC$.

The objective of blind MIMO equalization is to estimate the source signals $\mathbf{s}(n)$ from the only observation of the receiving sensor output $\mathbf{x}(n)$. This process involves ISI cancellation (time equalization) and CCI suppression (space equalization). These tasks can be performed by first identifying the channel taps

$$\underline{\mathbf{H}} = [\mathbf{H}(0), \mathbf{H}(1), \ldots, \mathbf{H}(M)] \tag{4}$$

which are then 'inverted' to estimate the sources. The block-Toeplitz channel matrix $\mathbf{H} \in \mathbb{C}^{P \times D}$ in Equation (2) must be full column rank. An obvious necessary condition is that $L > K$: the number of sensors must be strictly higher than the number of sources, i.e. sufficient spatio-temporal diversity must be available; also, $N \geqslant KM/(L-K)$, which sets a lower bound on the equalizer length. A sufficient condition for the invertibility of $\mathbf{H}$ is that the subchannels be coprime, that is, that they do not share any common zeros [12]. More elaborate sufficient conditions are given in Reference [33].

Even if the channel matrix is invertible, inherent indeterminacies exist. Without any further prior knowledge on the sources or the mixing system besides assumptions (A1) and (A3), the channel matrix taps $\mathbf{H}(k)$ can at best be identified up to a common post-multiplicative factor $\mathbf{\Lambda\Gamma}$, where $\mathbf{\Gamma} \in \mathbb{C}^{K \times K}$ is a permutation matrix and $\mathbf{\Lambda} \in \mathbb{C}^{K \times K}$ a non-singular diagonal matrix with unit-norm diagonal elements. These phase and permutation indeterminacies are unavoidable but admissible ambiguities in blind estimation.

In the sequel, it is assumed that the channel matrix $\mathbf{H}$ (or, equivalently, the channel tap matrix $\underline{\mathbf{H}}$) has been estimated through a suitable blind MIMO identification method (as those of, e.g. References [5, 16, 17, 32]). Our primary concern is the estimation (i.e. detection or equalization) of the source signals $\mathbf{s}$ from the sensor output $\mathbf{x}$ by using the identified channel. In blind space–time equalization techniques based on previous channel identification, ISI-CCI suppression is implicitly carried out during channel estimation, and actually takes effect at the detection stage.

3. ICA-AIDED DETECTION

3.1. Linear detection

Even if the channel is perfectly known, the estimation of the source signals in a noisy model like (1)–(2) is not a trivial task. The maximum likelihood sequence estimator is the optimal detector, but its computational load can be prohibitive in scenarios involving a large number of users and highly dispersive channels [3]. Trading off complexity for performance, linear receivers are based on the estimation of a linear transformation $\mathbf{G} \in \mathbb{C}^{P \times D}$ fulfilling certain (sub)optimality criterion; data are then detected as $\hat{\mathbf{s}}_n = \mathbf{G}^{\mathrm{H}}\mathbf{x}_n$. The zero forcing (ZF) detector aims at the joint minimization of ISI and CCI in the absence of noise, and can thus be expressed as the least-squares problem

$$\mathbf{G}_{\mathrm{ZF}} = \arg \min_{\mathbf{G}} \|\mathbf{G}^{\mathrm{H}}\mathbf{H} - \mathbf{I}_D\|_{\mathrm{F}}^2 \tag{5}$$

The solution to (5) is readily computed as $\mathbf{G}_{\mathrm{ZF}} = (\mathbf{H}\mathbf{H}^{\mathrm{H}})^{-1}\mathbf{H} = (\mathbf{H}^{\dagger})^{\mathrm{H}}$. The ZF detector can lead to severe noise amplification in noisy scenarios. This drawback is avoided by the minimum mean square error (MMSE) equalizer

$$\mathbf{G}_{\mathrm{MMSE}} = \arg \min_{\mathbf{G}} \mathrm{E}\{\|\mathbf{G}^{\mathrm{H}}\mathbf{x}_n - \mathbf{s}_n\|^2\} \tag{6}$$

with closed-form solution $\mathbf{G}_{\mathrm{MMSE}} = \mathbf{R}_x^{-1}\mathbf{H}$, where $\mathbf{R}_x = \mathrm{E}\{\mathbf{x}\mathbf{x}^{\mathrm{H}}\}$ represents the sensor-output covariance matrix. Due to its enhanced properties at low signal-to-noise ratio (SNR), we adhere to the MMSE detector in the following. The development is analogous for ZF equalization.

3.2. ICA refinement

Imprecisions, e.g. due to finite sample size, in the estimation of the channel matrix or the sensor covariance matrix have a negative impact on the detection of the transmitted data symbols. To alleviate this detrimental effect, the higher-order statistical independence of the users' signals can be exploited. Under the spatio-temporal independence assumption of (A1), model (2) corresponds to a problem of blind separation of independent sources in instantaneous linear mixtures, which can be solved with the statistical tool of ICA based on HOS [21]. From this perspective, the source estimation can be carried out without previous channel identification by applying an ICA method directly and then using a simple algorithm to identify and group each user's delays [24, 34, 35]. Although this fully blind ICA approach is conceptually simple, the computational complexity of separating $D = K(M + N)$ independent components can become excessive, even with a moderate number of users, in systems with long delay spreads as a result of high data rates [24].

The rationale behind ICA-assisted detection consists of taking advantage of the available channel estimate as an initial point in the ICA search. Two main benefits can be derived from this refinement. Firstly, since conventional detection (Equations (5)–(6)) only makes use (implicitly) of SOS, the exploitation of HOS by ICA is expected to mitigate performance drops caused by estimation errors at the channel identification stage. Secondly, if these channel identification errors are moderate, the initialization provided by the channel estimate may already be quite close to the ICA solution, thus decreasing the convergence time and computational complexity of the ICA post-processing block. The idea of ICA-refined detection was originally proposed in Reference [1] in the context of a DS-CDMA signal model. In

Reference [32], the ICA-based MMSE refinement was extended to the more general MIMO model, and is reproduced below for the sake of completeness.

Consider the whitened sensor output $\mathbf{z}_n = \mathbf{W}\mathbf{x}_n$, in which the whitening matrix $\mathbf{W} \in \mathbb{C}^{D\times P}$ constrains $\mathbf{R}_z = \mathbf{I}_D$. Matrix $\mathbf{W}$ can easily be computed from the eigenvalue decomposition (EVD) of $\mathbf{R}_x$, and involves second-order space–time decorrelation, power normalization and projection on the signal subspace. The MMSE estimate of $\mathbf{s}_n$ accepts the equivalent expression $\hat{\mathbf{s}}_n = \tilde{\mathbf{G}}^{\mathrm{H}}\mathbf{z}_n$, with

$$\tilde{\mathbf{G}} = \mathbf{W}\hat{\mathbf{H}} \tag{7}$$

In the noiseless case, detection matrix $\tilde{\mathbf{G}}$ is unitary. Hence, the whitened outputs can be regarded as a spatio-temporal unitary linear mixture of the users' data. To exploit the source statistical independence, an ICA method can operate on the whitened signals $\mathbf{z}_n$ with a separating matrix initialized at the conventional MMSE detection matrix $\tilde{\mathbf{G}}$. Final detection is then performed with the separating matrix $\hat{\mathbf{G}}$ provided by the ICA algorithm at convergence. The use of HOS constrains the users' data to be non-Gaussian (Assumption (A1)), which is verified by most digital modulations of practical significance. We select the fixed-point FastICA algorithm based on kurtosis optimization [21, 36] for its robustness and rapid (cubic) convergence properties. Assume that T consecutive whitened column vectors are stored in matrix $\mathbf{Z} = [\mathbf{z}_0, \mathbf{z}_1, \ldots, \mathbf{z}_{T-1}] \in \mathbb{C}^{D\times T}$. The FastICA algorithm can be outlined as follows [1, 21, 36]:

1. Initialize $\hat{\mathbf{G}}_0$ as the projection of $\tilde{\mathbf{G}}$ onto the set of unitary matrices.
2. For $k \geqslant 0$, repeat steps below until convergence.
3. $\hat{\mathbf{S}}_k = \hat{\mathbf{G}}_k^{\mathrm{H}}\mathbf{Z}$.
4. Update $\hat{\mathbf{G}}_{k+1} = \frac{1}{T}\mathbf{Z}(|\hat{\mathbf{S}}_k|^2 \odot \hat{\mathbf{S}}_k)^{\mathrm{H}} - \gamma\hat{\mathbf{G}}_k$.
5. Symmetric decorrelation $\hat{\mathbf{G}}_{k+1} \leftarrow \hat{\mathbf{G}}_{k+1}(\hat{\mathbf{G}}_{k+1}^{\mathrm{H}}\hat{\mathbf{G}}_{k+1})^{-1/2}$.

In Step 4, $\gamma = 3$ for real-valued sources (e.g. BPSK modulations) and $\gamma = 2$ for complex-valued sources. The orthogonal projection on the set of unitary matrices of Steps 1 and 5 admits an efficient implementation in terms of the singular value decomposition (SVD) $\hat{\mathbf{G}} = \mathbf{U}\boldsymbol{\Sigma}\mathbf{V}^{\mathrm{H}}$ as $\hat{\mathbf{G}} \leftarrow \mathbf{U}\mathbf{V}^{\mathrm{H}}$. As a statistically significant termination criterion we choose

$$\left|\frac{1}{D}\mathrm{trace}(|\hat{\mathbf{G}}_{k+1}^{\mathrm{H}}\hat{\mathbf{G}}_k|) - 1\right| < \frac{10^{-3}}{T} \tag{8}$$

That is, iterations are stopped when the column vectors of $\hat{\mathbf{G}}_{k+1}$ and $\hat{\mathbf{G}}_k$ lie in directions which are sufficiently close (in terms of a sample-size based threshold). In preliminary experiments, less than $2D$ iterations are typically required for convergence in high SNR environments and sufficient sample size. For low SNR or insufficient sample length, the algorithm may not converge, so the above maximum number of iterations is set as an additional termination test. Excluding the symmetric decorrelation step, the computational complexity of the FastICA algorithm is of order $O(DT)$ floating point operations (flops) per column of $\hat{\mathbf{G}}$ per iteration.

Note that the authors of Reference [1] were involved in extracting the signal of a single user of interest, whereas we aim at the simultaneous demodulation of all existing users (including all the spatially multiplexed data substreams of each user, if multiple transmit antennas are employed). Furthermore, the parameterization in the CDMA model of Reference [1] only accounts for channels with short delay spreads (more precisely, a delay spread of less than half the symbol period is considered in that reference). By contrast, the more general MIMO model of Equations (1)–(2) enables a more realistic characterization of wideband channels with longer

delay spreads.[‡] More importantly, Reference [1] extracts the user-of-interest's signal at a fixed delay. However, long delay spreads make it possible to extract the users' data at alternative delays, which can lead to potential performance improvements. Unlike fully blind ICA, where no control over the extracted delay is possible, we will see next that ICA-based MIMO equalization can be fine-tuned to carry out detection at the best delay for each user, thus improving performance while reducing computational cost.

3.3. Optimal delay selection

The previous sections have reviewed linear detectors that estimate all the components of the source vector $\mathbf{s}_n$ simultaneously, and how this conventional detection can be enhanced with the use of ICA. However, most of the detected signals are redundant, since $C = M + N$ time-shifted versions of each of the K users are recovered, whereas a single time delay suffices in practice. The time redundancy introduced by the multipath channel in the MIMO model (2) enables the choice of the equalization delay providing the best MMSE performance for each user. This choice is simplified thanks to the channel matrix estimate obtained in the blind identification stage.

The MMSE detector of the ith source signal, $1 \leqslant i \leqslant K$, with delay $0 \leqslant d \leqslant (C-1)$, is given by the corresponding column of $\mathbf{G}_{\mathrm{MMSE}}$:

$$\mathbf{G}_{i,d} = \mathbf{R}_x^{-1}\mathbf{h}_{i,d} \tag{9}$$

in which $\mathbf{h}_{i,d}$ denotes the $(Kd + i)$th column vector of channel matrix $\mathbf{H}$. The resulting MMSE can be obtained analytically as [28]

$$\mathrm{MMSE}_{i,d} = \mathrm{E}\{|\hat{s}_i(n-d) - s_i(n-d)|^2\} = 1 - \mathbf{h}_{i,d}^{\mathrm{H}}\mathbf{R}_x^{-1}\mathbf{h}_{i,d} \tag{10}$$

Optimum MMSE equalization for the ith user is achieved at delay

$$d_i = \arg\min_d \mathrm{MMSE}_{i,d} \tag{11}$$

Hence, from the available estimate of the channel matrix and the sensor output covariance matrix, it is possible to compute the equalizer that will detect each source signal with the lowest MMSE.

In practice, estimation errors caused by finite sample length may produce negative values of MMSE in Equation (10). However, in our experience the shape of the MMSE performance variation as a function of the equalization delay as well as the position of the optimum delay do not suffer significant changes relative to the theoretical solution.

3.4. Simplified ICA refinement

Once the optimal delay of each source has been selected, the corresponding columns of the estimated channel can be used to initalize the ICA post-processing stage. Let those columns be stored in matrix $\hat{\mathbf{H}}_K = [\mathbf{h}_{1,d_1}, \mathbf{h}_{2,d_2}, \ldots, \mathbf{h}_{K,d_K}]$. Then

$$\tilde{\mathbf{G}}_K = \mathbf{W}\hat{\mathbf{H}}_K \tag{12}$$

[‡] More details about the differences and relationships between channel models based on physical multipath parameters and on the channel impulse response can be found in Reference [4].

is the associated MMSE detector, which can serve as starting point for the ICA refinement (with the obvious modification of K for D in termination test (8)). In this manner, the ICA algorithm searches only for the K independent components associated with the users' signals at their respective optimum MMSE delay. This search for the optimum-delay components not only improves performance, but also leads to a reduction in computational complexity by a factor of C per iteration, which can be remarkable in highly time dispersive channels. In addition, since fewer independent components are sought, the ICA algorithm would also be expected to take fewer iterations to converge. These benefits will be put to the test in the experiments of Section 4.

This simplified MMSE-ICA detection scheme, which arises from the time redundancy induced by wideband multipath propagation, was originally proposed in Reference [32] for zero-delay equalization only. Herein, we improve on the original definition by allowing arbitrary delays and, in particular, those providing optimum MMSE performance for each user transmission.

3.5. Switching

The ICA refinement may converge to a solution far from optimal, worsening rather than improving the results of the conventional detector. Experimental results indicate that this undesirable outcome only occurs in low SNR scenarios or when processing short sample sizes. At low SNR, noise becomes dominant relative to the users' data in signal model (1)–(2). As a result, ICA will 'perceive' the noise as the actual sources, and thus will seek independence among the noise components. This misguided search will most probably yield a wrong equalization solution. Erroneous HOS estimation due to short observation windows can cause analogous adverse effects in the ICA refinement.

To avoid this degeneracy, a 'branch switching' criterion can be proposed along the lines of Reference [1]. By virtue of this criterion, the MMSE-ICA solution is deemed as favourable when the prior information provided by the conventional receiver is fairly preserved at the output of the ICA stage, that is, when the initial and final separating vectors (the columns of $\hat{\mathbf{G}}_0$ and $\hat{\mathbf{G}}$, respectively) are sufficiently correlated. This criterion can easily be extended to the MIMO model by switching to the MMSE-ICA solution of Section 3.2 whenever [32]

$$\xi \triangleq \frac{1}{D}\mathbb{R}\mathrm{e}(\mathrm{trace}(\hat{\mathbf{G}}^{\mathrm{H}}\hat{\mathbf{G}}_0)) > \tau \tag{13}$$

where $\tau \in]0,1[$ is a suitably selected threshold (e.g. Reference [1] chooses $\tau = 0.8$); the conventional MMSE detector is otherwise employed. Using K instead of D in the above expression, the switching rule is readily made applicable to the simplified MMSE-ICA solution of Section 3.4.

The usefulness of this switching strategy is arguable if the accuracy of the prior information acquired before detection (e.g. the proximity between the true and the identified channel) is poor. In such an event, the proposed switching could wrongly rule out ICA solutions that are actually advantageous compared to those of the linear MMSE receiver, which would be operating on erroneous information. This switching rule is tested in the simulations of next section.

4. EXPERIMENTAL RESULTS AND ANALYSIS

This section evaluates the comparative performance of the ICA-assisted equalizers under a variety of simulation conditions, and illustrates some points of the previous theoretical exposition. A communication system composed of $K = 5$ simultaneous QPSK-modulated users is simulated in a frequency-selective block fading channel introducing ISI from a maximum of $M = 4$ consecutive baud periods. The channel filter taps are randomly drawn from a complex Gaussian distribution and hence model (up to the pulse-shaping and receive filters) a Rayleigh propagation environment. A spatio-temporal oversampling level of $L = 10$ and a smoothing factor of $N = 5$ result in a 50×45 channel matrix $\mathbf{H}$. Additive white Gaussian noise with covariance matrix $\mathbf{R}_v = \sigma^2 \mathbf{I}_L$ is present at the sensor output; the SNR is given by

$$\mathrm{SNR} = \frac{\mathrm{trace}(\underline{\mathbf{H}}\,\underline{\mathbf{H}}^{\mathrm{H}})}{\sigma^2 L} \tag{14}$$

Equalization performance is measured by the signal mean square error (SMSE)

$$\mathrm{SMSE} = \frac{1}{K} \sum_{i=1}^{K} \mathrm{E}\{|\hat{s}_i(n - \hat{d}_i) - s_i(n - \hat{d}_i)|^2\} \tag{15}$$

where $\hat{d}_i$ represents the equalization delay selected for the ith user, which is obtained by the optimality criteria of Section 3.3 from the channel and covariance matrix estimates. Similarly, the channel identification accuracy can be assessed with the channel normalized mean square error (CMSE)

$$\mathrm{CMSE} = \frac{\|\hat{\underline{\mathbf{H}}} - \underline{\mathbf{H}}\|_{\mathrm{F}}^2}{\|\underline{\mathbf{H}}\|_{\mathrm{F}}^2} \tag{16}$$

where $\hat{\underline{\mathbf{H}}}$ is the estimated channel tap matrix. Performance parameters are averaged over v independent Monte Carlo (MC) iterations, with $vN_d \geqslant 10^5$, where N_d is the observation length in baud periods. As a quality index for the optimum-delay estimation performance we define the delay root mean square error (DRMSE)

$$\mathrm{DRMSE} = \sqrt{\frac{1}{v} \sum_{j=1}^{v} \frac{1}{K} \sum_{i=1}^{K} (\hat{d}_i^{(j)} - d_i)^2} \tag{17}$$

where $\hat{d}_i^{(j)}$ represents the ith-source delay estimate at MC iteration j, and theoretical values d_i are obtained from Equation (11) by plugging the true channel and covariance matrices in Equation (10).

4.1. Perfect channel knowledge

We first consider the scenario where the channel is assumed to be perfectly known or estimated, i.e. CMSE = 0. As a result, all errors in the MMSE equalizer are due exclusively to the finite-sample estimation of the sensor covariance matrix (or, equivalently in this case, of the noise variance), which is computed from N_d observed symbol periods. For instance, this scenario could simulate a training-based channel estimation preamble during transmission.

Performance vs sample size. Figure 1 shows the performance of the conventional MMSE, the MMSE-ICA and the simplified MMSE-ICA receivers against the sample size N_d, for SNR = 20 dB and a fixed channel matrix with condition number around 100. The ICA post-processing has difficulties to converge at low sample size, as shown by the number of FastICA iterations in Figure 2. A performance degradation is consequently observed when the switching criterion of

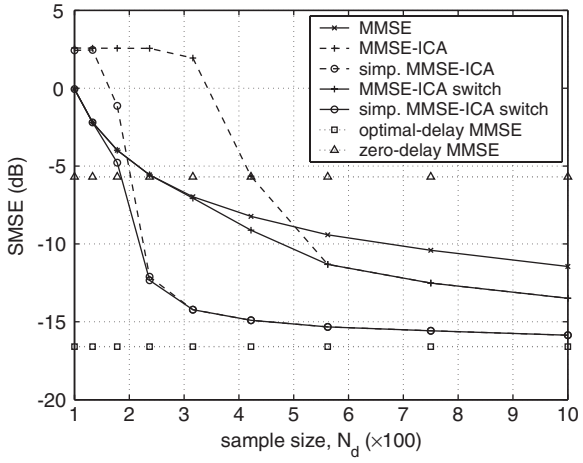

Figure 1. Equalization performance vs sample size, with CMSE = 0, SNR = 20 dB.

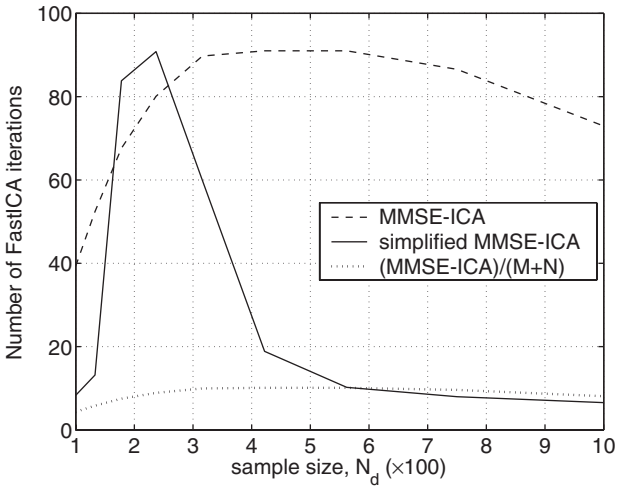

Figure 2. Number of FastICA iterations vs sample size in the simulation of Figure 1.

Section 3.5 is not implemented. However, as N_d gets sufficiently high the ICA receivers outperform the conventional equalizer, with the simplified MMSE-ICA obtaining the most efficient performance and approaching faster the theoretical lower bound. The iteration count of the latter then falls below $1/C$ times that of the full MMSE-ICA (Figure 2). According to Section 3.2, this means a reduction in flops by a factor of C^2.

Equalization delay. Figure 1 also compares the theoretical MMSE for the optimal- and the zero-delay equalizers, which emphasizes the gain that can be achieved by using the former. Illustrating this gain as well, Figure 3 plots the MMSE against the equalization delay for each source. The estimated optimum delay appears consistent and asymptotically unbiased, as shown in Figure 4. However, to keep the delay estimation accuracy more samples are needed as the SNR increases.

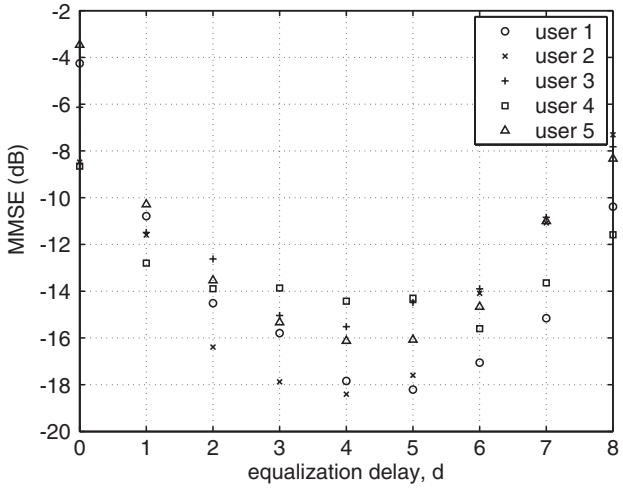

Figure 3. Theoretical MMSE performance vs equalization delay in the simulation conditions of Figure 1.

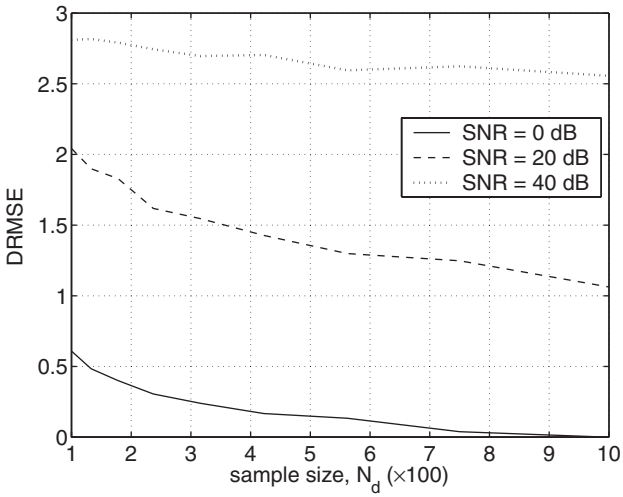

Figure 4. Optimum-delay estimation performance in the experiment of Figure 1, for several SNRs.

Switching threshold. In a bid to shed some light on the choice of the switching threshold τ, Figure 5 displays the loci of the average performance gain introduced by the ICA-aided detectors relative to the conventional MMSE, and their respective average correlation coefficient ξ, for various SNRs (0 , 20, 40, 60 dB, ∞). The plots indicate that $\tau \approx 0.8$ and $\tau \approx 0.6$ are good threshold choices for the MMSE-ICA and the simplified MMSE-ICA equalizer, respectively. In practice, the exact figures do not seem too critical. The 'switch' curves of Figure 1 were obtained with $\tau = 0.8$ for both ICA detectors, and such value has provided satisfactory results in all our experiments in a variety of different scenarios.

Performance vs SNR. The sensor covariance matrix estimation errors due to finite sample size cause interference flooring in the MMSE detector performance at high SNR, as soon as the

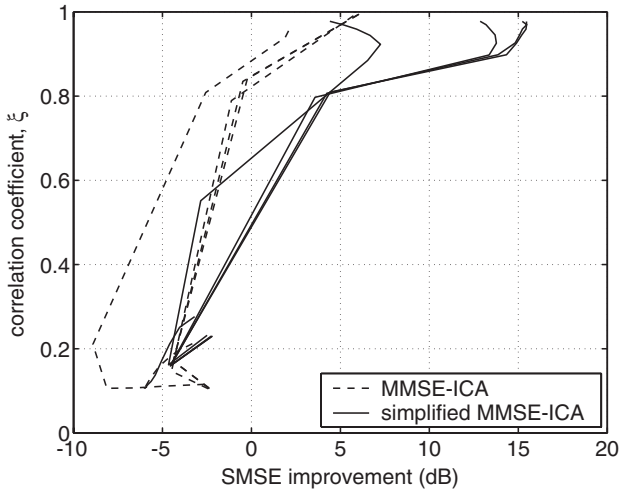

Figure 5. ICA performance gain vs correlation coefficient ξ for the scenario of Figure 1 and different SNRs.

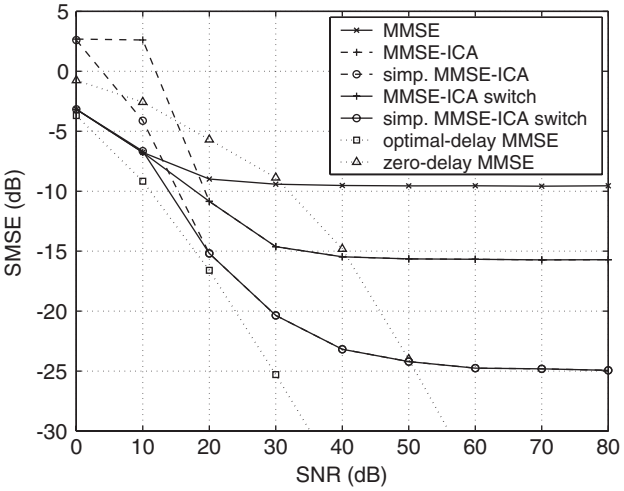

Figure 6. Equalization performance vs SNR, with CMSE $= 0$, $N_d = 500$.

sampling error overcomes the additive noise present at the sensor output. The success of ICA-based post-detection in tackling this adverse phenomenon is illustrated in Figure 6, which shows the performance of the different equalization schemes against the additive noise power, with an observation window of $N_d = 500$ baud periods and the same general conditions as above. MMSE-ICA alleviates the MMSE performance flooring by about 6 dB, whereas the simplified MMSE-ICA receiver provides a striking improvement of over 15 dB. Equivalently, the ICA detectors require about 3 and 12 times less samples, respectively, than the MMSE to achieve the same performance at high SNR.

Figure 7 shows that in low noise the MMSE-ICA actually converges in less iterations than the simplified MMSE-ICA. Hence, the ratio of C between both iteration counts seems to occur at moderate SNR levels only. On the other hand, Figure 8 illustrates again that more samples are needed to maintain the optimum-delay estimation quality as the SNR increases. This outcome, also observed in Figure 4, is closely related to the flooring effect commented above.

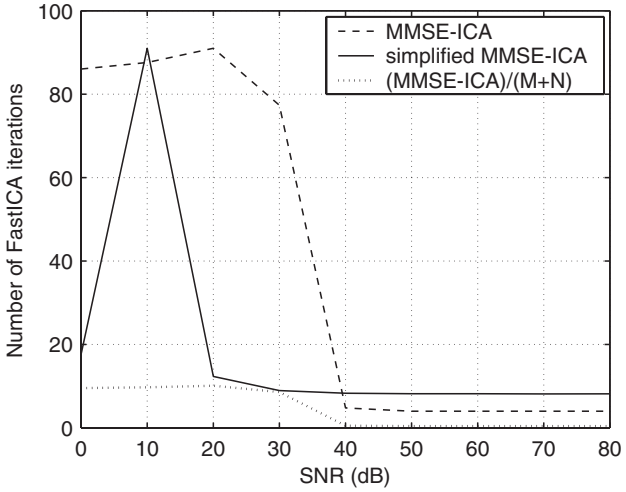

Figure 7. Number of FastICA iterations vs SNR in the experiment of Figure 6.

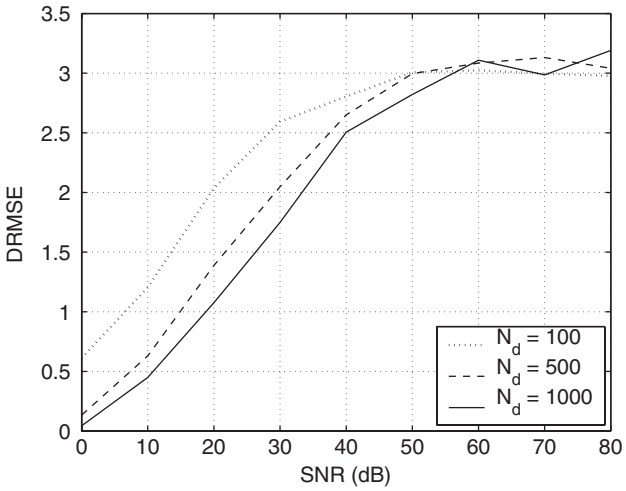

Figure 8. Optimum-delay estimation performance for the simulation conditions of Figure 6 and various sample lengths.

4.2. Blindly identified channel

In the experiments that follow, the channel is estimated from the sensor data using a suitable blind MIMO identification method. We choose the extension of the SIMO algorithm of Reference [12] followed by an ICA-based CCI-cancellation step, as explained in References [16, 24]. System parameters such as the channel order and the signal-subspace dimension are assumed as known.

Performance vs sample size. Figure 9 shows the detectors' performance as a function of the observed window size, when the sensor output SNR is 30 dB. The ICA-assisted equalizers

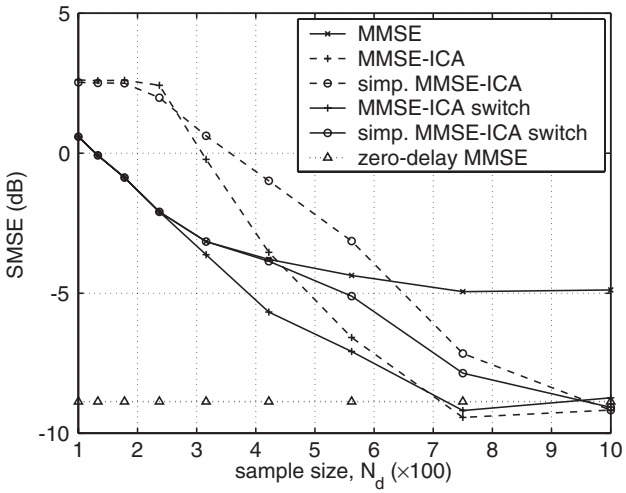

Figure 9. Blind equalization performance vs sample size, SNR = 30 dB.

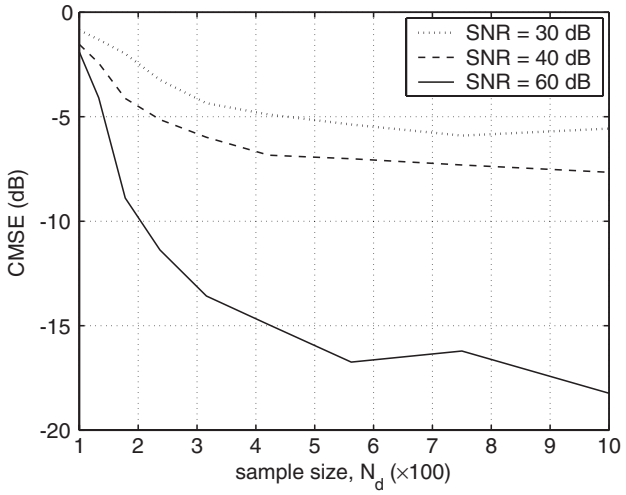

Figure 10. Blind channel identification performance for the simulation conditions of Figure 9 and several SNRs.

require around 500 samples to improve the conventional detector. This minimum sample length reduces for higher SNR (results for the noiseless case under similar simulation conditions can be found in Reference [32]). The theoretical optimal-delay MMSE lies around −25 dB, which the ICA methods are unable to reach due to an erroneous delay estimation (dashed line of Figure 11). Channel identification errors now join covariance matrix imprecisions in hindering an accurate delay detection. Indeed, the CMSE reaches only around −6 dB from about 700 samples in this simulation (dotted line in Figure 10). Despite the higher iteration count shown by the simplified MMSE-ICA in Figure 12, further experiments demonstrate that for high N_d and SNR both methods require approximately the same number of FastICA iterations.

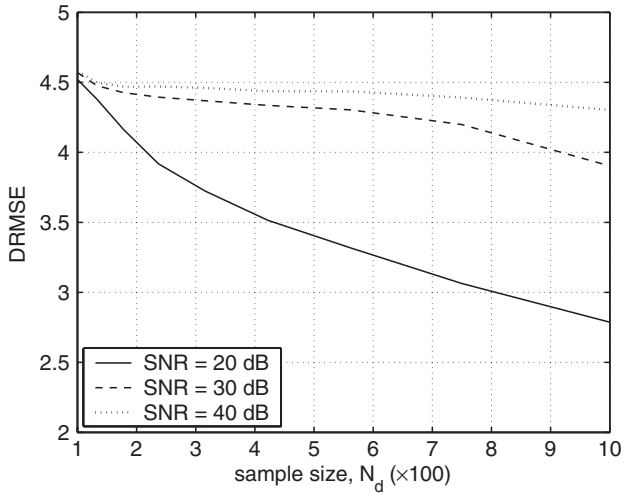

Figure 11. Delay estimation performance for the simulation conditions of Figure 9 and different SNRs.

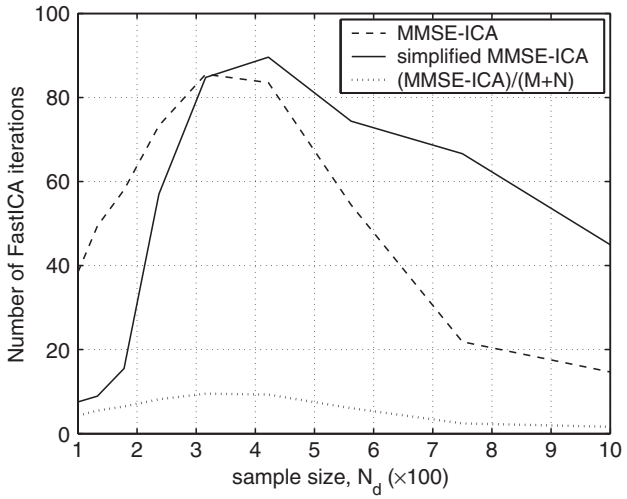

Figure 12. Number of FastICA iterations vs sample size in the simulation of Figure 9.

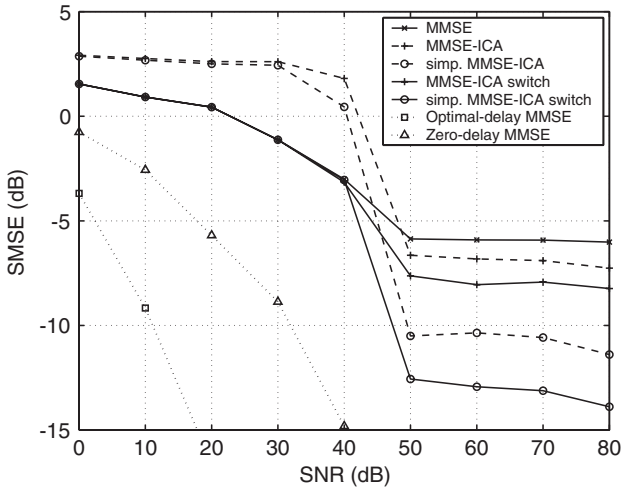

Figure 13. Blind equalization performance vs SNR, $N_d = 200$.

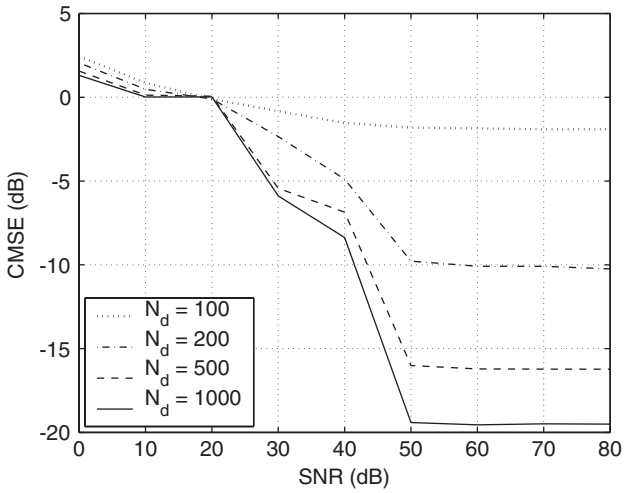

Figure 14. Blind channel identification performance for the simulation conditions of Figure 13 and various sample lengths.

Performance vs SNR. Figure 13 indicates that the ICA receivers outperform the MMSE detector with as few as $N_d = 200$ observed symbol periods, for a sensor output SNR above 40 dB. The benefits of the switching scheme can also be observed above that SNR value. The obtained CMSE at several sample lengths is shown in Figure 14. Delay estimation only accurate for sufficient window sizes at low SNR (Figure 15), as anticipated in the experiments with perfect channel knowledge. FastICA iteration counts for this simulation are displayed in Figure 16. The simplified MMSE-ICA method requires fewer iterations than the MMSE-ICA over

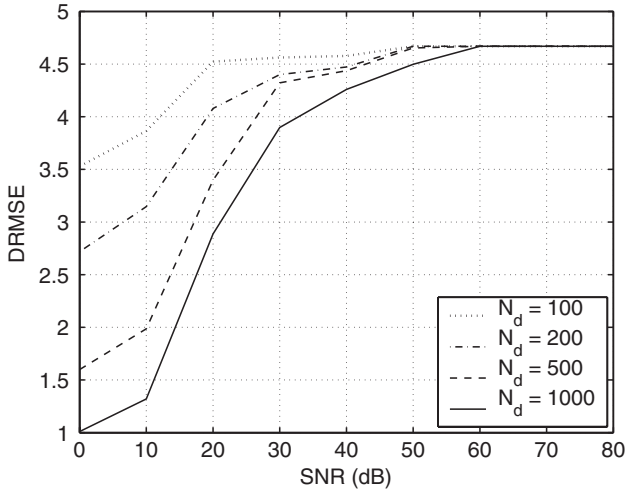

Figure 15. Delay estimation performance for the simulation conditions of Figure 13 and several sample lengths.

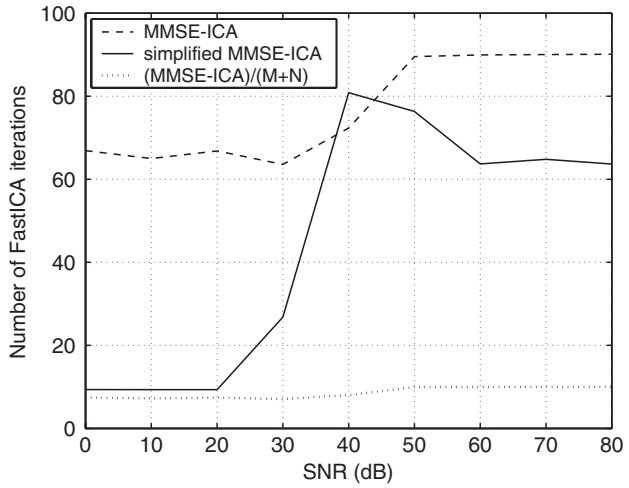

Figure 16. Number of FastICA iterations vs SNR for the simulation of Figure 13.

most of the SNR range, approaching the C factor at low SNR. In terms of flops, the simplified MMSE-ICA has proven less costly than the MMSE-ICA equalizer in all our experiments.

5. CONCLUSIONS

The users' statistical-independence, non-Gaussian, i.i.d. assumptions can be exploited to refine blind MIMO linear equalization through the use of ICA techniques based on HOS. The time diversity introduced by the wideband multipath channel leads to a simplification of the ICA-

assisted MMSE detector with improved performance and lower computational cost, by searching only for the equalization delays providing optimum MMSE for each user. The extension of these results to the SIMO model is straightforward.

It has been observed that a satisfactory optimum-delay detection depends on an accurate channel and sensor covariance matrix estimation, as well as a trade-off between SNR and observation length, whereby the required sample size increases as the noise power decreases. Nevertheless, even in situations where the channel and the delay estimates were rather inaccurate, the ICA-assisted detectors have been able to improve in all cases the conventional MMSE equalizer in moderate to high SNR and sample-size conditions. These conditions (e.g. just a few hundreds of observed baud periods) can be considered as realistic in practical scenarios.

Further work will consider the improvement of the optimum-equalization delay estimation, and will compare the ICA-aided methodology to other blind MIMO equalization schemes.

ACKNOWLEDGEMENTS

V. Zarzoso is in receipt of a Post-doctoral Research Fellowship awarded by the Royal Academy of Engineering of the U.K.

REFERENCES

1. Ristaniemi T, Joutsensalo J. Advanced ICA-based receivers for block fading DS-CDMA channels. *Signal Processing* 2002; **82**(3):417–431.
2. Wireless World Research Forum. *7th Meeting*, Eindhoven, The Netherlands, December 3–4 2002.
3. Proakis JG. *Digital Communications* (4th edn). McGraw-Hill: New York, 2000.
4. Paulraj AJ, Papadias CB. Space–time processing for wireless communications. *IEEE Signal Processing Magazine* 1997; **14**(6):49–83.
5. van der Veen A-J, Talwar S, Paulraj A. A subspace approach to blind space–time signal processing for wireless communication systems. *IEEE Transactions on Signal Processing* 1997; **45**(1):173–190.
6. Tugnait JK, Tong L, Ding Z. Single-user channel estimation and equalization. *IEEE Signal Processing Magazine* 2000; **17**(3):16–28.
7. Sato Y. A method of self-recovering equalization for multi-level amplitude modulation. *IEEE Transactions on Communications* 1975; **23**:679–682.
8. Godard DN. Self-recovering equalization and carrier tracking in two-dimensional data communication systems. *IEEE Transactions on Communications* 1980; **28**(11):1867–1875.
9. Benveniste A, Goursat M, Ruget G. Robust identification of a nonminimum phase system: blind adjustment of a linear equalizer in data communications. *IEEE Transactions on Automatic Control* 1980; **25**:385–399.
10. Shalvi O, Weinstein E. New criteria for blind deconvolution of nonminimum phase systems (channels). *IEEE Transactions on Information Theory* 1990; **36**(2):312–321.
11. Shalvi O, Weinstein E. Super-exponential methods for blind deconvolution. *IEEE Transactions on Information Theory* 1993; **39**(2):504–519.
12. Tong L, Xu G, Kailath T. Blind identification and equalization based on second-order statistics: a time domain approach. *IEEE Transactions on Information Theory* 1994; **40**(2):340–349.
13. Moulines E, Duhamel P, Cardoso J-F, Mayrargue S. Subspace methods for the blind identification of multichannel FIR filters. *IEEE Transactions on Signal Processing* 1995; **43**(2):516–525.
14. Slock DTM. Blind fractionally-spaced equalization, perfect-reconstruction filter banks and multichannel linear prediction. In *Proceedings of the ICASSP-94, 19th International Conference on Acoustics, Speech and Signal Processing*, vol. IV. Adelaide, Australia, April 19–22, 1994; 585–588.
15. Mansour A. A mutually referenced blind multiuser separation of convolutive mixture algorithm. *Signal Processing* 2001; **81**(11):2253–2266.
16. Zarzoso V, Nandi AK, García JI, Domínguez LV. Blind identification and equalization of MIMO FIR channels based on second-order statistics and blind source separation. In *Proceedings of the DSP-2002, 14th International Conference on Digital Signal Processing*, vol. I. Santorini, Greece, July 1–3, 2002; 135–138.

17. Zarzoso V, Nandi AK, Igual-García J, Vergara-Domínguez L. Blind identification and equalization of MIMO FIR channels based on subspace decomposition and independent component analysis. In *Proceedings of the 2nd IMA International Conference on Mathematics in Communications*, University of Lancaster, UK, December 16–18, 2002.
18. Talwar S, Viberg M, Paulraj A. Blind separation of synchronous co-channel digital signals using an antenna array. Part I: Algorithms. *IEEE Transactions on Signal Processing* 1996; **44**(5):1184–1197.
19. van der Veen A-J, Paulraj A. An analytical constant modulus algorithm. *IEEE Transactions on Signal Processing* 1996; **44**(5):1136–1155.
20. van der Veen A-J. Analytical method for blind binary signal separation. *IEEE Transactions on Signal Processing* 1997; **45**(4):1078–1082.
21. Hyvärinen A, Karhunen J, Oja E. *Independent Component Analysis*. John Wiley & Sons: New York, 2001.
22. Cardoso J-F, Souloumiac A. Blind beamforming for non-Gaussian signals. *IEE Proceedings-F* 1993; **140**(6):362–370.
23. Comon P. Independent component analysis, a new concept? *Signal Processing* 1994; **36**(3):287–314.
24. Zarzoso V, Nandi AK. Exploiting non-Gaussianity in blind identification and equalization of MIMO FIR channels. *IEE Proceedings—Vision, Image and Signal Processing* (*Special Issue on Nonlinear and non-Gaussian Signal Processing*) 2004;**151**(1):69–75.
25. Xu G, Liu H, Tong L, Kailath T. A least-squares approach to blind channel identification. *IEEE Transactions on Signal Processing* 1995; **43**(12):2982–2993.
26. Gesbert D, Duhamel P, Mayrargue S. On-line blind multichannel equalization based on mutually referenced filters. *IEEE Transactions on Signal Processing* 1997; **45**(9):2307–2317.
27. Giannakis GB, Halford SD. Blind fractionally spaced equalization of noisy FIR channels: direct and adaptive solutions. *IEEE Transactions on Signal Processing* 1997; **45**(9):2277–2291.
28. Shen J, Ding Z. Direct blind MMSE channel equalization based on second-order statistics. *IEEE Transactions on Signal Processing* 2000; **48**(4):1015–1022.
29. Gesbert D, Duhamel P, Mayrargue S. Blind multichannel adaptive MMSE equalization with controlled delay. In *Proceedings of the SSAP-1996, IEEE Statistical Signal and Array Processing Workshop*, Corfu, Greece, June 24–26, 1996; 172–175.
30. Gazzah H, Abed-Meraim K. Blind ZF equalization with controlled delay robust to order over estimation. *Signal Processing* 2003; **83**(7):1505–1518.
31. Prandini M, Campi MC, Leonardi R. Optimal delay estimation and performance evaluation in blind equalization. *International Journal of Adaptive Control and Signal Processing* 1997; **11**(7):621–640.
32. Zarzoso V. Exploiting independence for co-channel interference cancellation and symbol detection in multiuser digital communications. In *Proceedings of the ISSPA-2003, 7th International Symposium on Signal Processing and its Applications*, Paris, France, July 1–4, 2003.
33. Abed-Meraim K, Loubaton P, Moulines E. A subspace algorithm for certain blind identification problems. *IEEE Transactions on Information Theory* 1997; **43**(2):499–511.
34. Yang HH. On-line blind equalization via on-line blind separation. *Signal Processing* 1998; **68**(3):271–281.
35. Zhang Y, Kassam SA. Blind separation and equalization using fractional sampling of digital communications signals. *Signal Processing* 2001; **81**(12):2591–2608.
36. Hyvärinen A, Oja E. A fast fixed-point algorithm for independent component analysis. *Neural Computation* 1997; **9**(7):1483–1492.

NONLINEAR AND NON-GAUSSIAN SIGNAL PROCESSING

Exploiting non-Gaussianity in blind identification and equalisation of MIMO FIR channels

V. Zarzoso and A.K. Nandi

Abstract: The problem of blind identification and equalisation (BIE) of finite impulse response (FIR) channels in multiuser digital communications is investigated. The non-Gaussian nature and statistical independence of the users' data streams is exploited by resorting to blind signal separation (BSS) based on higher-order statistics (HOS). Two such techniques are put forward. The first technique is composed of an extension to the multiuser case of a second-order BIE method, followed by a BSS-based space-equalisation step. The second technique achieves joint space–time equalisation through the direct application of a HOS-based BSS method followed by a blind identification algorithm. In a number of numerical experiments, the first procedure proves less costly and more effective for short data records. Despite their computational complexity, interesting features such as constellation-independent channel identification and symbol recovery, and robustness to ill-conditioned channels in high SNR environments render HOS-BSS based BIE methods an effective alternative to BIE techniques exploiting other spatio-temporal structures.

1 Introduction

In digital communications, linear distortion effects such as multipath propagation and limited bandwidth cause inter-symbol interference (ISI) in the received signal, producing errors in symbol detection. A variety of equaliser designs can be employed to compensate for the channel effects [1]. As opposed to traditional techniques, blind channel identification and equalisation (BIE) methods do not require training sequences, and are thus able to use the bandwidth resources more efficiently and to perform in a wider range of communication environments. Due to their many desirable properties [2], blind methods have aroused great research interest.

Tong *et al*. first proved [3] that non-minimum phase (NMP) finite-impulse response (FIR) channels can be identified using only second-order statistics (SOS) if the received signal exhibits cyclostationarity. Cyclostationarity naturally leads to the so-called single-input multiple-output (SIMO) model, a multichannel signal structure with one input (the transmitted symbol sequence) and several outputs. By relying only on the subspace information contained within the sensor second-order correlation matrix, BIE is possible in SIMO systems [3, 4].

In multiuser communication environments (e.g. cellular wireless systems) the co-channel interference (CCI) caused by other users simultaneously transmitting across the same medium adds to multipath-induced ISI. To ensure reliable detection, space–time equalisation must be performed. Time equalisation aims at ISI removal, whereas space equalisation involves CCI elimination and the extraction of the signal(s) of interest. The exploitation of temporal and/or spatial diversity (fractional sampling and/or multiple sensors) results in multiple-input multiple-output (MIMO) signal models. Direct extensions of subspace-based SIMO methods to the MIMO case achieve time equalisation but are generally unable to separate the different source data streams, i.e. CCI remains in the form of an instantaneous linear mixture of the transmitted symbols [2, 5, 6]. To separate this spatial mixture, the fact that digital communication signals possess a finite alphabet (FA) can be exploited [2]. In a direct-sequence code-division multiple access (DS/CDMA) system, [6] reports an unsatisfactory performance of one such FA-based method, with probability of error well above 10% even in the noise-free case. Nevertheless, the spatial mixture can be resolved with the aid of the users' signature sequences [6], which are typically known in a CDMA scenario. This semi-blind method is not applicable to a general (i.e. using a multiple-access technique other than DS/CDMA) multiuser digital communication environment. The method of [6] is blind in that it spares training sequences. However, the use of signature sequences leads to a particular factorisation of the channel matrix, whereas fully blind methods generally avoid such parameterisations. Precisely there lies the robustness of these methods to deviations from the assumed prior information (e.g. calibration errors in beamforming) [7].

A more generic, fully blind approach sparing the prior knowledge of the users' signature sequences or FAs follows from the plausible hypothesis that the signals transmitted by different users are statistically independent. Hence, the remaining spatial mixture after the SOS-MIMO stage adopts a model of blind source separation (BSS) of instantaneous linear mixtures. In addition, digital communication signals are non-Gaussian, typically showing sub-Gaussian (or platykurtic [8]) probability density functions (pdfs), so BSS methods based on higher-order statistics (HOS) are applicable. In the case where the transmitted symbols are independent and identically distributed (i.i.d.), the source extraction can directly be solved by HOS-based BSS

IEE Proceedings online no. 20040278

doi: 10.1049/ip-vis:20040278

Paper received 4th September 2002 and in revised form 28th March 2003

The authors are with the Signal Processing and Communications Group, Department of Electrical Engineering and Electronics, The University of Liverpool, Brownlow Hill, Liverpool L69 3GJ, UK

techniques, as shown in [9–11]. However, the methods presented therein are not designed to identify the channel. A channel estimate may prove useful in a variety of tasks, such as power control, source localisation, propagation characterisation, or as a sensible initialisation for an adaptive receiver.

This contribution discusses the exploitation of the non-Gaussian i.i.d. source property in the FIR–MIMO BIE problem. In particular, we study two techniques which rely on such an assumption through the application of BSS. The first technique is composed of the extension to the MIMO case of a SOS-based SIMO method, completed by a BSS-based space-equalisation stage. The second technique consists of joint space–time equalisation through the direct application HOS-based BSS followed by a suitable algorithm for channel identification. The benefits and drawbacks of exploiting non-Gaussianity are also highlighted throughout.

A signal model is presented which will be used in the mathematical developments. The two BIE methods are put forward and simulation results are reported. Other relevant issues are also discussed.

Notations

$\mathbb{C}$ is the set of complex numbers. Vectors and matrices are represented, respectively, by boldface lower-case and upper-case symbols. $(\boldsymbol{A})_{ij}$ denotes the (i, j)-element of matrix $\boldsymbol{A}$. Symbol $\boldsymbol{I}_n$ refers to the $n \times n$ identity matrix, and

$$\boldsymbol{e}_i^{(n)} = [\underbrace{0, \ldots, 0}_{i-1}, 1, \underbrace{0, \ldots, 0}_{n-i}]^{\mathrm{T}}$$

is the ith canonic basis vector of $\mathbb{C}^n$. Superindices $(\cdot)^*$, $(\cdot)^{\mathrm{T}}$, $(\cdot)^{\mathrm{H}}$, $(\cdot)^{-1}$ and $(\cdot)^{\dagger}$ indicate the complex conjugate, transpose, Hermitian (conjugate-transpose), inverse and Moore–Penrose pseudoinverse operators, respectively. E[·] stands for mathematical expectation, and $\otimes$ denotes the Kronecker product.

2 Signal model

The signal model of [4] is extended to the multiple-input case. An oversampled single-sensor receiver is considered, although the model also holds for spatially separated multiple physical sensors. The system assumptions are:

(i) K data sources simultaneously transmit mutually-independent information-bearing non-Gaussian i.i.d. symbols $\{s_{k,m}\}_{k=1}^{K} \in \mathbb{C}$ at a known rate $1/T$ bauds, with $\mathrm{E}[s_{k,\cdot}] = 0$ and $\mathrm{E}[|s_{k,\cdot}|^2] = 1$.
(ii) The impulse responses $h_k(t)$ representing the propagation between the kth source and the sensor (including the effects of the transmitter and receiver filters, carrier-pulse shaping, etc.) span at most $M + 1$ data symbols.
(iii) The additive measurement noise $v(t)$ is white, zero-mean and uncorrelated with the data sequences; its variance is σ^2.

The implicit source power normalisation in assumption (i) stems from the fact that a complex scalar can be interchanged between the channel and the data without altering the received signal. This scalar factor is an admissible indeterminacy in blind equalisation, and cannot be resolved without resorting to further prior information.

In contrast to [2], herein source alphabets can be assumed unknown and not necessarily identical for all users; neither the alphabets need be constant modulus. The source data need not even be discrete. We only require that their kurtosis [8] be different from zero (at most one non-kurtic source is allowed [12]). Assumption (ii) demands channel stationarity, at least over the observation window. This hypothesis is verified in time non-selective scenarios, such as block-fading multipath channels, whose coherence time is large compared to the baud period [13].

With the above assumptions, the continuous-time complex baseband received signal can be expressed as

$$x(t) = \sum_{k=1}^{K} \sum_{m=-\infty}^{\infty} s_{k,m} h_k(t - mT) + v(t) \tag{1}$$

Sampling at a rate $1/T_s = L/T$, with L integer, from an initial instant $t_0 = 0$ s (without loss of generality) yields

$$x_n^{(i)} = \sum_{k=1}^{K} \sum_{m=0}^{M} s_{k,n-m} h_{k,m}^{(i)} + v_n^{(i)}, \quad i = 0, \ldots, L-1 \tag{2}$$

in which $x_n^{(i)} = x(iT_s + nT)$, $h_{k,n}^{(i)} = h_k(iT_s + nT)$ and $v_n^{(i)} = v(iT_s + nT)$. Hence, fractionally-spaced sampling effectively generates L virtual channels excited by the same input. Let us now store N consecutive output samples of virtual channel i in vector $\boldsymbol{x}_n^{(i)} = [x_n^{(i)}, \ldots, x_{n-N+1}^{(i)}]^{\mathrm{T}}$. Parameter N is referred to as the smoothing factor [14] or stacking level [9]. Similarly, gather the N samples of the L virtual channel outputs in vector $\boldsymbol{x}_n = [\boldsymbol{x}_n^{(0)^{\mathrm{T}}}, \ldots, \boldsymbol{x}_n^{(L-1)^{\mathrm{T}}}]^{\mathrm{T}}$ (with similar notations for the noise vector $\boldsymbol{v}_n$). Then, the following matrix model holds:

$$\boldsymbol{x}_n = \boldsymbol{H}\boldsymbol{s}_n + \boldsymbol{v}_n \tag{3}$$

where $\boldsymbol{s}_n = [\boldsymbol{s}_{1,n}^{\mathrm{T}}, \ldots, \boldsymbol{s}_{K,n}^{\mathrm{T}}]^{\mathrm{T}}$, $\boldsymbol{s}_{k,n} = [s_{k,n}, \ldots, s_{k,n-N-M+1}]^{\mathrm{T}}$; $\boldsymbol{H} = [\boldsymbol{H}_1, \ldots, \boldsymbol{H}_K]$ is the $LN \times K(M+N)$ channel filtering matrix, with $\boldsymbol{H}_k = [\boldsymbol{H}_k^{(0)^{\mathrm{T}}}, \ldots, \boldsymbol{H}_k^{(L-1)^{\mathrm{T}}}]^{\mathrm{T}}$, $\boldsymbol{H}_k^{(i)}$ representing the $N \times (M+N)$ Toeplitz convolution matrix associated with the linear filter $\boldsymbol{h}_k^{(i)} = [h_{k,0}^{(i)}, \ldots, h_{k,M}^{(i)}]^{\mathrm{T}}$. To abbreviate, in the sequel we denote $P \triangleq LN$, $C \triangleq M + N$ and $D \triangleq K(M+N) = KC$.

The objective of BIE is to estimate $\boldsymbol{H}$ (blind channel identification) and $\boldsymbol{s}_n$ (blind channel equalisation [ISI cancellation] and source separation [CCI cancellation]) from the only observation of the received vector $\boldsymbol{x}_n$. These tasks are equivalent to recovering the channel coefficient vector $\boldsymbol{h} = [\boldsymbol{h}_1^{\mathrm{T}}, \ldots, \boldsymbol{h}_K^{\mathrm{T}}]^{\mathrm{T}}$, with $\boldsymbol{h}_k = [\boldsymbol{h}_k^{(0)^{\mathrm{T}}}, \ldots, \boldsymbol{h}_k^{(L-1)^{\mathrm{T}}}]^{\mathrm{T}}$, and the source vector

$$\boldsymbol{s} = E_1^{\mathrm{H}} \boldsymbol{s}_n = [s_{1,n}, \ldots, s_{K,n}]^{\mathrm{T}} \tag{4}$$

where $E_i = \boldsymbol{I}_K \otimes \boldsymbol{e}_i^{(C)}$.

A necessary condition for blind identifiability is that the filtering matrix be full column rank, which can occur only if $\boldsymbol{H}$ has more rows than columns, $P \geq D$, or, equivalently, $L > K$ and $N \geq KM/(L-K)$. This condition is not sufficient. It is required that polynomial matrix $\boldsymbol{H}(z)$ be 'irreducible and column reduced', where $(\boldsymbol{H}(z))_{ij}$ is the z-transform of $h_j^{(i)}$ [5].

Note that with the information of assumptions (i)–(iii) we can obtain at best a channel estimate $\hat{\boldsymbol{H}}$ such that $\hat{\boldsymbol{H}}^{\dagger}\boldsymbol{H} = \boldsymbol{\Gamma}_K \otimes \boldsymbol{I}_C$, where $\boldsymbol{\Gamma}_K$ is an arbitrary $K \times K$ permutation matrix with unit-norm nonzero entries; signal blocks of different users present an order indeterminacy, which can only be surmounted if further information is available (e.g. users' signature sequences in a CDMA system).

3 SOS-based time equalisation and BSS-based space equalisation

3.1 Multiuser extension of SIMO methods

Tong *et al.* [3] realised that blind channel identification of NMP FIR channels is possible from SOS alone in the

single-user cyclostationary case, which results in the SIMO signal model. (The signal model in [3] is slightly different from that presented in the previous Section (with $K = 1$). Tong's signal model involves a different arrangement for the signal vectors and channel matrix, and allows for noninteger (fractional) values for the stacking level. However, both models are totally analogous, so that we can use the model of Section 2 without loss of generality.) Their approach takes advantage of the particular structure of the observed-vector correlation matrix $\boldsymbol{R}_x(m) = \mathrm{E}[\boldsymbol{x}_n \boldsymbol{x}_{n-m}^{\mathrm{H}}]$ at two different lags $(m = 0, 1)$. The direct application of this blind identification method to the MIMO case yields the following identifiability result [15].

Theorem 1: Suppose that $\boldsymbol{H}$ and $\boldsymbol{s}_n$ satisfy the linear model (3) and its constraints (i)–(iii). Then $\boldsymbol{H}$ is determined from $\boldsymbol{R}_x(0)$ and $\boldsymbol{R}_x(1)$ up to a post-multiplicative factor of the form $\boldsymbol{Q} \otimes \boldsymbol{I}_C$, where $\boldsymbol{Q} \in \mathbb{C}^{K \times K}$ is a $K \times K$ unitary matrix.

A similar indeterminacy is observed in the multiuser extension [2, 16] of the subspace method of [4], in which $\boldsymbol{Q}$ becomes an arbitrary $K \times K$ invertible matrix. Indeed, theorem 1 may be generalised to the MIMO extension of any SIMO BIE method [2].

According to the above result, the channel estimated by the extended Tong's method is of the form $\tilde{\boldsymbol{H}} = \boldsymbol{H}(\boldsymbol{Q} \otimes \boldsymbol{I}_C)$, with $\boldsymbol{Q}$ an unknown $K \times K$ unitary matrix. Should we want to carry out soft-symbol detection at this stage, the resulting zero-forcing (ZF) equaliser output would be

$$\boldsymbol{y}_n = \tilde{\boldsymbol{H}}^{\dagger} \boldsymbol{x}_n = (\boldsymbol{Q}^H \otimes \boldsymbol{I}_C)\boldsymbol{s}_n + \tilde{\boldsymbol{v}}_n \tag{5}$$

in which

$$\tilde{\boldsymbol{v}}_n = \tilde{\boldsymbol{H}}^{\dagger} \boldsymbol{v}_n \tag{6}$$

Now, defining $\boldsymbol{y} = \boldsymbol{E}_1^{\mathrm{H}} \boldsymbol{y}_n$, system (5) becomes

$$\boldsymbol{y} = \boldsymbol{Q}^{\mathrm{H}} \boldsymbol{s} + \tilde{\boldsymbol{v}} \tag{7}$$

where $\tilde{\boldsymbol{v}} = \boldsymbol{E}_1^{\mathrm{H}} \tilde{\boldsymbol{v}}_n$, and $\boldsymbol{s}$ is given by (4).

3.2 BSS-based space equalisation

Equation (7) represents a noisy unitary instantaneous linear mixture of the source symbols. That is, CCI elimination requires further processing. Since the components of $\boldsymbol{s}$ are statistically independent [assumption (i)], (7) corresponds to a BSS problem of instantaneous linear mixtures [17, 18]. Due to the i.i.d. assumption, SOS-based BSS methods fail, but the source non-Gaussianity can still be exploited through HOS. A few remarks indicate that HOS-based BSS seems well suited as a second processing step:

3.2.1 Complexity reduction: The BSS problem at this second stage has size $K \times K$, which is considerably reduced compared with the original dimensions of the BIE system (3).

3.2.2 Robustness to ill-conditioned channels: In the single-user case, the so-called uniform performance property enjoyed by many BSS methods [19] translates into a robust performance for ill-conditioned channels [9]. Note, however, that uniform performance is only expected to hold in the noiseless case [19].

3.2.3 Noise 'Gaussianisation': The central limit theorem and (6) guarantee that the equalised noise $\tilde{\boldsymbol{v}}$ will be close to Gaussian, even if the actual sensor noise $\boldsymbol{v}_n$ is not. The well known HOS immunity to Gaussian noise would then result in an increased robustness of the BIE method not only to Gaussian noise but also to other kinds of non-Gaussian noise, such as impulsive interference.

In the simulations of Section 5, we employ the joint approximate diagonalisation of eigenmatrices (JADE) BSS method [7]. This choice is somewhat arbitrary; we are concerned with the application of BSS as a general strategy, rather than assessing which particular BSS method provides the best performance. JADE optimises a HOS cost function through the joint diagonalisation of a particular set of fourth-order cumulant tensor 'slices'.

Once $\boldsymbol{Q}$ has been obtained via a HOS–BSS method, the full channel estimate can be calculated as $\hat{\boldsymbol{H}} = \tilde{\boldsymbol{H}}(\boldsymbol{Q}^{\mathrm{H}} \otimes \boldsymbol{I}_C)$. From the channel estimate, soft-symbol detection can then be accomplished from (3) as $\hat{\boldsymbol{s}}_n = \boldsymbol{G}^{\mathrm{H}} \boldsymbol{x}_n$ with the ZF and minimum mean square error (MMSE) equalisers

$$\boldsymbol{G}_{\mathrm{ZF}} = (\hat{\boldsymbol{H}}\hat{\boldsymbol{H}}^{\mathrm{H}})^{-1}\hat{\boldsymbol{H}} \tag{8}$$

$$\boldsymbol{G}_{\mathrm{MMSE}} = \boldsymbol{R}_x(0)^{-1}\hat{\boldsymbol{H}} \tag{9}$$

whose subspace version from the channel matrix singular value decomposition is given in [6].

Steps 2–5 of Table 1 summarise the BSS and detection stages, which, in combination with the extended Tong method, complete the first FIR–MIMO BIE algorithm proposed in this paper.

4 BSS-based joint space–time equalisation and channel identification

The i.i.d. assumption in (i) makes the components of the source vector $\boldsymbol{s}_n$ in (3) statistically independent. From this perspective, (3) itself can also be considered as a BSS model of instantaneous linear mixtures, and thus BSS techniques may be directly applied to resolve it [11].

The whitening step of Tong's method provides the outputs [15]

$$\boldsymbol{z}_n = \boldsymbol{W}\boldsymbol{x}_n = \boldsymbol{V}\boldsymbol{s}_n + \boldsymbol{w}_n \tag{10}$$

where $\boldsymbol{w}_n = \boldsymbol{W}\boldsymbol{v}_n$ and $\boldsymbol{W}$ represents the whitening matrix. In a second step, a HOS-based BSS method, such as JADE [7], can estimate the unitary mixing matrix $\boldsymbol{V}$. Detection can be carried out through ZF/MMSE equalisers (8)/(9).

Since in this case the BSS method operates over all the D whitened components, the complexity reduction remarked in the previous Section is lost. However, the key point to note in the direct application of BSS techniques to the BIE model is related to the source scale and order indeterminacies inherent to the BSS problem [17, 18]. These indeterminacies mean that a blind separation method can provide any solution $\hat{\boldsymbol{V}}$ such that $\hat{\boldsymbol{V}}^{\dagger}\boldsymbol{V}$ is an arbitrary permutation matrix with unit-norm non-zero entries. In our particular model (3), the arrangement and scale of the recovered source components as well as the corresponding columns of the filtering matrix are crucial, especially for

Table 1: Algorithm for SOS-based time equalisation and BSS-based space equalisation

1. Obtain first estimate of the filtering matrix $\tilde{\boldsymbol{H}}$ from the extended Tong method [15].
2. Compute ISI-free output (5).
3. Estimate matrix $\boldsymbol{Q}$ from (7) with a HOS-based BSS method.
4. Update estimate of channel matrix as $\hat{\boldsymbol{H}} = \tilde{\boldsymbol{H}}(\boldsymbol{Q}^{\mathrm{H}} \otimes \boldsymbol{I}_C)$.
5. Detect CCI-free source symbols [(8) and (9)].

channel identification purposes. Hence, the solution obtained via BSS needs to be refined if it is to be useful in the BIE scenario.

We propose the algorithm outlined in Table 2. First, the recovered source vector components are normalised to unit variance, and the component with the largest absolute normalised kurtosis is chosen. Given a unidimensional observation $x = s + v$, then

$$\tilde{\kappa}_4^x = \tilde{\kappa}_4^s \left(\frac{\text{SNR}}{1 + \text{SNR}} \right)^2$$

where $\tilde{\kappa}_4^x = \kappa_4^x / (\kappa_2^x)^2$, $\text{SNR} = \kappa_2^s / \kappa_2^v$ and κ_n^x and $\tilde{\kappa}_n^x$ represent the nth-order cumulant and normalised cumulant, respectively, of x [8]. Hence, if all sources have the same distribution, the highest normalised kurtosis criterion selects the least noisy component. Next, the correlation function between that and all other components is computed in turns. If the maximum absolute value of the correlation function is above certain threshold, the two components are considered to belong to the same source, their relative delay and phase being given by the delay and phase of their joint correlation function at its peak. (In the simulations of Section 5, an initial threshold value of 0.7 was used, with a multiplicative reduction factor (step 5 in Table 2) of 0.95.) Note that since the relative delays between two components of the same user's signal lie in the interval $[-C+1, C-1]$, the cross-correlation functions only need to be computed between those lag limits, with the consequent reduction in complexity. The components of the source vector and the channel matrix are then scaled and ordered accordingly. The process is repeated until no more source components remain to be arranged. In an ideal situation (perfect estimation), this algorithm outputs a channel estimate $\hat{\boldsymbol{H}}$ such that $\hat{\boldsymbol{H}}^{\dagger}\boldsymbol{H} = \boldsymbol{\Gamma}_K \otimes \boldsymbol{I}_C$.

Table 2: Algorithm for BSS-based joint space–time equalisation and channel identification

Repeat steps below until no more estimated source components remain to be ordered:

1. Select among remaining sources the component with largest normalised kurtosis, $\hat{\boldsymbol{s}}_i$.
2. Estimate (e.g. via time averaging) the cross-correlation functions
$$\boldsymbol{R}_{\hat{\boldsymbol{s}}_i \hat{\boldsymbol{s}}_j}(m) = \text{E}[\hat{\boldsymbol{s}}_i(n)\hat{\boldsymbol{s}}_j^*(n-m)]$$
for j within the group of components still to be arranged.
3. Obtain the lag position m_{ij} of the largest absolute value $|\rho_{ij}|$ of $\boldsymbol{R}_{\hat{\boldsymbol{s}}_i \hat{\boldsymbol{s}}_j}$
$$m_{ij} = \arg\max_m |\boldsymbol{R}_{\hat{\boldsymbol{s}}_i \hat{\boldsymbol{s}}_j}(m)|$$
$$\rho_{ij} = \boldsymbol{R}_{\hat{\boldsymbol{s}}_i \hat{\boldsymbol{s}}_j}(m_{ij})$$
4. If $|\rho_{ij}| >$ threshold, source pair $(\hat{\boldsymbol{s}}_i, \hat{\boldsymbol{s}}_j)$ belongs to the same user.
   (a) Correct phase: multiply $\hat{\boldsymbol{s}}_j$ by $e^{j<\rho_{ij}}$; multiply the jth column of $\hat{\boldsymbol{H}}$ by $e^{-j<\rho_{ij}}$.
   (b) Rearrange the elements of $\hat{\boldsymbol{s}}$ and the columns of $\hat{\boldsymbol{H}}$ according to the ordering of m_{ij}.
5. If no source pair was detected, reduce the threshold and return to step 4.

The above algorithm is based on the equalisation methods 'A' and 'C' of ([11], Section 5), but it improves them in that it is also able to accomplish channel identification.

5 Simulation results

A few numerical experiments illustrate the behaviour of the MIMO BIE methods presented in the previous Sections. We first define a number of performance parameters. A natural choice for the signal-to-noise ratio (SNR) is

$$\text{SNR} = \frac{\text{trace}(\boldsymbol{H}\boldsymbol{R}_s(0)\boldsymbol{H}^{\text{H}})}{\text{trace}(\boldsymbol{R}_v(0))} = \frac{1}{\sigma^2 P}\text{trace}(\boldsymbol{H}\boldsymbol{H}^{\text{H}}) \qquad (11)$$

which corresponds to the average source power contribution over the average noise power in the received signal. To measure the quality of the channel identification and the space–time equalisation results, we choose the channel mean square error (CMSE) and the average signal mean square error (SMSE), respectively, which are defined as

$$CMSE = \frac{\|\hat{\boldsymbol{h}} - \boldsymbol{h}\|^2}{\|\boldsymbol{h}\|^2} \qquad (12)$$

$$SMSE = \frac{1}{D}\text{E}\left[\|\hat{\boldsymbol{s}}_n - \boldsymbol{s}_n\|^2\right] \qquad (13)$$

The symbol error rate (SER) is computed as the number of erroneous symbols in the components of $\hat{\boldsymbol{s}}_n$ over the total number of symbols in $\boldsymbol{s}_n$. Before calculating these performance parameters, the estimated channel matrix and source vector are first rearranged to 'match' the original channel matrix and source vector, in a bid to correct the $\boldsymbol{\Gamma}_K \otimes \boldsymbol{I}_C$ ambiguity term. It is important to note that this rearrangement is based purely on the comparison of consecutive C-column blocks of the estimated and original channel matrices, so that the BIE results cannot possibly be altered (improved) in this process.

5.1 Performance against sample size

The first simulation tests the extension of Tong's method followed by BSS on (7) (ETBSS), and the full BSS method on (3) with the blind identification algorithm of Section 4 (FBSS). Two 4-QAM signals are transmitted over a dispersive multipath channel with a short delay spread of $M = 2$ symbol periods. Reception takes place in additive complex Gaussian noise. N_d symbol periods are observed, with oversampling factor $L = 6$ and stacking level $N = 2$. The channel coefficients are drawn from a complex Gaussian distribution, forming a fixed 12×8 channel matrix with condition number $\text{cond}(\boldsymbol{H}) = 5$. Performance parameters are averaged over ν Monte Carlo (MC) runs, with independent source and noise realisations at each run, and maintaining $\nu N_d = 10^4$. Figure 1 shows the CMSE and SMSE results for a varying observation window length N_d and several SNRs. At high enough SNR, ETBSS shows good performance for a low sample size. FBSS needs around 300 samples to provide satisfactory results, and then consistently outperforms the other method, becoming about twice as efficient. Figure 1*b* also shows that the methods tend asymptotically to the large-sample MMSE at each SNR value. In this experiment, SER counts are zero for both methods from $\text{SNR} = 30\,\text{dB}$ and $N_d > 300$ observed symbol periods, approximately.

5.2 Performance against noise level

The environment of the second simulation tests the effects of varying noise levels for different sample lengths, with

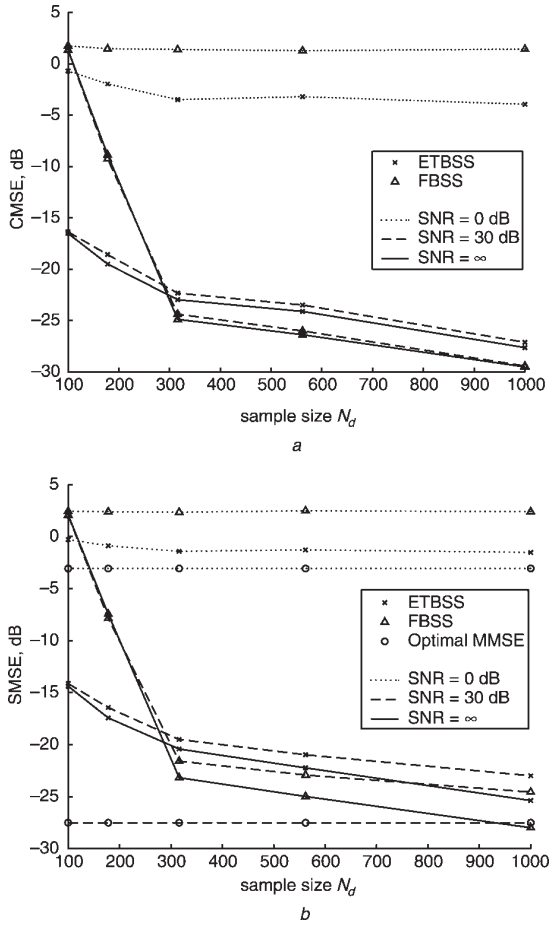

Fig. 1 *Performance against sample size for two 4-QAM sources, additive Gaussian noise, $M = 2$, $L = 6$, $N = 2$, cond($\boldsymbol{H}$) = 5, ν MC runs, $\nu N_d = 10^4$*

a CMSE
b SMSE with MMSE detection

$\nu N_d = 10^5$. Three 16-QAM modulations propagate in a more severe frequency-selective channel of order $M = 5$. We choose $L = 12$ and $N = 2$, which result in a 24×21 channel matrix with cond($\boldsymbol{H}$) = 30. Figure 2 shows that the ETBSS begins to obtain satisfactory BIE results from about SNR = 20 dB, even for low sample size, whereas FBSS requires a few thousand samples to start performing. However, for long observation windows, FBSS tolerates a noise level of around 10 dB higher than ETBSS. Both methods approach the optimal large-sample MMSE asymptotically, as displayed in Figs. 2*b* and 2*c*. In the SER plots, the 'optimal MMSE' curve corresponds to the probability of symbol error in the optimum detection (for an AWGN channel [13]) of a single component with MSE equal to the large-sample MMSE in the given simulation conditions (channel matrix and SNR).

5.3 Performance against noise distribution

Figure 3 explores the impact of the noise distribution on the BIE results, for large sample size ($N_d = 10^4$) at various SNRs. The sensor output is corrupted by additive noise with complex generalised Gaussian distribution (CGGD) of parameter α, whose pdf is given by $p(z) \propto \exp(-|z|^{\alpha})$. The CGGD becomes the complex Gaussian distribution for $\alpha = 2$, a super-Gaussian distribution for $\alpha < 2$ (e.g. the complex Laplacian variable for $\alpha = 1$), and a sub-Gaussian distribution for $\alpha > 2$. The methods' BIE results are

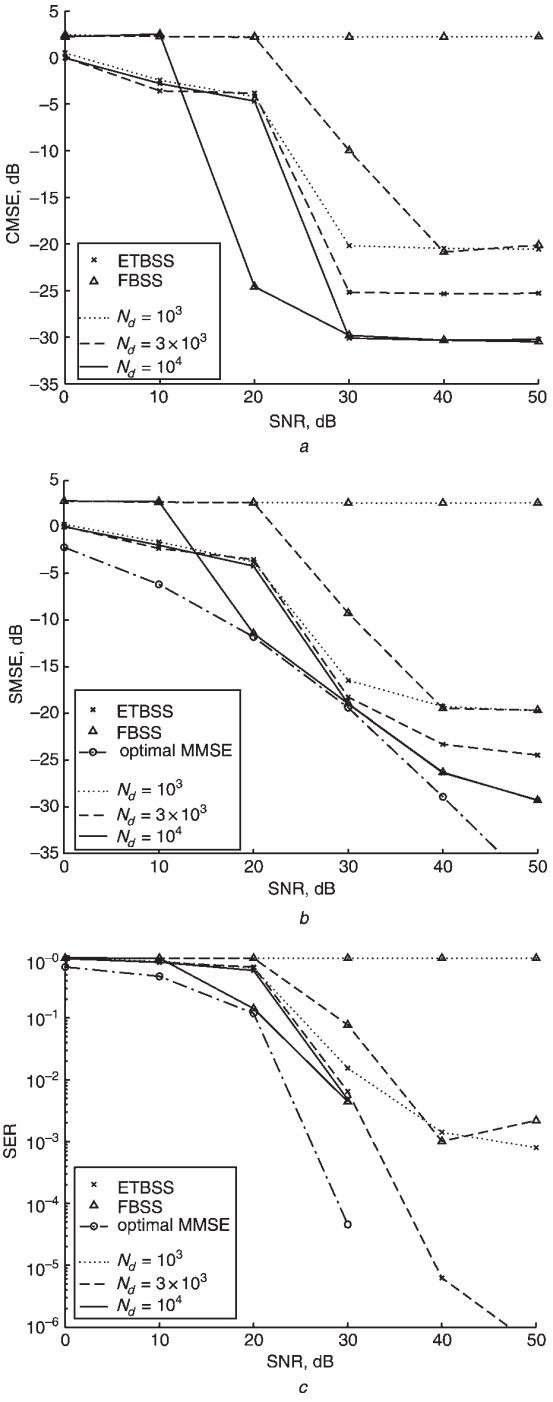

Fig. 2 *Performance against SNR for three 16-QAM sources, additive Gaussian noise, $M = 5$, $L = 12$, $N = 2$, cond($\boldsymbol{H}$) = 30, ν MC runs, $\nu N_d = 10^5$*

a CMSE
b SMSE with MMSE detection
c SER with MMSE detection

virtually identical over the tested range of noise distributions.

5.4 Performance against channel conditioning

The effects of the channel matrix conditioning are assessed in a final experiment, whose outcome is shown in Fig. 4. At each MC iteration, a channel matrix of a given condition

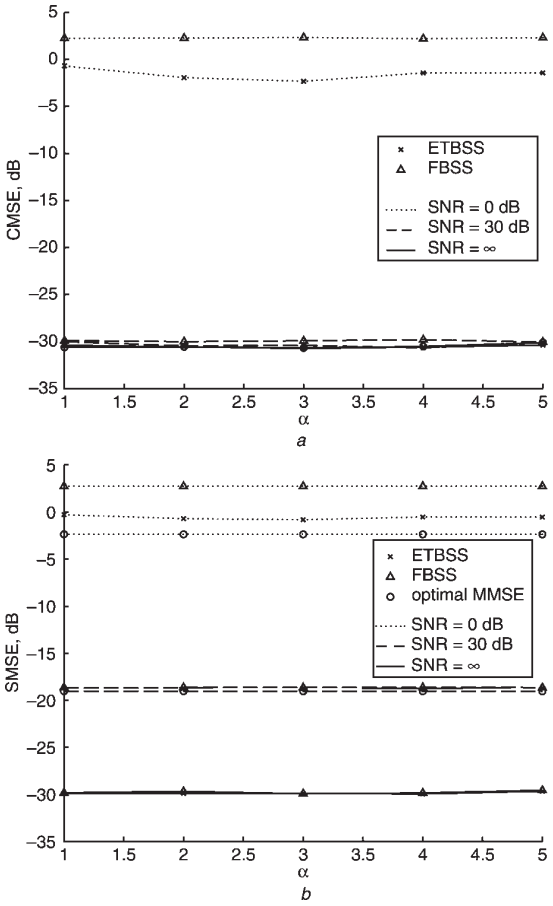

Fig. 3 *Performance against noise distribution for additive noise with CGGD of parameter α, three 16-QAM sources, $M = 5$, $L = 12$, $N = 2$, cond($\boldsymbol{H}$) = 30, $N_d = 10^4$ 10 MC runs*

a CMSE
b SMSE with MMSE detection

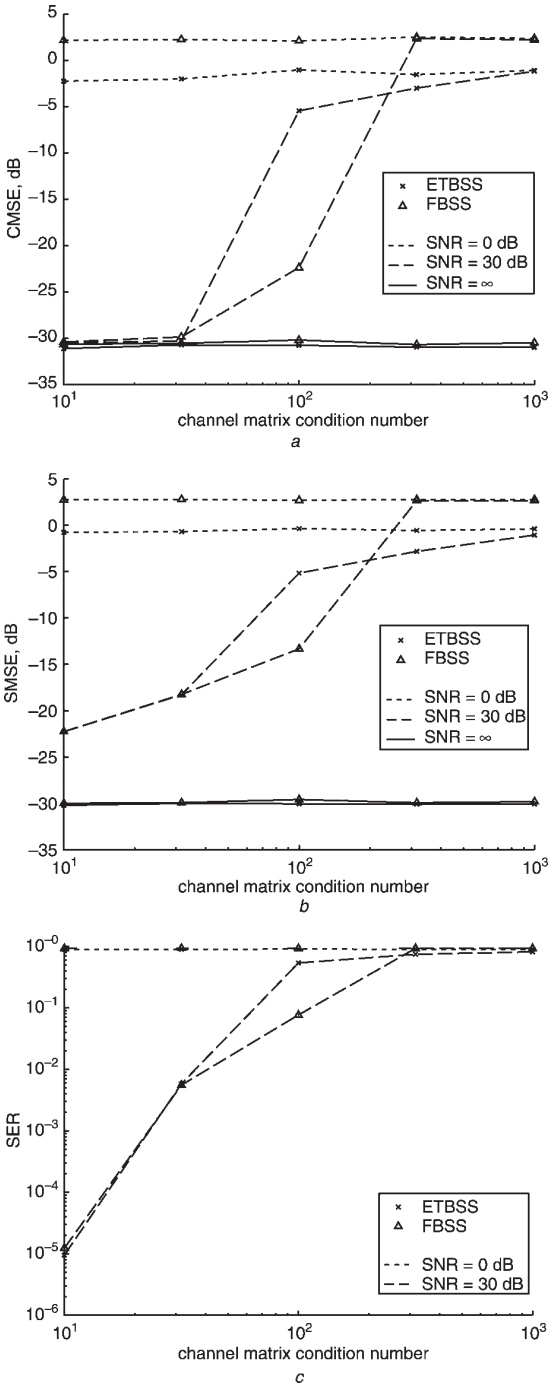

Fig. 4 *Performance against channel conditioning, for three 16-QAM sources, additive Gaussian noise, $M = 5$, $L = 12$, $N = 2$, $N_d = 10^4$, 10 MC runs*

a CMSE
b SMSE with MMSE detection
c SER with MMSE detection

number as well as independent source and noise realisations are randomly generated. For finite SNR, performance worsens as cond($\boldsymbol{H}$) increases. The ill conditioning of the channel matrix amplifies the noise in the whitening process, hampering the HOS processing stage, which 'sees' a lower SNR. In the noiseless case, no variation with the channel matrix condition number is observed. For illustration and comparison, the characteristics of some channels used in this paper and elsewhere in the literature are summarised in Table 3.

6 Discussion

A number of issues deserve special treatment, and are discussed next.

6.1 Computational complexity and choice of BSS method

The high cost involved in the computation of the higher-order cumulants/moments is probably the weakest aspect of HOS-based techniques. After Tong's method, JADE requires the calculation of the K^4 elements of the fourth-order cumulant tensor, followed by the diagonalisation of a $K^2 \times K^2$ matrix made from such cumulants. Consequently, the direct application of BSS exhibits a C^4-fold increase in computations. Indeed, JADE becomes computationally prohibitive for source vectors with many components, which may easily arise in more realistic scenarios with large delay spreads. Less costly schemes such as the FastICA algorithm [18] may prove more convenient in these practical situations. The methods of [12] and [20], which can be used in real-valued mixtures, show a complexity of the order of $K^{5/2}$ flops per vector sample. For coloured sources with different spectral content, computationally efficient BSS techniques using only SOS [17, 18, 21] are feasible after the application of a subspace method not relying on the i.i.d. assumption (e.g. [4]).

Table 3: Some channels used in the literature and in this paper

Reference	(*K*, *L*, *M*, *N*)	Description	Size	cond(***H***)
[3]	(1, 4, 5, 5)	SIMO, raised cosine carrier pulses, three-ray multipath, NMP subchannels	20×10	55.86
[9], case 1	(1, 2, 11, 11)	SIMO, similar impulse response to [3], NMP subchannels	22×22	2.96×10^4
[9], case 2	(1, 4, 5, 5)	SIMO, NMP subchannels	20×10	77.79
[11], example 1	(2, 8, 3, 1)	MIMO, squared-half-cosine carrier pulses, flat fading, NMP subchannels	8×8	181.14
Section 5.1	(2, 6, 2, 2)	MIMO, complex Gaussian channel taps, NMP subchannels	12×8	5
Sections 5.2 and 5.3	(3, 12, 5, 2)	MIMO, complex Gaussian channel taps, NMP subchannels	24×21	30

6.2 Blind identification from channel matrix structure

The blind identification algorithm from the BSS results proposed herein relies on preserving the source vector structure only. The joint exploitation of the block-Toeplitz structure of the channel matrix could lead to a reduction in the sample size required for satisfactory identification results. The minimum required sample size is ultimately limited by the use of HOS.

6.3 Channels with different delay spreads

In realistic communication environments, channel delay spreads of different users are likely to differ. The application of a SOS subspace method would then result, even under perfectly known channel orders, in a BSS problem of convolutive mixtures [5], which is a challenging area currently drawing intense research attention [18].

7 Conclusions

The present work has addressed the BIE of FIR channels in multiuser digital communication systems. The non-Gaussian property and statistical independence of the source data have been successfully exploited through HOS-based BSS techniques for CCI cancellation and for joint ISI-CCI suppression. The two proposed BSS-based techniques exhibit the same asymptotic performance, but the former is computationally more efficient, and proves more effective in short observation windows. Both approaches have shown their robustness, relative to the Gaussian-noise case, against non-Gaussian additive noise and impulsive interference. Other salient features of the BSS approach are its robustness to the channel matrix condition number in high SNR situations and its constellation-independent BIE capabilities. In conclusion, the BSS approach appears to be a strong alternative to FIR-MIMO BIE techniques relying on the exploitation of other spatio-temporal properties such as the users' finite alphabets, constant modulus or signature sequences.

8 Acknowledgments

V. Zarzoso is supported through a Postdoctoral Research Fellowship awarded by the Royal Academy of Engineering. Part of the research summarised in this work was carried out while on leave at the Departamento de Comunicaciones, Universidad Politécnica de Valencia, Spain, in collaboration with Dr. J. Igual and Prof. L. Vergara. The stay was framed within the programme 'PPI-02-01: Estancias en la UPV de Investigadores de Prestigio' (4372).

9 References

1 Tugnait, J.K., Tong, L., and Ding, Z.: 'Single-user channel estimation and equalization', *IEEE Signal Process. Mag.*, 2000, **17**, (3), pp. 16–28
2 Van Der Veen, A.-J., Talwar, S., and Paulraj, A.: 'A subspace approach to blind space-time signal processing for wireless communication systems', *IEEE Trans. Signal Process.*, 1997, **45**, (1), pp. 173–190
3 Tong, L., Xu, G., and Kailath, T.: 'Blind identification and equalization based on second-order statistics: a time domain approach', *IEEE Trans. Inf. Theory*, 1994, **40**, (2), pp. 340–349
4 Moulines, E., Duhamel, P., Cardoso, J.-F., and Mayrargue, S.: 'Subspace methods for the blind identification of multichannel FIR filters', *IEEE Trans. Signal Process.*, 1995, **43**, (2), pp. 516–525
5 Abed-Meraim, K., Loubaton, P., and Moulines, E.: 'A subspace algorithm for certain blind identification problems', *IEEE Trans. Inf. Theory*, 1997, **43**, (2), pp. 499–511
6 Wang, X., and Poor, H.V.: 'Blind equalization and multiuser detection in dispersive CDMA channels', *IEEE Trans. Commun.*, 1998, **46**, (1), pp. 91–103
7 Cardoso, J.-F., and Souloumiac, A.: 'Blind beamforming for non-Gaussian signals', *IEE Proc. F, Radar Signal Process.*, 1993, **140**, (6), pp. 362–370
8 Stuart, A., and Ord, J.K.: 'Kendall's advanced theory of statistics' Vol. I (Edward Arnold, London, 1994, 6th edn.)
9 Yang, H.H.: 'On-line blind equalization via on-line blind separation', *Signal Process.*, 1998, **68**, (3), pp. 271–281
10 Choi, S., and Cichocki, A.: 'Blind equalisation using approximate maximum likelihood source separation', *Electron. Lett.*, 2001, **37**, (1), pp. 61–62
11 Zhang, Y., and Kassam, S.A.: 'Blind separation and equalization using fractional sampling of digital communications signals', *Signal Process.*, 2001, **81**, (12), pp. 2591–2608
12 Comon, P.: 'Independent component analysis, a new concept?', *Signal Process.*, 1994, **36**, (3), pp. 287–314
13 Proakis, J.G.: 'Digital communications' (McGraw-Hill, New York, 2000, 4th edn.)
14 Liu, H., and Xu, G.: 'Closed-form blind symbol estimation in digital communications', *IEEE Trans. Signal Process.*, 1995, **43**, (11), pp. 2714–2723
15 Zarzoso, V., Nandi, A.K., García, J.I., and Domínguez, L.V.: 'Blind identification and equalization of MIMO FIR channels based on second-order statistics and blind source separation'. Proc. DSP-2002, 14th Int. Conf. on Digital signal processing, Santorini, Greece, 1–3 July 2002, Vol. I, pp. 135–138
16 Zarzoso, V., Nandi, A.K., Igual-García, J., and Vergara-Domínguez, L.: 'Blind identification and equalization of MIMO FIR channels based on subspace decomposition and independent component analysis'. Proc. 2nd IMA Int. Conf. on Mathematics in communications, University of Lancaster, UK, 16–18 Dec. 2002
17 Zarzoso, V., and Nandi, A.K.: 'Blind source separation', in Nandi, A.K. (Ed.): 'Blind estimation using higher-order statistics' (Kluwer Academic Publishers, Boston, MA, 1999), chap. 4, pp. 167–252
18 Hyvärinen, A., Karhunen, J., and Oja, E.: 'Independent component analysis' (John Wiley Sons, New York, 2001)
19 Cardoso, J.-F., and Laheld, B.H.: 'Equivariant adaptive source separation', *IEEE Trans. Signal Process.*, 1996, **44**, (12), pp. 3017–3030
20 Zarzoso, V., and Nandi, A.K.: 'Blind separation of independent sources for virtually any source probability density function', *IEEE Trans. Signal Process.*, 1999, **47**, (9), pp. 2419–2432
21 Belouchrani, A., Abed-Meraim, K., Cardoso, J.-F., and Moulines, E.: 'A blind source separation technique using second-order statistics', *IEEE Trans. Signal Process.*, 1997, **45**, (2), pp. 434–444

ATRIAL SIGNAL EXTRACTION IN ATRIAL FIBRILLATION ECGS EXPLOITING SPATIAL CONSTRAINTS

P. Bonizzi[1], *R. Phlypo*[3], *V. Zarzoso*[1], *O. Meste*[1] *and A. Fred*[2]

[1]I3S - UNSA/CNRS, 2000 Route des Lucioles, Les Algorithmes Euclide B, B.P. 121, 06903 Sophia Antipolis Cedex, France
[2]Instituto Superior Técnico - Torre Norte, Av. Rovisco Pais, 1, 1049-001, Lisbon, Portugal
[3]MEDISIP - IBBT, Ghent University, De Pintelaan 185, 9000 Ghent, Belgium
bonizzi@i3s.unice.fr

ABSTRACT

The accuracy in the extraction of the atrial activity (AA) from electrocardiogram (ECG) signals recorded during atrial fibrillation (AF) episodes plays an important role in the analysis and characterization of atrial arrhhythmias. The present contribution puts forward a new method for AA signal automatic extraction based on a blind source separation (BSS) formulation that exploits spatial information about the AA during the T-Q segments. This prior knowledge is used to optimize the spectral content of the AA signal estimated by BSS on the full ECG recording. The comparative performance of the method is evaluated on real data recorded from AF sufferers. The AA extraction quality of the proposed technique is comparable to that of previous algorithms, but is achieved at a reduced cost and without manual selection of parameters.

1. INTRODUCTION

Atrial Fibrillation (AF) represents the most common sustained cardiac arrhythmia in adults. It consists of a misfunction of the atrium characterized by a modification of the normal atrial activity (AA) pattern on the electrocardiogram (ECG) signal. Epidemiologic studies have shown that its prevalence and incidence doubles with each advancing decade beyond 50 years reaching 10% in people over 80 and has direct impact on mortality and morbidity [1, 2].

The accurate extraction of the AA signal from the ECG of AF is of great interest for subsequent analysis. For instance, when the behaviour of the atrioventricular node during AF is addressed, the precision in the relative amplitude of the AF estimated signal plays a critical role. A good estimate of the AA signal is also important for an accurate analysis of the temporal evolution of the spectral content of the AA signal. This analysis is justified by the evident correlation between the spontaneous termination of the episode and the decreasing trend of the AA signal main frequency [3].

It follows that the proper analysis and characterization of AF from ECG recordings requires the cancellation of the signal components associated with ventricular activity (VA), that is, the QRS-T complex. However, this is not a simple task. Indeed, a lot of facts hinder this operation. In particular, the much lower amplitude of the AA signal compared to the ventricular one and the spectral overlapping of the two phenomena, so that linear filtering solutions in the frequency domain are unsuccessful [4].

There exist in the literature two different families of methods applied to cancel out VA in the ECG. The first involves methods that aim for a direct suppression of the QRS-T complex, e.g., using an adaptive template in conjunction with the correct spatio-temporal alignment of every QRS-T complex [5, 6]. The second involves all the methods based on the blind source separation (BSS) approach. All the methods belonging to the first class share similar limitations such as high sensitivity to QRS morphological changes over time and inability to eliminate artifacts other than VA. Moreover, a common limitation to these methods is their inability to exploit the global spatial diversity of an ECG recording.

Starting from the key observation that AA and VA are decoupled, a new interesting perspective has been introduced recently which does not rely on direct elimination of the QRS-T complex [4]. Under this assumptions, the AA extraction problem accepts a formulation based on BSS of instantaneous linear mixtures, in which atrial and ventricular source contributions appear mixed at the electrode outputs in the ECG. First hopeful results obtained in the separation of AA sources through a BSS method gave rise to the definition of more suitable methods exploiting a priori information inside the BSS model.

The method proposed by Castells *et al.* in [7] used one complete independent component analysis (ICA) of the observed signals, followed by a second-order blind identification (SOBI). SOBI exploits the time coherence of the source signals and relies on stationary second-order statistics by performing a joint diagonalization of a set of covariance matrices. A limitation of this method is the presence of two parameters that are to be manually defined. Indeed, sources given by ICA are selected in relation with their kurtosis value, the first parameter. Only sources that satisfy a particular threshold are kept and introduced in SOBI. Moreover, also suitable correlation matrices' time lags must be manually defined. Our method, inspired to that presented by Hesse and James in [8], uses a spatial constraint as an a priori information inside the model. The spatial constraint used is based on an initial estimation of the AA source direction or spatial topography from the T-Q segments. Differently from [8], we use this spatial constraint not directly inside a suitable ICA model, but after a conventional ICA. In conjunction with a spectral concentration criterion, this topography is employed to enhance the separation of AA from VA and other artifacts in the whole recording.

2. METHODS

2.1 Data and Preprocessing

A dataset composed of 22 recordings (all presenting AF) was employed to analyze the proposed idea. All signals were recorded and digitized at a sampling rate of 1KHz. Among the segments employed in this analysis 20 were recorded us-

ing a standard 12-lead system while 2 were recorded using a 9-lead system. Pre-processing was done by applying a zero-phase high pass filter with a cut off frequency of 0.5Hz to remove physiologically irrelevant low frequency signal variations (<1Hz) [9], while a notch filter was implemented to suppress power line noise at 50Hz, applying it in a forward-backward way to eliminate any phase jump [10].

2.2 Blind Source Separation

The BSS consists of recovering a set of source signals from the observation of linear mixtures of the sources. The term blind underlines that little is known about the source signals or the mixing structure, the only hypothesis being the sources' mutual independence [11, 12]. Under this hypothesis, BSS can be carried out by ICA, a technique used to transform multisensor signals into statistically independent components [11]. Mathematically, given N observations of n time series $\mathbf{y}(t) \in \Re^n$, the observed signals, it is possible to write them as a linear combination $\mathbf{M} \in \Re^{n \times m}$ of the original sources $\mathbf{s}(t) \in \Re^m$ $(m \leq n)$. BSS searches for this linear combination and the corresponding sources given the observations. In the noiseless case, the BSS model for an instantaneous linear mixtures is:

$$\mathbf{y}(t) = \mathbf{M}\mathbf{s}(t) \tag{1}$$

where the ith column of M represents the spatial topography that links the ith source with the observed signals. ICA aims to estimate the sources $\hat{\mathbf{s}}(t)$ and the separating matrix $\hat{\mathbf{W}}$:

$$\hat{\mathbf{s}}(t) = \hat{\mathbf{W}}\mathbf{y}(t) \tag{2}$$

with $\hat{\mathbf{W}} \approx \mathbf{M}^\sharp$, and where the $\sharp$ operator stands for pseudo-inverse of the matrix.

Spatial whitening involves a linear transformation of the mean corrected observed signals $\mathbf{y}(t)$, which produces a set of uncorrelated waveforms with unit variance $\mathbf{z}(t)$:

$$\mathbf{z}(t) = \mathbf{V}\mathbf{y}(t) = \mathbf{V}\mathbf{M}\mathbf{s}(t) = \mathbf{H}\mathbf{s}(t) \tag{3}$$

The whitening matrix $\mathbf{V}$ can be obtained from the singular value decomposition (SVD) of the observation matrix $\mathbf{y}(t) = \mathbf{U}\mathbf{S}\mathbf{R}^\mathbf{T}$, and $\mathbf{V} = \sqrt{N}\mathbf{S}^{-1}\mathbf{U}^\mathbf{T}$. Since whitening identifies the independent components up to a rotation, the mixing matrix $\mathbf{H} = \mathbf{V}\mathbf{M}$ for whitened data is orthonormal, i.e. $\mathbf{H}^{-1} = \mathbf{H}^\mathbf{T}$ with unit norm columns. Therefore, sources estimated from whitened data $\hat{\mathbf{s}}(t) = \hat{\mathbf{H}}^T\hat{\mathbf{z}}(t)$ (with $\hat{\mathbf{H}} \approx \mathbf{H}$ and $\hat{\mathbf{z}}(t) = \hat{\mathbf{V}}\mathbf{y}(t)$) do not involve matrix inversion. This gives the possibility to apply the transpose of matrix $\hat{\mathbf{H}}$ on $\hat{\mathbf{z}}(t)$ directly, withouth further computations.

For the estimate of the a priori information that is used in the proposed method, a further model based only on the temporal segments in the observations free from any VA is needed. This model is obtained in the following way. Firstly, the set of ECG recordings under analysis (e.g. Fig. 1(a)) is taken and, after the QRS-T complexes detection, only the T-Q segments are isolated, so that $\mathbf{y}_{AA}(t) = \{\mathbf{y}(t_i) \mid t_i \notin QRS-T\}$. This new set of signals contains only AA and possible noise, but it is quite reasonable to suppose it free from any VA, confined in the QRS-T segment. Secondly, the BSS model for this new set is generated in two different ways, that is, applying either ICA or principal component analysis (PCA) (e.g., through SVD):

$$\mathbf{y}_{AA}(t) = \mathbf{M}_{AA}\mathbf{s}_{AA}(t) \tag{4}$$

$$\mathbf{y}_{AA}(t) = \mathbf{B}_{AA}\mathbf{z}_{AA}(t) \tag{5}$$

where $\mathbf{B}_{AA}^\sharp$ is the whitening matrix and $\mathbf{z}_{AA}(t)$ the set of decorrelated sources. In this way, two sets of independent (4) or simply decorrelated (5) sources respectively, formed by the components present in T-Q segments only, are obtained.

2.3 ICA and Spatial Constraint

In many BSS problems exploiting independence, one may only have particular interest in a component or a set of desired sources, and automatically discard the remainder of uninteresting signals or noise. To this end, ICA methods exploiting some a priori information as a referential constraint inside the problem have been presented in the literature. Both signal extraction and noise rejection essentially involve the estimation of a target source, in a more precise way than conventional ICA. Therefore, the achievement of a suitable constraint becomes a crucial task.

The observation that AA and VA are decoupled underlines the idea that their electrical vectors inside the heart should be different, and so their topographies. This naturally draws our attention to their spatial differences, rather than on their temporal ones. The importance of exploiting spatial diversity of an ECG recording is then clear. Therefore, a particular AA spatial constraint, as the AA spatial topography, can be used as a tool to get rid of the VA present in the ECG.

A spatial constraint can be defined either as an abstract prior knowledge (e.g., all the constraints defined on the mixing matrix structure, as orthogonality, orthonormality etc.) or in a more specific way. We use a specific spatial constraint, for each particular subject under analysis: the estimation of the AA spatial topography $\hat{\mathbf{m}}_{AA}$. As said before, this spatial constraint can be generated applying either ICA (4) or PCA (5) to the set $\mathbf{y}_{AA}(t)$. When the spatial constraint is constructed using ICA, as in the model described in (4), the second step is to search for the best AA source that describes the AF, $\hat{s}_{AA}$, inside the set of the estimated output sources $\hat{\mathbf{s}}_{AA}(t)$. The criterion used for selecting the best AA source is Spectral Concentration (SC) of the AA around its main peak, computed according to the following expression [7]:

$$SC = \frac{\int_{0.82f_c}^{1.17f_c} P_{AA}(f)\,df}{\int_0^{f_s/2} P_{AA}(f)\,df} \tag{6}$$

The above equation is a measure for the compactness of the spectrum around the central frequency f_c, that is the modal frequency in the 3-12Hz interval. P_{AA} is the power spectrum of the AA signal, $f_s/2$ is the half of the sampling frequency [7]. The column of the estimated mixing matrix $\hat{\mathbf{M}}_{AA}$ associated to the selected source is the topography of interest and defines the spatial constraint $\hat{\mathbf{m}}_{AA}$.

Alternatively, when the spatial constraint is constructed using PCA, as in the model described in (5), we can take as reference topography $\hat{\mathbf{m}}_{AA}$ the first column of the estimated matrix $\hat{\mathbf{B}}_{AA}$, that is the column associated with the decorrelated source with the highest energy. This is because AA is expected to be the component contributing to $\mathbf{y}_{AA}(t)$ with the highest variance. Moreover, it is possible to distinguish between spatial constraints of different severity, namely *hard* and *soft* spatial constraints, according to the uncertainty about their constraint topographies.

2.4 Hard constraints

If the degree of certainty about a particular spatial constraint topography $\hat{\mathbf{m}}_{AA}$ is quite high, it is possible to use it as a *hard* constraint. Indeed, in this case $\hat{\mathbf{m}}_{AA}$ can be used to define the weight vector of a spatial filter applied to the whitened set $\mathbf{z}(t)$ of observed signals. The spatial filter applies the AA signal topography on the prewhitened waveforms, for VA removal, as follows:

$$\hat{s}_{AA}(t) = \hat{\mathbf{h}}_{AA}^T \mathbf{z}(t) \tag{7}$$

where $\hat{s}_{AA}(t)$ is the output of the filter, that is, the estimated AF signal, and $\hat{\mathbf{h}}_{AA}$ is obtained by transformation of $\hat{\mathbf{m}}_{AA}$ as $\hat{\mathbf{h}}_{AA} = \mathbf{V}\hat{\mathbf{m}}_{AA}$. This transformation allows the projection of $\hat{\mathbf{m}}_{AA}$ on the whitened signal subspace insuring the appropriate use of the spatial constraint on the full recording.

2.5 Soft constraints

If the degree of uncertainty about the spatial constraint topography $\hat{\mathbf{m}}_{AA}$ is not negligible, it is better to introduce a *soft* constraint. With respect to other methods (e.g., [8]), we use this kind of a priori information on AF not directly inside a suitable ICA algorithm, but after a conventional ICA. First, AA spatial topography $\hat{\mathbf{m}}_{AA}$ is obtained, as explained in Section 2.3, and a conventional ICA is applied to the observed signals $\mathbf{y}(t)$, obtaining the set of independent sources $\hat{\mathbf{s}}(t)$ related to them, according to the model introduced in (1)-(3). Secondly, the best source that describes the AF, inside the set of output sources $\hat{\mathbf{s}}(t)$ is searched. The criterion used for selecting the best AF source is the SC of the AA source around its main peak [7]. We denote $\mathbf{m}$ the column of the mixing matrix associated with the selected source. Once we have obtained both the topography of the reference $\hat{\mathbf{m}}_{AA}$ and that of the source of interest $\hat{\mathbf{m}}$, we search for the topography $\hat{\mathbf{h}}'_{\text{opt}}$ maximizing the SC in the plane defined by the two whitened vectors $\hat{\mathbf{h}}_{AA}$ and $\hat{\mathbf{h}} = \mathbf{V}\hat{\mathbf{m}}$. An orthonormal basis of that plane can be defined as:

$$\mathbf{e}_1 = \hat{\mathbf{h}}_{AA} \tag{8}$$

$$\mathbf{e}_2 = \frac{\hat{\mathbf{h}} - \text{proj}_{\hat{\mathbf{h}}_{AA}}\hat{\mathbf{h}}}{\| \hat{\mathbf{h}} - \text{proj}_{\hat{\mathbf{h}}_{AA}}\hat{\mathbf{h}} \|} \tag{9}$$

where notation $\text{proj}_{\mathbf{c}}\mathbf{d}$ stands for the projection of vector $\mathbf{d}$ on vector $\mathbf{c}$. Accordingly,

$$\hat{\mathbf{h}}'_\alpha = \mathbf{e}_1\cos(\alpha) + \mathbf{e}_2\sin(\alpha) \tag{10}$$

$$\hat{s}'_\alpha(t) = \hat{\mathbf{h}}'^T_\alpha \hat{\mathbf{z}}(t) \tag{11}$$

where $\hat{\mathbf{h}}'_\alpha$ and $\hat{s}'_\alpha(t)$ represent respectively the generic spatial topography and the generic source, defined in the aforementioned plane, to be optimized. The source estimate associated with the largest SC value, $\hat{s}'_{\text{opt}}(t) = \hat{s}'_{\alpha_{\text{opt}}}(t)$, is taken as the best estimation of the AA source $\hat{s}_{AA}(t)$, its corresponding topography being $\hat{\mathbf{h}}'_{\text{opt}} = \hat{\mathbf{h}}'_{\alpha_{\text{opt}}}$, where

$$\alpha_{\text{opt}} = \arg\max_\alpha \mathbf{SC}(\hat{s}'_\alpha(t)) \tag{12}$$

The above SC optimization can be carried out algebraically at very little computational cost.

	$\mu_{SC} \pm \sigma_{SC}\,(\%)$	$\mu_k \pm \sigma_k\,(n.u.)$	$\mu_{f_c} \pm \sigma_{f_c}\,(Hz)$
COM2	52.00 ± 14.69	-0.0951 ± 0.5587	5.5154 ± 1.29
$\mathbf{SCICA}^{\mathbf{hard}}_{\mathbf{ICA}}$	46.56 ± 18.76	0.0519 ± 0.589	5.421 ± 1.2678
$\mathbf{SCICA}^{\mathbf{hard}}_{\mathbf{PCA}}$	36.09 ± 22.618	1.0329 ± 1.8245	4.6442 ± 1.2348
$\mathbf{SCICA}^{\mathbf{soft}}_{\mathbf{ICA}}$	58.39 ± 10.57	-0.2085 ± 0.4403	5.5154 ± 1.2656
$\mathbf{SCICA}^{\mathbf{soft}}_{\mathbf{PCA}}$	58.01 ± 12.14	-0.1717 ± 0.526	5.5209 ± 1.2736
SOBI	60.82 ± 9.21	-0.1391 ± 0.4967	5.3711 ± 1.3255
ST − Canc	57.01 ± 11.98	0.5511 ± 2.8898	5.4321 ± 1.2159

Table 1: Mean performance estimates of Spectral Concentration (SC), kurtosis (k) and characteristic frequency (f_c) for the different methods under analysis.

3. RESULTS

Since methods that exploit spatial constraints, even if in different ways from how presented here, already exist in the literature, the proposed method is named Spatial Constrained ICA (SCICA), choosing the same name of that proposed by Hesse and James [8]. This method for the automatic extraction of the AF from a set of observed ECG signals was applied to a dataset of 22 patients. Its performance is evaluated both for the PCA- and the ICA-defined constraints, and they are compared to those of some classical ones, among which, a conventional ICA (COM2) [11], a spatio-temporal cancellation approach (ST-Canc) [6] and a spatio-temporal BSS approach (SOBI) [7]. For completeness, the performance of the presented method, using either *hard* or *soft* constraints, was evaluated in terms of SC of the AA estimated source around its main peak, characteristic AF frequency value at the peak, and excess kurtosis of the estimated source. Mean value μ and standard deviation σ of each index are presented for each method.

Results are reported in Table 1, while an example of final estimation of the AF source $\hat{s}_{AA}(t)$ for different methods is shown in Fig. 1(b), when *soft* constraints are used for SCICA. Finally, Fig. 2 shows the box and whisker plot of the SC parameter only, for SCICA with *soft* constraints (both ICA and PCA defined), and for the other methods.

From the values of the performance indeces (Table 1), we note that SCICA shows good performances when *soft* constraints are used, obtained either using ICA or PCA, as in Section 2.3, according to the SC values found for the different methods. Whereas, performance is not so good when *hard* constraints are employed. Indeed, the variance of the AA set of sources estimated using *hard* constraints is quite high, attesting the strong correlation between the quality of the estimated source and the appropriateness of the chosen constraint.

4. DISCUSSION

This work has pointed out two important issues. Firstly, the importance of using a suitable a priori information in combination with the ICA algorithm when the extraction of the AF signal is addressed. Secondly, the use of SC as a preferential parameter in the search for the optimal AF signal estimate. The idea that AA and VA electrical vectors are spatially different supports the idea of using AF spatial topography esti-

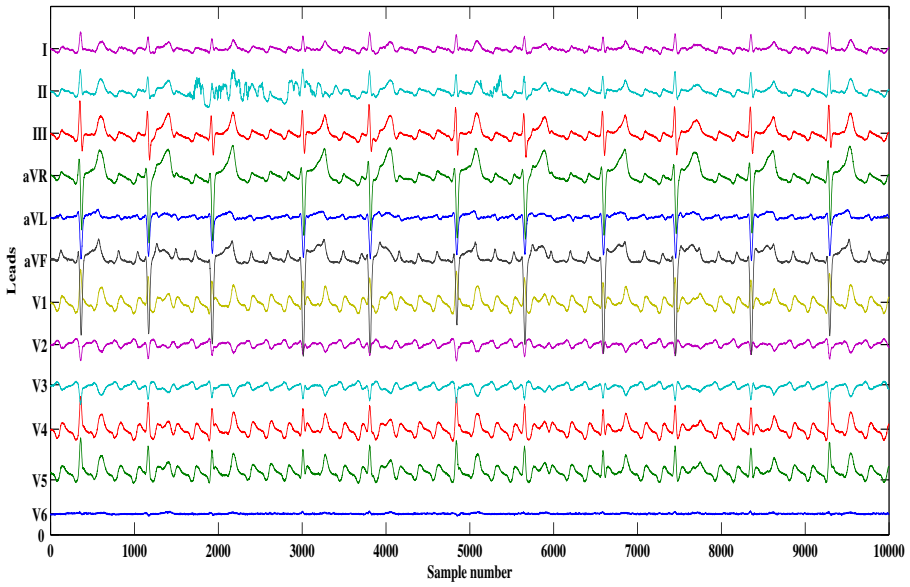

(a)

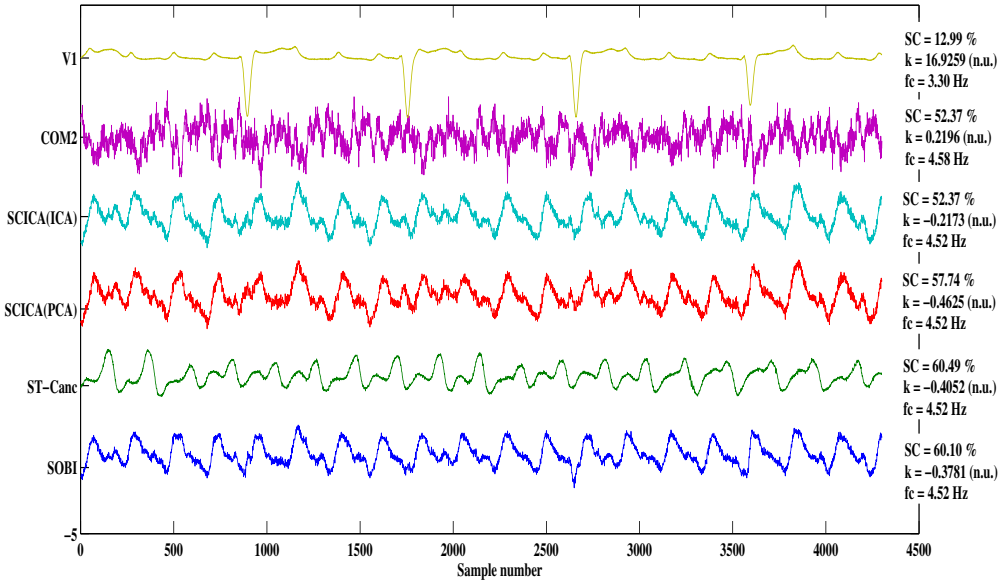

(b)

Figure 1: (a) Example of a 12-leads ECG recording. Signals in the figure are 10s long; leads, specific ECG leads. (b) V1 ECG lead and AA signals etimated using different methods. For SCICA only *soft* constraints are used. Values of Spectral Concentration(SC), kurtosis (k) and characteristic frequency (f_c) are presented for each signal. A 4.5s segment is represented for the bottom figure.

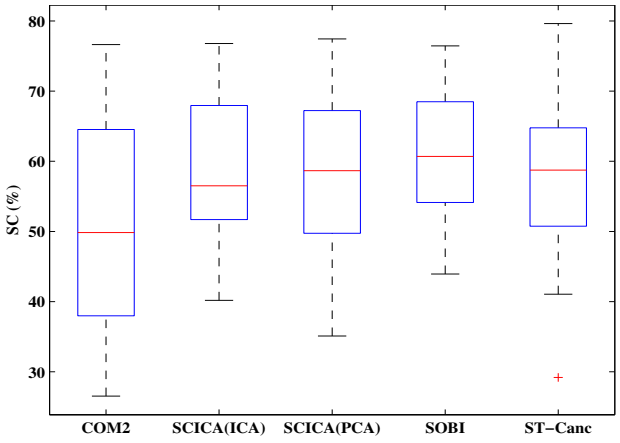

Figure 2: Box and whisker plot of the Spectral Concentration (SC) values for diffent methods. The box has lines at the lower quartile, median, and upper quartile values. The whiskers are lines extending from each end of the box to show the extent of the rest of the data. Outliers are data with values beyond the ends of the whiskers, and are represented as crosses; (%) percentage.

mate as spatial constraint.

The use of SC not simply as a performance parameter, but as an optimization criterion inside the AF signal extraction model seems to improve the AA estimation quality. This can be noted by looking at the ability of SCICA to get almost the same performance as other methods suitable for the extraction of the AF, but simply exploiting the statistical independence between AA and VA, and the optimization of SC.

An important result is the capability of getting similar performance for the proposed method when either SVD-defined or ICA-defined constraints are used in a *soft* way. This gives us the possibility to focus the attention mainly on their construction using SVD, with benefits in terms of complexity of the algorithm.

Finally, low performance values obtained when *hard* constraints are employed reveal it is inappropriate to apply the AA topography estimate directly on the observation set. To use it as *soft* constraint as a part of an optimization criterion seems to be a more appropriate option, as shown by the results.

5. CONCLUSION

A new fully automated method for the extraction of AA signals in ECG recordings of AF has been presented. The method is based on an initial estimation of the AA source direction or spatial topography from the T-Q segments. In conjunction with a spectral concentration criterion, this topography is employed to enhance the separation of AA from VA and other artifacts in the whole recording. Results show that the proposed methodology constitutes a cost-effective alternative to previous BSS-based methods. Indeed, a spatial reference computed from the PCA of the T-Q segments achieves a satisfactory performance while preventing the manual selection of parameters (e.g., kurtosis threshold or autocorrelation time lags).

Future works aim to exploit simultaneously reference AA topographies related not only to the AA source with the highest SC but also to other candidate AA sources in cases where more than one AA source may be present during an AF episode. A new definition of SC capable of describing the information contained in the harmonics of the characteristic frequency could allow a more efficient exploitation of this parameter.

Acknowledgements

The authors would like to express their gratitude to Leif Sörnmo and Francisco Castells for providing the real data. The work of Bonizzi Pietro is supported by the EU by a Marie-Curie Fellowship (EST-SIGNAL program : http://est-signal.i3s.unice.fr) under contract No MEST-CT-2005-021175.

REFERENCES

[1] W. K. Kannel, R. D. Abbott, D. D. Savage, and P. M. McNamara. Epidemiologic features of chronic atrial fibrillation: the Framingham study. *N Engl J Med*, 306:1018–22, 1982.

[2] A. D. Krahn, J. Manfreda, R. B. Tate, F. A. Mathewson, and T. E. Cuddy. The natural history of atrial fibrillation: incidence, risk factors, and prognosis in the Manitoba Follow-Up Study. *Am J Med*, 98:476–84, 1995.

[3] Petrutiul, S. and Sahakian, V. and Ng, J. and Swiryn, S. Analysis of the surface electrocardiogram to predict termination of atrial fibrillation: The 2004 computers in cardiology/physionet challenge. *Proc. Computers in Cardiology*, 31:105–108, 2004.

[4] J. J. Rieta, F. Castells, C. Sánchez, V. Zarzoso, and J. Millet. Atrial activity extraction for atrial fibrillation analysis using blind source separation. *IEEE Trans on Biomed Eng*, 51, No. 7:1176–86, July 2004.

[5] L. Sörnmo M. Stridh. Spatiotemporal QRST cancellation techniques for analysis of atrial fibrillation. *IEEE Trans. Biomed. Eng.*, 48:105–111, January 2001.

[6] O. Meste and N. Serfaty. QRST cancellation using bayesian estimation for the auricular fibrillation analysis. In *Engineering in Medicine and Biology*, 2005.

[7] F. Castells, J. J. Rieta, J. Millet, and V. Zarzoso. Spatiotemporal blind source separation approach to atrial activity estimation in atrial tachyarrhythmias. *IEEE Transactions on Biomedical Engineering*, 52(2):258–267, February 2005.

[8] C. W. Hesse and C. J. James. The FastICA algorithm with spatial constraints. *IEEE Signal Process. Lett.*, 12:792–795, 2005.

[9] Leif Sörnmo and Pablo Laguna. *Bioelectrical Signal Processing in Cardiac and Neurological Applications*. Elsevier Academic Press, 2005.

[10] S. K. Mitra. *Digital Signal Processing: A computer-based approach,* 2nd ed. McGraw-Hill, 2001.

[11] P. Comon. Independent component analysis: a new concept? *Signal Processing*, 36:287–314, 1994.

[12] Hyvrinen, A. and Karhunen, J. and Oja, E. *Independent Component Analysis*. Wiley, 2001.

30th Annual International IEEE EMBS Conference
Vancouver, British Columbia, Canada, August 20-24, 2008

Eigenvector Analysis for Separation of a Spectrally Concentrated Source from a Mixture

Ronald Phlypo, Vicente Zarzoso and Ignace Lemahieu

***Abstract*— An objective function is presented to recover a spectrally narrow band signal from multichannel measurements, as in electrocardiogram recordings of atrial fibrillation. The criterion can be efficiently maximized through the eigenvalue decomposition of some spectral correlation matrices of the whitened observations across appropriately chosen frequency bands. It is conjectured that the global optimum so attained recovers the source of interest when its spectral concentration around its modal frequency is maximal. Numerical experiments on synthetic data seem to support the validity of this hypothesis. Moreover, the components extracted from a patient data set with known atrial fibrillation show the characteristics of the associated f-wave as described in medical literature.**

I. INTRODUCTION

Atrial Fibrillation (AF) and atrial flutter (AFL) are the most prevalent cardiac arrhythmia encountered in clinical practice and accounts for approximately one third of the hospital admissions for cardiac rhythm disturbances. Its prevalence is about 0.4-1.0% in the general population and increases with age to reach up to 9% of the population aged 80 years and older. Amongst others, because of an aging population and more frequent monitoring, during the past 20 years there has been an increase of hospitalization of about 66%. This trouble is also associated with an augmented risk of stroke, heart failure and all-cause mortality [1].

Diagnostization and characterization of AF/AFL is mainly based on the noninvasive electrocardiographic (ECG) signals and has evolved from simple f-wave amplitude characterization to the estimation of spectral parameters [2]. However, the ventricular waveforms (QRS-T) have an amplitude many times larger than the atrial wave to be characterized and thus masks our signal of interest, as can be seen in Figure 1.

Proposed techniques to solve for this masking are based on the cancellation of the ventricular contribution in the ECG [3] or the decomposition into independent components (ICA) [4], whether or not with some priors on the signal of interest or its nullspace [5], [6]. Despite their popularity they suffer from some major drawbacks. The cancellation methods require a robust R-wave detection to synchronize the waveforms. Moreover, they neither make use of the spatial interdependencies of the leads, except for a possible rotation of the main electrical axis of the heart, neither do they account for individual waveform variations of the complexes. On the contrary, the spatial ICA based methods do take into account the spatial dependencies of the signals and are not affected by individual waveform variations, but they are generally not well suited for sources whose distribution parameters (higher order cumulants) are close to those of a Gaussian, unless its sub-Gaussian character is taken into account [5] or additional temporal information is used [6].

This work was supported by FWO contract number G.0095.05

R. Phlypo and I. Lemahieu are with Ghent University - IBBT, IbiTech-MEDISIP, Ghent, Belgium {ronald.phlypo, ignace.lemahieu}@ugent.be

V. Zarzoso is with I3S, University of Nice-Sophia Antipolis - CNRS, Sophia Antipolis, France zarzoso@i3s.unice.fr

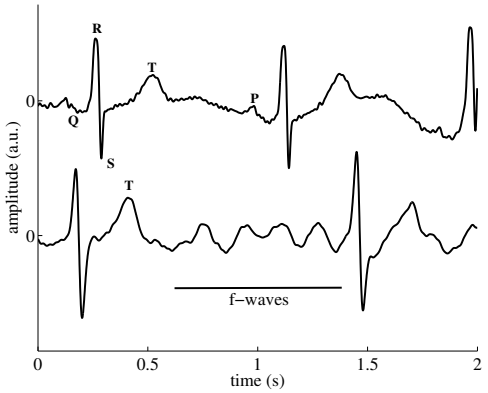

Fig. 1. Example of normal sinus rhythm (upper) and atrial fibrillation wave (lower)

However, the method of [5] deals only with the separation of two observations into two signals in its original version, namely the ventricular, respectively the atrial signal. The method of [6] makes use of an empirical parameter to threshold the cumulants of the signals obtained by ICA. The signals having cumulants below the threshold are subsequently fed to a spatiotemporal decorrelation method. However, the kurtosis threshold is chosen empirically, and the method is bound to provide poor results when the atrial activity cannot be fully separated from the ventricular activity by the initial ICA stage. All of the above methods are based on numerical optimization and even if some of them are feasible under multiple iterations of partial closed-form solutions, they all lack a final solution that can be represented as a global optimum for a well-defined function for AA estimation.

This contribution proposes the spectral concentration indicator of [6] as an explicit criterion for the extraction of an estimate of the AF/AFL source, and shows that it can be cost-effectively maximized by the eigenvalue decomposition of some well-chosen spectral correlation matrices of the available data.

II. METHODS

A. Notation

Scalars, constants, column vectors and matrices are represented by thin face lower case, light face upper case, bold

978-1-4244-1815-2/08/$25.00 ©2008 IEEE. 1863

face lower case and bold face upper case, respectively. The Fourier transform of a time series $x[n]$ is represented by $\tilde{x}(\omega)$.

B. Data and Preprocessing

We use 30 patient datafiles recorded at the Clinical University Hospital, Valencia, Spain, using a Prucka Eng. Cardiolab system with 12-leads, sampled at $f_s = 1000$ time samples per second [6]. All patients were under treatment of amiodarone. Baseline wander has been canceled out by a zero-phase 12^{th} order Chebychev filter with minimum passband ripple.

The simulated dataset is made up of 3 basis waveforms ($\mathbf{s}[n]$), namely a triangular waveform ($s_1[n]$), an impulsive waveform ($s_2[n]$) and stochastic non-Gaussian noise ($s_3[n]$) to simulate respectively AF/AFL, a QRS-wave complex and noise[1].

C. Linear Spatial Filtering

Consider N time samples taken from a 12-lead ECG, $\mathbf{y}[n] \in \mathbb{R}^{12}, n = 1 \dots N$ and a spatial mixing channel $\mathbf{a} \in \mathbb{R}^{12}$, such that $\mathbf{y}[n] = \mathbf{a}s[n] + \eta[n]$, where $s[n] \in \mathbb{R}$ is the atrial (fibrillatory or flutter) activity and $\eta \in \mathbb{R}^{12}$ is the activity in the recording $\mathbf{y}[n]$ that is not related to the atrial activity. This model can be seen as a first order approximation of a spatially fixed collection of oriented dipoles whose activity is measured at the body surface, assuming that the body tissues behave as a purely resistive propagation medium in the frequency range of interest [7]. From the measurement setup, it can easily be seen that η accounts for external noise and other physiological electrical source contributions, amongst others the ventricular activity.

Our goal is to inverse the above system by finding the linear filter $\mathbf{w}$ that recovers an estimate of the auricular activity $\hat{x}[n] = \mathbf{w}^T\mathbf{y}[n]$ at its output.

D. An objective function for AF/AFL

Consider now the spectral concentration (SC) indicator [6], given as:

$$\mathrm{SC}(x) = \frac{1}{\mathbf{P}_x} \int_{0.872 f_m}^{1.125 f_m} |\tilde{x}(f)|^2 \mathrm{d}f \qquad (1)$$

where $|\cdot|$ denotes the absolute value of $\tilde{x}(f)$, f_m is the modal frequency and $\mathbf{P}_x$ is the total power of x, i.e. $\int_0^N |x[n]|^2 \mathrm{d}n$. Now, under the assumption that our AF/AFL signal is narrow band around the modal frequency f_m and $\tilde{x}$ has maximum power in the frequency band $[0.875 f_m, 1.125 f_m]$Hz with respect to any other linear combination of η and s, (1) has a maximum for AF/AFL. Furthermore, the optimum is available under a closed form expression of eigenvalues, hence we call the method described next Eigenvalue-based Spectral Optimization (ESO).

Remark that since in this work $x[n] \in \mathbb{R}$, we have $\tilde{x}(f_1)\tilde{x}^\star(f_1) = \tilde{x}(f_s - f_1)\tilde{x}^\star(f_s - f_1) = |x(f_1)|^2$, where $\tilde{x}^\star$ is the complex conjugate of $\tilde{x}$. We can thus use uniquely positive frequency values without changing the value of (1).

[1]Matlab files containing the generators and the algorithm can be downloaded from http://users.ugent.be/∼rphlypo/software/

E. Prewhitening

Maximizing (1) can be done by maximizing the nominator under a constant denominator constraint. Therefore, we will subdivide our problem into two subproblems, as $s[n] = \mathbf{w}^T\mathbf{y}[n] = \mathbf{q}^T\mathbf{V}^T\mathbf{y}[n]$, where $\mathbf{q} \in \mathbb{R}^m$ and $\|\mathbf{q}\|_2 = 1$. The matrix $\mathbf{V} \in \mathbb{R}^{m \times m}$ is a matrix which will guarantee that the denominator in (1) will remain constant under unit norm projections. Denote by $\mathbf{z}[n]$ the transformed variables $\mathbf{V}^T\mathbf{y}[n]$, with $\mathcal{E}\{\mathbf{z}^T\mathbf{z}\} = \mathbf{I}_m$, where $\mathcal{E}\{\cdot\}$ is the expectation value and $\mathbf{I}_m$ the unit matrix in $\mathbb{R}^{m \times m}$. The expectation matrix can be reduced to the identity matrix by taking the columns of $\mathbf{V}$ as $\mathbf{e}_i/\sqrt{\lambda_i}$, where $\mathbf{e}_i$ is the eigenvector associated to the eigenvalue λ_i of the expectation matrix $\mathcal{E}\{\mathbf{y}\mathbf{y}^T\}$. For unit vectors $\mathbf{q}$, we then have

$$\mathbf{P}_x = \mathbf{q}^T \Phi_{\mathbf{z}}^{(0, f_s)} \mathbf{q} = 1 \ , \qquad (2)$$

where $\Phi_{\mathbf{z}}^{(f_1, f_2)} = \mathrm{Re}\left\{\int_{f_1}^{f_2} \tilde{\mathbf{z}}(f)\tilde{\mathbf{z}}^H(f)\mathrm{d}f\right\}$, where $\mathrm{Re}\{\cdot\}$ is the real part of its argument and $(\cdot)^H$ is the Hermitian transpose operator. The identity in (2) can directly be derived from Parseval's identity, $\mathcal{E}\{\tilde{\mathbf{z}}\tilde{\mathbf{z}}^T\} = \mathcal{E}\{\mathbf{z}\mathbf{z}^T\}$.

F. Spectral Optimization under Prewhitening

The only unknown that remains in the system is the vector $\mathbf{q}$. The vector $\mathbf{q}$ that is the solution to our problem is the one which maximizes the nominator in (1), i.e. the quadratic equation

$$\Psi(x) = \Psi\mathbf{q} = \mathbf{q}^T \Phi_{\mathbf{z}}^{(0.875 f_m, 1.125 f_m)} \mathbf{q} \ . \qquad (3)$$

The maximum of equation (3) can be found by looking for the eigenvector associated to the largest eigenvalue of (3). However, solving for the eigenvector requires the knowledge of the modal angular frequency f_m. In what follows we show that the modal frequency can be estimated by solving two maximum eigenvalue subproblems.

G. Estimation of $\hat{f}_m$

The modal frequency is not known *a priori* and should be estimated from the set of observations. We will rely here on the prior knowledge that the frequency of AF/AFL generally lies in the interval 3-9Hz [1]. However, as can be seen from Figure 2, this is also the frequency interval on which the T-wave has its major power contribution. We thus need to be able to distinguish between both activities. To this extent we make use of the fact that notwithstanding their spectral overlap, they do not share the same spectral parameters. Figure 2 shows that the AF/AFL spectrum is much more concentrated around the modal angular frequency than is the T-wave spectrum and that its modal frequency differs, and this is usually the case.

To separate the two activities, we propose to extract two intermediate components $\hat{x}_1$ and $\hat{x}_2$ by applying the filters according to the eigenvectors that are associated to the largest eigenvalues of the spectral matrices $\Phi_{\mathbf{z}}^{(3,6)}$, respectively $\Phi_{\mathbf{z}}^{(5,9)}$. For the two resulting estimates, $\hat{x}_1$ and $\hat{x}_2$, we estimate their respective modal frequency $\hat{f}_m^{x_1}$ and $\hat{f}_m^{x_2}$, together with their spectral concentration in the spectral band

TABLE I

THE PERCENTILES OF THE SPECTRAL CONCENTRATION DIFFERENCES BETWEEN $x_1[n]$ AND $s_1[n]$

percentile	0	1	25	50	75	99	100
ESO (%)	-4.93	-0.18	0.01	0.03	0.08	0.48	1.31
ST-BSS (%)	-26.20	-1.93	-0.27	-0.07	-0.01	0.20	2.10
ESO w.r.t. ST-BSS (%)	-4.84	-0.22	0.04	0.10	0.33	2.21	26.18

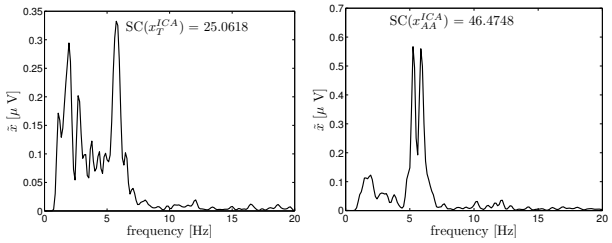

Fig. 2. Example of the power spectral density for the T-wave component (left) and atrial fibrillation (right) as estimated by the COM2 ICA algorithm [8] with SC (1) around $\hat{f}_m = \arg\max_f \tilde{x}(f)$ [in %].

as defined in (1). Finally, we use the estimate $\hat{f}_m = \hat{f}_m^{x_i}$, where i is associated with the intermediate component who has the highest spectral concentration. We then optimize for the spectral concentration around $\hat{f}_m$ as described above (section II-F).

III. RESULTS

A. Simulated Data

We will first show results on a simulated dataset, since it allows to compare the algorithm objectively with existing algorithms. The results over 1000 Monte Carlo realisations have been taken to extract $x_1[n]$ from the observations ($\mathbf{y}[n]$) generated through a full rank mixing ($\mathbf{A}$) of the above three sources $\mathbf{s}[n]$. The parameters of the algorithm have been set to look for the modal frequency in the 1-20 Hz frequency band prior to optimizing the spectral concentration. We compare it to a spatio-temporal blind source separation method ST-BSS [6] where the time delay vector for joint diagonalization has been adapted to include, next to 0 and 1, all prime numbers in the interval $[0, 100]$. This guarantees a lower susceptibility to the prior on the frequency band and is valid in the simulation case since we know from the set-up that there is only a single narrow banded source.

Results for the spectral concentration with respect to its value for the simulated waveform $s_1[n]$ are given in Table I for both the proposed method (ESO) and ST-BSS. The modal frequency has been estimated correctly in both cases with a mean value of zero and no significant outliers (p-value is 1 for a Wilcoxon rank sum test against a Dirac Delta distribution at zero with no rejection of the null-hypothesis at a 10^{-6} confidence level). The mean and standard deviation of the correlation coefficients between $x_1[n]$ and $s_1[n]$ amount to 0.9994 ± 0.0010 for ESO, respectively 0.9991 ± 0.0011 for ST-BSS (minima 0.9928 and 0.9933, maxima 1.0000 and 1.0000, respectively).

B. Patient Data

To evaluate the algorithm's performance we calculate the spectral concentration and estimate the modal frequency of the estimate obtained by the presented method optimized around $\hat{\omega}_m$ (ESO), respectively in the full 3-9Hz frequency band (ESO-fb), ST-BSS [6] (with the time delays as chosen in the original paper) and a maximum likelihood based blind source separation algorithm (ML-BSS) [5].

TABLE II

SC (1) AND $\hat{f}_m = \hat{\omega}_m f_s$ FOR THE SOURCE SIGNALS ESTIMATED WITH ESO AND TWO BSS METHODS ($\mu \pm \sigma$).

	SC	$\hat{f}_m$
ESO	51.11±17.25	5.31±1.22
ESO-fb	40.82±18.55	5.72±1.08
ST-BSS	42.21±17.15	5.13±1.39
ML-BSS	13.66±6.37	5.06±1.44

The results for the spectral concentration and the modal frequency estimate are given in table II as their mean and standard deviation obtained from the dataset.

Since the above results are unable to show the relation between the parameters calculated on the estimates by the different methods on the same data, we give the differences of the spectral concentration and modal frequency between the source $x[n]$ estimated by ESO and $x[n]$ as estimated by the methods ESO-fb, ST-BSS and ML-BSS, respectively, in Figure 3.

The correlation of the parameters over the methods is only obvious for ESO and ST-BSS ($\rho_{SC} = 0.88$ and $\rho_{\hat{\omega}_m} = 0.85$), while the ESO-fb method correlates only slightly with ESO and ST-BSS for the spectral concentration ($\rho_{SC} = 0.52$ in both cases), whilst the modal frequency correlation is $\rho_{\hat{\omega}_m} = 0.14$ with respect to both methods (and even negatively with respect to ML-BSS). The parameters of ML-BSS have no correlation that is beyond 0.25 for both spectral concentration values and modal angular frequencies.

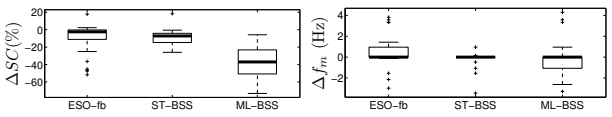

Fig. 3. Box-Whiskers plots of the differences between the parameters of the estimated sources with respect to the ESO method.

In Figure 4 we show a detail of an original data record and the estimated sources by ESO, ST-BSS and ML-BSS. The plots are given for illustrative purposes and show that the solution is physiologically interpretable and in line with medical expectations, namely a sawtooth wave with a modal frequency in the 4-9Hz band [1].

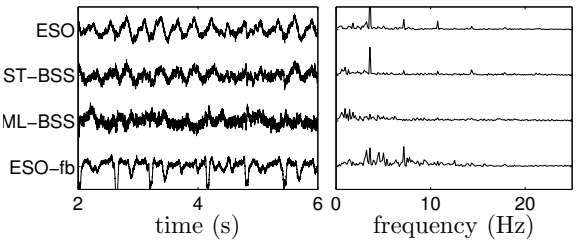

Fig. 4. Example of the AA source estimates on real data: (left) zoom on the V1-lead potentials and the estimated time courses with (right) the absolute values of their respective Fourier terms obtained by a FFT (all signals have arbitrary units).

IV. DISCUSSION

The results obtained from the simulations show that the presented method is able to extract a waveform with the same modal frequency and similar spectral concentration as the original waveform $s_1[n]$. Differences are noticeable through small changes in the spectral concentration value, because our model assumes total orthogonality between $s_1[n]$ and the other contributions $\eta[n]$. This orthogonality was not a prerequisite in the simulation set up and thus some source information might be wrongly estimated due to the mismatch of the simulations with our assumed model. However, as one can see from section III-A, the estimation is fairly close to the original source when considering the correlation coefficient.

Results on real data show that the frequencies estimated by the algorithm are in line with the results obtained by [6] and with clinical knowledge [1]. From Figure 3, it can be observed that the spectral concentration is greater almost everywhere when calculated from the ESO estimate than for the other two algorithms or the estimate in the whole 4-9Hz band. This result may not be surprising, since our algorithm optimizes explicitly for the spectral concentration.

Accordingly to this direct maximization of the spectral concentration for the ESO estimate, we observe that for the example given in Figure 4 the spectral noise floor is lowered and the multi-modality, or harmonic structure of the waveform, becomes more articulated. The former is a property that follows directly from the definition of our function (1) under a constant denominator, while the latter is connected to the application of a spatial filter. Since we optimize for the variance in the narrow band around the estimated frequency $\hat{f}_m$, the constant variance constraint assures that the variance outside this spectral band is kept as low as possible, which explains the lower noise floor. However, the spatial filter $\mathbf{q}$ requires that the estimated signal stems from a fixed spatial origin (not necessarily a single spatial point) and has a fixed orientation [7]. Because a spatial filter makes no distinction in spectral content and acts as a spatial band pass filter for all activity that stems from its physical origin(s), the source of interest with maximum spectral concentration in the band of interest (either 3-6Hz, either 5-9Hz), will be recuperated at the output of the filter $\mathbf{q}$ with its harmonics, even though they penalize SC (1).

In addition, the method is flexible and can easily be extended to optimize for non-stationary spectra, either through direct optimization of the (weighted) sum of the time-varying frequency covariance matrices around $\hat{\omega}_m[k]$ as defined in (1), where k represents the frame index, or through a joint diagonalization of these spectral covariance , along the lines of [9].

V. CONCLUSION

We propose to estimate the atrial activity in ECG recordings of AF by maximizing the spectral concentration of the linear extractor output signal. After prewhitening the multichannel data and estimating the modal frequency $\hat{f}_m$, the optimal spatial filter is found as the dominant eigenvector of the spectral correlation matrix of the whitened observations around that frequency. The global optimum of the criterion can be obtained by computationally efficient eigenvector analysis and, in experiments, is seen to extract the targeted source if it presents maximal spectral concentration around its modal frequency $\hat{f}_m$. The present technique is not limited to the extraction of atrial activity in AF ECGs, but can probably be extended with minor modifications to any problem requiring the estimation of narrowband signals from multichannel measurements, in biomedicine or other fields. Current work aims at determining the conditions under which the proposed criterion is indeed a contrast function for source extraction.

VI. ACKNOWLEDGMENTS

The authors gratefully acknowledge F. Castells and the Electrophysiology Laboratory of the University Clinical Hospital of Valencia, Spain for sharing the data with us.

REFERENCES

[1] ACC/AHA/Physician Consortium 2008, "Clinical performance measure for adults with nonvalvular atrial fibrillation or atrial flutter," *Circulation*, pp. 1100–1120, 2008 doi: 10.1161/CIRCULATIONAHA.107.187192.

[2] M. Stridh, L. Sörnmo, C. Meurling, and B. Olsson, "Sequential characterization of atrial tachyarrhythmias based on ECG time-frequency analysis," *IEEE Trans on Biomed Eng*, vol. 51, pp. 100–114, 2004.

[3] M. Stridh and L. Sörnmo, "Spatiotemporal qrst cancellation techniques for analysis of atrial fibrillation." *IEEE Trans Biomed Eng*, vol. 48, no. 1, pp. 105–111, Jan 2001.

[4] J. J. Rieta, F. Castells, C. Sánchez, V. Zarzoso, and J. Millet, "Atrial activity extraction for atrial fibrillation analysis using blind source separation." *IEEE Trans Biomed Eng*, vol. 51, no. 7, pp. 1176–1186, Jul 2004.

[5] F. Castells, J. Igual, J. Millet, and J. Rieta, "Atrial activity extraction from atrial fibrillation episodes based on maximum likelihood source separation," *Signal Processing*, vol. 85, pp. 523–535, 2005.

[6] F. Castells, J. Rieta, J. Millet, and V. Zarzoso, "Spatiotemporal blind source separation approach to atrial activity estimation in atrial tachyarrhythmias," *IEEE Transactions on Biomedical Engineering*, vol. 52, no. 2, pp. 258–267, Feb. 2005.

[7] J. Malmivuo and R. Plonsey, *Bioelectromagnetism: Principles and Applications of Bioelectric and Biomagnetic Fields*. New York: Oxford University Press, 1995.

[8] P. Comon, "Independent component analysis, a new concept?" *Signal Processing*, vol. 36, pp. 287–314, 1994.

[9] J.-F. Cardoso and A. Souloumiac, "Jacobi angles for simultaneous diagonalization." *SIAM Journ on Matrix Analysis and Applications*, vol. 17, no. 1, pp. 161–164, 1996.

Atrio-Ventricular Junction Behaviour During Atrial Fibrillation

P Bonizzi, V Zarzoso, O Meste

I3S Laboratory, University of Nice - Sophia Antipolis, France

Abstract

Up to now the functioning of the Atrio-Ventricular Junction (AVJ) during Atrial Fibrillation (AF) is still not completely understood. To shed some light on the AVJ behavior during AF episodes, this study analyses the existence of a possible relationship between the occurrence of a heart beat and the power of the atrial activity (AA) preceding this heart beat in an electrocardiogram (ECG) signal. AA power is measured in the interval of the ECG between the onset of the heart beat under analysis and the ending of the previous heart beat (T-Q interval). Our analysis has shown a difference in the distributions of AA power versus cardiac cycle length (RR interval on the ECG) between healthy and pathological subjects. In particular, a negative trend between these two parameters is discovered in pathological subjects. This negative relation shows a possible coherence between power arriving at the AVJ and the triggering of the heart beat, which is in line with the assumptions made in the quantitative model for the ventricular response during AF by Cohen [1].

1. Introduction

Atrial Fibrillation (AF) represents the most common sustained cardiac arrhythmia in adults. It consists of a misfunction of the atrium characterized by a modification of the normal atrial activity (AA) pattern on the electrocardiogram (ECG) signal. Epidemiologic studies have shown that its prevalence and incidence doubles with each advancing decade beyond 50 years reaching 10% in people over 80 and has direct impact on mortality and morbidity [2, 3].

Although the mechanism and effective treatments for most other supraventricular tachyarrhythmia have been discovered, the understanding of AF remains incomplete. In particular, no unifying mechanism has been found yet to explain the behaviour of the atrio-ventricular junction (AVJ) during AF. It is well known that heart rate variability is enhanced during AF [1, 4], while other studies have revealed a more complex relationship between AVJ behaviour and AF [5]. In addition, the variation of the RR interval during AF has been thought to result mainly from autonomic modulation of the electrophysiological properties of the atria and the AVJ [6]. Therefore, the characterization of the ventricular rhythm in AF has been controversial and its mechanism has been a subject of debate for decades [7], thus revealing that the prevailing ventricular rate during high atrial rate is a complex dynamic parameter.

Different hypothesis were introduced to explain the irregular ventricular response during AF, i.e., the dependence of the decremental conduction and repetitive concealment on the AF impulses within the AVJ [8], or yet the dependence of the electrotonic modulation on the AVJ propagation by concealed AF impulses [9].

Several quantitative models for the ventricular response during AF were developed [1, 7, 10] to deal with this problem. The AVJ model presented by Cohen *et al.* [1] introduced the hyphotesis that it can be treated as a lumped structure with well defined electrical properties, including the refractory period, the automaticity and a defined depolarization threshold. From this point, the present work analyzes the presence of a possible correlation between the occurrence of a heart beat and the power of the AA observable in the ECG signal during the T-Q interval preceding this heart beat. This analysis aims to test the presence of a dependence between the AA power arriving at the AVJ and the RR period, following the idea that the AVJ generates an activation wave when the AA power arriving at it exceeds a threshold value, intrinsic to the AVJ.

The study of AF and its characteristics can to a large extent be carried out through the analysis of the surface electrocardiogram (ECG), which has the advantage to be a noninvasive technique and is already reported to be useful [11].

2. Methods

A dataset composed of 23 real recordings (2 healthy subjects and 21 presenting AF) was employed to analyze the proposed idea. All signals were recorded and digitized at a sampling rate of 1 KHz. Among the segments em-

ISSN 0276–6574 561 Computers in Cardiology 2007;34:561–564.

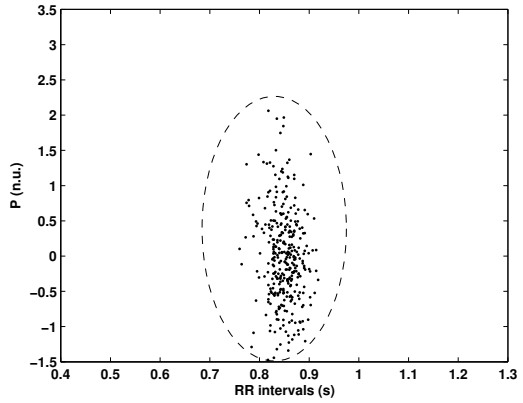

Figure 1. AA power versus RR interval distribution for a healthy subject. The shape distribution does not show the presence of any particular relation; n.u., normalized units; s, seconds.

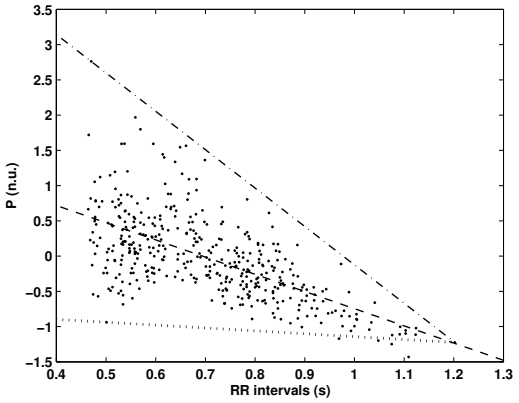

Figure 2. AA power versus RR interval distribution for a pathological subject. The shape distribution shows the presence of an inverse relation (dashed line), even if it is quite complex, due to the dispersion of the distribution (locked up between dotted and dashed-dotted lines); n.u., normalized units; s, seconds.

ployed in this analysis 19 were recorded using a standard 12-lead derivation system of 12s length (all AF) while 4 were recorded using a 9-lead derivation system of 300s length (2 healthy and 2 displaying AF). Pre-processing was done by applying a zero-phase low pass filter to remove physiologically irrilevant low frequency signal variations (<1 Hz) [12].

To allow the calculation of the AA power in each T-Q segment the algorithm of Zong *et al.* was employed to detect Q wave onset and T wave ending in each heart beat [13]. AA power in the T-Q interval referred to the *i*th heart beat on the *l*th lead was calculated as follows:

$$P_{AA_i}^{(l)} = \frac{1}{\#[Q_i - T_{i-1}]} \sum_{n=T_{i-1}}^{Q_i} x_{l,n}^2 \qquad (1)$$

where x_l is the digitized ECG signal recorded by the *l*th lead, T_{i-1} is the T wave ending instant of the *(i-1)*th heart beat, Q_i is the Q wave onset instant of the *i*th heart beat (the beat under analysis) and $Q_i - T_{i-1}$ is the number of samples contained in the *i*th T-Q interval.

Once each T-Q interval has been selected, AA power is calculated for each of all the leads ($P_{AA_i}^{(l)}$, with *l* generic lead, *i* generic beat).

To make use of the AA power of all leads, a normalization step is required. This is because a lead placed on the body surface records an electric activity whose amplitude depends on the distance between the electrode and the location of the recorded activities, on the electrical properties of the tissues and on the directions of the activities. Therefore, in each specific lead AA powers for all the T-Q segments are standardized in order to get a zero-mean and unit-variance normalization of power measurements on a lead-by-lead basis. This means that each AA power value is subtracted by the AA power mean value in that lead and devided by its standard deviation, as follows:

$$\tilde{P}_{AA_i}^{(l)} = \frac{P_{AA_i}^{(l)} - \overline{P_{AA}^{(l)}}}{\sigma_{P_{AA}^{(l)}}} \qquad (2)$$

where $\tilde{P}_{AA_i}^{(l)}$ is the normalized AA power of the T-Q*ith* interval, $\overline{P_{AA}^{(l)}}$ is the AA power mean value of the segments in the lead under analysis and $\sigma_{P_{AA}^{(l)}}$ is its standard deviation.

Subsequently, the mean value of the normalized AA powers occurring at the same heart beat in all leads is calculated for each heart beat as follows:

$$\overline{\tilde{P}_{AA_i}} = \frac{1}{L} \sum_{l=1}^{L} \tilde{P}_{AA_i}^{(l)} \qquad (3)$$

where L is the total number of leads. It is easy to see that $\overline{\tilde{P}_{AA_i}}$ is a summary of the whole AA preceding the *i*th heart beat. This normalizing procedure is necessary for exploiting at one time the spatial information contained in each lead as correctly as possible, keeping into account the arbitrary spatial differences among each electrode, as previously mentioned.

3. Results

The proposed approach for the analysis of AA power in the T-Q interval versus RR period was applied using a pa-

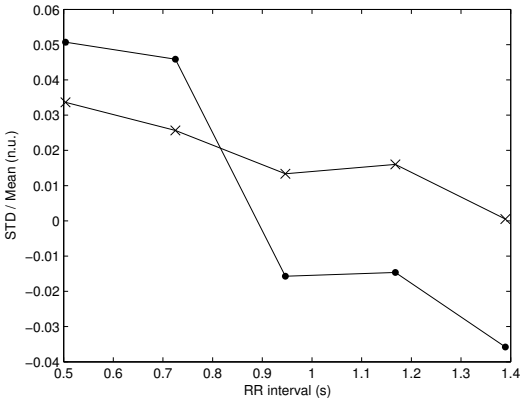

Figure 3. AA power meanvalues (point-marked line) and standard deviations (x-marked line) for all the pathological subjects split in five RR bins. Each point fixed in correspondence to the RR meanvalue of each bin; n.u., normalized units; s, seconds.

tient dataset of 23 recordings. Fig.1 and 2 plot the mean values of the normalized AA powers $\overline{\tilde{P}_{AA_i}}$ versus the RR_i intervals for a healthy and an unhealthy subject, respectively.

First of all, the difference in the $\overline{\tilde{P}_{AA_i}} = f(RR_i)$ shape distribution between healthy and pathologic subjects is remarkable. The healthy subject shows a rounded distribution, as in Fig. 1, while the pathological subjects seem to exhibit a triangular shape distribution, summarized by the dotted and dashed-dotted lines in Fig. 2. For pathological subjects an inverse relation appears between AA power arriving at the AVJ before each heart beat and the corresponding RR period (dashed line in Fig. 2). However, from the spread of the distribution it can be derived that it is not a linear relation. Possible explenations of this tendency are suggested in the discussion part of this paper.

Fig. 3 summarizes the general behaviour of the $\overline{\tilde{P}_{AA_i}} = f(RR_i)$ relation for all the pathological subjects under analysis. Indeed, it shows the trend of AA power mean values and standard deviations respectively, versus the RR intervals, after grouping RR intervals in five different classes and keeping the mean value of the $\overline{\tilde{P}_{AA_i}}$ (point-marked line) and of its standard deviations (x-marked line) in each class for all the subjects. Both the curves show clearly the inverse relation between AA power and RR interval.

4. Discussion and conclusions

In this study, the existence of a relationship between the occurrence of a heart beat and the power of the AA preceding this heart beat has been analyzed. First of all, the importance of a normalization step has been described, to give the possibility to exploit the spatial information kept in all leads, since the amplitude of the signal recorded by one lead can not be compared directly to that of another one.

The analysis of the $\overline{\tilde{P}_{AA_i}} = f(RR_i)$ relationship has shown a difference between healthy subjects, for which the presence of a relation is not evident (uniform scatter plot in Fig. 1), and pathological subjects, for which an inverse relation between these two parameters seems to be present (dashed line in Fig. 2), even if the distribution is quite spread (triangular scatter plot in Fig. 2). The presence of this relation is supported by the fact that the probability of having high AA power values associated to short RR intervals is higher than for long RR intervals, as clearly shown in Fig. 3. This finding suggests that the AVJ behaviour during AF is characterized by a power threshold value (in analogy with the electric depolarization threshold value), for which the likelihood of generating a cardiac beat by the AVJ is related to the amount of AA power carried by the AF activity arriving at it, in agreement with the AVJ models presented by Cohen *et al.* [1] and by Lian *et al.* [7]. Therefore, the higher the AA power arriving at the AVJ in a defined time, the higher the possibility to go over the threshold and to generate a beat (related to a shorter RR interval). The results shown in the previous section (Fig. 3), in agreement with these theoretical models, suggest that AF impulses arrival to the AVJ is a dominant factor in the AVJ excitation.

However, the great variance of $\overline{\tilde{P}_{AA_i}} = f(RR_i)$ distribution for short RR periods in the pathological subjects seems not to support the hypothesis of an inverse relation (behaviour summarized by the dotted line in Fig. 2). This can be explained in different ways. First, if it could be supposed that the leads placed on the body surface are not able to capture completely the three dimensionsal field related to AA, together with the fact that AF works randomly in time and space, then it can be assumed that what is recorded is sometimes only a partial vision of what is really happening, due to the leads' spatial resolution limit. Therefore, if a low AA power value associated to a short RR interval is observed (instead of a longer one, as would be suggested by the inverse relation), it can be supposed that the electrical activity recorded at that moment on the ECG is only a reduced portion of the real one (leads' placement unable to capture the main direction of AF). If this hyphothesis is correct, AA power in that particular moment must be actually greater, rising the related point in the $\overline{\tilde{P}_{AA_i}} = f(RR_i)$ plot nearer to the inverse relation (dashed line in Fig. 2). Thus, both the inverse relation and the hypothesis of dominance of AF impulses arriving at AVJ in generating its excitation are strengthened. On the other

hand, we could think the opposite,i.e., that leads placement works well in capturing all the AF electrical activity in any direction. Consequently, power variance trend in the $\overline{\tilde{P}_{AA_i}} = f(RR_i)$ distribution could be due to the amount of noise present in the AA signal and to the way the power is computed (the longer the RR periods for which AA energy is divided the lesser the variance of the estimator of the AA power mean). On the contrary, if the amount of noise in the AA signal is unimportant, it means that other factors must be taken into account for the understanding of the spread of the variance and the AVJ way of functioning.

Also, it must be taken into account that there is no certainty about the fact that AA recorded in the ECG before a heart beat is effectively what reachs the AVJ. Indeed, it is the global activity of the heart in a particular moment. The portion of this global activity that really arrives at the AVJ depends on the AA waves interaction, and so on their level of spatial and temporal organization.

In conclusion, the frequency content of AA is known to provide important physiological and clinical informations about AF [11]. This study has evidenced that alternative information such as the amplitude (power) of the AA signal can also shed some light on the understanding of the physiological mechanism behind this condition. Future work aims to analyze more deeply this finding, trying to exploit also the AA masked by the QRS complex [14, 15].

Acknowledgements

The authors would like to express their gratitude to Leif Sörnmo and Francisco Castells for providing the real data. The work of Bonizzi Pietro is supported by the EU by a Marie-Curie Fellowship (EST-SIGNAL program : http://est-signal.i3s.unice.fr) under contract No MEST-CT-2005-021175.

References

[1] Cohen RJ, Berger RD, Dushane TE. A quantitative model for the ventricular response during atrial fibrillation. IEEE 1983;781–796.

[2] Kannel WK, Abbott RD, Savage DD, McNamara PM. Epidemiologic features of chronic atrial fibrillation: the framingham study. N Engl J Med 1982;306:1018–22.

[3] Krahn AD, Manfreda J, Tate RB, Mathewson FA, Cuddy TE. The natural history of atrial fibrillation: incidence, risk factors, and prognosis in the Manitoba Follow-Up Study. Am J Med 1995;98:476–84.

[4] Fuster V, Ryden LE, Asinger RW. ACC/AHA/ESC guidelines for the management of patients with atrial fibrillation. JACC 2001;38:1266i–1266lxx.

[5] Garrigue S, Tchou PJ, Mazgalev TN. Role of the differential bombardment of atrial inputs to the atrioventricular node as a factor influencing ventricular rate during high atrial rate. Cardiovasc Res 1999;44:344–355.

[6] Toivonen L, Kadish A, Kou W, Morady F. Determinants of the ventricular rate during atrial fibrillation. J Am Coll Cardiol 1990;16:1194–1200.

[7] Lian J, Mussig D, Lang V. Computer modeling of ventricular rhythm during atrial fibrillation and ventricular pacing. IEEE Trans Biomed Eng 2006;53:1512–20.

[8] Watanabe Y, Watanabe M. Impulse formation and conduction of excitation in the atrioventricular node. J Cardiovasc Electrophysiol 1994;5:517–531.

[9] Meijler FL, Jalife J, Beaumont J, Vaidya D. AV nodal function during atrial fibrillation: The role of electrotonic modulation of propagation. J Cardiovasc Electrophysiol 1996; 7:843–861.

[10] Jorgensen P, Schafer C, Guerra PG, Talajic M, Nattel S. A mathematical model of human atrioventricular nodal function incorporating cocealed conduction. Bull Math Biol 2002;64:1083–1099.

[11] Bollmann A, Husser D, Mainardi L, Lombardi F, Langley P, Murray A, Rieta JJ, Millet J, Bertil Olsson S, Stridh M, Sornmo L. Analysis of surface electrocardiograms in atrial fibrillation: techniques, research, and clinical applications. Europace 2006;8:911–926.

[12] Sornmo L, Laguna P. Bioelectrical Signal Processing in Cardiac and Neurological Applications. Elsevier Academic Press, 2005.

[13] Zong W, Saeed M, Heldt T. A QT interval detection algorithm based on ecg curve length transform. In Computers in Cardiology. 2006; .

[14] Zarzoso V, Nandi AK. Noninvasive fetal electrocardiogram extraction: blind separation versus adaptive noise cancellation. IEEE Trans Biomed Eng 48;January 2001:12–18.

[15] Meste O, Serfaty N. QRST cancellation using bayesian estimation for the auricular fibrillation analysis. In Engineering in Medicine and Biology. 2005; .

Address for correspondence:

Pietro Bonizzi, Ph.D. Student
Laboratoire I3S - BIOMED UNSA - CNRS
2000, Route des Lucioles Les Algorithmes - bât. Euclide B
B.P. 121
06903 Sophia Antipolis - Cedex, France
E-mail: bonizzi@i3s.unice.fr

Proceedings of the 29th Annual International
Conference of the IEEE EMBS
Cité Internationale, Lyon, France
August 23-26, 2007.

Extraction of the Atrial Activity from the ECG based on Independent Component Analysis with Prior Knowledge of the Source Kurtosis Signs

Ronald Phlypo, Yves D'Asseler, Ignace Lemahieu
MEDISIP - IBiTech
University of Ghent
De Pintelaan 185, Blok B
9000 Ghent, Belgium
{ronald.phlypo, yves.dasseler, ignace.lemahieu}@ugent.be

Vicente Zarzoso
Laboratoire I3S
CNRS/UNSA
Les Algorithmes Euclides-B
2000, Route des Lucioles
06903 Sophia Antipolis Cedex
France
{phlypo, zarzoso}@i3s.unice.fr

Abstract— **In this work it will be shown that a contrast for independent component analysis based on prior knowledge of the source kurtosis signs (ica-sks) is able to extract atrial activity from the electrocardiogram when a constrained updating is introduced. A spectral concentration measure is used, only allowing signal pair updates when spectral concentration augments. This strategy proves to be valid for independent source extraction with priors on the spectral concentration. Moreover, the method is computationally attractive with a very low complexity compared to the recently proposed methods based on spatiotemporal extraction of the atrial fibrillation signal.**

I. INTRODUCTION

With a prevalence as high as 10% for people over the age of 70, atrial fibrillation (AF) and atrial flutter (AFL) are the most commonly encountered forms of cardiac arrhythmia. Since the origin and model of AF and AFL are barely understood until now [14], extraction of the electrical activity from the electrocardiogram (ECG) attributed to the AF/AFL is of great value for further understanding its underlying mechanisms. Therefore we propose a fully automated low complexity AF extraction technique. Contrary to the majority of the algorithms which try to unveil the atrial activity (AA) during AF periods by suppression of the QRS(-T) complex, the proposed method envisages the isolation of the AA as has been proposed in [5, and references therein].

However, most signal extraction techniques, whether in a single stage or in multiple stages are computationally expensive and are seldom fully automated, leaving the final component selection to the user. Moreover, there are only few methods that combine successfully both the spatial and temporal information without turning to an excessive computational cost.

The last point to tackle is surely the validation of the algorithms. The extraction of AF from the ECG is essentially an inverse problem where the unknown source is to be estimated from the total measurement. Hence, there is no objective performance index (i.e. based on the original sources or any a priori information about them) to compare against.

Ronald Phlypo would like to thank Vicente Zarzoso and the BIOMED research group at I3S for their kind hospitality

In this contribution we will compare a spatio-temporal two stage method for extraction of AA during AF/AFL episodes [5] against a novel single stage AA extraction technique based on limited *a priori* knowledge about its spectrum and source kurtosis signs (sks). The method is based on the contrast function in [11] and the adapted version in [10] to extract AF signals. It uses the prior information that in the 3-12Hz band the AF is characterised by a single frequency waveform and its harmonics with slow frequency and amplitude modulation [13]. Since the AA exhibits quasi-sinusoidal behaviour, we may thus use the contrast proposed in [11] with a negative sign for the AA kurtosis and a positive sign for the other sources.

II. DATA & METHODS

A. Data

For a validation of the results we turned to both simulations (of which the results are published in [11]) and real data. The dataset consisted of 51 patients, all being diagnosed with AF. The recordings were registered with a standard 12-lead ECG, including the bipolar limb leads I-III, the augmented unipolar limb leads aVR, aVF and aVL and the six unipolar chest leads V1-V6. Since there is abundance in the information in the leads, a second set was constructed with 8 leads including all six chest leads and recalculations from the limb leads to the electrode potentials between LL and LA, respectively RA. The latter set of potentials will be called the 8-lead system from hereon.

B. Independent Component Analysis

Solving the biomedical inverse problems often relies on the statistical properties of the underlying sources [9], [1]. Independent Component Analysis (ICA) has already proven to be an appropriate measure for decomposition of an ECG dataset into its source contributions according to a linear model [12]

$$\mathbf{y} = \mathbf{H}\mathbf{x} + \eta \quad , \tag{1}$$

where the projection of the source activities $\mathbf{x} \in \mathbb{R}^n$ onto the measurements $\mathbf{y} \in \mathbb{R}^m$ is determined by a linear mixing

1-4244-0788-5/07/$20.00 ©2007 IEEE

matrix $\mathbf{H} \in \mathbb{R}^{m \times n}$ up to some noise $\eta \in \mathbb{R}^m$. To solve Eq. 1, we need some *a priori* assumptions on the sources, e.g. statistical independence. In this paper, the noise η will be neglected or be taken as a source signal, reducing Eq. 1 to $\mathbf{y} = \mathbf{Hx}$. The system of equations is then solved by searching for $\mathbf{W}$ in $\hat{x} = \mathbf{W}^{-1}\mathbf{y}$ [1] which yields estimates $\hat{\mathbf{x}} = \mathbf{W}^{-1}\mathbf{Hx} = \mathbf{Qx}$ that are as independent as possible. From hereon, $\hat{\mathbf{x}}$ is considered a decorrelated version of $\mathbf{y}$. Left to estimate is the rotation matrix $\mathbf{Q}$, since they are the only group of matrices that preserve orthogonality in $\hat{\mathbf{x}}$. This paper presents the application of ICA based on sks (ica-sks) constrained in its updating by spectral concentration.

Any function $\Psi(\mathbf{Q})$ that can be optimised such that (1) Ψ is invariant under permutation and scaling and (2) it reaches its maximum if and only if $\mathbf{Q}$ yields maximally independent components $\hat{\mathbf{x}}$ is a contrast for independent component analysis (ICA) [6].

C. 2×2 Source Separation

For the case of 2 sources and 2 observations, an ICA contrast can be defined as a single planar rotation of the prewhitened data $\hat{\mathbf{x}}$. Since any rotation in a two dimensional plane can be expressed in matrix format as a Givens rotation

$$\mathbf{x} = \mathbf{Q}^T\hat{\mathbf{x}} \ \text{, where } \mathbf{Q}(\theta) = \begin{pmatrix} cos\theta & sin\theta \\ -sin\theta & cos\theta \end{pmatrix} , \quad (2)$$

the estimation is reduced to a single parameter and can be expressed in analytical form. The contrast that will be used here is based on independence and prior knowledge of source kurtosis signs and reads $\Psi(\mathbf{Q}) = \varepsilon_1\kappa_{1111} + \varepsilon_2\kappa_{2222}$, where $\kappa_{iiii} = \left\langle \hat{\mathbf{x}}_i^4 \right\rangle / \left\langle \hat{\mathbf{x}}_i^2 \right\rangle^2 - 3$ is the standardised kurtosis of $\hat{\mathbf{x}}_i$. ε_1 is chosen negative and ε_2 is chosen positive. This yields as the solution for θ [11], [16]:

$$\theta_{opt} = 0.5 \arctan 2 \left(\kappa_{1112} + \kappa_{2221}\right)\left(\kappa_{2222} - \kappa_{1111}\right)^{-1} , \quad (3)$$

where κ_{ijjj} is the bivariate moment defined as $\left\langle \hat{\mathbf{x}}_i \hat{\mathbf{x}}_j^3 \right\rangle$.

D. Higher Dimensional Data

For higher dimensional data ($n > 2$), it is possible to express the orthogonal mixing matrix $\mathbf{Q}$ as subsequent Givens rotations, updating the current source estimate $\hat{\mathbf{x}}$. Since for plane rotations in higher dimensional data it suffices to fix all axes but two, we can express the rotation of the subspace spanned by two components in $\hat{\mathbf{x}}$ by Eq. 2 while the other components undergo a identity transformation. Based on the fact that maximal mutual independence of each pair guarantees maximal independence of the set, pairwise rotations with a fixed updating order will yield a solution to ICA [7]. Being interested in a single component only - the one that contains the atrial fibrillation - we define one sweep as such that it will compare our best current estimate $\hat{\mathbf{x}}_i^{(k)}$ to every other $\hat{\mathbf{x}}_{j\neq i}^{(k)}$ and process these pairs according to

$$\begin{bmatrix} \hat{\mathbf{x}}_i^{(k+1)} \\ \hat{\mathbf{x}}_j^{(k+1)} \end{bmatrix} = \mathbf{Q}^T \begin{bmatrix} \hat{\mathbf{x}}_i^{(k)} \\ \hat{\mathbf{x}}_j^{(k)} \end{bmatrix} . \quad (4)$$

[1] Since $\mathbf{W}^{-1}$ is defined as the inverse of $\mathbf{H}$, m is limited to be equal to n, and $\mathbf{H}$ and $\mathbf{W}$ must be full column rank.

However, there is no guarantee that the source of interest is the only source with negative kurtosis, nor is it guaranteed that the algorithm will return the source with a basic frequency in the 3-12Hz band, the band of interest for AF signals. Hence the need to use a constrained optimisation criterion as given in the next paragraph.

E. Constrained Optimisation

To further optimise the algorithm for the extraction of AA we include a constraint in the update rule in the form of a decision rule. This decision rule will allow for rotation at step $k+1$ if and only if the rotation augments the spectral concentration of the best estimate found in iteration k. After calculating our potential candidates for $\hat{\mathbf{x}}_i^{(k+1)}$ and $\hat{\mathbf{x}}_j^{(k+1)}$ we apply a decision rule characterised by the detection of augmentation in spectral concentration:

$$\max\left(\mathrm{SC}\left(\hat{\mathbf{x}}_i^{\star(k)}\right), \mathrm{SC}\left(\hat{\mathbf{x}}_j^{\star(k)}\right)\right) > \mathrm{SC}\left(\hat{\mathbf{x}}_i^{(k)}\right) , \quad (5)$$

where the function SC calculates the ratio of the power spectral density (PSD) in the 90-110% range of the frequency with maximal power in the 3-12Hz band to the PSD of half the spectrum (i.e. from 0Hz to half the sampling frequency Fs) given by:

$$\mathrm{SC}(a) = \frac{\int_{0.9f_c}^{1.1f_c} P_a(\tau) e^{-2\pi\tau f} df}{\int_{0}^{0.5\mathrm{Fs}} P_a(\tau) e^{-2\pi\tau f} df} . \quad (6)$$

If the decision rule of Eq. (5) is fulfilled, the new estimate $[\hat{\mathbf{x}}_i^{(k+1)}\hat{\mathbf{x}}_j^{(k+1)}]^T$ is replaced by the candidates $[\hat{\mathbf{x}}_i^{\star}\hat{\mathbf{x}}_j^{\star}]^T$ the component with the highest SC as the new reference. If not fulfilled the estimates do not get updated and the pair $\left(\hat{\mathbf{x}}_i, \hat{\mathbf{x}}_{j+1}\right)$ is processed. The updating process is finished when a full sweep has passed without finding candidates augmenting the spectral concentration, which is generally of the order of 3 sweeps.

F. Spatio-temporal Source Separation

As a reference technique we will use the technique proposed by Castells *et al.* [5] based on spatio-temporal source decomposition. The algorithm consists essentially out of an ICA step (FastICA [8]) with elimination of the components with a kurtosis higher than the threshold of 1.5 followed by a temporal decorrelation step, namely Second Order Blind Identification (SOBI) [3]. The iterative algorithm RobustICA [15] was used here as an implementation of FastICA. SOBI is known to be quite robust to estimation errors in the used time lags, but there is no rule on how to choose the optimal set. Therefore we also include a temporal decorrelation algorithm known as Canonical Correlation Analysis (CCA) [2] based solely on a single sample shift, to compare with.

TABLE I

THE DIFFERENCES IN ESTIMATION OF THE CENTRAL FREQUENCIES FOR 12-LEADS[1], 8-LEADS[2] AND 12-LEADS VERSUS 8-LEADS[3].

	rICA+SOBI	rICA+CCA	ica-sks	combEML
rICA+SOBI	0.85^3	1.38^1	1.09^1	1.05^1
rICA+CCA	0.69^2	0.16^3	-0.29^1	-0.32^1
ica-sks	-0.26^2	-0.95^2	-0.50^3	-0.03^1
combEML	-0.32^2	-1.02^2	-0.06^2	-0.53^3

TABLE II

SPECTRAL CONCENTRATION FOR THE SET OF 51 PATIENTS. 12-LEADS (UPPER ROW) AND 8-LEADS (LOWER ROW)

rICA+SOBI	rICA+CCA	ica-sks	combEML
29.80 ± 12.44	43.16 ± 14.99	57.89 ± 11.33	56.12 ± 10.47
40.36 ± 15.66	39.87 ± 14.21	53.72 ± 14.52	51.17 ± 10.29

TABLE III

COMPUTATIONAL COMPLEXITY PER ITERATION AND SOME AVERAGE NUMBERS OF ITERATIONS NEEDED FOR CONVERGENCE.

method	computational complexity	iterations until convergence
rICA	$\mathcal{O}((5n+12)nT)$	10
SOBI	$\mathcal{O}\left(17n^2T+2(n-1)(n-2)\right)$	$1+\lfloor\sqrt{n}\rfloor$
CCA	$\mathcal{O}\left(4nT^2+4n^2T+\frac{62}{3}n^3\right)$	1
ica-sks	$\mathcal{O}(7(n-1)T)$	5
combEML	$\mathcal{O}(8(n-1)T)$	10

G. Preprocessing

Having no significant information for AF in the frequency bands below 0.5Hz and above 30Hz, we apply a 12^{th} order Butterworth bandpass filter with the specified frequencies as -3dB points. This has no effect on the end results since the preprocessing is done before feeding any data to the algorithms and thus the PSD in the denominator of the RHS of Eq. 6 does not change by replacing the lower and upper limits by 0.5Hz and 30Hz respectively. This will only result in a nonlinear rescaling of all spectral concentration coefficients due to the nominator, although no large changes can be noted if AF is extracted because the signal power linked to AF in the rejected frequencies is negligible.

III. RESULTS

A. Frequency Estimation

As a first evaluation measure the mean of the differences in estimated central frequencies are presented in table I. The upper right triangle shows the differences in frequencies for the estimation of the algorithm given in the top row versus the one in the left column based on 12 lead ECG systems, while the lower left triangle gives those values for the 8-lead (re-referenced) system. Values on the diagonal compare the results of the algorithms in their 12-lead setting versus their 8-lead setting. The table compares RobustICA + SOBI (rICA+SOBI), RobustICA + CCA (rICA+CCA), ica-sks and the combined EML (combEML) algorithm as proposed in [16] but with the decision rule in the update.

B. Spectral Concentration

The spectral concentration measure is the same as in the updating criterion. The spectral concentration is a valid measure since it's value has not directly been used to update the contrast function, but it has been used as a constraint. The results in table II show the typical values of spectral concentration for each of the methods used. The upper row gives the mean values with standard deviation for the 12 leads system, whereas the lower row show results for the 8 leads system.

C. Computational Complexity

To see the performance of the algorithms against their computational complexity, we show for each method the approximate complexity as a function of the number of samples T, the number of measurements n and the number of sources to extract m. Given that the EML based algorithms only need to estimate a single source ($m = 1$) and the RobustICA needs to do a full decomposition before the kurtosis based selection ($m = n$), the entries for RobustICA, ica-sks and combEML do not depend on m. It is worth mentioning that the n for SOBI and CCA is usually much smaller than the n taken in the other methods, since there has been done a dimension reduction through component selection based on kurtosis values. Table III gives the order of magnitude for each of the methods with the predefined lags in SOBI taken as in [5], being 17 equally spaced lags of 20ms (i.e. a range of 0 to 320 ms).

D. Graphical Results

In Fig. 1 and Fig. 2 the results are shown for the ica-sks algorithm for a simulated and a patient dataset, respectively. The simulated dataset has been constructed as to mimic cardiac electrical activity based on AF simulations as presented in [13] and ventricular activity or QRS waveforms based on a function given in [11].

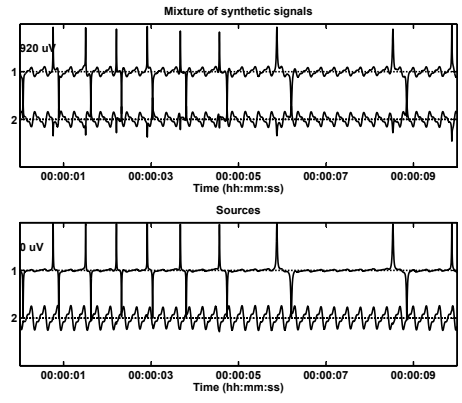

Fig. 1. Separation of a simulated AF signal from a high kurtotic QRS-like signal.

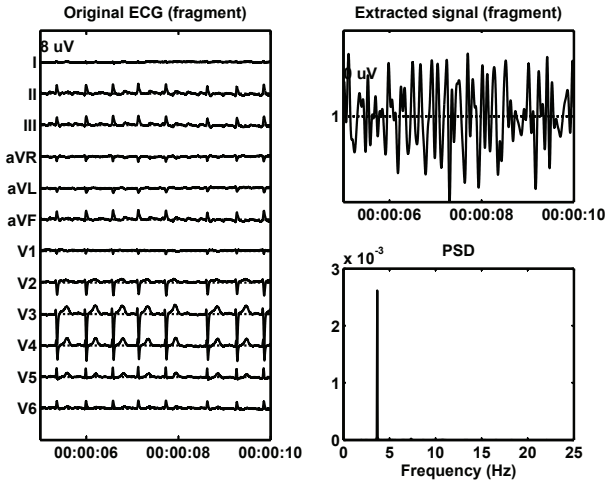

Fig. 2. Extraction of the AF from patient ECG using ica-sks.

IV. DISCUSSION

Although comparison of algorithms to solve inverse problems is not an easy task, results in this paper show that our method has acceptable results when compared to the spatiotemporal method presented in [5]. The results in table I clearly show that the used methods are comparable when the central frequency has to be estimated. However due to a lack of an objective measure of performance we do not have the possibility to make a statement about the accuracy of the estimate.

Referring to table II, we observe that the EML based methods using the constrained updating outperform the spatiotemporal methods based on a standard ICA implementation followed by a second order decorrelation method. We used the implementation RobustICA for the ICA method since it generally returned higher SC. To omit the selection procedure of the time lags introduced in SOBI, we also compared to the method of CCA, based on a single lag.

From Fig.(1) it is clear that the contrast works well on two artificial signals without using the constrained updating. Since the AF signal is generally subgaussian and the ventricular activity supergaussian [4], the contrast based on prior knowledge of the source kurtosis signs [11] is excellently suited for the two sources, two observations case. However, in the higher dimensional ECG subspace the exact prior knowledge of the sks is absent and thus we need to turn to constrained updating.

One of the most interesting features, however, is the low computational complexity of the source extraction methods based on EML (see table III). Based on a single stage only, and estimation of a single source, the flops required per iteration are heavily reduced compared to a dual stage algorithm yet yielding comparable results.

V. CONCLUSIONS

We presented a new method for extraction and estimation of the AA from the ECG of AF/AFL patients, namely ica-sks. The method is based on an ICA contrast exploiting prior knowledge about the desired source kurtosis signs and the spectral concentration in the 3-12 Hz band. As opposed to the method in [5], our method is able to exploit both properties simultaneously, resulting in an attractively low computational complexity.

VI. ACKNOWLEDGMENTS

We are grateful to F. Castells, J.J. Rieta and J. Millet from the Universidad Politecnica de Valencia, Spain, for sharing the dataset of AF patient registrations.

REFERENCES

[1] M. Babaie-Zadeh and C. Jutten. Semi-blind approaches for source separation and independent component analysis. In *Proceedings of 14th European Symposium on Artificial Neural Networks (ESANN) 2006*, pages 301–312, Bruges, Belgium, 2006.

[2] M. Borga and H. Knutsson. A canonical correlation approach to blind source separation. report liu-imt-ex-0062. Technical report, Department of Biomedical Engineering, Linköping University, 2001.

[3] J.-F. Cardoso and A. Souloumiac. Blind beamforming for non-gaussian signals. *IEE Proc.-F*, 140(6):362–370, 1993.

[4] F. Castells, J. Igual, J. Millet, and J. Rieta. Atrial activity extraction from atrial fibrillation episodes based on maximum likelihood source separation. *Signal Processing*, 85:523–535, 2005.

[5] F. Castells, J. Rieta, J. Millet, and V. Zarzoso. Spatiotemporal blind source separation approach to atrial activity estimation in atrial tachyarrhythmias. *Biomedical Engineering, IEEE Transactions on*, 52(2):258–267, Feb. 2005.

[6] P. Comon. Analyse en composantes indépendantes et identification aveugle. *Traitement du signal*, 7(3):435–450, 1990. Numero special non lineaire et non gaussien.

[7] P. Comon. Independent component analysis, a new concept? *Signal Processing*, 36:287–314, 1994.

[8] A. Hyvärinen and E. Oja. A fast fixed-point algorithm for independent component analysis. *Neur Comp*, 9:1483–1492, 1997.

[9] S. Makeig, A. J. Bell, T.-P. Jung, and T. J. Sejnowski. Independent component analysis of electroencephalographic data. In *Advances in Neural Information Processing Systems*, volume 8, pages 145 – 151, 1996.

[10] R. Phlypo, V. Zarzoso, P. Comon, Y. D'Asseler, and I. Lemahieu. Extraction of atrial activity from the ECG by spectrally constrained ICA based on kurtosis sign. In S. A. A. M E Davies, C J James and M. D. Plumbley, editors, *ICA 2007: 7th International Conference on Independent Component Analysis and Signal Separation*, London, UK, 2007.

[11] R. Phlypo, V. Zarzoso, P. Comon, Y. D'Asseler, and I. Lemahieu. ISRN I3S/RR-2007-13-FR: A contrast for ICA based on the knowledge of source kurtosis signs http://www.i3s.unice.fr/˜mh/RR/2007/liste-2007.html. Technical report, I3S, Sophia Antipolis, France, 2007.

[12] J. J. Rieta, F. Castells, C. Sánchez, V. Zarzoso, and J. Millet. Atrial activity extraction for atrial fibrillation analysis using blind source separation. *IEEE Trans Biomed Eng*, 51(7):1176–1186, Jul 2004.

[13] M. Stridh and L. Sörnmo. Spatiotemporal qrst cancellation techniques for analysis of atrial fibrillation. *IEEE Trans Biomed Eng*, 48(1):105–111, Jan 2001.

[14] D. G. Wyse and B. J. Gersh. Atrial fibrillation: a perspective: thinking inside and outside the box. *Circulation*, 109(25):3089–3095, Jun 2004.

[15] V. Zarzoso and P. Comon. How fast is FastICA? In *Proceedings of the 14th European Signal Processing Conference (EUSIPCO)*, Firenze, Italy, September 2006.

[16] V. Zarzoso, A. K. Nandi, F. Hermann, and J. Millet-Roig. Combined estimation scheme for blind source separation with arbitrary source PDFs. *IEE Electronics Letters*, 37(2):132–133, 2001.

ALPHABET-BASED DEFLATION FOR BLIND SOURCE EXTRACTION IN UNDERDETERMINED MIXTURES

Vicente Zarzoso and Pierre Comon
Laboratoire I3S, Université de Nice – Sophia Antipolis / CNRS
Les Algorithmes – Euclide-B, 2000 route des Lucioles, BP 121
06903 Sophia Antipolis Cedex, France
{zarzoso, pcomon}@i3s.unice.fr

ABSTRACT

The deflation approach to blind source extraction estimates the source signals one by one. The contribution of the latest source estimate is computed via linear regression and subtracted from the observations before performing a new extraction. In the context of digital communications, novel alphabet-based contrast criteria can naturally be defined, leading to the recently proposed parallel deflation concept. We analyse the use of such criteria in the challenging scenario of underdetermined mixtures, where the sources outnumber the sensors. Due to the limitations of linear extraction, projection on the signal alphabet before the regression-subtraction stage is shown to be capital for a successful source estimation. It is also demonstrated that alphabet-based criteria outperform the constant modulus (CM) principle, even for CM-type sources. More interestingly, classical deflation can improve on parallel deflation, but requires a refinement to render its performance robust to the extraction ordering.

Keywords: alphabet-based criteria, blind source separation, deflation, digital communications, MIMO transmission, underdetermined mixtures.

1 INTRODUCTION

The goal of blind source separation (BSS) is to recover the unknown source signals from their observed mixtures. The deflation approach to BSS consists of estimating the source signals one after another. Originally proposed by Delfosse-Loubaton [3] in the context of instantaneous linear mixtures, deflation was later applied with success by Tugnait in the convolutive scenario [10]. After estimating a single source signal using a suitable cost or contrast function, its contribution to the sensor output is estimated (via linear regression, for instance) and subtracted from the observations. The process is then repeated until all sources have been extracted. In multiple-input multiple-output (MIMO) digital communications, deflation (or symbol cancellation) has also been employed by the popular V-BLAST detection algorithm [5], which requires an accurate channel matrix estimate and is thus non-blind.

Despite its appealing simplicity, deflation presents two main drawbacks. Firstly, estimation errors caused in each extraction-deflation stage accumulate through successive stages. As a result, the source estimation quality deteriorates progressively as more sources are obtained. Secondly, since a linear extractor is usually employed, the maximum number of sources that can be separated is limited by the available spatial diversity, i.e., it is generally impossible to extract more sources than sensors. This limits the applicability of deflation in the interesting scenario of underdetermined mixtures.

The discrete nature of digital modulation sources, characterized by a finite number of symbols composing the signal alphabet or constellation, can help alleviate these shortcomings. The present contribution analyses and compares these alphabet-exploiting techniques for deflation-based source extraction in underdetermined mixtures. A simple modification improves the robustness of classical deflation to the source extraction ordering, and outperforms the recently proposed parallel deflation [8] in estimating all sources with low error probability more often.

2 PROBLEM AND ASSUMPTIONS

A noisy mixture $\mathbf{x} = [x_1, x_2, \ldots, x_L]^{\mathrm{T}} \in \mathbb{C}^L$ of K uncorrelated sources $\mathbf{s} = [s_1, s_2, \ldots, s_K]^{\mathrm{T}} \in \mathbb{C}^K$ is observed at the output of an L-sensor array, where $^{\mathrm{T}}$ denotes transposition. In matrix form, the sensor output can be expressed as:

$$\mathbf{x} = \mathbf{H}\mathbf{s} + \mathbf{n} = \sum_{k=1}^{K} \mathbf{h}_k s_k + \mathbf{n} \qquad (1)$$

where $\mathbf{H} \in \mathbb{C}^{L\times K}$ represents the unknown full-rank mixing matrix with columns $\{\mathbf{h}_k\}_{k=1}^K$, and $\mathbf{n} \in \mathbb{C}^L$ the additive noise, which is also unknown, uncorrelated with the sources, and has covariance matrix $\sigma_n^2\mathbf{I}_L$. Eqn. (1) models (but is not limited to) a flat-fading MIMO transmission system. BSS aims at estimating the realizations of random

In *Proc. ICA Research Network International Workshop*, Liverpool, UK, Sept. 18-19, 2006, pp. 21-24.

vector $\mathbf{s}$ from the observation of the corresponding realizations of the mixture $\mathbf{x}$. To this end, we seek an extracting vector $\mathbf{w} \in \mathbb{C}^L$ so that the linear extractor output

$$y = \mathbf{w}^{\mathrm{H}}\mathbf{x} \tag{2}$$

optimises some cost function or contrast criterion. Symbol $^{\mathrm{H}}$ represents the Hermitian (conjugate-transpose) operator. After a source signal has been estimated in this fashion, its contribution is computed and subtracted (cancelled) from the observations, which then become 'deflated'. The source estimation and deflation process is repeated until all signals have been extracted.

In the challenging underdetermined mixture scenario, the number of sources is higher than the number of sensors, $K > L$. In that case, it is generally not possible to estimate all sources linearly, even in the absence of noise, as the rows of the mixing matrix only span an L-dimensional subspace of $\mathbb{C}^K$. Similarly, linear extraction severely limits the capabilities of conventional deflation, as will be seen later, calling for the design of alternative extraction and/or deflation criteria.

The novelty of the present approach lies in the exploitation of the discrete character of digital communication signals. In the sequel, it will be assumed that the sources can be divided into R different groups, $\sum_{r=1}^{R} K_r = K$, where group r contains K_r sources with the same digital modulation $\mathcal{A}_r$. Each digital modulation is characterized by its alphabet or constellation $\mathcal{A}_r = \{a_{r,m}\}_{m=1}^{M}$, whose discrete symbols can be represented by the roots of a polynomial $\psi_r(z) = \prod_{m=1}^{M}(z - a_{r,m})$.

3 ALPHABET-BASED EXTRACTION

Under the signal model and assumptions of the previous section, it follows that functional

$$\mathcal{J}_r(y) = \mathrm{E}\{|\psi_r(y)|^2\}$$

is a contrast function for sources with alphabet $\mathcal{A}_r$ under rather general assumptions [2]. In particular, a constellation may not be a subset of another. This criterion, originally proposed in [6], is known as alphabet polynomial fitting (APF) and becomes the so-called constant power (CP) criterion for M-PSK modulations [11]. The APF presents the advantage of targeting a specific signal modulation, in contrast to alternative criteria typically used in the separation of digital communication sources such as the constant modulus (CM) or the kurtosis maximisation (KM) principles [4, 9]. As opposed to independence-based contrast criteria, the APF can separate spatially correlated and spectrally coloured sources. To estimate a source signal of given modulation, a simple yet efficient gradient-descent procedure with optimal step size can drive a linear extractor in the search of the corresponding APF contrast-function minima [11].

4 CLASSICAL DEFLATION

At the end of a successful iterative search (leading to the optimisation of the corresponding contrast function $\mathcal{J}_r$), the extractor output y contains an estimate $\hat{s}$ of a source signal s with alphabet $\mathcal{A}_r$. In regression-based classical deflation, the contribution of the extracted source to the observations is estimated as:

$$\hat{\mathbf{h}} = \arg\min_{\mathbf{h}} \mathrm{E}\{\|\mathbf{x} - \mathbf{h}\hat{s}\|^2\} \;\Rightarrow\; \hat{\mathbf{h}} = \frac{\mathrm{E}\{\mathbf{x}\hat{s}^*\}}{\mathrm{E}\{|\hat{s}|^2\}} \tag{3}$$

symbol * denoting complex conjugation, and then subtracted to yield the deflated sensor output:

$$\mathbf{x} \;\leftarrow\; \mathbf{x} - \hat{\mathbf{h}}\hat{s}. \tag{4}$$

If a linear extractor is employed, as in eqn. (2), it is easy to prove that the rank of the sensor-output covariance matrix (related to the available spatial diversity) necessarily decreases by one at each deflation step, regardless of the achieved source estimation quality. As a result, only L out of the K sources can at most be estimated by this procedure. This fundamental limitation renders plain classical deflation inappropriate in the underdetermined case.

5 ALPHABET-BASED DEFLATION

5.1 Parallel Deflation

Estimation errors accumulate through successive stages in classical deflation. Parallel deflation [8] tries to overcome this limitation by exploiting the discrete nature of digital sources and alphabet diversity, which arises when $R > 1$. Sources from alphabet $\mathcal{A}_r$ are extracted using the corresponding APF criterion. To minimise the impact of error accumulation, the deflation process used for the sources with a given modulation is carried out from the original observations, that can be processed in parallel by the appropriate APF contrasts. As a result, one such parallel deflation processes 'perceives' a mixture of K_r sources on L sensors, which should be easier to deal with than the L mixtures of K sources 'seen' by conventional deflation over all sources. Nevertheless, the extraction of sources from group r may be severely hampered by the interfering sources from the other groups.

5.2 Projection on the Source Alphabet

As pointed out earlier, the linear estimate of a source signal reduces the rank of the deflated sensor-output covariance matrix, making it impossible to extract all sources in an underdetermined mixture. To circumvent this difficulty, let us assume that the source has been perfectly estimated: $\hat{s} = s_k$, for some $k \in \{1, \ldots, K\}$. Then, under the source uncorrelation assumption, the deflation procedure described by eqns. (3)–(4) would produce $\hat{\mathbf{h}} = \mathbf{h}_k$ and the new set of observations $\mathbf{x} = \sum_{p \neq k} \mathbf{h}_p s_p + \mathbf{n}$; that is, the interference caused by that source to the remaining sources would be perfectly cancelled. Since the rank of the deflated sensor-output covariance matrix would not necessarily decrease, the rest of the sources might still be extracted at later stages.

Obviously, it will generally be difficult to have $\hat{s} = s_k$. A simple manner to try to obtain this perfect estimate is by projecting the linear extractor output on the known source constellation before deflation, as in the V-BLAST detection algorithm [5]. This non-linear processing can

be carried out cost-effectively by the minimum-distance detector.

5.3 Optimal Ordering in Classical Deflation

Classical deflation reduces the remaining interference as more sources are extracted. The amount of interference reduction depends on the quality of the source estimate. To minimise error accumulation, the 'strongest' or best estimated sources should be extracted and deflated first. The prior knowledge of the channel matrix simplifies the optimal ordering in terms of the output signal-to-noise ration (SNR), as in the V-BLAST algorithm [5]. For the blind scenario, we propose the following ordering method which, for simplicity but without loss of generality, is developed for M-PSK modulations.

The symbol error probability in the detection of a M-PSK signal contaminated by complex Gaussian noise can be accurately approximated by [7]:

$$P_e = 2Q\left(\sqrt{\mathrm{SNR}}\sin\left(\frac{\pi}{M}\right)\right), \quad M > 2 \qquad (5)$$

where $Q(x) = \frac{1}{\sqrt{2\pi}}\int_x^\infty \mathrm{e}^{-t^2/2}dt$. Now, given the set $\{\hat{s}_p, \hat{\mathbf{h}}_p, \mathbf{w}_p\}_{p=1}^K$ provided by an initial deflation sweep, the signal-to-interference-and-noise ratio (SINR) in the estimation of source k can be computed as:

$$\mathrm{SINR}_k = \frac{|\mathbf{w}_k^{\mathrm{H}}\hat{\mathbf{h}}_k|^2}{\sum_{p\neq k}|\mathbf{w}_k^{\mathrm{H}}\hat{\mathbf{h}}_p|^2 + \hat{\sigma}_n^2\|\mathbf{w}_k\|^2}. \qquad (6)$$

The noise variance estimate $\hat{\sigma}_n^2$ can be obtained from the sensor-output residual after all sources have been deflated. To estimate the probability of error P_e in (5), the SNR can be replaced with the SINR given above. Deflation can then be repeated in ascending order of P_e or, equivalently, descending order of $\sqrt{\mathrm{SINR}}\sin(\pi/M)$. To target a specific source while trying to alleviate the increased computational cost, the linear extractor found in the original deflation is used to initialise the iterative optimisation of the corresponding alphabet-matched contrast function (the CP criterion for M-PSK signals). The whole process may be repeated until the ordering converges, or just for a fixed number of deflation iterations.

6 EXPERIMENTAL STUDY

Influence of extraction criterion and alphabet projection. An underdetermined instantaneous linear mixture of 4 sources with QPSK modulation is observed at the output of a 3-sensor array in blocks of 150 data symbols. The sensor output is corrupted by additive white complex circular Gaussian noise, with a varying spatially averaged received SNR defined as in [5], which can be expressed as $\mathrm{SNR} = \mathrm{trace}(\mathbf{H}\mathbf{H}^{\mathrm{H}})/(L\sigma_n^2)$. The mixing matrix elements are randomly drawn from a normalised complex Gaussian distribution at each of the 200 Monte Carlo iterations. In the first experiment, two extraction criteria (CM and CP) together with two deflation methods (classical deflation and classical deflation with projection), giving rise to the methods labelled as CM-D, CM-P-D (projection on $|s| = 1$), CP-D and CP-P-D (projection on the alphabet). The search for the CM and the CP contrast function minima is carried out with the optimal step-size technique of [11]. ZF V-BLAST with perfect channel estimate is implemented as in [5]. The linear MMSE detector and the non-linear MAP detector serve as performance bounds.

Figure 1 (top) shows the symbol-error-rate (SER) averaged over the 4 estimated sources. Figure 1(bottom) displays the probability of extracting all 4 sources with an SER below 10%. The CM-D and the CP-D, where deflation is based on conventional linear regression, are unable to extract the four sources satisfactorily. Likewise, the MMSE extractor and V-BLAST are also severely limited by the lack of linear invertibility of the channel matrix. Although the CM-P-D visibly improves on the CM-D, the combination of alphabet projection and alphabet-based extraction appears most effective. Indeed, the CP-P-D approaches the MAP bound and, for sufficient SNR, is able to extract all four sources at low SER with probability close to one.

Classical vs. parallel deflation. Influence of extraction ordering. The second experiment simulates a mixture of 6 sources, three with BPSK and three with 3-PSK modulation, observed at the output of 4 sensors, in the same general conditions as above and 150 Monte Carlo iterations. Only CP-based extraction is considered: classical deflation with direct ordering (targeting the BPSK sources first), with inverse ordering (aiming at the 3-PSK sources first), and with the optimal ordering presented in the previous section (with a single extra deflation sweep after ordering). These methods are also compared with the parallel deflation approach of [8] with alphabet projection.

As observed in Fig. 2, the performance of classical deflation depends strongly on the extraction ordering, with the proposed optimal ordering achieving the best results at almost twice the average number of optimal step-size gradient-descent iterations (around 550) required by the two other classical deflation methods (300). Parallel deflation entails the lowest computational cost (just over 200 iterations) but shows a performance near classical deflation with inverse ordering, marginally improving on the MMSE's average SER at high SNR.

7 CONCLUSIONS

We have exploited the discrete nature of digital communication signals to address the deflation-based blind source extraction in underdetermined mixtures. As already noticed in other works (e.g., [1]), some type of non-linear processing is necessary to extract all sources satisfactorily. Herein, projection on the signal alphabet before deflation has been shown to ameliorate the performance of linear extraction, with an alphabet-based criterion (CP) clearly outperforming the traditional CM principle, even for sources verifying the CM assumption. An alphabet-matched linear extraction criterion followed by projection on the signal alphabet can considerably improve the performance of classical regression-based deflation in extracting all sources from an underdetermined mixture with a reasonably low probability of error. Also, the gradual interference suppression of classical deflation seems to have

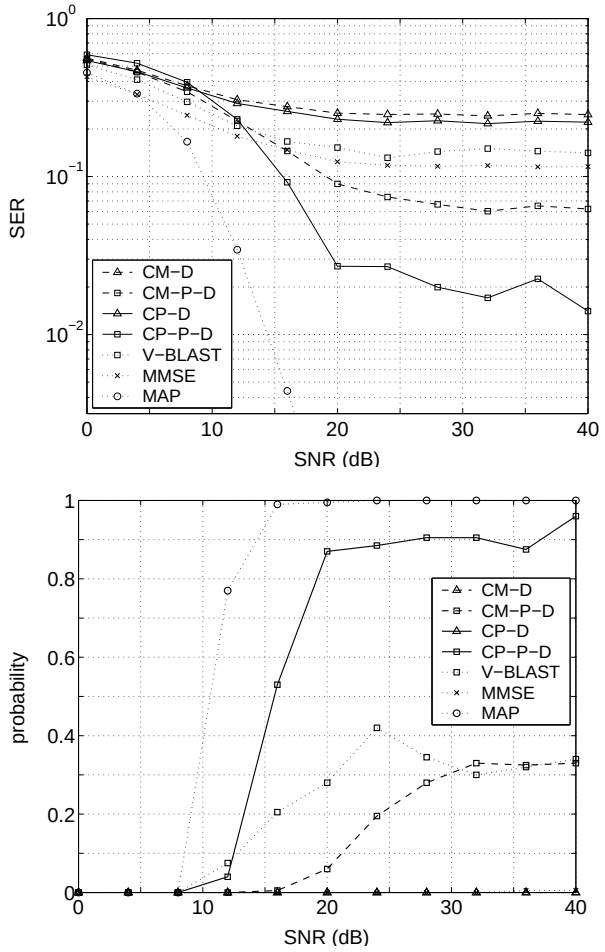

Figure 1: Source extraction results in the underdetermined (3×4) scenario with QPSK sources, signal blocks of 150 symbols and 200 Monte Carlo runs. Top: average separator output SER. Bottom: probability of extracting the 4 sources with SER < 0.1.

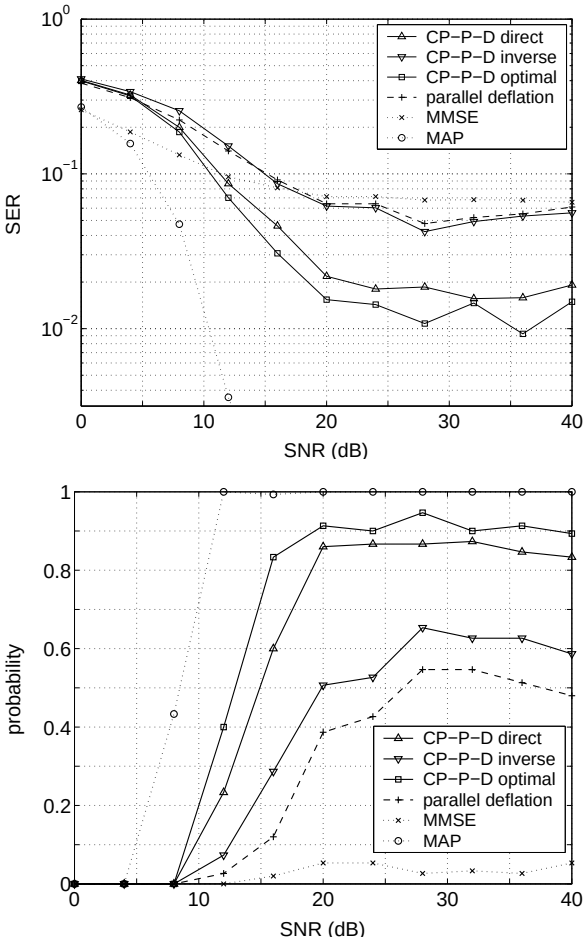

Figure 2: Source extraction results in the underdetermined (4×6) scenario with three BPSK and three 3-PSK sources, signal blocks of 150 symbols and 150 Monte Carlo runs. Top: average separator output SER. Bottom: probability of extracting the 6 sources with SER < 0.1.

a more significant positive impact than the reduced error accumulation of parallel deflation. The further performance enhancement provided by the proposed method for optimising the extraction order may not compensate for the additional computational cost. The method is reminiscent of the V-BLAST technique [5], but requires no training and can handle scenarios of less sensors that sources with possibly different modulations.

References

[1] P. Comon. Blind identification and source separation in 2×3 under-determined mixtures. *Transactions on Signal Processing*, 52(1):11–22, Jan. 2004.

[2] P. Comon. Contrasts, independent component analysis, and blind deconvolution. *International Journal of Adaptive Control and Signal Processing (Special Issue on Blind Signal Separation)*, 18(3):225–243, Apr. 2004.

[3] N. Delfosse and P. Loubaton. Adaptive blind separation of independent sources: a deflation approach. *Signal Processing*, 45(1):59–83, July 1995.

[4] D. N. Godard. Self-recovering equalization and carrier tracking in two-dimensional data communication systems. *IEEE Trans. Comms.*, 28(11):1867–1875, Nov. 1980.

[5] G. D. Golden, G. J. Foschini, R. A. Valenzuela, and P.W. Wolniansky. Detection algorithm and initial laboratory results using V-BLAST space-time communication architecture. *Electronics Letters*, 35(1):14–15, Jan. 1999.

[6] O. Grellier and P. Comon. Blind separation of discrete sources. *IEEE Sig. Proc. Lett.*, 5(8):212–214, Aug. 1998.

[7] J. G. Proakis. *Digital Communications*. McGraw-Hill, New York, 4th edition, 2000.

[8] L. Rota, V. Zarzoso, and P. Comon. Parallel deflation with alphabet-based criteria for blind source extraction. In *Proc. SSP-2005*, Bordeaux, France, July 17–20, 2005.

[9] O. Shalvi and E. Weinstein. New criteria for blind deconvolution of nonminimum phase systems (channels). *IEEE Trans. Information Theory*, 36(2):312–321, Mar. 1990.

[10] J. K. Tugnait. Identification and deconvolution of multichannel non-Gaussian processes using higher order statistics and inverse filter criteria. *IEEE Transactions on Signal Processing*, 45:658–672, Mar. 1997.

[11] V. Zarzoso and P. Comon. Blind and semi-blind equalization based on the constant power criterion. *IEEE Transactions on Signal Processing*, 53(11):4363–4375, Nov. 2005.

HOW FAST IS FASTICA?

Vicente Zarzoso, Pierre Comon

Laboratoire I3S, CNRS/UNSA
Les Algorithmes – Euclide-B, BP 121
06903 Sophia Antipolis Cedex, France
{zarzoso, comon}@i3s.unice.fr

Mariem Kallel

Departement TIC, Laboratoire U2S, ENIT
Campus Universitaire "Le Belvédère"
1002 Tunis, Tunisia

ABSTRACT

The present contribution deals with the statistical tool of Independent Component Analysis (ICA). The focus is on the deflation approach, whereby the independent components are extracted one after another. The kurtosis-based FastICA is arguably one of the most widespread methods of this kind. However, its features, particularly its speed, have not been thoroughly evaluated or compared, so that its popularity seems somewhat unfounded. To substantiate this claim, a simple quite natural modification is put forward and assessed in this paper. It merely consists of performing exact line search optimization of the contrast function. Speed is objectively measured in terms of the computational complexity required to reach a given source extraction performance. Illustrative numerical results demonstrate the faster convergence and higher robustness to initialization of the proposed approach, which is thus referred to as RobustICA.

1. INTRODUCTION

Independent Component Analysis (ICA) transforms an observed random vector into mutually statistically independent components [1]. Its numerous applications have spurred an increasing research interest in this technique; for instance, ICA is the basic statistical tool to perform Blind Source Separation (BSS) [1, 2, 3]. In its original definition (see [1, 4], among other early works), ICA extracts all the sources jointly or simultaneously; this is the so-called "symmetric" approach. ICA can also be performed by estimating the sources sequentially or one by one. This alternative procedure, referred to as *deflation*, was originally proposed in [5], and used successfully in the separation of convolutive mixtures [6]. Deflation has later been widely promoted in the machine learning community [3]. Joint algorithms are usually thought to outperform deflationary algorithms due to errors accumulated in successive subtractions (regressions) of the estimated source contribution to the observation. This shortcoming is generally claimed to be compensated by a significant gain in computations, although this claim still requires closer examination.

The FastICA [7, 8], originally put forward in deflation mode, features among the most popular ICA algorithms. Although it appeared when many other ICA methods had already been proposed, the deflationary FastICA has never been compared by the authors of [3] with earlier joint algorithms such as COM2 [1], JADE [4], COM1 [9], or the deflation methods by Tugnait [6] or Delfosse-Loubaton [5]. In fact, to our knowledge, FastICA (both in its deflation and symmetric implementations) has only been compared with neural-based adaptive algorithms and principal component analysis (PCA), that most ICA algorithms are known to outperform. Its popularity has been justified on the grounds of the satisfactory performance offered by the method in several applications, as well as its simplicity. However, these features, and in particular its speed, have never been substantiated by a thorough comparison with other techniques. A first serious attempt has been made in [10], where FastICA is found to fail for weak or highly spatially correlated sources. In spite of its comprehensiveness, the comparative analysis of [10] is perhaps unfortunate in contrasting the deflationary FastICA with joint methods such as COM2, JADE and COM1. On the other hand, recent studies have put in evidence some deficiencies of FastICA, such as the detrimental effects of saddle points on its performance [11].

Given the assiduous attention the method has received over the last decade, these gaps are somewhat surprising. Indeed, it does not seem difficult to envisage a very simple, quite natural deflation algorithm that would outperform FastICA. The goal of this work is to put forward such a method, which we refer to as *RobustICA*, and compare it with FastICA. The new method simply consists of carrying out exact line search of the contrast function, the normalized kurtosis [12]. Exact line search is achieved at low cost, since the optimal step size (OS) leading to the global maximum along the search direction can algebraically be found at each iteration among the roots of a low-degree polynomial. The OS methodology, which has already been proposed in the time equalization context [13, 14, 15, 16], can be used in conjunction with a variety of alternative criteria such as the constant modulus [17] and the constant power [14, 18]. As part of our experimental study, we evaluate the computational complexity required to reach a given source extraction performance. The algorithms' speed and efficiency can thus be compared objectively.

It is now generally acknowledged that adaptive (also known as on-line, recursive or sample-by-sample) algorithms are not always computationally cheaper than block (off-line, windowed) algorithms, and that they are rarely better in terms of precision. On this account, block implementations are the focus of this paper.

2. MODEL AND NOTATION

Let an L-dimensional random vector $\mathbf{x}$ denote the observation, which is assumed to stem from the linear sta-

In *Proc. EUSIPCO-2006*, Florence, Italy, Sept. 4-8, 2006.

tistical model:

$$\mathbf{x} = \mathbf{H}\mathbf{s} + \mathbf{v}. \quad (1)$$

The source vector $\mathbf{s} = [s_1, s_2, \ldots, s_K]^{\mathrm{T}}$ is made of K statistically mutually independent components. The noise term $\mathbf{v}$ will be ignored throughout, except in the numerical experiments. In fact, its distribution is assumed to be unknown, so that it can at most be considered as a nuisance; otherwise, a maximum likelihood approach could be employed, which is beyond the scope of the present comparison. The goal of ICA can be expressed as follows: given a sensor-output signal block composed of T samples, estimate the corresponding T-sample realization of the source vector.

Vectors and matrices will be typeset in boldface lowercase and boldface uppercase symbols, respectively; superscripts $(^{\mathrm{T}})$, $(^{\mathrm{H}})$, and $(^*)$ denote respectively transposition, conjugate transposition, and complex conjugation. Unless otherwise specified, the components of random vectors $\mathbf{x}$, $\mathbf{s}$ and $\mathbf{v}$ take their values in the complex field.

3. OPTIMALITY CRITERIA

The deflation approach to ICA consists of searching for an extracting vector $\mathbf{w}$ so that its scalar output

$$z \stackrel{\text{def}}{=} \mathbf{w}^{\mathrm{H}}\mathbf{x} \quad (2)$$

maximizes some optimality criterion or contrast function. A widely used contrast is the normalized kurtosis of the separator output:

$$\mathcal{K}(\mathbf{w}) = \frac{\mathrm{E}\{|z|^4\} - 2\mathrm{E}^2\{|z|^2\} - |\mathrm{E}\{z^2\}|^2}{\mathrm{E}^2\{|z|^2\}}. \quad (3)$$

This criterion is easily seen to be insensitive to scale, i.e., $\mathcal{K}(\lambda\mathbf{w}) = \mathcal{K}(\mathbf{w})$, $\forall\lambda \neq 0$. This scale indeterminacy is inherent in BSS, and we can thus impose $\|\mathbf{w}\| = 1$ for numerical convenience. Other criteria are the widespread constant modulus (CM) [17]:

$$\mathcal{C}(\mathbf{w}) = \mathrm{E}\{\big(|z|^2 - 1\big)^2\} \quad (4)$$

and the constant power (CP) [14, 18]:

$$\mathcal{P}_r(\mathbf{w}) = \mathrm{E}\{|z^r - 1|^2\}. \quad (5)$$

Another type of objective functions need the data to be *prewhitened*, so that the sensor outputs are assumed to have an identity covariance matrix, $\mathbf{R}_x \stackrel{\text{def}}{=} \mathrm{E}\{\mathbf{x}\mathbf{x}^{\mathrm{H}}\} = \mathbf{I}$. One criterion that we shall be particularly interested in is the separator-output fourth-order moment:

$$\mathcal{M}(\mathbf{w}) = \mathrm{E}\{|z|^4\}. \quad (6)$$

This criterion must be optimized under a constraint to avoid arbitrarily large values of z. Assuming $\|\mathbf{w}\| = 1$, it is simple to realize that (6) is equivalent to (3) after prewhitening in two cases: if all sources and mixtures are real-valued, and if the sources are complex-valued but second-order circular, i.e., the non-circular second-moment matrix $\mathbf{C}_x \stackrel{\text{def}}{=} \mathrm{E}\{\mathbf{x}\mathbf{x}^{\mathrm{T}}\}$ is null. For instance, in the case where the mixture and noise are complex but the sources are real, criteria (6) and (3) are not equivalent.

4. KURTOSIS-BASED FASTICA

The stationary values of the kurtosis contrast $\mathcal{K}(\mathbf{w})$ are given by the cancellation of its gradient, which is proportional to:

$$\mathrm{E}\{\mathbf{x}zz^{*2}\} - (\mathbf{w}^{\mathrm{T}}\mathbf{C}_x^*\mathbf{w})\mathbf{C}_x\mathbf{w}^* - (\mathbf{w}^{\mathrm{H}}\mathbf{R}_x\mathbf{w})^{-1}\big[\mathrm{E}\{|z|^4\} - |\mathbf{w}^{\mathrm{H}}\mathbf{C}_x\mathbf{w}^*|^2\big]\mathbf{R}_x\mathbf{w}. \quad (7)$$

Under the constraint $\|\mathbf{w}\| = 1$, the stationary points of $\mathcal{M}(\mathbf{w})$ are obtained for the collinearity condition on $\mathrm{E}\{\mathbf{x}zz^{*2}\}$:

$$\mathrm{E}\{(\mathbf{w}^{\mathrm{H}}\mathbf{x}\mathbf{x}^{\mathrm{H}}\mathbf{w})\mathbf{x}\mathbf{x}^{\mathrm{H}}\}\mathbf{w} = \lambda\mathbf{w} \quad (8)$$

where λ is some Lagrangian multiplier. It is easy to verify that the same result is obtained by performing the unconstrained optimization of $\mathcal{M}(\mathbf{w})/\|\mathbf{w}\|^4$.

Equation (8) is a fixed-point equation as claimed in [7] only when λ is known, which is not the case here; λ must be determined so as to satisfy the constraint, and thus unfortunately it depends again on $\mathbf{x}$ and $\mathbf{w}$. In [3, 7], λ is arbitrarily set to a deterministic fixed value, which allows to spare computations. For this reason, as eventually pointed out in [8], FastICA is actually an approximate standard Newton algorithm rather than a fixed-point algorithm. As a result of the Hessian matrix approximation carried out under the prewhitening assumption, the kurtosis-based FastICA reduces to a conventional gradient-descent algorithm with a fixed step size, and is hence a particular case of [6]. In the real-valued scenario, FastICA's update rule reads:

$$\mathbf{w}^+ = \mathbf{w} - \frac{1}{3}\,\mathrm{E}\{\mathbf{x}(\mathbf{w}^{\mathrm{T}}\mathbf{x})^3\} \quad (9)$$

$$\mathbf{w}^+ \leftarrow \mathbf{w}^+/\|\mathbf{w}^+\|. \quad (10)$$

The Hessian matrix approximation is somewhat fortunate in that, under the source statistical independence assumption, it theoretically endows the resulting method with global cubic convergence. It is likely that the algorithms described in the next section inherit analogous convergence properties. Nevertheless, the FastICA algorithm sometimes gets stuck at saddle points, particularly for short sample sizes [11].

5. OPTIMAL STEP SIZE: ROBUSTICA

As we have just recalled, FastICA attempts to maximize the normalized kurtosis of the extractor output by means of a approximate Newton algorithm. The Hessian simplification reduces the Newton update to a gradient-based update with fixed step size. For the kurtosis as well as analogous contrast functions commonly encountered in blind signal processing, a more efficient optimization method exists that can improve performance while accelerating convergence. This method, theoretically straightforward yet effective in practice, is exact line maximization.

Line maximization of a generic cost function $\mathcal{J}(\mathbf{w})$ consists of finding its global maximum along a given

search direction:

$$\mu_{\text{opt}} = \arg\max_{\mu} \mathcal{J}(\mathbf{w} + \mu\mathbf{g}). \tag{11}$$

The direction is typically (but not necessarily) the gradient: $\mathbf{g} = \nabla_{\mathbf{w}}\mathcal{J}(\mathbf{w})$. Exact line search is in general computationally intensive and presents other limitations [19], which explains why, despite being a well-known optimization method, it has largely been disregarded. However, for criteria such as the kurtosis, the CM and the CP contrasts, $\mathcal{J}(\mathbf{w} + \mu\mathbf{g})$ is a low-degree rational function in μ. As a result, the optimal step size μ_{opt} can be found algebraically (in closed form) among the roots of a simple polynomial of degree D:

$$p(\mu) = \sum_{k=0}^{D} a_k \mu^k. \tag{12}$$

At each iteration, optimal step size (OS) optimization performs the following steps:

S1) Compute OS polynomial coefficients
S2) Extract OS polynomial roots $\{\mu_k\}_{k=1}^{D}$
S3) Obtain $\mu_{\text{opt}} = \arg\max_{k} \mathcal{J}(\mathbf{w} + \mu_k\mathbf{g})$
S4) Update $\mathbf{w}^+ = \mathbf{w} + \mu_{\text{opt}}\mathbf{g}$. (13)

The application of the OS methodology on the kurtosis, the CM and the CP criteria results in the OS kurtosis maximization algorithm (OS-KMA), the OS CM algorithm (OS-CMA), and the OS CP algorithm (OS-CPA), respectively. Note that the above procedure also applies when the contrast function is to be minimized: the minimization of the CM and CP criteria can be achieved through the maximization of $-\mathcal{C}(\mathbf{w})$ and $-\mathcal{P}_r(\mathbf{w})$, respectively. Some important aspects of OS optimization are briefly developed next.

Coefficient computation (step S1). The polynomials associated with the OS-KMA has degree $D = 4$. The derivation of its coefficients is tedious but otherwise straightforward. As summarized in the Appendix, they can be obtained at each iteration from the observed signal block and the current values of $\mathbf{w}$ and $\mathbf{g}$. An alternative version is based on the sensor-output statistics computed once before starting the iterations. This statistics-based version becomes more costly than the data-based version for large values of L. The expressions for the OS-CMA polynomial, which has degree $D = 3$, can be found in [15, 16].

Root extraction and selection (steps S2–S3). The roots of polynomial at orders 3 and 4 can be found with standard algebraic procedures such as Cardano's and Ferrari's formulas, respectively [19]. Preliminary experiments point out that, although complex-valued roots may appear as favourite in the sense of the maximization of $\mathcal{J}(\mathbf{w} + \mu_k\mathbf{g})$, the best real-valued candidate root should typically be preferred.

Normalization. To improve numerical conditioning in the determination of μ_{opt}, the normalized version of the gradient vector should be used in the above steps.

Table 1: Computational complexity per iteration of the deflationary ICA algorithms compared in this paper, for signal blocks of T samples observed at the output of L sensors, assuming real-valued sources and mixtures. The figures in the second row are for the simulation scenario of Sec. 7 and Figs. 1–2.

		RobustICA	
	FastICA	OS-KMA	OS-CMA
(L, T)	$2(L+1)T$	$(5L+12)T$	$(3L+10)T$
$(4, 150)$	1500	4800	3300

As observed in Sec. 3, the kurtosis criterion is scale invariant, so that the new extracting vector $\mathbf{w}^+$ should be normalized as in (10) after each OS-KMA iteration.

Computational complexity. The computational cost per iteration of FastICA and the two OS methods (data-based versions) presented above is shown in Table 1. Only the most significant terms have been retained. These dominant terms are of order $\mathrm{O}(T)$, and provide accurate approximations of the exact cost for sufficient sample size T. Complexity is measured in floating point operations (flops). A flop is considered as a real product.

The OS technique in the blind and semi-blind equalization context is fully developed in [14, 15, 16]; details are omitted here due to space limitations. By design, and as confirmed by simulations, OS optimization provides some robustness to local extrema and reduced overall complexity relative to conventional fixed step-size optimization. In the ICA context, the OS methodology naturally gives rise to what could be referred to as *RobustICA* algorithms. Indeed, improved faster convergence and increased robustness to the initial value of the extracting vector will be illustrated in the experiments of Sec. 7.

6. DEFLATION

After convergence, output signal z contains an estimate $\hat{s}_k$ of source component s_k. In most deflation algorithms (except, e.g., [5]), the extracted-source contribution to the sensor output is estimated by linear regression as $\hat{\mathbf{x}}_k = \hat{\mathbf{h}}_k \hat{s}_k$, with

$$\hat{\mathbf{h}}_k = \mathrm{E}\{\mathbf{x}\hat{s}_k^*\}/\mathrm{E}\{|\hat{s}_k|^2\}. \tag{14}$$

This contribution is then subtracted from the observations, producing a new observed vector

$$\mathbf{x} \leftarrow \mathbf{x} - \hat{\mathbf{x}}_k. \tag{15}$$

From the 'deflated' observations, the next source is estimated by running again the same extraction procedure. The deflation procedure is repeated until no sources are left. In practice, the expectations in (14) are substituted by sample averages over the signal block, which accept efficient matrix-vector product formulations.

7. NUMERICAL EXPERIMENTS

Since FastICA heavily relies on the whitening assumption, only real orthogonal mixtures are considered in the

following numerical study, as if prewhitening had been previously carried out. By contrast, a feature of deflation algorithms in general, and RobustICA in particular, is that they can directly operate on the observed sensor output without prewhitening. Hence, the orthogonal mixture scenario benefits the FastICA implementation.

A mixture of $K = 4$ independent unit-power BPSK sources is observed at the output of a $L = 4$ element array in signal blocks of 150 samples. Isotropic additive white real Gaussian noise is present at the sensor output, with signal-to-noise ratio:

$$\mathrm{SNR} = \frac{\mathrm{trace}(\mathbf{H}\mathbf{H}^{\mathrm{T}})}{\sigma_v^2 L} = \frac{1}{\sigma_v^2}. \tag{16}$$

Equivalent thresholds on the separating vector variation and a higher limit of $100L = 400$ iterations are employed as convergence tests. Once all sources have been estimated, they are optimally scaled and permuted to allow a meaningful comparison with the original sources. The signal mean square error (SMSE), defined as

$$\mathrm{SMSE}_k = \mathrm{E}\{|s_k - \hat{s}_k|^2\} \tag{17}$$

is used as separation quality index. The minimum mean square error (MMSE) receiver, which jointly estimates the separating vectors assuming that all transmitted symbols are used for training, provides a performance bound. Computational complexity is measured in terms of the number of floating point operations (flops) required to reach a solution. Performance parameters are averaged over 1000 independent random realizations of the sources, the noise and the mixing matrix.

A single-tap initialization, $\mathbf{w}_0 = [0, 1, 0, 0]^{\mathrm{T}}$, is used for all sources to be extracted. Fig. 1(a) shows the SMSE performance variation as a function of SNR. The first source extracted by OS-KMA and OS-CMA attains the MMSE bound, whereas the first source by FastICA can only achieve the performance of the second source by the other two methods. As expected, performance degrades for subsequent extractions. On average, the RobustICA algorithms clearly outperform FastICA, which shows a worse finite sample-size flooring effect due to the increased misadjustment introduced by its constant step size.

The algorithms' computational complexity is displayed in Fig. 1(b). Flop counts are obtained as the number of iterations times the number of flops per iteration (Table 1). OS-CMA's cost decreases as the SNR increases and as more sources are extracted. The OS-KMA shows a similar trend except for the last source, but its average complexity lies just below OS-CMA's. FastICA is only efficient when extracting the first source in sufficient SNR, and often goes over the iteration-count limit for the remaining sources. On average, FastICA turns out to be well over an order of magnitude more expensive than RobustICA in these experiments, even though its cost per iteration (Table 1) is less than a half and a third of OS-CMA's and OS-KMA's, respectively.

To assess their efficiency, the three methods' average extraction quality as a function of complexity is summarized by the '+'-marked plots in Fig. 2. RobustICA's higher efficiency is remarkable, despite its heavier cost per iteration (Table 1). Note that the MMSE is not an iterative method, and so its cost is irrelevant here; its SMSE value is shown in Fig. 2 for reference only. Also displayed in that figure is the average performance for other initial values of the extracting vector: canonical basis and random. In the former, the separating vector aiming to extract the kth source is initialized with the kth canonical basis vector, $\mathbf{e}_k = [\underbrace{0, \ldots, 0}_{(k-1)}, 1, \underbrace{0, \ldots, 0}_{(L-k)}]^{\mathrm{T}}$, $k = 1, \ldots, K$. In the latter, the initial values of the extracting vector taps are independently drawn from a normalized Gaussian distribution. As observed in these plots, RobustICA's consistent behaviour contrasts with FastICA's sensitivity to initialization.

8. CONCLUSIONS

The main purpose of this contribution was to show that FastICA is probably not the best ICA algorithm, and that its popularity is not based on a solid scientific comparison with earlier algorithms. Its fair simplicity is appealing, but its satisfactory fast performance has long been taken for granted by many researchers in the field. The superior efficiency and increased robustness to initialization of the simple RobustICA technique demonstrate that FastICA can indeed be easily improved. The OS methodology giving rise to RobustICA is not exclusive to the kurtosis criterion, but is applicable to any contrast function that can be expressed as a rational function in the step size. Further work will consider the use of the OS strategy for simultaneous ICA, and its comparison with other techniques.

9. APPENDIX: OS-KMA POLYNOMIAL

The OS polynomial of contrast $\mathcal{K}$ at $\mathbf{w}$ along direction $\mathbf{g}$ has coefficients:

$$\begin{aligned} &a_0 = -2h_0 i_1 + h_1 i_0, && a_1 = -4h_0 i_2 - h_1 i_1 + 2h_2 i_0 \\ &a_2 = -3h_1 i_2 + 3h_3 i_0, && a_3 = -2h_2 i_2 + h_3 i_1 + 4h_4 i_0 \\ &a_4 = -h_3 i_2 + 2h_4 i_1 \end{aligned}$$

with

$$\begin{aligned} h_0 &= \mathrm{E}\{|a|^2\} - 2\mathrm{E}^2\{|a|\} - |\mathrm{E}\{a\}|^2 \\ h_1 &= 4\mathrm{E}\{|a|d\} - 8\mathrm{E}\{|a|\}\mathrm{E}\{d\} - 4\mathbb{R}\mathrm{e}(\mathrm{E}\{a\}\mathrm{E}\{c^*\}) \\ h_2 &= 4\mathrm{E}\{d^2\} + 2\mathrm{E}\{|ab|\} - 8\mathrm{E}^2\{d\} - 4\mathrm{E}\{|a|\}\mathrm{E}\{|b|\} \\ &\quad -4|\mathrm{E}\{c\}|^2 - 2\mathbb{R}\mathrm{e}(\mathrm{E}\{a\}\mathrm{E}\{b^*\}) \\ h_3 &= 4\mathrm{E}\{|b|d\} - 8\mathrm{E}\{|b|\}\mathrm{E}\{d\} - 4\mathbb{R}\mathrm{e}(\mathrm{E}\{b\}\mathrm{E}\{c^*\}) \\ h_4 &= \mathrm{E}\{|b|^2\} - 2\mathrm{E}^2\{|b|\} - |\mathrm{E}\{b\}|^2 \\ i_0 &= \mathrm{E}\{|a|\}, \quad i_1 = 2\mathrm{E}\{d\}, \quad i_2 = \mathrm{E}\{|b|\} \\ a &= y^2, \quad b = g^2, \quad c = yg, \quad d = \mathbb{R}\mathrm{e}(yg^*) \\ y &= \mathbf{w}^{\mathrm{H}}\mathbf{x}, \quad g = \mathbf{g}^{\mathrm{H}}\mathbf{x}. \end{aligned}$$

REFERENCES

[1] P. COMON, "Independent component analysis, a new concept?," *Signal Processing, Elsevier*, vol. 36, no. 3, pp. 287–314, Apr. 1994, Special Issue on Higher-Order Statistics.

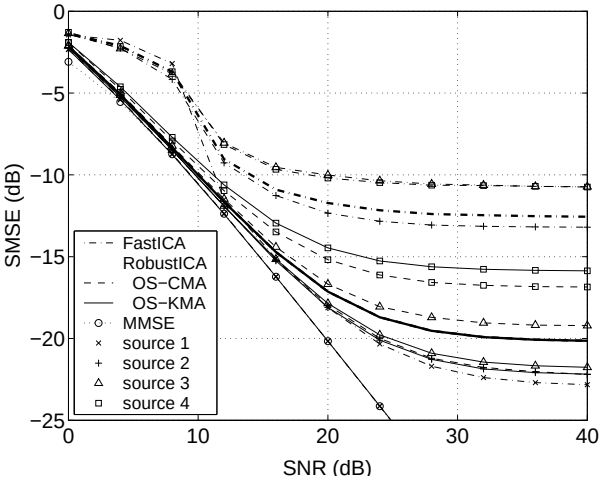

(a)

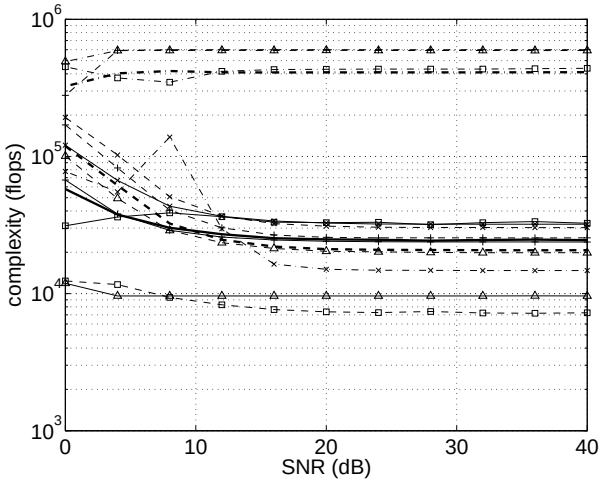

(b)

Figure 1: Performance of deflationary ICA algorithms for single-tap initialization: (a) signal extraction quality, (b) computational complexity. Unmarked thick lines represent performance indices averaged over the 4 sources.

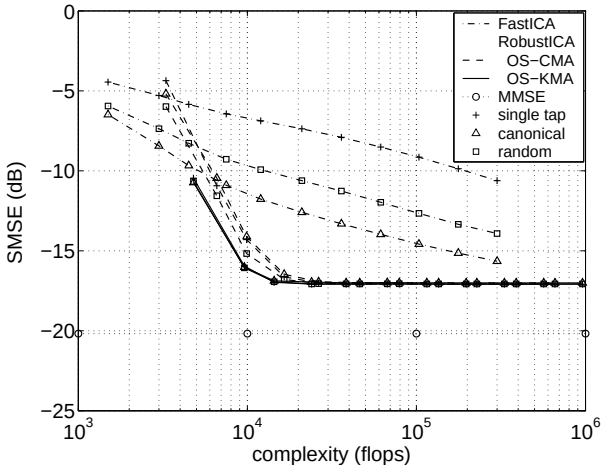

Figure 2: Average extraction quality against computational cost at 20-dB SNR for different extracting vector initializations.

[2] J. F. CARDOSO, "High-order contrasts for independent component analysis," *Neural Computation*, vol. 11, no. 1, pp. 157–192, Jan. 1999.

[3] A. HYVÄRINEN, J. KARHUNEN, and E. OJA, *Independent Component Analysis*, John Wiley & Sons, 2001.

[4] J. F. CARDOSO and A. SOULOUMIAC, "Blind beamforming for non-Gaussian signals," *IEE Proceedings - Part F*, vol. 140, no. 6, pp. 362–370, Dec. 1993, Special issue on Applications of High-Order Statistics.

[5] N. DELFOSSE and P. LOUBATON, "Adaptive blind separation of independent sources: a deflation approach," *Signal Processing*, vol. 45, pp. 59–83, 1995.

[6] J. K. TUGNAIT, "Identification and deconvolution of multichannel non-Gaussian processes using higher order statistics and inverse filter criteria," *IEEE Trans. Sig. Proc.*, vol. 45, pp. 658–672, Mar. 1997.

[7] A. HYVÄRINEN, "A family of fixed-point algorithms for independent component Analysis," in: *Proc. ICASSP*, Munich, Germany, April 20-24 1997, pp. 3917–3920.

[8] A. HYVÄRINEN, "Fast and robust fixed-point algorithms for independent component analysis," *IEEE Trans. Neural Networks*, vol. 10, no. 3, pp. 626–634, 1999.

[9] P. COMON and E. MOREAU, "Improved contrast dedicated to blind separation in communications," in: *Proc. ICASSP*, Munich, April 20-24 1997, pp. 3453–3456.

[10] P. CHEVALIER, L. ALBERA, P. COMON, and A. FERREOL, "Comparative performance analysis of eight blind source separation methods on radiocommunications signals," in: *Proc. Intl. Joint Conf. on Neural Networks*, Budapest, Hungary, July 25–29, 2004.

[11] P. TICHAVSKÝ, Z. KOLDOVSKÝ, and E. OJA, "Performance analysis of the FastICA algorithm and Cramér-Rao bounds for linear independent component analysis," *IEEE Trans. Sig. Proc.*, vol. 54, no. 4, pp. 1189–1203, Apr. 2006.

[12] O. SHALVI and E. WEINSTEIN, "New criteria for blind deconvolution of nonminimum phase systems (channels)," *IEEE Transactions on Information Theory*, vol. 36, no. 2, pp. 312–321, Mar. 1990.

[13] P. COMON, "Independent component analysis, contrasts and convolutive mixtures," in: *Proc. 2nd IMA Conference on Mathematics in Communications*, Lancaster, UK, Dec. 16-18, 2002, pp. 10–17, invited.

[14] V. ZARZOSO and P. COMON, "Blind and semi-blind equalization based on the constant power criterion," *IEEE Trans. Sig. Proc.*, vol. 53, no. 11, Nov. 2005, pp. 4363–4375.

[15] V. ZARZOSO and P. COMON, "Blind channel equalization with algebraic optimal step size," in: *Proc. EUSIPCO, XIII European Signal Processing Conference*, Antalya, Turkey, Sept. 4–8, 2005.

[16] V. ZARZOSO and P. COMON, "Optimal step-size constant modulus algorithm," *IEEE Transactions on Communications*, submitted.
(`www.i3s.unice.fr/%7Emh/RR/2004/RR-04.23-V.ZARZOSO.pdf`)

[17] D. N. GODARD, "Self-recovering equalization and carrier tracking in two-dimensional data communication systems," *IEEE Transactions on Communications*, vol. 28, no. 11, pp. 1867–1875, Nov. 1980.

[18] O. GRELLIER and P. COMON, "Blind separation of discrete sources," *IEEE Signal Processing Letters*, vol. 5, no. 8, Aug. 1998, pp. 212–214.

[19] W. H. PRESS, S. A. TEUKOLSKY, W. T. VETTERLING, *et al.*, *Numerical Recipes in C. The Art of Scientific Computing*, 2nd Ed., Cambridge University Press, 1992.

BLIND CHANNEL EQUALIZATION WITH ALGEBRAIC OPTIMAL STEP SIZE

Vicente Zarzoso[1*] *and Pierre Comon*[2]

[1] Department of Electrical Engineering and Electronics, The University of Liverpool, Liverpool L69 3GJ, UK
vicente@liv.ac.uk

[2] Laboratoire I3S, Les Algorithmes – Euclide-B, BP 121, 06903, Sophia Antipolis, France
comon@i3s.unice.fr

ABSTRACT

The constant modulus algorithm (CMA) is arguably the most widespread iterative method for blind equalization of digital communication channels. The present contribution studies a recently proposed technique aiming at avoiding the shortcomings of conventional gradient-descent implementations. This technique is based on the computation of the step size leading to the absolute minimum of the CM criterion along the search direction. For the CM as well as other equalization criteria, this optimal step size can be calculated algebraically at each iteration by finding the roots of a low-degree polynomial. After developing the resulting optimal step-size CMA (OS-CMA), the algorithm is compared to its conventional constant step-size counterpart and more recent alternative CM-based methods. The optimal step size seems to improve the conditioning of the equalization problem as in prewhitening (e.g., via a prior QR decomposition of the data matrix), although it becomes more costly for long equalizers. The additional exploitation of the i.i.d. assumption through prewhitening can further improve performance, an outcome that had not been clearly interpreted in former works.

1. INTRODUCTION

An important problem in digital communications is the recovery of the data symbols transmitted through a distorting medium. The constant modulus (CM) criterion is probably the most widespread blind channel equalization principle [1]. The CM criterion generally presents local extrema — often associated with different equalization delays — in the equalizer parameter space [2]. This shortcoming renders the performance of gradient-based implementations, such as the well-known constant modulus algorithm (CMA), very dependent on the equalizer impulse response initialization. Even when the absolute minimum is found, convergence can be severely slowed down for initial equalizer settings with trajectories in the vicinity of saddle points [3, 4]. Also, the constant value of the step-size parameter (or adaption coefficient) must be carefully selected to ensure a stable operation while balancing convergence rate and final accuracy (misadjustment or excess mean square error). The stochastic gradient CMA (SG-CMA) drops the expectation operator and approximates the gradient of the criterion by a one-sample estimate, much in the LMS fashion. This rough approximation generally leads to slow convergence and poor misadjustment, even if the step size is carefully selected.

Block (or fixed-window) methods obtain a more precise gradient estimate from a batch of channel output samples, improving convergence speed and accuracy [5]. Tracking capabilities are preserved as long as the channel remains stationary over the observation window. The block-gradient CMA (simply denoted as CMA hereafter) is particularly suited to burst-mode transmission systems. Unfortunately, the multimodal nature of the CM criterion sustains the negative impact of local extrema in block implementations. The block CMA method of [5] is based on a preliminary QR decomposition of the data matrix, followed by power iterations on an equivalent kurtosis minimization criterion. An appropriate choice of the step size ensures the monotonic convergence of this algorithm (referred to as QR-CMA herein), although global convergence is not guaranteed. The recursive least squares CMA (RLS-CMA) [6], which operates on a sample-by-sample basis, also proves notably faster and more robust than the SG-CMA. The derivation of the RLS-CMA relies on an approximation to the CM cost function in stationary or slowly varying environments, where block implementations may actually prove more efficient in exploiting the available information (the received signal burst). Moreover, the problems posed by local extrema are not explicitly addressed by the RLS approach. Another attempt to improve convergence is based on an adaptive control tuner that adjusts the second derivative of the equalizer tap estimates [7]. This accelerating adaptive filtering CMA (AAF-CMA) presents enhanced convergence rate and tracking capabilities relative to the SG-CMA, and is able to avoid shallow local extrema.

A recently proposed methodology to avoid the shortcomings derived from the multimodality of the CM criterion consists of performing consecutive one-dimensional absolute minimizations of the cost function. This technique, known as exact line search or steepest descent, is generally considered inefficient [8]. However, it was first observed in [9] that the value of the adaption coefficient that leads to the absolute minimum of most blind cost functions along a given search direction can be computed algebraically. It was conjectured that the use of this algebraic optimal step size could not only accelerate convergence but also avoid local extrema in some cases. The present contribution carries out the theoretical development and experimental evaluation of the optimal step-size CMA (OS-CMA) derived from this idea, which was briefly presented in [10] under a different name. The OS-CMA is then compared to other CM-based implementations such as the CMA, the QR-CMA, the RLS-CMA and the AAF-CMA.

2. CONSTANT MODULUS EQUALIZATION

Zero-mean data symbols $\{s_n\}$ are transmitted at a known baud-rate $1/T$ through a time dispersive channel with impulse response $h(t)$. The channel is assumed linear and time-invariant (at least over the observation window), with a stable, causal and possibly non-minimum phase transfer function, and comprises the transmitter pulse-shaping and receiver front-end filters. Assuming perfect synchronization and carrier-residual elimination, baud-spaced sampling yields the discrete-time channel output

$$x_n = \sum_k h_k s_{n-k} + v_n \qquad (1)$$

in which $x_n = x(nT)$, $x(t)$ denoting the continuous-time baseband received signal. Similar definitions hold for h_k

* Royal Academy of Engineering Research Fellow.

In *Proc. EUSIPCO*, Antalya, Turkey, Sept. 4-8, 2005.

and the additive noise v_n. Eqn. (1) represents the so-called single-input single-output (SISO) signal model. This model applies to scenarios where diversity in the form of time oversampling or multiple receive sensors is not available. The interest in the SISO model lies in its 'hardness': in general, FIR channels cannot be perfectly equalized using FIR filters. By contrast, in multichannel configurations, giving rise to multiple-output models (SIMO, MIMO), FIR channels accept zero-forcing FIR equalizers under relatively mild length-and-zero conditions [11]. The results presented in this paper are easily transposable to multichannel models [10,13].

To recover the original data symbols from the received signal, a linear equalizer is employed with finite impulse response spanning L baud periods $\mathbf{f} = [f_1,\, f_2,\, \ldots,\, f_L]^{\mathrm{T}} \in \mathbb{C}^L$, This filter produces the output signal $y_n = \mathbf{f}^{\mathrm{H}}\mathbf{x}_n$, where $\mathbf{x}_n = [x_n,\, x_{n-1},\, \ldots,\, x_{n-L+1}]^{\mathrm{T}} \in \mathbb{C}^L$. The equalizer vector can be blindly estimated by minimizing the CM cost function [1]:

$$J_{\mathrm{CM}}(\mathbf{f}) = \mathrm{E}\big\{\big(|y_n|^2 - \gamma\big)^2\big\} \tag{2}$$

where $\gamma = \mathrm{E}\{|s_n|^4\}/\mathrm{E}\{|s_n|^2\}$ is a constellation-dependent parameter. The CMA is a gradient-descent iterative procedure to minimize the CM cost. Its update rule reads

$$\mathbf{f}' = \mathbf{f} - \mu\mathbf{g} \tag{3}$$

where $\mathbf{g} \stackrel{\mathrm{def}}{=} \nabla J_{\mathrm{CM}}(\mathbf{f}) = 4\mathrm{E}\big\{(|y_n|^2 - \gamma)y_n^*\mathbf{x}_n\big\}$ is the gradient vector at point $\mathbf{f}$, and μ represents the step-size parameter. In the sequel, we assume that a block of length N_d baud periods x_n is observed at the channel output, from which $N = (N_d - L + 1)$ vectors $\mathbf{x}_n$ can be constructed.

3. OPTIMAL STEP-SIZE CMA

3.1 Steepest-Descent Minimization

Steepest-descent minimization consists of finding the absolute minimum of the cost function along the line defined by the search direction (typically the gradient) [8]:

$$\mu_{\mathrm{opt}} = \arg\min_{\mu} J_{\mathrm{CM}}(\mathbf{f} - \mu\mathbf{g}). \tag{4}$$

In general, exact line search algorithms are unattractive because of their relatively high complexity. Even in the one-dimensional case, function minimization must usually be performed using costly numerical methods. However, it was originally observed in [9] that the CM cost $J_{\mathrm{CM}}(\mathbf{f} - \mu\mathbf{g})$ is a low-degree rational function in the step size μ. Consequently, it is possible to find the optimal step size μ_{opt} in closed form among the roots of a simple polynomial in μ. Exact line minimization of function (2) can thus be performed at relatively low complexity.

3.2 Algebraic Optimal Step Size: the OS-CMA

In effect, some algebraic manipulations show that the derivative of $J_{\mathrm{CM}}(\mathbf{f} - \mu\mathbf{g})$ with respect to μ is the 3rd-degree polynomial

$$p(\mu) = d_3\mu^3 + d_2\mu^2 + d_1\mu + d_0 \tag{5}$$

with real-valued coefficients given by

$$\begin{array}{ll} d_3 = 2\mathrm{E}\{a_n^2\}, & d_2 = 3\mathrm{E}\{a_n b_n\} \\ d_1 = \mathrm{E}\{2a_n c_n + b_n^2\}, & d_0 = \mathrm{E}\{b_n c_n\} \end{array} \tag{6}$$

where $a_n = |g_n|^2$, $b_n = -2\mathbb{R}\mathrm{e}(y_n g_n^*)$, and $c_n = (|y_n|^2 - \gamma)$, with $g_n = \mathbf{g}^{\mathrm{H}}\mathbf{x}_n$.

Alternatively, the coefficients of the OS-CMA polynomial can be obtained as a function of the sensor-output statistics as:

$$\begin{array}{ll} d_3 = C_{\mathbf{gggg}}, & d_2 = -3\mathbb{R}\mathrm{e}(C_{\mathbf{gggf}}) \\ d_1 = 2C_{\mathbf{ffgg}} + \mathbb{R}\mathrm{e}(C_{\mathbf{fgfg}}) - \gamma C_{\mathbf{gg}}, & d_0 = \mathbb{R}\mathrm{e}(\gamma C_{\mathbf{fg}} - C_{\mathbf{fffg}}) \end{array} \tag{7}$$

where

$$C_{\mathbf{abcd}} \stackrel{\mathrm{def}}{=} \mathrm{E}\{\mathbf{a}^{\mathrm{H}}\mathbf{x}\mathbf{x}^{\mathrm{H}}\mathbf{b}\mathbf{c}^{\mathrm{H}}\mathbf{x}\mathbf{x}^{\mathrm{H}}\mathbf{d}\} = \sum_{ijkl} \mathrm{E}\{x_i x_j^* x_k x_l^*\} a_i^* b_j c_k^* d_l$$

and $C_{\mathbf{ab}} \stackrel{\mathrm{def}}{=} \mathbf{a}^{\mathrm{H}}\mathbf{R}_x\mathbf{b}$, with $\mathbf{R}_x = \mathrm{E}\{\mathbf{x}\mathbf{x}^{\mathrm{H}}\}$ denoting the sensor-output covariance matrix. This second procedure needs to compute in advance the sensor-output covariance matrix $\mathbf{R}_x$ and 4th-order moments $\mathrm{E}\{x_i x_j^* x_k x_l^*\}$, $1 \leqslant i,\, j,\, k,\, l \leqslant L$. Coefficients (6)–(7) are derived in the Appendix.

Having obtained its coefficients through any of the above equivalent procedures, the roots of polynomial (5) can be extracted as explained in Sec. 3.3. The optimal step size corresponds to the root attaining the lowest value of the cost function, thus accomplishing the *global* minimization of J_{CM} in the gradient direction. Once μ_{opt} has been determined, the filter taps are updated as in (3), and the process is repeated with the new filter and gradient vectors, until convergence. This algorithm is referred to as *optimal step-size CMA (OS-CMA)*. Specifically, we call OS-CMA-1 the method resulting from coefficient computation (6), and OS-CMA-2 that obtained from (7). Note that both methods are equivalent in equalization performance and convergence rate measured in terms of iterations. The only difference lies in their computational cost in number of operations (Sec. 3.5).

To improve numerical conditioning in the determination of μ_{opt}, gradient vector $\mathbf{g}$ should be normalized beforehand. Since the relevant parameter is the search direction $\tilde{\mathbf{g}} = \mathbf{g}/\|\mathbf{g}\|$, this normalization does not cause any adverse effects. Accordingly, vector $\mathbf{g}$ is substituted by $\tilde{\mathbf{g}}$ when computing the polynomial coefficients (6)–(7) and in the update rule (3).

3.3 Root Extraction

Standard analytical procedures such as Cardano's formula, or more efficient iterative methods [12], are readily available for obtaining the roots of 3rd-degree polynomial (5); an efficient MATLAB implementation, valid for polynomials with real or complex coefficients, is given in [13]. Concerning the nature of the roots, two options are possible: either all three roots are real, or one is real and the other two form a complex conjugate pair. If all three roots are real valued, we check which of the three real roots provides the lowest value of $J_{\mathrm{CM}}(\mathbf{f} - \mu\mathbf{g})$. In our experiments, when one root was real and the other two formed a complex conjugate pair, the real root typically provided the lowest value of the cost function. Even when the real root did not yield the lowest J_{CM}, it generally produced better output mean square error (MSE) than the complex roots. Hence, the real root should be preferred.

3.4 Preliminary Convergence Analysis

By design of steepest-descent methods, gradient vectors at consecutive iterations are orthogonal, which, depending on the initialization and the shape of the cost-function surface, may slow down convergence [8]. In the OS-CMA, gradient orthogonality is mathematically represented by relation $\mathbb{R}\mathrm{e}(\mathbf{g}^{\mathrm{H}}\mathbf{g}') = 0$, with $\mathbf{g}' = \nabla J_{\mathrm{CM}}(\mathbf{f}')$. In our experiments, the OS-CMA always converged in less iterations than its constant step-size counterpart [13]. Likewise, fast convergece and improved stability have been independently reported in [10]. In addition, the frequency of misconvergence to local extrema is diminished with the use of the optimal step-size strategy, as empirically demonstrated in [13] and briefly in Section 4.

3.5 Computational Complexity

The computational load of the OS-CMA is mainly due to the calculation of the polynomial coefficients (6) or (7). Mathe-

Table 1: Computational cost in number of flops for several CM-based algorithms (single-input case). L: number of taps in equalizer vector; N: number of data vectors in observed signal burst.

	initialization	per iteration
SG-CMA	—	$2(L+1)$
CMA	—	$2N(L+1)$
OS-CMA-1	—	$N(6L+15)$
OS-CMA-2	$N\left[\binom{L+3}{4}+\binom{L+1}{2}\right]$	$6L^4+3L^2+2L$
QR-CMA	$4L^2N$	$2(L+2)N$
RLS-CMA	—	$L(4L+7)$
AAF-CMA	—	$6L$

matical expectations are in practice approximated by sample averaging across the observed signal burst. The computational cost of these averages in (6) is of order $\mathrm{O}(NL)$ per iteration, for data blocks composed of N sensor vectors $\mathbf{x}_n$. The cost per iteration of the alternative procedure (7) is approximately of order $\mathrm{O}(L^4)$. However, the second procedure needs to compute in advance the sensor-output 4th-order statistics, $\mathrm{E}\{x_i x_j^* x_k x_l^*\}$, $1 \leqslant i, j, k, l \leqslant L$, incurring in an additional cost of $\mathrm{O}(NL^4)$ operations. Depending on the number of iterations for convergence and the relative values of N and L, this initial load may render the second method more costly.

Table 1 provides the figures for the OS-CMA computational cost in terms of the number of real floating point operations or *flops* (a flop represents a multiplication or a division followed by an addition or a subtraction). Also shown are the values for other CM-based methods. Only dominant terms in the relevant parameters (L, N) are retained in the flop-count calculations. Real-valued signals and filters are assumed, although analogous values can similarly be obtained for the complex-valued scenario. The cost of extracting the roots of the step-size polynomial does not depend on (L, N) and can thus be considered negligible (see Section 3.3).

3.6 Variants

The algebraic optimal step-size technique can also be applied to other blind equalization criteria. The kurtosis maximization (KM, also known as Shalvi-Weinstein) criterion [14] can be globally minimized along a given direction by rooting a polynomial of degree 4 in μ (details are omitted due to the lack of space). This would give rise to the OS-KMA, with a computational cost per iteration similar to that of the OS-CMA. The optimal step-size technique remains applicable if the received data are prewhitened, e.g., using a QR decomposition of the data matrix, as in the QR-CMA method of [5]. Accordingly, we refer to the optimal step-size KM algorithm with prewhitening as OS-QR-KMA. Prewhitening improves conditioning and may lead to faster convergence under the i.i.d. input assumption.

4. EXPERIMENTAL RESULTS

The following experiments evaluate the comparative performance of the OS-CMA. Bursts of $N_d = 200$ baud periods are observed at the output of a baud-spaced order-4 channel excited by an i.i.d. BPSK source ($\gamma = 1$) and corrupted by AWGN with 10-dB SNR. To test robustness to the channel configuration, the channel impulse response coefficients are randomly drawn from a zero-mean unit-variance real-valued Gaussian distribution before processing each of 500 independent signal bursts. The typical center-tap filter serves as equalizer tap vector initialization. Iterations are stopped when $\|\mathbf{f}' - \mathbf{f}\|/\|\mathbf{f}\| < 0.1\mu/\sqrt{N}$, where $\|\cdot\|$ denotes the Euclidean norm, and μ is the constant step size chosen for the conventional CMA. To limit complexity, a higher bound of $500L$ iterations is set. The final equalizer vector is scaled to provide the lowest MSE value among all possible extraction delays. The same signal bursts, channel impulse response, and termination test are used for all methods under study. Regarding the methods' parameters, an adaption coefficient $\mu = 10^{-4}$ is chosen in a bid to prevent divergence of the conventional block CMA. The QR-CMA operates with the optimal value of [5, Secs. 4–5] ($\alpha = 2/3$). The RLS-CMA is run with the typical forgetting factor $\lambda = 0.99$ and inverse covariance matrix initialized at the identity ($\delta = 1$). The values $m_1 = 0.15$, $\kappa = 100$, $\mu = 0.5$ are used for the AAF-CMA, as suggested in [7]. In the latter two methods, which operate on a sample-by-sample basis, the received signal block is re-used as many times as required.

The average output MSE after convergence as a function of the equalizer length L is shown in Fig. 1, where the same 500 signal bursts are used at each value of L. Also plotted as a reference is the performance of the minimum MSE (MMSE) equalizer with optimum delay. Since the optimum-delay MMSE equalizer typically lies close to the CM-cost global extrema [4], the distance to the MMSE-bound curve provides an indication of global convergence. The average overall computational complexity (flops) for convergence in the same experiment appears in Fig. 2. The complexity of the OS-QR-KMA is very close to that of the OS-CMA (with a small extra cost due to prewhitening) and has not been plotted for the sake of clarity.

The OS-CMA considerably improves its conventional constant-step counterpart and the AAF-CMA; also, it slightly outperforms the RLS-CMA over the whole equalizer-length range, and the QR-CMA for short equalizer lengths. Hence, the OS-CMA ability to escape local extrema [9, 13] seems more evident in lower-dimensional equalizer spaces. As expected, the OS-CMA-2 is more complex than the OS-CMA-1 for long equalizers, due to the extra complexity introduced by the computation of the sensor-output 4th-order moments before starting the iterations. The OS-CMA-1 complexity remains above that of the other non-conventional methods in this scenario. Nevertheless, the OS-CMA appears less complex than the conventional CMA, as it converges in over an order of magnitude fewer iterations. Just like the QR-CMA, the OS-QR-KMA takes advantage of both the constellation and the i.i.d. character of the input signal. With the incorporation of the algebraic optimal step-size, the OS-QR-KMA is able to outperform the QR-CMA, getting closer to the MMSE bound and requiring up to an order of magnitude less iterations, yet becoming more costly for longer equalizers.

5. CONCLUSIONS

Global line minimization of the CM cost function can be carried out algebraically by finding the roots of a 3rd-degree polynomial with real coefficients. The resulting blind equalization algorithm, the OS-CMA, has been studied in this contribution, which expands the brief description of this technique independently developed in [10]. The OS-CMA clearly outperforms in equalization quality and cost the conventional constant step-size CMA; it is also able to improve other non-conventional methods for short equalizer lengths. The exploitation of the i.i.d. assumption through prewhitening (e.g., based on a QR decomposition of the data matrix) can further improve performance regardless of the criterion employed (CM, KM); this feature has not been clearly interpreted in previous works [5]. The optimal step size seems to have a conditioning effect similar to prewhitening, as both techniques yield very similar results, the former becoming less costly for short equalizer settings. The optimal step-size strategy, which is not exclusive to the CM criterion [15, 16], can also be easily implemented in semi-blind

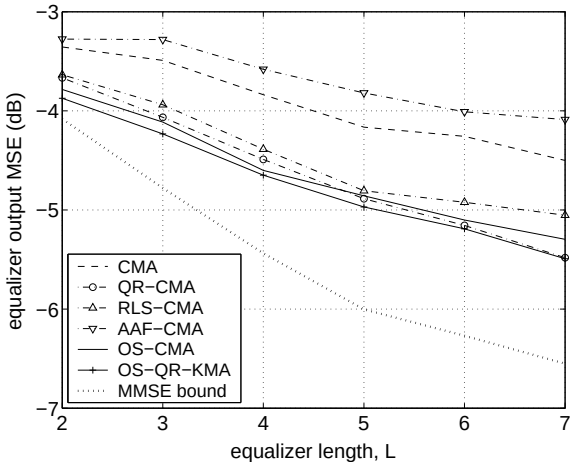

Figure 1: Equalizer output MSE after convergence.

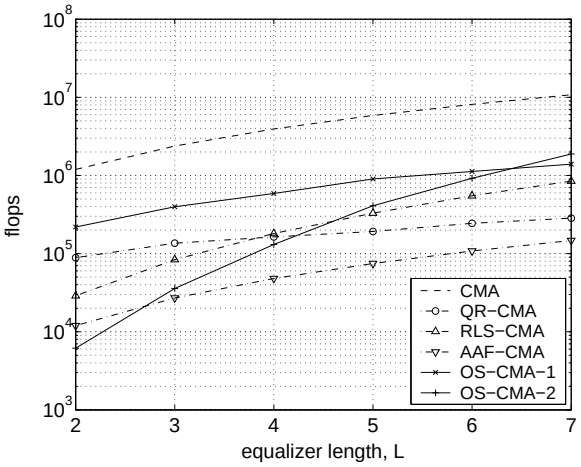

Figure 2: Computational cost for convergence.

operation [16, 17], and its extension to multichannel configurations (e.g., the SIMO model) is straightforward [13]. In consequence, this strategy arises as a promising approach to improving the performance of blind equalizers in burst-mode transmission systems. Further work should include a more comprehensive performance evaluation and comparison in a wider variety of equalization scenarios, and the search for new variants aiming at a reduced complexity in large equalizer spaces.

Appendix: Coefficients of Step-Size Polynomial

Method 1: Let $\mathbf{f}' = \mathbf{f} - \mu\mathbf{g}$. Then $J_{\mathrm{CM}}(\mathbf{f}') = \mathrm{E}\{(|\mathbf{f}'^{\mathrm{H}}\mathbf{x}_n|^2 - \gamma)^2\}$. Calling $y_n = \mathbf{f}^{\mathrm{H}}\mathbf{x}_n$ and $g_n = \mathbf{g}^{\mathrm{H}}\mathbf{x}_n$, we have $|\mathbf{f}'^{\mathrm{H}}\mathbf{x}_n|^2 = \mu^2|g_n|^2 - 2\mu\mathbb{R}\mathrm{e}(y_n g_n^*) + |y_n|^2$. Hence, $J_{\mathrm{CM}}(\mathbf{f}') = \mathrm{E}\{(a_n\mu^2 + b_n\mu + c_n)^2\}$, with $a_n = |g_n|^2$, $b_n = -2\mathbb{R}\mathrm{e}(y_n g_n^*)$ and $c_n = (|y_n|^2 - \gamma)$. Expanding the square results in $J_{\mathrm{CM}}(\mathbf{f}') = \mu^4\mathrm{E}\{a_n^2\} + 2\mu^3\mathrm{E}\{a_n b_n\} + \mu^2\mathrm{E}\{b_n^2 + 2a_n c_n\} + 2\mu\mathrm{E}\{b_n c_n\} + \mathrm{E}\{c_n^2\}$. Taking the derivative with respect to μ and eliminating common constant factors, we finally arrive at the polynomial with the coefficients shown in (6).

Method 2: $J_{\mathrm{CM}}(\mathbf{f}') = \mathrm{E}\{\left(|\mathbf{f}'^{\mathrm{H}}\mathbf{x}|^2 - \gamma\right)^2\} = \mathrm{E}\{|\mathbf{f}'^{\mathrm{H}}\mathbf{x}|^4\} - 2\gamma\mathrm{E}\{|\mathbf{f}'^{\mathrm{H}}\mathbf{x}|^2\} + \gamma^2$. In the first place, $\mathrm{E}\{|\mathbf{f}'^{\mathrm{H}}\mathbf{x}|^2\} = \mathrm{E}\{\mathbf{f}'^{\mathrm{H}}\mathbf{x}\mathbf{x}^{\mathrm{H}}\mathbf{f}'\} = \mu^2 C_{\mathbf{gg}} - 2\mu\mathbb{R}\mathrm{e}(C_{\mathbf{fg}}) + C_{\mathbf{ff}}$, where $C_{\mathbf{ab}} = \mathbf{a}^{\mathrm{H}}\mathbf{R}_x\mathbf{b}$, $\mathbf{R}_x = \mathrm{E}\{\mathbf{x}\mathbf{x}^{\mathrm{H}}\}$, $\mathbf{a}, \mathbf{b} \in \mathbb{C}^L$. Similarly, let us denote

$$C_{\mathbf{abcd}} = \mathrm{E}\{\mathbf{a}^{\mathrm{H}}\mathbf{x}\mathbf{x}^{\mathrm{H}}\mathbf{b}\mathbf{c}^{\mathrm{H}}\mathbf{x}\mathbf{x}^{\mathrm{H}}\mathbf{d}\} = \sum_{ijkl=1}^{L} \mathrm{E}\{x_i x_j^* x_k x_l^*\} a_i^* b_j c_k^* d_l$$

with $\mathbf{a}, \mathbf{b}, \mathbf{c}, \mathbf{d} \in \mathbb{C}^L$, which shows the symmetry properties $C_{\mathbf{abcd}} = C_{\mathbf{cdab}} = C_{\mathbf{cbad}} = C_{\mathbf{adcb}} = C_{\mathbf{badc}}^*$. Then, after some algebraic simplifications, we can express

$$\begin{aligned}\mathrm{E}\{|\mathbf{f}'^{\mathrm{H}}\mathbf{x}|^4\} &= \mu^4 C_{\mathbf{gggg}} - 4\mu^3\mathbb{R}\mathrm{e}(C_{\mathbf{ggg f}}) \\ &\quad + 2\mu^2[2C_{\mathbf{ffgg}} + \mathbb{R}\mathrm{e}(C_{\mathbf{fgfg}})] - 4\mu\mathbb{R}\mathrm{e}(C_{\mathbf{fffg}}) + C_{\mathbf{ffff}}.\end{aligned}$$

Combining the previous expressions, taking the derivative with respect to variable μ and eliminating common constant factors, one arrives at the polynomial with the coefficients given in (7).

Acknowledgement. The authors would like to thank one of the reviewers for pointing out reference [10].

REFERENCES

[1] D. N. Godard, "Self-recovering equalization and carrier tracking in two-dimensional data communication systems," *IEEE Transactions on Communications*, vol. 28, no. 11, pp. 1867–1875, Nov. 1980.

[2] Z. Ding, C. R. Johnson, and R. A. Kennedy, "On the (non)existence of undesirable equilibria of Godard blind equalizers," *IEEE Transactions on Signal Processing*, vol. 40, no. 10, pp. 2425–2432, Oct. 1992.

[3] S. Lambotharan, J. Chambers, and C. R. Johnson, "Attraction of saddles and slow convergence in CMA adaptation," *Signal Processing*, vol. 59, no. 3, pp. 335–340, June 1997.

[4] C. R. Johnson, P. Schniter, I. Fijalkow, L. Tong, *et al.*, "The core of FSE-CMA behavior theory," in *Unsupervised Adaptive Filtering, Vol. II: Blind Deconvolution*, S. S. Haykin, Ed. New York: John Wiley & Sons, 2000, ch. 2, pp. 13–112.

[5] P. A. Regalia, "A finite-interval constant modulus algorithm," in *Proc. ICASSP-2002*, vol. III, Orlando, FL, May 13–17, 2002, pp. 2285–2288.

[6] Y. Chen, T. Le-Ngoc, B. Champagne, and C. Xu, "Recursive least squares constant modulus algorithm for blind adaptive array," *IEEE Transactions on Signal Processing*, vol. 52, no. 5, pp. 1452–1456, May 2004.

[7] M. T. M. Silva, M. Gerken, and M. D. Miranda, "An accelerated constant modulus algorithm for space-time blind equalization," in *Proc. EUSIPCO-2004*, Vienna, Austria, Sept. 6–10, 2004, pp. 1853–1856.

[8] W. H. Press, S. A. Teukolsky, W. T. Vetterling, and B. P. Flannery, *Numerical Recipes in C. The Art of Scientific Computing*, 2nd ed. Cambridge, UK: Cambridge University Press, 1992.

[9] P. Comon, "Contrasts, independent component analysis, and blind deconvolution," *International Journal of Adaptive Control and Signal Processing (Special Issue on Blind Signal Separation)*, vol. 18, no. 3, pp. 225–243, Apr. 2004.

[10] C. Xu and J. Li, "A batch processing constant modulus algorithm," *IEEE Communications Letters*, vol. 8, no. 9, pp. 582–584, Sept. 2004.

[11] Y. Li and Z. Ding, "Global convergence of fractionally spaced Godard (CMA) adaptive equalizers," *IEEE Transactions on Signal Processing*, vol. 44, no. 4, pp. 818–826, Apr. 1996.

[12] C. Lanczos, *Applied Analysis*. New York: Dover, 1988.

[13] V. Zarzoso and P. Comon, "Optimal step-size constant modulus algorithm," *IEEE Transactions on Communications*, Oct. 2004, submitted.

[14] O. Shalvi and E. Weinstein, "New criteria for blind deconvolution of nonminimum phase systems (channels)," *IEEE Trans. on Information Theory*, vol. 36, no. 2, pp. 312–321, Mar. 1990.

[15] L. Rota and P. Comon, "Blind equalizers based on polynomial criteria," in *Proc. ICASSP-2004*, vol. IV, Montreal, Canada, May 17–21, 2004, pp. 441–444.

[16] V. Zarzoso and P. Comon, "Blind and semi-blind equalization based on the constant power criterion," *IEEE Transactions on Signal Processing*, 2005, to appear in Oct.–Nov. 2005.

[17] ——, "Semi-blind constant modulus equalization with optimal step size," in *ICASSP-2005*, vol. III, Philadelphia, PA, Mar. 18–23, 2005, pp. 577–580.

PARALLEL DEFLATION WITH ALPHABET-BASED CRITERIA FOR BLIND SOURCE EXTRACTION

Ludwig Rota[†], *Vicente Zarzoso*[‡*], *Pierre Comon*[†]

[†]Laboratoire I3S, UNSA/CNRS
2000 route des Lucioles, BP 121
06903 Sophia Antipolis Cedex, France
{rota, comon}@i3s.unice.fr

[‡]Dept. of Electrical Eng. & Electronics
The University of Liverpool
Brownlow Hill, Liverpool L69 3GJ, UK
vicente@liv.ac.uk

ABSTRACT

Blind source extraction aims at estimating the source signals which appear mixed at the output of a sensor array. A novel approach to blind source extraction is presented in this contribution, which exploits the discrete character (finite alphabet property) of digital modulations in the case where sources with different alphabet exist. An alphabet polynomial fitting (APF) criterion matched to the specific signal constellation is employed to extract, through deflation, the sources with the same modulation. Using the appropriate APF criteria, the sources with different modulations can be extracted in parallel. This new concept, referred to as parallel deflation, presents the potential of reducing both the signal estimation errors that typically accumulate in the conventional deflationary approach and the spatio-temporal diversity required for a satisfactory source extraction. In addition, APF criteria can be optimized through a cost-effective optimal step-size technique that can escape local extrema.

Keywords : blind equalization, deflation, finite alphabet, MIMO, parallel processing, underdetermined mixtures.

1. INTRODUCTION

Channel equalization aims to reconstruct the transmitted signals that have distorted by the propagation medium. Blind equalization has been the subject of intense research interest since the pioneering work of Sato [1] and Godard [2]. The main advantage of blind techniques is arguably that training sequences are not required, so that the effective transmission rate, and thus the spectral efficiency, are increased. In multiple-input multiple-output (MIMO) scenarios, the spatial mixing of several transmitted sources adds to the inter-symbol interference introduced by the time dispersive channel. Blind signal extraction can be accomplished through a deflation approach, where the input signals are estimated one after another [3, 4]. The major limitation of classical deflation is that estimation errors accumulate along successive extraction stages. Also, sufficient diversity must be available in general; i.e., for a satisfactory equalization, the number of sensors needs to be higher than the number of sources.

The present contribution addresses the problem of blind extraction of discrete signals, particularly in the underdetermined case where there are less sensors than sources. The originality of this work lies in the use of a polynomial criterion named *alphabet polynomial fitting (APF)*, which exploits the knowledge of the modulation alphabet in order to accomplish the source extraction [5, 6]. In contrast to traditional source-distribution independent principles such as constant modulus [2] or kurtosis maximization (KM) [7], the APF criterion targets a specific modulation. This feature leads to the novel concept of parallel deflation: a polynomial criterion can be used in a deflationary process to extract the signals of each modulation. Parallel deflation can thus reduce the diversity required for the extraction of all sources from a mixture while extracting different modulations simultaneously. As a result, this new approach can increase the extraction performance while reducing the computational cost compared to classical deflation.

Moreover, APF criteria can be optimized by efficient gradient- or Newton-descent procedures based on an optimal step size computed algebraically at each iteration. The optimal step-size strategy is able to avoid local extrema at an affordable computational cost.

2. BLIND SOURCE EXTRACTION

2.1. Problem and Signal model

We consider a time-dispersive MIMO linear time-invariant (LTI) system with the input-output relationship

$$\boldsymbol{w}(n) = \sum_{k=0}^{L_c} \mathbf{C}_k \boldsymbol{s}(n-k) + \boldsymbol{b}(n), \quad n \in \mathbb{N}$$

[*] Royal Academy of Engineering Research Fellow.

In *Proc. SSP-2005, 13th IEEE Workshop on Statistical Signal Processing*, Bordeaux, France, July 17-20, 2005.

where

$\boldsymbol{s}(n) \in \mathbb{C}^N$	source signal vector,
$\boldsymbol{w}(n) \in \mathbb{C}^P$	channel output signal vector,
$\boldsymbol{b}(n) \in \mathbb{C}^P$	noise vector,
$\mathbf{C}_k \in \mathbb{C}^{P\times N}$	channel impulse response.

The sequence $\mathbf{C}_k$, $k = 0, \ldots, L_c$ corresponds to the impulse response matrix taps of the finite impulse response (FIR) MIMO channel. An equalizer described by the impulse response matrix taps $\mathbf{H}_k \in \mathbb{C}^{N\times P}$, $k = 0, \ldots, L_h$, processes the channel output signals and aims at extracting the sources. The output signal vector is thus given by

$$\hat{\boldsymbol{s}}(n) = \sum_{k=0}^{L_h} \mathbf{H}_k \boldsymbol{w}(n-k), \quad n \in \mathbb{N}.$$

The extraction of the pth output component $\hat{s}_p(n)$ can alternatively be expressed as:

$$\hat{s}_p(n) = \boldsymbol{h}_p{}^{\intercal} \tilde{\boldsymbol{w}}(n) \tag{1}$$

where $\tilde{\boldsymbol{w}}(n) = [\boldsymbol{w}(n)^{\intercal}, \boldsymbol{w}(n-1)^{\intercal}, \ldots, \boldsymbol{w}(n-L_h)^{\intercal}]^{\intercal} \in \mathbb{C}^{P(L_h+1)}$ (symbol $^{\intercal}$ stands for transposition) and $\boldsymbol{h}_p = [(\boldsymbol{H}_0)_{(p,:)}, (\boldsymbol{H}_1)_{(p,:)}, \ldots, (\boldsymbol{H}_{L_h})_{(p,:)}]^{\intercal} \in \mathbb{C}^{P(L_h+1)}$, notation $(\boldsymbol{H}_j)_{(p,:)}$ denoting the pth row of the equalizer matrix tap $\boldsymbol{H}_j$.

2.2. Classical deflation

Classical deflation aims at extracting one by one the N source signals mixed at the output of P sensors. This scheme can be employed with a source-distribution independent criterion such as the CM or KM principles; for instance, the KM cost function [7] is used in the original paper [3]. Thus, a unique criterion is applied to extract each source from the observations. In order to avoid extracting the same signal twice, the contribution of the extracted source has to be estimated (e.g., via correlation techniques) and subtracted from the sensors. This procedure is repeated until the N sources are extracted. The required diversity for the N-source extraction is limited by a number of sensors $P \approx N$. Moreover, estimation errors accumulate with the number of extractions, so that the extraction quality gradually decreases. Classical deflation is illustrated in Fig. 1.

3. ALPHABET-BASED SOURCE EXTRACTION

3.1. Alphabet-based criteria

In the sequel, $N = \sum_i K_i$ denotes the total number of emitted signals, where K_i is the number of signals having the same alphabet $\mathcal{A}_i$. This corresponds to the following additional hypothesis about the input signals:

S1. Sources $\mathbf{s}^{(i)} = [s_1^{(i)}, \ldots, s_{K_i}^{(i)}]^{\intercal}$ belong to a finite alphabet $\mathcal{A}_i$, characterized by d_i complex distinct roots of the polynomial $Q_i(s(n)) = 0$, where d_i corresponds to the total number of possible symbols in the constellation.

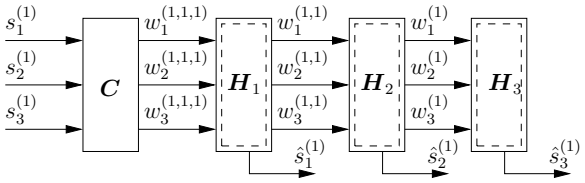

Fig. 1. Classical deflation. Extraction of 3 signals $\{s_p^{(1)}\}_{p=1}^3$, typically (but not necessarily) having the same modulation $\mathcal{A}_1$. Conventional deflation estimates the input signals one by one.

Modulation	$\mathcal{A}$	$Q(s)$
BPSK	$\{-1, +1\}$	$s^2 - 1$
q-PSK	$\{e^{\jmath 2k\pi/q}\}\vert_{k\in 0,\ldots,q-1}$	$s^q - 1$
QAM-16	$\{\pm 1, \pm 3\} + \{\pm\jmath, \pm 3\jmath\}$	$\sum_{k=0}^{4} \alpha_k s^{4k}$

$\alpha_0 = 50625/256, \alpha_1 = 12529/16, \alpha_2 = -221/8,$
$\alpha_3 = 17, \alpha_4 = 1.$

Table 1. Alphabets and associated polynomials of some discrete modulations.

This hypothesis is essential to alphabet-based criteria. For instance, a q-PSK modulated signal s is characterized by the roots of polynomial $Q(s) = s^q - 1$. Thus, each discrete modulation can be associated with an APF criterion, as illustrated by the examples in Table 1.

Considering hypothesis **S1** on the discrete inputs of a MIMO channel, it is possible to perform source extraction by minimizing the following polynomial criterion [5]:

Theorem 1 *: Consider $\mathcal{S}_i$ the set of processes taking their values in alphabet $\mathcal{A}_i$, and $\mathcal{H}$ the set of FIR filters. Criterion:*

$$\mathcal{J}_{APF}^{(i)}(\boldsymbol{H}_i, \hat{\mathbf{s}}^{(i)}) = \sum_{n=1}^{K_i} \sum_{m} \left| Q_i\big(\hat{s}_n^{(i)}(m)\big) \right|^2 \tag{2}$$

*is a contrast function under hypothesis **S1**.*

An APF criterion can be used for classical deflation when the emitted signals have all the same alphabet, i.e., $N = K_1$ and $K_i = 0, \forall i > 1$. However, novel extraction approaches are enabled by the discriminating character of APF criteria, which is stronger than that of traditional principles such as CM and KM. The new approaches consist of extracting the sources with different alphabets in parallel, thus the terms of parallel extraction and parallel deflation, which are explained next.

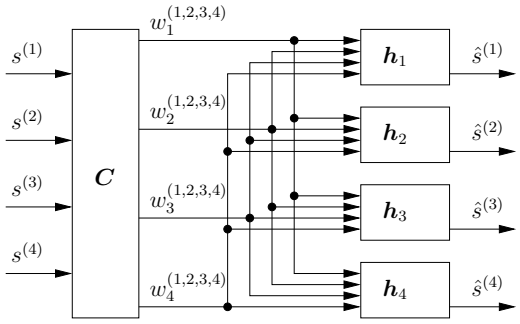

Fig. 2. Parallel Extraction. From the observed sensor output, parallel extraction allows the simultaneous separation of source signals having different modulations.

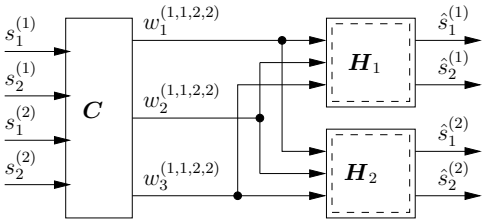

Fig. 3. Parallel deflation in an underdetermined case. The extraction of more sources than sensors is possible with parallel deflation, provided that enough diversity is available for extracting the sources of each alphabet.

3.2. Parallel extraction

Parallel extraction can take place when the N emitted signals all have different modulations, i.e., $K_i = 1, \forall i$. Each equalizer is computed from an APF criterion corresponding to one alphabet. Thus, the equalizers for each modulation can be determined in parallel from the observed sensor output. Fig. 2 shows an example of parallel extraction of signals $\{s^{(i)}\}_{i=1}^4$ with alphabets $\{\mathcal{A}_i\}_{i=1}^4$, respectively. Parallel extraction can be considered as a particular case of the more general parallel deflation.

3.3. Parallel deflation

In the general case, the sensor output observes mixtures of M groups of sources where the ith group is composed of K_i signals having the same modulation. Thus we have $N = \sum_{i=1}^{M} K_i$. Then, it is possible to extract the sources of the same group by means of a deflation approach operating on a criterion matched with the corresponding modulation. This process can be carried out in parallel for other groups having a different modulation and hence their own APF criterion. Consequently, the discriminating property of APF criteria is able to decouple a separating problem of N signals into M extraction problems of K_i sources, $i = 1, \ldots, M$. Contrary to classical deflation, the required diversity for parallel deflation is reduced to $P \approx \max(K_i)$. This diversity improvement offers further advantages in terms of performance (e.g., less error accumulation), computational complexity and cost. Parallel deflation reduces to parallel extraction when $M = N$, so that deflation is no longer required.

4. OPTIMIZATION OF APF CRITERIA

In order to estimate a source with alphabet $\mathcal{A}_i$, contrast function (2) must be minimized with respect to the equalizer tap vector $\boldsymbol{h}$, which is used to extract a single component as in eqn. (1). After a suitable initialization (e.g., via the conventional center-tap filter), the equalizer vector is iteratively updated in the descent direction $\boldsymbol{g}$:

$$\boldsymbol{h}' = \boldsymbol{h} - \mu \boldsymbol{g}$$

In a gradient-based algorithm, we have $\boldsymbol{g} = \nabla \mathcal{J}_{APF}^{(i)}(\boldsymbol{h})$, whereas a Newton-based algorithm would involve the Hessian of $\mathcal{J}_{APF}^{(i)}$ as well.

The interesting feature of APF criteria is that $\mathcal{J}_{APF}^{(i)}(\boldsymbol{h}')$ is a $2q$th-degree polynomial in the step size μ, for constellations composed of q symbols. This feature is not exclusive of APF contrasts, but it is also shared by other equalization criteria such as CM and KM [5]. As a result, steepest descent minimization of contrast (2) can be carried out by finding the optimal step size

$$\mu_{\text{opt}} = \min_{\mu} \arg \mathcal{J}_{APF}^{(i)}(\boldsymbol{h} - \mu \boldsymbol{g})$$

among the roots of the $(2q-1)$th-degree polynomial $\partial \mathcal{J}_{APF}^{(i)}(\boldsymbol{h} - \mu \boldsymbol{g})/\partial \mu$. In some cases, this root finding can be accomplished algebraically: the APF criterion matched to BPSK signals and the CM criterion are associated with respective 3rd-degree polynomials, solved by Cardano's formula; the normalized KM criterion involves a 4th-degree polynomial whose roots are obtained by Ferrari's formula. The coefficients of these polynomials are simple polynomial functions of the observed data vectors and the current equalizer and gradient vectors [6, 8]. Consequently, the incorporation of the optimal step-size technique only entails a moderate increase in computational complexity. In return, since μ_{opt} yields the global minimum of $\mathcal{J}_{APF}^{(i)}$ along direction $\boldsymbol{g}$, the optimal step-size technique shows an improved robustness against local extrema relative to conventional gradient-descent minimization [9].

After convergence of the equalizer vector, the contribution of the estimated source signal to the observations is

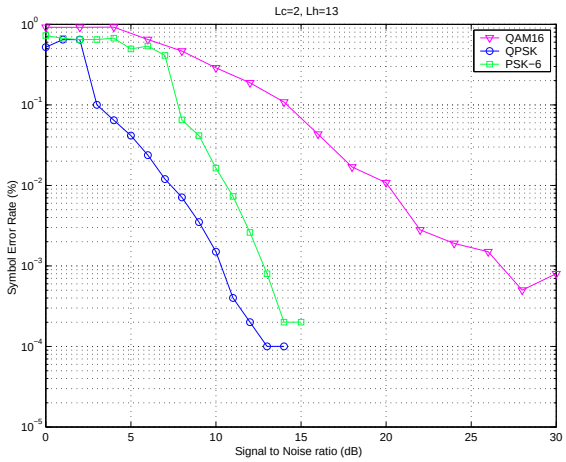

Fig. 4. Parallel extraction of 3 different sources for various SNRs.

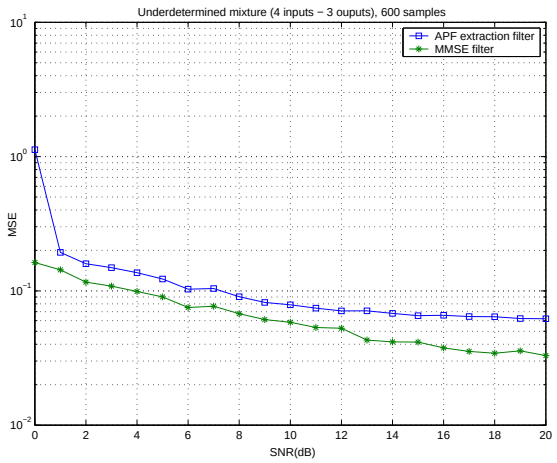

Fig. 5. APF extraction of a QPSK signal from an underdetermined mixture.

calculated and subtracted from the sensor output, to prevent extracting the same source twice. This contribution is easily obtained as the cross-correlation between the estimated source signal and the sensor output vector. To extract the next source, the APF criterion needs to be minimized again, but using the sensor output data without the contribution from the source previously extracted. This process is repeated until all sources with the same modulation have been obtained In parallel deflation, the deflation processes of the different APF criteria can be executed in parallel.

5. PRELIMINARY EXPERIMENTAL RESULTS

5.1. Parallel extraction

In this experiment, $N = 3$ sources with different modulations (QPSK, QAM-16, PSK-6) are mixed by a length-3 channel ($L_c = 2$). $P = 3$ noisy observations are processed by a parallel extraction algorithm made up of the APF criteria associated with each modulation. The channel coefficients are randomly drawn from a Gaussian distribution, and so is the noise added to the observations. Fig. 4 summarizes the parallel extraction performance for different signal-to-noise ratios (SNRs).

5.2. Parallel deflation

The second experiment tests a channel spanning two baud periods ($L_c = 1$) and mixing $N = 4$ source signals (2 QPSK and 2 QAM16, i.e., $M = 2$) at the output of only $P = 3$ sensors:

$$C(z) = C_0 + C_1 z^{-1}$$

with

$$C_0 = \begin{bmatrix} -0.66 & -0.19 & 0.65 & 0.92 \\ 0.22 & -0.96 & 0.43 & -0.85 \\ -0.30 & -0.76 & 0.95 & 0.85 \end{bmatrix}$$

$$C_1 = \begin{bmatrix} 0.75 & -0.98 & -0.75 & -0.38 \\ -0.97 & 0.27 & 0.90 & 0.53 \\ 0.95 & 0.65 & 0.30 & -0.52 \end{bmatrix}$$

Hence, this situation describes the underdetermined mixture context. The extraction of one of the QPSK signals is illustrated in Fig. 5. Note that, despite the hardness of the underdetermined scenario, the APF extraction performance lies very close to the MMSE bound.

6. CONCLUSIONS

The use of contrast functions matched to the signal modulation enables the definition of a novel approach to blind source extraction whereby sources with different constellations can be extracted in parallel, provided that no alphabet be a subset of another. Parallel deflation may prove useful when different modulations coexist in the same transmission environment. Such a scenario is likely in future-generation wireless communication networks, where signal constellations will be dynamically allocated according to the service required and the channel conditions, analogously to the bit-loading schemes used in multicarrier communications [10]. The preliminary experiments reported in this paper are encouraging. More detailed experimental results illustrating the performance of the parallel deflation approach will be presented at the conference.

7. REFERENCES

[1] Y. SATO, "A method of self recovering equalization for multilevel amplitude-modulation systems," *IEEE Trans. on Com.*, vol. 23, pp. 679–682, June 1975.

[2] D. GODARD, "Self recovering equalization and carrier tracking in two dimensional data communication systems," *IEEE Trans. on Signal Processing*, vol. 28, no. 11, pp. 1867–1875, Nov. 1980.

[3] N. DELFOSSE and P. LOUBATON, "Adaptive blind separation of independent sources: A deflation approach," *Signal Processing*, vol. 45, pp. 59–83, 1995.

[4] J.R. TREICHLER and M.G. LARIMORE, "New processing techniques based on the constant modulus algorithm," *IEEE Trans. on Acoust. Speech Sig. Proc.*, vol. 33, no. 2, pp. 420–431, April 1985.

[5] P. COMON, "Contrasts, independent component analysis, and blind deconvolution," *International Journal of Adaptive Control and Signal Processing (Special Issue on Blind Signal Separation)*, vol. 18, no. 3, pp. 225–243, Apr. 2004.

[6] L. ROTA and P. COMON, "Blind Equalizers Based on Polynomial Criteria," in *Proc. ICASSP*, Montreal, Quebec, 17-21 May 2004.

[7] O. SHALVI and E. WEINSTEIN, "New criteria for blind deconvolution of nonminimum phase systems (channels)," *IEEE Trans. on Information Theory*, vol. 36, no. 2, pp. 312–321, Mar. 1990.

[8] V. ZARZOSO and P. COMON, "Blind channel equalization with algebraic optimal step size," in *EUSIPCO-2005, XIII European Signal Processing Conference*, Antalya, Turkey, Sept. 4–8, 2005.

[9] V. ZARZOSO and P. COMON, "Optimal step-size constant modulus algorithm," *IEEE Transactions on Communications*, Oct. 2004, submitted (`http://www.i3s.unice.fr/%7Emh/RR/2004/RR-04.23-V.ZARZOSO.pdf`).

[10] Z. WANG and G. B. GIANNAKIS, "Wireless multicarrier communications," *IEEE Signal Processing Magazine*, vol. 17, no. 3, pp. 29–48, May 2000.

SEMI-BLIND CONSTANT MODULUS EQUALIZATION WITH OPTIMAL STEP SIZE

Vicente Zarzoso[*]

Department of Electrical Engineering and Electronics
The University of Liverpool
Brownlow Hill, Liverpool L69 3GJ, UK
vicente@liv.ac.uk

Pierre Comon

Laboratoire I3S, CNRS/UNSA
Les Algorithmes – Euclide-B, BP 121
06903 Sophia Antipolis, France
comon@i3s.unice.fr

ABSTRACT

Channel equalization is an important problem in digital communications. This contribution studies a hybrid equalization criterion combining the constant modulus (CM) property and the minimum mean square error (MMSE) between the equalizer output and the known pilot sequence. An efficient semi-blind block gradient-descent algorithm is put forward, in which the step size globally minimizing the cost function along the search direction is algebraically computed at each iteration. The use of the optimal step size notably accelerates convergence and can further reduce the impact of local extrema on the semi-blind algorithm's performance. The proposed approach is not restricted to the CM-MMSE principle, but it can benefit alternative equalization criteria as well.

1. INTRODUCTION

The equalization of digital communication channels consists of recovering the unknown data transmitted through a distorting propagation medium. Blind equalization techniques typically rely on certain known properties of the input modulation, such as the finite alphabet or constant modulus (CM) of its data symbols [1]. Although the blind approach is versatile, bandwidth efficient and especially attractive in broadcast/multicast scenarios, the exploitation of training or pilot sequences (data symbols known by the receiver) can considerably increase equalization performance and robustness (e.g., reduce the volume of data required for successful equalization). From an alternative point of view, the semi-blind approach can also be interpreted as the regularization of the conventional training-based minimum mean square error (MMSE) receiver, whose performance degrades for insufficient pilot-sequence length [2]. The fact that current as well as future communication systems encompass training sequences in their definition standards provides another strong motivation for the development of semi-blind equalization techniques.

The CM criterion is the most widespread blind equalization principle, probably due its simplicity and flexibility [1]. Indeed, the CM criterion is easy to implement, and can also tackle non-CM modulations, at the expense of an increased misadjustment due to constellation mismatch. As its major shortcoming, the CM cost function presents local stationary points associated with spurious non-equalizing solutions. The existence of spurious solutions degrades the performance of conventional gradient- and Newton-descent procedures, which is very dependent on the initial value of the equalizer tap vector [1, 3]. Spurious convergence can be alleviated to some extent by taking into account training symbols, as shown by the semi-blind criterion of [2]. This criterion is composed of a blind part exploiting the CM property of the (unknown) data symbols and a training part based on the MMSE between the equalizer output and the pilot sequence.

Another approach to avoiding misconvergence are closed-form solutions. Both blind and semi-blind CM-based equalization can be carried out algebraically or in closed form, that is, without iterative optimization. The analytical CM algorithm (ACMA) requires a joint diagonalization stage (a costly QZ iteration) in the general case where multiple solutions exist [4], although its complexity can be relaxed if the solutions are simply delayed versions of each other [5]. The semi-blind ACMA (SB-ACMA) proposed in [6] spares the costly joint diagonalization step of its blind counterpart by constraining the spatial filter (beamformer) to lie on certain subspace associated with the pilot-sequence vector. Nevertheless, the uniqueness of this semi-blind solution remains to be studied in more detail, and so does its performance in the presence of noise. Although closed-form solutions are only exact in the noiseless case, they can always be used as judicious initial points to iterative optimization criteria.

The present contribution focuses on the semi-blind equalization principle of [2]. We propose to minimize this hybrid CM-MMSE cost function by means of an efficient gradient-descent algorithm whereby the optimal step size is computed algebraically at each iteration as the rooting of a 3rd-degree polynomial. As shown in simulations, the use of the optimal step size greatly speeds up convergence and can further reduce the impact of spurious local extrema on the equalization performance, which closely approaches the MMSE lower bound from just a few pilot symbols.

2. PROBLEM AND SIGNAL MODEL

For simplicity, we deal with the basic single-input single-output (SISO) channel model. Consider the discrete-time channel output

$$x_n = \sum_k h_k s_{n-k} + v_n \tag{1}$$

in which s_n represents the transmitted symbols, h_k are the channel impulse-response taps, and v_n is the additive noise. The goal of channel equalization is to recover the original data symbols from the received signal corrupted by the convolutive channel effects (intersymbol interference) and noise. To achieve this objective, a baud-spaced linear equalizer with impulse response taps $\mathbf{f} = [f_1, \ldots, f_L]^{\mathrm{T}} \in \mathbb{C}^L$ is sought so that the equalizer output $y_n = \mathbf{f}^{\mathrm{H}}\mathbf{x}_n$ is a close estimate of the source symbols s_n, where $\mathbf{x}_n = [x_n, x_{n-1}, \ldots, x_{n-L+1}]^{\mathrm{T}}$. A similar signal model holds, with analogous objectives, if multiple spatially-separated sensors

[*]In receipt of a Post-Doctoral Research Fellowship awarded by the Royal Academy of Engineering, UK.

In *Proc. ICASSP*, Philadelphia, PA, March 18-23, 2005, Vol. III, pp. 577-580. Updated version

are available (spatial oversampling), or when several users simultaneously transmit, giving rise to additional co-channel interference. The results presented in this paper can readily be extended to multichannel (e.g., MIMO) configurations.

3. SEMI-BLIND CONSTANT MODULUS CRITERION

Practical communication systems typically feature pilot sequences to aid synchronization and channel equalization. Exploiting this available information can improve blind equalization performance. The minimization of the following hybrid cost function constitutes a semi-blind CM-MMSE criterion:

$$J_{\rm SB}(\mathbf{f}) = \lambda J_{\rm MMSE}(\mathbf{f}) + (1-\lambda) J_{\rm CM}(\mathbf{f}) \qquad (2)$$

where

$$J_{\rm MMSE}(\mathbf{f}) = \frac{1}{N_t} \sum_{n=0}^{N_t-1} \left| y_n - s^{\rm t}_{n-d} \right|^2 \qquad (3)$$

is the pilot-based MMSE cost function and

$$J_{\rm CM}(\mathbf{f}) = \frac{1}{N_b} \sum_{n=N_t}^{N-1} \left(|y_n|^2 - \gamma \right)^2 \qquad (4)$$

is the CM cost function. In the above expressions, $\{s^{\rm t}_n\}$ denotes the training sequence, d represents the equalization delay, $\gamma = {\rm E}\{|s_n|^4\}/{\rm E}\{|s_n|^2\}$ is an alphabet-dependent constant, and $N_b = (N - N_t)$ is the number of equalizer output samples used in the blind part of the criterion (corresponding to unknown, or 'blind', transmitted symbols). The total number of observed symbol periods per burst is $N_d = (N + L - 1)$. Parameter $\lambda \in [0,\, 1]$ can be considered as the relative degree of confidence between the blind- and the training-based parts of the criterion. Without loss of generality, the training sequence is assumed to appear at the beginning of the transmitted burst.

The above semi-blind cost function (using the "CMA 1-2" cost instead of the "CMA 2-2") was first put forward in [2]. The original motivation was to overcome the deficiencies of the LS solution to (3) when the pilot sequence is not long enough, an enhancement known as regularization. On the other hand, it was also shown that the incorporation of the pilot sequence is capable of reducing the probability of convergence to spurious solutions typically arising from the non-convexity of the CM cost function.

The simple technique presented in the next section further reduces the effects of local extrema while notably accelerating convergence.

4. OPTIMAL STEP-SIZE ALGORITHM

Unconstrained optimization of cost function (2) can be performed via conventional gradient descent by updating the equalizer filter weights as:

$$\mathbf{f}_{k+1} = \mathbf{f}_k - \mu \mathbf{g}_k, \qquad k = 0,\, 1,\, \ldots \qquad (5)$$

where $\mathbf{g}_k \stackrel{\rm def}{=} \nabla J_{\rm SB}(\mathbf{f}_k) = \lambda \nabla J_{\rm MMSE}(\mathbf{f}_k) + (1-\lambda) \nabla J_{\rm CM}(\mathbf{f}_k)$, and μ is the step size or adaption coefficient. We refer to this iterative method as semi-blind CMA (SB-CMA). A Newton descent is employed in [2] for the minimization of (2). However, misconvergence problems due to the non-convexity of the cost function still occur in Newton-based minimization [7].

A simple effective alternative is obtained by observing that $J_{\rm SB}(\mathbf{f} - \mu\mathbf{g})$ is a rational function in the step size parameter μ. Consequently, it is possible to perform steepest descent of function (2) by finding the optimal step size $\mu_{\rm opt} = \arg\min_{\mu} J_{\rm SB}(\mathbf{f} - \mu\mathbf{g})$ among the roots of a polynomial in μ. In effect, the derivative of $J_{\rm SB}(\mathbf{f} - \mu\mathbf{g})$ with respect to μ is the 3rd-degree polynomial

$$p(\mu) = \lambda p_{\rm MMSE}(\mu) + (1-\lambda) p_{\rm CM}(\mu) \qquad (6)$$

where $p_{\rm MMSE}(\mu) = \alpha_1 \mu + \alpha_0$, with

$$\alpha_1 = \frac{1}{N_t} \sum_{n=0}^{N_t-1} |g_n|^2 \qquad (7)$$

$$\alpha_0 = -\frac{1}{N_t} \sum_{n=0}^{N_t-1} \mathbb{R}{\rm e}\{g_n^*(y_n - s^{\rm t}_n)\} \qquad (8)$$

$g_n = \mathbf{g}^{\rm H}\mathbf{x}_n$, and $p_{\rm CM}(\mu) = \beta_3\mu^3 + \beta_2\mu^2 + \beta_1\mu + \beta_0$, with

$$\beta_3 = \frac{2}{N_b} \sum_{n=N_t}^{N-1} a_n^2, \qquad \beta_2 = \frac{3}{N_b} \sum_{n=N_t}^{N-1} a_n b_n$$

$$\beta_1 = \frac{1}{N_b} \sum_{n=N_t}^{N-1} (2a_n c_n + b_n^2), \qquad \beta_0 = \frac{1}{N_b} \sum_{n=N_t}^{N-1} b_n c_n \qquad (9)$$

$a_n = |g_n|^2$, $b_n = -2\mathbb{R}{\rm e}(y_n g_n^*)$, $c_n = (|y_n|^2 - \gamma)$. Gradient vector $\mathbf{g}$ should be normalized beforehand in order to improve numerical conditioning. The roots of this polynomial can be found through standard non-iterative analytical procedures such as Cardano's formula, or efficient iterative methods [8]. The optimal step size corresponds to the root attaining the absolute minimum in μ of the cost function, thus accomplishing the *global* minimization of $J_{\rm SB}$ in the gradient direction. Once $\mu_{\rm opt}$ has been determined, the filter taps are updated as in (5), and the process is repeated with the new filter and gradient vectors, until convergence. We refer to this algorithm as *optimal step-size semi-blind CMA (OS-SB-CMA)*. For $\lambda = 1$ the above iterative procedure reduces to the optimal step-size version of the well-known least mean squares (LMS) algorithm for supervised MMSE equalization.

The computational cost of the above sample averages is of order ${\rm O}(LN)$ per iteration, for data blocks composed of N sensor vectors $\mathbf{x}_n$. Alternatively, the coefficients of the step-size polynomial can be obtained as a function of the sensor-output statistics, computed once before starting the algorithm (along the lines of [9]; details are omitted here due to space limitations). The cost per iteration of this alternative procedure is of order ${\rm O}(L^4)$, with an additional burden of ${\rm O}(L^4 N)$ operations due to the computation of the sensor-output 4th-order moments.

5. EXPERIMENTAL RESULTS

A zero-mean unit-variance QPSK-modulated input excites the order-6 non-minimum phase FIR channel $H_2(z)$ of [5, Sec. V], whose output is corrupted by additive white complex circular Gaussian noise. An FIR filter with length $L = 5$ is used to equalize the channel, aiming at the optimal MMSE delay ($d_{\rm opt} = 6$ at 20-dB SNR). Bursts of length $N_d = 100$ symbols are observed at the channel output, yielding a total of $N = 96$ sensor-output vectors. We choose $\lambda = 0.5$, and $\mu = 10^{-3}$ for the constant step-size algorithms. Iterations are stopped as soon as $\|\mathbf{f}_{k+1} - \mathbf{f}_k\| / \|\mathbf{f}_k\| < 0.1\mu/\sqrt{N}$. Equalization quality is measured in terms of the symbol error rate (SER), which is estimated by averaging over 500 independent bursts. The first experiment

compares several fully-blind methods ($N_t = 0$, $N_b = N$). The closed-form solution of [5, Sec. II-B] is referred to as 'DK-top'. Iterative solutions are obtained from the constant gradient-descent CMA with three different initializations: first-tap filter, center-tap filter and the DK-top solution. As a reference, a conventional receiver is simulated by computing the LS solution to the MMSE criterion assuming that 10% of the transmitted symbols are available for training. Accordingly, we refer to the LS solution with the whole burst used for training as 'MMSE bound'. Fig. 1 shows that the closed-form solution is only useful as an initial point to the blind iterative receiver, whose performance depends on the actual initialization.

In the same scenario, the performance of the SB-CMA criterion (2) with constant step size is summarized in Fig. 2. The SB-ACMA closed-form solution [6] is also considered, whereas semi-blind operation of the DK-top solution (SB-DK-top) is enabled by the SVD-based procedure described in [10, 11]. Even though the inclusion of training information enhances DK-top relative to the blind case (Fig. 1), SB-ACMA proves superior, and outperforms the conventional receiver for sufficient SNR. Nevertheless, SB-ACMA can be further improved if used as a starting point for the iterative SB-CMA, whose performance becomes nearly independent of initialization at low to moderate SNR. A flooring effect is observed at high SNR values. As observed in Fig. 4, the number of iterations for convergence increases compared to the blind scenario. This increase is probably due to the flattening of the CM cost function when training is incorporated. A similar effect in semi-blind operation (although for a different equalization criterion) is remarked in [12]. By contrast, Figs. 3–4 show that the performance of the OS-SB-CMA is virtually independent of initialization, while dramatically reducing the iteration count by about two orders of magnitude. Also, the flooring effect at high SNR observed in the constant step-size SB-CMA now disappears.

A second experiment (Figs. 5–6) evaluates the performance variation as a function of the percentage of symbols in the transmitted burst used for training, calculated as $N_t/N \times 100\%$, for 10-dB SNR. The OS-CMA using only the 'blind' symbols is also tested for two different initializations. The SB-ACMA closed-form solution only improves the conventional receiver for short pilot sequences, and always benefits from gradient-descent iterations. The OS-SB-CMA slightly improves the SB-CMA for short training and for all initializations ('$\times$': first tap; '$+$': center tap; '$\triangle$': SB-DK-top; '$\square$': SB-ACMA), while maintaining its computational superiority across the whole training-length range. For reasonable pilot-length values, the semi-blind methods are able to attain the conventional MMSE receiver performance while increasing the spectral efficiency (decreasing the pilot length), thus improving the effective data rate. Properly initialized, fully-blind operation outperforms the semi-blind methods in short training, as if using too few pilot symbols could 'confuse' the blind receiver; a similar effect is observed for sufficient training, where the 'blind' symbols seem to divert the conventional receiver from its satisfactory solution. However, the performance of the OS-CMA in this scenario depends on initialization, although the optimal step-size approach endows the fully-blind CMA with some immunity to local extrema [9].

6. CONCLUSIONS

The semi-blind equalization criterion of [2] can be globally minimized along any given search direction. This contribution has presented the closed-form expression for the polynomial allowing the derivation of the optimal value of the step size. Experimental results demonstrate that this simple procedure remarkably accelerates convergence and can further reduce the negative impact of local extrema on the algorithm's performance. The optimal step-size strategy is not exclusive to the CM-MMSE principle but can also be incorporated to alternative equalization criteria with a rational cost function or which may be well approximated by a rational function in the adaption coefficient [7, 12].

Further work includes the comparison with alternative step-size optimality and acceleration approaches [13, 14], and the determination of the optimum value of confidence parameter λ.

7. REFERENCES

[1] C. R. Johnson, P. Schniter, I. Fijalkow, L. Tong, et al., "The core of FSE-CMA behavior theory," in *Unsupervised Adaptive Filtering, Vol. II: Blind Deconvolution*, S. S. Haykin, Ed., chapter 2, pp. 13–112. John Wiley & Sons, New York, 2000.

[2] A. M. Kuzminskiy, L. Féty, P. Foster, and S. Mayrargue, "Regularized semi-blind estimation of spatio-temporal filter coefficients for mobile radio communications," in *Proc. XVIème Colloque GRETSI*, Grenoble, France, Sept. 15–19, 1997, pp. 127–130.

[3] Z. Ding, R. A. Kennedy, B. D. O. Anderson, and C. R. Johnson, "Ill-convergence of Godard blind equalizers in data communication systems," *IEEE Transactions on Communications*, vol. 39, no. 9, pp. 1313–1327, Sept. 1991.

[4] A.-J. van der Veen and A. Paulraj, "An analytical constant modulus algorithm," *IEEE Transactions on Signal Processing*, vol. 44, no. 5, pp. 1136–1155, May 1996.

[5] K. Doğançay and R. A. Kennedy, "Least squares approach to blind channel equalization," *IEEE Transactions on Signal Processing*, vol. 47, no. 11, pp. 1678–1687, Nov. 1999.

[6] A. L. Swindlehurst, "A semi-blind algebraic constant modulus algorithm," in *Proc. ICASSP-2004, 29th International Conference on Acoustics, Speech and Signal Processing*, Montreal, Canada, May 17–21, 2004, vol. IV, pp. 445–448.

[7] P. Comon, "Contrasts, independent component analysis, and blind deconvolution," *International Journal of Adaptive Control and Signal Processing (Special Issue on Blind Signal Separation)*, vol. 18, no. 3, pp. 225–243, Apr. 2004.

[8] C. Lanczos, *Applied Analysis*, Dover, New York, 1988.

[9] V. Zarzoso and P. Comon, "Optimal step-size constant modulus algorithm," *IEEE Transactions on Communications*, Oct. 2004, submitted.

[10] O. Grellier and P. Comon, "Closed-form equalization," *Proc. SPAWC-99, 2nd IEEE Workshop on Signal Processing Advances in Wireless Communications*, pp. 219–222, May 9–12, 1999.

[11] P. Comon, "Blind equalization with discrete inputs in the presence of carrier residual," in *Proc. 2nd IEEE International Symposium on Signal Processing and Information Theory*, Marrakech, Morocco, Dec. 2002.

[12] V. Zarzoso and P. Comon, "Blind and semi-blind equalization based on the constant power criterion," *IEEE Transactions on Signal Processing*, in press.

[13] P. A. Regalia, "A finite-interval constant modulus algorithm," in *Proc. ICASSP-2002, 27th International Conference on Acoustics, Speech and Signal Processing*, Orlando, FL, May 13–17, 2002, vol. III, pp. 2285–2288.

[14] M. T. M. Silva, M. Gerken, and M. D. Miranda, "An accelerated constant modulus algorithm for space-time blind equalization," in *EUSIPCO-2004, XII European Signal Processing Conference*, Vienna, Austria, Sept. 6–10, 2004, pp. 1853–1856.

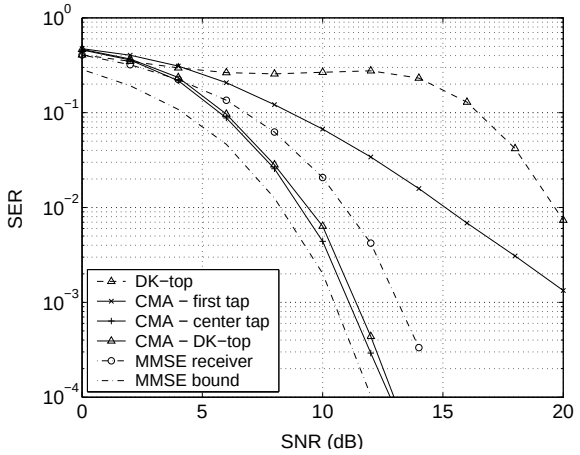

Fig. 1. Blind equalization performance. Solid lines: constant step-size gradient-descent CMA with different initializations.

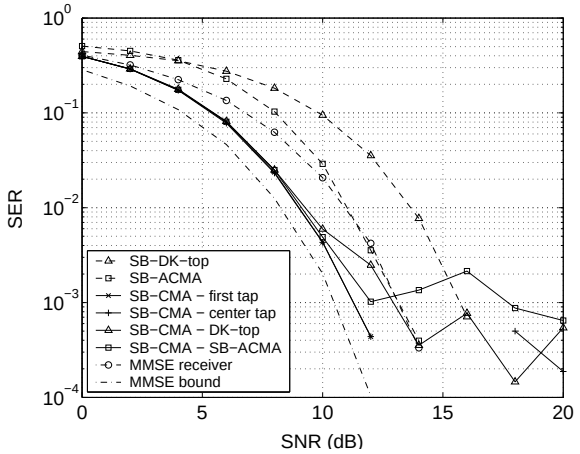

Fig. 2. Semi-blind equalization performance. Solid lines: constant step-size SB-CMA with different initializations.

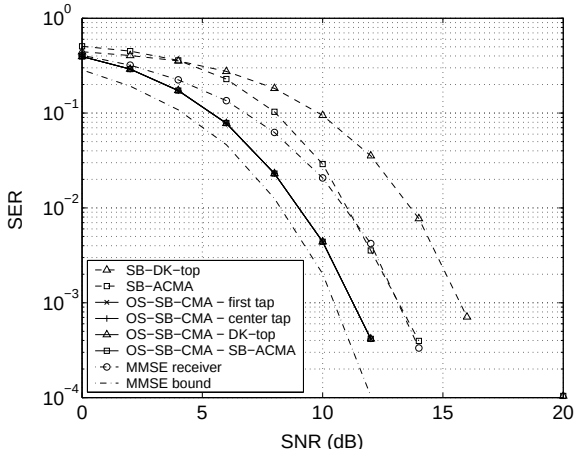

Fig. 3. Semi-blind equalization performance. Solid lines: OS-SB-CMA with different initializations.

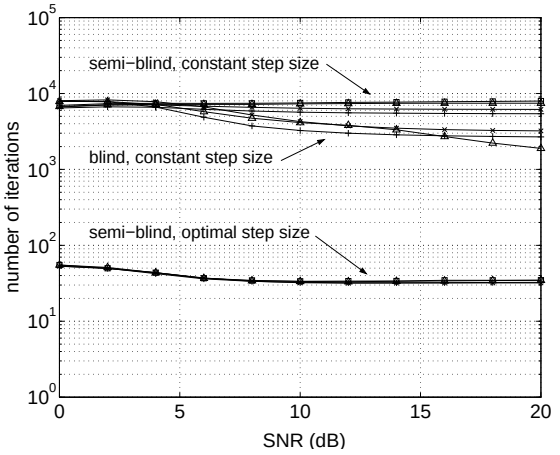

Fig. 4. Number of iterations for convergence of the iterative methods in the simulations of Figs. 1–3.

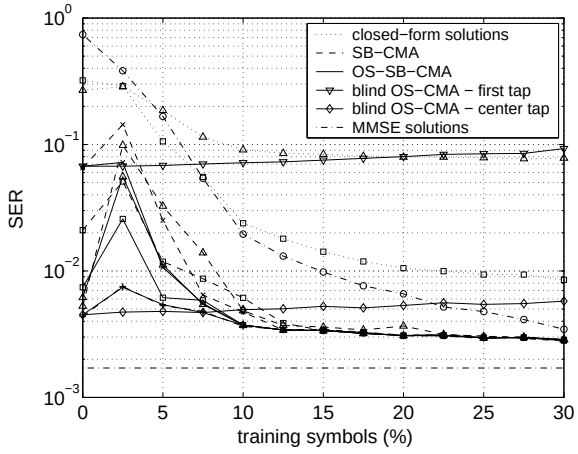

Fig. 5. Equalization performance for a varying number of pilot symbols in the transmitted burst.

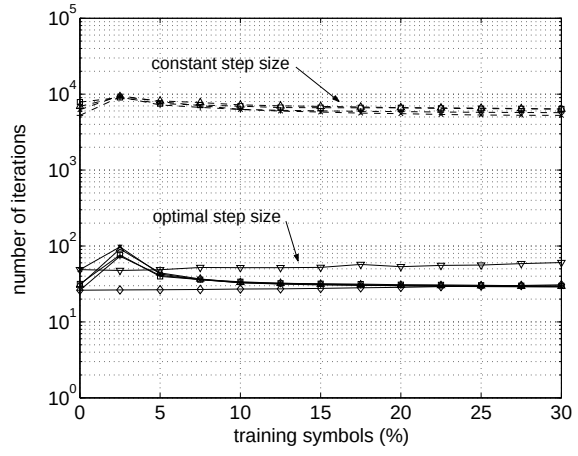

Fig. 6. Number of iterations for convergence of the iterative methods in the simulation of Fig. 5.

Surface-ECG Atrial Activity Extraction via Blind Source Separation: Spectral Validation

J Millet-Roig, JJ Rieta, *V Zarzoso, A Cebrián, F Castells, ~C Sánchez, +R García-Civera

BET- DIEo Universidad Politécnica de Valencia, Valencia, Spain
*Signal Processing Department, University of Liverpool, Liverpool, England
~Departamento de Electronica, Universidad Castilla la Mancha, Cuenca, Spain
+Laboratorio de Electrofisiologia Cardiaca, Hospital Clinico Valencia, Valencia , Spain

Abstract

The isolation of atrial activity (AA) from the surface electrocardiogram (ECG) remains a challenging unsolved problem. Different methods based on the ventricular activity (VA) cancellation have been proposed, validated from the performance obtained over synthesized AF recordings where the AA is known. This performance is measured by comparison (e.g. correlation and quadratic error) of real and estimated AA lead by lead. Other methods estimate one AA as a global contribution of all leads, and so, performance can not be computed in the same way. In this case, the present work explores this problem from a spectral-domain perspective. Several AA extracted from real atrial fibrillation (AF) and atrial flutter (AFL) patients have been analyzed. A spectral analysis reveals the existence of characteristic patterns.

1. Introduction

Higher amplitude of ventricular activity (VA) masks atrial repolarization, as well as despolarization in noisy environments. The observation of Atrial activity (AA) is further hindered when the AA becomes arrhythmic, or even chaotic, as in atrial fibrillation (AF) episodes. For the study of AF and atrial flutter (AFL) from the surface ECG several techniques have been put forward and validated by means of synthetic signals where the simulated AA component was directly available. However, in real ECG recordings AA is by nature unknown, and so its correlation with the estimated AA signal cannot be computed. Some validation criteria have been proposed in the time domain, but lack thoroughness, reproducibility and simplicity. The present work explores this problem from a spectral-domain perspective.

Malign ventricular arrhythmias have extensively been characterized since the 1980's. In this sense, different algorithms have been implemented to automatically detect Ventricular Fibrilation (VF) and other common ventricular arrhythmias as Ventricular Tachycardia (VT). Research in the frequency domain is fundamentally based on the fact that the energy of the fibrillation signal is concentrated around a main peak, and is contained within a certain frequency band [1,2]. In fig 1 Sinusal Rhythm (SR), VT and VF episodes with their corresponding power spectrum density are illustrated.

Nygards and Hulting [3] performed this type of analysis to implement an automatic monitorization system capable of detecting the presence of VF. Forster and Weaver [4] in turn based the detection of VF on the calculation of the relation between the RMS levels of the signal in the VF and low-frequency bands. Barro et al. [5], based on the power spectrum density, defined four parameters: the normalized first spectral moment and three others representing the energy distribution by bands. Nolle et al. [6] employed a series of parameters characteristic of VF, such as total power in the 1.5 to 24.2 Hz band or the maximum power components within the detection band. Millet et al. [7] reproduced these parameters plus other ones in the frequency and time domain after wavelet Transform applied.

So, a variety of spectral features have been found to be common to most such as spectrum concentration around a main frequency, bounded interval containing the main frequency, harmonic presence/absence at the main frequency, etc.

This paper considers such indices in the characterization of the AA estimated via blind source separation (BSS) from surface ECG signals. Bearing in mind the anatomic and other differences between atrium and ventriculum, it can be assumed that the spectral content of correctly extracted AA episodes should closely match those characteristics.

2. Database

Recordings of AF and AFL from 14 patients are enrolled in this study. All of them were provided by the

0276–6547/02 $17.00 © 2002 IEEE

Computers in Cardiology 2002;29:605–608.

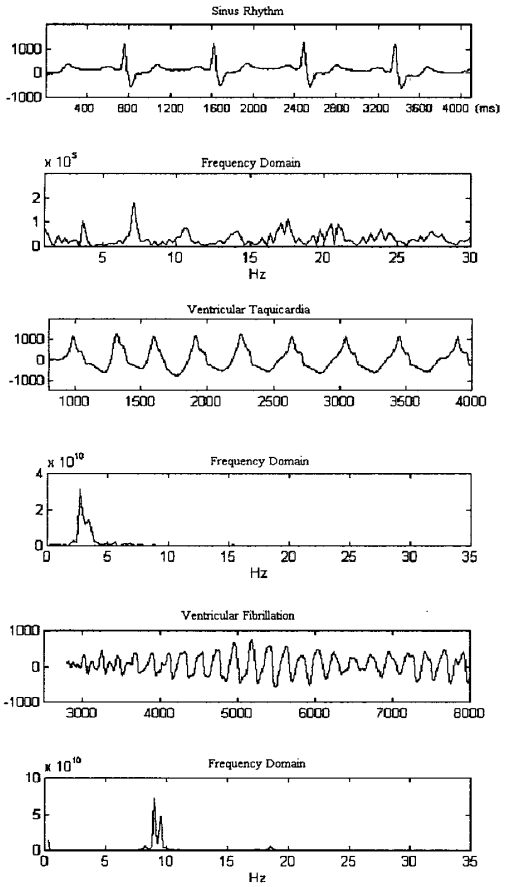

Fig. 1. Sinus Rhythm, Ventricular Tachycardia and Ventricular Fibrillation episodes with their corresponding spectral analysis.

Cardiac Electrophysiological Laboratory (Prucka Eng.) from 'Hospital Clínico de Valencia'. These recordings consist of 8 seconds segments of standard 12-lead ECGs sampled (or resampled) at 1000Hz.

3. Methods

All records were pre-processed by means of a band-pass filter with cut-off frequencies of 0.5Hz and 60Hz. Notch filter was applied to remove power line interference.

Each episode was introduced in a BSS model based on higher-order statistics. 12 Independent source signals were obtained, among of them there should be at least one AA candidate [8]. In fig. 2 it is represented an

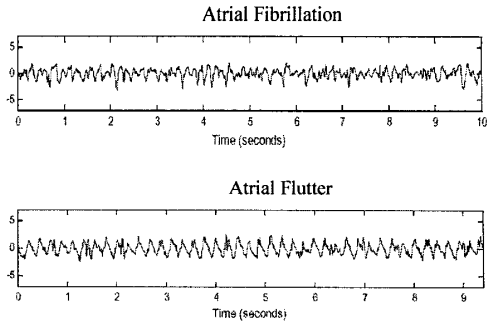

Fig. 2. Atrial activity extracted after BSS processing from atrial fibrillation and atrial flutter recordings.

example of AA extracted from AF and AFL recordings respectively.

3.1. Spectral parameters computation

Once the spectrum frequency has been calculated, it should be parameterized in order to find specific characteristics for each atrial arrhythmia. In this study we propose a set of spectral parameters [3-7] that have already shown their effectiveness in the characterization and discrimination of ventricular arrhythmias. These parameters are:

a) Main Frequency Peak (F_p): Spectral component with maximal power content.

b) Spectral Content below the main peak (A1):

$$A1 = \frac{\sum_{i=0.7324}^{F_p/2} xi}{\sum_{i=0.7324}^{20F_p} xi} \quad (1)$$

c) Spectral Concentration in the Band of the Peak (SCBP):

$$SCBP = \frac{\sum_{i=0.7F}^{1.4F} xi}{\sum_{i=0.7324}^{20F} xi} \quad (2)$$

d) First Order Moment (M1):

$$M1 = \frac{\sum_{i=0.7324}^{20F} xi \cdot fi}{\sum_{i=0.7325}^{20F} xi} \quad (3)$$

e) Normalized First Order Spectral Moment (NFSM):

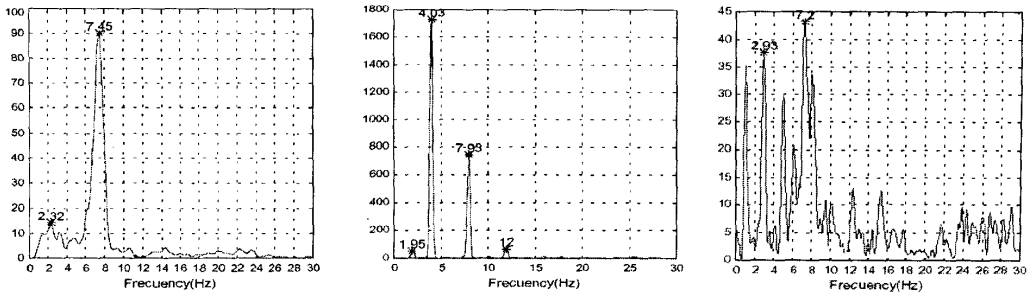

a b c

Fig.2: a) Spectrum of the estimated atrial source during an AF episode. b) Spectrum of the estimated atrial source during an AFL episode. c) Spectrum of a normal sinus rhythm.

$$NFSM = \frac{1}{F_p} \frac{\sum_{i=0.7324}^{20F} xi \cdot fi}{\sum_{i=0.7325}^{20F} xi} \quad (4)$$

f) Second Order Moment (M2):

$$M2 = \frac{\sum_{i=fsub}^{fsup} xi \cdot (fi - M1)^2}{\sum_{i=fsub}^{fsup} xi} \quad (5)$$

g) Main Peak Amplitude to First Harmonic Amplitude Ratio (MPFHR):

$$MPFHR = \frac{x(F_p)}{x(2F_p)} \quad (6)$$

where xi is the spectral amplitude at the frequency fi.

3.2. Statistical analysis

Statistical description (mean value, standard deviation, range, etc.) has been computed for each parameter and for each rhythm by means of SPSS program tool. Box Whisker & Dot Plots has been displayed to quick illustrate performance of each parameter between NSR vs Atrial arrhythmias (AFl & AF) and AF vs AFl. Statistical significance analysis for each parameter and for both groups has also been done.

4. Results and discussion

Once spectral analysis of different episodes was computed they were checked. As it was expected, ventricular sources presented a spectrum very close to the spectrum of a normal sinus rhythm (NSR), i.e. with high spectral content in the frequency range [0.5..60]Hz. Meanwhile atrial sources showed a spectrum that differs from the spectra of ventricular sources.

Inspection of spectrum atrial sources (fig. 2 as an example) confirm what we expected:

- Narrowband for AF-AFl vs. Wideband for NSR.
- Main peak amplitude vs several peaks amplitude.
- Harmonic presence for AFl vs absence for AF.

And some others not so expected:

- Main frequency peak is overlapped against NSR-Atrial Arrhythmias. Mainly in AFL vs NSR episodes. As we can see in fig. 2, main frequency peak was located around 4.3Hz in the case of AFL and within the interval [6..8] Hz in the case of AF.
- Peak amplitude strongly higher in AFl episodes than AF.

Table 1 summarizes mean and standard deviation of some of spectral parameters described above for AF and AFl.

Table 1. Spectral Parameters

	AF		AFL	
	Mean	Std	Mean	Std
F_p (Hz)	6.32	0.9	4.27	0.3
A1	0.21	0.096	0.055	0.028
SCBP	0.47	0.12	0.59	0.05
M1	6.18	0.95	4.13	0.25
NFSM	1.46	0.47	1.6	0.12
M2	0.695	0.087	0.49	0.016
MPFHR	43.52	50.33	2.88	0.31

As it can be observed, some of them show strong differences, i.e. the main peak frequency, the spectral content below the main peak, the main peak to first harmonic ratio, etc. In the case of main peak frequency the range is [2.3,6.83] for NSR, [5.13,7.32] for AF and [4.03,4.64] for AFl. So Fp is very good localized for AFl but completed overlapped with NSR. So, on one hand this parameter by itself is not able to discriminate

between NSR and Afl, while on the other hand it is perfect to discriminate between AF vs AFl. Other parameters as MPFHR are not consistent since ranges for AF and AFL are overlapped.

First and second order moments arise to be parameters with no overlapped ranges and hence, appropiated for characterization and further discrimination.

Significant analysis corroborate the observation for AF vs Atrial Arrhtymias: SCBP, M1, M2 parameters are significant ($p<0.05$). Meanwhile this is not the case for Fp ($p=0.43$). For AF vs AFl: Fp, M2, A1,SCBP,MPFHR and M1 parameters are significant ($p<0.05$). Fp or M2 parameters are enough for completed discrimination (100% of accuracy).

It has be remarked that some parameters could be redundant. For example, the main peak frequency and the first order moment are strongly correlated for AF vs AFl study.

5. Conclusions

Spectral characterization proves a straightforward, efficient methodology for validating the effectiveness of AA extraction techniques (both local and global contribution) from the surface ECG. In addition, the proposed methodology substantiates the suitability of BSS to this problem and offers simple guidelines for the implementation of future BSS-based automatic AA-extraction algorithms.

Furthermore, the spectral parameterization proposed in this study show a different characterization for different atrial arrhythmias: AF and AFL. These parameters have also proven their success for the classification of other ventricular arrhytmias. All these considerations lead the authors to anticipate promising prospects for the further characterization of other existing atrial arrythmias as well as for their automatic identification.

References

[1] Clayton RH, Murray A, Campbell RWF. Analysis of the Body Surface ECG measured in independent leads during ventricular fibrillation in humans. PACE 1995; 18: 1876-1881.

[2] Chorro FJ, Guerrero J, Cánoves J, Martínez-Sober M, Mainar L, Sanchis J, et al. Quantification of the modifications in the dominant frequency of ventricular fibrillation under conditions of ischemia and reperfusion: an experimental study. PACE 1998; 21: 1716-1723.

[3] Nygards ME, Hulting J. Recognition of ventricular fibrillation from the power spectrum of the ECG. Comput Cardiol 1977: 393-397.

[4] Forster FK, Weaver WD. Recognition of ventricular fibrillation, other rhythms and noise in patients developing the sudden cardiac death syndrome. Comput Cardiology 1982: 245-248.

[5] Barro S, Ruiz R, Cabello D, Mira J. Algorithmic sequential decision-making in the frequency domain for life threatening ventricular arrhythmias and imitiative artifacts: a diagnostic system. Journal Biomedical Engineering 1989; 11: 320-328.

[6] Nolle FM, Bowser RW, Badura FK, et al. Evaluation of a frequency-domain algorithm to detect ventricular fibrillation in the surface electrocardiogram. Computers in Cardiology 1989: 337-340.

[7] Millet-Roig J., López JJ, Mocholí A., Ruiz R., Chorro F.J. Study of frequency and Time domain parameters extracted by means of wavelet transform applied to ECG to distnguish between VF and other arrhytmias. Computers in Cardiology, vol. 25; Cleveland, 1998

[8] J. J. Rieta, V. Zarzoso, J. Millet-Roig, R. García-Civera and R. Ruiz-Granell, "Atrial Activity Extraction Based on Blind Source Separation as an Alternative to QRST Cancellation for Atrial Fibrillation Analysis" in: *Computers in Cardiology, Vol. 27, Boston, MA, September 24-27, 2000, pp. 69-72.*

Address for correspondence.

Name: José Millet Roig
Full postal address: ETSIT Telecomunicaciones
Camí de Vera s/n
46020 Valencia
SPAIN
E-mail address: jmillet@eln.upv.es

CLOSED-FORM SEMI-BLIND SEPARATION OF THREE SOURCES FROM THREE REAL-VALUED INSTANTANEOUS LINEAR MIXTURES VIA QUATERNIONS

Vicente Zarzoso and Asoke K. Nandi

Signal Processing and Communications Group, Department of Electrical Engineering and Electronics,
The University of Liverpool, Brownlow Hill, Liverpool L69 3GJ, UK
Tel/Fax: +44 151 794 4525/4540, e-mail: {vicente, aknandi}@liv.ac.uk
http://www.liv.ac.uk/{~vicente, EEE/staff/nandi.htm}

ABSTRACT

In the problem of blind source separation from instantaneous linear mixtures, a unitary transformation remains unknown after second-order spatial whitening. We present a novel approach for the identification of the orthogonal matrix in the real-valued three-signal scenario which, in contrast to existing procedures, operates in a single closed-form step, with no iterations. The new approach is based on intuitive geometrical notions and the theory of quaternions, and develops into a practical semi-blind method requiring certain prior knowledge on the source statistics. A simple numerical experiment illustrates the proposed algorithm.

1. INTRODUCTION

Consider the linear model:

$$\mathbf{y} = M\mathbf{x}, \tag{1}$$

where $\mathbf{y} \in \mathbb{R}^p$, $\mathbf{x} \in \mathbb{R}^q$ and $M \in \mathbb{R}^{p\times q}$. Blind source separation (BSS) aims to recover the unknown source signals $\mathbf{x}$ and mixing matrix M from the observed mixture $\mathbf{y}$ [1]. The above model holds, for instance, when unknown transmitted radio signals impinge on an antenna array whose layout is unknown or difficult to model. The BSS problem is also encountered in a variety of areas such as multi-user communications, radar/sonar, biomedical signal processing and seismic exploration.

The crucial assumption allowing the source extraction and mixing-matrix identification is the statistical independence of the source signals. Mathematically, this assumption can be formulated in terms of the source joint probability density function (pdf) $p_{\mathbf{x}}(\mathbf{x})$:

$$p_{\mathbf{x}}(\mathbf{x}) = \prod_{s=1}^{q} p_{x_s}(x_s), \tag{2}$$

Vicente Zarzoso would like to thank the Royal Academy of Engineering for supporting this work through the award of a Post-doctoral Research Fellowship.

where p_{x_s} is the marginal pdf of the sth component of $\mathbf{x}$. From this perspective, BSS can be accomplished through the independent component analysis (ICA) of the observations. ICA searches for a transformation on the observed vector yielding independent components or, at least, as independent as possible in the sense of the optimization of a suitable independence criterion [2]. Certain identifiability conditions guarantee that the vector obtained via ICA corresponds to the sources, up to, perhaps, irrelevant permutation and scale factors affecting its components. The evident complexity in operating directly over the pdf is alleviated by means of more tractable approximations, or contrasts, based on higher-order statistics [2, 3].

In this paper, we aim to achieve ICA by adopting a more intuitive geometrical viewpoint. After diagonalization of the observed covariance matrix (pre-whitening) — carried out through conventional second-order techniques (principal component analysis)— the mixing reduces to an unknown orthogonal transformation $Q \in \mathbb{R}^{q\times q}$, which can be considered as a rotation in a q-dimensional space. The resulting whitened sensor-output $\mathbf{z} \in \mathbb{R}^q$ then reads:

$$\mathbf{z} = Q\mathbf{x}. \tag{3}$$

Accordingly, $p_{\mathbf{z}}(\mathbf{z}) = p_{\mathbf{x}}(Q^{\dagger}\mathbf{z})$, where symbol † stands for the transpose operator, so that the pdf of $\mathbf{x}$ undergoes an analogous transformation in the whitened observation signal subspace. In such subspace, the source directions correspond to the columns of Q. The estimated rotation must be such that, when applied on the whitened observations, it aligns the source directions with the observation frame of reference, thus resulting in the pdf of a signal vector with independent components [eqn. (2)].

In the fundamental two-signal case ($q = 2$) the above geometrical concepts are illustrated in Fig. 1. The bottom plots display the scatter diagrams —representations of the form $\big(x_1(\tau), x_2(\tau)\big)$, τ denoting a time index— which are sample approximations of the true pdfs. The unknown unitary transformation reduces to a planar rotation of angle θ, whose estimation can be carried out in closed form [2, 3,

In *Proc. 6th International Symposium on Signal Processing and its Applications*, Kuala Lumpur, Malaysia, August 13-16, 2001, Vol. I, pp. 1-4.

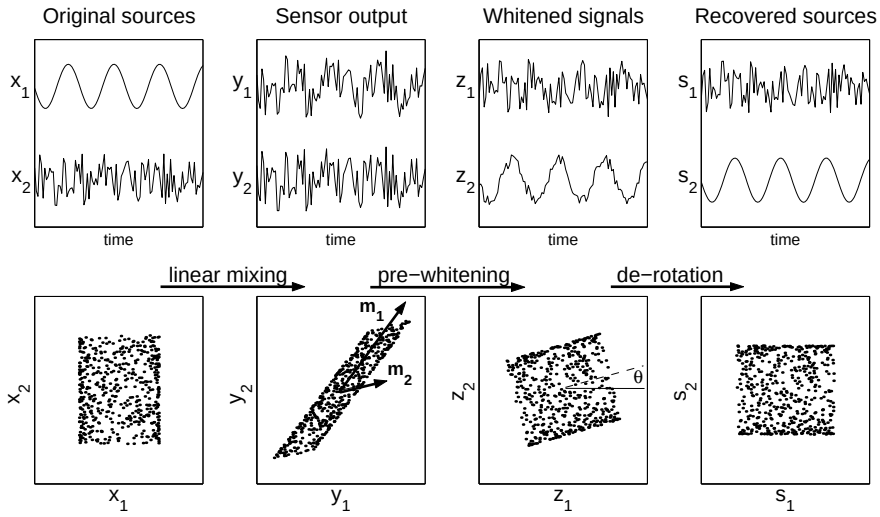

Figure 1: BSS of two instantaneous linear mixtures, with sources composed of a sinusoid and a uniformly distributed process. The top plots show the time variation of the signals, whereas the bottom plots represents the respective scatter plots. Vectors $\mathbf{m}_1$ and $\mathbf{m}_2$ refer to the source directions (or signatures) in the observation signal subspace. After diagonalizing the sensor-output covariance matrix, the source directions simply become the whitened signal subspace basis vectors rotated by an unknown angle θ.

4, 5, 6, 7, 8]. Fourth-order cumulants are directly employed in the algebraic and contrast-based approaches of [4] and [2, 6]. When the sources present symmetric marginal pdfs, a simple yet insightful geometrical standpoint can be taken by exploiting the various symmetries of the resulting scatter plot [5]. The restricted approximate ML criterion of [3] is extended in [7, 8], where the scatter-plot samples are conveniently expressed as complex numbers $(z_1 + iz_2)$, $i^2 = -1$. Higher-order expectations of these representations are shown to generate explicit expressions for the estimation of the relevant parameter.

More than two sources can be separated through the iterative application of a two-signal method over all signal pairs [2]. In the three-signal case ($q = 3$), iterations on three signal pairs are required, sometimes over several sweeps. In a bid to obtain a more efficient separation scheme, the present contribution is devoted to extending the single-step (i.e., non-iterative) closed-form estimation of Q to the three-signal scenario. The mathematical tool which allows us to accomplish this task is the quaternion algebra.

2. QUATERNIONS

Quaternions were invented by Sir William Rowan Hamilton, the most important Irish mathematician of all time, in the 1840's [9]. In his original motivation, Hamilton developed quaternions as quotients of three-dimensional (3D) vectors. Algebraically, a quaternion is a four-dimensional entity that can be represented as a linear combination of the four quaternion units 1, i, j, and k: $\mathbb{A} = a + a_1 i + a_2 j + a_3 k$, $a,\, a_m \in \mathbb{R}$, $1 < m < 3$. These units form the basis for the quaternion space, and fulfil the famous fundamental relations $i^2 = j^2 = k^2 = ijk = -1$, which give the basic rules for quaternion multiplication. Quaternions are the natural extension of complex numbers, with the remarkable feature that their product is not commutative [9]. In fact, they constituted the first non-Abelian ring to be discovered [10]. The most salient properties of quaternions are summarized below [11]:

(P1) Quaternion $\mathbb{A}$ can be expressed as the combination of a scalar part, $a \in \mathbb{R}$, and a vector part, $\mathbf{a} = [a_1,\, a_2,\, a_3]^\dagger \in \mathbb{R}^3$: $\mathbb{A} = [\![a,\, \mathbf{a}]\!]$. We denote $\mathrm{vec}(\mathbb{A}) = \mathbf{a}$.
(P2) Conjugate: $\mathbb{A}^* = [\![a,\, -\mathbf{a}]\!]$.
(P3) Norm: $|\mathbb{A}| = (\mathbb{A}\mathbb{A}^*)^{\frac{1}{2}} = (\mathbb{A}^*\mathbb{A})^{\frac{1}{2}} = \sqrt{a^2 + |\mathbf{a}|^2}$.
(P4) Inverse: $\mathbb{A}\mathbb{A}^{-1} = \mathbb{A}^{-1}\mathbb{A} = 1 \;\Rightarrow\; \mathbb{A}^{-1} = \mathbb{A}^*|\mathbb{A}|^{-2}$.
(P5) Product:

$$\mathbb{A}\mathbb{B} = [\![ab - \mathbf{a}\cdot\mathbf{b},\, a\mathbf{b} + b\mathbf{a} + \mathbf{a}\times\mathbf{b}]\!], \qquad (4)$$

where $\mathbb{B} = [\![b,\, \mathbf{b}]\!]$, symbol '$\cdot$' represents the inner (or dot) product and '$\times$' the vector (or cross) product. Quaternion product is associative, $(\mathbb{A}\mathbb{B})\mathbb{C} = \mathbb{A}(\mathbb{B}\mathbb{C})$, but not commutative, i.e., in general $\mathbb{A}\mathbb{B} \neq \mathbb{B}\mathbb{A}$. Also: $(\mathbb{A}\mathbb{B})^* = \mathbb{B}^*\mathbb{A}^*$.
(P6) Exponential form: $\mathbb{A} = |\mathbb{A}|\mathrm{e}^{\mathbf{n}\phi}$, where

$$\mathrm{e}^{\mathbf{n}\phi} = [\![\cos\phi,\, \mathbf{n}\sin\phi]\!], \qquad (5)$$

and $\mathbf{n} = \mathbf{a}/|\mathbf{a}|$. In addition: $(\mathrm{e}^{\mathbf{n}\phi})^* = \mathrm{e}^{-\mathbf{n}\phi}$, and $\mathrm{e}^{\mathbf{n}\phi}\mathrm{e}^{\mathbf{n}\theta} = \mathrm{e}^{\mathbf{n}\theta}\mathrm{e}^{\mathbf{n}\phi} = \mathrm{e}^{\mathbf{n}(\phi+\theta)}$, $\forall\phi, \theta \in \mathbb{R}$.

One of the most attractive features of quaternions is their ability to represent and perform operations in the 3D space, including affine transformations, projections and, specially, rotations. A point in a 3D Euclidean space, $\mathbf{x} \in \mathbb{R}^3$, can be represented by the pure quaternion $\mathbb{X} = [\![0, \mathbf{x}]\!]$. A rotation of angle θ around an axis —or *pole*— $\mathbf{n}$ generates vector $\mathbf{z}$. This rotated point is found in the vector part of another pure quaternion $\mathbb{Z}$ given by the so-called canonical transformation [11]:

$$\mathbb{Z} = \mathrm{e}^{\mathbf{n}\theta/2}\mathbb{X}\,\mathrm{e}^{-\mathbf{n}\theta/2}. \tag{6}$$

Applications of quaternions include molecular and nuclear physics, cryptography, image processing [12], robotics and computer vision [13], computer theory, electromagnetism, and mechanical design. For the first time, this contribution applies quaternions to the problem of source separation.

3. SOURCE SEPARATION VIA QUATERNIONS

3.1. General Approach

The connection between BSS in the three-signal case and quaternions soon becomes apparent. The 3D source and whitened vectors can be represented by quaternions $\mathbb{X}$ and $\mathbb{Z}$, respectively. The unitary transformation Q linking the sources and sensor-output after pre-whitening [eqn. (3)] can similarly be characterized by a pole $\mathbf{n}$ and a rotation angle θ that are both unknown. The quaternion formulation of this transformation is then given by (6). Hence, the problem reduces to the estimation of rotation parameters $(\mathbf{n}, \theta)$ from $\mathbb{Z}$. If the sources were known, the problem could be solved by the algorithm described next.

Algorithm 1 (Identification of 3D rotation parameters). Given two linearly independent source samples $\mathbf{x}_1$, $\mathbf{x}_2$, and their respective whitened observations, $\mathbf{z}_1$, $\mathbf{z}_2$, the rotation parameters can be identified as follows:

- Step 1. Compute the displacement vectors

$$\mathbf{d}_m = \mathbf{z}_m - \mathbf{x}_m, \qquad m = 1, 2. \tag{7}$$

- Step 2. Estimate the rotation axis (Appendix 6.1):
  - If $\mathbf{d}_1 = \mathbf{d}_2 = \mathbf{0}$ then $\theta = 0$ and, since there is no rotation, the actual value of $\mathbf{n}$ is irrelevant. Second-order analysis has already performed the source separation.
  - Else, if $\mathbf{d}_1 = \mathbf{0}$, $\mathbf{d}_2 \neq \mathbf{0}$ (resp. $\mathbf{d}_1 \neq \mathbf{0}$, $\mathbf{d}_2 = \mathbf{0}$) then $\mathbf{n} = \mathbf{x}_1$ (resp. $\mathbf{n} = \mathbf{x}_2$).
  - Else, $\mathbf{n} = \mathbf{d}_1 \times \mathbf{d}_2$. If $\mathbf{n} = \mathbf{0}$ then $\mathbf{n} = \mathbf{x}_1 \times \mathbf{x}_2 \times \mathbf{d}_m$ ($m = 1$ or $m = 2$).
- Step 3. Normalize pole: $\mathbf{n} := \mathbf{n}/|\mathbf{n}|$.
- Step 4. Set up $\mathbb{N} = [\![0, \mathbf{n}]\!]$, $\mathbb{X}_m = [\![0, \mathbf{x}_m]\!]$, and $\mathbb{Z}_m = [\![0, \mathbf{z}_m]\!]$, $m = 1, 2$. Obtain the rotation quaternion as (Appendix 6.2):

$$\mathrm{e}^{\mathbf{n}\theta/2} = \left[(\mathbb{N}\mathbb{Z}_m - \mathbb{Z}_m\mathbb{N})(\mathbb{N}\mathbb{X}_m - \mathbb{X}_m\mathbb{N})^{-1}\right]^{\frac{1}{2}}, \tag{8}$$

  with $m = 1$ or $m = 2$ according to Step 2.

3.2. A Practical Semi-Blind Method

Since, by definition, the source signals are not available, the above procedure cannot be applied directly. Instead, we adopt a *semi-blind* approach, by assuming that we have prior knowledge of the source statistics at least at two different orders. The conditions that these statistics must fulfil will be determined later. First, let us define the r*th-order quaternion moment* [12] as:

$$\overline{\mathbb{X}}_r = \mathrm{E}[\underbrace{\mathbb{X}\mathbb{X}^*\cdots}_{r}], \tag{9}$$

where $\mathrm{E}[\cdot]$ represents the mathematical expectation. Denoting the $(r+s+t)$th-order moment of the source signals as $\mu^x_{rst} = \mathrm{E}[x_1^r x_2^s x_3^t]$, and assuming zero-mean unit-power sources, the first source quaternion moments are:

$$\overline{\mathbb{X}}_1 = 0, \qquad \overline{\mathbb{X}}_2 = 3 \tag{10a}$$

$$\overline{\mathbb{X}}_3 = \mu^x_{300} i + \mu^x_{030} j + \mu^x_{003} k \tag{10b}$$

$$\overline{\mathbb{X}}_4 = \mu^x_{400} + \mu^x_{040} + \mu^x_{004} + 6 \tag{10c}$$

$$\overline{\mathbb{X}}_5 = (\mu^x_{500} + 4\mu^x_{300})i + (\mu^x_{050} + 4\mu^x_{030})j + (\mu^x_{005} + 4\mu^x_{003})k \tag{10d}$$

From the basic properties of quaternions outlined in Section 2, the whitened-signal quaternion moments turn out to be [cf. eqn. (6)]:

$$\overline{\mathbb{Z}}_r = \mathrm{e}^{\mathbf{n}\theta/2}\overline{\mathbb{X}}_r\mathrm{e}^{-\mathbf{n}\theta/2}, \qquad \forall r \geqslant 1. \tag{11}$$

That is, the source quaternion moments are affected, at any order, by the same rotation as the quaternion samples. If we select two orders r_1 and r_2 such that $\overline{\mathbb{X}}_{r_1}$ and $\overline{\mathbb{X}}_{r_2}$ are not proportional, the corresponding moment vectors $\overline{\mathbf{x}}_{r_m} = \mathrm{vec}(\overline{\mathbb{X}}_{r_m})$, $m = 1, 2$, are linearly independent. As a conclusion, the rotation parameters can be identified by appropriate substitution of $\overline{\mathbb{X}}_{r_m}$, $\overline{\mathbb{Z}}_{r_m}$, $\overline{\mathbf{x}}_{r_m}$ and $\overline{\mathbf{z}}_{r_m} = \mathrm{vec}(\overline{\mathbb{Z}}_{r_m})$ for $\mathbb{X}_m$, $\mathbb{Z}_m$, $\mathbf{x}_m$ and $\mathbf{z}_m$, $m = 1, 2$, resp., in Algorithm 1.

3.3. Identifiability

The identifiability condition of the proposed method reduces to the linear independence of source quaternion moments $\overline{\mathbb{X}}_{r_1}$ and $\overline{\mathbb{X}}_{r_2}$. For this condition to be fulfilled at orders $r_1 = 3$ and $r_2 = 5$, for instance, at least a pair of asymmetrically distributed sources must show dissimilar 3rd- to 5th-order moment ratios. In particular, at most one symmetric distribution is allowed among the sources.

4. ILLUSTRATIVE RESULTS

As an illustrative numerical example, we select $r_1 = 3$, $r_2 = 5$, and source signals composed of 5×10^3 i.i.d. samples with exponential, Rayleigh and uniform distribution. Hence, $\overline{\mathbb{X}}_3 = 2i + 0.63j$ and $\overline{\mathbb{X}}_5 = 52i + 8.52j$ [eqns. (10)], which comply with the conditions set out in Section 3.3. The pole and angle of rotation are $\mathbf{n} = [0.21,\ -0.52,\ 0.83]$ (vector $[2,\ -5,\ 8]$ normalized) and $\theta = 30^{\text{o}}$, which correspond to an orthogonal mixing matrix $Q = \begin{bmatrix} 0.87 & -0.43 & -0.24 \\ 0.40 & 0.90 & -0.16 \\ 0.28 & 0.05 & 0.96 \end{bmatrix}$. The application of the proposed algorithm on the resulting unitary mixtures produces the estimates $\hat{\mathbf{n}} = [0.03 \pm 0.32,\ -0.54 \pm 0.23,\ 0.72 \pm 0.17]$ and $\hat{\theta} = 36.1^{\text{o}} \pm 17.8^{\text{o}}$, where the "mean $\pm$ standard deviation" values are obtained by averaging over 10^3 independent Monte Carlo runs. The interference-to-signal ratio (ISR) [1], a performance index that measures the distance between the original and the estimated mixing matrices, yields an average of $\text{ISR}(Q, \widehat{Q}) = -14.7$ dB, corresponding to a successful source separation.

5. CONCLUSIONS AND OUTLOOK

We have presented a novel approach for three-dimensional linear ICA which enables the closed-form identification of the remaining orthogonal transformation after second-order analysis in a single step, i.e., without iterations of any kind. The approach is based on the algebra of quaternions, and is able to perform non-iterative semi-blind separation of three source signals from three instantaneous linear mixtures.

At the orders considered ($r_1 = 3$, $r_2 = 5$) the applicability conditions of the suggested algorithm are indeed restrictive. Additional work is required to increase the range of source distributions that can be treated. Nevertheless, the basic foundations for the use of quaternions in ICA/BSS have been laid down, and we envisage that the applicability domain of quaternion theory in this exciting signal processing problem will be broadened in future investigations. Further efforts could begin by focusing on the performance analysis of the proposed identification scheme, its comparison with iterative procedures, and the application of quaternion algebra to contrast-based approaches.

6. APPENDICES

6.1. Rotation Identification

We prove that the rotation axis of Q can be identified from two linearly independent source samples $\mathbf{x}_1$, $\mathbf{x}_2$, and their associated observations $\mathbf{z}_1$, $\mathbf{z}_2$, as in Algorithm 1. First, consider the following remarks:
(R1) The eigenspace of rotation $Q \neq I$ (I being the identity matrix) is spanned by its pole $\mathbf{n}$, with associated eigenvalue $\lambda = 1$.
(R2) From $\mathbf{d}_m = (Q - I)\mathbf{x}_m$ and the linear independence of $\mathbf{x}_m$, it follows that $\mathbf{d}_m = \mathbf{0}$, $\forall m$, iff $Q = I$.
(R3) If $\mathbf{d}_m = \mathbf{0}$ then $\mathbf{x}_m$ belongs to the eigenspace of $Q \neq I$.
(R4) When $\mathbf{d}_m \neq \mathbf{0}$ are parallel, vectors $\mathbf{n}$, $\mathbf{x}_1$ and $\mathbf{x}_2$ are coplanar.
(R5) If $Q \neq I$, the rotation pole lies in the plane perpendicular to any non-null displacement vector $\mathbf{d}_m$.

Therefore:
• If $\mathbf{d}_1 = \mathbf{d}_2 = \mathbf{0}$ then, according to (R2), there is no rotation to be identified: $\theta = 0$.
• Else, if $\mathbf{d}_1 = \mathbf{0}$, $\mathbf{d}_2 \neq \mathbf{0}$ (resp. $\mathbf{d}_1 \neq \mathbf{0}$, $\mathbf{d}_2 = \mathbf{0}$) then, from (R1)–(R3), the rotation axis is spanned by $\mathbf{x}_1$ (resp. $\mathbf{x}_2$).
• Else, $\mathbf{d}_1 \times \mathbf{d}_2 = 0$ implies that $\mathbf{d}_m$ are parallel and hence, from (R4)–(R5), $\mathbf{n}$ can be computed from the intersection of the plane spanned by vectors $\mathbf{x}_m$ and the plane perpendicular to either $\mathbf{d}_m$. If $\mathbf{d}_m$ are not parallel, (R5) guarantees that $\mathbf{n}$ can be obtained from their vector product.

6.2. Rotation Quaternion

It is shown next that the quaternion associated with a rotation around a pole $\mathbf{n}$ applied to point $\mathbf{x}$ resulting in another point $\mathbf{z}$ is given by

$$\mathrm{e}^{\mathbf{n}\theta/2} = \left[(\mathbb{NZ} - \mathbb{ZN})(\mathbb{NX} - \mathbb{XN})^{-1}\right]^{\frac{1}{2}}, \tag{12}$$

where $\mathbb{N} = [\![0,\ \mathbf{n}]\!]$, $\mathbb{X} = [\![0,\ \mathbf{x}]\!]$ and $\mathbb{Z} = [\![0,\ \mathbf{z}]\!]$.

From quaternion product (4), we have that $\mathbf{u} = \text{vec}(\mathbb{NZ} - \mathbb{ZN}) = 2(\mathbf{n} \times \mathbf{z})$ and, similarly, $\mathbf{v} = \text{vec}(\mathbb{NZ} - \mathbb{ZN}) = 2(\mathbf{n} \times \mathbf{z})$. Now, since $\mathbf{x}$ is rotated around $\mathbf{n}$ by θ radians to yield $\mathbf{z}$, it turns out that $\mathbf{u}$ and $\mathbf{v}$ are perpendicular to $\mathbf{n}$, and separated by the same angular distance. Considering the associated pure quaternions $\mathbb{U} = [\![0,\ \mathbf{u}]\!]$, $\mathbb{V} = [\![0,\ \mathbf{v}]\!]$, and from the properties summarized in Section 2: $\mathbb{VU}^{-1} = [\![\mathbf{u} \cdot \mathbf{v},\ \mathbf{u} \times \mathbf{v}]\!]|\mathbf{u}|^{-2} = [\![\cos\theta,\ \mathbf{n}\sin\theta]\!] = \mathrm{e}^{\mathbf{n}\theta}$, from which result (12) readily follows. Finally, observe that, since scalars do commute in the quaternion product, quaternion $(-\mathbb{N})$ also yields $\mathrm{e}^{\mathbf{n}\theta/2}$ in (12). In such a case, the equivalent rotation parameters $(-\mathbf{n},\ -\theta)$ are estimated instead of $(\mathbf{n},\ \theta)$.

7. REFERENCES

[1] V. Zarzoso and A. K. Nandi, "Blind Source Separation," in *Blind Estimation Using Higher-Order Statistics*, A. K. Nandi (Ed.), pp. 167–252. Kluwer Academic Publishers, Boston, 1999.

[2] P. Comon, "Independent Component Analysis, A New Concept?," *Sig. Proc.*, Vol. 36, No. 3, pp. 287–314, Apr. 1994.

[3] F. Harroy and J.-L. Lacoume, "Maximum Likelihood Estimators and Cramer-Rao Bounds in Source Separation," *Sig. Proc.*, Vol. 55, No. 2, pp. 167–177, Dec. 1996.

[4] P. Comon, "Separation of Sources Using Higher-Order Cumulants," in *Proc. SPIE*, San Diego, CA, 1989, Vol. 1152, pp. 170–181.

[5] R. E. Bogner, *Blind Separation of Sources*, Memo. No. 4559, Defence Research Agency, Malvern, UK, May 1992.

[6] F. Herrmann and A. K. Nandi, "Maximisation of Squared Cumulants for Blind Source Separation," *IEE Electronics Letters*, Vol. 36, No. 19, pp. 1164–1165, 2000.

[7] V. Zarzoso and A. K. Nandi, "Blind Separation of Independent Sources for Virtually Any Source Probability Density Function," *IEEE Trans. Sig. Proc*, Vol. 47, No. 9, pp. 2419–2432, Sept. 1999.

[8] V. Zarzoso, *Closed-Form Higher-Order Estimators for Blind Separation of Independent Source Signals in Instantaneous Linear Mixtures*, Ph.D. thesis, The University of Liverpool, UK, Oct. 1999.

[9] W. R. Hamilton, *Elements of Quaternions*, Longmans, Green & Co., London, 1866.

[10] J. A. Gallian, *Contemporary Abstract Algebra*, Houghton Mifflin, Boston, MA, 4th edition, 1998.

[11] S. L. Altmann, *Rotations, Quaternions and Double Groups*, Clarendon Press, Oxford, 1986.

[12] S.-C. Pei and C.-M. Cheng, "Color Image Processing by Using Binary Quaternion-Moment-Preserving Thresholding Technique," *IEEE Transactions on Image Processing*, Vol. 8, No. 5, pp. 614–628, May 1999.

[13] R. Smith, A. Frost, and P. Probert, "Sensor System for the Navigation of an Underwater Vehicle," *International Journal of Robotics Research*, Vol. 18, No. 7, pp. 697–710, 1999.

WEIGHTED CLOSED-FORM ESTIMATORS FOR BLIND SOURCE SEPARATION

Vicente Zarzoso, Frank Herrmann and Asoke K. Nandi

Signal Processing and Communications Group, Department of Electrical Engineering and Electronics,
The University of Liverpool, Brownlow Hill, Liverpool L69 3GJ, UK
Tel/Fax: +44 151 794 4525/4540, e-mail: {vicente, fherrm, aknandi}@liv.ac.uk
http://www.liv.ac.uk/~{vicente, fherrm, aknandi}

ABSTRACT

This paper investigates a novel closed-form estimation class, so-called weighted estimator (WE), for blind source separation in the basic two-signal problem. Proper combination of previously proposed estimators yields consistent estimates of the separation parameters under general conditions. In the real-mixture case, we determine analytic expressions for the WE asymptotic (large-sample) variance and the source-dependent weight value of the most efficient estimator in the class. By means of the bicomplex-number formalism, the WE is extended to the complex-mixture scenario, for which Cramér-Rao bounds are also derived. Simulations compare the WE with other methods, demonstrating its potential.

Keywords: blind source separation, estimation theory, higher-order statistics, non-Gaussian signal processing, sensor array processing.

1. INTRODUCTION

The problem of blind source separation (BSS) arises in a great variety of applications, in fields as diverse as wireless communications, seismic exploration and biomedical signal processing. BSS aims to reconstruct an unknown set of q mutually independent source signals $\mathbf{x} \in \mathbb{C}^q$ which appear mixed at the output of a p-sensor array $\mathbf{y} \in \mathbb{C}^p$, $p \geqslant q$. In the noiseless instantaneous linear case, sources and observations are linked through an unknown mixing transformation $M \in \mathbb{C}^{p \times q}$:

$$\mathbf{y} = M\mathbf{x}. \tag{1}$$

The problem consists of estimating the source vector $\mathbf{x}$ and the mixing matrix M from the exclusive knowledge of sensor vector $\mathbf{y}$. Neither the ordering nor the power and phase-shift of the sources can be identified in the model above, so we may assume, with no loss of generality, an identity source covariance matrix.

When the time structure of the signals cannot be exploited (e.g., due to the source spectral whiteness), one needs to resort to higher-order statistics (HOS) [1]. The success of the separation then relies on the non-Gaussian nature of the sources. A previous spatial whitening process (entailing second-order decorrelation and power normalization) helps to reduce the number of unknowns, resulting in a set of normalized uncorrelated components $\mathbf{z} \in \mathbb{C}^q$:

$$\mathbf{z} = Q\mathbf{x}, \tag{2}$$

with $Q \in \mathbb{C}^{q \times q}$ unitary. As the general scenario $p > 2$ can be tackled through an iterative approach over the signal pairs [2], the two-signal case, $p = q = 2$, is of fundamental importance. The unitary transformation Q is then a complex elementary Givens rotation matrix:

$$Q = \begin{bmatrix} \cos\theta & -\mathrm{e}^{-j\alpha}\sin\theta \\ \mathrm{e}^{j\alpha}\sin\theta & \cos\theta \end{bmatrix}. \tag{3}$$

Hence, the source-signal extraction and mixing-matrix identification reduce to the estimation of angular parameters $\theta,\ \alpha \in \mathbb{R}$.

In the real-valued mixture case, $\alpha = 0$ and only θ is unknown. The performance of the first closed-form solution for the estimation of θ, based on the output 4th-order cross-cumulant nulling [3], was later shown to depend on θ itself [4, 5]. The maximum-likelihood (ML) approach on the Gram-Charlier expansion of the source probability density function (pdf) produced the solution of [6], whose validity was broadened through the extended ML (EML) and the alternative EML (AEML) estimators [4, 7, 8]. Such estimators lose their consistency for zero source kurtosis sum (sks) and source kurtosis difference (skd), respectively. This deficiency was overcome in [8] and [9]. In the latter, adopting the framework of [6] the two estimators were joined into a single analytic expression, the approximate ML (AML). The MaSSFOC estimator [10], derived from the approximate maximization of a contrast function made up of the sum of output squared kurtosis [2], exhibits a strikingly resembling form. The notion of linearly combining estimation expressions using arbitrary weights was originally put forward in [9], giving rise to the so-called weighted AML (WAML) estimator. It was suggested that the weight parameter could be adjusted by taking advantage of a priori information on the source pdfs, although no specific guidelines were given on how the actual choice should be made.

The present contribution fills this gap by studying in finer detail this weighted estimator (WE) for BSS and emphasizing its potential benefits. In the real-mixture case, we capitalize on the complex-centroid notation used in the EML and AEML estimators in order to provide an analytic formula for the WE large-sample variance. From this formula, the weight parameter of the asymptotically most efficient WE is obtained as a function of the source statistics. In addition, the WE is neatly extended to the complex-valued mixture case with the bicomplex number formalism developed in [4, 11]. We deduce Cramér-Rao lower bounds (CRLBs) for the pertinent parameters, and show in simulations that the WE is able to follow the CRLB trend of an objective separation-quality performance index. The connections between the WE and other analytic solutions are also highlighted throughout the paper.

First, we summarize a few mathematical notations. Symbol $\mu^x_{mn} = \mathrm{E}[x_1^m x_2^n]$, where $\mathrm{E}[\cdot]$ denotes the mathematical expectation, stands for the $(m+n)$th-order moment of the source signals $\mathbf{x} = (x_1, x_2)$. For convenience, the cumulants of complex vector $\mathbf{z} = (z_1, \ldots, z_q)$ are defined as $\mathrm{Cum}^z_{i_1 i_2 i_3 \ldots} =$

Vicente Zarzoso would like to thank the Royal Academy of Engineering for supporting this work through the award of a Post-doctoral Research Fellowship.

In *Proc. 11th IEEE Workshop on Statistical Signal Processing*, Orchid Country Club, Singapore, August 6-8, 2001, pp. 456-459.

$\mathrm{Cum}[z_{i_1}^*, z_{i_2}, z_{i_3}^*, \dots]$, $1 \leqslant i_k \leqslant q$, with the convention, in the two-component case, $\kappa^z_{n-r,\,r} = \mathrm{Cum}^z_{\underbrace{1\dots1}_{n-r}\,\underbrace{2\dots2}_{r}}$. We also define $\gamma = \kappa^x_{40} + \kappa^x_{04}$ (sks) and $\eta = \kappa^x_{40} - \kappa^x_{04}$ (skd). Symbol $\angle a$ represents the principal value of the argument of $a \in \mathbb{C}$.

2. REAL-MIXTURE CASE

2.1. Fourth-Order Weighted Estimator

The WAML estimator [9] accepts a more convenient formulation when adopting the EML/AEML approach [4, 5, 7, 8], which is based on the polar representation of real-valued bivariate random vector $\mathbf{z} = (z_1, z_2)$ as $\rho \mathrm{e}^{j\phi} = z_1 + jz_2$, $j = \sqrt{-1}$. Higher-order expectations then generate complex-valued linear combinations (*centroids*) of the whitened-sensor statistics which lead to explicit estimation expressions for the parameter of interest. Accordingly, the EML is expressed as

$$\hat{\theta}_{\mathrm{EML}} = \tfrac{1}{4}\angle(\gamma\xi_4), \tag{4}$$

where ξ_4 is the 4th-order complex centroid:

$$\xi_4 = \mathrm{E}[\rho^4 \mathrm{e}^{j4\phi}] = (\kappa^z_{40} + \kappa^z_{04} - 6\kappa^z_{22}) + j4(\kappa^z_{31} - \kappa^z_{13}), \tag{5}$$

and the sks can be estimated from the array output through $\gamma = \mathrm{E}[\rho^4] - 8 = \kappa^z_{40} + \kappa^z_{04} + 2\kappa^z_{22}$. Similarly, the AEML [4, 8] reads:

$$\hat{\theta}_{\mathrm{AEML}} = \tfrac{1}{2}\angle\xi_2, \tag{6}$$

$$\xi_2 = \mathrm{E}[\rho^4 \mathrm{e}^{j2\phi}] = (\kappa^z_{40} - \kappa^z_{04}) + j2(\kappa^z_{31} + \kappa^z_{13}). \tag{7}$$

Under mild conditions [4, 7], centroids ξ_4 and ξ_2 are consistent estimators of $\gamma\mathrm{e}^{j4\theta}$ and $\eta\mathrm{e}^{j2\theta}$, respectively, so that $\hat{\theta}_{\mathrm{EML}}$ and $\hat{\theta}_{\mathrm{AEML}}$ consistently estimate θ as long as $\gamma \neq 0$ and $\eta \neq 0$, respectively. It follows that

$$\hat{\theta}_{\mathrm{WE}} = \tfrac{1}{4}\angle\xi_{\mathrm{WE}}, \qquad \text{with} \tag{8}$$

$$\xi_{\mathrm{WE}} = w\gamma\xi_4 + (1-w)\xi_2^2, \qquad 0 < w < 1. \tag{9}$$

is a consistent estimator of θ for *any* source distribution (besides when the sources are both Gaussian). Eqn. (8) is essentially the WAML estimator [9] written in centroid form. Nonetheless, we adhere to the more general denomination of *weighted estimator (WE)*, since its ML nature becomes unclear when extended to the complex-signal domain (Section 3).

Some special cases of the WE are:

(i) $w = 0$: AEML estimator of [4, 8].
(ii) $w = 1/3$: AML estimator of [9].
(iii) $w = 1/2$: MaSSFOC estimator of [10].
(iv) $w = 1$: EML estimator of [4, 7].

2.2. Performance Analysis

Along the lines of [4, 5], and omitting tedious algebraic details, the asymptotic (large-sample) variance of the WE (8) is determined as:

$$\sigma^2_{\hat{\theta}_{\mathrm{WE}}} = \frac{\mathrm{E}\Big\{\big[w\gamma(x_1^3x_2 - x_1x_2^3) + (1-w)\eta(x_1^3x_2 + x_1x_2^3)\big]^2\Big\}}{T\big[w\gamma^2 + (1-w)\eta^2\big]^2}, \tag{10}$$

where T is the number of samples. Remark that:

(i) $\sigma^2_{\hat{\theta}_{\mathrm{WE}}}$ reduces to the asymptotic variance of the AEML and EML estimators [4, 5] for $w = 0$ and $w = 1$, respectively.

(ii) When $\gamma = 0$ (resp. $\eta = 0$), WE performance reduces to that of the AEML (resp. EML) estimator, for any $0 < w < 1$.

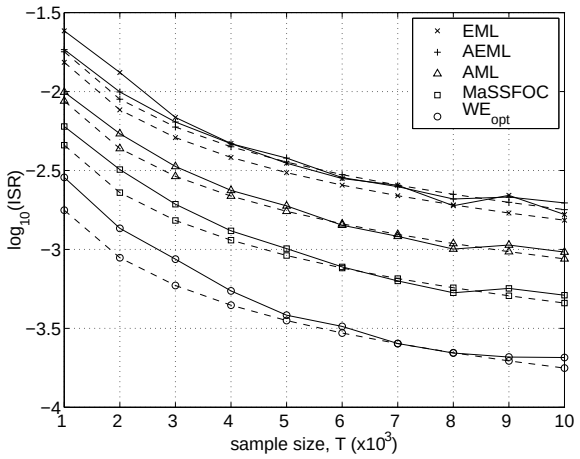

Fig. 1. ISR vs. sample size. Uniform–Rayleigh sources, $\theta = 15^{\mathrm{o}}$, ν independent Monte Carlo runs, with $\nu T = 5 \times 10^6$. Solid lines: average empirical values. Dashed lines: asymptotic variances (10).

2.3. Optimal Large-Sample Performance

If $|\kappa^x_{40}| \neq |\kappa^x_{04}|$, the derivative of eqn. (10) with respect to w cancels at:

$$w_{\mathrm{opt}} = \frac{1}{2} + \frac{\mu^x_{40}\mu^x_{04}\big[(\kappa^x_{40})^2 - (\kappa^x_{04})^2\big] + \kappa^x_{40}\kappa^x_{04}(\mu^x_{60} - \mu^x_{06})}{2\big[(\kappa^x_{40})^2\mu^x_{06} - (\kappa^x_{04})^2\mu^x_{60}\big]}. \tag{11}$$

Since $\partial^2(\sigma^2_{\hat{\theta}_{\mathrm{WE}}})/\partial w^2\big|_{w_{\mathrm{opt}}} > 0$, w_{opt} corresponds to the minimum variance estimator of the WE family. Hence, given the source statistics, one can select the WE with optimal asymptotic performance. If $w_{\mathrm{opt}} \notin [0, 1]$, we choose between $w_{\mathrm{opt}} = 0$ (AEML) and $w_{\mathrm{opt}} = 1$ (EML) the value that gives the lowest $\sigma^2_{\hat{\theta}_{\mathrm{WE}}}$ in (10).

2.4. Simulation Results

A few simulations illustrate the benefits of the WE and show the goodness of asymptotic approximation (10). First, observe that any angle estimate of the form $\hat{\theta} = \theta + n\pi/2$, $n \in \mathbb{Z}$, provides a valid separation solution up to the indeterminacies mentioned in Sec. 1. The interference-to-signal ratio (ISR) performance index [1] approximates the variance of $\hat{\theta}$, $\sigma^2_{\hat{\theta}}$, around any valid separation solution [4]. The ISR is an objective measure of separation performace, for it is method independent.

Fig. 1 shows the ISR results obtained by the EML, AEML, AML, MaSSFOC and optimal WE, together with the expected asymptotic variances, for varying sample size and i.i.d. sources with uniform and Rayleigh distributions [$w_{\mathrm{opt}} = 0.7141$, from eqn. (11)]. Centroids are computed from their polar forms. The optimal WE substantially outperforms the other estimators, being, e.g., five and ten times as efficient [12] as the AML and the AEML, respectively. The fitness of asymptotic approximation (10) is very precise in all cases.

The generalized Gaussian distribution (GGD) with shape parameter λ, $p(x) \propto \exp(-|x|^\lambda)$, is used as source pdf in the simulation of Fig. 2. We fix $\kappa^x_{04} = 0.5$ and smoothly vary κ^x_{40} to generate

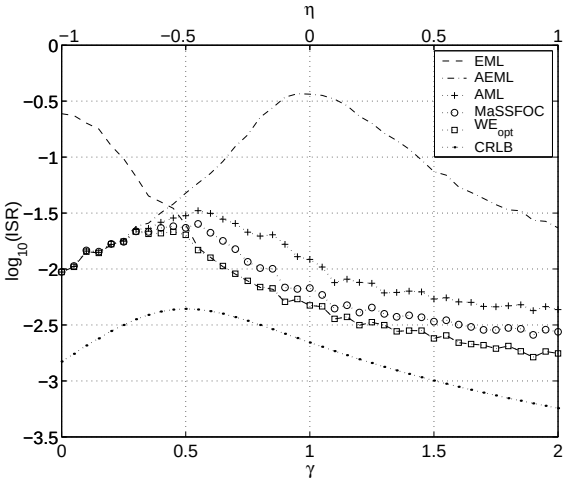

Fig. 2. ISR vs. sks γ and skd η. GGD sources, $\kappa_{04}^x = 0.5$, $\theta = 15^{\rm o}$, $T = 5 \times 10^3$ samples, 10^3 Monte Carlo runs.

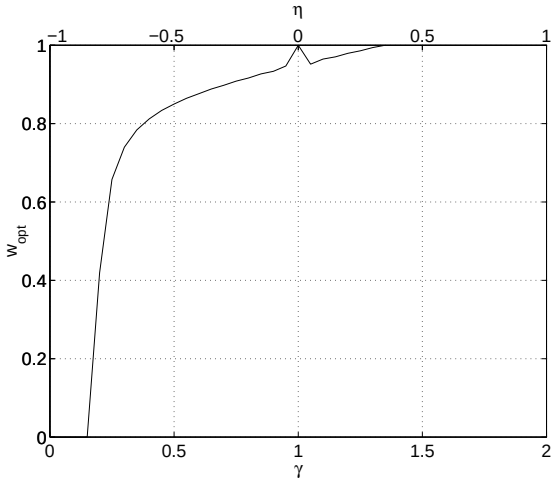

Fig. 3. Optimal value of the WE weight parameter in the separation scenario of Fig. 2.

a range of sks and skd values. The optimal WE, with $w_{\rm opt}$ calculated as in Sec. 2.3 and shown in Fig. 3, is compared with other analytic solutions and the CRLB obtained in [9] for the real case. The optimal WE follows the CRLB more closely than any of the other methods.

3. COMPLEX-MIXTURE CASE

3.1. Bicomplex Numbers

In [4, 11], the so-called bicomplex numbers prove useful in simplifying the development of closed-form estimators in the complex-mixture scenario. Given a unitary matrix $Q = \left[\begin{smallmatrix} a & -b^* \\ b & a^* \end{smallmatrix}\right]$, $a,\, b \in \mathbb{C}$, where * denotes complex conjugation, the associated bicomplex number is defined as $\bar{x} = a + \jmath b$. Though analogous to j, the *bimaginary unit* $\jmath$ is actually a distinct algebraic element. Terms $a = \mathbb{R}{\rm e}(\bar{x})$ and $b = \mathbb{I}{\rm m}(\bar{x})$ are the *breal* and *bimaginary* parts of $\bar{x}$, respectively. The product of two bicomplex numbers $\bar{x}_1 = a_1 + \jmath b_1$ and $\bar{x}_2 = a_2 + \jmath b_2$ is defined in accordance with the product of unitary transformations:

$$\bar{x}_1 \bar{x}_2 = (a_1 a_2 - b_1^* b_2) + \jmath (b_1 a_2 + a_1^* b_2). \tag{12}$$

In this manner, an isomorphism is created between the set of unitary matrices under usual matrix product and the set of bicomplex numbers under the above product operation. Note that, as with j, $\jmath^2 = -1$. A special class of bicomplex numbers arises when the associated unitary transformation shows the shape of (3):

$$\mathrm{e}_\alpha^{\jmath\theta} = \cos\theta + \jmath \mathrm{e}^{j\alpha} \sin\theta, \tag{13}$$

which we call bicomplex exponential.

3.2. Fourth-Order Weighted Estimator

By means of the bicomplex formalism, one can easily generalize centroids (5) and (7) to the complex-mixture case. Effectively,

$$\bar{\xi}_4 = (\kappa_{40}^z + \kappa_{04}^z - 6\kappa_{22}^z) + \jmath 4(\kappa_{31}^z - \kappa_{13}^z) \tag{14}$$

and

$$\bar{\xi}_2 = (\kappa_{40}^z - \kappa_{04}^z) + \jmath 2(\kappa_{31}^z + \kappa_{13}^z) \tag{15}$$

are consistent estimators of $\gamma \mathrm{e}_\alpha^{\jmath 4\theta}$ and $\eta \mathrm{e}_\alpha^{\jmath 2\theta}$, respectively, under the same general conditions as in the real case. Centroid (14) gives rise to the complex EML (CEML) estimator [4, 11], whereas (15) yields the complex AEML (CAEML) estimator [4]. Bearing in mind the bicomplex product (12), it follows immediately that the linear combination

$$\bar{\xi}_{\rm CWE} = w\gamma\bar{\xi}_4 + (1-w)\bar{\xi}_2^2 \tag{16}$$

consistently estimates $\big(w\gamma^2 + (1-w)\eta^2\big)\mathrm{e}_\alpha^{\jmath 4\theta}$. The sks γ may be obtained from the available data just as in the real case. For $w \in [0,\, 1]$, parameters $(\theta,\, \alpha)$ are estimated through

$$\begin{cases} 4\hat{\theta}_{\rm CWE} = \angle\big(\mathbb{R}{\rm e}(\bar{\xi}_{\rm CWE}) + j|\mathbb{I}{\rm m}(\bar{\xi}_{\rm CWE})|\big) \\ \hat{\alpha}_{\rm CWE} = \angle\, \mathbb{I}{\rm m}(\bar{\xi}_{\rm CWE}), \end{cases} \tag{17}$$

which is the *complex WE (CWE)*.

3.3. Cramér-Rao Lower Bounds

Assuming circularly distributed source signals composed of T independent samples, the Fisher information matrix (FIM) for the estimation of parameters $(\theta,\, \alpha)$ in model (2)–(3) reads:

$$\mathrm{FIM}_{(\theta,\,\alpha)} = T \begin{bmatrix} I & 0 \\ 0 & \frac{1}{4} I \sin^2 2\theta \end{bmatrix}, \tag{18}$$

where

$$I = I_1 + I_2 - 4,$$
$$I_k = \frac{1}{2} \iint\limits_{\mathsf{D}_k} \frac{1}{p_k} \left[\left(\frac{\partial p_k}{\partial u} \right)^2 + \left(\frac{\partial p_k}{\partial v} \right)^2 \right] \mathrm{d}u\,\mathrm{d}v, \tag{19}$$

and $p_k(u,\, v)$ is the pdf of the kth source signal $x_k = u_k + jv_k$, $u_k,\, v_k \in \mathbb{R}$, $k = 1,\, 2$. Integration extends over the definition domain D_k of the corresponding random variable.

It is interesting to note that:
(i) The CRLBs of θ and α are decoupled, and therefore:

$$\mathrm{CRLB}_\theta = (TI)^{-1} \tag{20}$$

$$\mathrm{CRLB}_\alpha = 4(TI\sin^2 2\theta)^{-1} \tag{21}$$

(ii) For sources with complex generalized Gaussian distribution (CGGD) of shape parameter λ, given by

$$p(u,\, v) \propto \exp\{-(u^2+v^2)^{\frac{\lambda}{2}}\}, \quad \lambda > 0, \tag{22}$$

we have

$$I_k = \tfrac{1}{2}\lambda_k^2 \Gamma(4/\lambda_k)/\Gamma^2(2/\lambda_k). \tag{23}$$

Then, the FIM is zero, and hence the model unidentifiable, iff $\lambda_1 = \lambda_2 = 2$, i.e., both sources are Gaussian.

(iii) When $\theta = n\pi/2,\ \forall n \in \mathbb{Z}$, estimation of α becomes unfeasible. However, in such cases the correct estimation of α does not affect the source extraction, e.g., if $\theta = 0,\ Q$ in (3) is just an identity matrix; if $\theta = \pi/2,\ Q$ only contains off-diagonal phase factors which are 'absorbed' by the source signals.

(iv) Endorsing the previous point we have that, for accurate estimates of $(\theta,\, \alpha)$, ISR $\approx \sigma^2_{\hat\theta} + \frac{1}{4}\sigma^2_{\hat\alpha}\sin^2 2\theta$, so that ISR is lower bounded by $2 \times \mathrm{CRLB}_\theta$. When $\theta = n\pi/2,\ n \in \mathbb{Z}$, and if $\hat\theta$ is still precise enough, this bound decreases to CRLB_θ. That is, the lower bound of separation-performance objective measure ISR is independent of θ and is (asymptotically) determined by the source statistics only [via I in (19)].

3.4. Simulation Results

A simple simulation experiment compares the behaviour of the CEML, CAEML and CWE (with $w = 1/3$ and $w = 1/2$, which would correspond to the complex extensions of AML and MaSS-FOC, resp.). Two independent CGGDs are used as sources. Average ISR results as a function of sks and skd are displayed in Fig. 4. As expected, the CEML and CAEML worsen near $\gamma = 0$ and $\eta = 0$, respectively. By contrast, the CWE maintains a satisfactory separation in both tested cases over all γ and η range, and, as occurred in the real case (Fig. 2), its performance follows closely the CRLB trend.

4. CONCLUSIONS AND OUTLOOK

A new class of closed-form estimators of the separation parameters in the fundamental two-signal instantaneous linear mixture BSS problem has been investigated. A weighted estimator (WE) arises from the linear combination of the EML and AEML centroids, and produces consistent estimates under rather general conditions (essentially, if at most one source is Gaussian). For real-valued mixtures, prior knowledge on the source statistics can be exploited by selecting the WE with optimal large-sample performance (minimum asymptotic variance). With the aid of the bicomplex numbers the WE has also been extended to the complex-mixture case, where it has shown a performance variation similar to the CRLB, that we have derived for circular sources.

Paths of further research include the asymptotic performance analysis of the WE in the complex environment, which is of relevance in areas as important as digital communications. Also, in order to enable a fully blind operation, it is necessary to develop the optimal weight coefficient as a function of the array-output statistics. The estimator's behaviour in the presence of additive noise and impulsive interference needs to be explored as well.

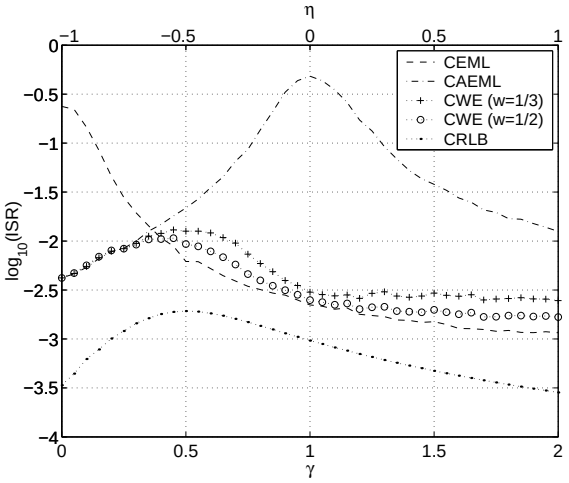

Fig. 4. ISR vs. sks γ and skd η. CGGD sources, $\kappa^x_{04} = 0.5$, $\theta = 15^o$, $\alpha = 65^o$, $T = 5 \times 10^3$ samples, 10^3 independent Monte Carlo iterations.

5. REFERENCES

[1] V. Zarzoso and A. K. Nandi, "Blind Source Separation," in *Blind Estimation Using Higher-Order Statistics*, A. K. Nandi (Ed.), pp. 167–252. Kluwer Academic Publishers, Boston, 1999.

[2] P. Comon, "Independent Component Analysis, A New Concept?," *Signal Processing*, Vol. 36, No. 3, pp. 287–314, Apr. 1994.

[3] P. Comon, "Separation of Sources Using Higher-Order Cumulants," in *Proc. SPIE*, San Diego, CA, 1989, Vol. 1152, pp. 170–181.

[4] V. Zarzoso, *Closed-Form Higher-Order Estimators for Blind Separation of Independent Source Signals in Instantaneous Linear Mixtures*, Ph.D. thesis, The University of Liverpool, UK, Oct. 1999.

[5] V. Zarzoso and A. K. Nandi, "Unified Formulation of Closed-Form Estimators for Blind Source Separation in Real Instantaneous Linear Mixtures," in *Proc. ICASSP*, Istanbul, Turkey, June 2000, Vol. V, pp. 3160–3163.

[6] F. Harroy and J.-L. Lacoume, "Maximum Likelihood Estimators and Cramer-Rao Bounds in Source Separation," *Signal Processing*, Vol. 55, No. 2, pp. 167–177, Dec. 1996.

[7] V. Zarzoso and A. K. Nandi, "Blind Separation of Independent Sources for Virtually Any Source Probability Density Function," *IEEE Transactions on Signal Processing*, Vol. 47, No. 9, pp. 2419–2432, Sept. 1999.

[8] V. Zarzoso, A. K. Nandi, F. Herrmann, and J. Millet-Roig, "Combined Estimation Scheme for Blind Source Separation with Arbitrary Source PDFs," *IEE Electronics Letters*, Vol. 37, No. 2, pp. 132–133, Jan. 18, 2001.

[9] M. Ghogho, A. Swami, and T. Durrani, "Approximate Maximum Likelihood Blind Source Separation with Arbitrary Source Pdfs," in *Proc. IEEE SSAP Workshop*, Pocono Manor Inn, PA, Aug. 2000.

[10] F. Herrmann, *Independent Component Analysis with Applications to Blind Source Separation*, Ph.D. thesis, The University of Liverpool, UK, Sept. 2000.

[11] V. Zarzoso and A. K. Nandi, "Unified Formulation of Closed-Form Estimators for Blind Source Separation in Complex Instantaneous Linear Mixtures," in *Proc. EUSIPCO*, Tampere, Finland, Sept. 2000, Vol. I, pp. 597–601.

[12] E. L. Lehmann, *Theory of Point Estimation*, Wadsworth, Inc., Pacific Grove, CA, 1991.